VOLUME 75 OCTOBER 14, 1971 NUMBER 21

JPCHAx

THE JOURNAL OF PHYSICAL CHEMISTRY

PUBLISHED BIWEEKLY BY THE AMERICAN CHEMICAL SOCIETY

FIGHT FUZZINESS

WITH THE NEW REAL-TIME

256 POINT CORRELATOR

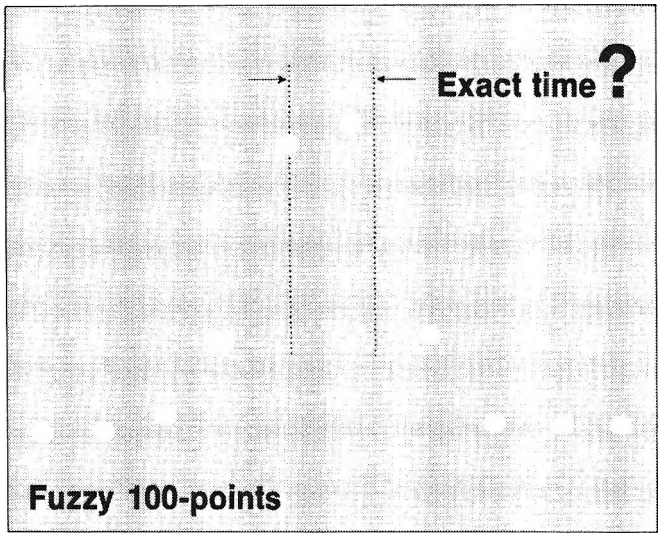

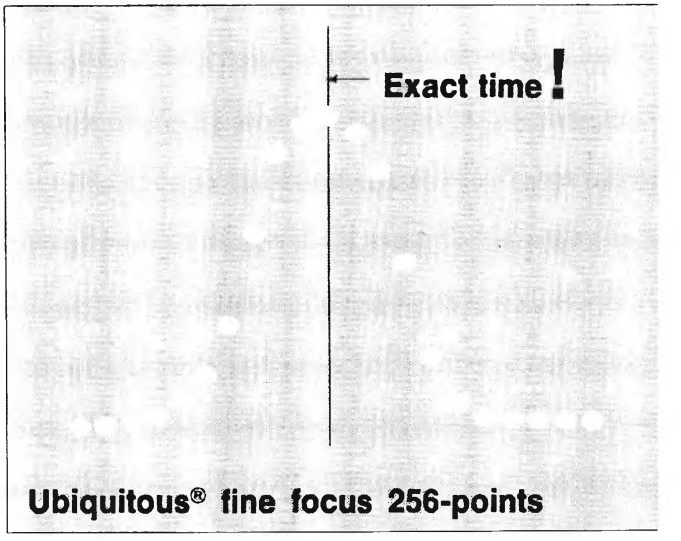

The new UC-201A Ubiquitous® Correlator is a complete time-domain measurement laboratory for real-time auto and cross-correlation • signal enhancement • probability

For underwater acoustics, fluid dynamics, medical research, vibration analysis, noise source identification, aerodynamics, radio astronomy, geophysics, hydrodynamics.

Features:

- exact time measurements with digital dial
- computes the integral and differential of any stored function (converts probability density to cumulative distribution without rerunning data)
- precomputational delay built-in (256 samples)
- sampling increments from ½ usec to 2 se
- complete external (computer) control plu digital outputs
- built-in test s gnals for all modes
- small, portable, easy t use
- reasonably priced

Options:

- exponential (running) av eraging
- additional precomputa tional delay (2048 samples)
- centering (128) dela switch

federal scientific

From FEDERAL SCIENTIFIC, originators of the Ubiquitous Spectrum Analyzer, the most widely used real-time unit of its type in the free world.

FEDERAL SCIENTIFIC CORPORATION, SUBSIDIARY OF ELGIN NATIONAL INDUSTRIES, INC
615 W. 131st ST., N.Y., N.Y. 10027. TEL: (212) 286-4400

THE JOURNAL OF

PHYSICAL CHEMISTRY

BRYCE CRAWFORD, Jr., *Editor*
STEPHEN PRAGER, *Associate Editor*
ROBERT W. CARR, Jr., FREDERIC A. VAN-CATLEDGE, *Assistant Editors*

EDITORIAL BOARD: A. O. ALLEN (1970–1974), R. BERSOHN (1967–1971), J. R. BOLTON (1971–1975), S. BRUNAUER (1967–1971), M. FIXMAN (1970–1974), H. S. FRANK (1970–1974), J. R. HUIZENGA (1969–1973), M. KASHA (1967–1971), W. J. KAUZMANN (1969–1973), W. R. KRIGBAUM (1969–1973), R. A. MARCUS (1968–1972), W. J. MOORE (1969–1973), J. A. POPLE (1971–1975), B. S. RABINOVITCH (1971–1975), H. REISS (1970–1974), S. A. RICE (1969–1975), R. E. RICHARDS (1967–1971), F. S. ROWLAND (1968–1972), R. L. SCOTT (1968–1972), R. SEIFERT (1968–1972)

CHARLES R. BERTSCH, *Manager, Editorial Production*

AMERICAN CHEMICAL SOCIETY, *1155 Sixteenth St., N.W., Washington, D. C. 20036*
FREDERICK T. WALL, *Executive Director*

Books and Journals Division
JOHN K CRUM, *Director (Acting)*
JOSEPH H. KUNEY, *Head, Business Operations Department*
RUTH REYNARD, *Assistant to the Director*

©Copyright, 1971, by the American Chemical Society. Published biweekly by the American Chemical Society at 20th and Northampton Sts., Easton, Pa. 18042. Second-class postage paid at Washington, D. C., and at additional mailing offices.

All manuscripts should be sent to *The Journal of Physical Chemistry*, Department of Chemistry, University of Minnesota, Minneapolis, Minn. 55455.

Additions and Corrections are published once yearly in the final issue. See Volume 74, Number 26 for the proper form.

Extensive or unusual alterations in an article after it has been set in type are made at the author's expense, and it is understood that by requesting such alterations the author agrees to defray the cost thereof.

The American Chemical Society and the Editor of *The Journal of Physical Chemistry* assume no responsibility for the statements and opinions advanced by contributors.

Correspondence regarding accepted copy, proofs, and reprints should be directed to Editorial Production Office, American Chemical Society, 20th and Northampton Sts., Easton, Pa. 18042. Manager: CHARLES R. BERTSCH. Assistant Editor: EDWARD A. BORGER. Editorial Assistant: EVELYN J. UHLER.

Advertising Office: Century Communications Corporation, 142 East Avenue, Norwalk, Conn. 06851.

Business and Subscription Information

Remittances and orders for subscriptions and for single copies, notices of changes of address and new professional connections, and claims for missing numbers should be sent to the Subscription Service Department, American Chemical Society, 1155 Sixteenth St., N.W., Washington, D. C. 20036. Allow 4 weeks for changes of address. Please include an old address label with the notification.

Claims for missing numbers will not be allowed (1) if received more than sixty days from date of issue, (2) if loss was due to failure of notice of change of address to be received before the date specified in the preceding paragraph, or (3) if the reason for the claim is "missing from files."

Subscription rates (1971): members of the American Chemical Society, $20.00 for 1 year; to nonmembers, $40.00 for 1 year. Those interested in becoming members should write to the Admissions Department, American Chemical Society, 1155 Sixteenth St., N.W., Washington, D. C. 20036. Postage to Canada and countries in the Pan-American Union, $4.00; all other countries, $5.00. Single copies for current year: $2.00. Rates for back issues from Volume 56 to date are available from the Special Issues Sales Department, 1155 Sixteenth St., N.W., Washington, D. C. 20036.

This publication and the other ACS periodical publications are now available on microfilm. For information write to: MICROFILM, Special Issues Sales Department, 1155 Sixteenth St., N.W., Washington, D. C. 20036.

Notice to Authors last printed in the issue of June 10, 1971

Reprints from Chemical & Engineering News

Keeping broadly informed challenges every person today. If you missed these features from recent issues of C&EN, you can still get copies by filling in the coupon below.

Population

A 2-part feature
David M. Kiefer, C&EN
Oct. 7 & 14, 1968 **75¢**

Mr. Kiefer finds that population is growing unchecked in much of the world, and that U.S. population will expand 50% in the next 30 years or so. Social as well as technological innovation is needed to thwart this advance. **10148**

Computers in Chemical Education

Dr. Frederick D. Tabbutt
Reed College
Portland, Oregon
January 19, 1970 **50¢**

A number of experiments with computers in education have been undertaken in the past few years. Some of the approaches to computer-assisted education now show promise as useful adjuncts as surrogate teachers. **11970**

Arthritis

A 3-part feature
Howard J. Sanders, C&EN
July 22, 29, & Aug. 12, 1968 **75¢**

Causes of arthritis are still a mystery, although more and more evidence points to infection as a possible trigger. Mr. Sanders discusses and examines the possible causes and the past, present, and future of treatment. **07228**

Industrial Research Careers

Howard Reiss
University of California
Los Angeles
June 29, 1970 **50¢**

A major concern of those beginning careers in science is, of course, where to carry out their careers—in a university, private industry, a foundation or wherever. An industrial research career can be a rewarding one, both professionally and financially. **62970**

Public Policy and the Environment

February 9, 1970 **50¢**

Speaking at the 158th ACS National Meeting, Lee DuBridge, Herbert Doan, and Barry Commoner urged cooperation among government, industry, and university in tackling environmental improvement. **02970**

Pollution Control Instrumentation

Michael Heylin, C&EN
February 15, 1971 **50¢**

Efforts to control air and water resources intelligently depends on the ability to detect and to monitor pollutants. The challenge to produce better instrumentation for this purpose is now receiving intense attention from industry and government researchers. **21571**

Allergy

Howard J. Sanders, C&EN
May 11, 1970 **50¢**

Although hay fever, bronchial asthma, and other allergies will not be conquered, they will be better understood and better treated. The expanding study of these diseases in fundamental scientific terms, using the latest research techniques, allergic disorders will yield more and more of their secrets that only a few years ago seemed almost unfathomable. **51170**

Food Additives

Howard J. Sanders, C&EN
October 10, 1966 **75¢**

Makers of food additives are keeping their eyes on the spectacular growth of new foods and the shifting moods of regulation-minded Washington. An array of chemicals enhances the wholesomeness, attractiveness, convenience, and nutritional value of American foods. **10176**

Technology Assessment

David M. Kiefer, C&EN
October 5, 1970 **50¢**

Technology assessment is an attempt—still halting and uncertain—to establish an early-warning system to control, direct, and, if necessary, restrain technological development so as to maximize the public good while minimizing the public risks. **10570**

Chemistry and the Atmosphere

Howard J. Sanders, C&EN
March 28, 1966 **75¢**

The earth's atmosphere is a vast, churning mixture of gases and trace quantities of liquids and solids. Held to the earth by the pull of gravity, it is the transparent envelope without which life on earth would cease to exist. **32866**

Career Opportunities The New Priorities

March 8, 1971 **50¢**

C&EN's annual career guide for chemists and chemical engineers. In the search for new priorities, new opportunities are emerging. Here C&EN looks at three such areas—food, shelter, and health. **03871**

Chaos in Science Teaching

Dr. Conrad E. Ronneberg
Professor Emeritus, Denison University
June 1, 1970 **50¢**

To many people familiar with the stiuation in teaching introductory science courses, both in high school and college, the situation is utter chaos. To place attempts to improve science teaching in proper perspective requires a brief review of the progress of science teaching since World II. **06170**

Artificial Organs

A 2-part feature
Howard J. Sanders, C&EN
April 5 and 12, 1971 **75¢**

The implanting of a total artificial heart in a human has been the most dramatic single advance to date in the field of artificial organs. In recent years, however, many other artificial organs have also been developed, and scientists foresee a vast increase in the number of body parts that, in the years ahead, will be replaceable by mechanical devices. **04571**

Scientific Societies and Public Affairs

K. M. Reese, C&EN
May 3, 1971 **50¢**

Scientific and engineering societies for many years have fostered research, published papers, and sponsored meetings without great regard for the world beyond their particular disciplines. Only in the past decade or so have the learned societies edged into the realm of public affairs. **05371**

1 to 49 copies—single copy price 50 to 299 copies—20% discount

Prices for larger quantities available on request

☐ 10148 ☐ 11970 ☐ 07228
☐ 62970 ☐ 02970 ☐ 51170
☐ 21571 ☐ 10176 ☐ 10570 ☐ 32866
☐ 03871 ☐ 06170 ☐ 04571 ☐ 05371

TO: REPRINT DEPARTMENT

ACS Publications
1155 Sixteenth St., N.W.
Washington, D.C. 20036

FROM:

Name _____

Street _____

City _____

State _____ Zip Code

Amount enclosed $ _____

THE JOURNAL OF

PHYSICAL CHEMISTRY

Volume 75, Number 21 October 14, 1971

NOTES

COMMUNICATIONS TO THE EDITOR

AUTHOR INDEX

In papers with more than one author the name of the author to whom inquiries about the paper should be addressed is marked with an asterisk in the by-line.

THE JOURNAL OF
PHYSICAL CHEMISTRY

Registered in U. S. Patent Office © *Copyright, 1971, by the American Chemical Society*

VOLUME 75, NUMBER 21 OCTOBER 14, 1971

Kinetics of the Shock Wave Thermolysis of 1,1,2,2-Tetrafluoroethane[1a]

by G. E. Millward,[1b] R. Hartig,[1b] and E. Tschuikow-Roux*

Department of Chemistry, University of Calgary, Calgary 44, Alberta, Canada (*Received April 5, 1971*)

Publication costs borne completely by The Journal of Physical Chemistry

The kinetics of the thermal decomposition of a dilute mixture of 1,1,2,2-tetrafluoroethane in argon has been studied in a single-pulse shock tube in the temperature range 1190–1450°K at total reflected shock pressures of about 2900–4000 Torr. The major reaction is the elimination of hydrogen fluoride, $CHF_2CHF_2 \xrightarrow{k_1} CHFCF_2 + HF$, with the first-order rate constant given by $\log (k_1, \text{sec}^{-1}) = 13.3 \pm 0.4 - (69.4 \pm 3.1 \text{ kcal})/2.303RT$. Theoretical calculations of the activation energy and preexponential factor showed reasonable agreement with the observed values. At temperatures above 1310°K significant production of CH_2F_2 and C_2F_4 was also observed. These additional products are explained in terms of radical reactions resulting from the carbon-carbon bond scission in CHF_2CHF_2. The activation energy for the symmetric dissociation, $CHF_2CHF_2 \rightarrow 2CHF_2$, was found to be 91.4 ± 3.7 kcal mol^{-1} and provides an estimate of the C–C bond dissociation energy in 1,1,2,2-tetrafluoroethane.

Introduction

Earlier chemical activation,[2] subsonic flow,[3] and static system[4] investigations of HF elimination from alkyl fluorides indicate that α fluorination decreases the activation energy, whereas β-fluoro substitution increases it. The RRK treatment of chemical activation data on fluoroethanes has been recently criticized by Pritchard and Perona.[5] Reexamination[6] of these data in terms of the more appropriate RRKM theory has reversed the earlier conclusion indicating that an increase in fluorination should lead to an increase in activation energy. This prediction has been substantiated by the recent chemical activation work of Chang and Setser[7] and by pyrolysis studies in two laboratories employing the single-pulse shock tube (SPST)[6,8–10] technique.

Thus, the different results obtained in subsonic flow and static systems may be due to an experimental artifact. These techniques may be subject to problems of temperature gradients and heterogeneous effects. In a SPST the sample is heated rapidly and homogeneously, the reaction being free from heterogeneous complications. This is not to say that this technique has not been criticized.[11] However, the gas dynamics[10,12,13] and the methods of estimating shock parameters[14,15]

(1) (a) Work supported by the National Research Council of Canada; (b) Postdoctoral Fellow.

(2) D. C. Phillips and A. F. Trotman-Dickenson, *J. Chem. Soc. A*, 1144 (1968).

(3) D. Sianesi, G. Nelli, and R. Fontanelli, *Chim. Ind. (Milan)*, **50**, 619 (1968).

(4) M. Day and A. F. Trotman-Dickenson, *J. Chem. Soc. A*, 233 (1969).

(5) G. O. Pritchard and M. J. Perona, *Int. J. Chem. Kinet.*, **2**, 281 (1970).

(6) P. Cadman, M. Day, A. W. Kirk, and A. F. Trotman-Dickenson, *Chem. Commun.*, 203 (1970).

(7) H. W. Chang and D. W. Setser, *J. Amer. Chem. Soc.*, **91**, 7648 (1969).

(8) P. Cadman, M. Day, and A. F. Trotman-Dickenson, *J. Chem. Soc. A*, 2498 (1970).

(9) E. Tschuikow-Roux, W. J. Quiring, and J. M. Simmie, *J. Phys. Chem.*, **74**, 2449 (1970).

(10) E. Tschuikow-Roux and W. J. Quiring, *ibid.*, **75**, 295 (1971).

(11) R. A. Strehlow, "A Review of Shock Tube Chemistry," Technical Report AAE 68-1, University of Illinois, 1968.

(12) E. Tschuikow-Roux, *Phys. Fluids*, **8**, 821 (1965).

(13) A. Lifshitz, A. Bar-Nun, P. C. T. De Boer, and E. L. Resler, Jr., *J. Chem. Phys.*, **53**, 3050 (1970).

have been firmly established using the well-studied unimolecular decomposition reactions of perfluorocyclobutane[13,14] and ethyl chloride.[10] Thus, the potential of these instruments, for pyrolytic studies, has been clearly demonstrated.

The present work is an extension of previous investigations in this series and represents the first *pyrolysis* of an α,β-substituted fluoroethane. Further, if the trend of increasing activation energy with additional fluorosubstitution continues, then the influence of the radical reactions must become progressively more important. This is so since the magnitude of the rate constant for the C–C bond dissociation will become comparable to that for HF elimination. As will be seen below the nature of the radical reactions has indeed been established.

Experimental Section

The operation of the modified SPST equipped with a ball valve has been described in detail.[12,16] Prior to each experiment the tube was evacuated to 10^{-5} Torr, and the leak rate did not exceed 10^{-3} Torr min^{-1}. The tube was then filled with pure argon (150 Torr), and the ball valve was filled with the dilute reaction mixture (0.6% $C_2H_2F_4$ in Ar) to the same pressure. The wave forms were generated in the tube by bursting a scribed aluminum diaphragm using helium as the driver gas.

Two pressure transducers (Kistler, Model 603A/623F), of rise time 1 μsec, were located 10 and 20 cm, respectively, from the end plate. The amplified signals from the transducers were fed to two universal counters (Hewlett-Packard, Model 5325A), which recorded the transit times of the incident and reflected shocks. The signals were also fed to an oscilloscope (Tektronix, Model 535A with CA plug-in), so that the wave history could be recorded photographically.

The 1,1,2,2-$C_2H_2F_4$ was kindly donated by the E. I. du Pont de Nemours Co., and a gc analysis indicated it had a purity of 99.95%. A similar purity was found for $CHFCF_2$ and CH_2F_2, the gases being obtained from Peninsular Chemresearch Inc. C_2F_4 was prepared by heating polytetrafluoroethylene (Teflon) shavings *in vacuo*. Bulb-to-bulb distillation of the product resulted in a purity of 99.9%. The argon was obtained from Matheson, and it had a stated purity of 99.998%. The dilute reaction mixture was prepared in a large stainless steel tank and allowed to mix thoroughly before use.

Following each shock the reactant and products were effectively isolated in the end section of the tube by closure of the ball valve. After mixing, a sample of the gases was withdrawn for analysis by gas chromatography. The chromatograph (Varian 1740-1) was equipped with a flame ionization detector in conjunction with a 12-ft silica gel column. Analyses were carried out isothermally at 150°, with helium as a carrier gas at 30 $cm^3\ min^{-1}$. Quantitative identification was achieved by means of standard mixtures of the products and reactant in argon prepared for calibration purposes. The extent of the reaction varied from ~0.4%, at about 1200°K, to ~60%, at 1450°K.

Results

The reflected shock temperatures, T_5, and pressures, P_5, were calculated from measured incident and reflected shock velocities, as described previously.[15] The reaction or dwell time, t, was determined accurately by a previously described method,[12] using shock transit times and photographic oscilloscope recordings of the wave history near the reflecting wall of the SPST. These results are set out in Table I.

The thermal decomposition of 1,1,2,2-$C_2H_2F_4$ at temperatures between 1190 and 1310°K yielded C_2HF_3 as the major product. Above 1310°K significant amounts of additional products were formed, which were identified by gc and mass spectrometry as being CH_2F_2 and C_2F_4. Two other products, whose combined total was less than 1% of the total product formation, could not be identified as either C_1 or C_2 fluoro hydrocarbons. They were ignored in the present analysis. The product yields, in Table I, are expressed as ratios of product to reactant.

Kinetic Analysis

The decomposition of 1,1,2,2-tetrafluoroethane over the entire temperature range of this study (1190–1450°K) is complex. To facilitate the analysis we have quite arbitrarily divided the pyrolysis results into two ranges. Below 1310°K the observed C-containing product is almost exclusively C_2HF_3, and we conclude that HF elimination is the predominant reaction

$$CHF_2CHF_2 \xrightarrow{k_1} C_2HF_3 + HF$$

Accordingly, the rate constant was evaluated from the first-order rate law

$$k_1 = [1 - (\epsilon/t)]^{-1}(1/t) \ln (1 + R_1) \qquad (1)$$

where R_1 is the product/reactant ratio, $[C_2HF_3]/[C_2H_2F_4]$, t is the calculated reaction time,[12] and the first factor corrects for the finite cooling rate[10,12] by the rarefaction wave.

At temperatures above 1310°K product analysis indicates that other reaction paths become significant and must be considered. Among primary processes the homolytic bond scission of the CF and CH bonds can be ruled out on thermochemical grounds. Thus the bond energies of the CF and CH bonds in $C_2H_2F_4$ are about 110 and 103 kcal mol^{-1},[17] respectively, and these

(14) J. M. Simmie, W. J. Quiring, and E. Tschuikow-Roux, *J. Phys. Chem.*, **73**, 3831 (1969).

(15) E. Tschuikow-Roux, J. M. Simmie, and W. J. Quiring, *Astronaut. Acta*, **15**, 511 (1970).

(16) W. J. Quiring, Ph.D. Thesis, University of Calgary, 1971.

(17) B. de B. Darwent, NSRDS-NBS, 31 (1970).

Table I: Experimental Results

Mach no. W_{11}	Mach no. W_{21}	P_2, Torr	T_2, °K	P_5, Torr	T_5, °K	t, μsec	Product ratios[a] R_1	R_2	R_3	k', sec^{-1}	k_1, sec^{-1}	$k' - k_1$, sec^{-1}
2.216	1.265	888	705	2912	1193	788	0.0035	...	...	...	3.91	...
2.203	1.306	873	697	2956	1199	843	0.0045	...	...	...	5.02	...
2.216	1.310	883	701	3007	1210	534	0.0031	...	...	...	5.20	...
2.234	1.295	899	711	3027	1219	929	0.0052	...	...	...	5.26	...
2.244	1.314	907	715	3104	1236	651	0.0066	...	...	...	9.18	...
2.256	1.300	917	719	3107	1238	740	0.0093	...	...	...	11.2	...
2.267	1.303	927	724	3151	1249	813	0.0155	...	...	...	17.3	...
2.295	1.285	951	745	3192	1277	711	0.0144	...	...	...	17.9	...
2.280	1.329	938	731	3256	1275	767	0.0189	...	...	...	24.4	...
2.284	1.308	941	731	3216	1265	889	0.0282	...	...	...	29.1	...
2.349	1.302	998	761	3408	1316	842	0.0316	0.0105	0.0095	53.7	36.9	16.8
2.322	1.335	974	746	3409	1307	899	0.0538	0.0183	0.0157	84.2	57.6	26.6
2.313	1.336	967	747	3384	1309	916	0.0653	0.0216	0.019	80.0	68.7	21.3
2.337	1.334	987	754	3454	1319	928	0.0717	0.0243	0.0226	108.0	73.4	34.3
2.389	1.330	1033	773	3616	1353	818	0.0649	...	...	71.0	71.0	...
2.352	1.349	1001	761	3546	1341	1000	0.1335	0.0404	0.0461	182.0	122.0	60.0
2.367	1.338	1013	767	3564	1346	855	0.149	0.0441	0.0528	235.0	157.0	78.0
2.405	1.350	1048	785	3725	1387	823	0.226	0.082	0.116	396.0	233.0	163.0
2.402	1.372	1045	784	3776	1396	860	0.206	0.109	0.128	380.0	202.0	178.0
2.386	1.349	1031	777	3661	1371	924	0.248	0.0693	0.120	367.0	226 0	141.0
2.432	1.384	1072	790	3914	1415	1049	0.530	0.166	0.530	725.0	337.0	388.0
2.424	1.354	1065	793	3798	1402	961	0.491	0.118	0.300	640.0	370.0	270.0
2.443	1.401	1082	801	4000	1445	876	0.794	0.163	0.621	1045.0	554.0	491.0

[a] $R_i = [X_i]/[CHF_2CHF_2]$ where X_i = $CHFCF_2$, CH_2F_2, C_2F_4 for i = 1, 2, 3, respectively, and R_i is determined experimentally.

reactions cannot be competitive with the HF elimination reaction. The activation energy for molecular elimination of hydrogen, a process which could give rise to the observed C_2F_4, is difficult to assess. We note, however, that for the somewhat analogous reaction, $C_2H_6 \rightarrow H_2 + C_2H_4$, one calculates[18] an activation energy of 74 kcal mol^{-1} at 298°K which is not much higher than the experimentally observed activation energy for the HF elimination. On the other hand, based on the known heats of formation (values in kilocalories per mole) of HF (−64.8),[19] C_2HF_3 (−118.5),[20] C_2F_4 (−157.2),[20] and a calculated value of $\Delta H_f°$ (CHF_2CHF_2) ≃ −209 kcal mol^{-1} [21] we find that the difference in the heats of reaction at 298°K for H_2 and HF elimination is $\Delta(\Delta H)$ = 26 kcal mol^{-1}.

$$CHF_2CHF_2 \longrightarrow HF + C_2HF_3 \qquad \Delta H = 26 \text{ kcal mol}^{-1}$$

$$\longrightarrow H_2 + C_2F_4 \qquad \Delta H = 52 \text{ kcal mol}^{-1}$$

Using this evidence we choose to ignore the contribution (if any) of the last reaction. Finally we consider the symmetric dissociation of CHF_2CHF_2 by C–C bond rupture. By analogy with C_2F_6 [22] this reaction must have an activation energy of about 90–93 kcal mol^{-1}. However, compensating for this high activation energy there will be a high preexponential factor which is associated with a very loose transition state for such reactions.[22,23] In this case reaction products should be observed which involve the CHF_2 radical as a precursor. A reaction scheme which is consistent with our product analysis is given in eq I–VIII.

$$CHF_2CHF_2 \xrightarrow{k_1} C_2HF_3 + HF \qquad \text{(I)}$$

$$\xrightarrow{k_2} 2CHF_2 \qquad \text{(II)}$$

$$2CHF_2 \xrightarrow{k_{-2}} CHF_2CHF_2 \qquad (-\text{II})$$

$$\xrightarrow{k_3} CH_2F_2 + CF_2 \qquad \text{(III)}$$

$$CHF_2 + CHF_2CHF_2 \xrightarrow{k_4} CH_2F_2 + CHF_2CF_2 \qquad \text{(IV)}$$

$$2CF_2 \xrightarrow{k_5} C_2F_4 \qquad \text{(V)}$$

$$CHF_2CF_2 \xrightarrow{k_6} C_2F_4 + H \qquad \text{(VI)}$$

$$H + CHF_2CHF_2 \xrightarrow{k_7} CHF_2CF_2 + H_2 \qquad \text{(VII)}$$

$$H + CHF_2CF_2 \xrightarrow{k_8} CHF_2CHF_2 \qquad \text{(VIII)}$$

It should be noted that this mechanism has not been tested for the effects of pressure, concentration, and inhibitors. The secondary processes included in the above scheme are worthy of some discussion. The CHF_2 radicals have three possible reaction manifolds:

(18) Evaluated from the known heat of reaction, ΔH = 32.7 kcal mol^{-1}, and the activation energy for the reverse four-center addition reaction, E_r = 41.3 kcal mol^{-1} (ref 36).

(19) D. D. Wagman, W. H. Evans, V. B. Parker, I. Halow, S. M. Bailey, and R. Schumm, National Bureau of Standards Technical Note 270-3, 1968.

(20) L. R. Lacher and H. A. Skinner, *J. Chem. Soc. A*, 1034 (1968).

(21) E. Tschuikow-Roux, unpublished data.

(22) E. Tschuikow-Roux, *J. Chem. Phys.*, **43**, 2251 (1965).

(23) C. P. Quinn, *Proc. Roy. Soc., Ser. A*, **275**, 190 (1963).

combination, disproportionation, and hydrogen abstraction from the parent compound. The disproportionation of two difluoromethyl radicals to yield a difluorocarbene,[24] reaction III, was first reported by Bellas, *et al.*,[25] who established the disproportionation/combination ratio $k_3/k_{-2} = 0.19$. A recent photolysis study of $(CHF_2)_2CO$ showed k_3/k_{-2} to be constant[26] at ~0.17 in the temperature range 297–443°K. Thus, the inclusion of reaction −II has the consequence that reaction III must play an important role. At this point it is important to stress the experimental fact that only minute amounts of C_3 and C_4 compounds were observed. Thus, the tetrafluoroethyl radical combination reaction $2CHF_2CF_2 \rightarrow C_4H_2F_8$ and the cross combination $CHF_2 + CHF_2CF_2 \rightarrow C_3H_2F_6$ must be very unfavorable. This may be due to low radical concentrations or the chemically activated adducts undergo a rapid reverse C–C bond scission. Therefore the above reactions are excluded from the scheme. Having eliminated these reactions we must then omit the corresponding disproportionation reactions, since in general these are less favorable than the former.[27] The existence of only small amounts of C_3 compounds is also important in discussing the fate of the difluorocarbene, CF_2, species. It is known that CF_2 does not undergo insertion into CH bonds.[28] However, it is more difficult to justify omitting the addition reaction of CF_2 to the olefins present in this system, although the latter reaction would require an activation energy,[29] whereas the combination reaction V does not. Finally, reactions involving the consecutive elimination of HF from C_2HF_3 and CH_2F_2 are not included in the mechanism. We note that HF elimination of alkenyl fluorides have considerably higher activation energies than the corresponding alkyl fluorides.[30–32] Further, no evidence of C_2F_2 was found in the qualitative analysis of products. The studies of Politanskii and Shevchuk[33,34] indicate that in the case of CH_2F_2 some HF elimination, $CH_2F_2 \rightarrow CHF + HF$, can be expected to occur. However, no significant CHFCHF was found and for this reason the reaction has been omitted from the scheme.

For simplicity we write: (A) = $[CHF_2CHF_2]$; (B) = $[CHFCF_2]$; (C) = $[CHF_2]$; (D) = $[CH_2F_2]$; (E) = $[CHF_2CF_2]$; (F) = $[CF_2CF_2]$; (G) = $[CF_2]$, and (H) is the hydrogen atom concentration. From a theoretical analysis of the material balance it was found that

$$A_0 = A + B + {}^1/_2D + F \quad (2)$$

or in terms of the observed product/reactant ratios

$$A_0/A = 1 + R_1 + {}^1/_2R_2 + R_3 \quad (3)$$

From the general stationary-state equations for transient species we obtain

$$k_2(A) - k_{-2}(C)^2 - k_3(C)^2 - k_8(H)(E) = 0 \quad (4)$$

It is reasonable to assume that (C) > (H) or (E) at least on a trial basis, since H and CHF_2CF_2 are produced in secondary processes. Thus, we can obtain an approximate relationship for the concentration of the CHF_2 radical, which is given by

$$(C) = k_2^{1/2}(A)^{1/2}/(k_{-2} + k_3)^{1/2} \quad (5)$$

The rate of disappearance of A is given by

$$-d(A)/dt = k_1(A) + k_2(A) - k_{-2}(C)^2 + k_4(C)(A) + k_7(H)(A) - k_8(H)(E) \quad (6)$$

Using the stationary-state equations for the transient species (C), (H), and (F) eq 6 can be reduced to

$$-d(A)/dt = k_1(A) + 2k_2(A) - 2k_{-2}(C)^2 - k_3(C)^2 + k_7(H)(A) \quad (6a)$$

Neglecting the last term[35] in (6a) and making use of eq 5 yields

$$-d(A)/dt = k'(A) \quad (7)$$

where

$$k' = k_1 + k_2k_3/(k_{-2} + k_3) \quad (8)$$

Integrating (7) with the appropriate boundary conditions that $(A) = (A)_0$ at $t = 0$ gives

$$k' = (1/t) \ln [(A)_0/(A)] = (1/t) \ln (1 + R_1 + {}^1/_2R_2 + R_3) \quad (9)$$

The values of k' obtained from eq 9 are shown in Table I.

The formation of B is given by

$$d(B)/dt = k_1(A) = k_1(A)_0e^{-k't} \quad (10)$$

Integrating (10) with (B) = 0 at $t = 0$ and substituting k' from (9) we obtain, after correction for the finite cooling rate

$$k_1 = R_1 \ln (1 + R_1 + {}^1/_2R_2 + R_3)/(R_1 + {}^1/_2R_2 + R_3)[1 - (\epsilon/t)]t \quad (11)$$

(24) J. M. Tedder and J. C. Walton, *Progr. React. Kinet.*, **4**, 37 (1967).

(25) M. G. Bellas, O. P. Strausz, and H. E. Gunning, *Can. J. Chem.*, **43**, 1022 (1965).

(26) G. O. Pritchard and M. J. Perona, *Int. J. Chem. Kinet.*, **1**, 509 (1969).

(27) A. F. Trotman-Dickenson and G. S. Milne, NSRDS-NBS, 9 (1967).

(28) R. A. Mitsch, private communication.

(29) R. A. Mitsch and A. S. Rodgers, *Int. J. Chem. Kinet.*, **1**, 439 (1969).

(30) J. M. Simmie, W. J. Quiring, and E. Tschuikow-Roux, *J. Phys. Chem.*, **74**, 992 (1970).

(31) J. M. Simmie and E. Tschuikow-Roux, *ibid.*, **74**, 4075 (1970).

(32) P. Cadman and W. J. Engelbrecht, *Chem. Commun.*, 453 (1970).

(33) S. F. Politanskii and V. U. Shevchuk, *Kinet. Katal.*, **8**, 12 (1967).

(34) S. F. Politanskii and V. U. Shevchuk, *ibid.*, **9**, 496 (1968).

(35) Neglect of the term $k_7(H)(A)$ is justified in this case since it can be shown that at temperatures > 1350°K and under the experimental conditions cited the rate of abstraction is slower than combination, *i.e.*, $k_7(H)(A) < k_{-2}(C)^2$.

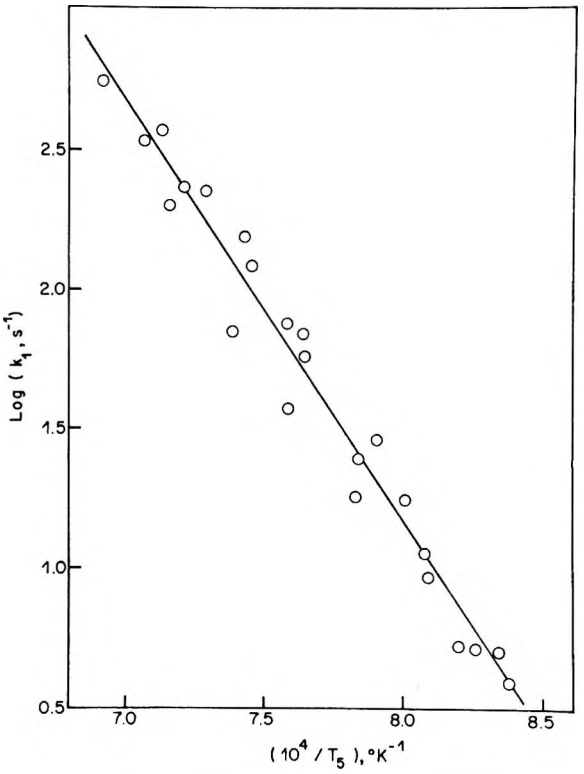

Figure 1. Temperature dependence of the rate constant k_1 for HF elimination from CHF_2CHF_2.

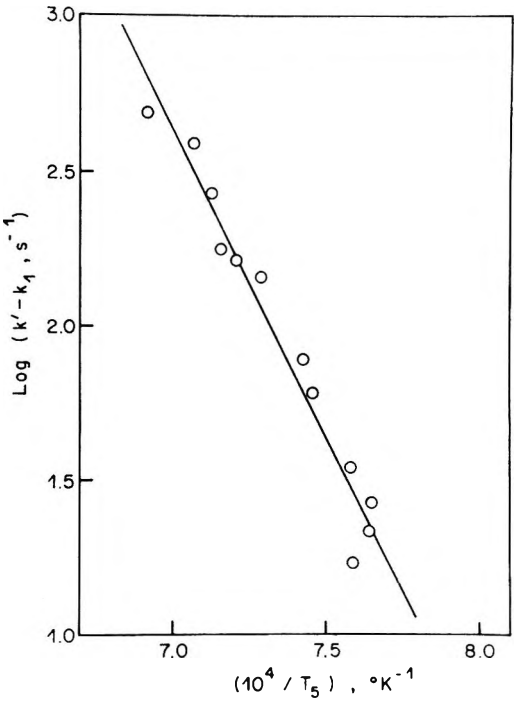

Figure 2. Temperature dependence of $(k' - k_1)$.

The values of k_1 obtained from the experimental results are shown in Table I and the temperature dependence is plotted in Figure 1.

Rearranging (8) we obtain

$$k' - k_1 = k_2/(k_{-2}/k_3 + 1) \qquad (12)$$

which yields an estimate of the rate constant for the C–C bond scission, k_2, provided the value of the disproportionation/combination ratio, k_3/k_{-2}, for CHF_2 radicals is known at high temperatures. The values of $k' - k_1$ are given in Table I, and the temperature dependence is plotted in Figure 2.

Discussion

The rate constants, k_1, reported in Table I are high-pressure limiting values, as has been shown by previous considerations.[9] A least-squares analysis of the data of Figure 1 yields the Arrhenius expression

$$k\ (\text{sec}^{-1}) = 10^{13.3\pm0.4} \exp[-(69.4 \pm 3.1)/RT]$$

where R is in kilocalories per mole and the error limits are standard deviations. This result fits into the currently observed pattern[6-10] of increasing activation energy with increasing fluorination. The preexponential factor is also consistent with the previously determined values. However, the increase in activation energy, between CH_3CF_3 and CHF_2CHF_2, ~0.7 kcal mol^{-1}, is not as dramatic as that observed between CH_3CHF_2 and CH_3CF_3, ~6.8 kcal mol^{-1}. Thus, although there is an increase in the activation energy due to the additional fluorine atom, this increase is not as large as one might expect because of fluorine substituents on the β-carbon atom. This appears to support the hypothesis that β substitution tends to decrease the *change* in activation energy.

In Figure 2 the logarithm of the rate constant difference $(k' - k_1)$ is plotted as a function of $1/T_5$. A least-squares analysis of the data gives

$$k' - k_1 = k_2/[(k_{-2}/k_3) + 1] = 10^{16.6\pm0.4} \exp[-(91.4 \pm 3.7)/RT]\ (\text{sec}^{-1})$$

where R is in kilocalories per mole and again the error limits are standard deviations. The ratio k_3/k_{-2} has been evaluated at temperatures up to 440°K and found to lie between 0.17 and 0.20.[25,26] The lowest temperature in this study is ~1200°K, in which case the value of k_3/k_{-2} may be somewhat different. It is noted that reactions −II and III have little temperature dependence in the exponential term, since they have approximately zero activation energies. However, there may be some temperature dependence in the preexponential ratio A_3/A_{-2} which is derived from the difference in the transition states for the two processes. This may favor the disproportionation reaction. For the purposes of this calculation we choose $k_3/k_{-2} = 0.2$ and assume it to be constant over the temperature range of this study. Therefore

$$k_2\ (\text{sec}^{-1}) = 10^{17.4\pm0.4} \exp[-(91.4 \pm 3.7)/RT]$$

It should be noted that the choice of $k_3/k_{-2} = 0.2$ results in $k_1/k_2 < 1$ over the whole temperature range. The value of the activation energy for reaction II does

not change, however, if k_3/k_{-2} is constant, and provides us with the first experimental estimate of the C–C bond dissociation energy in CHF_2CHF_2. This value lies intermediate between that of C_2H_6[23] and C_2F_6[22] as might be anticipated.

It is of interest to calculate the activation energy for the four-center HF elimination reaction using the electrostatic semi-ion pair model of Benson and Haugen.[36] The activation energy may be calculated from the sum of the enthalpy change for reaction I and the activation energy, E_r, for the reverse addition reaction. The theory is strictly applicable in the case of nonpolar olefins. Nevertheless, as will be shown below, through suitable adjustment of bond parameters partial agreement has been found. The necessary input parameters were either taken from the literature or evaluated as shown below. Thus the dipole moments are $\mu^\circ_{HF} = 1.82$ D[37] and $\mu^\circ_{CHFCF_2} = 1.4$ D.[37] The ground-state polarizability of HF is $\alpha^\circ_{HF} = 0.96$ Å^3,[38] while that of $CHFCF_2$, $\alpha^\circ_{CHFCF_2} = 5.54$ Å^3 was calculated from the bond additivity rules.[39] For the semi-ion pair, α_{HF}, lies halfway between the ground-state polarizability and the mean free ion pair polarizability and is given by

$$\alpha_{HF} = (2\alpha^\circ_{HF} + \alpha_{H^+} + \alpha_{F^-})/4$$

where $\alpha_{F^-} = 1.23\alpha^\circ_{HF}$[40] and the value of α_{H^+} is equated to that for $\alpha_{H_2^+} = 0.37$ Å^3.[41] The transition-state polarizability of $CHFCF_2$ is given by

$$\alpha_{CHFCF_2} = (\alpha^\circ_{CHFCF_2} - \alpha_{C=C}) + \alpha_{C\dot{-}C}$$

where $\alpha_{C=C}$[39] is the longitudinal molar polarizability of the C=C bond and $\alpha_{C\dot{-}C}$[38] is that of a C—C bond in benzene. Thus, we calculate $\alpha_{HF} = 0.87$ Å^3 and $\alpha_{CHFCF_2} = 4.91$ Å^3. The bond lengths in the transition state were evaluated according to the following procedure. In this case, a bond order of 3 is conserved in the reactants (*i.e.*, a bond order of 2 in C=C and 1 in H—F) and in the products (*i.e.*, 1 in C—C, C—H, and C—F). It is thus reasonable to assume that the bond order is 3 in the transition state. However, the transition state is a loosely bonded four-center semi-ion pair complex, as shown in Figure 3. This means that the "effective" bond order is 2.5, since a total of one electron is used in creating the semi-ion pair. Although this electron, corresponding to a bond order of 0.5, is involved in a role other than covalent bonding, we stipulate that the total bond order of 3 is conserved. Fractional bond lengths were then evaluated using the bond length–bond order rule of Pauling[42]

$$r = r_s - 0.6 \log n \qquad (12)$$

where r is the bond length in ångströms, corresponding to a bond order n and r_s is the single bond length. The C$\dot{-}$C bond length was set at 1.4 Å ($n = 1.5$) and the HF bond length at 1.318 Å ($n = 0.24$), as prescribed by Benson and Haugen.[36] The remaining bond order,

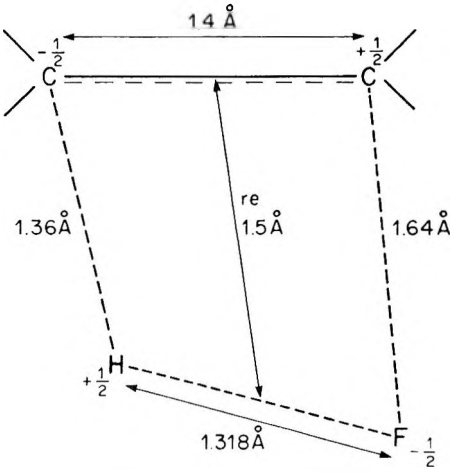

Figure 3. Semiion pair transition-state model for HF elimination from CHF_2CHF_2. r_e is the average of the equilibrium distances C–H and C–F.

0.76, was then shared equally between the two forming bonds, C–H and C–F. The calculated distances are shown in Figure 3.

From the above parameters E_r is calculated to be 38 kcal mol^{-1}. Addition of this quantity to the enthalpy of the reaction, 26 kcal mol^{-1}, gives an activation energy of 64 kcal mol^{-1} for the elimination reaction. This is below the observed value but shows better agreement than was obtained in the cases of CH_3CHF_2 and CH_3CF_3.

It is of interest to compare the experimental A factor with one calculated in terms of a predicted entropy of activation,[43] $\Delta S^\dagger$, given by

$$\Delta S^\dagger = (S_{tors}{}^\dagger - S_{hir}) + \Delta S_{int}{}^\dagger + R \ln g$$

where $(S_{tors}{}^\dagger - S_{hir})$ is the intrinsic entropy change in passing from the hindered internal rotation of the ground state to the torsional mode of the cyclic complex. For $C_2H_2F_4$ the barrier to internal rotation is taken as 3.5 kcal mol^{-1}, by comparison with other fluoroethanes.[44] This gives rise to an entropy contribution of 8.74 eu at 1350°K. The torsional mode can be

(36) S. W. Benson and G. R. Haugen, *J. Amer. Chem. Soc.*, **87**, 4036 (1965).

(37) "Handbook of Chemistry and Physics," Chemical Rubber Co., Cleveland, Ohio, 1971.

(38) Landolt-Börnstein, "Zahlenwerte und Funktionen," Band I, "Atom und Molekular Physik," Teil 3, Springer Verlag, Berlin, 1951, p 511.

(39) R. J. W. Le Fèvre, *Advan. Phys. Org. Chem.*, **3**, 1 (1965).

(40) G. R. Haugen and S. W. Benson, *Int. J. Chem. Kinet.*, **2**, 235 (1970).

(41) Landolt-Börnstein, "Zahlenwerte und Funktionen," Band I, "Atom und Molekular Physik," Teil 1, Springer Verlag, Berlin, 1950, p 401.

(42) L. Pauling, *J. Amer. Chem. Soc.*, **69**, 542 (1947).

(43) H. E. O'Neal and S. W. Benson, *J. Phys. Chem.*, **71**, 2903 (1967).

(44) A. B. Tipton, C. O. Britt, and J. E. Boggs, *J. Chem. Phys.*, **46**, 1606 (1967).

assigned a value of 350 cm^{-1},[45] and the corresponding entropy contribution is 3.94 eu. The entropy change in this mode is therefore −4.8 eu. $\Delta S_{int}^{\dagger} = \sum_{i}^{3N-8} S_i^{\dagger} - \sum_{i}^{3N-7} S_i$ is the residual intrinsic vibrational entropy change due to all the other modes. If all the other frequency changes are neglected, with the exception of the CF stretch (1100 cm^{-1}) which is taken as the reaction coordinate in the transition state, then $\Delta S_{int}^{\dagger} = -1.8$ eu. Thus, with a reaction path degeneracy of $g = 4$ the net change in entropy is −3.8 eu. From this we obtain log A (sec^{-1}) = 13.1, which shows good agreement with the observed value of 13.3.

Acknowledgment. We thank Dr. R. F. Hein of E. I. du Pont de Nemours Co. for a sample of 1,1,2,2-$C_2H_2F_4$.

(45) S. W. Benson, private communication.

Recoil Reaction Products of Carbon-11 in C_5 Hydrocarbons[1]

by G. L. Jewett and A. F. Voigt*

Institute for Atomic Research and Department of Chemistry, Iowa State University, Ames, Iowa 50010
(Received June 14, 1971)

Publication costs assisted by Ames Laboratory, U. S. Atomic Energy Commission

Gaseous and liquid radioactive products up to C_6 compounds produced by the $^{12}C(\gamma,n)^{11}C$ reaction in liquid *n*-pentane, isopentane, pentene-1, cyclopentane, and cyclopentene were separated and analyzed by radio gas chromatography. Results were interpreted in terms of insertion reactions by the carbon atom and methylene radical, and the relative probabilities of fragmentation and stabilization reactions following their insertion in the parent molecules were determined.

Experiments have been conducted to determine the yields of gaseous and liquid products from the reactions of recoil ^{11}C with the liquid hydrocarbons, *n*-pentane, isopentane, pentene-1, cyclopentane, and cyclopentene. The yields of the gaseous products were reported in earlier papers;[2,3] those of the higher boiling products have been presented[4] but not published.

Experimental Section

The technique used has been described[5,6] and further details are available.[7] Briefly, small liquid samples, 0.2 ml, in glass bulbs were irradiated with 70-MeV bremsstrahlung to cause the $^{12}C(\gamma,n)^{11}C$ reaction. After approximately 20 min to allow ^{15}O produced in the glass to decay, monitor counts of the bulbs were made with an NaI(Tl) counter. The bulbs were broken in a stream of helium, and the products and parent compound were separated by conventional radio gas chromatography with the counting cell previously described.[2]

The liquids irradiated were Research grade obtained from Phillips Petroleum Co. with purities listed from 99.82 to 99.99 mol %. They were used without further purification. In the scavenger experiments with the aliphatic pentanes saturated solutions of iodine were used. In cyclopentane, several iodine concentrations below saturation were also used.

For the separation columns Chromosorp P was the solid support with the following liquid phases: 2-ethylhexyl acetate for the gases, tripropionin for C_3 to C_6 compounds, and Apiezon Oil for the highly unsaturated C_6 compounds.

Results and Discussion

Results given in Tables I and II are based on the total ^{11}C produced, following calibration techniques which have previously been described.[3] Because of limitations of the chromatograph system, products with volatilities much less than that of the parent compounds were not carried through the column and detected. Thus products in which a carbene formed by carbon

(1) Work was performed in the Ames Laboratory of the U. S. Atomic Energy Commission, Contribution No. 3036.

(2) A. F. Voigt, D. E. Clark, and F. G. Mesich, "Chemical Effects of Nuclear Transformations," Vol. I, International Atomic Energy Agency, Vienna, 1965, p 385.

(3) D. E. Clark and A. F. Voigt, *J. Amer. Chem. Soc.*, 89, 1528 (1967).

(4) A. F. Voigt and G. L. Jewett, Abstracts, 152nd National Meeting of the American Chemical Society, New York, N. Y., Sept 1966, No. R46.

(5) G. F. Palino and A. F. Voigt, *J. Amer. Chem. Soc.*, 91, 242 (1969).

(6) R. L. Williams and A. F. Voigt, *J. Phys. Chem.*, 73, 2538 (1969).

(7) G. L. Jewett, Ph.D. Thesis, Iowa State University, Ames, Iowa, 1967.

Table I: Products from Pentanes and Pentene

Product	Per cent yield from: *n*-Pentane	*n*-Pentane + I_2	Isopentane	Isopentane + I_2	Pentene-1
Methane	6.36 ± 0.12	3.78 ± 0.02	6.45 ± 0.03	3.21 ± 0.03	1.47 ± 0.03
Ethane	1.14 ± 0.07	0.81 ± 0.10	1.75 ± 0.15	1.17 ± 0.15	0.35 ± 0.05
Ethylene	8.35 ± 0.25	7.21 ± 0.01	12.5 ± 0.5	11.0 ± 0.06	4.16 ± 0.08
Acetylene	17.5 ± 0.5	18.6 ± 0.1	21.7 ± 0.14	22.1 ± 0.07	17.4 ± 0.1
Propane	1.00 ± 0.03	0.27 ± 0.04	1.07 ± 0.02	0.40 ± 0.05	0.17 ± 0.01
Propylene	4.44 ± 0.20	3.92 ± 0.02	4.21 ± 0.02	3.49 ± 0.14	2.66 ± 0.04
Allene	1.09		0.97 ± 0.08		1.37 ± 0.04
Methyl acetylene	2.62 ± 0.18	2.07 ± 0.11			2.31 ± 0.06
Butanes	0.65 ± 0.03	0.26 ± 0.04	0.72 ± 0.10		0.18 ± 0.03
Butenes	2.84 ± 0.02	2.22 ± 0.07	1.26 ± 0.07	0.61 ± 0.19	1.29 ± 0.05
Butadiene					2.71 ± 0.06
n-Hexane	8.8 ± 0.3	6.7 ± 0.2			
2-Methylpentane	6.2 ± 0.1	4.2 ± 0.2	9.0 ± 0.2[a]	7.7 ± 0.2[a]	
3-Methylpentane	3.3 ± 0.4	2.0 ± 0.1	7.73 ± 0.04	5.10 ± 0.05	
2,2-Dimethylbutane			2.15 ± 0.10	1.10 ± 0.15	
Total hexanes	18.3	12.9	17.9	13.9	
Total hexenes	14.9 ± 0.5	12.0 ± 0.3	12.4 ± 0.4	7.9 ± 0.1	5.14 ± 0.03
Hexadienes					12.0 ± 0.5
Hexyne-1					1.67 ± 0.35
Unidentified product					4.85 ± 0.04
Methyl iodide					

[a] Includes 2,3-dimethylbutane.

Table II: Products from Cyclopentane and Cyclopentene

Product	Per cent yield from: Cyclopentane	Cyclopentane + I_2	Cyclopentene
Methane	7.6 ± 0.4	4.4 ± 0.9	2.89 ± 0.08
Ethane	0.43 ± 0.06	0.33 ± 0.02	0.14 ± 0.02
Ethylene	3.22 ± 0.13	2.39 ± 0.11	1.28 ± 0.07
Acetylene	16.4 ± 0.5	17.0 ± 0.3	14.3 ± 0.3
Propylene	1.22 ± 0.22	0.79 ± 0.07	0.20 ± 0.01
Allene	1.59 ± 0.08	0.75 ± 0.1	0.86 ± 0.01
Methylacetylene	1.15 ± 0.05	1.6–0.25[a]	0.56 ± 0.02
Butenes	1.15 ± 0.02	1.1–0.8[a]	0.23 ± 0.05
Butadiene	0.53 ± 0.07		1.79 ± 0.02
Hexene-1	3.0 ± 0.3	3.4–1.7[a]	
Hexadienes	2.3 ± 0.2	1.2 ± 0.2	3.2 ± 0.2
Methylcyclopentane	16.3 ± 0.5	16.6–11.6[a,b]	
Methylenecyclopentane	6.3 ± 0.3	7.0–2.2[a]	1.28 ± 0.11
Methylcyclopentenes			6.9 ± 0.3
Cyclohexene	4.3 ± 0.6	7.8–4.0[a]	2.18 ± 0.09
Bicyclo[3.1.0]hexane	5.2 ± 0.1	4.4–2.5[a]	3.7 ± 0.5
1,3-Cyclohexadiene			3.6 ± 0.1
Benzene			2.0 ± 0.2
2 Unidentified products			3.5 ± 0.4
Methyl iodide		6.8–8.1[c]	

[a] Yield decreases with increase in iodine concentration. [b] May include some 1,5-hexadiene. [c] Yield increases with increase in iodine concentration.

atom insertion into one molecule of parent reacts with a second molecule to form a large product, *e.g.*, C_{11} from C_5, could not be observed. The formation of products of this kind is a possible explanation for the rather low total recovery found for several of the compounds.

The general reaction scheme shown in Figure 1 applies to reactions in *n*-pentane, isopentane, and, with minor changes, in cyclopentane. For the unsaturated molecules, reaction with the π system of the double bond must also be considered. The relative contribution of alternate routes to the same product was not established in these experiments, and it is probable that mechanisms other than the ones shown also contribute. For example, although ethylene is shown only as a

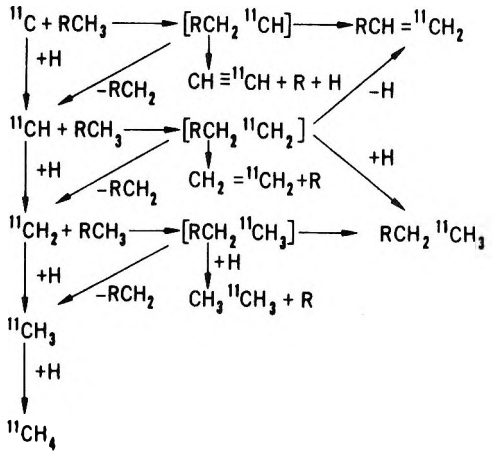

Figure 1. Reaction pathways: $^{11}C + RCH_3$.

product of methyne insertion followed by cleavage, an alternate path involving carbon atom insertion, cleavage, and hydrogen abstraction is quite probable.

Certain points can be established. The formation of the olefin from the preceding paraffin, *e.g.*, hexene-1 from *n*-pentane, most likely involves insertion of the bare carbon atom, followed by stabilization of the carbene.[8] Similarly, the most probable reaction for the formation of the hexanes from pentane is methylene insertion.[9] Thus one can classify (Table III) reactions of bare carbon atoms and methylene into fragmentation, yielding acetylene, ethane, C_3, and C_4 products, and stabilization, yielding C_6 hydrocarbons. Products which can logically be attributed to reactions of methyne and methyl radicals are also listed in Table III without implying that these are the necessary pathways.

For the reactions attributable to the carbon atom the percentage of products resulting from stabilization ranges from 23 to 34, while for the reactions of methylene, this percentage is 84 to 90. It is certainly not unexpected that the carbon atom carries with it more energy so that after insertion, stabilization is less likely than would be the case for methylene.

It is of interest to examine the yields attributable to methylene insertion for statistical behavior since such examination has previously been made for products from ^{14}C recoil experiments.[10] In *n*-pentane the formation of the three hexanes on a purely statistical basis would give the ratio *n*-hexane:2-methylpentane:3-methylpentane = 3:2:1. The observed ratios are 2.66:1.88:1 for the unscavenged and 3.33:2.1:1 for the scavenged system, probably a statistical distribution within experimental error. Wolf[10] reported this ratio as 3.2:2.1:1 for ^{14}C results with *n*-pentane.

The four hexanes possible from isopentane were not completely resolved, but for the three fractions separated the expected ratio would be 3-methylpentane:(2-methylpentane + 2,3-dimethylbutane):2,2-dimethylbutane = 6:5:1. The unscavenged system gave the ratio 3.6:4.2:1 and the scavenged system 4.6:7.0:1. The 3-methylpentane, formed by attack at one of the two adjacent methyl groups, apparently has less than a statistical yield, possibly for steric reasons.

Table III: Reaction Pathways, Pentanes

	Yields, %			
	n-Pentane		Isopentane	
Pathway	Pure	Scavenged	Pure	Scavenged
Reacting as C				
Acetylene	17.5	18.6	21.7	22.1
Unsaturated C_3	8.2	6.0	5.2	3.5
Unsaturated C_4	2.8	2.2	1.3	0.6
Unsaturated C_6	15.0	12.0	12.4	7.9
Total	43.5	38.8	40.6	34.1
% Stabilization	34.5	30.9	30.5	23.2
Reacting as CH				
Ethylene	8.3	7.2	12.5	10.9
Reacting as CH_2				
Ethane	1.1	0.8	1.8	1.2
Saturated C_3	1.0	0.3	1.1	0.4
Saturated C_4	0.6	0.3	0.7	0
Saturated C_6	18.3	12.9	18.9	13.9
Total	21.0	14.5	22.5	15.5
% Stabilization	87.2	90.3	84.0	89.7
Reacting as CH_3				
Methane	6.4	3.8	6.4	3.2
Methyl iodide	...	...	...	5.4
Total	6.4	3.8	6.4	8.6
Total recovered	79.2	64.3	82.0	69.1

The results from cyclopentane can also be classified as due to carbon atoms and methylene reactions (Table IV) showing definite but less striking differences. In this case 50% of the products of carbon atom reactions result from stabilization processes. The production of ethylene can be attributed to methylene without involving hydrogen loss or pickup and it has been included in the methylene products. Since the ethylene yield is much lower here than in the aliphatic compounds, this change is not drastic. Results in parentheses were obtained if ethylene was not included as a methylene fragmentation product.

A similar analysis has been made for the two compounds with double bonds (Table V). This may not be as valid a comparison as the other cases since reactions occur at the double bond as well as at the CH bonds. It is noted that a considerably smaller fraction of the total yield is attributable to methylene reactions, and the fraction of the ^{11}C which remains unbound until it has picked up enough hydrogen to form methane has become very small.

(8) G. Stöcklin and A. P. Wolf, *J. Amer. Chem. Soc.*, **85**, 229 (1963).

(9) See reviews by A. P. Wolf, *Advan. Phys. Org. Chem.*, **2**, 201 (1964); R. Wolfgang, *Progr. React. Kinet.*, **3**, 97 (1965).

(10) A. P. Wolf, "Chemical Effects of Nuclear Transformations," Vol. II, International Atomic Energy Agency, Vienna, 1961, p 3.

Table IV: Reaction Pathways, Cyclopentane

Pathway	Yields, % Pure	Yields, % Scavenged
Reacting as C		
Acetylene	16.4	17.0
Diunsaturated C_3, C_4	3.2	1.6
Unsaturated C_5	20.5	18.6
Total	40.1	37.2
% Stabilization	51	50
Reacting as CH_2		
Ethane	0.4	0.3
Ethylene[a]	3.2	2.4
Monounsaturated C_3, C_4	2.5	1.8
Saturated C_6	19.4	19.4
Total	25.5	23.9
% Stabilization	76 (87)[a]	81 (90)[a]
Reacting as CH_3		
Methane	7.6	4.4
Methyl iodide		7.3
Total	7.6	11.7
Total recovered	73	73

[a] See text.

Table V: Reaction Pathways, Pentene and Cyclopentene

Pathway	Yields, % Pentene	Yields, % Cyclopentene
Reacting as C		
Acetylene	17.4	14.3
Diunsaturated C_3, C_4	6.4	3.2
Polyunsaturated C_6	16.5	9.0
Total	40.3	26.5
% Stabilization	41	34
Reacting as CH		
Ethylene	4.2	1.3
Reacting as CH_2		
Monounsaturated C_3, C_4	4.1	0.2
Monounsaturated C_6	5.0	14.3
Diunsaturated noncyclic C_6		3.3
Total	9.1	17.8
% Stabilization	55	99
Reacting as CH_3		
Saturated C_2–C_4	0.7	
Methane	1.5	2.9
Total	2.2	2.9
Total recovered	56	49

In both scavenger systems in which methyl iodide was determined, isopentane and cyclopentane, its yield more than compensates for the reduction in methane yield. Thus the iodine must react in part with a precursor to the methyl radical. Other iodinated products such as methylene iodide would not have been detected, which may help to account for the lower total recovery in the scavenged systems.

The Mercury-Sensitized Photodecomposition of Nitrous Oxide in the Presence of Mixtures of Carbon Monoxide and Methane

by R. Simonaitis, Julian Heicklen,*

Department of Chemistry, Ionosphere Research Laboratory, and Center for Air Environment Studies, The Pennsylvania State University, University Park, Pennsylvania 16802

M. M. Maguire, and R. A. Bernheim

Department of Chemistry, The Pennsylvania State University, University Park, Pennsylvania 16802

(Received February 18, 1971)

Publication costs borne completely by The Journal of Physical Chemistry

The mercury-photosensitized decomposition of N_2O in the presence of CO–CH_4 mixtures was studied at 548°K. From the competition between CO and CH_4 for $O(^3P)$, the ratio k_1/k_2 was found to be 2.0, where the reactions are (1) $O(^3P) + CO \rightarrow CO_2$ and (2) $O(^3P) + CH_4 \rightarrow CH_3 + HO$. Reaction 1 is second order at the pressures used in this study (>250 Torr, mainly N_2O). Furthermore, the HO radical produced in reaction 2 can react with either CO ($HO + CO \rightarrow H + CO_2$, reaction 3) or CH_4 ($HO + CH_4 \rightarrow H_2O + CH_3$, reaction 4). An approximate value of $k_4/k_3 = 1.0$ was obtained. A reexamination of the determination of k_2 suggests that its value at 548°K is about one-tenth as large as previously reported. In runs in the absence of CO or CH_4, the $O(^3P)$ produced in the primary process appears as O_2, but there is a noticeable induction period in O_2 formation. Experiments with added CH_4 have established that the oxygen atoms are efficiently adsorbed by the wall of the quartz reaction vessel. Thus because of the inhomogeneity of the light absorption, $O(^3P)$ atoms can be removed by the walls even in the presence of an $O(^3P)$ scavenger. Furthermore, results with two different mercury resonance lamps are quantitatively different, because of the difference in pressure broadening of the incident radiation.

Introduction

Recently[1] we have examined the reaction of $O(^3P)$

$$O(^3P) + CO \longrightarrow CO_2 \qquad (1)$$

with CO at 298–472°K by studying the competition between CO and 2-trifluoromethylpropene for oxygen atoms produced in the mercury-photosensitized decomposition of N_2O. We found this reaction to be intermediate between second and third order at pressures of 200–800 Torr with N_2O as the principal gas. Furthermore, at any pressure the reaction became more second order as the temperature was raised. The limiting low- and high-pressure rate constants were found to fit the expressions $k_0 = 1.29 \times 10^9 \exp(-4070/RT)$ M^{-2} sec^{-1} and $k_\infty = 3.40 \times 10^6 \exp(-2930/RT)$ M^{-1} sec^{-1}.

In view of the unusual behavior found for the rate constant and the discrepancies found in the literature[2,3] with regard to the rate constant and the order of the reaction, it seemed appropriate to examine reaction 1 in a different system. In this paper the same technique for generating oxygen atoms is used at 548°K, but the competing gas was CH_4 rather than 2-trifluoromethylpropene, so that reaction 1 was studied in competition with reaction 2

$$O(^3P) + CH_4 \longrightarrow HO + CH_3 \qquad (2)$$

Since HO radicals are produced in reaction 2, it was hoped that, in addition to obtaining k_1/k_2, it also would be possible to measure k_3/k_4

$$HO + CO \longrightarrow H + CO_2 \qquad (3)$$

$$HO + CH_4 \longrightarrow H_2O + CH_3 \qquad (4)$$

Measuring the competition between reactions 3 and 4 is difficult because reaction 1 produces CO_2 which complicates the analysis of the data. Nevertheless, an estimate for k_3/k_4 could be made.

As the study was in progress, it became apparent that some of the oxygen atoms were being removed by a reaction other than reaction 2. Thus it was necessary to study this route of oxygen atom disappearance. This was done in several series of runs with CO absent, and those results are also reported here.

Experimental Section

Most of the experiments utilized conventional static photochemical techniques. Matheson CP grade N_2O was purified in several ways. For some runs the N_2O was passed over ascarite and degassed at −196°. In other runs the N_2O was distilled at −160°, and the

(1) R. Simonaitis and J. Heicklen, *J. Chem. Phys.*, in press.

(2) D. L. Baulch, D. D. Drysdale, and A. C. Lloyd, "High Temperature Reaction Rate Data," No. 1, Department of Physical Chemistry, Leeds University, 1968.

(3) N. Cohen and J. Heicklen, "Comprehensive Chemical Kinetics," C. H. Bamford and C. F. H. Tipper, Ed., Elsevier, to be published in Vol. 6.

middle fraction was used. A third procedure was to preirradiate N_2O–Hg mixtures and then to degas at −196°. All three methods of purification gave N_2O free of impurities (<10 ppm) as determined by both gas chromatography and mass spectrometry. Specifically NO, O_2, N_2, and hydrocarbons were absent. Furthermore, the photochemical results were the same regardless of the methods of purification, except with N_2O alone at 275°. For these runs a different cylinder of N_2O was used, and the oxygen quantum yields were lower if the N_2O was distilled at −160° to remove any NO_2.

Matheson "ultrapure" methane was purified by repeated degassing at −196° and distillation at −186°. The remaining impurities were N_2 (100 ppm), O_2 (<10 ppm), and C_2H_6 (<20 ppm). At high pressures of CH_4 a small correction for the presence of these impurities was made. However, for most runs the correction was negligible.

Matheson CP grade CO was purified by passage over glass beads at −196°, degassing at −196°, and distillation from liquid argon. The O_2 impurity was reduced to <10 ppm, but 190 ppm N_2 remained.

The reactants were saturated with mercury vapor before being mixed in the reaction vessel which was a cylindrical quartz cell 5 cm in diameter and 10 cm long. The reaction vessel was jacketed in a wire-wound aluminum furnace with quartz windows. Irradiation was from a Hanovia flat-spiral, low-pressure mercury resonance lamp. The radiation passed through a Corning 9-54 filter before entering the reaction cell to remove all radiation below 2200 Å. For some runs without CO present, a North American Phillips Model 93109E low-pressure mercury resonance lamp was used.

After irradiation the cell contents were condensed in a trap at −196°. The noncondensables (N_2, H_2, CO, and O_2) were collected in a Toepler pump and analyzed for N_2 and O_2 by gas chromatography using a 0.25-in. diameter by 10-ft long 5A molecular sieve column operating at 25°. Corrections for background N_2 were made in computing the rate of N_2 formation, $R\{N_2\}$. The fraction condensable at −196° was analyzed for C_2H_6 and CO_2 on a 0.25-in. diameter by 20-ft long Porapak Q column at 25°.

Some experiments were done using electron paramagnetic resonance spectroscopy to follow continuously the rate of production of O_2 *in situ* in the mercury-sensitized decomposition of N_2O alone. The 25-cc photolysis cell used consisted of a length of Suprasil quartz tubing placed in the X-band cavity of a Varian 4502 epr spectrometer and extending about 15 cm below it. A 50-W spiral low-pressure mercury lamp, obtained from Ultra-violet Products, Inc., was placed around the extension immediately below the cavity. A Corning 7-54 filter could be inserted between the quartz tubular cell and the spiral lamp to eliminate the 1849-Å mercury spectral line.

Results

CO Absent. Initially, the mercury-sensitized photodecomposition of 100 Torr N_2O at 23° was studied as a function of irradiation time. The results are listed in Table I for N_2 and O_2 productions. Since $\Phi\{N_2\} = 1.00$, the ratio of O_2 to N_2 is $\Phi\{O_2\}$.

Table I: Effect of Irradiation Time on the Mercury-Photosensitized Decomposition of N_2O

Irradiation time, min	$10^8 \times R\{N_2\}$, mol/l. sec	$\Phi\{O_2\}$
T = 23°, $[N_2O]$ = 100 Torr, Phillips 93109E Lamp		
60.0	0.108	0.200
63.0	0.127	0.236
64.0	0.117	0.254
180.0	0.115	0.339
398.0	0.152	0.414
600.0	0.118	0.337
1200.0	0.064	0.221
T = 275°, $[N_2O]$ = 53 Torr, Hanovia Lamp		
33.0	0.42	0.038
210.0	0.64	0.20

The irradiation time was varied from 60 to 1200 min. For about 600 min the rate of N_2 production, $R\{N_2\}$, was nearly constant, where $R\{N_2\}$ is computed as the N_2 produced divided by the irradiation time. For 1200-min exposure, $R\{N_2\}$ dropped noticeably indicating that HgO was formed, which inhibited the reaction. The production of HgO in the later part of the reaction is attributed to the sequence of steps

$$O + O_2 + M \longrightarrow O_3 + M$$

$$O_3 + Hg \longrightarrow HgO + O_2$$

The measured quantum yield of O_2 formation is very much less than 0.5 for short irradiation times and increases with exposure time, reaching a maximum value of about 0.42 for about 400-min exposure. Further irradiation decreases the yield. Our peak value of $\Phi\{O_2\} \simeq 0.42$ occurs for a total N_2 production of 36 μmol/l. Cvetanović[4] obtained $\Phi\{O_2\} = 0.47$ for a total N_2 production of 6–50 μmol/l. Our results compare favorably even though Cvetanović's intensity was about five to ten times ours. The falloff of $\Phi\{O_2\}$ as the irradiation time increases is due to the O_2 consumption *via* the above reactions. The low values for $\Phi\{O_2\}$ at short exposures were unexpected and indicate that some of the oxygen atoms have formed products other than O_2.

At 275°, the induction period in oxygen formation is even more pronounced. For the 210-min run almost 1 Torr of oxygen atoms is missing.

(4) R. J. Cvetanović, *J. Chem. Phys.*, 23, 1203 (1955).

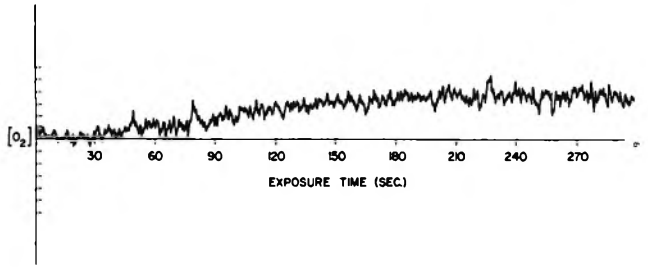

Figure 1. Plot of $[O_2]$ *vs.* time as obtained by epr spectroscopy during the mercury-sensitized photolysis of 20 Torr N_2O at 25°. The intensity of the $K = 11, J = 12 \rightarrow 10, M_s = -2 \rightarrow -1$ transition of O_2 was monitored. This transition occurred at a magnetic field of 5961.4 G with a klystron frequency of 9208.5 MHz.

To check the induction period in O_2 formation, epr experiments were done so that O_2 could be monitored continuously. The $K = 11, J = 12 \rightarrow 10, M_s = -2 \rightarrow -1$ transition at X-band frequencies is useful for this type of experiment. The cell was filled with 20 Torr N_2O and irradiated in the absence of mercury vapor and with no filter. Under these conditions the direct photolysis of N_2O produces $O(^1D)$ which reacts with N_2O and produces O_2 instantaneously; the epr signal appears with no delay. With the filter in place O_2 is not detected.

When the cell is filled with 20 Torr N_2O and allowed to stand overnight over a small amount of mercury, the spectrum of O_2 appears with an induction period upon irradiation with filtered light from the spiral lamp. The curve of growth is shown in Figure 1. After a 30-sec induction period the O_2 grows at a rate of 2.34×10^{-8} mol/l. sec until it levels off and reaches a constant value of 3.5 μmol/l. The limiting value can be attributed to HgO formation which was observed on the surface of the mercury pool at the bottom of the cell. The induction period represents a loss of 1.4 μmol/l. or 26 μ of oxygen atoms.

We looked for the epr signal due to NO with no success. However, the epr spectrum of O_2 is so intense in the region where the NO transitions are expected to occur that they may be obscured. This problem could be circumvented by using a cavity with a Stark modulation system rather than Zeeman modulation. A search for the signal due to $O(^3P_2)$ yielded negative results, thus indicating a steady-state pressure of $O(^3P_2)$ of ≤ 1 μ.

Table II shows the results of the mercury-photosensitized decomposition of N_2O at 275° in the presence of CH_4. The products measured were C_2H_6, CO_2, and CO. No oxygen was found. Methane is very much less efficient than N_2O in scavenging $Hg(6^3P_1)$.[5a] However to be certain that $\Phi\{N_2\}$ remained 1.00 in the presence of CH_4, a few runs were done with a few Torr of C_3H_6 present (to scavenge the oxygen atoms) with CH_4 both present and absent. The rate of N_2 formation was unaffected. In the N_2O–CH_4 system the oxygen atom can react with CH_4 leading to

$$O + CH_4 \longrightarrow CH_3 + OH \quad (2)$$

$$OH + CH_4 \longrightarrow H_2O + CH_3 \quad (4)$$

If any O_2 is produced, it is scavenged by CH_3

$$CH_3 + O_2 + M \longrightarrow CH_3O_2 + M \quad (a)$$

$$CH_3O_2 + CH_4 \longrightarrow CH_3O_2H + CH_3 \quad (b)$$

An alternate fate of CH_3O_2 could be self-annihilation. However, since its rate constant[5b] is about 10^{10} M^{-1} sec^{-1}, this reaction will be unimportant in our system if $k_b > 10^2$ M^{-1} sec^{-1}. Our results are consistent with this hypothesis. The CH_3OOH presumably decomposes to H_2O and CH_2O, the latter being further oxidized to CO and CO_2. Thus, for every oxygen atom reacting with CH_4, one molecule of C_2H_6 is produced.

The ethane yield, $\Phi\{C_2H_6\}$, increases from 0.12 to 0.57 as the CH_4 pressure is raised from 5 to 99 Torr. However, $\Phi\{C_2H_6\}$ is almost independent of a 30-fold change in N_2O pressure or a 300-fold change in $R\{N_2\}$ (*i.e.*, the absorbed intensity, I_a).

Most of the runs were done for similar conversions. However, two runs were done at greatly reduced conversions (the 2- and 10-min runs). $\Phi\{C_2H_6\}$ decreased from 0.35 to 0.22 as the irradiation time increased from 2 to 66 min for otherwise identical runs. The reason for the drop may be that at longer conversions more O_2 is produced which enhances reaction a and thus leads to some loss of CH_3 *via* reaction a followed by self-annihilation of CH_3O_2. However, the drop in $\Phi\{C_2H_6\}$ is not very pronounced considering the 33-fold variation in extent of conversion. At any rate, all the other runs are for similar conversions and should be directly comparable.

The effect of conversion was further checked under other conditions. These results are shown in Table III. A ninefold variation in the extent of conversion had no noticeable effect on $\Phi\{C_2H_6\}$.

Another series of runs was made to test the effect of N_2O pressure and these results are shown in Table IV. Contrary to the results in Table II where the N_2O pressure had almost no effect, the results in Table IV show that $\Phi\{C_2H_6\}$ noticeably drops as $[N_2O]$ increases. The effect is more pronounced with 9.8 Torr CH_4 than with 110 Torr CH_4. However, even in the former case, the effect is much less than linear, a 35-fold increase in $[N_2O]$ gives only a 4.3-fold drop in $\Phi\{C_2H_6\}$. The difference between the two sets of experiment listed in Tables II and IV is that two different types of mercury resonance lamp were used. These results were carefully checked, and the different results caused by the two types of lamps are real.

Table V contains another set of experiments illustrating that $\Phi\{C_2H_6\}$ increases with $[CH_4]$. $\Phi\{C_2H_6\}$

(5) (a) R. J. Cvetanović, *Progr. React. Kinet.*, **2**, 39 (1964); (b) J. Heicklen, *Advan. Chem. Ser.*, **No. 76**, 23 (1968).

Table II: Mercury-Photosensitized Decomposition of N_2O–CH_4 Mixtures at 275° with a Hanovia Flat-Spiral, Low-Pressure Mercury Resonance Lamp

$[N_2O]$, Torr	$[CH_4]$, Torr	Irradiation time, min	$10^8 \times R\{N_2\}$, mol/l. sec	$\Phi\{C_2H_6\}$	$\Phi\{CO_2\}$	$\Phi\{CO\}$
30.0[a]	5.00	65.00	0.50	0.120	...	0.165
615	5.00	65.00	0.55	0.103	0.068	...
32.0	5.05	66.00	0.43	0.128	0.080	0.118
610	5.10	65.00	0.57	0.080	...	...
30.0	5.90	4.00	6.5	0.133	0.043	...
600	9.80	1010.00	0.041	0.204	...	...
660	9.80	4.00	9.9	0.089	...	...
20.0	10.0	65.00	0.43	0.217	...	...
615	10.0	65.00	0.58	0.165	...	...
635	10.0	65.00	0.57	0.160	0.050	0.124
220	10.1	65.00	0.58	0.202	0.033	...
22.0	10.1	66.00	0.43	0.224	0.065	...
22.3	10.2	10.00	0.44	0.27	...	...
22.3	10.2	2.00	0.44	0.35	...	...
614	13.5	65.00	0.56	0.213	0.045	0.119
642	23.0	4.00	8.4	0.214	...	...
630	25.0	840.00	0.032	0.262	0.146	0.042
604	56.0	4.00	9.9	0.37	0.028	...
540	99.0	65.00	0.56	0.57	0.027	...

[a] 390 Torr CF_4 also present.

Table III: Effect of Irradiation Time on the Mercury-Photosensitized Decomposition of N_2O–CH_4 Mixtures at 275°; Phillips 93109E Lamp

$[N_2O]$, Torr	$[CH_4]$, Torr	Irradiation time, min	$10^8 \times R\{N_2\}$, mol/l. sec	$\Phi\{C_2H_6\}$	$\Phi\{CO_2\}$
100	102	12.0	0.326	0.61	...
97	103	14.0	0.348	0.54	0.025
100	100	30.0	0.346	0.59	0.014
100	97	81.0	0.286	0.63	0.012
100	98	155.0	0.224	0.61	0.011

Table IV: Effect of N_2O Pressure on the Mercury-Photosensitized Decomposition of N_2O–CH_4 Mixtures at 275°; Phillips 93109E Lamp

$[N_2O]$, Torr	$10^8 \times R\{N_2\}$, mol/l. sec	$\Phi\{C_2H_6\}$	$\Phi\{CO_2\}$
$[CH_4]$ = 110 ± 10 Torr, Irradiation Time = 30 min			
13.5	0.195	0.81	0.17
17	0.214	0.82	0.025
30	0.214	0.85	0.12
100	0.347	0.60	0.014
112	0.337	0.67	0.011
117	0.325	0.61	0.011
244	0.438	0.62	...
$[CH_4]$ = 9.8 ± 0.2 Torr, Irradiation Time = 60 min			
13.0	0.063	0.57	...
54.0	0.172	0.33	...
123	0.235	0.25	...
228	0.302	0.198	...
310	0.34	0.193	...
460	0.47	0.132	...

Table V: Effect of CH_4 Pressure on the Mercury-Photosensitized Decomposition of N_2O–CH_4 Mixtures at 275°; Phillips 93109E Lamp

$[N_2O]$, Torr	$[CH_4]$, Torr	Irradiation time, min	$10^8 \times R\{N_2\}$, mol/l. sec	$\Phi\{C_2H_6\}$	$\Phi\{CO_2\}$
80	5.0	15.0	0.393	0.062	...
75	5.5	30.0	0.426	0.060	...
54	9.8	60.0	0.172	0.295	...
42	13.0	64.0	0.180	0.39	...
31	19	30.0	...	0.23	...
45	23.0	60.0	0.146	0.51	
27	29	30.0	...	0.30	...
60	36	30.5	0.390	0.44	...
80	62	30.0	0.344	0.60	...
100	100	870.0	0.0087	0.49	0.002
100	100	1080.0	0.0096	0.47	0.037
45	112	30.0	0.271	0.64	...
51	316	30.0	0.366	0.79	0.012
57	354	30.0	0.406	0.80	0.009
53	374	30.0	0.424	0.68	0.008
51	434	30.0	0.424	0.87	0.009

increases from 0.06 to 0.87 as $[CH_4]$ is raised from 5.0 to 434 Torr.

CO Present. When the mercury-photosensitized decomposition of N_2O is studied in the presence of mixtures of CO and CH_4 at 548°K, the products of the reaction are N_2, C_2H_6, CO_2, H_2, and presumably H_2O. The first four products were found, but no effort was made to find H_2O. Oxygen was not produced under our reaction conditions.

The present study was complicated by the occurrence of a heterogeneous dark reaction between N_2O and CO

to give CO_2 and N_2 at high pressures of CO. It was also observed that this dark reaction became more important as the cell aged. Therefore, the rates of formation of CO_2 and N_2 were not useful at high CO pressures. Actinometry had to be done in separate runs in which CO was not present. For the experiments at low pressures of CO, which were also the first to be performed, the dark reaction was negligible. This dark reaction also became more important as the temperature was raised above 548°K, thus prohibiting us from performing experiments at more elevated temperatures.

A further complication was the disappearance of H_2 in the dark. Over a period of 1–2 hr 30–50% of a known amount of H_2 (~30 μ) introduced into the cell in the presence of reactants at 548°K disappeared; over a period of 12 hr, all the H_2 vanished. Thus the rate of H_2 formation could not be measured reliably. Fortunately C_2H_6 is unaffected in the dark in the presence of the reactants at 548°K.

The best regime to study the competition between reactions 1 and 2 is at high $[CO]/[CH_4]$ where the quantum yield of ethane formation, $\Phi\{C_2H_6\}$, is small (see Discussion). Results of experiments at high $[CO]/[CH_4]$ at 548°K with two different radiation sources are given in Table VI. For the runs with CO present, the CO pressure was varied from 7.6 to 204 Torr; the CH_4 pressure, from 4.80 to 182 Torr; and the N_2O pressure, from 146 to 652 Torr. In all the runs the relative amounts of N_2O, CH_4, and CO were such that at least 90% of the excited mercury atoms were scavenged by N_2O as computed from the known quenching constants.[5a] The ratio $[CO]/[CH_4]$ ranged from 0.084 to 20; $\Phi\{C_2H_6\}$ dropped regularly as the ratio was raised and was reduced to 0.020 at the highest ratio. Two runs were done with the intensity reduced by a factor of 47, and $\Phi\{C_2H_6\}$ was only slightly altered.

At lower ratios of [CO] to $[CH_4]$, the relative importance of reaction 1 compared to reaction 2 is reduced, and the competition between reactions 3 and 4 can be studied. Results at reduced values of $[CO]/[CH_4]$ are shown in Table VII. The pressure of CO was varied from 3.4 to 9.3 Torr; of CH_4, from 94 to 379 Torr; and of N_2O, from 22 to 465 Torr. As for the studies listed in Table VI, the gas pressures were such that at least 90% of quenching of the excited mercury atom was done by N_2O. The ratio $[CH_4]/[CO]$ was changed by a factor of 4 in these experiments, and two runs were done at very reduced intensities. Neither the quantum yield of C_2H_6 nor CO_2 was much influenced by the variation in experimental parameters. $\Phi\{C_2H_6\}$ remained between 0.49 and 0.75. $\Phi\{CO_2\}$ showed slightly more variation, ranging from 0.052 to 0.160.

Table VI: Mercury-Photosensitized Decomposition of N_2O at 548°K in the Presence of CH_4 and High Pressures of CO

[CO], Torr	[CH_4], Torr	[N_2O], Torr	Irradiation time, min	$10^7 I_a$, einsteins/l. min	$\Phi\{C_2H_6\}$
		Hanovia Lamp			
0.0	4.90	146	66.0	3.30	0.127
53	4.80	167	89.0	3.30	0.029
53	182	184	68.0	3.30	0.61
57	9.70	161	69.0	3.30	0.068
58	4.85	162	67.0	3.30	0.037
59	9.75	287	75.0	3.30	0.055
60	10.00	652	67.0	3.30	0.041
61	165	574	67.0	3.30	0.49
103	10.00	617	1245.0	0.0745	0.055
105	9.80	290	65.0	3.30	0.041
108	9.90	623	66.0	3.30	0.035
186	11.00	600	1257.0	0.0745	0.035
196	9.75	584	65.0	3.30	0.020
		Phillips Lamp			
0.0	19.0	306	60.0	2.31	0.31
0.0	26.5	370	60.0	2.63	0.31
7.6	90.0	496	60.0	2.63	0.53
13.0	34.0	567	60.0	2.63	0.28
19.0	19.0	290	60.0	2.22	0.137
27.0	75.0	515	60.0	2.63	0.37
37.5	26.5	560	60.0	2.63	0.147
50	16.5	585	60.0	2.63	0.070
51	11.0	552	60.0	2.63	0.048
51	38.0	588	60.0	2.63	0.204
53	8.0	294	60.0	2.31	0.055
73	26.0	565	60.0	2.63	0.12
95	19.5	290	60.0	2.43	0.084
104	26.0	305	60.0	2.43	0.092
127	27.5	592	60.0	2.63	0.076
137	26.0	562	60.0	2.63	0.062
204	26.0	594	60.0	2.63	0.044

Table VII: Mercury-Photosensitized Decomposition of N_2O at 548°K with the Phillips Lamp in the Presence of CH_4 and Low Pressures of CO

[CO], Torr	[CH_4], Torr	[N_2O], Torr	Irradiation time, min	$10^7 I_a$, einsteins/l. min	$\Phi\{C_2H_6\}$	$\Phi\{CO_2\}$
3.4	126	92	30.0	2.11	0.54	0.052
4.4	117	190	30.0	2.22	0.48	0.057
4.5	112	44	30.0	1.58	0.64	0.073
5.7	212	22	60.0	1.59	0.75	0.056
6.2	96	287	60.0	1.95	0.56	0.110
6.2	181	351	60.0	2.32	0.68	0.088
6.3	94	95	966.0	0.070	0.61	0.120
6.3	101	465	60.0	1.91	0.52	0.130
6.5	98	186	60.0	2.40	0.49	0.085
7.5	94	32	970.0	0.050	0.54	0.110
8.2	203	106	30.0	2.31	0.62	0.086
8.9	104	350	60.0	1.94	0.49	0.160
9.3	379	128	30.0	2.75	0.69	0.065

Discussion

CO Absent. It is clear from our results that there is a considerable delay in O_2 production in the mercury-sensitized photolysis of pure N_2O. Furthermore, the amount of unaccounted for oxygen atoms is sufficiently large to eliminate the possibility of reaction with either

Hg or an impurity since their initial pressures are less than a few microns. An apparent explanation is given by the sequence of steps

$$O(^3P) + N_2O \longrightarrow 2NO \quad (c)$$

$$O(^3P) + NO + M \longrightarrow NO_2 + M \quad (d)$$

$$O(^3P) + NO_2 \longrightarrow NO + O_2 \quad (e)$$

The initial product of the reaction is NO, which conforms to Cvetanović's[4] finding that oxides of nitrogen are produced. The best values[6] for the rate constants k_d and k_e at room temperatures are $k_d = 3.6 \times 10^{10}$ M^{-2} sec^{-1} with O_2 as a chaperone and $k_e = 2.6 \times 10^9$ M^{-1} sec^{-1}. Even if reaction d is more efficient with N_2O than with O_2, which is likely, k_2 is still sufficiently large so that $[NO_2]/[NO]$ is always much less than unity for all our experiments; the steady-state approximation on NO_2 is valid.

An approximate value for k_c can be estimated from the expression $k_c = k_d[NO]$ when the rates of reaction c and d are equal. The results indicate that this occurs for $[NO] \sim 10$ μ. Then $k_c \sim 2 \times 10^4$ M^{-1} sec^{-1} at room temperature.

Reaction c has been studied in the shock tube by several investigators at temperatures of 1000–2000°.[7] The best rate constant is $2.3 \times 10^{10} \exp(-24{,}100/RT)$ M^{-1} sec^{-1}, which gives 1.3×10^{-10} M^{-1} sec^{-1} when extrapolated to 300°K. This value is 14 orders of magnitude smaller than estimated above. Furthermore, it is not clear why the reaction of $O(^3P)$ with N_2O should give only NO at room temperature and not O_2 plus N_2, as it does at higher temperatures.[7] Also, attempts to find NO by both gas chromatography and mass spectrometry were unsuccessful.

Other difficulties with this mechanism come from the results with CH_4 present. The reaction of oxygen atoms with N_2O would lead to products which will scavenge CH_3 radicals, thus leading to a strong dependence of $\Phi\{C_2H_6\}$ on $[N_2O]$ contrary to our findings. Finally, if NO were produced, it should scavenge CH_3 ultimately to produce CH_2NOH.[8] Therefore, we conclude that the oxygen atoms are not reacting with N_2O, contrary to an earlier report by us.[9]

The only remaining possibility is that the oxygen atoms are being removed by adsorption on the walls of the reaction vessel.

$$O \xrightarrow{\text{wall}} O_{ads} \quad (5)$$

The mechanism would then predict

$$\Phi\{C_2H_6\}^{-1} - 1 = k_5/k_2[CH_4] \quad (I)$$

Figure 2 is a log–log plot of this expression using the data of Table II with the two low conversion points omitted. The slight effect of N_2O pressure is observed, the low-pressure points lying below those at high pressure. The best straight line of unit slope is drawn through the high-pressure points, and the intercept

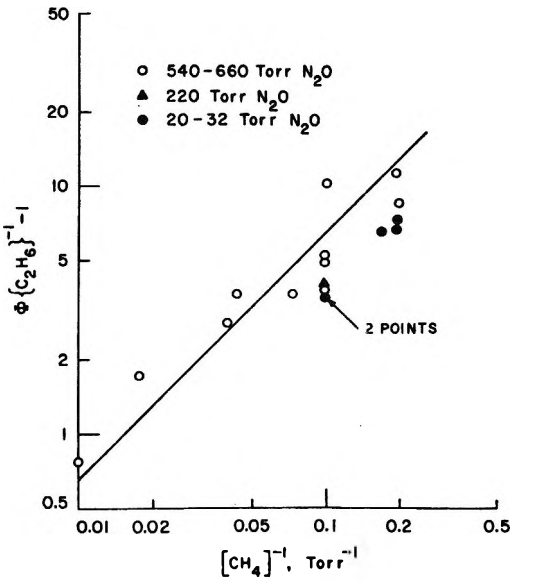

Figure 2. Plot of $\Phi\{C_2H_6\}^{-1} - 1$ *vs.* $[CH_4]^{-1}$ in the mercury-photosensitized decomposition of N_2O–CH_4 mixtures at 275°, using a Hanovia flat-spiral, low-pressure mercury resonance lamp.

yields $k_5/k_2 = 65$ Torr. The three points lying furthest above the line are those at highest intensity. Under these conditions some methyl radicals might be removed by interaction with oxygen atoms[10,11]

$$O + CH_3 \longrightarrow CH_2O + H$$

thus yielding low values for $\Phi\{C_2H_6\}$.

There are two apparent difficulties with the wall removal mechanism. First, diffusion from the interior of the reaction vessel is much too slow to compete with reaction 2 which has a rate constant of 5.1×10^6 M^{-1} sec^{-1} at 275°.[12] Second, the diffusion rate should vary inversely with the total pressure, whereas we observe only a slight pressure dependence.

Both of these apparent discrepancies can be explained by the fact that the absorption of radiation is nonuniform and occurs mainly near the front window of the reaction cell; thus diffusion distances are small. In fact, because of pressure broadening the absorption occurs nearer the window at higher pressures, and this effect apparently compensates for the reduced diffusion rates.

(6) "DASA Reaction Rate Handbook," 1967.

(7) D. L. Baulch, D. D. Drysdale, D. G. Horne, and A. C. Lloyd, "High Temperature Reaction Rate Data," No. 4, Department of Physical Chemistry, Leeds University, 1969.

(8) J. Heicklen and N. Cohen, *Advan. Photochem.*, **5**, 157 (1968).

(9) R. Simonaitis, J. Heicklen, M. M. Maguire, and R. Bernheim, Ionosphere Research Laboratory Scientific Report No. 340, The Pennsylvania State University, 1969.

(10) H. Niki, E. E. Daby, and B. Weinstock, 12th Symposium (International) on Combustion, 1969, p 277.

(11) J. T. Herron and R. D. Penzhorn, *J. Phys. Chem.*, **73**, 191 (1969).

(12) J. T. Herron, *Int. J. Chem. Kinet*, **1**, 527 (1969).

The experimental results tend to verify the above arguments. The Hanovia lamp operates at relatively low temperatures, and the incident mercury radiation is sharp. Measurements of $R\{N_2\}$ as a function of $[N_2O]$ show that about 75% of the radiation is absorbed at 20 Torr and essentially all the radiation is absorbed above 50 Torr of N_2O. Only a small effect of N_2O pressure on k_5 is observed. On the other hand, the Phillips lamp operates at higher temperatures and thus the incident mercury radiation is considerably broader. $R\{N_2\}$ increases markedly with N_2O pressure, and even at 600 Torr of N_2O, all the radiation is not absorbed. Thus, at low pressure more of the radiation is absorbed in the interior of the vessel, k_5 is correspondingly reduced, and $\Phi\{C_2H_6\}$ is enhanced as shown in Table IV.

The efficient removal of oxygen atoms by adsorption on the walls of the vessel has also been shown to be the case in the vacuum ultraviolet photolysis of CO_2,[13] thus accounting for the oxygen deficiency in that system. A very recent publication[14] has shown that Pyrex surfaces efficiently adsorb oxygen atoms and that these atoms do not combine to form O_2. Our results with N_2O are consistent with these findings.

CO Present. The reaction scheme is certainly the following

$$Hg + h\nu\ (2537\ \text{Å}) \longrightarrow Hg(6^3P_1)$$

$$Hg(6^3P_1) + N_2O \longrightarrow Hg + N_2 + O(^3P)$$

$$O + CO \longrightarrow CO_2 \quad (1)$$

$$O + CH_4 \longrightarrow HO + CH_3 \quad (2)$$

$$HO + CO \longrightarrow CO_2 + H \quad (3)$$

$$HO + CH_4 \longrightarrow H_2O + CH_3 \quad (4)$$

$$O \longrightarrow \text{wall} \quad (5)$$

$$2CH_3 \longrightarrow C_2H_6 \quad (6)$$

$$H + CH_4 \longrightarrow H_2 + CH_3 \quad (7)$$

$$H + N_2O \longrightarrow HO + N_2 \quad (8)$$

All of the listed reactions, except reaction 5, are well known and have been reported in numerous studies. As shown above, reaction 5 occurs in our reaction vessel, and with experiments using the Hanovia lamp, k_5/k_2 is 65 Torr at 548°K. Another radical–molecule reaction which might be considered is

$$HO + N_2O \longrightarrow HO_2 + N_2$$

No evidence has ever been advanced for this reaction, though it is exothermic and conserves spin. In the absence of CO, the rate of N_2 formation is not enhanced in the mercury-photosensitized decomposition of N_2O at 548°K by introducing HO radicals into the system. Thus this reaction must be slow and can be neglected.

Radical–radical reactions involving O, HO, and H have also been neglected in the above scheme. If such reactions were important, then a reduction in intensity would reduce their relative importance, and $\Phi\{C_2H_6\}$ should increase. The runs at reduced intensity gave slightly higher values for $\Phi\{C_2H_6\}$, but considering the factor of 47 change in I_a, this increase is minor. Consequently, competitions between radical–radical and radical–molecule reactions cannot be important. This is not true at lower temperatures where experiments were also attempted. At 475°K and below, there is a pronounced intensity effect which prohibited meaningful experiments from being done at those temperatures.

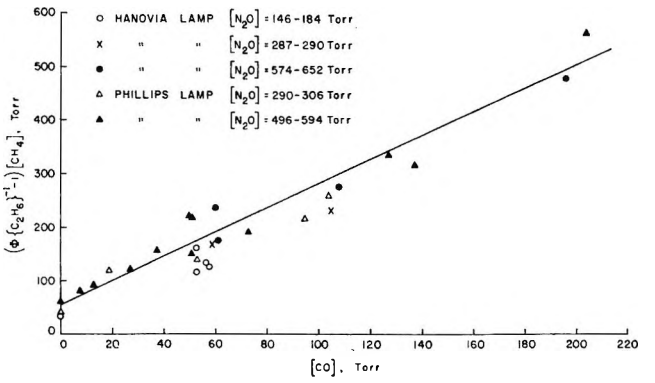

Figure 3. Plot of $(\Phi\{C_2H_6\}^{-1} - 1)[CH_4]$ *vs.* [CO] in the mercury-photosensitized decomposition of N_2O at 548°K in the presence of CH_4 and high pressures of CO.

Determination of k_1/k_2. The mechanism leads to the following rate law for C_2H_6 production

$$(\Phi\{C_2H_6\}^{-1} - 1)[CH_4] = k_5/k_2 + k_1[CO]/k_2 \quad (II)$$

Figure 3 is a plot of the left-hand side of the equation *vs.* [CO] for the data in Table VI. In spite of the significant scatter, the plot can reasonably be fitted by a straight line, showing that reaction 1 is second order as expected from the results at lower temperatures.[1] The intercept of 65 Torr corresponds to the value of k_5/k_2 found with the Hanovia lamp above. The data with the Phillips lamp are for high total pressures, and pressure broadening is sufficient to ensure complete absorption of the radiation. Thus the differences between the two lamps are negligible (as seen from Tables II and IV at total pressures above 200 Torr) and the data from the two lamps fit the same plot. The slope of 2.0 corresponds to k_1/k_2. Close examination of Figure 3 reveals that the data points at high N_2O pressures lie slightly higher than those at low N_2O pressures, thus indicating that k_1 may be just into the pressure-falloff region.

Value of k_2. The value of k_2 has been reported by many investigators, and the results were recently reviewed by Herron.[12] Most of the investigators measured

(13) T. G. Slanger, *J. Chem. Phys.*, **45**, 4127 (1966).
(14) J. A. Riley and C. F. Giese, *ibid.*, **53**, 146 (1970).

Table VIII: Rate Constants of Importance in the Reaction of $O(^3P)$ with CH_4; Units of M^{-1} sec^{-1}

Rate constant expression	Value at 548°K	Reference
$k_4 = 2.9 \times 10^{10} \exp(-5000/RT)$	2.9×10^8	Wilson and Westenberg[a]
$k_7 = 12.6 \times 10^{10} \exp(-11,900/RT)$	2.19×10^6	Walker[b]
$k_9 = 1.3 \times 10^{10}$	1.3×10^{10}	Baulch, *et al.*[c]
$k_{10} = 10^{10} \exp(-3300/RT)$	4.8×10^8	McNesby, *et al.*[d]
$k_{11} = \sim 10^{10} \exp(-3500/RT)$	3.9×10^8	*e*
$k_{12} = 4.0 \times 10^{10}$	4.0×10^{10}	*f*

[a] Reference 17. [b] R. W. Walker, *J. Chem. Soc. A*, 2391 (1968). [c] D. L. Baulch, D. D. Drysdale, and A. C. Lloyd, "High Temperature Reaction Rate Data," No. 3, Department of Physical Chemistry, Leeds University, 1969. [d] J. R. McNesby, M. D. Scheer, and R. Klein, *J. Chem. Phys.*, **32**, 1814 (1960). [e] Preexponential factor assumed equal to that of k_{10}. Activation energy determined from value of $k_{11} = 2.6 \times 10^7$ at 300°K [W. R. Brennan, I. D. Gay, G. P. Glass, and H. Niki, *J. Chem. Phys.*, **43**, 2569 (1965)]. [f] Hoare[18] found $k_{12}/k_4 = 33 \pm 6$ at 525°K. Thus 4.0×10^{10} is an upper limit to k_{12} at 548°K.

the loss of oxygen atoms in a flow tube experiment and, between 350 and 2000°K, their results fit the expression

$$-d[O]/dt[O][CH]_4 = 8.0 \times 10^{10} \exp(-9050/RT)\ M^{-1}\ \text{sec}^{-1} \quad \text{(III)}$$

Westenberg and deHaas[15] measured the ratio of oxygen atom to CH_4 consumption and found a ratio of 3.8 ± 0.4. On this basis the rate constant for reaction 2 was assumed to be given by the right-hand side of expression III divided by 3.8. However the stoichiometry was not measured under the same conditions as the rate experiments. Herron[12] has pointed out that the stoichiometric factor should be higher. Even if the stoichiometric factor is correct, the conclusion that the rate constant is the rate divided by the stoichiometric factor will only be valid if CH_4 is removed exclusively by oxygen atoms and not by other species. In fact, this is not the case, and the complete mechanism is

$$O + CH_4 \longrightarrow HO + CH_3 \quad (2)$$

$$HO + CH_4 \longrightarrow H_2O + CH_3 \quad (4)$$

$$H + CH_4 \longrightarrow H_2 + CH_3 \quad (7)$$

$$HO + O \longrightarrow O_2 + H \quad (9)$$

$$O + CH_2O \longrightarrow HO + HCO \quad (10)$$

$$H + CH_2O \longrightarrow H_2 + HCO \quad (11)$$

$$HO + CH_2O \longrightarrow H_2O + HCO \quad (12)$$

$$CH_3 + O \longrightarrow CH_2O + H \quad (13)$$

$$HCO + O \longrightarrow HO + CO \quad (14)$$

$$HCO + H \longrightarrow H_2 + CO \quad (15)$$

Both O_2 and H atoms were found as products of the reaction, but CH_2O was not. For this reason all the investigators rejected reaction 13, though it since has been shown to be important.[11,16] Since $k_9 \gg k_4$, then under the conditions of the experiments, the rate of reaction 4 is small compared to that for reaction 9 and can be neglected, for simplicity. If reaction 12 is also neglected, and the steady-state assumption is made for HO, CH_3, HCO, and CH_2O, the above mechanism leads to the prediction

$$-d[O]/dt = \{(3 + 2\alpha + 2\beta)k_2[O] + (1 + 2\alpha + 2\beta)k_7[H]\}[CH_4] \quad \text{(IV)}$$

where

$$\alpha \equiv k_{10}[O]/(k_{10}[O] + k_{11}[H]) \quad \text{(V)}$$

$$\beta \equiv k_{14}[O]/(k_{14}[O] + k_{15}[H]) \quad \text{(VI)}$$

The values for k_{14} and k_{15} are not known, but they should be similar. Values for the other pertinent rate constants are listed in Table VIII.

Let us first consider the erroneous assumptions that reaction 7 is unimportant. Reaction 7 can only be unimportant if [H]/[O] is sufficiently small. Under these conditions, reactions 11 and 15 are also unimportant; α and β both become 1; and eq IV reduces to

$$k_{obsd} = -d[O]/dt[O][CH_4] = 7k_2 \quad \text{(VII)}$$

Thus, even for these assumptions, $k_2 = k_{obsd}/7$ and not $k_{obsd}/3.8$.

Actually, reaction 7 cannot be negligible as hydrogen atoms are seen as a product of the reaction. To have made meaningful measurements, most of the oxygen atoms must have been consumed and [H] ~ [O]; k_2 would be even smaller than deduced from eq VII.

The above conclusions are consistent with the assumption that reaction 12 is less important than reactions 10 plus 11 at 548°K if $[CH_4] \leq 300\ \mu$ pressure, which was generally the case. Furthermore, the steady-state value for $[CH_2O]$ becomes less than 10^{-2}. $[CH_4]$, which is below the detection limit of the analytical schemes and explains why CH_2O was not found as a product.

From an extrapolation of our previous work,[1] the high-pressure limiting value of k_1 is computed to be

(15) A. A. Westenberg and N. deHaas, *J. Chem. Phys.*, **46**, 490 (1967).

(16) H. Niki, E. E. Daby, and B. Weinstock, *ibid.*, **48**, 5279 (1968).

$1.05 \times 10^6\ M^{-1}\ \text{sec}^{-1}$. Thus k_2 should be about $5 \times 10^5\ M^{-1}\ \text{sec}^{-1}$ at 548°K, since $k_1/k_2 = 2.0$.

Determination of k_3/k_4. The mechanism consisting of steps 1–8 leads to the prediction

$$\left(\frac{\Phi\{CO_2\}}{\Phi\{C_2H_6\}} - \frac{k_1[CO]}{k_2[CH_4]}\right)^{-1} = \frac{k_7[CH_4]}{k_7[CH_4] + k_8[N_2O]} + \frac{k_4[CH_4]}{k_3[CO]} \quad \text{(VIII)}$$

For the data in Table VII, the left-hand side of eq VIII is always much greater than unity, whereas the first term on the right-hand side of the equation necessarily must be less than 1 and can be neglected. A plot of the left-hand side of eq VIII *vs.* $[CH_4]/[CO]$ is shown in Figure 4. The data are badly scattered owing to the fact that the ordinate is a small difference of two similar numbers. Nevertheless, the log–log plot is fitted by the best line of slope 1 and yields an approximate value for $k_4/k_3 = 1.0$, with an uncertainty of about a factor of 2.

The value of k_3 can be obtained from the expression $k_3 = 4.2 \times 10^8 \exp(-1080/RT)\ M^{-1}\ \text{sec}^{-1}$ given by Baulch, *et al.*,[2] to be $1.56 \times 10^8\ M^{-1}\ \text{sec}^{-1}$ at 548°K. Using the value[17] of 2.9×10^8 for k_4 at 548°K gives $k_4/k_3 = 1.86$. Within the experimental uncertainty our results give the same value. However, k_4/k_3 was measured directly by Hoare[18] at 400–650°. An extrapolation of his data gives $k_4/k_3 = 0.25$ at 548°K, considerably lower than our value.

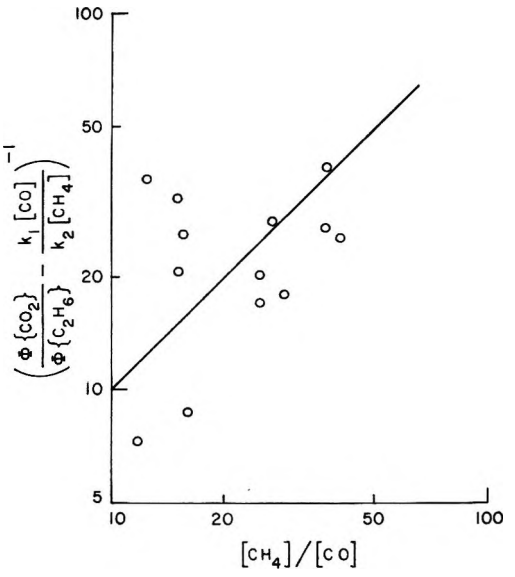

Figure 4. Log–log plot of $(\Phi\{CO_2\}/\Phi\{C_2H_6\} - k_1[CO]/k_2[CH_4])^{-1}$ *vs.* $[CH_4]/[CO]$ in the mercury-photosensitized decomposition of N_2O at 548°K in the presence of CH_4 and low pressures of CO.

Acknowledgment. This work was supported by the National Science Foundation under Grants GA-12385 and GP-10829, for which we are grateful.

(17) W. E. Wilson and A. A. Westenberg, 11th Symposium (International) on Combustion, 1967 p 1143.

(18) D. E. Hoare, *Proc. Roy. Soc., Ser. A*, **291**, 73 (1966).

The Photochemistry of the Fluorotoluenes. I. Quantum Yields of Fluorescence and Intersystem Crossing in 1-Fluoro-2-, 1-Fluoro-3-, and 1-Fluoro-4-methylbenzenes

by Khalid Al-Ani and David Phillips*

Department of Chemistry, The University, Southampton, SO9 5NH, United Kingdom *(Received March 19, 1971)*

Publication costs borne completely by The Journal of Physical Chemistry

The photochemistry of the fluorotoluenes has been studied in the gas phase at 2653, 2537, and 2482 Å at 25°. Fluorescence yields at 2653 Å were found to be about 0.22 for the 1,2 and 1,3 isomers and 0.35 for the 1,4 isomer. Self-quenching was shown to be absent in all three compounds at this wavelength. Quantum yields of triplet-state formation were measured by two methods and found at long wavelengths to be 0.66, 0.75, and 0.62 for the 1,2, 1,3, and 1,4 isomers, respectively, by the olefin isomerization technique, and 0.53, 0.73, and 0.73 by the biacetyl phosphorescence technique. Fluorescence and triplet-state yields were found to decrease with increasing photon energy.

Introduction

The work reported here is part of a study into the effect of simple substitution upon the basic photochemistry of benzene in the gas phase. Extensive previous work upon the fluorine-substituted benzenes[1-12] has been reported and recently work has been completed upon some trifluoromethyl-substituted benzenes.[13] Toluene has been studied in detail,[14,15] but the effect of two substituents of different types upon fluorescence yields and triplet state yields in benzene has not been investigated, apart from a brief report on 2-fluorotoluene.[16] It was therefore decided to investigate the photochemistry of 2-, 3-, and 4-fluorotoluenes in detail in the gas phase to elucidate the effect of substitution by two different species. Part II of this work will report on the quenching of the excited states of the compounds by added molecules.

Experimental Section

The apparatus and techniques used in this study have been described adequately in a previous report.[8]

Materials. 1-Methyl-2-fluorobenzene, 1-methyl-3-fluorobenzene, and 1-methyl-4-fluorobenzene were obtained from Koch Light Laboratories Ltd. Analysis by gas–liquid partition chromatography showed them to contain about 0.3% impurity, and they were used without attempts at further purification.

cis-But-2-ene was obtained from Cambrian Chemicals Ltd., as a research grade chemical. It contained 0.07% *trans*-but-2-ene as an impurity.

trans-But-2-ene was obtained from Phillips Petroleum Co., as a research grade chemical and contained 0.05% *cis*-but-2-ene as an impurity.

Benzene was Chromatoquality obtained from Matheson Coleman and Bell and contained no detectable impurities.

Biacetyl was obtained from British Drug Houses Ltd. It contained no impurities detectable by gas–liquid partition chromatography on a 20% Carbowax 20M column and was stored in a blackened bulb at room temperature.

Results

The absorption spectra of all three fluorotoluene isomers are similar to that of benzene in the vapor phase in that prominent vibrational progressions appeared even under moderate resolution (see Figure 1). Mean radiative lifetimes calculated from integrated absorption spectra[17] of the three compounds indicate that the

(1) I. Unger, *J. Phys. Chem.*, **69**, 4284 (1965).

(2) D. Phillips, *ibid.*, **71**, 1839 (1967).

(3) M. E. MacBeath, G. P. Semeluk, and I. Unger, *ibid.*, **73**, 995 (1969).

(4) F. W. Ayer, F. Griess, G. P. Semeluk, and I. Unger, *Ber. Bunsenges. Phys. Chem.*, **72**, 282 (1968).

(5) J. L. Durham, G. P. Semeluk, and I. Unger, *Can. J. Chem.*, **46**, 3177 (1968).

(6) G. P. Semeluk, R. D. S. Stevens, and I. Unger, *ibid.*, **47**, 597 (1969).

(7) I. Unger and G. Scholz, *ibid.*, **48**, 2324 (1970).

(8) K. Al-Ani and D. Phillips, *J. Phys. Chem.*, **74**, 4046 (1970).

(9) D. Phillips, *J. Chem. Phys.*, **46**, 4679 (1967).

(10) E. Ratajczak, *Rocz. Chem.*, **44**, 447 (1970).

(11) I. Haller, *J. Chem. Phys.*, **47**, 1117 (1967).

(12) A. Bergomi and F. Gozzo, *Chim. Ind. (Milan)*, **50**, 745 (1968).

(13) D. Gray and D. Phillips, *J. Chem. Phys.*, in press.

(14) C. S. Burton and W. A. Noyes, Jr., *ibid.*, **49**, 1705 (1968).

(15) S. L. Lem, G. P. Semeluk, and I. Unger, *Can. J. Chem.*, **47**, 4711 (1969).

(16) R. B. Cundall, A. S. Davies, and K. Dunnicliff, "The Triplet State," Beirut Symposium, A. B. Zahlan, Ed., 1967, p 183.

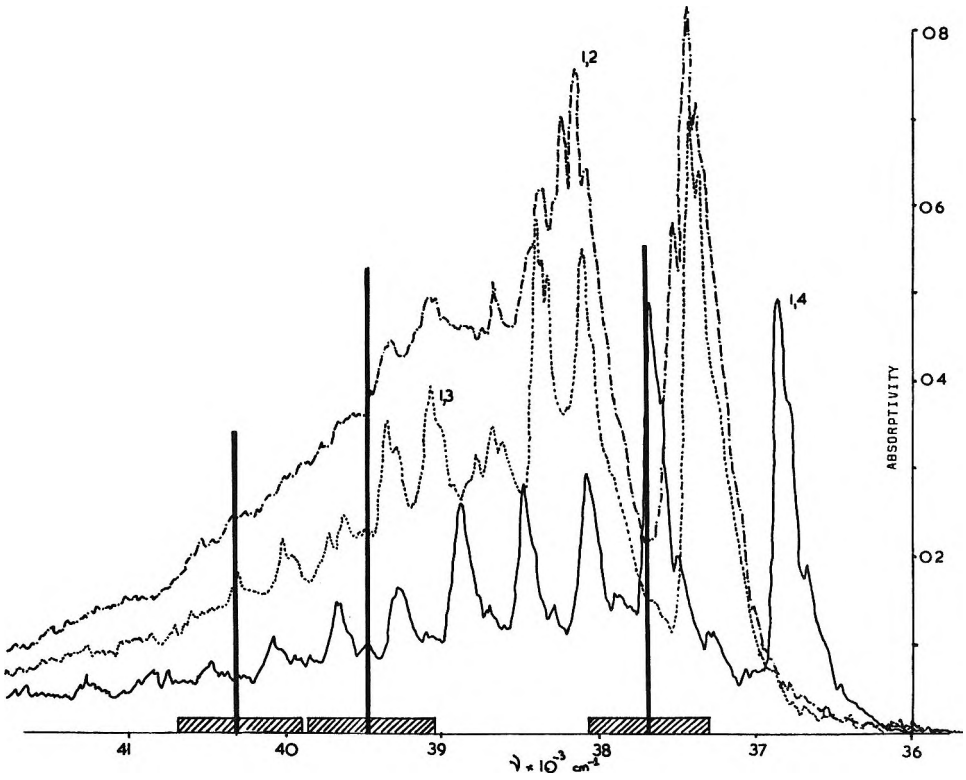

Figure 1. Absorption spectra of fluorotoluenes in vapor phase: -·-·-·, 1-fluoro-2-methylbenzene, 2 Torr; ------, 1-fluoro-3-methyl-benzene, 2 Torr; ——, 1-fluoro-4-methylbenzene, 1 Torr. Solid lines represent mercury lines for excitation at 2653, 2537, and 2482 Å. Cross-hatched blocks give bandpass of monochromator at each wavelength corresponding to slit width used.

1,2 and 1,3 isomers have lifetimes of 1.1×10^{-7} and 1.3×10^{-7} sec, respectively, whereas the 1,4 isomer has the shorter lifetime of 0.8×10^{-7} sec. Comparison of these values with those of the fluorobenzenes shows that the 1,2 and 1,3 isomers have natural lifetimes very similar to those of 1,2- and 1,3-difluorobenzenes and other fluorobenzenes with C_{2v} symmetry. The mean radiative lifetime of the 1,4-fluorotoluene, however, is longer than that of 1,4-difluorobenzene (5×10^{-8} sec), indicating that the methyl and fluoro substituents behave somewhat differently, as might be expected. The 0–0 transition in the 1,2 and 1,3 isomers is estimated to be at 270 nm; that of the 1,4 isomer, at 275 nm.

Fluorescence. The difficulties experienced in obtaining accurate measurements of fluorescence quantum yields in compounds with highly structured absorption spectra have been pointed out.[18] Unless intense narrow-band light sources are employed, use of T-shaped fluorescence cells as in this study can lead to apparent self-quenching of the fluorescence which is caused by the geometrical arrangement of the viewing system. Great care must therefore be taken in calculation of fluorescence yields under such circumstances. Uncorrected values of the fluorescence quantum yield of the three at 2653 ± 25, 2537 ± 25, and 2482 ± 25 Å are shown in Figures 2–4. The bandpasses of the monochromator at the wavelengths used in this study are shown in Figure 1. Because the exciting radiation comes from mercury emission lines, the majority of the intensity of light passing through the monochromator will be contained within a spectral bandpass at each wavelength much smaller than that shown in Figure 1.

It can be seen that for 1-fluoro-2-methylbenzene at 2482 and 2537 Å and for the 1-fluoro-3-methyl and 1-fluoro-4-methyl isomers at 2482 Å, absorption occurs in a region where strong vibrational prominences are absent. The crude quantum yields of fluorescence shown in Figures 2–4 are thus easily corrected for geometrical effects using the method described earlier,[18] and these results are also shown in Figures 2–4. However, for all isomers at the remaining wavelengths, it can be seen that the exciting wavelength spans two or more strong vibrational bands in the spectrum of the aromatic. To correct for geometrical effects, we have used the extinction coefficients obtained from the absorption spectra in Figure 1 at the exact wavelength of the exciting mercury line and a "viewing length"[18] of 4 cm. The results of applying these corrections to the compounds above (and to the benzene standard) are shown in Figures 2–4. It proves very difficult to apply an adequate correction to the results at 2653 Å for the 1-fluoro-4-methylbenzene at higher pressures be-

(17) M. Ballester, J. Palau, and J. Riera, *J. Quant. Spectrosc. Radiat. Transfer*, **4**, 819 (1964).

(18) D. Gray, K. Al-Ani, and D. Phillips, *J. Chem. Soc. A*, 905 (1971).

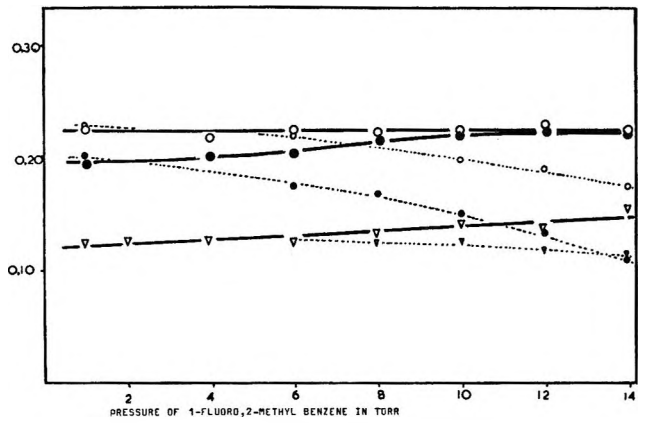

Figure 2. Fluorescence yield of 1-fluoro-2-methylbenzene at various wavelengths as function of pressure: O, 2653 Å; ●, 2537 Å; ▽, 2482 Å; ——, results corrected for effect of viewing geometry; ----, uncorrected results.

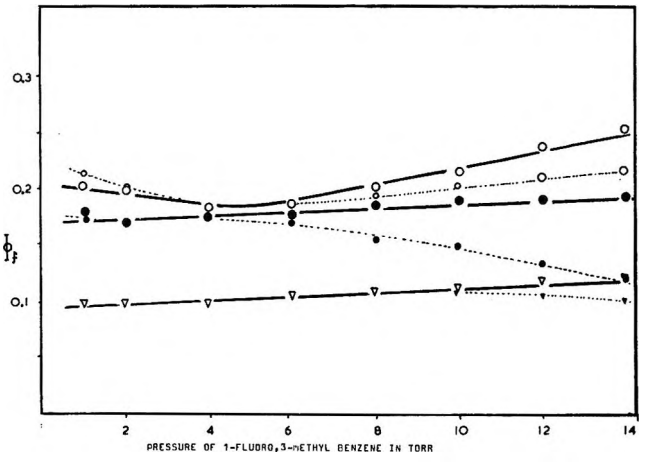

Figure 3. Fluorescence yield of 1-fluoro-3-methylbenzene as function of pressure: O, 2653 Å; ●, 2537 Å; ▽, 2482 Å; ——, results corrected for geometry of system; ----, uncorrected results.

cause of the very high extinction coefficient at this wavelength. However, other techniques indicate that self-quenching is absent in this compound under these circumstances.

Triplet State. The usual techniques of the sensitization of phosphorescence of biacetyl[19] and of the cis–trans isomerization of but-2-ene[20] were used to calculate triplet-state yields for the three isomers studied. Both techniques require some interpretation of the data and will be dealt with in turn.

But-2-ene Experiments. At 2650 Å, addition of large pressures of *cis*- or *trans*-but-2-ene to each of the isomers did not cause any significant change in the fluorescence yield of each compound, and it may thus be concluded that quenching of the excited singlet state of the fluorotoluenes by but-2-ene does not occur. Results of the biacetyl sensitization experiments indicated that the lifetimes of the triplet state of the fluorotoluenes were approximately the same and of the

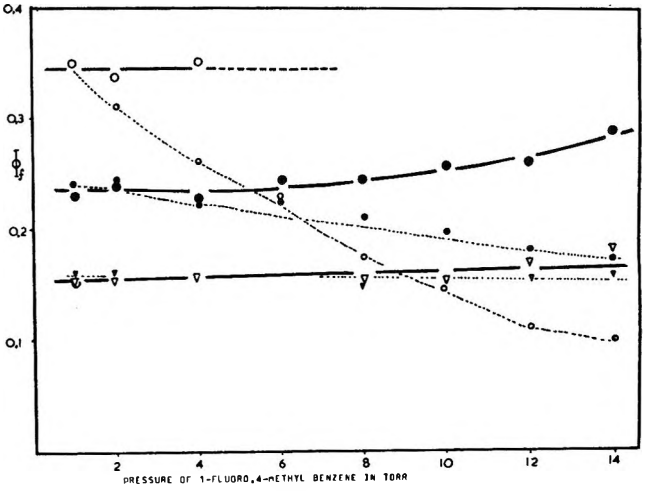

Figure 4. Fluorescence quantum yield of 1-fluoro-4-methylbenzene as a function of pressure: O, 2653 Å; ●, 2537 Å; ▽, 2482 Å; ——, results corrected for viewing geometry; ----, uncorrected results.

same order of magnitude as that of fluorobenzene. Consequently to obtain triplet-state yields, 70 Torr *cis*-but-2-ene was used completely to quench the aromatic triplet. Cundall has shown this to be a sufficient pressure for one of the isomers.[16] To calculate triplet-state yields from yields of sensitized cis–trans isomerization of the but-2-ene, it is necessary to carry out actinometry or calibration with a standard (in this case benzene, for which Φ_T was taken as 0.70[21]) and also to know the so-called "branching ratio" for the but-2-ene when sensitized by each aromatic molecule. The branching ratio is the relative rate of relaxation of excited triplet but-2-ene to the ground-state cis and trans isomers. We have established that for the three aromatic molecules studied here, "branching ratios" are all within experimental error of unity,[22] as for benzene.[23] Calculation of triplet-state yields for the 1,2, 1,3, and 1,4 isomers at this wavelength is thus simple and the results are shown in Table I.

At the shortest wavelengths studied, addition of *cis*- or *trans*-but-2-ene was found to enhance the fluorescence yield of the aromatic molecules, presumably *via* vibrational relaxation. The "branching ratio" has not been measured for sensitization at the shorter wavelengths, and the figure of unity obtained at 2650 Å was employed. The values of isomerization quantum yields under these conditions at 70 Torr *cis*-but-2-ene pressure are shown in Table I, together with values corrected for the effect

(19) H. Ishikawa and W. A. Noyes, Jr., *J. Amer. Chem. Soc.*, **84**, 1502 (1962).

(20) R. B. Cundall and T. F. Palmer, *Trans. Faraday Soc.*, **56**, 1211 (1960).

(21) W. A. Noyes, Jr., W. A. Mulac, and D. A. Harter, *J. Chem. Phys.*, **44**, 2100 (1966).

(22) D. Gray, K. Al-Ani, and D. Phillips, *J. Chem. Soc. A*, in press.

(23) E. K. C. Lee, H. O. Denschlag, and G. A. Haninger, Jr., *J. Chem. Phys.*, **48**, 4547 (1968).

Table I: Quantum Yields of Sensitized Cis–Trans Isomerization of But-2-ene; $\Phi_{c\rightarrow t}$, Aromatic Pressure 4 Torr, *cis*-But-2-ene 70 Torr, 25°

Sensitizer	Wavelength, Å	$\Phi_{c\rightarrow t}$	Φ_F°/Φ_F[a]	Φ_T°
1-Fluoro-2-methylbenzene	2653	0.33	1.00	0.66
	2537	0.31	1.00	0.62
	2482	0.26	0.86	0.45
1-Fluoro-3-methylbenzene	2653	0.375	1.00	0.75
	2537	0.36	1.00	0.72
	2482	0.26	0.78	0.40
1-Fluoro-4-methylbenzene	2653	0.31	1.00	0.62
	2537	0.29	1.00	0.58
	2482	0.29	0.71	0.42

[a] Φ_F°/Φ_F is the ratio of quantum yields of fluorescence of the aromatic at zero pressure *cis*-but-2-ene and 70 Torr, respectively. The triplet-state yield of the aromatic in the absence of olefin is given by $2\Phi_{c\rightarrow t} \times \Phi_F^\circ/\Phi_F$.

of *cis*-but-2-ene pressure upon the singlet state of the aromatic. The effect of variation in pressure of aromatic on the quantum yield of cis–trans isomerization of the but-2-ene is shown in Figure 5.

Biacetyl Sensitization. Uncorrected data using this method are shown in Figures 6–8. Two corrections must be applied to the data to obtain meaningful quantum yields for triplet-state formation. The first arises because of the fact that an emission measurement is made, and thus the geometry of the viewing system is again important assuming that no diffusion of excited biacetyl molecules away from the physical region of the fluorescence cell in which absorption by the aromatic occurred before the biacetyl emits. The second and more important correction arises because the singlet states of the aromatics are quenched significantly by biacetyl.

It may be seen from Figures 6–8 that comparatively high pressures of biacetyl are necessary to obtain a maximum in the yield of sensitized emission, indicating a short lifetime for the triplet states of the fluorotoluenes. At the pressures of biacetyl used to obtain the maximum emission, significant quenching of the singlet state of the aromatic occurs and, moreover, the biacetyl itself absorbs exciting radiation. The approach of Ishikawa and Noyes has been used to correct for the latter,[19] but it should be noted that for the highest pressures of biacetyl used, the correction will not be valid and its use leads to artificially high values for the sensitized emission. We have tabulated (Table II) values of the triplet-state yield for each compound at each wavelength obtained by division of the value of the maximum sensitized emission yield corrected for singlet quenching and geometrical effects by the value of the phosphorescence yield of biacetyl (0.15). Comparison with Table I shows that the two methods of measurement of

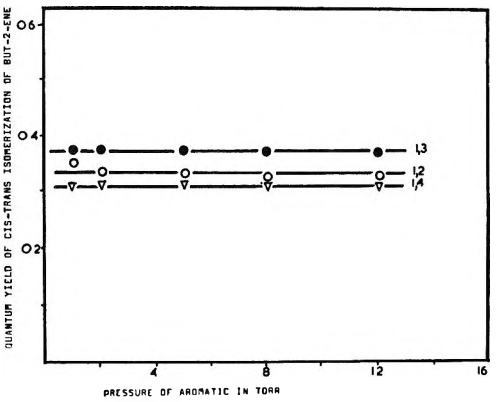

Figure 5. Quantum yields of cis–trans isomerization of but-2-ene by fluorotoluenes at 2653 Å as function of aromatic pressure; pressure of olefin 70 Torr, 25°: ○, 1-fluoro-2-methylbenzene; ●, 1-fluoro-3-methylbenzene; ▽, 1-fluoro-4-methylbenzene.

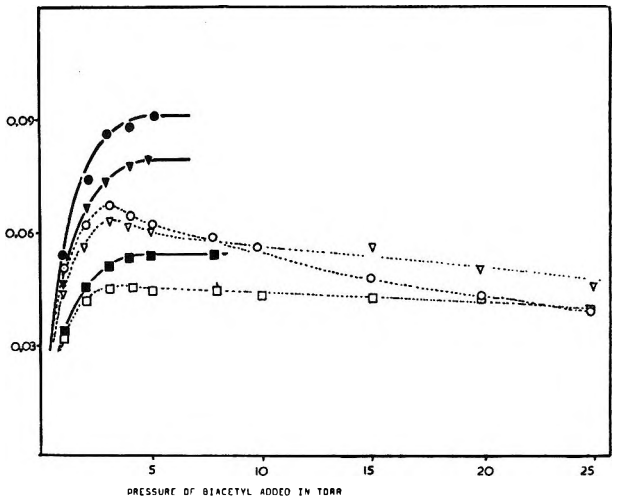

Figure 6. Quantum yield of phosphorescence of biacetyl sensitized by 1-fluoro-2-methylbenzene excited at various wavelengths as function of pressure of added biacetyl: —○---○---, 2653 Å, uncorrected for singlet quenching; —●—●—, 2653 Å, corrected results; —▽---▽---, 2537 Å, uncorrected for singlet quenching; —▼—▼—, 2537 Å, corrected results; ---□---□---, 2482, Å, uncorrected for singlet quenching; —■— ■—, 2482 Å, corrected.

triplet-state yields give comparable results. It should be noted that in the biacetyl experiments the spectral distribution of the sensitized emission has not been determined. However, this emission can be completely quenched by addition of but-2-ene, which does not affect biacetyl excited directly and has only a slight effect upon the singlet excited states of the aromatics. It may therefore be concluded that the sensitized emission observed can only be phosphorescence from biacetyl.

Discussion

The radiative lifetimes of the singlet states of the fluorotoluenes are all in the region of a factor of 4 shorter than that of benzene, and it is well established

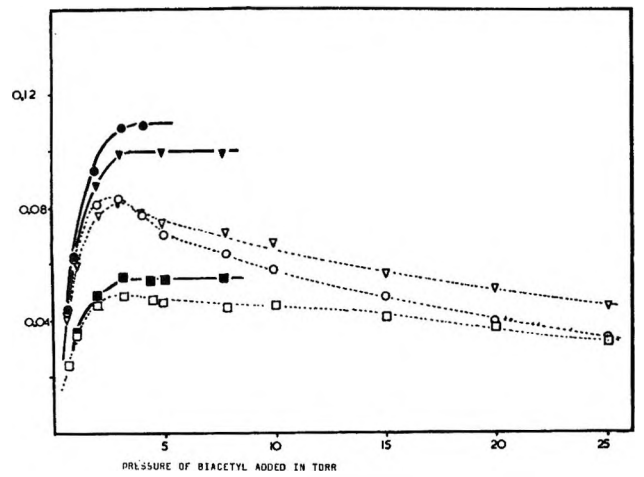

Figure 7. Quantum yield of phosphorescence of biacetyl sensitized by 1-fluoro-3-methylbenzene at various wavelengths as function of pressure of added biacetyl: ---O---O—, 2653 Å, uncorrected for singlet quenching; —●—●—, 2653 Å, corrected results; ---▽---▽—, 2537 Å, uncorrected for singlet quenching; —▼—▼—, 2537 Å, corrected results; —□---□—, 2482 Å, uncorrected for singlet quenching; —■—■—, 2472 Å, corrected.

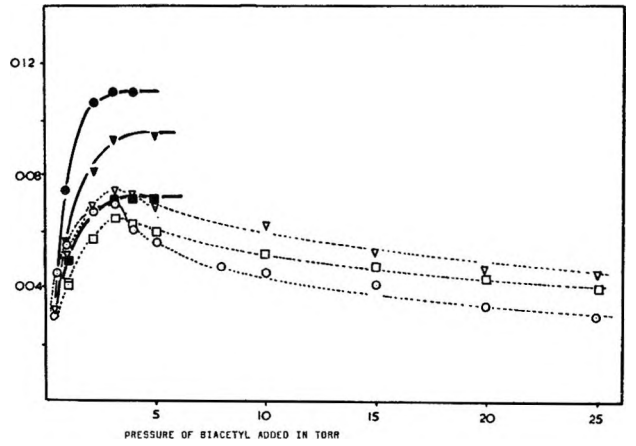

Figure 8. Quantum yield of phosphorescence of biacetyl sensitized by 1-fluoro-4-methylbenzene excited at various wavelengths as function of pressure of added biacetyl: ---O---O—, 2653 Å, uncorrected for singlet quenching; —●—●—, 2653 Å, corrected results; —▽—▽—, 2537 Å, uncorrected for singlet quenching; —▼—▼—, 2537 Å, corrected results; —□---□---, 2482 Å, uncorrected for singlet quenching; —■—■—, 2482 Å, corrected.

that a pressure of 20 Torr is required completely to vibrationally relax the excited singlet state of the benzene molecule. It seems clear, therefore, that at the pressures used in this study, the fluorescence observed from the fluorotoluenes must be resonance fluorescence occurring from higher vibrational levels of the excited singlet state. This has been shown to be the case in a spectroscopic study on fluorobenzene[24] at similar pressures. We may use the following simple scheme therefore to explain the results.

$$A + h\nu \longrightarrow {}^1A_n \quad (1)$$

$$^1A_n \longrightarrow A + h\nu_r \quad (2)$$

$$^1A_n \longrightarrow {}^3A_m \quad (3)$$

$$^1A_n \longrightarrow \text{product} \quad (4)$$

$$^1A_n + M \longrightarrow {}^1A_0 + M \quad (5)$$

$$^1A_0 \longrightarrow A + h\nu_n \quad (6)$$

$$^1A_0 \longrightarrow {}^3A_n \quad (7)$$

$$^1A_0 \longrightarrow A \quad (8)$$

where A is the aromatic molecule, superscripts refer to multiplicity, subscripts to excess vibrational energy content, and $h\nu_r$ and $h\nu_n$ to resonance and normal fluorescence, respectively. The behavior of each compound at the three wavelengths studied may be discussed with reference to this scheme.

Table II: Sensitized Phosphorescence Yields of Biacetyl at 25°; Pressure of Aromatic 4 Torr

Sensitizer	Wavelength, Å	$\Phi_{s,max}$	$\Phi_{s,max}$ (cor)	Φ_T[a]
1-Fluoro-2-methylbenzene	2653	0.066	0.086	0.57
	2537	0.063	0.074	0.49
	2482	0.046	0.058	0.39
1-Fluoro-3-methylbenzene	2653	0.083	0.109	0.73
	2537	0.083	0.100	0.67
	2482	0.050	0.056	0.37
1-Fluoro-4-methylbenzene	2653	0.070	0.11	0.73
	2537	0.075	0.092	0.61
	2482	0.065	0.074	0.49

[a] $\Phi_T = \Phi_{max}(cor)/0.15$.

2653 Å. For 1-fluoro-2-methylbenzene, it is clear that although excitation at 2653 Å produces an excited state with 0.08-eV excess vibrational energy there is little significant variation in fluorescence quantum yield with pressure of aromatic or with pressure of added chemically inert gas. We may therefore assume that for this compound the state produced at 2653 Å behaves as if it were equilibrated, and therefore the quantum yield of fluorescence ($\Phi_{F_{2653}}$) will be given by

$$\Phi_{F_{2653}} = k_6/(k_6 + k_7 + k_8) \quad (I)$$

The value of this is shown in Table III.

At 2653 Å, 1 fluoro-3-methylbenzene is produced in an excited state with 0.08-eV excess vibrational energy. Although the results in Figure 3 indicate some variation of quantum yield of fluorescence with pressure of aromatic, addition of high pressures of chemically inert gases does not significantly alter the value of the quantum yield of emission, and eq I has been applied to this

(24) K. Nakamura, *J. Chem. Phys.*, **53**, 998 (1970).

Table III: Summary of Data on Fluorotoluenes[a]

Sensitizer	Wavelength, Å	Φ_F	Φ_T (butene)	Φ_T (biacetyl)	$\Delta\Phi = 1 - (\Phi_F + \Phi_T)$
1-Fluoro-2-methylbenzene	2653	0.22	0.66	0.57	0.12
	2537	0.19	0.615	0.49	0.20
	2482	0.12	0.45	0.39	0.43
1-Fluoro-3-methylbenzene	2653	~0.21	0.75	0.73	0.04
	2537	0.17	0.72	0.67	0.11
	2482	0.09	0.40	0.37	0.51
1-Fluoro-4-methylbenzene	2653	0.35	0.62	0.73	0.03
	2537	0.23	0.58	0.61	0.19
	2482	0.15	0.42	0.49	0.43

[a] For $\Delta\Phi$, Φ_T obtained by the butene method has been used.

compound also, as well as to the 1,4 isomer for a similar reason.

It will be noted that a self-quenching step (9) has been omitted from the scheme above, despite indications from other studies that this step may be of importance in some other simply substituted benzenes. Inclusion of step 9 in the sequence above would lead to

$$^1A_0 + A \longrightarrow A + A \qquad (9)$$

a pressure dependence upon the quantum yield of fluorescence which is not observed here. However, because of the corrections necessary to obtain quantum yields of fluorescence, an independent check has been carried out which confirms that (9) is unimportant. In the presence of *cis*-but-2-ene at 2653 Å, the following additional steps are necessary.

$$^3A_n + M \longrightarrow {}^3A_0 + M \qquad (10)$$

$$^3A_0 \longrightarrow A \qquad (11)$$

$$^3A_0 + cis\text{-Bu} \longrightarrow {}^3cis\text{-Bu} + A \qquad (12)$$

$$^3cis\text{-Bu} \longrightarrow cis\text{-Bu} \qquad (13)$$

$$\longrightarrow trans\text{-Bu} \qquad (14)$$

The quantum yield of sensitized cis → trans isomerization of but-2-ene is then given by

$$\Phi_{c\to t} = \frac{k_7}{k_6 + k_7 + k_8 + k_9[A]} \frac{k_{12}[cis\text{-Bu}]}{k_{11} + k_{12}[cis\text{-Bu}]} \times \frac{k_{14}}{k_{13} + k_{14}} \qquad (II)$$

Thus at constant pressure of *cis*-but-2-ene, variation in pressure of aromatic should cause a change in the cis–trans isomerization quantum yield if (9) is of importance. It can be clearly seen from Figure 5 that no such variation occurs in any of the isomers studied here, and thus (9) is justifiably neglected. As a further check, the fluorescence lifetimes of these compounds as a function of pressure are currently being investigated.

The triplet-state yields of the isomers at 2653 Å are simply obtained from expression II, since a pressure of *cis*-but-2-ene was used such that $k_{12}[cis\text{-Bu}] > k_{11}$, and $k_{14}/(k_{13} + k_{14})$ has been measured as 0.50.[22]

Thus

$$\Phi_{2653} = 2\Phi_{c\to t\ 2653}$$

The addition of biacetyl requires the additional steps

$$^1A_0 + Bi \longrightarrow A + Bi^{II} \qquad (15)$$

$$^3A_0 + Bi \longrightarrow A + {}^3Bi_n \qquad (16)$$

$$^3Bi_n + M \longrightarrow {}^3Bi_0 + M \qquad (17)$$

$$^3Bi_0 \longrightarrow Bi + h\nu_p \qquad (18)$$

$$^3Bi_0 \longrightarrow Bi \qquad (19)$$

The quantum yield of sensitized phosphorescence from biacetyl, Φ_s, is given by

$$\Phi_{s_{2653}} = \frac{k_7}{k_6 + k_7 + k_8 + k_{15}[Bi]} \frac{k_{16}[Bi]}{k_{11} + k_{16}[Bi]} \times \frac{k_{18}}{k_{18} + k_{19}} \qquad (III)$$

Results obtained from the quenching of the fluorescence of the aromatic molecules by biacetyl give values of

$$\frac{\Phi_{F_{2653}}^{\circ}}{\Phi_{F_{2653}}} = \frac{k_6 + k_7 + k_8 + k_{15}[Bi]}{k_6 + k_7 + k_8}$$

where $\Phi_{F_{2653}}^{\circ}$ is the quantum yield of fluorescence in the absence of biacetyl, and Φ_F, that at a given pressure of biacetyl.

Thus the triplet-state yield of the molecule is given by

$$\Phi_{T_{2653}} = \frac{k_7}{k_6 + k_7 + k_8} = \Phi_{s_{2653}} \frac{\Phi_{F_{2653}}^{\circ}}{\Phi_{F_{2653}}} \frac{1}{0.15}$$

$k_{16}[BiA] \gg k_{11}$ and $k_{18}/(k_{18} + k_{19}) = 0.15$.

2537 Å. At this wavelength, excited singlet states of the 1,2, 1,3, and 1,4 isomers are produced with 0.29, 0.29, and 0.37 eV of excess energy, respectively. The total quantum yield of fluorescence will be given by

$$\Phi_{F_{2537}} = \frac{k_2}{k_2 + k_3 + k_4 + k_5[M]} + \frac{k_6}{k_6 + k_7 + k_8} \frac{k_5[M]}{k_2 + k_3 + k_4 + k_5[M]} \qquad (IV)$$

The variation of this expression with pressure [M] is complex but tends to the limits

$$\Phi_{F_{2537}}^{\circ} = \frac{k_2}{k_2 + k_3 + k_4} \qquad (V)$$

$$\Phi_{F_{2537}}^{\infty} = \frac{k_6}{k_6 + k_7 + k_8} = \Phi_{F_{2482}} \qquad \text{(VI)}$$

Thus at high pressures the fluorescence yields at 2540 Å should tend toward those at the longer wavelengths. Inspection of Figures 2–4 shows this to be the case. At low pressures, the fluorescence yields should tend to a constant value. Zero-pressure extrapolations must be done with caution depending on the pressure region in which measurements are taken. In the present case the mean radiative lifetimes of the excited aromatic molecules are such that collision should not occur at pressures of around 1 Torr and below. Since the values of $\Phi_{F_{2537}}$ at 1 Torr pressure indicate significant nonradiative decay for each molecule, the actual lifetimes of the excited singlet molecules at this pressure will be much shorter. If we assume that the nonradiative decay process (or processes) are first order, then the fluorescence yields at low pressures shown in Figures 2–4 may be safely extrapolated to give a value of $\Phi_{F_{2537}}^{\circ}$. These are shown in Table III. It is of interest to note that the values decrease as the wavelength of excitation decreases, as has been found for many compounds whereas for benzene[25] (and for α,α,α-trifluoromethylbenzene[26]) values of the fluorescence yield are higher from some upper vibrational levels than the equilibrated level, indicating a higher radiative probability (or lower nonradiative probability) from these upper vibrational states.

The estimation of triplet-state yields is made difficult by the fact that in the butene isomerization method the olefin which must be added undoubtedly contributes toward vibrational relaxation *via* reaction 5, while in the case of the biacetyl sensitization the excited singlet state of the aromatic will be quenched by the added biacetyl. Nevertheless, a consideration of the effects of addition of the two gases allows the estimation of triplet yields under the conditions specified shown in Tables I and II.

2482 Å. Similar considerations to those at 2537 Å apply, and values of fluorescence and triplet yields are summarized in Table I and II.

Some other features of the photochemistry of these fluorotoluenes in addition to those already discussed are worthy of mention. Firstly, the compounds show close analogy to the corresponding difluorobenzenes in that for the 1,2 and 1,3 isomers the radiative lifetimes are all similar, as are fluorescence and triplet-state yields, whereas the 1,4 isomers have shorter radiative lifetimes and higher fluorescence yields.

It is interesting to note that the triplet energy of the 1,4-fluorotoluene must lie higher than that of *cis*-but-2-ene in that the aromatic can sensitize the isomerization of the olefin, and the "branching ratio" is normal (unity). The 1,4-difluorobenzene has been reported to lie lower than that of *cis*-but-2-ene, and recently it has been found that substitution with trifluoromethyl groups in the 1,4 positions causes anomalies in the "branching ratio" which may be indicative of a low-lying aromatic triplet energy.[22,26] Phosphorescence spectra in EPA glasses at 77°K indicate that the triplet energies of the fluorotoluences are approximately at 3.43, 3.58, and 3.49 eV for the 1,2, 1,3, and 1,4 isomers, respectively.[27]

All compounds exhibit the by now familiar behavior in that as excitation wavelength is shortened, a process other than fluorescence or intersystem crossing becomes important. As in other aromatics, this process may be valence isomerization, and since this can easily be checked with disubstituted benzenes, work is in progress to determine the extent of such reactions.

Acknowledgments. This work has been supported in part by NATO Office of Scientific Research, Europe. We thank the Science Research Council, United Kingdom, for equipment grants and K. A-A. wishes to thank the British Council for payment of fees during the tenure of a postgraduate studentship.

(25) E. M. Anderson and G. B. Kistiakowsky, *J. Chem. Phys.*, **51**, 182 (1969).

(26) D. Gray, Ph.D. Thesis, University of Southampton, Sept 1970.

(27) M. Tobin and D. Phillips, unpublished results.

Effects of Optical Bleaching on Luminescence Decay and Trapped Electron Concentrations in γ-Irradiated 3-Methylpentane at 77°K

by K. Funabashi,* C. Hebert, and J. L. Magee

Department of Chemistry and the Radiation Laboratory,[1] University of Notre Dame, Notre Dame, Indiana 46556
(Received March 31, 1971)

Publication costs assisted by the U. S. Atomic Energy Commission

The luminescence decay of γ-irradiated 3-methylpentane (3MP) has been studied in the dark and with ir (1600 nm) and uv (265, 325 nm) bleaching for times as long as 8 hr. Bleaching with ir increases the decay rate and bleaching with uv retards it. The emission under all conditions was found to consist of the same two bands: one with a maximum at 380 nm and the other (much smaller) with a maximum at 230 nm. An added hole trap, 2-methylpentene-1 (2MP-1), was found to increase the decay rate with and without bleaching light and, as in pure 3MP, ir increases the decay rate and uv retards it. The decay rates of trapped electron concentrations have been measured in the dark and with ir and uv bleaching. The absorption spectrum has been found to be the same under all conditions and for all times studied. For the dark decay the luminescence intensity is proportional to the rate of decrease in trapped electron concentrations; deviations from this proportionality are observed for both ir and uv bleaching and these are partially explained. It seems that there are two kinds of traps for electrons in γ-irradiated 3MP.

I. Introduction

It has long been known[1,2] that γ irradiation of 3-methylpentane (3MP) at 77°K produces trapped electrons which absorb at long wavelengths (~1600 nm). Samples containing such trapped electrons emit luminescence,[2a] and it has generally been assumed that the cause of this effect is the combination of the trapped electrons with positive ions. The concentration of trapped electrons decreases with time on standing in the dark at 77°K and can be accelerated by infrared light in the absorption band of the electrons.[2b] It has also been realized that the disappearance of the trapped electrons is more complicated than just recombination with ions: a "completely" bleached sample emits a very large flash of light on warming,[3] and this is probably the result of the neutralization of separated charges remaining in the bleached samples. The same bleached samples exhibit electrical conductivity[4] while being warmed, and this must be taken as further proof of the existence of a second kind of trapped electron (deeply trapped) at 77°K which does not absorb at 1600 nm. The expression "trapped electron" usually refers to the species which absorbs at 1600 nm and if the expression is not further qualified will have that meaning here.

Ekstrom, Suenram, and Willard[5] made spectroscopic measurements on γ-irradiated 3MP which had been subsequently bleached with ir light and found absorption in the 250–400-nm region some of which they attributed to deeply trapped electrons. In exploratory work, the authors of this paper found that irradiation with ultraviolet light (~300 nm) increases the concentration of trapped electrons in partially bleached samples of γ-irradiated 3MP. The work reported here was undertaken primarily as a study of the importance of various kinds of trapping of electrons in 3MP at 77°K. Three kinds of bleaching (in the dark, with ir and uv radiation) are compared for both luminescence and trapped electron concentrations, and these experimental results are interpreted in the light of other results from this laboratory and elsewhere.

II. Experimental Section

A. Sample Preparation. Phillips "pure-quality" 3MP was further purified by passage through a 6-ft column of silica gel which had been freshly activated by heating at 400° for 8 hr. The material was then distilled through a spinning-band column with a reflux-to-takeoff ratio of 10:1. (Gas chromatography of the distillate indicated less than 2×10^{-4} *M* impurity, identified as 2-methylpentane.) The purified 3MP was then transferred to a storage container on a vacuum rack. A cold finger built into the vacuum system above the storage container was filled with acetone and repeatedly chilled by a piece of copper tubing inserted in a dewar of liquid nitrogen. During each such chilling the container was pumped as the 3MP refluxed in the

(1) The Radiation Laboratory of the University of Notre Dame is operated under contract with the U. S. Atomic Energy Commission. This is AEC Document No. COO-38-651.

(2) (a) M. Burton, M. Dillon, and R. Rein, *J. Chem. Phys.*, **41**, 2228 (1964); (b) D. W. Skelly and W. H. Hamill, *ibid.*, **44**, 289 (1966).

(3) K. Funabashi, P. J. Herlev, and M. Burton, *ibid.*, **43**, 3939 (1965).

(4) B. Wiseall and J. E. Willard, *ibid.*, **46**, 4387 (1967).

(5) A. Ekstrom, R. Suenram, and J. E. Willard, *J. Phys. Chem.*, **74**, 1888 (1970).

system. This procedure removed most of the dissolved gases before individual samples were prepared. Individual samples were prepared by distilling a large amount (usually about 30 ml) of liquid from the storage flask onto a sodium–potassium (NaK) mirror and allowing the 3MP to stand in the mirror flask overnight. The purpose of this procedure was to remove CO_2 and O_2. On the following day, Suprasil cells made of 1 cm square tubing were attached to the manifold and evacuated. Each was then filled with 6 ml of 3MP and sealed off at low pressure. To prepare solutions, the same procedure was used except that, after the solvent was distilled into the Suprasil cells, the system was brought up to atmospheric pressure with dry nitrogen and the solute was injected into the cell through a rubber septum on a Y branch above the cell. The samples were then degassed by three freeze–pump–thaw cycles and sealed off at low pressure.

The frozen samples maintained at 77°K in a dewar filled with liquid nitrogen were irradiated in a 4-kCi ^{60}Co underwater source for 2 min at a dose rate of 2.18×10^{18} eV g^{-1} min^{-1}. Roughly, this amount of irradiation is adequate to "liberate" about 10^{17} electrons/g.

B. Luminescence Apparatus. Irradiated samples in cells were transferred to a quartz dewar mounted on an optical bench. Light emitted by the sample went through windows in the dewar and was collected by a lens system mounted directly behind a chopper operated at 83 Hz. The light then passed through the entrance slits of a Bausch and Lomb 250-mm monochromator using a Bausch and Lomb 33-53-08-02 grating with 1200 grooves/mm and a blaze wavelength of 200 nm. The grating dispersion was 3.3 nm/mm. This monochromator was also equipped with a remotely controlled scanning motor which produced a scanning rate of 100 nm/min. The beam from the monochromator was focused and reflected by a front surface mirror into the front window of a 9635 QD EMI photomultiplier tube having a pair of magnetic focusing rings preceding the photocathode to reduce the active area to 8.0 mm in diameter. The photomultiplier was operated at an overall gain of 2000 A/lm by supplying the cathode with 1430 V dc from a Hamner Model N-4035 power supply. Current from the photomultiplier anode was fed into the input circuit of a Princeton Applied Research (PAR) Model JB-5 lock-in amplifier. The output from the PAR amplifier was recorded on a Sargent recorder (Model S-72151). The monochromator–photomultiplier system was calibrated by using a IP 28 calibrated RCA photomultiplier. An I-Lite of known intensity and spectral emission was used to determine the absolute sensitivity of the combination at 520 nm, and an efficiency curve was generated by comparing the relative intensities of various lines emitted by a Hanovia low-pressure mercury lamp to the known intensities. Lines from the mercury lamp were also used to calibrate the wavelength scale on the monochromator.

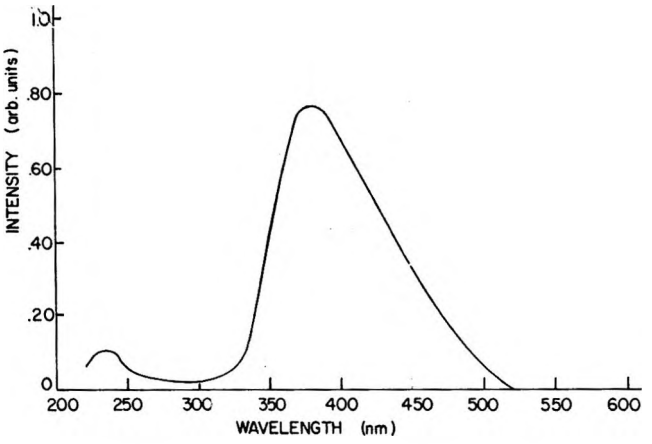

Figure 1. Emission spectrum of 3MP γ irradiated at 77°K at a dose of 4.4×10^{14} eV g^{-1}.

The hydrocarbon sample in the dewar could be bleached by either or both of two different sources of light during emission. One was a 200-W Hanovia xenon lamp and the other was a Sylvania Sun Gun tungsten lamp. A Bausch and Lomb high-intensity monochromator, which could be used with either source, was equipped with ultraviolet (200–400 nm), visible (350–800 nm), and lower infrared (700–1600 nm) gratings. The xenon lamp was used primarily for bleaching in the ultraviolet and visible ranges, while the tungsten lamp was used in the infrared region.

C. Infrared Absorption. The method of measurement of the infrared absorption spectrum is identical with that of Skelly and Hamill.[2b]

III. Results

Figure 1 shows the emission spectrum of 3MP γ irradiated at 77°K at a dose of 4.4×10^{18} eV g^{-1}. Because the decay rate during the initial 10 min was so fast in comparison to the time required for scanning the entire spectrum (~4 min), the emission was allowed to decay for 10 min in the dark before scanning. The emission spectrum during the initial 10 min of decay, however, was identical with that of Figure 1 after correction. Other samples of 3MP were prepared, frozen, and irradiated in the same manner, and the emission was scanned during bleaching of the irradiated hydrocarbon by either infrared or ultraviolet light. The infrared light was produced by the tungsten lamp with a Corning 2030 filter (transmission $\lambda > 750$ nm). Scans were made at photon fluxes of 1.6×10^{16} and 3.2×10^{16} photons cm^{-2} sec^{-1}. The emission spectrum found in every case was identical with that given in Figure 1. Ultraviolet bleaching at 265 nm with photon fluxes of 2.9×10^{15} and 7.2×10^{15} photons cm^{-2} sec^{-1} with a 20-nm bandpass gave identical results after correction for scattered bleaching light. The spectrum given in Figure 1 is slightly different from the one previously published[2a] because of improved correction for wavelength, monochromator transmission efficiency,

and photomultiplier sensitivity in the present work. It also contains an additional peak at around 230 nm which appears in both irradiated glassy and liquid 3MP.

The emission at 230 nm has already been observed by Merkel and Hamill[6] in γ-irradiated 3MP at 77°K and is probably related to fluorescence in hydrocarbon liquids observed by Hirayama and Lipsky,[7] while the emission at 380 nm has been assumed to be related to a low-lying triplet state.[6] These assignments are consistent with the measured lifetime of the 380-nm peak (4.4 sec) and the estimated lifetime of the 230-nm peak (≤ 2 μsec). The luminescence decay in this paper refers to that of the 380-nm band, which is the 415-nm band in Merkel–Hamill work[6] (the difference is due to our improved correction for the wavelength dependence of the photomultiplier).

Figure 2 shows the effect of ir bleaching on the luminescence decay. The upper curve is the dark decay and the lower two curves are for bleaching with photon intensities of 1.5×10^{16} and 3.1×10^{16} photons cm^{-2} sec^{-1} of 1600-nm radiation, respectively. The bleaching light was turned on immediately after the termination of the γ irradiation. On the ordinate 100 is estimated to correspond to 10^8 photons sec^{-1} emitted from the sample.

Figure 3 shows the effect of uv bleaching on the luminescence decay. Again the decay appears, this time as the lower curve. The upper curves are for bleaching intensities of 2.9×10^{15} and 7.2×10^{15} photons cm^{-2} sec^{-1} of 265-nm radiation, respectively.

In Figures 2 and 3, the time zero corresponds to 30 sec after termination of irradiation and the wavelength monitored is 380 nm. The 230-nm peak followed the same decay pattern as that of the 380 nm. Most observations have involved shorter time intervals than we have used (8 hr). All of our observations on dark decay and on luminescence during various kinds of bleaching can be adequately represented in terms of the equation

$$L = N_1 e^{-\lambda_1 t} + N_2 e^{-\lambda_2 t} + N_3 e^{-\lambda_3 t} \qquad (1)$$

It is not possible to fit the decay curves in terms of simple first- or second-order kinetic schemes. It is, however, possible to represent the curves also in terms of a polynomial function of time. Accuracies of the curve fitting for a polynomial function and the form 1 are comparable. It is, however, much easier to give physical meanings to the constants and parameters in the case of eq 1. In Table I the constants for the curves of Figures 2 and 3 are summarized.

It is important to relate the luminescence results to the direct observation of trapped electrons in the samples by absorption measurements. Figure 4 shows the effect of ir bleaching on the decay of optical density at 1600 nm. The upper curve is the dark decay, and the lower two curves are for the same ir intensities used previously. Figure 5 shows the effect of uv bleaching on the decay of optical density of 1600 nm. Again the dark decay is included and the two upper curves are for the uv intensities used previously. In Figures 4 and 5, intermittent measurements of the optical density at 1600 nm are represented by the triangular, square, and circular markings, while the luminescence intensities of Figures 2 and 3 do not have these experimental points because the emission intensities were measured continuously. Because of this difference in measurements of the luminescence and the optical density, the decay constants for the optical density, which could have been obtained from Figures 4 and 5, are not expected to be as accurate as those given in Table I and consequently

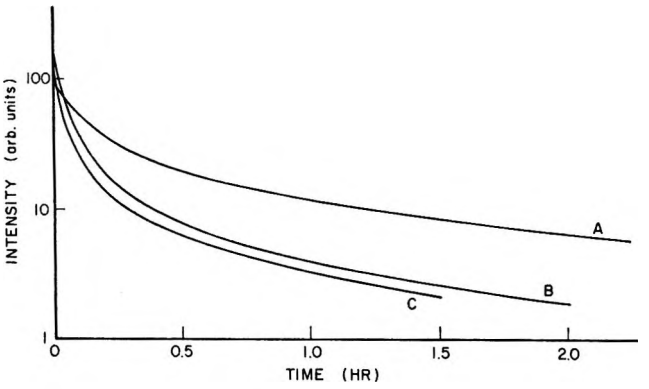

Figure 2. Effect of ir bleaching of the luminescence decay of γ-irradiated 3MP. Curve A is for decay without bleaching light. Curves B and C are bleaching with photon intensities of 1.5×10^{14} and 3.1×10^{16} photons cm^{-2} sec^{-1} of 1600-nm radiation, respectively.

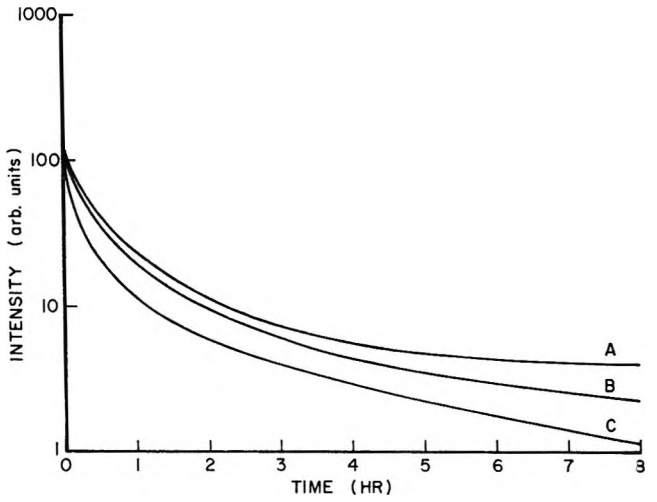

Figure 3. Effect of uv bleaching on the luminescence decay of γ-irradiated 3MP. Curve C is for decay without bleaching light (it is the same curve as A of Figure 2 except that the time scale is longer here). Curves A and B are for bleaching with photon intensities of 7.2×10^{15} and 2.9×10^{15} photons cm^{-2} sec^{-1} of 265-nm radiation, respectively.

(6) P. B. Merkel and W. H. Hamill, *J. Chem. Phys.*, **53**, 3414 (1970).
(7) F. Hirayama and S. Lipsky, *ibid.*, **51**, 3616 (1969).

Table I: Decay Parameters for 3MP

Curve	$1/\lambda_1$, min	$1/\lambda_2$, min	$1/\lambda_3$, min	N_1[a]	N_2	N_3	Bleaching light: Intensity, photons cm^{-2} sec^{-1}	Bleaching light: Wavelength, nm
A, Figure 2	2.80	17.8	122.0	44.21	32.15	23.63	None	
B, Figure 2	2.44	32.3	312.5	136.6	23.21	1.72	1.5×10^{16}	1500
C, Figure 2	2.38	30.3	294.1	327.15	14.66	1.78	3.06×10^{16}	1500
A, Figure 3	7.14	40.0	208.3	41.79	22.61	50.51	7.18×10^{15}	265
B, Figure 3	5.88	30.3	185.2	36.85	43.03	16.01	2.85×10^{15}	265
C, Figure 3	Same as A, Figure 2							

[a] N_i's scaled to give $I(0) = 100$ for the dark decay.

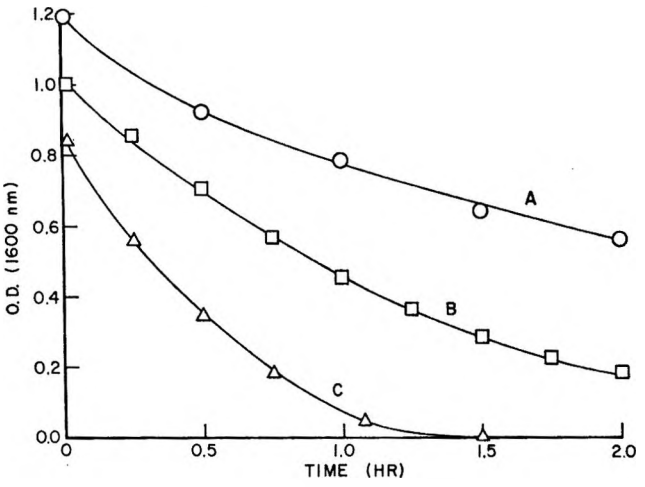

Figure 4. Effect of ir bleaching on decay of optical density at 1600 nm of γ-irradiated 3MP. Curve A is for decay without bleaching light. Curves B and C are for the same bleaching intensities as for curves B and C of Figure 2.

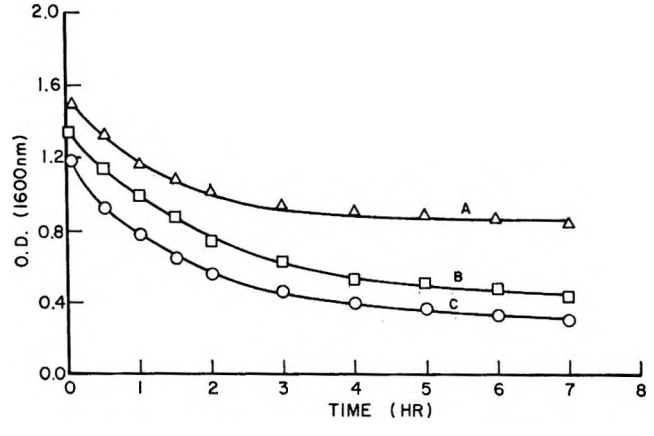

Figure 5. Effect of uv bleaching on decay of optical density at 1600 nm of γ-irradiated 3MP. Curve C is for decay without bleaching (it is the same curve as A of Figure 4 except that the time scale is longer here). Curves A and B are for the same bleaching intensities as for curves A and B of Figure 3.

cannot be compared in a meaningful way with the luminescence decay. For this reason, we have not analyzed the decay constants for the optical density.

Figure 6 shows a sequence of observations carried out

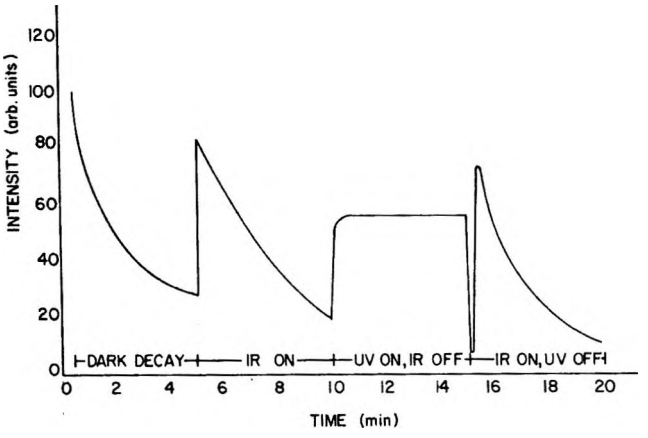

Figure 6. Luminescence decay sequence. The first ir intensity is 1.5×10^{16} photons cm^{-2} sec^{-1}. The uv intensity is 2.9×10^{15} photons cm^{-2} sec^{-1}. The last ir intensity is 3.0×10^{16} photons cm^{-2} sec^{-1}.

on a sample of irradiated 3MP to summarize the bleaching studies in pure 3MP. The sample is first allowed to decay in the dark and then partially bleached with ir. Irradiation with uv restores the trapped electron concentration and the luminescence. It is quite apparent that the decay rate is extremely small during the uv irradiation; on this time scale it appears as a constant. Irradiation again with ir rapidly bleaches the trapped electrons.

There has always been a question regarding the role of the positive charge in the bleaching process. Systems in which it is known that only the negative charge can move (photoionized TMPD in 3MP)[8] behave in a qualitatively similar manner to γ-irradiated systems.[4] In pure 3MP the identity of the positive ion is not known for certain, but it has frequently been assumed to be $3MP^+$. If this is the case there may be a certain amount of positive-charge mobility, and it may have an effect on the bleaching process. Figure 7 shows some results obtained with an added hole trap. Solutions of 5×10^{-3} M 2-methylpentene-1 (2MP-1) in 3MP were frozen and γ irradiated, and the luminescence was ob-

(8) K. G. Cadogan and A. C. Albrecht, *J. Phys. Chem.*, 72, 929 (1968).

Table II: Decay Parameters for 3MP with Added 2MP-1

Curve	$1/\lambda_1$, min	$1/\lambda_2$, min	$1/\lambda_3$, min	N_1[a]	N_2	N_3	Bleaching light: Intensity, photons cm^{-2} sec^{-1}	Bleaching light: Wavelength, nm
A, Figure 7	0.66	2.50	20.0	93.6	1.4	1.0	1.6×10^{16}	1500
B, Figure 7	7.14	2.77	32.3	22.1	1.6	1.3	None	
C, Figure 7	7.51	3.03	50.0	38.6	2.9	2.3	4.8×10^{15}	265

[a] Curves are normalized to $I(0) = 100$ for pure 3MP dark decay.

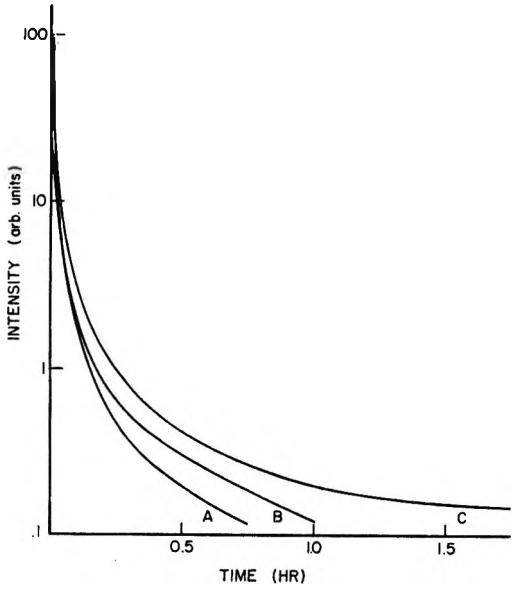

Figure 7. Luminescence decay of γ-irradiated 3MP with 5×10^{-3} M 2-methylpentene-1 added. Curve B is for the dark decay. Curve A is for bleaching with ir photon intensity of 1.6×10^{16} photons cm^{-2} sec^{-1} and curve C is for bleaching with uv photon intensity of 4.8×10^{15} photons cm^{-2} sec^{-1}.

served as for the pure 3MP samples, including dark decay and ir and uv bleaching. The first thing one notices from Figure 7 is the qualitative agreement with the pure 3MP samples: ir bleaching increases the decay of luminescence and uv bleaching decreases it. In a quantitative way, however, it is clear that the dark decay is much faster than for the pure 3MP and that the ir and uv effects in acceleration and retardation are much smaller. Parameters for the curves of Figure 7 are summarized in Table II.

The same experiments were performed with 5×10^{-3} M benzene added. Benzene is known to trap both positive holes and electrons.[9] The results were identical with those shown in Figure 7. In this case, however, a spectroscopic study showed that the light emission was entirely from benzene, whereas with the 2MP-1 additive it was the same as that from pure 3MP.

These experiments suggest that the positive charge is mobile in 3MP glasses at 77°K. The concentration of additive is at the level of 1 molecule per 1600 molecules of 3MP, and any mechanism for an effect as large as we have observed requires motion of the positive charge. This evidence also supports the assumption that the positive charge in 3MP is $3MP^+$; at 77°K the charge can only move in a resonant process because there is no molecular diffusion. Alternatively, one could propose a mechanism involving a triplet energy transfer from 3MP to 2MP-1 to account for the effect of 2MP-1. However, the relevant triplet energy level for 3MP is not known and also the notion that our 380-nm emission is related to 3MP triplet is still a matter of conjecture.

Although the luminescence is decreased, the concentration of trapped electrons is increased by the hole-trapping additive 2MP-1.[9] The decay of the optical density was not observed in our experiments, but the concentrations of trapped electrons is known to be larger at all times than those in undoped samples.[10] The decrease of luminescence in these samples means that the disappearance of trapped electrons is not associated with a light emission process. Presumably the positive ions are $2MP\text{-}1^+$ and do not emit radiation on neutralization. It is well known that olefin molecules do not radiate from their excited states, and it is assumed that an efficient degradation process associated with the double bond is responsible.

In Figure 7 the ir bleaching curve A indicates an acceleration of the decay process in the same manner as for pure 3MP. The uv bleaching curve C, however, may have another phenomenon involved. In addition to releasing electrons from deep traps the uv radiation may be able to move the positive charges from 2MP-1 back again to 3MP where they would be mobile. The quantitative nature of these curves has not been studied enough to be sure that this effect is required.

IV. Discussion

There is no molecular diffusion in glassy 3MP on the time scale of interest here, and all processes involved in decay of luminescence and trapped electron concentrations are electronic in nature. The concepts of solid-state physics have generally been used in discussions of excess

(9) J. P. Guarino and W. H. Hamill, *J. Amer. Chem. Soc.*, **86**, 777 (1964); T. Shida and W. H. Hamill, *J. Chem. Phys.*, **44**, 2375, 4372 (1966).

(10) J. B. Gallivan and W. H. Hamill, *ibid.*, **44**, 1279 (1966).

electrons and such electrons are normally considered to be either free (in a conduction band) or trapped. It has sometimes been recognized that there may be different kinds of traps,[5] but for the most part by "trapped electron" the shallow trapped electron which has an absorption maximum near 1600 nm is meant. We shall follow convention and call such electrons "trapped electrons" and refer to this concentration (in number per unit volume) as n_s; we shall also discuss another type of trapped electron which is deeper trapped and refer to its concentration as n_d.

The G value for creation of trapped electrons in γ irradiation of 3MP is known to be near unity,[2b,5] and we shall assume this value applies here although it was not measured. In hydrocarbons at room temperature it is known from scavenger studies that the maximum G value for scavengeable electrons is approximately 4.[11] It is generally assumed that the smaller electron yield of the 3MP glass is a result of early recombination. In a sense it is surprising that any electrons remain uncombined for times of the order of minutes in a glass of pure 3MP. Maruyama[12] has measured the mobility of electrons in this glass at 77°K and found it to be 0.11 $cm^2\ V^{-1}\ sec^{-1}$. Electrons with a mobility of such a magnitude would recombine with a geminate ion in a time less than 1 nsec if no other process were involved. We can understand these facts on the assumption that the trapping process requires an activation energy and that the electron accelerated in the strong field of their geminate ions are more rapidly trapped than under the conditions used by Maruyama.

The early trapped electron decay (first hour or so) is known to be "first order" in the sense that the fractional decay is independent of dose.[2b,5,9] This result has been assumed to indicate that the decay takes place in the various spurs independently.

We are interested in the relationship between the luminescence and trapped electron concentration as shown in Figures 2–5. Since presumably electron disappearance must accompany luminescence, the relationship

$$L \propto -\frac{dn_s}{dt} \tag{2}$$

is suggested where L is the luminescence intensity at time t. To test eq 2 using the data of Figures 2–5 we take the integral form

$$\int_0^t L dt \propto n_s^0 - n_s \tag{3}$$

where n_s^0 is the concentration n_s at the initial time. In Figures 8 and 9 plots of the quantity

$$[n_s^0 - n_s]^{-1} \int_0^t L dt$$

as a function of time are shown as obtained from the data of Figures 2 and 4 and Figures 3 and 5, respectively.

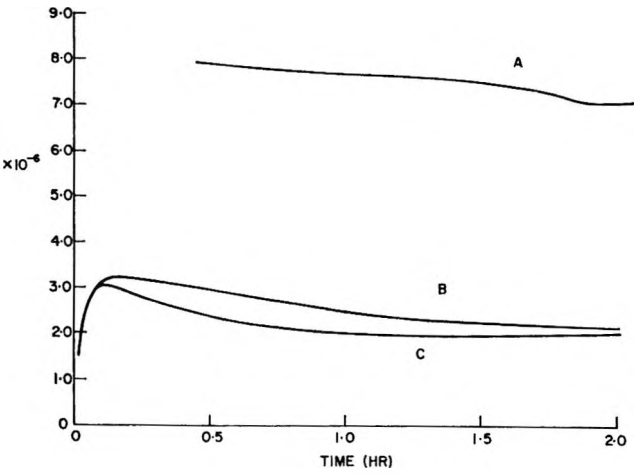

Figure 8. Effect of ir bleaching on the quantity $[n_s^0 - n_s]^{-1}\int_0^t L dt$. Curve A is for dark decay. Curves B and C are for bleaching with photon intensities of 1.5×10^{16} and 3.1×10^{16} photons $cm^{-2}\ sec^{-1}$ of 1600-nm radiation, respectively.

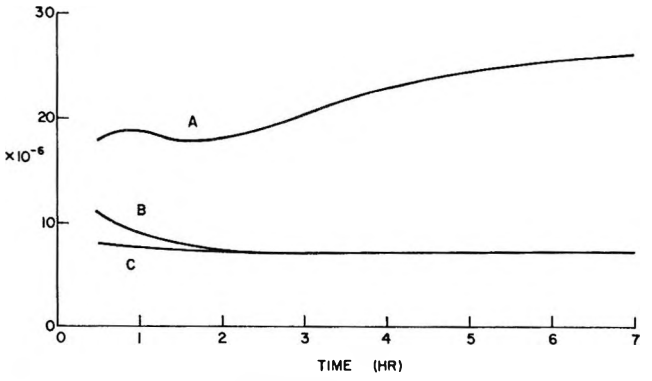

Figure 9. Effect of uv bleaching on the quantity $[n_s^\circ - n_s]^{-1}\int_0^t L dt$. Curve C is for dark decay. Curves B and A are for bleaching with photon intensities of 2.8×10^{15} and 7.2×10^{15} photons $cm^{-2}\ sec^{-1}$ of 265-nm radiation, respectively.

After an initial transient period eq 2 and 3 apply quite well to all of the cases except the stronger uv bleaching. However the ratio of photons out to electrons lost is not the same for all. Calling the proportionality constant q we can write

$$L = -q\frac{dn_s}{dt} \tag{4}$$

Equation 1 for L can be integrated analytically giving an explicit relationship between the luminescence parameters and n_s

$$n_s = \frac{N_1}{q\lambda_1}e^{-\lambda_1 t} + \frac{N_2}{q\lambda_2}e^{-\lambda_2 t} + \frac{N_3}{q\lambda_3}e^{-\lambda_3 t} + n_c \tag{5}$$

(11) J. M. Warman, K. D. Asmus, and R. H. Schuler, *J. Phys. Chem.*, **73**, 931 (1969).

(12) Y. Maruyama, private communication on work performed at the Radiation Laboratory, University of Notre Dame.

where n_c is a constant of integration of dimension concentration. According to eq 1 the luminescence intensity goes to zero exponentially at long times, and it might be expected that the constant n_c should be taken as zero. On the other hand, eq 1 is not known to be correct for times much longer than 8 hr and so we cannot assume that all of the electrons are involved in the decay given by eq 1. The constant n_c can very well be nonzero.

Equation 5 was used to calculate electron concentrations for all of the pure 3MP cases. The results are given in Figures 10 and 11. The parameters q and n_c were obtained by requiring that the initial concentration and the concentration at 7 hr agree with experiment for the dark decay and the uv bleaching. For the ir bleaching cases the initial concentration was taken as 4.0×10^{16} and n_c was taken as zero. In Figures 10 and 11 the experimental curves are also shown as the dashed lines.

Figure 11 shows that the luminescence and electron concentration measurements are in satisfactory agreement for pure 3MP in dark decay. The fraction 7×10^{-6} of recombinations lead to the emission of a photon. The constant n_c is found to be 0.93×10^{16} electrons cm^{-3} which means that about 25% of the trapped electrons are involved in a very long-time decay process. The absorption spectrum was studied very carefully at long times and, as well as we can tell, it is the same as that observed at early times.

The experimental data on luminescence and electron concentrations for the weaker uv bleaching case are also in satisfactory agreement. The q value is the same as that for dark decay which must mean that the neutralization process is the same as that for dark decay. Such a process depends on the excited state formed and can therefore be sensitive to energy. The creation of mobile electrons by absorption of the uv photons has not changed the energetics of the electron–ion recombination process.

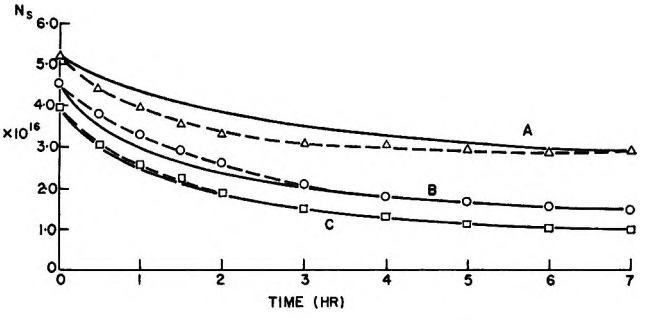

Figure 10. Electron concentrations as a function of time. The solid curves are calculated from luminescence curves using eq 5 and the dashed curves are obtained from measured optical densities. Curve A is for the dark decay, and curves B and C are for bleaching with photon intensities of 1.5×10^{16} and 3.1×10^{16} photons cm^{-2} sec^{-1} of 1600-nm radiation, respectively.

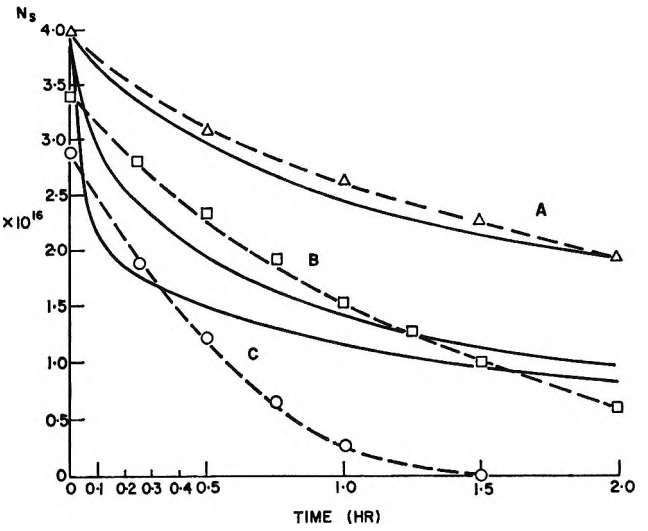

Figure 11. Electron concentrations as a function of time. The solid curves are calculated from luminescence curves using eq 5, and the dashed curves are obtained from measured optical densities. Curve C is for the dark decay and curves A and B are for bleaching with photon intensities of 7.2×10^{15} and 2.9×10^{16} photons cm^{-2} sec^{-1} of 265-nm radiation, respectively.

The reason for the uv bleaching experiments was to investigate the role of deeper trapped electrons. It is apparent from Figures 2 and 4 that the uv photons have an appreciable effect on both luminescence and electron concentrations. Figure 5 shows that the electron concentration n_s is increased at the earliest times by the uv bleaching light. We interpret this result as a photostationary[4] state between mobile electrons and shallow-trapped and deep-trapped electrons. There is much evidence that photostationary states are formed in organic glasses which contain trapped electrons.[13] The theory of such states is presumably similar to that for the better understood solid-state semiconductors.[14]

A simple kinetic model can be developed as follows. Let n_s = concentration of shallow-trapped electrons, n_d = concentration of deep-trapped electrons, n_f = concentration of mobile electrons, and N = total concentration of electrons with

$$n_s + n_d + n_f = N$$

$$\frac{dn_f}{dt} = \sigma I n_d + k_s n_s - (k_s' + k_d' + k')n_f \qquad (6)$$

$$\frac{dn_s}{dt} = k_s' n_f - k_s n_s \qquad (7)$$

$$\frac{dn_d}{dt} = k_d' n_f - \sigma I n_d \qquad (8)$$

Here I is the bleaching light intensity, and it is assumed that this light is absorbed only by the deep-trapped

(13) G. E. Johnson and A. C. Albrecht, *J. Chem. Phys.*, **44**, 3162 (1966).

(14) P. Bräunlich and P. Kelly, *Phys. Rev. B*, **1**, 1596 (1970).

electrons (cross section σ). The k's and k''s are first-order rate constants for the processes by which electrons change their states. Notice that the rate constant k_d for thermal activation of the deep-trapped electrons to the mobile state is neglected. We assume that the activation energy is too large for this process to occur at an appreciable rate.

Addition of the set of equations gives

$$\frac{d}{dt}(n_f + n_s + n_d) = \frac{dN}{dt} = -k'n_f$$

which means that the total pool of electrons is only depleted by neutralization. We are interested in a photostationary state established in seconds and so we can take N as constant. Furthermore, since

$$n_f \ll n_s, n_d$$

we can use

$$n_s + n_d = N = \text{constant}$$

With these approximations eq 7 and 8 both reduce to

$$\frac{dn_s}{dt} = -\frac{k_s k_d' + k_s'\sigma I}{K'} n_s + \frac{k_s'\sigma I N}{K'} \qquad (9)$$

where we have set

$$K' = k_s' + k_d'$$

and taken k' to be zero.

Equation 9 describes the photostationary state and, of course, the transient leading to it. The transient time constant is given by

$$\frac{1}{\tau} \approx \frac{k_s k_d' + k_s'\sigma I}{K'} = \frac{k_s(k_d'/k_s')\sigma I}{1 + (k_d'/k_s')} \qquad (10)$$

The flux used is 3×10^{15} protons cm^{-2} sec^{-1}, and if we take the cross section to be 10^{-16} cm^2 (based on the assumption of unity for the oscillator strength), the term σI is 0.3. The ratio k_d'/k_s' is most likely less than unity. The rate constant k_s is for the thermal release of electrons from traps, and we estimate it to be 10^{-2} or smaller. We are left with an estimate of the time constant for the photostationary state of 3 sec

$$1/\tau \approx 0.3 \text{ or } \tau \approx 3 \text{ sec}$$

In Figure 6 the sequence of dark–ir bleach–uv bleach–ir bleach shows the response to the uv radiation as almost instantaneous. It is this time constant we are discussing. This transient has been observed as carefully as the experimental equipment allows and is indeed of the order of a few seconds.

At the photostationary state $dn_s/dt \approx 0$ and we have

$$\frac{n_s}{N} = \frac{\sigma I}{k_s k_d'/k_s' + \sigma I} \qquad (11)$$

The experimental results shown in Figure 5 give us values of n_s (presumably in photostationary states) for two different fluxes. We have the following values: $I = 2.9 \times 10^{15}$, $n_s = 4.54 \times 10^{16}$; $I = 7.2 \times 10^{15}$, $n_s = 5.20 \times 10^{16}$. We can solve the two equations simultaneously and get values of N and $k_s k_d'/k_s'$ considered as unknowns. This calculation yields the values

$$N = 5.75 \times 10^{16}$$

$$k_s k_d'/k_s' = 0.08$$

The value of n_s in the sample initially was 4.0×10^{16}. This analysis is consistent with the presence of 1.75×10^{16} additional electrons in the sample in "deep traps."

It is difficult to imagine another source for the electrons which appear within a few seconds of the start of uv bleaching. One might think of ionization process involving a triplet state

$$^3[3MP] \xrightarrow{uv} 3MP^+ + e$$

The probability of this process depends on the triplet energy level and the ionization potential of 3MP in the solid. If one assumes the 380-nm emission is related to the triplet–singlet transition, uv illumination with 265 and 325 nm, which generate the same effect, would excite 3MP to about 8 and 7 eV above the ground state, respectively. Although the ionization potential of 3MP in the solid is not known, these values seem too low for ionization energy.

The deep-trapped electron may be in intrinsic traps of the matrix or as negative ions of radicals formed by the γ irradiation. The results (Figure 11) for the larger uv flux indicate that the situation is more complicated than that described by this simple model. The q value (photons emitted in luminescence per electron disappearing) is about three times as large as that of the dark decay and the weaker uv bleaching. This probably indicates that the uv light is producing additional ionization. Since the weaker flux does not produce the effect, it is probably a 2-photon process in a radical. An intermediate state with a lifetime of the order of 1 sec could be ionized by the larger flux (7×10^{15} photons cm^{-2} sec^{-1}).

The three curves shown in Figure 4 for the effect of ir bleaching on electron concentrations all start at the same value at zero time (the value for dark decay). It appears that the time constants for the initial electron *decreases* for the ir bleaching cases are as short as those for the electron *increases* in the uv cases shown in Figure 5. The way in which these experiments were done makes accurate measurement of the transients difficult, but we believe the phenomenon involved is different. The electron decrease is not just the change in the distribution of electrons in a pool with the formation of a photostationary state as in the uv cases, but a rapid loss of electrons to neutralization or deep traps. The curves shown in Figure 10 calculated from eq 5

show the same very steep initial drop which is found in the experimental curves. The agreement between the model and the experimental results is rough and not entirely satisfactory.

The quantum yield for bleaching with ir has been investigated.[2,15] The initial quantum yield has been given as near unity, and it has been observed to decrease to small values as the bleaching progressed. The ir bleaching reported here has a quantum yield calculated over the first 3 min of 5×10^{-3} and over the first hour of $\sim 10^{-4}$. The "initial value" calculated for the first few photons may be much larger, near unity, but over most of the bleaching, at the intensities used here, the quantum yield is extremely small. For the uv bleaching the decay is actually slowed up by the light, and one would have to say that the quantum yield for bleaching is *negative*. This is true even in the case of the weaker bleaching where there is no production of additional electrons. Apparently quantum yield is not a useful concept here.

It would be desirable to have a kinetic model which describes the decay of γ-irradiated 3MP. We shall not present such a model at this time, but it is worthwhile to consider some of its properties. The approximate validity of eq 5 shows that the luminescence and electron concentrations fit into the same pattern. The form of eq 5 as a linear combination of exponentials suggests that a set of first-order differential equations could be the basis of a kinetic model. This in turn suggests that the geminate pair is the basic entity whose properties determine all the phenomena.

In any case a model must deal both with electron energy and spatial distribution. At the present time most investigators seem to have a preoccupation with the spatial distribution to the exclusion of energetics. We have seen that both deep traps and shallow traps are required. Analysis of the photostationary state created by the uv bleaching gives an estimate that there are about half as many deep-trapped electrons as shallow-trapped electrons initially in 3MP. The dark decay leaves about one-fourth of the shallow-trapped electrons with a time constant much larger than 8 hr. Burton, Dillon, and Rein[2a] have observed a group of trapped electrons with an activation energy of 0.25 eV for neutralization as contrasted with the activation energy of 0.1 eV for the early dark decay. It is likely that it is a second kind of shallow-trapped electron which is involved. The absorption spectrum has been observed to remain constant and so such a slightly deeper trapped electron would have to have essentially the same optical properties as the more abundant species.

A compelling requirement for a kinetic model is a proper treatment of the mobility of the positive charge. There is ample evidence that this motion is important, for example, the decay of the 2MP-1-doped sample of 3MP reported here (Figure 7). It has, to the present time, not been given its proper role.

Acknowledgment. J. L. M. wishes to thank Professor Sir Frederick Dainton for the hospitality of the Physical Chemistry Laboratory at Oxford University where the paper was partially written.

(15) P. J. Dyne and O. A. Miller, *Can. J. Chem.*, **43**, 2696 (1965).

The Photolysis of Rhodium(III) 1,10-Phenanthroline Chelates in Glassy Solution. An Electron Spin Resonance Study[1]

by Keith DeArmond* and Warren Halper

Department of Chemistry, North Carolina State University, Raleigh, North Carolina 27607 *(Received April 12, 1971)*

Publication costs assisted by the U. S. Army Research Office (Durham)

The sensitized photolytic decomposition of ethanol glass solutions (77°K) containing luminescent rhodium(III) chelates has been investigated utilizing electron spin resonance (esr) spectroscopy. A metal-containing radical and a solvent radical have been identified in the photolysis of those rhodium chelates containing the 1,10-phenanthroline ligand. The reaction pathway involves production of a solvent radical by a two-photon process involving the long-lived triplet of the solute and the subsequent attack of the solvent radical upon the chelate in the ground state. A general structure for the metal chelate radical is proposed.

Deactivation of excited electronic states in molecules may be divided into two categories: (1) physical processes and (2) chemical processes. Photolysis, a chemical process, is competitive with luminescence, a physical process, and can decrease luminescence yields in large molecules. Photolysis of first transition series d^6 Co(III) and d^3 Cr(III) systems[2,3] typically involves solvolysis of monodentate ligands in the coordination sphere or redox reactions of the central ion (Co(III) complexes only). The irreversible[4] photolysis of transition metal complexes with chelate type ligands is known for only a few complexes with the oxalate complex photolysis most thoroughly studied.[5] Photolysis of second- and third-row complexes does not appear to be a common deactivation pathway, a fact consistent with the nonlabile character of second- and third-row complexes and generally stable oxidation states of their ions.

Luminescence from d^6 Rh(III) and Ir(III) chelates[6-8] has been observed with a variety of energy level schemes, but no evidence for photolysis has been presented in these studies. Preliminary esr studies of the luminescent excited state of Rh(III) 2,2′-dipyridyl and 1,10-phenanthroline chelates at high light intensities produced evidence for a radical photolysis process.

A detailed esr study was initiated to determine the significance of this photolysis process to the overall relaxation processes and to minimize line broadening of the triplet-state resonance caused by this radical photolysis process. The main purposes of this study were (1) identification of the primary photolysis products and (2) determination of the reaction pathway. From a description of the radical products and the relative formation rates, the photolysis reaction can be identified as a unimolecular (bond-breaking or photoionization) or a bimolecular (solvent–solute or solute–solute) reaction. Product identification should enable determination of the reactive site. Determination of the reaction pathway should permit a description of the role of the luminescent triplet state in this radical photolysis.

Experimental Section

All alcohol solutions were prepared using commercial 95% ethanol dried by treatment with CaO, then dried with CaH_2 to remove any residual trace quantities of water. Water present in the ethanol can cause severe cracking when the solution is frozen. The $MgCl_2$–H_2O solvent was prepared using the technique of Zuloaga and Kasha.[9] The 1,10-phenanthroline (phen) monohydrate and 2,2′-dipyridyl (dip) were obtained from Aldrich Chemical Co. and were not further purified.

$[Rh(phen)_2Cl_2]X$ and $[Rh(dip)_2Cl_2]X$ (where X = Cl^- and ClO_4^-) were prepared by the method of Gillard, *et al.*[10] $[Rh(phen)_3]X_3$ and $[Rh(dip)_3]X_3$ (where X = Cl^- and ClO_4^-) were prepared using this same method with a stoichiometric amount of complexing ligand added after 3 hr of refluxing to convert the bis complex to the tris complex. The reflux was continued for at least 12 hr and the compound was purified using Gillard's procedures. $[Rh(dip)_2(phen)]Cl_3$ and $[Rh(phen)_2(dip)]Cl_3$ were prepared by analogous methods. The

(1) Supported by the Army Research Office (Durham) (AROD).

(2) E. L. Wehry, *Quart. Rev. (London)*, 21, 213 (1967).

(3) A. W. Adamson, W. L. Waltz, E. Zinato, D. W. Watts, P. D. Fleischauer, and R. D. Lindholm, *Chem. Rev.*, **68**, 541 (1968).

(4) Reversible bond breaking and recombination may be a dominant process in the deactivation of Cr(III) chelates. See S. T. Spees and A. W. Adamson, *Inorg. Chem.*, **1**, 531 (1962).

(5) K. V. Krishnamurty and G. M. Harris, *Chem. Rev.*, **61**, 213 (1961).

(6) M. K. DeArmond and J. E. Hillis, *J. Chem. Phys.*, **49**, 466 (1968).

(7) D. H. W. Carstens and G. A. Crosby, *J. Mol. Spectrosc.*, **34**, 113 (1970).

(8) M. K. DeArmond and J. E. Hillis, *J. Chem. Phys.*, in press.

(9) F. Zuloago and M. Kasha, *Photochem. Photobiol.*, **7**, 549 (1968).

(10) R. D. Gillard, J. A. Osborn, and G. Wilkinson, *J. Chem. Soc.*, 1951 (1965).

$[Rh(dip)_2Cl_2]Cl$ and $[Rh(phen)_2Cl_2]Cl$ were converted by the addition of stoichiometric quantities of *o*-phenanthroline and 2,2′-dipyridyl, respectively, followed by 24 hr of refluxing. These materials were purified using Gillard's method.

Anal. Calcd for $[Rh(dip)_2(phen)]Cl_3 \cdot 5H_2O$: C, 48.5; H, 4.33; N, 10.6. Found: C, 48.0; H, 4.43; N, 11.0. Calcd for $[Rh(phen)_2(dip]Cl_3 \cdot 5H_2O$: C, 50.1; H, 4.20; N, 10.3. Found: C, 50.4; H, 4.26; N, 9.86.

$[Ir(phen)_2Cl_2]Cl$ was prepared by the method of Harris and McKenzie.[11] Degassed samples were prepared by freeze-pump-thaw recycling a minimum of three times. The tubes were sealed under a vacuum.

Electron spin resonance measurements were done with a JEOLCO ME-3X spectrometer operating at X-band frequency equipped with a cylindrical mode TE-012 cavity. Quartz windows in the cavity permit efficient irradiation at room and liquid nitrogen temperature. An Osram 500-W mercury lamp was used for irradiation. Magnetic field measurements were made with a Magnion G-502 Gaussmeter and Hewlett-Packard 5245L frequency counter. Klystron frequency measurements were done using a DPPH powder standard. All measurements were done in cylindrical 5-mm quartz esr tubes. Esr variable temperature measurements were made using the JEOLCO JES-UCT-2X attachment.

Optical spectra at room temperature and 80°K were determined with a Cary 14 spectrometer. The 80°K spectra were obtained using a copper block cryostat constructed for use with the Cary 14. Luminescence spectra were determined with an Aminco Bowman spectrophotofluorometer (SPF) equipped with a phosphorimeter attachment. Lifetimes were determined with the phosphorimeter and various flash lamps in conjunction with a Tektronix 564 oscilloscope. The luminescence data have been reported[7,8] for all except the mixed ligand complexes.

Results

A. Tris Complexes. The esr spectra obtained for the irradiated tris complexes of Rh(III) in alcohol glass at 77°K are given in Figure 1. All $[Rh(phen)_3]^{3+}$ samples gave a purple color after irradiation with a structured esr signal in the free radical region (g = 2.00) and a broad band showing partially resolved structure centered at g = 2.16. The $[Rh(dip)_3]^{3+}$ samples, in contrast, gave only a free radical signal with the solution turning brown after lengthy irradiation. Both chloride and perchlorate salts of $[Rh(phen)_3]^{3+}$ gave similar coloration and esr spectra upon irradiation. Warming of the irradiated $[Rh(phen)_3]^{3+}$ sample (below the glass point) caused the free radical signal to disappear at −140°, both signals decreasing in intensity as the temperature is raised. At the glass point temperature, (T = −117°), the g = 2.16 signal typically remained as did the purple color.

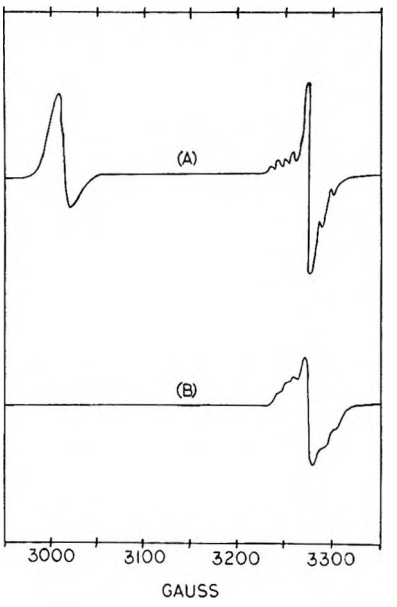

Figure 1. Esr spectra of irradiated $[Rh(phen)_3]Cl_3$ (A) and $[Rh(dip)_3]Cl_3$ (B) in ethanol glass at 77°K; $\nu \approx 9.182$ GHz.

Degassed samples of these complexes produced the same esr spectra in the g = 2.16 region as the aerated samples. The g = 2.00 spectrum was slightly dependent upon O_2 in the glass. Irradiated $MgCl_2 \cdot xH_2O$ glassy solutions of $[Rh(phen)_3]^{3+}$ exhibited no color or esr signal.

Table I compares the integrated intensities for the g = 2.00 and g = 2.16 signals of the $[Rh(phen)_3]^{3+}$ as a function of initial concentration and irradiation time. Relative concentrations of paramagnetic species within each g value region were measured by integrating signal areas. Comparison of absolute radical concentrations between the two g value regions is not valid since line shapes are different. Comparison of the ratio of the two signals at different times is appropriate if the same radical species are present at all times during irradia-

Table I: Integrated Intensities for the g = 2.00 and g = 2.16 Esr Signals for $[Rh(phen)_3]^{3+}$ as a Function of Initial Concentration and Irradiation Time

Concn, M	Irradiation time, min	Integrated intensity g = 2.16	Integrated intensity g = 2.00
0 (ethanol only)	30	0	336
1.8×10^{-4}	30	689	346
	5	269	311
9.0×10^{-4}	30	1392	607
	5	316	251
1.8×10^{-3}	30	2004	662
	5	347	226

(11) C. M. Harris and R. D. McKenzie, *J. Inorg. Nucl. Chem.*, **25**, 171 (1963).

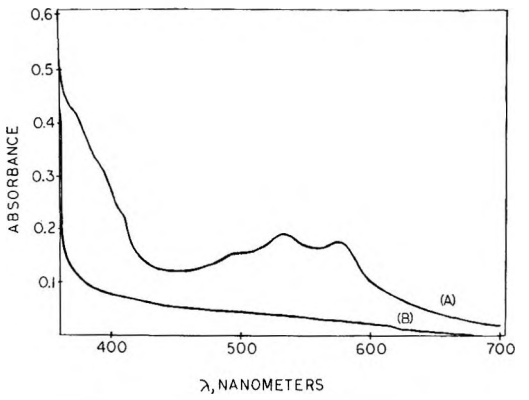

Figure 2. Uv-visible spectra of irradiated (A) (6.3×10^{-3} *M* after 0.5 hr irradiation in a 1-cm² cell with a 500-W high-pressure mercury lamp) and nonirradiated (B) $[Rh(phen)_3]Cl_3$ in ethanol glass at 80°K.

tion. Table II indicates the dependence of the paramagnetic species production upon lamp intensity. The uv-visible spectrum of the photolyzed $[Rh(phen)_3]_3^+$ sample is shown (Figure 2) with the unirradiated $[Rh(phen)_3]^{3+}$ spectra. The purple sample was allowed to thaw and the color disappear. The uv-visible spectrum was then identical with the unirradiated sample.

Table II: The Dependence of $g = 2.00$ Paramagnetic Species Production on Lamp Intensity[a]

Incident lamp intensity, I[b]	I dependence[c]	Integrated intensity of $g = 2.00$ signal
7.95		162
	2.5	
15.9		948
	1.36	
35.5		2816
	1.03	
100		8220

[a] Sample 3.6×10^{-3} *M* $[Rh(phen)_3]Cl_3$ in ethanol glass irradiated for 45 min. [b] Perkin-Elmer reference screens used. [c] The power to which the ratio of incident lamp intensities needs to be raised in order to equal the ratio of integrated $g = 2.00$ signal intensities.

B. Mixed Ligand Complexes. Irradiation of $[Rh(phen)_2(dip)]^{3+}$ produces an esr spectrum closely resembling that produced by irradiation of $[Rh(phen)_3]^{3+}$. In addition to the $g = 2.00$ signal there was observed a signal centered at 2.16. The phosphorescence spectrum for this complex produced an emission with vibrational structure similar to that of the $[Rh(phen)_3]^{3+}$ complex and an emission lifetime of 44.3 msec comparable to that of the $[Rh(phen)_3]^{3+}$ complex.[8]

Irradiation of $[Rh(dip)_2(phen)]^{3+}$ produced the $g = 2.00$ signal and a weak signal centered at $g = 2.16$. The ratio of the $g = 2.16$ to the $g = 2.00$ signal was smaller for this mixed ligand complex than for the other tris or bis Rh(III) complexes. Phosphorescence spectra for the mixed ligand complex produces an emission spectrum with vibrational structure similar to that of the $[Rh(dip)_3]^{3+}$ complex and two emission lifetimes of 5 and 40 msec.[12]

C. Bis Complexes. Esr spectra for the irradiated alcohol glass solutions of $[Rh(phen)_2Cl_2]^+$ gave a signal at $g = 2.00$ similar to that of the tris complex. An additional signal centered at $g = 2.18$ is narrower than that observed for the $[Rh(phen)_3]^{3+}$ complex. The shorter luminescence lifetime (47 μsec) of this bis Rh(III) complex as compared to 48 msec for $[Rh(phen)_3]^{3+}$ necessitated longer irradiation periods to obtain measurable signal intensities (see Discussion). The relative growth rates of the two esr bands are similar to that observed for the $[Rh(phen)_3]^{3+}$ solution. The purple color was again in evidence and the temperature dependence of the two signals is similar to that of the $[Rh(phen)_3]^{3+}$. The esr spectrum of the $[Rh(dip)_2Cl_2]^+$ in glassy solution produced only the $g = 2.00$ signal. Photolysis of an alcohol glass solution of the $[Ir(phen)_2Cl_2]^+$ complex produces no esr signal.

D. Ligands and Solvent. Photolysis of alcohol glass solutions of 1,10-phenanthroline monohydrate produced a yellow-green solution with an esr spectrum in the $g = 2.00$ region similar to that for the chelate complexes. Irradiation of the alcohol glass solution of the 2,2′-bipyridyl produces a brown colored solution. Both solutions gave a structured signal in the $g = 2.00$ region.

Photolysis of a pure alcohol glass solution produced a purple color with a $g = 2.00$ signal. The purified solvent mixture always produced a weak long-lived blue phosphorescence due to trace quantities of aromatic impurity.

Discussion

The description of the photolysis process in the metal chelates requires identification of the radical products and the reaction pathway. The ratio $g = 2.16/g = 2.00$ at short irradiation time being markedly different from this same ratio at longer irradiation times (Table I), the absence of the $g = 2.16$–2.18 signal from the Rh(III) complexes containing only dipyridyl, or dipyridyl and chloride ligands, and the separation of the two esr signals indicates that at least two radicals are produced in the photolysis of the $[Rh(phen)_3]^{3+}$, $[Rh(phen)_2Cl_2]^+$, $[Rh(dip)_2(phen)]^{3+}$, and $[Rh(phen)_2(dip)]^{3+}$ chelates. The magnitude of the g shift for the $g = 2.16$–2.18 signal implies that this radical contains a *heavy metal*. The $g = 2.00$ signal must result from a species containing only light atoms.

The presence of the $g = 2.00$ signal for all alcohol glass solvent samples including the sample blank indicates that this signal is generated from the ethanol

(12) M. K. DeArmond and W. Halper, to be published.

Table III: Results of Uv Irradiation of Ethanol Glasses Containing Various Solutes

Compound	τ_p, sec	Triplet type	Irradiation result[a] Color	Qualitative intensity of esr signals g = 2.00	g = 2.16
1,10-Phenanthroline	1.52	Delocalized orbital	Yellow-green	Strong	...
$[Rh(phen)_3]Cl_3$	4.84×10^{-2}	Delocalized orbital	Violet	Strong	Strong
$[Rh(phen)_2Cl_2]Cl$	4.69×10^{-5}	Localized orbital	Violet	Medium	Medium
$[Ir(phen)_2Cl_2]Cl$	7.30×10^{-6}	Delocalized orbital	...	...	...
2,2′-Dipyridyl	9.55×10^{-1}	Delocalized orbital	Brown	Strong	...
$[Rh(dip)_3]Cl_3$	2.21×10^{-3}	Delocalized orbital	Brown-violet	Strong	...
$[Rh(dip)_2Cl_2]Cl$	4.61×10^{-6}	Localized orbital	Brown-violet	Weak	...
$[Rh(phen)_2(dip)]Cl_3$	4.43×10^{-2}	Delocalized orbital	Violet	Strong	Medium
$[Rh(dip)_2(phen)]Cl_3$	5.0×10^{-3}, 4.0×10^{-2}	Delocalized orbital	Violet	Strong	Very weak

[a] Glasses are 10^{-3} M in solute concentration and are irradiated for at least 0.5 hr in quartz tubes at 77°K.

solvent. The absence of any radical signal for the $MgCl_2 \cdot xH_2O$ glass is additional verification of this process. Comparison of the spectra produced here with those published[13,14] indicates that these g = 2.00 signals are due to $CH_3CH_2\cdot$, $CH_3CHOH\cdot$, $CH_3\cdot$, and $CH_3CO\cdot$ radicals.

The absence of the g = 2.16–2.18 peak for the complexes not containing the 1,10-phenanthroline ligand suggests that the reactive site is associated with the ligand ring system rather than the metal ion. Photooxidation involving the ring π-electron system[15,16] is unlikely in view of the large positive charge of this cationic species. Further, the absence of the g = 2.16–2.18 peak for the dipyridyl complexes is inconsistent with a photooxidation explanation, since the two ligands would be expected to have similar ionization potentials. Anion variation did not alter the general appearance of the esr spectra; therefore a redox reaction involving electron transfer from the anion to the chelate cation is not an appropriate explanation of the photolysis. Consequently, the reactive site must be the bond between carbons 5 and 6 in the 1,10-phenanthroline ring. The width and structure of the g = 2.16 signal implies that the unpaired electron is delocalized. A hyperfine splitting of ~18 G was resolved for the tris complexes. Further, the slow decay of the radical signal above the glass point implies that the radical moiety is large.

Symons and Townsend[17] irradiated ethanol glasses containing photochemically active compounds and observed the glasses to be paramagnetic, violet, and to contain a single broad absorption with a maximum at 517 nm. This spectrum was attributed to the production of $CH_3\dot{C}HOH$ from ethanol by hydrogen atom abstraction. The uv-visible spectrum determined for the $[Rh(phen)_3]^{3+}$ contains three peaks in the 520-nm region contrasting with the single peak observed by Symons and Townsend and therefore cannot be due only to solvent photolysis.

Siegel, *et al.*, concluded that the solvent radicals are formed by a two-photon process involving a long-lived triplet intermediate.[13,14] The dependence of the solvent radical production here upon the excitation intensity is consistent with this two photon mechanism. Siegel and Eisenthal[13] have utilized the Δm = 2 esr signal to measure directly the triplet-state concentration of a napthalene solute (τ = 2.3 sec) with alcohol, ether, and hydrocarbon solvent. They obtained a 1.5 to 2.5 lamp intensity dependence. The absence of any excited-state esr signal for these samples precludes such a technique here. However, lamp intensities, sample volumes, and concentrations used here are comparable to those described by Siegel and Eisenthal. The shorter lifetimes of these metal chelate solutes is compensated by the increased irradiation efficiency of the esr cavity utilized for these experiments. Therefore, the approach of the intensity dependence of the solvent radical production to 1 (Table II) suggests, as for the napthalene solute, that a large fraction of the molecules have been excited to the triplet state. Since the solvent radical production rate is proportional to the triplet population, it is proportional to the lifetime of emitting triplet state (chelate and/or solvent impurity). The solvent radical intensities are qualitatively consistent with the triplet lifetimes of the metal chelates (Table III). The magnitude of the solvent radical growth rate for the pure solvent implies that the emission lifetime of the impurity in the solvent is greater than 100 msec. An aromatic π–π^* phosphorescence typically has a lifetime of 1 sec magnitude or longer.[18] In concentrated (greater than 10^{-3} M) metal chelate solutions, energy transfer from the solvent impurity emitting state to that of the emitting state in

(13) S. Siegel and K. Eisenthal, *J. Chem. Phys.*, **42**, 2494 (1965).
(14) H. S. Judeikis and S. Siegel, *ibid.*, **43**, 3625 (1965).
(15) K. D. Cadogan and A. C. Albrecht, *ibid.*, **43**, 2550 (1965).
(16) H. Pilloff and A. Albrecht, *ibid.*, **49**, 4891 (1968).
(17) M. C. R. Symons and M. Townsend, *ibid.*, **25**, 1299 (1957).
(18) J. C. Calvert and J. N. Pitts, "Photochemistry," Wiley, New York, N. Y., 1968.

the metal chelate is likely. The metal chelate lifetime would then determine the radical production.

The solvent radical attack upon the C_5–C_6 bond may occur in either the ground or the excited triplet state of the solute. Extinction of the excitation source quenches production of both the solvent and the metal radicals and therefore produces no evidence for or against direct solute triplet state participation in production of the metal radical. The *ratio* of the metal to the solvent radical concentration is the same for the tris and bis phen complexes, although the triplet lifetimes are markedly different. This implies that the rate of formation of the metal radical by solvent radical attack is independent of the solute excited triplet concentration. Secondly, the bis and tris Rh(III) complexes produce the metal radical although the luminescent triplet for the tris complex is *delocalized orbital* ($\pi \rightarrow \pi^*$) while that of the bis complex is a *metal localized* orbital (d–d).[8] These two facts suggest that the solvent radical does not attack the chelate in the triplet state. The absence of an esr signal for the photolyzed $[Ir(phen)_2Cl_2]^{1+}$ sample may be due to quadrupole broadening ($I = {}^3/_2$ for ^{191}Ir, ^{193}Ir). The weak metal radical signal observed for the $[Rh(dip)_2(phen)]^{3+}$ complex can be explained if the solvent radical attack in the glassy solution involves a cage reaction with nearest-neighbor solvent molecules. The emission spectrum and lifetime of this mixed ligand complex suggest that excited triplet may be localized on the dipyridyl ligands.[12] Such an excited state would activate nearest-neighbor solvent molecules and would produce fewer metal radicals since the 1,10-phenanthroline ligand would not be readily attacked by solvent radicals adjacent to the dipyridyl ligands.

Conclusion

The photolysis of $[Rh(phen)_3]^{3+}$ in alcohol glass solution produces a metal radical with the general structure (Figure 3). The attacking radical is likely $CH_3CHOH\cdot$, but $CH_3CH_2\cdot$, $CH_3CO\cdot$, or $CH_3\cdot$ may also attack. The CH_3CHOH radical is the primary

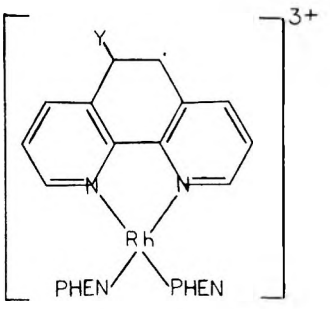

Figure 3. The proposed general structure (Y = CH_3CHOH, CH_3CH_2, CH_3, or CH_3CO) of the metal radical product of irradiated $[Rh(phen)_3]^{3+}$ in ethanol glass at 77°K.

solvent photolysis product and does dominate the free radical region of the esr spectrum.

A reaction sequence suggested by the data is given where M is a metal chelate, $M^*(S_1)$ is the metal chelate in an excited singlet, $M^{**}(T_1)$ is the metal chelate in the excited triplet, and M^{***} is the chelate in an undefined high-energy state capable of transferring energy to the solvent for radical decomposition. R is an alkyl group.

$$M + h\nu_1 \longrightarrow M^*(S_1) \quad (1)$$

$$M^*(S_1) \longrightarrow M^{**}(T_1) \quad (2)$$

$$M^{**}(T_1) + h\nu_1 \longrightarrow M^{***} \quad (3)$$

$$M^{***} + ROH \longrightarrow M + RO\cdot + H\cdot \quad (4)$$

$$RO\cdot \longrightarrow R' + R''O\cdot \quad (4a)$$

or

$$RO\cdot \longrightarrow R'\cdot + R''O \quad (4b)$$

$$RO\cdot + M \longrightarrow \dot{M}\text{–}OR \quad (5)$$

or

$$R'\cdot + M \longrightarrow M\text{–}\dot{R} \quad (5a)$$

or

$$R''O\cdot + M \longrightarrow M\text{–}R''O\cdot \quad (5b)$$

Matrix Reactions of Fluorohalomethanes with Alkali Metals: Infrared Spectrum and Bonding in the Monofluoromethyl Radical

by James I. Raymond and Lester Andrews*

Chemistry Department, University of Virginia, Charlottesville, Virginia 22901 *(Received June 7, 1971)*

Publication costs borne completely by The Journal of Physical Chemistry

When CH_2FBr diluted in argon is codeposited with a beam of atomic lithium at 15°K, the free radicals CH_2F and CH_2Br are stabilized in sufficient concentration for observation of several infrared absorptions. Studies utilizing CD_2FBr and CH_2FCl help confirm the spectral identity of the monofluoromethyl free radical. The new absorptions are assigned to the symmetric C–F stretching vibration of the CH_2F and CD_2F radicals, and the DCD bending mode of CD_2F. The vibrational potential function giving the best fit of symmetric vibrational frequencies is determined and bonding in CH_2F is discussed.

Introduction

The monofluoromethyl radical has been postulated as a chemical intermediate. CH_2F has been produced for kinetic studies by the reactions of Na with CH_2FCl[1] and Br with CH_3F.[2] The esr spectrum[3] of CH_2F has been observed in krypton and xenon matrices near liquid nitrogen temperature following 2.8-MeV electron irradiation of CH_3F. In this work, Fessenden and Schuler[3] observed ^{13}C hyperfine splittings which enabled them to determine the pyramidal angle (θ) to be about 5° or less. Two subsequent[4,5] molecular orbital calculations have suggested that the CH_2F radical is slightly nonplanar. Recent matrix studies of the vacuum-ultraviolet photolysis[6] of CH_3F have yielded species identified as CH_2F in addition to CF and HCF. Matrix reactions of alkali metal atoms with CH_2ClX and CH_2BrX precursors in this laboratory[7,8] have yielded the CH_2Cl and CH_2Br free radicals. To understand the bonding and structure in these radicals, further studies of CH_2F have been done using the matrix reaction of CH_2FX with alkali metals. A detailed description of these experiments follows.

Experimental Section

The cryogenic refrigeration system, alkali atom source, and experimental technique have been described in detail.[9] Isotopically enriched samples of lithium metal, 99.99% ^7Li and 95.6% ^6Li, 4.4% ^4Li (ORNL), and sodium metal (J. T. Baker, lump) were used without purification. Bromofluoromethane was synthesized by the Hunsdiecker method as described by Haszeldine.[10] The reaction was carried out in iron pipe (3 ft of 0.25 in. pipe connected to 3 in. of 0.5 in. pipe) equipped with a pressure gauge and a needle valve for venting off the gaseous product into a liquid nitrogen cooled trap. The silver salt precursor (silver monofluoroacetate) was prepared by dissolving sodium monofluoroacetate in ice–water and stirring in an equimolar amount of silver nitrate. The insoluble product was separated by filtration and dried for 24 hr *in vacuo*. A 11.0-g (0.060 mol) sample of the silver salt was placed in the reaction apparatus and cooled to liquid nitrogen temperature. Bromine 10.5 g (0.065 mol), was added to the salt, and the vessel was sealed and evacuated. Instantaneous reaction occurred at room temperature, the pressure rising to 150 psi. The gaseous product was vented into the receiver and purified by trap-to-trap distillation using an acetone slush. The yield was less than 10%. The bromofluoromethane-d_2 was prepared by deuterating the methylenic carbon of monofluoroacetamide in a basic methanol-*d* solution, converting back into the silver salt, and repeating the previously described reaction sequence. Mass spectra showed the fractionated product to be a 2:1:1 mixture of the dideuterio-, monodeuterio-, and hydrogen bromofluoromethanes, respectively. Iodofluoromethane was synthesized by reacting stoichiometric quantities of methylene iodide and crystalline mercuric fluoride in a glass apparatus. The reaction mixture was heated to 150° and then recooled quickly to room temperature. The liquid residue remaining in the pot was fractionated on a vacuum line, and samples were prepared immediately from these

(1) J. F. Reed and B. S. Rabinovitch, *J. Phys. Chem.*, **61**, 598 (1957).

(2) A. M. Tarr, J. W. Coomber, and E. Whittle, *Trans. Faraday Soc.*, **61**, 1182 (1965).

(3) R. W. Fessenden and R. H. Schuler, *J. Chem. Phys.*, **43**, 2704 (1965).

(4) K. Morokuma, L. Pedersen, and M. Karplus, *ibid.*, **48**, 4801 (1968).

(5) D. L. Beveridge, P. A. Dobosh, and J. A. Pople, *ibid.*, **48**, 4802 (1968).

(6) M. E. Jacox and D. E. Milligan, *ibid.*, **50**, 3252 (1969).

(7) L. Andrews and D. W. Smith, *ibid.*, **53**, 2956 (1970).

(8) D. W. Smith and L. Andrews, *ibid.*, in press.

(9) L. Andrews, *ibid.*, **48**, 972 (1968).

(10) R. N. Haszeldine, *J. Chem. Soc.*, 4259 (1952).

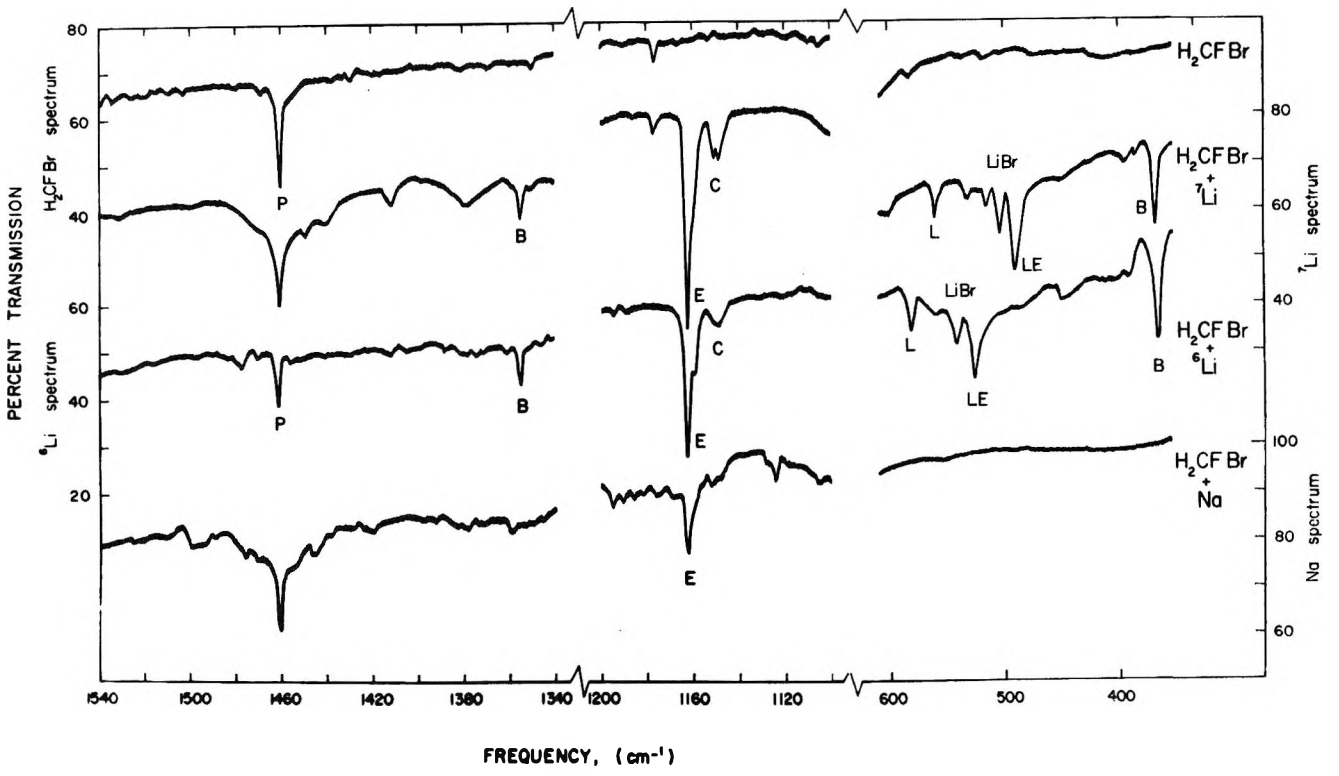

Figure 1. Infrared spectra in the 1340–1540-, 1100–1200-, and 350–600-cm^{-1} spectral region for CH_2FBr in argon (M/R = 200:1) deposited at 15°K without alkali metal, deposited with ^7Li (matrix/alkali = M/A = 200:1), deposited with ^6Li (M/A = 200:1), and deposited with Na (M/A = 200:1).

purified cuts. The infrared spectrum showed the product to be pure iodofluoromethane with small amounts of 1,2-difluoroethane and methylene iodide as the major impurities. Chlorofluoromethane (DuPont, Fluorocarbon 31), methylene fluoride (DuPont, Fluorocarbon 32), and argon (Air Products, 99.995%) were used without purification.

Samples of bromofluoromethane, chlorofluoromethane, iodofluoromethane, and methylene fluoride in argon (matrix/reactant = M/R = 200:1) were codeposited with an atomic beam of lithium or sodium (matrix/alkali = M/A = 200:1) on a cesium iodide window maintained at 15°K. Deposition times ranged from 18 to 24 hr. Infrared spectra were recorded during and after deposition using a Beckman IR-12 filter-grating spectrophotometer in the 200–4000-cm^{-1} spectral region. Frequency accuracy is ±0.5 cm^{-1}, and spectral slit widths are 0.8 cm^{-1} at 1100 cm^{-1} and 900 cm^{-1}, 0.9 cm^{-1} at 700 cm^{-1}, and 2.1 cm^{-1} at 500 cm^{-1}.

Results

Bromofluoromethane with Alkali Metals. The gas phase spectrum of CH_2FBr, previously unreported, compared favorably with the spectrum of CH_2FCl gas[11] and CH_2FBr isolated in an argon matrix. The spectra obtained after reaction of ^6Li and ^7Li (M/A = 200:1) with CH_2FBr (M/R = 200:1) were compared with the spectrum of CH_2FBr deposited without the metals. Several new absorptions were present after reaction with lithium which were not present in experiments without Li. Weak new absorptions occurred at 521.2, 504.2, 837.9, and 843.0 cm^{-1} in the ^7Li experiments and at 541.4, 887.6, and 891.5 cm^{-1} in the ^6Li experiments. The 521.2- and 504.2-cm^{-1} bands agree with argon matrix values for the ^7LiBr monomer and the 541.4-cm^{-1} absorption agrees with that of ^6LiBr monomer as reported by Schlick and Schnepp.[12] The bands at 837.9 and 843.0 cm^{-1} in the ^7Li runs and the bands at 887.6 and 891.5 cm^{-1} in the ^6Li experiments agree with the observed argon matrix frequencies for ^7LiF and ^6LiF, respectively.[13] The intensities of the LiF and LiBr are approximately comparable in individual experiments. Although precise data are not available concerning the concentration dependence of these intensities, it appears that more bromine than fluorine was abstracted. The very fact that fluorine abstraction competes with bromine abstraction indicates that the CF bond dissociation energy in the precursor may not be as great as empirically expected. Unfortunately, precise data concerning the bond dissociation energies are not available.

Other bands occurring for the Li–CH_2FBr–Ar sys-

(11) E. K. Plyler and M. A. Lamb, *J. Res. Nat. Bur. Stand.*, **45**, 204 (1950).

(12) S. Schlick and O. Schnepp, *J. Chem. Phys.*, **41**, 463 (1964).

(13) M. J. Linevsky, *ibid.*, **38**, 658 (1963).

Table I: Infrared Absorptions Resulting from the Deposition of H_2CFBr in Argon without Alkali Metal and with ^6Li, ^7Li, and Na[a]

Identification	H_2CFBr–no Li	H_2CFBr–^6Li	H_2CFBr–^7Li	H_2CFBr–Na
P	1460.0 (0.18)	1461.2 (0.089)	1460.0 (0.20)	1460.5 (0.16)
B		1355.9 (0.054)	1356.0 (0.044)	
P	1311.4 (1.2)	1312.0 (0.81)	1311.5 (1.3)	1311.8 (0.68)
CH_4	...	1306.0 (0.089)	1306.0 (0.066)	1306.5 (0.13)
P	1276.3 (0.084)	1277.1 (0.041)	1277.0 (0.066)	1277.2 (0.050)
P	1245.0 (0.057)	1245 (w)	1245 (w)	1244.6 (0.039)
P	1227.5 (0.23)	1227.2 (0.13)	1227.9 (0.17)	1227.6 (0.14)
E		1162.9 (0.33)	1162.8 (0.35)	1163.0 (0.090)
		1159.3 (sh)		
C		1151.6 (0.049)	1151.0 (0.055)	
U				1125.1 (0.026)
U				1100.0 (0.034)
U				1080.5 (0.21)
$(CH_2F)_2$			1078.9 (0.085)	
P	1059.9 (0%T)	1059.9 (0%T)	1059.9 (0%T)	1059.9 (1.2)
P	1046.3 (0.88)	1046.2 (0.51)	1046.4 (0.33)	1046.5 (0.52)
U		950.0 (0.049)		
LiF		891.5 (0.045)	843.0 (0.067)	
		887.6 (0.070)	837.9 (0.11)	
B		693.4 (0.078)	693.5 (0.067)	
P	641.7 (0%T)	642.0 (0%T)	642.2 (0%T)	642.0 (0%T)
P	619.4 (0.19)	620.3 (0.080)	619.6 (0.13)	620.2 (0.15)
L		578.5 (0.087)	567.3 (0.050)	
LiBr			521.2 (0.078)	
		541.4 (0.072)	504.2 (0.062)	
U			533.7 (0.050)	
LE		525.5 (0.18)	491.3 (0.12)	
B		368.0 (0.23)	367.5 (0.10)	
NaBr				275.1 (0.043)

[a] Frequencies are expressed in cm^{-1} and optical densities (OD) are given in parentheses. All M/R and M/A = 200:1. sh = shoulder, w = weak; U = unidentified absorption; P = parent absorption.

tems are shown for selected spectral regions in Figure 1. All absorptions occurring in the 300–1500-cm^{-1} region along with their identifications are listed in Table I. Parent (CH_2FBr) absorptions are designated by the symbol P and unidentified absorbers by U. Several absorptions in the 500–600-cm^{-1} region show lithium isotope shifts and are identified as L and LE. It seems plausible that the 525.5-cm^{-1} band in the ^6Li experiment which shifts to 491.3 cm^{-1} in the ^7Li experiment is a Li–CH_2X species, probably $LiCH_2F$. Molecules of this type have previously been described by Andrews.[14,15] Another set of absorptions labeled L, 578.5 and 567.3 cm^{-1} in the -6 and -7 experiments, respectively, shows a lithium isotopic shift, but their identity has not been deduced. It is clear that bands showing a lithium isotopic shift cannot be due to an isolated free radical. The bands B, E, and C designated in the figure appeared when either ^6Li or ^7Li (M/A = 200:1) was allowed to react with CH_2FBr in argon (M/R = 200:1). The B absorptions, which occur at 1355.9, 693.4, 368.0 cm^{-1} and 1356.0, 693.5, 367.5 cm^{-1} in the -6 and -7 runs, respectively, are due to the CH_2Br radical.[8] The E bands appeared at 1162.9 (^6Li) and 1162.8 cm^{-1} (^7Li), and the C bands at 1151.6 (^6Li) and 1151.0 cm^{-1} (^7Li). In addition, an absorption at 1306.0 cm^{-1} was present in both lithium isotope experiments and is the argon matrix frequency of methane.[16]

When CH_2FBr was deposited simultaneously with Na, the band designated E was observed at 1163.0 cm^{-1} although the intensity was reduced (Figure 1, Table I). Another weak absorption was present only in the Na experiments at 275.1 cm^{-1} and has been assigned to the argon matrix frequency of the NaBr monomer.[8] Three other bands exclusive to the sodium–bromofluoromethane experiment were found at 1125.1, 1100.0, and 1080.5 cm^{-1} and are labeled U in Table I, representing unidentified frequencies. The peaks previously noted as B and C are absent here, while the absorption attributed to methane (1306.5 cm^{-1}) was observed.

Sample-warming experiments were carried out for the ^7Li– and ^6Li–CH_2FBr–Ar experiments; the deposited samples were warmed to 35°K and then recooled to 15°K. The intensities of the B, E, and C absorptions decreased or disappeared entirely relative

(14) L. Andrews, *J. Chem. Phys.*, **47**, 4834 (1967).
(15) L. Andrews and T. G. Carver, *J. Phys. Chem.*, **72**, 1743 (1968).
(16) F. H. Frayer and G. E. Ewing, *J. Chem. Phys.*, **48**, 781 (1968).

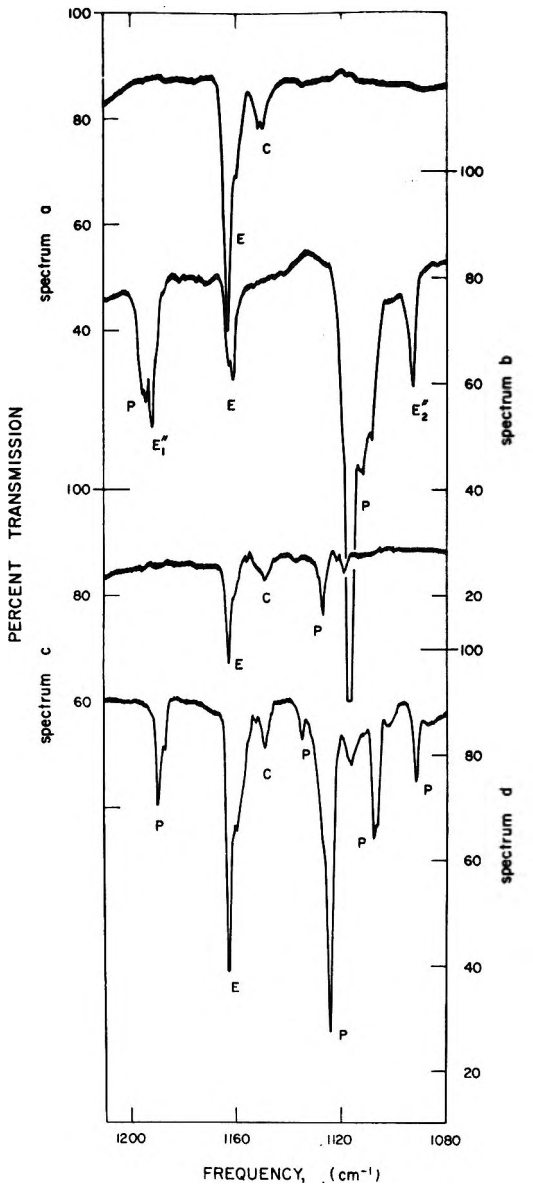

Figure 2. Infrared spectra in the 1080–1210-cm^{-1} region for the reaction of ^{7}Li (M/A = 200:1) with the following substituted methanes in argon (M/R = 200:1) deposited at 15°K: a, CH_2FBr; b, CD_2FBr; c, CH_2FCl; and d, CH_2FI.

to the unchanged parent absorptions. Owing to scattering conditions no quantitative data could be obtained. No new absorptions were observed after the diffusion experiments.

Chlorofluoromethane with Alkali Metals. When CH_2FCl (M/R = 200:1 in argon) reacted with the two lithium isotopes, several new absorptions appeared which were common to both expriments. Figure 2 shows the 1080–1210-cm^{-1} spectral region for the ^{7}Li–CH_2FCl–Ar system and Table II lists absorptions of interest for this reaction system, which occurred at 1390.8, 826.3, 820.4, and 396.6 cm^{-1}. In addition, absorptions at 1162.7 and 1149.3 cm^{-1} appeared which correspond to the E and C bands of the Li–CH_2FBr experiments. Weak unidentified absorptions (labeled U) are present at 1073.2 and 682.0 cm^{-1} for both ^{6}Li and ^{7}Li reactions with CH_2FCl. Two other sets of medium intensity peaks occurred at 842.3 and 837.4 cm^{-1} in the ^{7}Li experiment and at 891.5 and 887.0 cm^{-1} in the ^{6}Li experiment. These correspond to the reported frequencies for ^{7}LiF and ^{6}LiF, respectively.[13] No LiCl absorptions were detected due to the low yield of this reaction.

When Na was deposited with a sample of CH_2FCl in argon, the only new absorption that appeared was a weak band at 1162.8 cm^{-1} (E), which is common to all of the preceding alkali metal–CH_2FBr and –CH_2FCl experiments.

Iodofluoromethane with Alkali Metals. When CH_2FI in argon (M/R = 200:1) was codeposited with ^{7}Li metal (Table II) an intense absorption appeared at 447.5 cm^{-1}, which is exclusive to this experiment; its assignment to ^{7}LiI follows.[17] The E and C absorptions at 1162.7 and 1148.5 cm^{-1} were present, but the E absorption was slightly more intense here than in the previous experiments utilizing the other halofluoromethanes as precursors. The E and C bands, at 1162.6 and 1149.2 cm^{-1}, respectively, were also found in the spectrum of the ^{6}Li–CH_2FI–Ar system.

Methylene Fluoride with Lithium. Difluoromethane in argon (M/R = 200:1) was deposited simultaneously with ^{7}Li (M/A = 200:1) for 20 hr. An analogous run was carried out using ^{6}Li (M/A = 200:1). No new absorptions appeared which could be attributed to lithium fluoride, the CH_2F radical, or other known species.

Bromofluoromethane-d_2 with Lithium. Several experiments were carried out depositing CD_2FBr (M/R = 200:1) in argon without Li, and with ^{6}Li (M/A = 200:1) and ^{7}Li (M/A = 200:1). The spectrum of CD_2FBr, though unreported in the literature, appears reasonable in comparison to the spectrum of its analog, CH_2FBr. The major impurities in the series of experiments were attributed to the incomplete deuteration of the bromofluoromethane. CH_2FBr and CDHFBr were present in equivalent amounts comprising a total of 50% of the starting material used to prepare the samples. Hereafter the use of the symbol CD_2FBr will refer to this 2:1:1 mixture just discussed. Figure 2 shows the 1080–1210-cm^{-1} spectral region for the reaction of ^{7}Li with the CD_2FBr, and Table II lists particular absorptions of interest for the ^{7}Li–CD_2FBr–Ar system.

When CD_2FBr (M/R = 200:1) in argon was codeposited with a beam of ^{7}Li (M/A = 200:1), the ^{7}LiF and ^{7}LiBr bands were again present in addition to two major new absorptions at 1191.4 and 1093.0 cm^{-1}, labeled E_1'' and E_2'', respectively. The band designated E in past experiments was apparent here as an

(17) L. Andrews and G. C. Pimentel, *J. Chem. Phys.*, 47, 3637 (1967).

Table II: Infrared Absorptions in the 1080–1210-cm^{-1} Region Plus Other Bands of Interest for the Matrix Reaction of Lithium-7 (M/A = 200:1) with H_2CFBr, D_2CFBr, H_2CFCl, and H_2CFI in Argon (M/R = 200:1) at 15°K[a]

Identification	ν, cm^{-1}	OD	Identification	ν, cm^{-1}	OD
	H_2CFBr			D_2CFBr[b]	
(B)	1356.0	(0.044)	(P)	1193.8	(0.15)
(E)	1162.8	(0.35)	(E_1'')	1191.4	(0.19)
(C)	1151.0	(0.055	(E)	1162.8	(0.10)
(^{7}LiF)	843.0	(0.067)		1161.2	(0.12)
	837.9	(0.11)		1117.2	(0%T)
(B)	693.5	(0.067)	(P)	1112.0 (sh)	
(^{7}LiBr)	521.2	(0.078)		1108.7 (sh)	
	504.2	(0.062)	(E_2'')	1093.0	(0.14)
(LE)	491.3	(0.12)	(D_2CBr)	1016.2	(0.040)
(B)	367.5	(0.10)	(^{7}LiF)	843.0	(0.11)
				837.5	(0.13)
			(^{7}LiBr)	504.2	(0.11)
			(LE, LE', LE'')	490.0	(0.23)
			(B)	367.0	(0.048)
			(DHCBr)	315 ± 2	(0.14)
			(D_2CBr)	262.6	(0.11)
	H_2CFCl			H_2CFI	
(H_2CCl)	1390.8	(0.074)	(P)	1189.1	(0.11)
(E)	1162.7	(0.12)		1186.5 (sh)	
(C)	1149.3	(0.028)	(E)	1162.7	(0.36)
(P)	1126.8	(0.063)	(C)	1148.5	(0.033)
(P)	1118.8	(0.023)	(P)	1135.0	(0.031)
(U)	1073.2	(0.18)	(P)	1124.2	(0.47)
(^{7}LiF)	842.3	(0.25)	(P)	1116.1	(0.034)
	837.4	(0.23)	(P)	1108.0	(0.12)
(H_2CCl)	826.3	(0.23)	(P)	1091.8	(0.070)
	820.4	(0.089)	(P,$(CH_2F)_2$)	1078.5	(0.54)
(U)	682.0	(0.029)	(^{7}LiI)	447.5	(0.20)
(H_2CCl)	396.6	(0.53)			

[a] ν are given in cm^{-1}; optical densities (OD) and band identification are given in parentheses. [b] Actually a 2:1:1 mixture, respectively, of D_2CFBr–$DHCFBr$–H_2CFBr.

absorption at 1161.2 cm^{-1} with a less intense side band at 1162.8 cm^{-1}. One of the previously noted B absorptions (367.0 cm^{-1}) occurred again but reduced in intensity. In addition to E_1'' and E_2'', several bands appeared at 1016.2, 490.0, 315 ± 2, and 262.6 cm^{-1}, which were absent from the alkali metal–CH_2FBr runs. The intense, broad 490-cm^{-1} absorption is labeled in Table II as LE, LE', LE''. This absorption is close in frequency to the 491.3-cm^{-1} (LE) band noted in the ^{7}Li–CH_2FBr–Ar system, and it is tentatively assigned to the substituted methyllithium compound ($LiCH_2F$). The corresponding broad absorption here is probably due to the three possible species, *i.e.*, $LiCH_2F$, LiCHDF, and $LiCD_2F$. The 1016- and 263-cm^{-1} bands are due to CD_2Br and the 315-cm^{-1} feature arises from CHDBr.[8]

When ^{6}Li (M/A = 200:1) was deposited with CD_2FBr (M/R = 200:1), the absorptions at 1191.4 (E_1'') and 1093.0 cm^{-1} (E_2'') were observed in addition to both lithium-6 halide monomers. All of the other previous new absorptions noted for the ^{7}Li–CD_2FBr–Ar system were present, with the exception of the 490.0-cm^{-1} band which was shifted to 525.0 cm^{-1}.

Discussion

The task at hand is to identify absorptions which can be attributed to the monofluoromethyl free radical and use these data to provide information about its structure and vibrational potential function.

Monofluoromethyl Identity. The observation of weak bands corresponding to LiBr in the Li–CH_2FBr and –CD_2FBr experiments indicates that the free radicals CH_2F and CD_2F are likely products. The absorption designated E (1162.8 cm^{-1}), which is found in all the experiments utilizing CH_2FBr, CH_2FCl, and CH_2FI as precursors, shows no shift when the two lithium isotopes are used. The band is also observed in the two lithium-6 and -7 experiments with CD_2FBr, though the intensity of the absorption is reduced by three-quarters. (It should be recalled that the CD_2FBr sample used was in actually a 2:1:1 mixture, respectively, of CD_2FBr, HCDFBr, and CH_2FBr.) Similarly, when sodium is substituted for lithium and allowed to react with CH_2FBr and CH_2FCl, the 1163-cm^{-1} (E) absorption again appears though less intensely than in the case of the lithium isotopic experiments. Thus, the absorber

responsible for E likely contains no alkali metal atom since the position of the band is invariant with the mass of the alkali metal used in the experiment. It seems reasonable therefore to suggest that the CH_2F free radical is responsible for the absorption designated E. In addition, the observation of an absorption at 1079 cm^{-1} in the ^7Li–CH_2FBr experiment identified as $(CH_2F)_2$ is consistent with production of CH_2F by the matrix reaction. Jacox and Milligan,[6] using vacuum ultraviolet photolysis of methyl fluoride in argon, have in fact observed a band at 1163 cm^{-1} and assigned it to the free radical CH_2F.

The weak absorptions labeled C which occur when ^6Li and ^7Li are deposited with CH_2FBr, CH_2FCl, and CH_2FI appear in close proximity to the absorption assigned to CH_2F. The C bands maintain approximately constant relative intensity with the radical absorptions. An absorption in this region is totally lacking in the Na experiments with these precursors. It seems reasonable that the bands are likely due to an LiBr–CH_2F complex in the case of the CH_2FBr reactant, and LiCl–CH_2F in the case of CH_2FCl, and an LiI–CH_2F complex for the CH_2FI precursor. The small spectral shift (*ca.* 10 cm^{-1}) between the radical fundamental and the complex frequency is probably due to the fact that the lithium halide perturbation is small and produces only a small change in the frequency for this motion.

When CD_2FBr is codeposited with Li two identical bands labeled E_1'' and E_2'' appear in each isotope experiment at 1191.4 and 1093.0 cm^{-1}, respectively. Assignment of these absorptions to the CD_2F free radical in the present work confirms the previous[6] choice of assignments to C–F modes of DCF (1183 cm^{-1}) and D_2CF (1191 cm^{-1}) based on an argon–nitrogen matrix shift argument.

Vibrational Assignment. The ^{13}C hyperfine esr spectrum of CH_2F has been interpreted by Fessenden and Schuler[3] to indicate that the pyramidal angle θ is about 5° or less. Recent molecular orbital calculations[4,5] have suggested that the CH_2F radical is slightly nonplanar. Group theoretical notations for the slightly nonplanar C_s structure will be used.

CH_2F has six infrared active vibrational modes for the C_s or C_{2v} structure. The symmetric C–H stretch $\nu_1(a')$ has not been observed here, probably due to its low intensity and greater sample scattering in the high-frequency spectral region. The symmetric HCH valence angle bending mode $\nu_2(a')$ has also escaped detection in spite of the careful search in the 1400–1600-cm^{-1} region. The CF stretching mode $\nu_3(a')$ is the assignment for the intense 1162.8-cm^{-1} feature observed here and previously.[6]

The out-of-plane bending modes for CH_2Cl and CH_2Br, which are believed to be planar radicals,[7,8] are observed at 397 and 367 cm^{-1}. If CH_2F were planar, its out-of-plane mode could reasonably be expected in the 400–500-cm^{-1} region. An intensive study of the 400–600-cm^{-1} range reveals no symmetric bending mode $\nu_4(a')$. In previous studies[7] of lithium matrix reactions with CH_2ClBr, the LiBr product absorption is approximately as intense as the out-of-plane mode of CH_2Cl. In the lithium reaction with CH_2FBr, the out-of-plane mode of CH_2Br is about twice as intense as the LiF product. Hence, the out-of-plane bend for a planar CH_2F is reasonably expected to be at least comparable in intensity with the product LiBr absorption (0.08 OD in several CH_2FBr experiments). The fact that no such band is observed for CH_2F may suggest that it is slightly nonplanar which should affect the position, nature, and intensity of this normal mode.

No other features are produced by the alkali metal reaction which could be due to the antisymmetric (a'') modes of CH_2F. The 940–1020-cm^{-1} spectral region is free of absorption in these experiments. The weak band at 996 cm^{-1} tentatively assigned to CH_2F by Jacox and Milligan[6] must be due to some other photolysis product or impurity in their sample. The 1163-cm^{-1} absorption of these workers[6] appears to be about 0.12 OD, a somewhat lower yield than the 0.36 OD produced in the present work.

Of the two new absorptions observed following the reaction of CD_2FBr with lithium atoms, the 1191-cm^{-1} feature is assigned to $\nu_3(a')$ the C–F stretch and the 1093-cm^{-1} band is assigned to $\nu_2(a')$ the D–C–D valence angle bend. This latter assignment is supported by the observation of the analogous modes[7,8] of CD_2Cl, CD_2Br, and CD_2I at 1045.0, 1016.0, and 994.5 cm^{-1}. The shift of the C–F mode to higher frequency following deuteration is due to interaction between ν_2 and ν_3 whose frequency ordering reverses following deuteration. This phenomenon has been observed for difluoromethyl[18] and fluoroform.[19] No other bands are observed which can be assigned to CD_2F presumably due to their low intensity relative to the bands observed here.

Force Constant Calculations. One of the purposes for this work was to determine the CF stretching force constant of CH_2F. A reasonably good approximate C–F force constant can be determined using the FG matrix method with symmetry coordinates and the following assumptions. For the nonplanar radical the a' symmetry block contains four modes. The highest frequency C–H mode is clearly separable to an excellent approximation. The lowest frequency vibration ν_4 is of a different symmetry if the radical is planar and is rigorously separable under this condition. However, for the slightly nonplanar radical interaction of ν_4 with ν_2 and ν_3 should be approximately negligible due to the almost planar geometry and the expected lower frequency of ν_4 (which may fall between CH_3 (611 cm^{-1}) and CH_2Cl (397 cm^{-1}).

(18) T. G. Carver and L. Andrews, *J. Chem. Phys.*, **50**, 5100 (1969).

(19) V. Galasso, G. de Alti, and G. Costa, *Spectrochim. Acta*, **21**, 699 (1965).

Calculations were done using the program FADJ for the a′ symmetry block using 120° bond angles, where ν_4 is rigorously separable, C–H bond lengths of 1.079 Å and a C–F bond length of 1.36 Å. Since the symmetric H–C–H mode of CH_2Cl is observed at 1391 cm^{-1}, this provides a lower limit for ν_2 of CH_2F.

The ratio of this mode for (CH_2Cl/CD_2Cl) is 1.332 which predicts that ν_2 of CH_2F is 1458 cm^{-1}, based on ν_2 of CD_2F (1093 cm^{-1}). However, this latter mode is shifted to lower frequency by interaction with ν_3 of CD_2F, hence a higher value of ν_2 of CH_2F is expected, perhaps near 1485 cm^{-1}. Calculations were performed for estimated CH_2F ν_2 frequencies of 1485, 1515, 1545, 1575, and 1605 cm^{-1}. Symmetry coordinate force constants F_{11}, F_{12}, F_{13} were fixed at 5.38, 0.0, and 0.0 mdyn/Å as in the calculations for CH_2Cl.[7] For this range of CH_2F ν_2 frequencies, the average difference between calculated and observed frequencies is 18.6, 12.7, 6.8, 1.0, and 6.8 cm^{-1}. Clearly the 1605-cm^{-1} estimate of ν_2 is too high since the frequency fit is poorer and frequency departure from harmonic is not in the correct direction for a cubic anharmonic term. For all of these calculations the C–F force constant varies from 6.73 to 6.46 mdyn/Å. We feel that 1515 cm^{-1} represents the best estimate of ν_2 for CH_2F. Table III lists these potential constants with limits influenced by the estimate of ν_2 for CH_2F.

Table III: Potential Constants for the Symmetric Block of CH_2F Assuming a Planar Structure

	Frequencies, cm^{-1}		
	CH_2F	CD_2F	Potential constants[a]
ν_2	1515 ± 30	1093.0	F_{11} = 5.38
ν_3	1162.8	1191.0	$F_{12} = F_{13}$ = 0.0
			F_{22} = 6.64 ± 0.15
			F_{23} = −0.57 ± 0.02
			F_{33} = 0.76 ± 0.05

[a] Units: F_{11}, F_{22} mdyn/Å, F_{23} mdyn/rad, F_{33} mdyn Å/rad².

Precursor Reactivity. It is of chemical interest to compare the reactivities of the precursors CH_2F_2, CH_2FCl, CH_2FBr, and CH_2FI with lithium and sodium atoms. The matrix reaction of lithium with CH_2F_2 produced no detectible CH_2F or LiF. Lithium atoms reacted preferentially with the fluorine in CH_2FCl producing an intense LiF band (0.25 OD), and no detectable LiCl although some CH_2F was observed in addition to an excellent yield of CH_2Cl. For the CH_2FBr reaction with lithium atoms, comparable LiBr and LiF absorptions (0.08 OD) were observed along with CH_2F and CH_2Br radicals. Reaction of lithium with CH_2FI yielded only LiI and CH_2F. No CH_2I or LiF were detected with the CH_2FI reaction. The sodium atom reaction with CH_2FCl yielded only a weak (0.02 OD) CH_2F band. Similarly, the sodium reaction with CH_2FBr yielded only CH_2F (0.07 OD). A contrasting piece of data is the earlier reaction of CCl_3F with lithium atoms in this laboratory,[20] which yielded only LiCl and CCl_2F with no detectible LiF or CCl_3 radical. The reaction of CH_2ClBr with lithium and sodium yielded almost completely CH_2Cl and the alkali metal bromide.

The lack of fluorine abstraction by lithium from CH_2F_2 is not surprising due to the strength of CF bonds particularly when two fluorines are bonded to the same carbon (C–F length is 1.358 Å).[21] In spite of the weaker C–F bond in CCl_3F (C–F length is 1.40–1.44 ± 0.04 Å), the chlorines are apparently irresistible to lithium. In view of these facts, it is perhaps surprising that lithium abstracts fluorine from CH_2FCl (C–F length is 1.378 Å) and CH_2FBr.

Using single fluorine, chlorine, and bromine carbon bond dissociation energies of 107, 80, and 67 kcal/mol and alkali metal halide bond energies from Vedeneyev, *et al.*,[22] the lithium abstraction reactions of F, Cl, and Br are each exothermic by 33 ± 3 kcal/mol. However, the abstraction of F by Na is less exothermic than Cl or Br abstraction by about 12 kcal/mol, which justifies the preference of Cl or Br abstraction over F abstraction by sodium.

Perhaps accurate C–F and C–Cl bond dissociation energies for the CH_2FCl molecule will yield a slight thermodynamic preference for decomposition of a 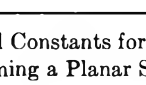

activated complex into CH_2Cl + LiF. This is suggested by bond lengths in CH_2FCl where C–Cl is 1.759 ± 0.003 Å, shorter than in CH_2Cl_2 (1.7724 ± 0.0005 Å) and C–F in 1.378 ± 0.006 Å, longer than CH_2F_2 (1.358 ± 0.001 Å). Also pertinent is the fact that CH_2Cl may exhibit more electronic stabilization (4 ± 1 kcal/mol) than CH_2F (2 ± 1 kcal/mol), which may enhance the rate of decomposition of the transition state $H_2CFCl\cdots Li$ into CH_2Cl and LiF as opposed to CH_2F and LiCl.

Clearly major factors affecting the decomposition of the $H_2CXY\cdots M$ transition state are the alkali–X (or Y) bond strengths relative to carbon–X (or Y) and the electronic stabilization of the radical CH_2X (or Y). We suggest that the electronic stabilization of CH_2F is about 2 kcal/mol less than CH_2Cl and CH_2Br which is influencial in fluoride abstraction from the CH_2ClF and CH_2BrF molecules.

Conclusions

The potential constants of monofluoromethyl were determined for their reflections on the bonding in this free radical.

(20) L. Andrews, unpublished results.

(21) Bond lengths from L. E. Sutton, *Chem. Soc. (London), Spec. Publ.*, No. 11 (1958).

(22) V. I. Vedeneyev, L. V. Gurvick, V. N. Kondrat'yev, V. A. Medvedev, and Y. L. Frankevich, "Bond Energies," E. Arnold, London, 1966.

Potential Constants. Bending Force Constants. The H–C–H symmetric bending force constant for CH_2F is $0.76 \pm 0.05 \times 10^{-11}$ erg/rad^2, which is slightly higher than that for CH_2Cl (0.62 ± 0.01) and near values for other CH_2 groups.[7] The C–F stretch, H–C–H bending interaction force constant $(-0.57 \pm 0.02) \times 10^{-3}$ dyn/rad is somewhat higher than that for CH_2Cl (-0.32 ± 0.02),[7] which is no surprise since these modes interact more for CH_2F and CD_2F due to their close proximity. The negative sign has been rationalized in terms of hybridization.[7]

C–F Force Constant. The C–F force constant deduced here for CH_2F (6.64 ± 0.15 mdyn/Å) exceeds that for CH_3F (5.79 mdyn/Å).[23] Comparison to methylene fluoride[24] and fluoroform[19] is less meaningful due to the well-known strengthening of C–F bonds as the number of such bonds to a single carbon is increased from one to four. Since CH_2F is nearly planar, fluorine bonded to an sp^2-hybridized carbon is expected to have a higher force constant than its sp^3 counterparts. The possibility of additional strengthening of the C–F bond in CH_2F will be discussed below.

Bonding in Fluoromethyl Radicals. Comparison of the bond dissociation energies and ionization potentials in Table IV indicates that no electronic stabilization is present in CF_3 relative to CH_3, in direct contrast to the observations for CCl_3. In spite of difficulties[25] in calculating reliable potential functions for AX_3 molecules, the reported C–F force constant[26] for CF_3 is consistent with the absence of electronic stabilization as discussed earlier.[18] The data of Table IV for CHF_2 suggest a small amount of electronic stabilization; however, the C–F force constant[18] for CHF_2 is not sufficiently accurate to attest this point.

The bond dissociation energies in Table IV suggest that 1–2 kcal/mol of electronic stabilization may be attributed to CH_2F. Some stabilization is indicated by the lower ionization potential of CH_2F relative to CH_3. Perhaps this small amount of electronic stabilization in CH_2F is responsible for the higher C–F force constant in CH_2F than in CH_3F.

For a planar or very nearly planar CH_2F radical, the p orbitals on carbon and fluorine perpendicular to the molecular plane are of appropriate symmetry to form bonding and antibonding π-molecular orbitals. Three electrons occupy these M.O.'s, two are bonding and one is antibonding, giving a net of one π-bonding electron for the C–F bond in addition to the σ bond. Such π bonding probably occurs in the isoelectronic OF radical whose force constant (5.40 mdyn/Å) is higher than in OF_2 (4.0 mdyn/Å).[27] Hence, π bonding in CH_2F could account for the electronic stabilization and increased C–F force constant. Clearly, departure from planarity decreases overlap of fluorine and carbon 2p orbitals for a fluoromethyl radical. Hence, the pyramidal[3] CF_3 radical (F–C–F = 111°) cannot be effectively stabilized by π bonding. Furthermore, the higher electronegativity of fluorine may reduce its participation in π bonding to a free radical carbon 2p orbital.

Table IV: Ionization Potentials and Bond Dissociation Energies Involving Fluoromethyl Radicals

R	D_{R-H}, kcal/mol	I_R, eV
CH_3	104.2 ± 0.7[a]	9.95[c]
CH_2F	≤ 102.8[b]	9.35
CHF_2	≤ 103.3[b]	9.45
CF_3	106.7 ± 0.5[a]	10.1

[a] J. C. Amphlett and E. Whittle, *Trans. Faraday Soc.*, **64**, 2130 (1968). [b] A. M. Tarr, J. W. Coomber, and E. Whittle, *ibid.*, **61**, 1182 (1965). [c] F. P. Lossing, P. Kebarle, and J. B. DeSousa, "Ionization Potentials of Alkyl and Halogenated Alkyl Free Radicals" in "Advances in Mass Spectroscopy," Pergamon Press, London, 1959. See also R. S. Neale, *J. Phys. Chem.*, **68**, 143 (1964).

Acknowledgments. The authors gratefully acknowledge financial support for this research by the National Science Foundation under Grant GP-8587. J. I. R. acknowledges fellowship support by the National Defense Education Act.

(23) J. Aldous and I. M. Mills, *Spectrochim. Acta*, **19**, 1567 (1963).
(24) A. G. Meister, J. M. Dowling, and A. J. Bielechi, *J. Chem. Phys.*, **25**, 941 (1956).
(25) I. W. Levin, *ibid.*, **47**, 4685 (1967).
(26) D. E. Milligan and M. E. Jacox, *ibid.*, **48**, 2265 (1968).
(27) L. Andrews and J. I. Raymond, *ibid.*, in press.

Spectroscopy of Titanium Oxide and Titanium Dioxide Molecules in Inert Matrices at 4°K

by N. S. McIntyre, K. R. Thompson, and W. Weltner, Jr.*

Department of Chemistry, University of Florida, Gainesville, Florida 32601 *(Received April 15, 1971)*

Publication costs assisted by the National Science Foundation

The lowest-lying $^3\Pi$ state of TiO has been observed as a weak system at 8406 Å in absorption in a neon matrix at 4°K. The ultraviolet bands recently observed by Pathak and Palmer in the gas phase and attributed to TiO have also been observed at 3100 Å in a neon matrix. As in the gas phase, the vibrational progressions seem to be due to two overlapping systems which are strongly perturbing each other so that a definite analysis for either $Ti^{16}O$ or $Ti^{18}O$ was not possible. The electronic transitions of TiO in the visible region have also been observed in krypton and xenon matrices. The infrared spectrum of trapped TiO_2 yields the stretching frequencies, and a bond angle of ~110° is obtained from Ti isotope splittings. An emission system of TiO_2 was observed at ~5300 Å, terminating in the ground state.

Introduction

The molecule TiO has been studied more thoroughly by optical spectroscopy than any other diatomic transition metal molecule. While the astrophysical importance of the molecule prompted earlier investigations,[1-5a] more recently theoretical calculations[6-9] have broadened the basis for a thorough understanding of the electronic structure of TiO.

Five band systems, two triplet (α, γ) and three singlet (β, δ, φ), have been rather thoroughly analyzed by gas phase emission spectroscopy.[10-13] These are indicated in Figure 1. Emission bands observed in the red-orange region[4] have been tentatively identified as arising from as many as three new systems.[14] One of these systems, γ', has been confirmed to be a triplet–triplet transition by its appearance, along with the α and γ bands, in the absorption spectrum of TiO trapped in solid neon and argon matrices.[15] Two singlet states, $^1\Delta$ and $^1\Sigma$, observed as lower levels in emission studies[11,12] are expected to lie close in energy to the $^3\Delta_r$ ground state,[7,8] and Phillips[16] has placed the lowest $^1\Delta$ level at about 581 cm^{-1} above the $X^3\Delta$. However, the accuracy of that number is probably low, and it must be considered as uncertain by at least several hundred wave numbers.

Spin-forbidden transitions, which would definitely locate the singlet manifold relative to the triplet manifold, have not been identified in the gas phase spectra. One might expect more ready relaxation of the spin selection rule in this heavier molecule than in many cases where such transitions have been observed.[17,18] It was hoped that these weak transitions could be observed in the less-crowded matrix spectra or that they could be induced to appear in the solid state.[19] For that reason the spectra of trapped TiO have here been measured over a greater energy range than in the previous work.[15] Also, the spectra have been observed in krypton and xenon matrices, where presumably the selection rules would be more easily broken down.[19] Although there are no definite indications of spin-forbidden transitions, two new allowed systems have been observed, one of which is the uv system recently detected by Pathak and Palmer.[20]

The molecule TiO_2 has also been studied more thor-

(1) A. Christy, *Phys. Rev.*, **33**, 701 (1929).

(2) F. Lowater, *Proc. Phys. Soc. (London)*, **41**, 557 (1927).

(3) K. Wurm and H. J. Meister, *Z. Astrophys.*, **13**, 199 (1936).

(4) F. P. Coheur, *Bull. Soc. Roy. Sci. Liege*, **12**, 98 (1943).

(5) (a) J. G. Phillips, *Astrophys. J.*, **111**, 314 (1950); **114**, 152 (1951); (b) see ref 17 for the spectroscopic symbolism used here.

(6) R. A. Berg and O. Sinanoglu, *J. Chem. Phys.*, **32**, 1082 (1960).

(7) K. D. Carlson and C. Moser, *J. Phys. Chem.*, **67**, 2644 (1963).

(8) K. D. Carlson and R. K. Nesbet, *J. Chem. Phys.*, **41**, 1051 (1964).

(9) K. D. Carlson and C. R. Clayton, "Advances in High Temperature Chemistry," Vol. 1, Academic Press, New York, N. Y., 1967, p 43.

(10) R. W. B. Pearse and A. G. Gaydon, "The Identification of Molecular Spectra," 3rd ed, Wiley, New York, N. Y., 1963.

(11) A. V. Petterson, *Ark. Fys.*, **16**, 185 (1959).

(12) A. V. Petterson and B. Lindgren, *ibid.*, **22**, 491 (1962).

(13) C. Linton and R. W. Nicholls, *J. Phys. B (Atom. Molec. Phys.)*, **2**, 490 (1969).

(14) B. Rosen, "4th International Meeting on Molecular Spectroscopy, 1959," Vol. 2, Pergamon Press, Elmsford, N. Y., 1962, p 533.

(15) W. Weltner, Jr., and D. McLeod, Jr., *J. Phys. Chem.*, **69**, 3488 (1965).

(16) J. G. Phillips, *Astrophys. J.*, **115**, 567 (1952).

(17) G. Herzberg, "Spectra of Diatomic Molecules," Van Nostrand, Princeton, N. J., 1950.

(18) G. Herzberg, *Mem. Soc. Roy. Sci. Liege, Collect. 8*, **17**, 121 (1968) (published 1969).

(19) G. W. Robinson, *J. Mol. Spectrosc.*, **6**, 58 (1961); *J. Chem. Phys.*, **46**, 572 (1967).

(20) C. M. Pathak and H. B. Palmer, *J. Mol. Spectrosc.*, **33**, 137 (1970).

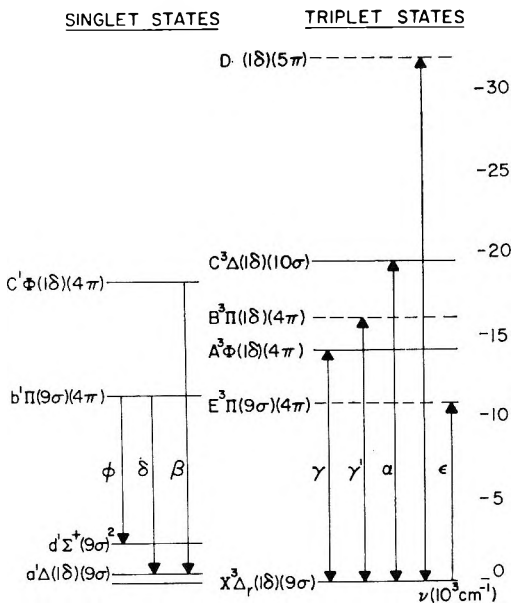

Figure 1. Known energy levels and observed transitions of TiO. Arrow heads indicate whether transitions were observed in emission or absorption or both. For discussion of dashed levels, see text. For symbolism used to indicate electronic configurations, see ref 28.

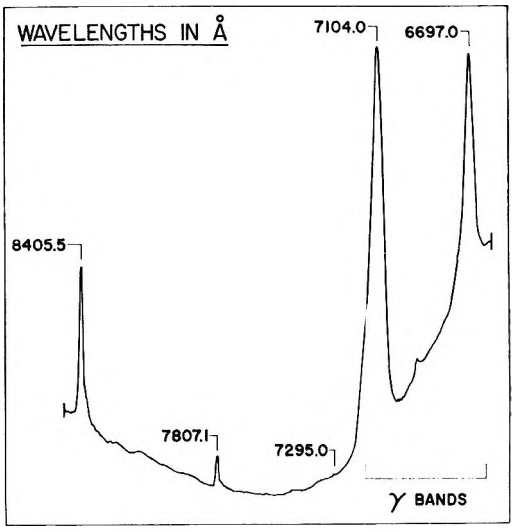

Figure 2. Absorption bands (ε system) of $Ti^{16}O$ in a neon matrix at 4°K.

oughly in the infrared, and an emission spectrum observed in the visible has been attributed to it.

Experimental Section

The design of the furnace and cryostat assemblies used in this work has been described previously.[15,21] A molecular beam of $Ti^{16}O$ was produced by the inductive or resistive heating of solid TiO_2 (Fisher reagent) in degassed tungsten or tantalum Knudsen cells at temperatures between 2200 and 2400°K. The beam was trapped on a CsI or CaF_2 window at 4°K along with neon or argon gas in a concentration of ~1:1000. $Ti^{18}O$ was prepared by passing $^{18}O_2$ (Miles-Yeda Ltd.) over an equimolar amount of powdered titanium (Spex Co.) at 1600°K in an inductively heated tungsten cell. High-purity neon, argon, and krypton gases (Linde) were precooled before deposition.

The condensed TiO_2 system was observed to react with tungsten above 1900°K to produce various complex tungsten oxides with vibrational spectra in the region 1020–650 cm^{-1} of the infrared spectrum.[22] The intensity of these absorptions could be reduced, but not eliminated, by heating the loaded cell at operating temperature for about 1 hr. The conditioned cell was then reloaded with fresh TiO_2 prior to the actual deposition. To identify unambiguously the new electronic transitions in TiO and TiO_2, the molecule was also evaporated from tantalum cells and the resultant tantalum oxide species were identified from an earlier matrix study of that system.[23]

Electronic transitions to states lying below 9000 Å in energy could be investigated using a CaF_2 prism interchange installed in a Perkin-Elmer 621 infrared spectrophotometer. The near-infrared region from 7000 to 10,000 Å could be scanned at higher resolution using a Jarrell-Ash Ebert spectrometer equipped with an RCA 7104 photomultiplier tube cooled to 77°K. The uv region (2000–3500 Å) was investigated using a deuterium lamp source and an RCA 7200 photomultiplier detector. Interchangeable gratings with blaze appropriate for each spectral region were calibrated with mercury emission lines. Emission of TiO_2 molecules in neon matrices was excited with an AH-6 high-pressure mercury lamp.

Results

I. Near-Infrared and Visible Absorption Spectra of TiO. The visible absorption spectrum of a transparent neon matrix containing TiO molecules evaporated at 2300°K included the three strong band systems described previously.[15] A strong infrared absorption at 997.2 cm^{-1} could be identified with the TiO $^3\Delta$ ground-state vibration frequency in the gas phase, $\Delta G_{1/2}'' = 1000.0$ cm^{-1}.[5] A new system of sharp absorption bands, labeled ε, was observed with (0,0) band at 8405.5 Å in neon (see Figure 2). The ε system, of lower overall intensity than the previously observed α, γ, and γ′ bands, also had a weaker (1,0) band than observed in previous systems. Table I lists band positions and vibrational analysis for both $Ti^{16}O$ and $Ti^{18}O$. The ratio of $\Delta G_{1/2}'(Ti^{18}O)/\Delta G_{1/2}'(Ti^{16}O) = 0.9539$ is in good agreement with the calculated $\nu'(Ti^{18}O)/\nu'(Ti^{16}O) = 0.9574$.

(21) W. Weltner, Jr., "Advances in High Temperature Chemistry," Vol. 2, Academic Press, New York, N. Y., 1970, p 85; *Science*, **155**, 155 (1967).

(22) W. Weltner, Jr., and D. McLeod, Jr., *J. Mol. Spectrosc.*, **17**, 276 (1965).

(23) W. Weltner, Jr., and D. McLeod, Jr., *J. Chem. Phys.*, **42**, 882 (1965).

Table I: Infrared Absorption Bands of TiO in Neon and Argon Matrices at 4°K (ϵ System)

	Neon						Argon		
	$Ti^{16}O$			$Ti^{18}O$			$Ti^{16}O$		
v′	λ, Å	ν, cm^{-1}	$\Delta G_{v+1/2}'$, cm^{-1}	λ, Å	ν, cm^{-1}	$\Delta G_{v+1/2}'$, cm^{-1}	λ, Å	ν, cm^{-1}	$\Delta G_{v+1/2}'$, cm^{-1}
0	8405.5	11,894		8403.0	11,897		8394	11,910	
			911			870			910
1	7807.1	12,805		7830.7	12,767		7798	12,820	
			899						
2	7295.0	13,704							

$Ti^{16}O$ in argon gives a relatively strong band at 8394 Å and weaker ones at 8297, 8166, and 7798 Å. The 8394-Å band does appear to be the counterpart of the 8406-Å band in neon so that the 7798-Å band could be assigned as indicated in Table I. However, without the neon results, one would find such an interpretation of the argon spectrum rather dubious. There are also some bands in that region of the krypton spectrum, but an assignment is even more doubtful there.

Although the γ bands in neon and argon matrices are quite distinct and easily assigned in krypton and xenon, there is anomalous absorption in that region. The two spectra are rather similar, each showing only two definite bands, one relatively weak and the other strong and rather broad. The weaker band is at 6975 Å in krypton and at 7097 Å in xenon, and it seems likely that it is the (1,0) bands of the γ system. The (0,0) bands would then lie at ~7360 and ~7580 Å in krypton and xenon, respectively, about where one would expect them to be shifted in these heavier matrices. There appears to be strong very broad background absorption in this region which does not occur in the lighter matrices. The two stronger bands occur at 6660 Å in krypton and 6797 Å in xenon and are not assignable to any of the three allowed systems, γ, γ', or α. This could be a desired singlet ← triplet absorption, but there is no confirming evidence other than the possible intensity enhancement in the heavier matrices. The (1,0) bands for these transitions would lie at about the (0,0) positions of the γ' system.

The progressions in the γ' system and especially the stronger α system are easily observed in the heavier matrices. All of the observed bands of TiO in krypton and xenon matrices are listed in Table II.

II. Ultraviolet Absorption Spectrum of TiO. The ultraviolet absorption spectrum of a neon matrix containing TiO had a series of strong absorption bands in the spectral region from 3200 to 2600 Å. The major portion of the spectrum is shown in Figure 3. The spectrum has the shape of a broad Franck–Condon envelope with individual bands spaced about 500 cm^{-1} apart and with increased complexity at the blue end of the spectrum. As Figure 3 indicates subtitution of ^{18}O resulted in considerable alteration of the general appearance of the system, as well as shifts in individual band positions.

Table II: Absorption Bands of TiO in Krypton and Xenon Matrices at 4°K

	Krypton[a]		Xenon[a]	
System	λ, Å	ν, cm^{-1}	λ, Å	ν, cm^{-1}
γ (1,0) ?	6926	14,434	7118	14,045
?	6697	14,928	6829	14,639
?	6644	15,047		
γ' (0,0)	6328	15,798	6445	15,512
(1,0)	6013	16,626	6118	16,341
(2,0)	5716	17,490	5791	17,263
α (0,0)	5484	18,230	5590	17,884
(1,0)	5257	19,017	5379	18,586
(2,0)	5043	19,824	5162	19,367
(3,0)	4846	20,630	4963	20,143
(4,0)	4658	21,462	4772	20,950
(5,0)			4572	21,852

[a] Bands were generally broad so that peak positions were determined to ±15 Å.

The ultraviolet spectrum of tungsten oxide species has very few bands in this region,[22] and they are not part of the observed system. Moreover, these same spectra were observed when several evaporations of TiO were made in the presence of excess titanium, thus precluding the presence of TiO_2 vapor on the basis of earlier mass spectrometric studies at high temperature.[24]

The flame spectrum of TiO in this spectroscopic region has recently been reported by Pathak and Palmer.[20] A triplet–triplet emission system, D–$X^3\Delta$, was proposed, having $\Delta G_{1/2}' = 1035$ cm^{-1} and $\Delta G_{1/2}'' = 1004$ cm^{-1}. The latter is in approximate agreement with the ground-state value of 1000 cm^{-1}. The mean wavelength for the four bands assigned to the (0,0) head is 3130 Å (31,940 cm^{-1}). Other than the (0,1), (0,0), and (1,0) bands those authors were not able to assign the vibrational progressions because the spacing was irregular. Unfortunately, the 4°K spectrum also shows the same kinds of features and seems to indicate that these bands arise from at least two perturbing electronic states.

In analyzing the neon matrix spectrum the strongest bands have been treated as two overlapping systems belonging to TiO. The similar appearance and in-

(24) J. Berkowitz, W. A. Chupka, and M. G. Inghram, *J. Phys. Chem.*, **61**, 1569 (1957).

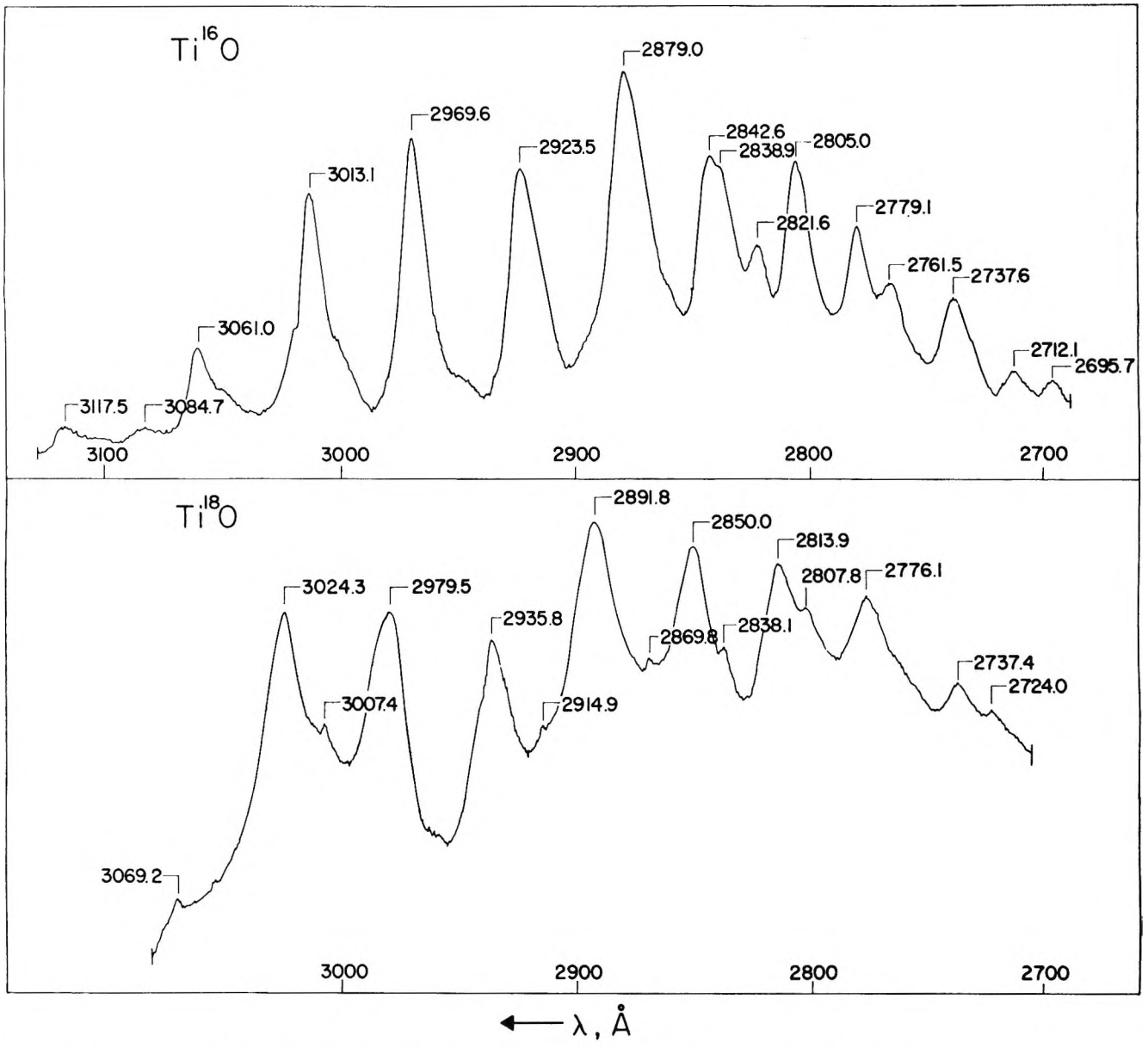

Figure 3. Ultraviolet absorption bands of $Ti^{16}O$ and $Ti^{18}O$ in a neon matrix at 4°K (wavelengths in ångstroms).

tensity pattern of alternate bands is taken as evidence of this. Table III lists band positions and differences between bands on the basis of such an assignment.

Assuming the same magnitude of gas-neon matrix blue shift observed for other TiO triplet band systems,[15] the first band in system I at 3117.5 Å corresponds satisfactorily with the assigned (0,0) band in the gas phase study. The matrix value for $\Delta G_{1/2}'$, however, does not agree with that for the gas phase, nor do the other differences in either system I or II exhibit any regular anharmonic behavior. Both systems thus appear to be perturbed at several vibrational levels, as is perhaps also the case in the gas phase. The substitution of ^{18}O for ^{16}O, useful in an earlier study for the removal of perturbations,[22] apparently decreases the perturbation in one area, but intensifies it in another. It does not appear to be possible to satisfactorily explain the appearance of the spectrum in Figure 3 by a simple energy level scheme based on mutual repulsion of vibrational levels in just systems I and II. Also the (0,0) bands in the matrix are not clearly determined so that the numbering of vibrational levels in Table III is indefinite.

There also appeared to be some weaker bands in the spectra which were not part of the system I and II bands. These have been listed at the bottom of Table III. These less intense bands were for the most part visible only in the regions where systems I and II appeared to be most perturbed.

III. Spectroscopic Studies of TiO_2. The mass spectrometric study of the evaporation of $TiO_2(s)$[24] reported the gas phase molecule TiO_2 as having an

Table III: Ultraviolet Absorption Bands of TiO in a Neon Matrix at 4°K

Band system	v′	$Ti^{16}O$ λ, Å	$Ti^{16}O$ ν, cm^{-1}	$Ti^{16}O$ $\Delta G_{v+1/2}'$, cm^{-1}	$Ti^{18}O$ λ, Å	$Ti^{18}O$ ν, cm^{-1}	$Ti^{18}O$ $\Delta G_{v+1/2}'$, cm^{-1}
I	n′ + 0	3117.5	32,068	1111	3131.7	31,922	1134
	n′ + 1	3013.1	33,179	1017	3024.3	33,056	996
	n′ + 2	2923.5	34,196	973	2935.8	34,052	1025
	n′ + 3	2842.6	35,169	803	2850.0	35,077	934
	n′ + 4	2779.1	35,972	1112	2776.1	36,011	1038
	n′ + 5	2695.7	37,084	1027	2698.3	37,049	
	n′ + 6	2623.1	38,111				
II	n″ + 0	3061.0	32,660	1005	3069.2	32,512	1041
	n″ + 1	2969.6	33,665	1062	2979.5	33,553	1017
	n″ + 2	2879.0	34,724	916	2891.8	34,570	951
	n″ + 3	2805.0	35,640	1221	2813.9	35,521	999
	n″ + 4	2712.1	36,861	828	2737.4	36,520	
	n′ + 5	2651.9	37,698				
Other TiO bands		3178.5	31,452	979			
		3084.7	32,409				
					3008.3	33,232	1042
					2916.8	34,274	
		2839.8	35,212	947			
		2764.5	36,162				
					3050.4	32,773	946
					2964.8	33,719	981
					2881.0	34,700	
		2821.5	35,432	1086			
		2737.6	36,518	962			
		2668.0	37,470				

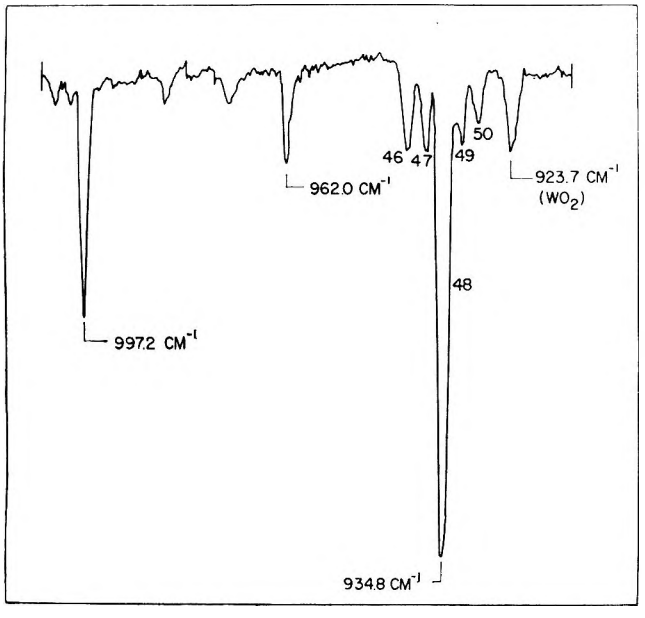

Figure 4. Stretching frequencies in the infrared spectra of TiO and TiO_2 molecules trapped in a neon matrix at 4°K.

enthalpy of sublimation slightly greater than that of TiO. In agreement with the previous matrix isolation study,[14] evaporation of a fresh sample of TiO_2 into a neon matrix resulted in the appearance of a strong infrared absorption band at 934.8 cm^{-1}. Closer examination (see Figure 4) revealed four weaker bands symmetrically bracketing the main peak that are attributable to the less-abundant isotopes of titanium. The overall intensity distribution of the five peaks closely corresponded with the natural abundances of the titanium isotopes. Annealing of the matrix resulted in no isolated changes in this group of bands. Individual positions were $^{46}TiO_2$, 940.7 cm^{-1}; $^{47}TiO_2$, 937.6 cm^{-1}; $^{48}TiO_2$, 934.8 cm^{-1}; $^{49}TiO_2$, 931.8 cm^{-1}, and $^{50}TiO_2$, 928.7 cm^{-1}. All measurements have a relative precision of ±0.2 cm^{-1}.

In addition to weak tungsten oxide bands, observed in earlier work, and the TiO band at 997.2 cm^{-1}, a new infrared absorption of moderately weak intensity was found at 962.0 cm^{-1} which only appeared when the 934.8-cm^{-1} band was present. For a bent triatomic oxide (C_{2v} symmetry) two stretching frequencies are allowed. The strong band at 934.8 cm^{-1} is assigned to ν_3, the asymmetric stretch and the weaker band at 962.0 cm^{-1} to ν_1, the symmetric stretch. The bending frequency, ν_2, was not found.

Weak emission bands in the green region were observed when a neon matrix containing TiO_2 was irradiated at ~3800 Å using an AH-6 mercury lamp (see Figure 5). Analysis of the bands in Table IV indicates only one progression with $\Delta G_{1/2}'' = 959$ cm^{-1}. A bent-bent or linear-bent electronic transition between excited and ground states will lead to a progression in ν_1 and/or ν_2. Thus the close agreement between $\Delta G_{1/2}''$ and the infrared band at 962.0 cm^{-1} is considered as support for assignment of the latter as ν_1, if,

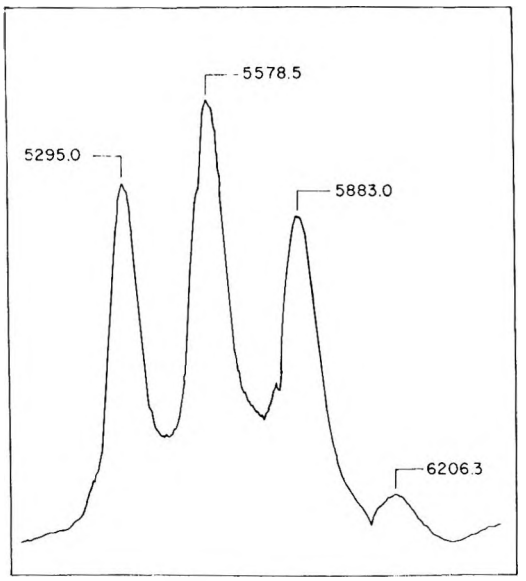

Figure 5. Emission spectrum of TiO_2 in a neon matrix at 4°K (wavelengths in ångstroms).

Table IV: Emission System of TiO_2 in a Neon Matrix at 4°K

Transition	λ, Å	$\bar{\nu}$, cm^{-1}	$\Delta G_{v+1/2}''$, cm^{-1}
(0,0,0)-(0,0,0)	5295.0 ± 2	18,880	959 ± 12
(0,0,0)-(1,0,0)	5578.5 ± 2	17,921	928 ± 12
(0,0,0)-(2,0,0)	5883.0 ± 2	16,993	884 ± 20
(0,0,0)-(3,0,0)	6206 ± 4	16,109	

as seems likely, the emission terminates in the ground state.

The isotopic shifts observed for ν_3, the asymmetric stretching frequency, can be used to calculate an approximate O–Ti–O bond angle. For a C_{2v} molecule, the angle α is obtained from the relation[25]

$$\left[\frac{\omega_3(1)}{\omega_3(2)}\right]^2 = \frac{[\mu(^{16}O) + \mu(Ti(1))(1 - \cos\alpha)]}{[\mu(^{16}O) + \mu(Ti(2))(1 - \cos\alpha)]}$$

where μ is the reciprocal mass of the isotope in question and ω_3 is the harmonic asymmetric stretching frequency. Taking all possible combinations of the five isotopes, the calculated bond angle was 110 ± 15°.

Discussion

TiO. The excited electron configurations and electronic states of the TiO molecule have been discussed previously,[15,26,27] and the present status is indicated in Figure 1. The $B^3\Pi$ state has not been definitely identified in the gas state,[4,14] but a series of strong absorption bands do appear in neon matrix spectra[15] and have been designated as the γ' bands, after Coheur.[4] The only as yet unidentified triplet state expected to be located in the infrared region is the $^3\Pi(9\sigma)(4\pi)$,[28] and it seems reasonable to assign the weak matrix ϵ bands to this $E^3\Pi \leftarrow X^3\Delta$ transition. There are, however, several points to be noted about the observations relative to this assignment.

The upper state of the E–X transition in neon falls at T_{00} = 11,894 cm^{-1}. Assuming that Phillips' value of 581 cm^{-1} is correct for the $a^1\Delta$–$X^3\Delta$ spacing, the $b^1\Pi(9\sigma)(4\pi)$ state (in the gas) is found to lie at T_{00} = 11,854 cm^{-1}, which is then actually below the assigned $E^3\Pi$ state. The reverse is expected to be true, but this discrepancy can be removed if the a–X spacing is really larger than 581 cm^{-1}, which could easily be the case (particularly in the matrix). However, it seems likely that the $b^1\Pi$–$E^3\Pi$ spacing would probably be less than about 1000 cm^{-1} even then. Such a singlet–triplet spacing would then be of the same order of magnitude as the $a^1\Delta$–$X^3\Delta$ energy of the $(1\delta)(9\sigma)$ configuration, but it is considerably smaller than the $C^1\Phi$–$A^3\Phi$ spacing of the $(1\delta)(4\pi)$ configuration (4200 cm^{-1}). The relatively low-lying electronic states of TiO are associated with orbitals which are largely atomic 3d and 4s centered on the metal atom,[7-9] and these configurations can perhaps be more informatively designated as $\sigma_{4s}\pi_{3d}^*$, $\sigma_{4s}\delta_{3d}$, and $\delta_{3d}\pi_{3d}^*$ [corresponding to $(9\sigma)(4\pi)$, $(1\delta)(9\sigma)$, and $(1\delta)(4\pi)$, respectively]. On this basis, similar correlation energies in the $\sigma_{4s}\pi_{3d}^*$ and $\sigma_{4s}\delta_{3d}$ configurations as compared to the $\delta_{3d}\pi_{3d}^*$ seems reasonable.[29]

A second point to examine in the assignment of the ϵ bands is the distribution of intensity in the observed vibrational progression in the neon spectrum. The (0,0) band is considerably stronger (see Figure 2) than the (1,0) whereas longer progressions have been observed in the other matrix systems.[15] However, upper state vibrational frequencies in these α, γ, and γ' systems are all considerably lower, ranging from 866 to 838 cm^{-1}, than the $\Delta G_{1/2}'$ = 911 cm^{-1} (see Table I) derived from the ϵ bands for the $E^3\Pi$ level. If the vibrational frequency can be used, as is often approximately true, as an indication of the rotational constant in that state, then one expects a B value in the $E^3\Pi$ state closer to that in the ground state. Then the intensity in the vibrational progression in the E–X transition should be shifted toward the (0,0) band relative to the other matrix systems, as observed.

The remaining question is why the overall intensity of this system is so small. It is significant here that the $E^3\Pi \leftarrow X^3\Delta$ transition is the only one in the triplet manifold which, if classified in terms of metal atom orbitals, involves a d–d transition; all others observed

(25) G. Herzberg, "Infrared and Raman Spectra of Polyatomic Molecules," Van Nostrand, Princeton, N. J., 1945.

(26) C. J. Cheetham and R. F. Barrow, "Advances in High Temperature Chemistry," Vol. 1, Academic Press, New York, N. Y., 1967, p 7.

(27) L. Brewer and D. W. Green, *High Temp. Sci.*, 1, 26 (1969).

(28) The symbolism for the electronic configurations of TiO used here is that of ref 7, 8, and 9.

(29) K. D. Carlson and C. Moser, *J. Chem. Phys.*, 46, 35 (1967).

involve excitation of the 4s electron into a σd or πd orbital.

The ultraviolet spectra of TiO in matrices supports the findings of Pathak and Palmer,[20] indicating that there is at least one triplet D level at about 32,000 cm^{-1}. The matrix bands indicate the probable presence of at least two states lying close to one another. These two triplet states are indicated in Figure 1 by a dashed line and derived from a configuration $(1\delta)(5\pi)$ where the 5π orbital is assumed to be largely titanium 4p. In the isoelectronic ScF molecule two states, $^1\Pi$ and $^3\Phi$, have been observed to occur in this energy region and probably also arise from that configuration.[26,27] Large Franck–Condon envelopes for the TiO bands indicate a large change in bond distance in the upper states, supporting Cheetham and Barrow's suggestion[26] that p electrons contribute little to the bonding in these molecules.

TiO_2. Electric deflection investigation[30] of molecular TiO_2 indicates that it has a permanent dipole moment and therefore a bent structure. This is corroborated by our infrared work. However, a comparison of the bond angle derived here (110 ± 15°) with that of the isoelectronic molecule CaF_2 (140 ± 5°)[31] indicates that there is little geometric similarity.

CeO_2 may also be considered as isoelectronic with TiO_2, and it is interesting that the emission systems of these two molecules observed in neon matrices are so much alike. The (0,0) band of CeO_2 [32] occurs at 5100 Å as compared to 5300 Å for TiO_2, and the Franck–Condon envelopes are quite similar. The emission lifetime, which in the case of CeO_2 is very long (~0.2 sec), was not measured for TiO_2.

It can also be noted that TiO_2 is another molecule, like CeO_2, TaO_2, ThO_2, and ZrO_2, which contradicts the general rule that $\nu_3 > \nu_1$ for the ground-state vibrational frequencies.[32]

Acknowledgment. This work was supported by the National Science Foundation under Grant NSF GP-25411.

(30) M. Kaufman, J. Muenter, and W. Klemperer, *J. Chem. Phys.*, 47, 3365 (1967).

(31) G. V. Calder, D. E. Mann, K. S. Seshadri, M. Allavena, and D. White, *ibid.*, 51, 2093 (1969).

(32) R. L. DeKock and W. Weltner, Jr., *J. Phys. Chem.*, 75, 514 (1971).

Infrared Study of Boron Trichloride Chemisorbed on Silica Gel[1]

by Victor M. Bermudez

U. S. Naval Research Laboratory, Washington, D. C. 20390 *(Received May 3, 1971)*

Publication costs assisted by the U. S. Naval Research Laboratory

The mid-infrared spectrum of BCl_3 chemisorbed on aerosil silica gel, in the form of a loose powder supported on a transparent plate, has been measured, together with the spectrum of the hydrolysis product. The spectra are quite rich in the 1500–500-cm^{-1} region, and the effect of high-temperature evacuation of the substrate prior to chemisorption suggests that a distinction must be made between reaction with isolated and with geminal free hydroxyl groups. A proposed model for the chemisorption, whereby isolated hydroxyls form a nonbridging species $\equiv$Si—O—BCl_2, geminal groups a bridging species =Si(—O—)$_2$BCl, and hydrogen-bonded hydroxyls another bridging species ($\equiv$Si—O—)$_2$BCl, is shown to be consistent with the trends observed in the spectra and with earlier studies of BCl_3–SiO_2 systems and capable of resolving the discrepancies in the value of the free hydroxyl concentration obtained by different methods. An attempt is made to assign the observed absorptions to specific normal modes of each species, although the mid-infrared spectra alone provide insufficient data for a complete assignment. The experimental problems involved in obtaining spectra of small concentrations of highly reactive surface species are discussed in detail.

Introduction

The reactions of the surface hydroxyls of silica gel and porous glass with inorganic and organic halides (particularly chlorides), both in gas phase and in solution, have been the object of numerous studies during the past decade.[2] Much of the effort has been directed toward achieving an understanding of the surface structure of silica-based adsorbents by utilizing these quantitative reactions to measure the concentration of surface hydroxyls and to distinguish among the possible configurations (*i.e.*, vicinal, geminal, or isolated).

(1) Supported in part by the Advanced Research Projects Agency, Order No. 418.

(2) See ref 3–7, 9, and 10 and references quoted therein.

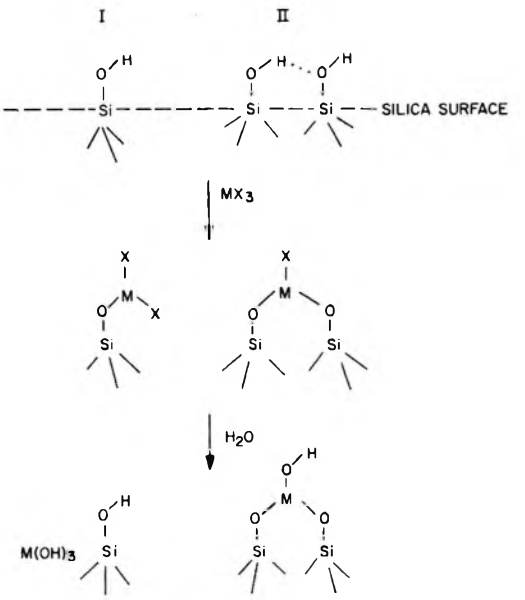

Figure 1. A schematic representation of the two modes of chemisorption of a trihalide MX_3 on a hydroxylated silica surface, together with the respective hydrolysis reactions.

Some work has also been motivated by the possibility of developing new catalytic materials based on a silica surface modified by the chemisorption of metal halides.

For trivalent halides of the form MX_3, the chemisorbed species are generally thought to exist in two forms, shown in Figure 1. Evidence for this model consists mainly of two observations. One is the dependence of the ratio of the concentration of M to the concentration of X in the reaction product on the prior heat treatment of the silica substrate. Increasing the temperature of silica gel is known[3] to cause increasing condensation of adjacent, hydrogen-bonded hydroxyl groups, thereby reducing the concentration of sites favoring a type-II species and yielding a value of [X]/[M] approaching 2/1. Boehm and coworkers[4] have performed this experiment with BCl_3 and obtained a value for [Cl]/[B] of 1.8 for silica evacuated at 550°, and Armistead and coworkers[5] have employed a similar technique to estimate (under the assumption that all free hydroxyls form a type-I product) that the fully hydroxylated silica surface contains approximately 1.4 "free hydroxyls" and 1.6 pairs of hydrogen-bonded hydroxyls per 100 Å^2. Tyler and coworkers[6] have demonstrated the microporous structure of pressed aerosil disks by showing that an appreciable number of hydroxyls are unavailable for reaction with BCl_3 or exchange with D_2O.

Further evidence, at least for the existence of the type-II species, derives from the observation[7] of a band at about 3700 cm^{-1} in the spectrum of the hydrolyzed reaction product, which is believed to be characteristic of a BOH group bridging two SiO groups on the silica surface, similar to that found[8] in porous Vycor glass.

Thus far, there has been virtually no direct observation of the spectra of the chemisorbed halides themselves,[9] largely as a result of the numerous experimental difficulties, the greatest being the low concentration (a statistical monolayer or less) of chemisorbed molecules and the very intense infrared absorption by silica in the region of interest. Furthermore, most of fundamentals of the heavier inorganic halides occur in or near the far-infrared, where spectrometer sensitivity is relatively low. Rhee and Basila[10] have studied the chemisorption of BF_3 on various oxide surfaces. Although a few bands believed to be due to chemisorbed species were observed, failure to compensate for absorption by the oxide substrate prevented recording of the complete spectrum. The Raman spectra of $SbCl_3$ on silica gel and porous glass have been reported;[11] however, the fact that evacuation of the system near the boiling point of $SbCl_3$ resulted in the disappearance of all observed bands indicates that the spectrum was most probably that of the physically adsorbed trihalide.

This paper reports the results of mid-infrared ($\omega >$ 250 cm^{-1}) studies of BCl_3 chemisorbed on aerosil silica, together with a detailed discussion of experimental techniques. BCl_3 was selected because earlier studies[4-7,10] provide some indication of what can be expected and because all four fundamentals (two of which are doubly degenerate) lie in the accessable region of the spectrum,[12] although this need not be the case for the chemisorbed species. Unfortunately, the extreme reactivity of the boron trihalides, especially with water vapor, contributes to the experimental problems.

Experimental Section

Materials. A possible complication is the migration

(3) J. A. Hockey, *Chem. Ind. (London)*, **84**, 57 (1965); M. L. Hair, "Infrared Spectroscopy in Surface Chemistry," Marcel Dekker, New York, N. Y., 1967, Chapter 4.

(4) H. P. Boehm, M. Schneider, and F. Arendt, *Z. Anorg. Allg. Chem.*, **320**, 43 (1963).

(5) C. G. Armistead, A. J. Tyler, F. H. Hambleton, S. A. Mitchell, and J. A. Hockey, *J. Phys. Chem.*, **73**, 3947 (1969). The technique used in this study cannot distinguish isolated free hydroxyls from geminal free hydroxyls. It has been shown Hair and Hertl, ref 29] that approximately 40% of the free hydroxyls are isolated and the rest geminal.

(6) A. J. Tyler, F. H. Hambleton, and J. A. Hockey, *J. Catal.*, **13**, 35 (1969).

(7) (a) F. H. Hambleton and J. A. Hockey, *Trans. Faraday Soc.*, **62**, 1694 (1966); (b) B. Camara, H. Dunken and P. Fink, *Z. Chem.*, **8**, 155 (1968).

(8) M. J. D. Low and N. Ramasubramanian, *J. Phys. Chem.*, **70**, 2740 (1966); M. L. Hair in "Clean Surfaces," G. Goldfinger, Ed., Marcel Dekker, New York, N. Y., 1970, p 269.

(9) However, bands due to the metal–oxygen vibrations of the products of the hydrolysis of $TiCl_4$ and $GeCl_4$ on silica gel have been observed; see S. I. Kol'tsov, *J. Appl. Chem. USSR*, **42**, 975 (1969); S. I. Kol'tsov and V. B. Aleskovskii, *ibid.*, **42**, 1838 (1969); A. M. Shevyakov, G. N. Kuznetsova, and V. B. Aleskovskii, in "Chemistry of High-Temperature Materials," N. A. Toropov, Ed., Consultants Bureau, New York, N. Y., 1969, p 162.

(10) K. H. Rhee and M. R. Basila, *J. Catal.*, **10**, 243 (1968).

(11) E. V. Pershina and Sh. Sh. Raskin, *Sov. Phys. Dokl.*, **8**, 583 (1963).

(12) B. Latimer and J. P. Devlin, *Spectrochim. Acta*, **21**, 1437 (1965).

of molecular water from within the silica gel particles to the surface and the subsequent hydrolysis of the chemisorbed boron halide, a process known[5] to occur when the chemisorption product is held at elevated temperatures. Precipitated gels, unlike aerosils, have been shown[13,14] to be microporous and capable of retaining significant quantities of molecular water after evacuation at room temperature. Therefore, a high surface area aerosil, Cabosil Grade S-17 (Cabot Corp., Boston, Mass.), was used. The surface area, as determined by the BET method using nitrogen adsorption at 77°K, was found to be 295 $m^2/g \pm 10\%$.

BCl_3 (99.9% pure) was used as received from the Matheson Co.

Infrared Spectra. All spectra were recorded on a Perkin-Elmer Model 521, a grating instrument with KBr optics. Between 640 and 250 cm^{-1}, a brass cell with $^1/_{16}$-in. thick high-density polyethylene windows was used. The windows were "wedged" by repeated striking with a ball-peen hammer to eliminate interference fringes. The inner surface of the cell was coated with Teflon; the windows were attached with brass flanges and the seal made vacuum-tight with Teflon gaskets and halocarbon stopcock lubricant. The cell was fitted with a stopcock and ball-joint for connecting to the vacuum manifold. Since BCl_3 reacts slowly with polyethylene, fresh windows were used at the beginning of each new run. Spectra in this region were calibrated using a mixture of equal parts (by weight) of indene, camphor, and cyclohexanone.[15]

Above 500 cm^{-1}, a modified version of the variable temperature cell used by Wagner and Hornig,[16] shown in Figure 2, was employed. KCl windows were used (to eliminate possible halogen exchange), and all metallic parts of the cell were Teflon-coated. Above 700 cm^{-1}, the spectra were calibrated using pure indene.[17] The flattened sampling area permits use of small samples and windows without vignetting of the light beam, a useful feature when very thin pressed disks (less than 0.1 mm thick) are employed, which cannot be made very large. All joints and stopcocks were lubricated with halocarbon grease; in addition, the large jacketed joint was provided with a ring of silicone grease on the upper half to improve the vacuum seal. Unfortunately, the necessity for using the halocarbon lubricant precluded the study of chemisorbed BBr_3. A comparison of the spectrum of the cell (with KBr windows) containing BBr_3 (K & K Laboratories, 99.5% pure) at the room-temperature vapor pressure with spectra of pure BBr_3[18] and the mixed boron halides[19] showed strong impurity peaks at 951 ($^{11}BCl_2Br$) and 918 cm^{-1} ($^{11}BClBr_2$). A similar comparison involving BCl_3 (200 mm, KCl windows) showed no evidence of mixed halides (pure BCl_3 spectrum given in ref 12).

Reaction between the BCl_3 and water adsorbed on the alkali halide windows can complicate the spectra with

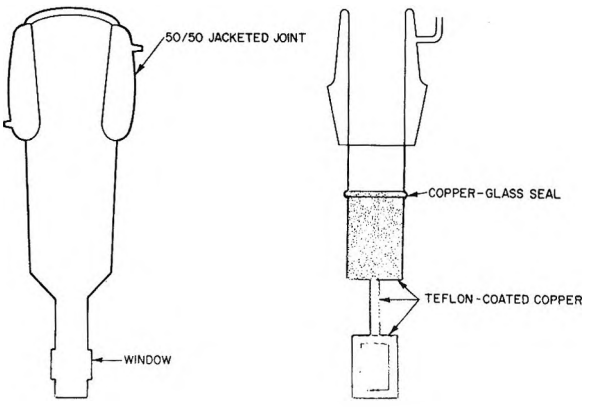

Figure 2. The variable temperature infrared cell, modified for use with samples of minimal size, employed above 500 cm^{-1}.

$B(OH)_3$ bands. Attaching the windows with silicone resin, following Little and coworkers,[20] and heating with an infrared lamp desiccated the windows but contaminated the substrate as the resin outgassed. Therefore, the windows were sealed with Apiezon W, checked after each run for spurious absorptions, and reground and repolished when necessary.

Sample Preparation. The sample was used in the form of a thin layer of powder deposited on a thin plate of the appropriate material—polyethylene or KCl—from a suspension in *n*-pentane (previously dried over sodium), a technique that has been known for some time.[21] Pressed disks cannot be used in spectroscopic studies below about 1200 cm^{-1} because a sufficiently transparent sample is too fragile; furthermore, scattering by the powdered sample was negligible for $\lambda > \sim 7$ μ and tolerable for $\lambda > \sim 5$ μ. To observe the weak bands, due to the chemisorbed BCl_3, in the presence of the very strong absorption by the silica substrate, it was necessary to compensate by having equal quantities of aerosil and window material in both beams of the instrument. The uniformity of the deposited layer of silica significantly affects the quality of the spectra; although the number and position of the peaks are reproducible from sample to sample, bands that are strong and sharp in the uniform specimen are often broad or distorted in the non-uniform sample.

(13) F. H. Hambleton, J. A. Hockey, and J. A. G. Taylor, *Trans. Faraday Soc.*, 62, 795 (1966).

(14) J. A. Cusumano and M. J. D. Low, *J. Phys. Chem.*, 74, 1950 (1970).

(15) R. N. Jones, P. K. Faure, and W. Zaharias, *Rev. Univ. Mines*, 15, 417 (1959).

(16) E. L. Wagner and D. F. Hornig, *J. Chem. Phys.*, 18, 296 (1950).

(17) R. N. Jones, N. B. W. Jonathan, M. A. MacKenzie, and A. Nadeau, *Spectrochim. Acta*, 17, 77 (1961).

(18) T. Wentink and V. H. Tiensuu, *J. Chem. Phys.*, 28, 826 (1958).

(19) L. P. Lindeman and M. K. Wilson, *ibid.*, 24, 242 (1956).

(20) L. H. Little, H. E. Klauser, and C. H. Amberg, *Can. J. Chem.*, 39, 42 (1961).

(21) H. A. Benesi and A. C. Jones, *J. Phys. Chem.*, 63, 179 (1959).

The assembled cell, with sample, was evacuated at room temperature to remove physically adsorbed water, and background spectra were taken to determine the proper degree of reference-beam compensation. The sample was then subjected to two passes of BCl_3 at 0.5 atm and evacuated several hours to remove adsorbed gases. All reactions were conducted at room temperature, since direct attack on siloxane (Si–O–Si) linkages can be expected at elevated temperatures.[12,22] Furthermore, the chemisorption of BCl_3 is known[7a] to proceed rapidly and quantitatively at room temperature. Hydrolyses were conducted by opening the cell to degassed, distilled water, at the room temperature vapor pressure, on the vacuum manifold.

As an aid in assigning observed bands to type-I or type-II sites, spectra were also taken of BCl_3 chemisorbed on silica that had been previously subjected to evacuation at high temperature to eliminate type-II chemisorption sites. Drying of silica under vacuum is known[23] to remove virtually all hydrogen-bonded hydroxyls, and the resulting surface is very much less hydrophilic than that of silica dried at lower temperature (<400°). Figure 3 shows spectra (in the OH stretching region) of aerosil dried under vacuum in a fused silica tube at 800° and pressed into a pellet in air at room temperature. Even after long exposure to room air, the surface hydroxyls are predominantly isolated (sharp, high-frequency peak) with small but increasing amounts of interacting hydroxyls (broad, low-frequency band).

The actual high-temperature samples, henceforth referred to as "H.T.," were kept under vacuum while cooled to room temperature, then transferred directly to sodium-dried *n*-pentane in a nitrogen-filled drybox. Spectroscopic samples were prepared as previously described, with the exception that all manipulations were performed in the drybox, and the assembled cell was evacuated immediately. Under these conditons, and in view of the very low hydrophilicity of H.T. silica, the material present in the cell is expected to be identical with that initially formed during the heat treatment.

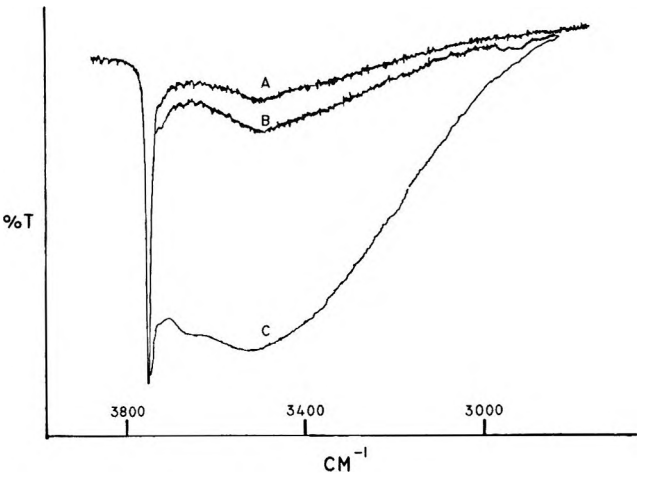

Figure 3. Spectra of pressed (0.22 mm thick) disks of aerosil: A, evacuated 15 hr at 800° before pressing in air at room temperature; B, pressed after 6 hr in room air; C, specimen pressed from "as received" aerosil.

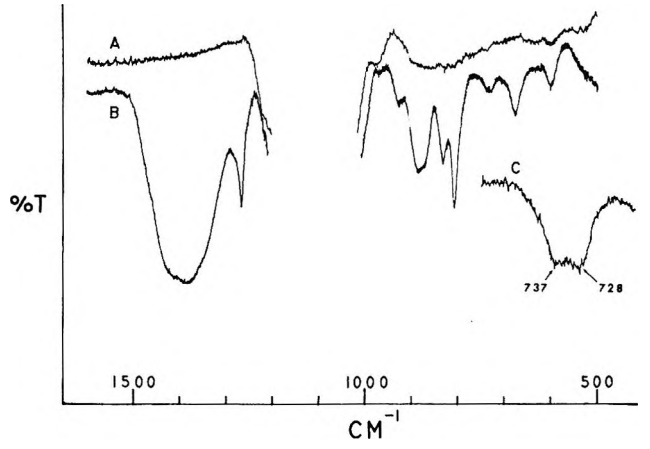

Figure 4. Spectrum of BCl_3 on silica gel: A, background after 5 hr evacuation at 25°; B, after chemisorption of BCl_3 and 12 hr evacuation at 25°; C, weak overlapping bands at 730 cm^{-1} re-scanned with fivefold expansion of transmission and frequency scales. Blank section indicates the region where instrument response is poor.

Results

The spectra obtained are shown in Figures 4–6, and the results are tabulated in Table I; in all cases, spectra were re-scanned on an expanded frequency scale for calibration. When the thickness of the silica substrate was such that satisfactory instrument response was not attainable in the 1200–1000-cm^{-1} region, the experiment was repeated with a thinner (and, inevitably, less uniform) sample. Spectra obtained under a fivefold expansion of the transmission and frequency scales revealed no additional weak absorptions except where noted. Furthermore, no bands were observed below 540 cm^{-1}, although spectra taken with either of the two cells show a band somewhere between 490 and 530 cm^{-1}. This feature is not reproducible in position from sample to sample and may be due to incomplete compensation of the strong silica absorption at 470 cm^{-1}. With polyethylene windows, a band is seen at about 444 cm^{-1}; it disappears after several hours of evacuation and is also seen in a "blank" cell, containing no silica. This absorption is most probably the ν_2 mode of $^{11}BCl_3$ (observed at 457 cm^{-1} in the gas phase[12]) which has diffused into the plastic or strongly adsorbed to it. The H.T. spectra were similar to the R.T. spectra, subject to the changes in intensity listed in Table I, with the exception that the band at ~883 cm^{-1} in the H.T./H_2O sample is more distinct than the corresponding shoulder in the R.T. spectrum.

(22) J. A. Hockey, *J. Phys. Chem.*, **74**, 2570 (1970).
(23) J. B. Peri, *ibid.*, **70**, 2937 (1966).

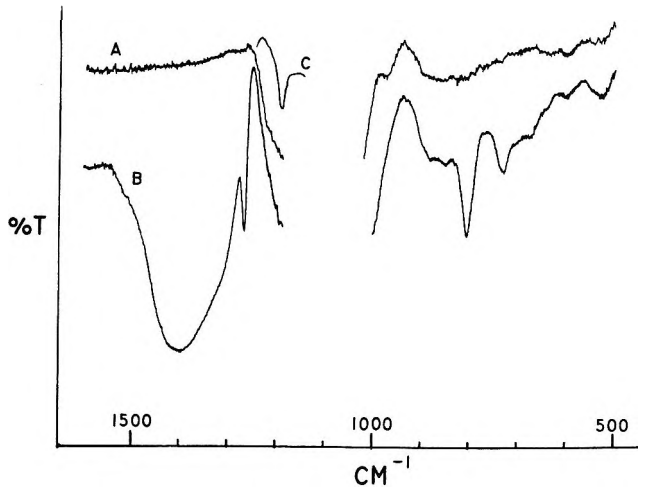

Figure 5. Spectrum of BCl_3 on silica gel after hydrolysis: A, background; B, sample as in Figure 4B after hydrolysis and 5 hr evacuation at 25°; C, repeat of B with thinner substrate.

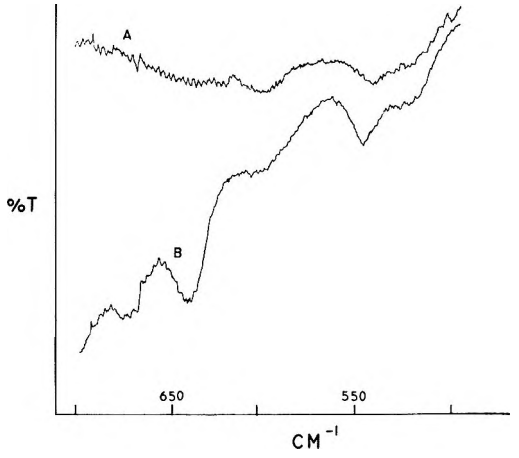

Figure 6. A, background; B, fivefold expansion of the 700-500-cm^{-1} region of the hydrolysis product spectrum.

The possibility that HCl, a by-product of the chemisorption reactions, might react with the silica surface was considered. However, it has been well documented[23,24] that HCl vapor does not react with the surface silanols of silica gel even at 700°. Contributions to the spectrum from physically adsorbed BCl_3 can also be ruled out, since none of the observed bands (with the exception of the weak absorption at 927 cm^{-1}) are in the vicinity of the frequencies of molecular BCl_3 and evacuation of the sample (after exposure to BCl_3) for 7 and 12 hr produce identical spectra.

Recently, Van Cauwelaert and coworkers,[25] on the basis of the heat of adsorption of methyl bromide on aerosil silica as a function of prior heat treatment, have concluded that aerosils do retain molecular water on the surface even after evacuation at 90°. This conflicts with the results of earlier spectroscopic and adsorption experiments,[2,13] and almost certainly the condensation of hydrogen-bonded hydroxyls contributes to the observed trends in the heat of adsorption. While it is not intended to dispute the work of Van Cauwelaert with the results of the present study, it seems unlikely that hydrolysis (rather than chemisorption) of the BCl_3 by molecular water remaining after evacuation at room temperature has produced the observed spectra. First, evacuation of the aerosil (at room temperature) for 5 hr and 15 hr before admission of the BCl_3 produced identical spectra. Second, the striking changes in the spectrum produced by hydrolysis and the general lack of coincidence between the spectra of hydrolyzed and unhydrolyzed samples leads to the conclusion that no spectroscopically detectable hydrolysis products are present in the unhydrolyzed system.

Table I: The Infrared Spectrum of BCl_3 Chemisorbed on Aerosil[a]

R.T.[b]	R.T./H_2O[c]	H.T.[d]	H.T./H_2O
1410 (sh)		1410 (sh)	
	1400 (vs, b, a)		1400 (vs, b, a)
1380 (vs, b, a)		1380 (vs, b, a)	
1265 (s)	1267 (s)	1265 (s)	1267 (s)
	*1192 (m)		*1192 (m)
927 (w, sh)		~930 (sh)	
		889 (s)	
	883 (m, sh)		884 (m)
880 (s, a)			
	850 (vw, sh)		
832 (m)		830 (m)	
808 (s)	807 (s)	809 (s)	809 (s)
737 (w)			
	730 (m)		732 (w)
728 (w)		729 (w)	
677 (m)		677 (m)	
	*674 (vw)		*675 (vw)
	*642 (vw)		*647 (vw)
596 (m)			
	*546 (vw)		*546 (vw)

[a] All frequencies are ±1 cm^{-1}, except for broad bands, which are ±4 cm^{-1}. Bands indicated with an asterisk (*) are due to $B(OH)_3$ (see ref 31). Abbreviations are: vs = very strong, s = strong, m = moderate, w = weak, vw = very weak, b = broad, sh = shoulder, a = asymmetric. [b] R.T. (room temperature)—aerosil evacuated at room temperature before exposure to BCl_3. [c] R.T. sample after hydrolysis. [d] H.T. (high temperature)—aerosil evacuated at 800° before exposure to BCl_3 (see text).

Discussion

If the scheme shown in Figure 1 were strictly correct, certain bands present in the sample evacuated at room temperature (henceforth referred to as "R.T.") would be absent in the H.T. specimen. These, then, would be the absorptions due to the type-II species, (≡Si—O—)$_2$BCl. Similarly, the only bands observed in the H.T./H_2O (hydrolyzed H.T. sample) spectrum would

(24) M. L. Hair and W. Hertl, *J. Phys. Chem.*, **73**, 2372 (1969).

(25) F. H. Van Cauwelaert, J. B. Van Assche, and J. B. Uytterhoeven, *ibid.*, **74**, 4329 (1970).

be those of $B(OH)_3$, and their subtraction from the R.T./H_2O data would yield the bands due to $(\equiv Si-O-)_2BOH$. What one finds instead is that many of the bands in the R.T. samples are also present in the H.T. specimens with more or less the same intensity, and among these are several peaks in the H.T./H_2O spectrum which are clearly not due to $B(OH)_3$. Since it is virtually certain that all but a negligible concentration of interacting hydroxyls are removed by the high-temperature evacuation, the only satisfactory explanation for both the similarity between the H.T. and R.T. spectra and the presence of bands in the H.T./H_2O spectrum not due to $B(OH)_3$ is that geminal free hydroxyl sites are present and react with BCl_3, as shown in Figure 7, to form a second type of bridging species, II′.

Very recently, Kunawicz and coworkers[26] have reported evidence that hydrogen-bonded interacting hydroxyls are more reactive toward hydrogen sequestering reagents than are isolated free hydroxyls and that the siloxane bridges resulting from the high-temperature (700°) evacuation are more reactive than the remaining free hydroxyls. Although the observed effect of hydrogen bonding on the reaction rate is entirely reasonable, the possibility that BCl_3 may react with siloxane bridges does not significantly affect the present interpretation. Although BCl_3 may react in the manner described, the resulting nonbriding, type-I species would not in themselves account for the present observations. Many of the conclusions reached by Kunawicz and coworkers are based on changes in intensity of very strong bands plotted on a linear % transmission (rather than linear absorbance) scale; for instrumental reasons, quantitative comparisons of band intensities under such conditions are difficult.

First, a comment on the structural parameters of the II′ species is in order. Taking 1.37 Å for the B–O bond length[27] and 120° for the O–B–O bond angle, one finds an O–O distance of 2.37 Å. For an Si–O distance of 1.62 Å and a tetrahedral O–Si–O angle, as in vitreous silica,[28] the O–O distance is 2.63 Å. This discrepancy is not forbiddingly large, and an increase in the O–B–O angle on the order of 10% (with a similar decrease in the O–Si–O angle) is sufficient to satisfy the bond angle requirements of the II′ structure.

The results obtained by Camara and coworkers[7b] provide compelling evidence for the existence of a type-II′ hydrolysis product. Spectra of aerosil silica evacuated at 700° showed only free-hydroxyl absorption. The sample after treatment with BCl_3, hydrolysis, and re-evacuation at 600° showed an intense peak at 3710 cm^{-1}, which has been assigned to the bridging =BOH unit. Clearly bridging chemisorbed species are formed even when only free hydroxyls are present on the silica surface.

Recognition of the existence of the type-II′ chemisorption product resolves the discrepancy between the

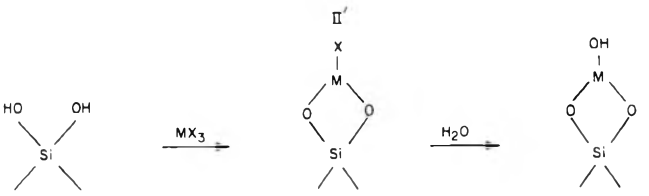

Figure 7. The chemisorption reaction at geminal free hydroxyl sites.

values of the free hydroxyl concentration measured by reaction with CH_3OH[29a] (1.70 OH/100 Å^2) and by reaction with BCl_3[5] (1.4 ± 0.1 OH/100 Å^2) under the assumption that all free hydroxyls form a type-I product with BCl_3. If the free silanol concentration obtained by methanolysis is indeed the true value (and there is general agreement on this point[30]) and the ratio of concentrations of single and geminal units of 2/3 obtained by Hair and Hertl[29] is correct, then the erroneously small value obtained by residual chlorine analysis of the BCl_3 chemisorption product is the result of the reaction of 60% of the geminal sites to form a type-II product.

We next consider the normal modes of the three surface species and the extent to which an assignment of the bands listed in Table I is possible. An approximate analysis of the local symmetry of each species can be formulated by treating each surface silicon atom as an infinitely massive point particle. Thus the type-I and -II′ halogenated structures are viewed as five-atom molecules and the type-II bridging species as a six-atom molecule. Such a model will not, of course, yield realistic selection rules or allow proper consideration of the coupling between the vibrations of the silica lattice and those of the chemisorbed molecules. Nevertheless, the approach is useful in describing the local symmetry of the normal modes of the surface species. The results of the analysis are summarized in Table II and do not include the three torsional modes of each species derived from the rotational degrees of freedom. Evidently, the total number of normal modes is too great, in comparison with the number of bands observed, to permit calculation of meaningful potential functions. However, an attempt at a partial assignment is possible by analogy with $B(OH)_3$,[31] crystalline,[32] and glassy[33-35]

(26) J. Kunawicz, P. Jones, and J. A. Hockey, *Trans. Faraday Soc.*, 67, 848 (1971).

(27) V. F. Ross and J. O. Edwards in "The Chemistry of Boron and Its Compounds," E. L. Muetterties, Ed., Wiley, New York, N. Y., 1967, Chapter 3.

(28) R. L. Mozzi and B. E. Warren, *J. Appl. Cryst.*, 2, 164 (1969).

(29) (a) M. L. Hair and W. Hertl, *J. Phys. Chem.*, 73, 4269 (1969); (b) W. Hertl and M. L. Hair, *ibid.*, 75, 2181 (1971).

(30) See, for example, B. Evans and T. E. White, *J. Catal.*, 11, 336 (1968).

(31) J. R. Durig, W. H. Green, and A. L. Marston, *J. Mol. Struct.*, 2, 19 (1968).

(32) I. I. Plysnina and Yu. A. Kharitonov, *J. Struct. Chem. USSR*, 4, 506 (1963).

Table II: Classification of the Normal Modes of Chemisorbed Surface Species in Terms of Local Symmetry

Type	Point group	No. of normal modes	Activity
I, ≡Si—O—BCl_2	C_s	7A′ + 2A″	A′, A″ ir and Raman
II, (≡Si—O—)$_2$BCl	C_{2v}	$5A_1 + 1A_2 + 2B_1 + 4B_2$	A_1, B_1, B_2 ir and Raman; A_2 Raman
II′, =Si(—O—)$_2$BCl	C_{2v}	$4A_1 + 2B_1 + 3B_2$	

borosilicates, trichloroboroxine,[12] $(BOCl)_3$, B_2H_6 chemisorbed on silica gel,[36] and the mixed halides BX_2Cl and $BXCl_2$.[19,37]

Identification of absorptions due to $B(OH)_3$ in the hydrolysis product spectra is relatively straightforward. They appear with similar intensity in both R.T./H_2O and H.T./H_2O samples and correspond closely to known $B(OH)_3$ infrared bands as tabulated by Durig and coworkers.[31] Although several workers report a strong, broad band in $B(OH)_3$ centered in the 800–825-cm^{-1} vicinity, it is an order of magnitude too broad to be identified with the strong, sharp band at about 809 cm^{-1} in BCl_3–SiO_2 spectra both before and after hydrolysis. Similarly, the weak band reported in the $B(OH)_3$ spectrum at about 880 cm^{-1} is too weak to be identified with the band at 883 cm^{-1} in the R.T./H_2O and H.T./H_2O spectra.

There are, in all, three different chlorine-containing and two different chemisorbed hydrolyzed species, and the first requirement is to decide which bands belong to each species. With regard to the hydrolyzed species, any band in the H.T./H_2O spectrum not belonging to $B(OH)_3$ can be safely assigned to the type-II′ site. Similarly, any band in the R.T./H_2O spectrum not appearing in the H.T./H_2O spectrum is associated with the type-II species. For near coincidences between the two, one must rely on a comparison of the relative intensities. If a particular band (at 1267 cm^{-1}, for example) appears with comparable intensity in both spectra, it is probably due to the type-II′ site; whereas, a lesser intensity in the H.T./H_2O spectrum would indicate a frequency common to both type-II and -II′ species. Similar reasoning can be applied to the spectra obtained before hydrolysis, with the added complication that the H.T. spectrum contains bands belonging to two species, type I and II′.

Comparing intensities in this manner can be misleading for two reasons. First, estimation of intensities is difficult when bands are overlapping, distorted, or present as shoulders set against more intense bands or a sloping background. It can be seen that many of the bands in the accompanying spectra fall into one or more of these categories. Second, the environment of a chemisorbed molecule on the silica surface is quite different for the R.T. and H.T. spectra. In the former, the surface is covered with fairly densely packed chemisorbed species and strained siloxane linkages. In the latter, the chemisorption sites are more sparse and the siloxanes more concentrated and, perhaps, somewhat annealed if the temperature during evacuation is sufficiently high. The effect this has on the band intensities is unknown, although probably not completely negligible. It appears that the positions of some of the bands in the H.T. spectra are very slightly dependent on the duration of the high-temperature evacuation, shifting a few wave numbers to higher frequency with prolonged treatment. Rhee and Basila[10] have observed that the position of the band at 1394 cm^{-1} in the spectrum of BF_3 chemisorbed on aerosil varies by ±10 cm^{-1} from sample to sample and increases in intensity when the chemisorption product is evacuated at high temperature.

Tables III and IV present summaries of the assignments made. Bands listed between two columns cannot be definitely assigned to one or the other and may, in fact, be common to both species.

Table III: Tentative Assignment of Absorption Bands in the Spectra of the Hydrolyzed Chemisorption Product

Type II, (≡Si—O)$_2$-BOH		Type II′, =(Si—O—)$_2$-BOH	
3695[a]		3710[b]	OH stretch
	1400		antisym. BO stretch
		1267	antisym. SiO stretch
		883	sym. BO stretch
850			
		807	"ring deformation" or torsion
	731		

[a] From ref 7a. [b] From ref 7b.

The most unambiguous assignments in Tables III and IV (aside from the OH stretching frequencies) are those of the higher frequency BO stretching modes, since a wide variety of materials containing SiOB units yield a strong band between 1370 and 1400 cm^{-1}. Upon hydrolysis, the band at 1380 cm^{-1} shifts to 1400 cm^{-1}, consistent with the replacement of Cl by a smaller mass. No band appears at higher frequency, implying that the shoulder at 1410 cm^{-1} is associated with ≡$SiOBCl_2$. This is, however, somewhat higher than

(33) P. E. Jellyman and J. P. Procter, *J. Soc. Glass Tech.*, **39**, 173T (1955).
(34) W. A. Pliskin, *Proc. IEEE*, **52**, 1468 (1964).
(35) Y. Haneta, *Jap. J. Appl. Phys.*, **8**, 274 (1969).
(36) J. J. Fripiat and M. VanTongelen, *J. Catal.*, **5**, 158 (1966).
(37) H. E. Pence and G. L. Humphrey, *Proc. West. Va. Acad. Sci.*, **341**, 71 (1962).

Table IV: Tentative Assignment of Absorption Bands in the Spectra of the Unhydrolyzed Chemisorption Product

Type I, ≡Si—O—BCl_2	Type II′, =Si(—O—)$_2$BCl	Type II, (≡Si—O—)$_2$BCl	
1410			BO stretch
	1380		antisym. BO stretch
	1265		antisym. SiO stretch
927			antisym. BCl stretch
	889		sym. BO stretch
		880	sym. BO stretch
831			SiOB bending
	808		"ring deformation" or torsion
		737	BCl stretch
728			
	677		
		596	

the BO stretch frequency in simple borates,[38] 1340 ± 10 cm^{-1}. The band at 1380 cm^{-1} (1400 cm^{-1}) in the H.T. (H.T./H_2O) spectrum is considerably less broad than the band in the R.T. (R.T./H_2O), indicating a lower total concentration of BO bonds, as expected. The peak at 1265 cm^{-1} is clearly due to a vibration of the type-II′ species not involving significant motion of the Cl atom, since it shifts only slightly after replacement of Cl by OH. The frequency is much too high to be a BO vibration and about 150 cm^{-1} higher than typical SiO stretching frequencies. However, the strain in the four-membered ring of the type-II′ species is expected to shift the SiO stretching frequency to high frequencies by increasing the relative amount of s character in the SiO bond.[38]

The weak band at 927 cm^{-1} appears with comparable intensity in both the R.T. and H.T. samples, and it cannot be decided *a priori* whether the band belongs to the type-I or -II′ species. However, the antisymmetric BCl stretching frequencies in the $BXCl_2$ mixed halides all fall in the 1000–940-cm^{-1} region, *e.g.*, 993, 951, and 942 cm^{-1} for $^{11}BFCl_2$,[19] $^{11}BBrCl_2$,[19] and $BICl_2$,[37] respectively. Similarly the band at 889 cm^{-1} in the H.T. spectrum may be associated with either of the two species, but—together with the strong, asymmetric band at 880 cm^{-1} in the R.T. spectrum—has been assigned to the symmetric BO stretching mode, in analogy with the totally symmetric (A_g) BO stretching vibration in $B(OH)_3$. The band at 831 cm^{-1}, observed with comparable intensity in the R.T. and H.T. spectra (but not in the hydrolyzed samples) is assigned to the SiOB bending mode in the type-I species.

The sharp, intense band at 808 cm^{-1} can be unambiguously assigned to a type-II′ vibration. $(BOCl)_3$ exhibits a "ring deformation" band at 807 cm^{-1} in the Raman spectrum,[12] and the borates and borosilicates, in general, have a bending mode close to 800 cm^{-1}. The apparent lack of sensitivity to hydrolysis suggests that the vibration may instead be a torsional mode involving oscillation of the ring about the BCl axis. The weak band at 737 cm^{-1} in the R.T. spectrum is assigned to the BCl stretching vibration in the type-II species, in analogy with $(BOCl)_3$. Several bands seen at lower frequencies cannot be assigned with any degree of certainty.

The preceding, somewhat hypothetical assignment cannot be improved without more spectroscopic data. Laser Raman spectroscopy appears promising, since powdered oxides tend to be very poor Raman scatterers and thus do not present the complications intrinsic to the infrared experiments. Several organic molecules physically adsorbed on silica gel have been studied,[39] but, to date, no chemisorbed species have been observed (with the possible exception of acetaldehyde[40]). Since pressed aerosil disks are transparent below about 300 cm^{-1}, far-infrared spectra should be obtainable without the restrictions on substrate thickness; however, the low concentration of chemisorbed species demands good instrument sensitivity.

In conclusion, the infrared spectrum of a simple molecule, BCl_3, chemisorbed on silica gel has, for the first time, been observed in the region of strong substrate absorption. The lack of strong dependence of the spectrum on the high-temperature evacuation of the silica, prior to chemisorption, and the presence of bands not due to $B(OH)_3$ in the spectrum of the hydrolysis product of the thermally treated sample suggest that geminal free hydroxyl sites must be considered as a distinct type of chemisorption site. Geminal hydroxyl pairs—like adjacent, hydrogen-bonded hydroxyl pairs—form a bridging chemisorption product with BCl_3 which remains intact during hydrolysis. It has, in the past, been tacitly assumed that geminal sites react as do isolated free hydroxyls, forming a nonbridging species subsequently destroyed by hydrolysis.[41-45]

(38) L. J. Bellamy, "The Infrared Spectra of Complex Molecules," 2nd ed, Wiley, New York, N. Y., 1958.

(39) See, for example, R. O. Kagel, *J. Phys. Chem.*, **74**, 4518 (1970); P. J. Hendra and E. J. Loader, *Trans. Faraday Soc.*, **67**, 828 (1971).

(40) P. J. Hendra and E. J. Loader, *Nature (London)*, **217**, 637 (1968).

(41) NOTE ADDED IN PROOF. Very recently, Peglar and coworkers[42]

have reported the results of infrared, mass spectrometric and gravimetric studies of the chemisorption of $AlMe_3$ on aerosil. Their data indicate that the resulting type-I species $\equiv Si—O—AlMe_2$ can undergo a rearrangement reaction with a nearby siloxane bridge to form a type-II bridging species and a $\equiv Si—Me$ group. The possibility that a similar process may occur in the BCl_3–SiO_2 system constitutes an alternative explanation for the presence of bridging species in the H.T. samples. Nevertheless, for the system under consideration, there are reasons for favoring the present interpretation over the rearrangement theory, although none is so conclusive as to definitely rule out at least some contribution from rearrangement. First, no absorption in the 450–550 cm^{-1} region, characteristic of the Si–Cl single bond,[43] was observed in any of the spectra, although spectra in this region are of questionable quality. Second, if rearrangement were the dominant process, then the H.T. and R.T. spectra should be identical in the number and position of absorption maxima, which is not the case. However, the differences are not overwhelming, and it could be argued that they result from the effects of the heat treatment on the substrate. Finally, using bond energies calculated from standard heats of formation,[44] one obtains a value of ΔH for the breaking and forming of bonds in the rearrangement process of about 4 kcal/mol as compared to about 26 kcal/mol for the $AlMe_3$–SiO_2 system.[44] These values of ΔH do not include the contribution from the strain energy of the siloxane bridge, but it appears reasonable to state that the rearrangement process in the BCl_3–SiO_2 system is less favorable than in the $AlMe_3$–SiO_2 system by about 22 kcal/mol.

(42) R. J. Peglar, F. H. Hambleton, and J. A. Hockey, *J. Catal.*, **20**, 309 (1971).

(43) A. L. Smith, *Spectrochim. Acta*, **16**, 87 (1960).

(44) R. C. Weast, Ed., "Handbook of Chemistry and Physics," 52nd ed, Chemical Rubber Publishing Co., Cleveland, Ohio, 1971.

(45) D. J. C. Yates, G. W. Dembinski, W. R. Kroll, and J. J. Elliott, *J. Phys. Chem.*, **73**, 911 (1969).

The Electronic Structure of Furanquinones. I. The Absorption Spectra of Dinaphtho[2,1-2′,3′]furan-8,13-dione and Dinaphtho[1,2-2′,3′]furan-7,12-dione

by M. S. Walker,* J. E. Kuder, and R. L. Miller

Research Laboratories, Xerox Corporation, Rochester, New York 14603 *(Received April 19, 1971)*

Publication costs assisted by the Xerox Corporation

The electronic absorption and fluorescence excitation polarization spectra of the isomeric quinones, dinaphtho[2,1-2′,3′]furan-8,13-dione (I) and dinaphtho[1,2-2′,3′]furan-7,12-dione (II) have been recorded. The spectra provide some support for the weakly interacting chromophore model of quinones proposed by Morton and Earlam. Transition energies and moment polarizations are in fair agreement with those predicted by the Hückel molecular orbital theory. The long wavelength π–π^* absorption in these molecules involves significant intramolecular charge transfer. The calculated dipole moment change involved in this transition, −17.3 and −22.4 D for I and II, respectively, is in accord with the solvent-induced frequency shifts of the transition observed in absorption.

Introduction

The electronic structures of polycyclic quinones have received considerable experimental and theoretical attention due to the importance of quinones as dyes,[1] their implication in biological processes,[2] and the subsequent interest in their photophysical and photochemical properties.

Morton and Earlam[3] interpreted the absorption spectra of 1,4-naphthoquinone and 9,10-anthraquinone in terms of a weakly interacting chromophore model. They assigned the absorption bands as originating in the benzenoid or quinonoid chromophoric groups of the molecules according to a similarity, in wavelength and extinction coefficients, with the absorption bands of salicylaldehyde and *p*-benzoquinone, respectively. Subsequently, several authors[4,5] have used this empirical model to interpret the spectra of simple *p*-quinones. The model finds support in the general similarity of the spectra of *p*-quinones,[6] as pointed out by Sidman,[7] who suggested that higher *p*-quinones might be treated simply as vinyl derivatives of *p*-benzoquinone. Further, the alternating bond lengths in the quinoid chromophore, observed by X-ray crystallographic analysis,[8,9] suggest that electron delocalization in these molecules may not be extensive.

Drott and Dearman[10] have assigned the n–π^* and π–π^* states of 9,10-anthraquinone using the method of

(1) K. Venkataraman, "The Chemistry of Synthetic Dyes," Academic Press, New York, N. Y., 1952.

(2) R. A. Morton, "Biochemistry of Quinones," Academic Press, New York, N. Y., 1965.

(3) R. A. Morton and W. T. Earlam, *J. Chem. Soc.*, 159 (1941).

(4) R. H. Peters and H. H. Sumner, *ibid.*, 2101 (1953).

(5) I. Singh, R. T. Ogata, R. E. Moore, C. W. J. Chang, and P. J. Scheuer, *Tetrahedron*, **24**, 6053 (1968).

(6) V. H. Hartmann and E. Lorenz, *Z. Naturforsch. A*, **7**, 360 (1952).

(7) J. W. Sidman, *J. Amer. Chem. Soc.*, **78**, 4567 (1956).

(8) S. N. Sen, *Indian J. Phys.*, **31**, 347 (1948).

(9) J. Gaultier and C. Hauw, *Acta Crystallogr.*, **18**, 179 (1965).

(10) H. R. Drott and H. H. Dearman, *J. Chem. Phys.*, **47**, 1896 (1967).

photoselection and have theoretically interpreted their observations by adopting a weakly interacting chromophore model for the molecule. Transition moment directions in several other quinones have also been deduced from polarization absorption spectra.[11,12]

The π-electronic excitation energies of *p*-benzo-, naphtho-, and anthraquinones have been calculated using a simple molecular orbital treatment[13,14] and more recently using the Pariser–Parr–Pople method.[15,16] Results of these calculations are not in total agreement.

Though furanquinones have been known for some time[17] and have been reported to be suitable as vat dyes,[18] little is known about their electronic structure. Frohlinde and Werner[19] in their studies of the photorearrangement of binaphthyl(2,2′)diquinone(1,4-1′,4′) reported the ultraviolet and visible absorption spectra of dinaphtho[1,2-2′,3′]furan-7,12-dione and its 5-hydroxy and 5-acetoxy derivatives, while several authors have reported absorption bands in the region 400 to 500 nm for dinaphthofurandiones.[20,21] Reported here are the results of a spectroscopic and molecular orbital study of the electronic structure of dinaphtho[2,1-2′,3′]-furan-8,13-dione and its structural isomer dinaphtho-[1,2-2′,3′]furan-7,12-dione (Figure 1).

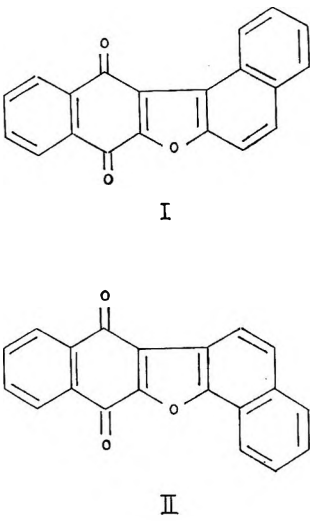

Figure 1. Molecular structure of dinaphtho[2,1-2′,3′]furan-8,13-dione (I) and dinaphtho[1,2-2′,3′]furan-7,12-dione (II).

Experimental Section

Dinaphtho[2,1-2′,3′]furan-8,13-dione (I) and dinaphtho[1,2-2′,3′]furan-7,12-dione (II) were synthesized by refluxing 2,3-dichloro-1,4-naphthoquinone with β-naphthol and α-naphthol, respectively, in anhydrous pyridine.[22,23] The quinones were recrystallized from methanol several times and then vacuum sublimed. Melting points were 271° (I) and 230–231° (II); literature values are 271 and 231°, respectively. Microanalysis of I gave H, 3.60%; C, 80.64% and for II, H, 3.50%; C, 80.12%. The molecular formula $C_{20}H_{10}O_3$ requires H, 3.40%; C, 80.50%.

Ultraviolet and visible absorption spectra were recorded on a Cary 14 recording spectrophotometer using 1- or 10-cm path length matched quartz cells. Fluorescence and fluorescence excitation polarization spectra were recorded on a Aminco-Kiers spectrophotofluorometer fitted with a Glan-prism polarizer assembly. Excitation and emission bandwidths were kept at 2 nm. The polarization (P) of the fluorescence excitation spectrum was measured using the formula due to Azumi and McGlynn[24] where

$$P = \frac{I_{EE} - I_{EB}(I_{BE}/I_{BB})}{I_{EE} + I_{EB}(I_{BE}/I_{BB})} \quad (1)$$

and I_{EE}, I_{EB}, I_{BE}, I_{BB} refer to the recorded fluorescence intensities for the four different orientations of the prism polarizers at each wavelength of excitation. The subscripts of E and B refer to the electric vector in the vertical and horizontal planes, respectively. Four excitation spectra were recorded successively corresponding to the prism orientations EE, EB, BE, and BB, and a minimum of four measurements of P were made to check reliability.

Solvents were Matheson Coleman and Bell "Spectroquality" reagent and solute concentrations were typically 10^{-5} to 10^{-4} M. The solutions were not deoxygenated. Absorption and emission spectra were recorded at ambient and 77°K temperatures, respectively.

Hückel molecular orbital (HMO) calculations were performed using a program written in FORTRAN IV for the UNIVAC 1108 computer. The heteroatom parameters used are those suggested by Streitwieser:[25] h_0(furan) = 2.00, k_{CC} = 0.80, h_0(carbonyl) = 1.00, $k_{C=O}$ = 1.00, $h_{c(x)} = 0.1h_x$. Resonance integrals of 0.80β and 1.10β, respectively, were used for the carbon–carbon single and double bonds of the quinone portion of the molecule. These values were chosen on the basis of the bond lengths reported for *p*-benzoquinone[26] and

(11) J. W. Sidman, *J. Amer. Chem. Soc.*, **78**, 2363 (1956).
(12) H. Labhart, *Chimica (Aarau)*, **15**, 20 (1961).
(13) L. E. Orgel, *Trans. Faraday Soc.*, **52**, 1172 (1956).
(14) A. Kuboyama, *Bull. Chem. Soc. Jap.*, **31**, 752 (1958).
(15) A. Kuboyama and K. Wada, *ibid.*, **39**, 1874 (1966).
(16) C. Leibovici and J. Deschamps, *Theoret. Chim. Acta*, **4**, 321 (1966).
(17) S. Kostanecki, *Chem. Ber.*, **36**, 2193 (1903).
(18) B. D. Tilak and M. R. Venkiteswaran, *J. Sci. Ind. Res.*, **16B**, 400 (1957).
(19) D. S. Frohlinde and V. Werner, *Chem. Ber.*, **94**, 2726 (1961).
(20) M. F. Sartori, *J. Org. Chem.*, **24**, 1756 (1959); *ibid.*, **26**, 3152 (1961).
(21) A. J. Shand and R. H. Thomson, *Tetrahedron*, **19**, 1919 (1963).
(22) Ng. P. B. Hoi, *J. Chem. Soc.*, 489 (1952).
(23) Ng. P. B. Hoi and P. Demerseman, *ibid.*, 4699 (1952).
(24) T. Azumi and S. P. McGlynn, *J. Chem. Phys.*, **37**, 2413 (1962).
(25) A. Streitwieser, "Molecular Orbital Theory," Wiley, New York, N. Y., 1962, p 135.
(26) J. M. Robertson, *Proc. Roy. Soc., Ser. A*, **150**, 106 (1935).

the variation of resonance integral with bond length as discussed by Streitwieser.[25] Molecular coordinates used in the dipole moment and transition moment calculations were obtained from Dreiding stereo models (Rinco Instrument Co.).

Results

Absorption and Polarization Spectra. The ultraviolet and visible absorption spectra, recorded at ambient temperatures, for quinones I and II in hexane solvent are shown in Figures 2 and 3, respectively. In polar solvents the spectra show a general red shift of the absorption bands with some loss in vibrational structure. The spectra show no evidence of long wavelength weak carbonyl n–π^* transitions.

The polarization (P) of the fluorescence excitation spectra for quinones I and II in EPA solvent (−196°) are also shown in Figures 2 and 3, respectively. The uncorrected fluorescence maxima for the quinones in EPA glass occur at 508 and 493 nm, respectively. Polarization of the fluorescence is positive and constant over the emission bandwidth in both cases. Polarization spectra were recorded for the quinones in EPA due to the somewhat low solubility and low fluorescence yield of these molecules in hydrocarbon solvents. Further their absorption spectra showed only small wavelength shifts and some loss in structure in the polar glass. The angle θ between the absorption transition moment and the emission oscillator was calculated for several of the absorption bands using the formula[27]

$$P = \frac{3\cos^2\theta - 1}{\cos^2\theta + 3} \qquad (2)$$

For quinone I, the following angles, 16, 45, 28, and <30°, were calculated for the absorption bands centered at 430, 330, 295, and 240 nm, respectively. While for quinone II, angles of 14, 19, and 45° were calculated for the bands centered at 415, 335, and 310 nm, respectively. The rapidly changing degree of polarization below 300 nm in the polarization spectrum of II excluded the calculation of any meaningful value of θ for transitions lying below this wavelength. These angles have not been corrected for depolarization effects inherent in the measurements.

Solvent-Induced Frequency Shifts. Several authors have discussed solvent effects on electronic transitions and interpreted solvent-induced frequency shifts in terms of dispersive and static dipole interactions. The simplified formula due to McRae[28] relating the frequency shift ($\Delta\nu$) of a transition to the solvent refractive index (n) and dielectric constant (D) is given as

$$\Delta\nu = (AL_0 + B')\left[\frac{n^2 - 1}{2n^2 + 1}\right] + C\left[\frac{D - 1}{D + 2} - \frac{n^2 - 1}{n^2 + 2}\right] \qquad (3)$$

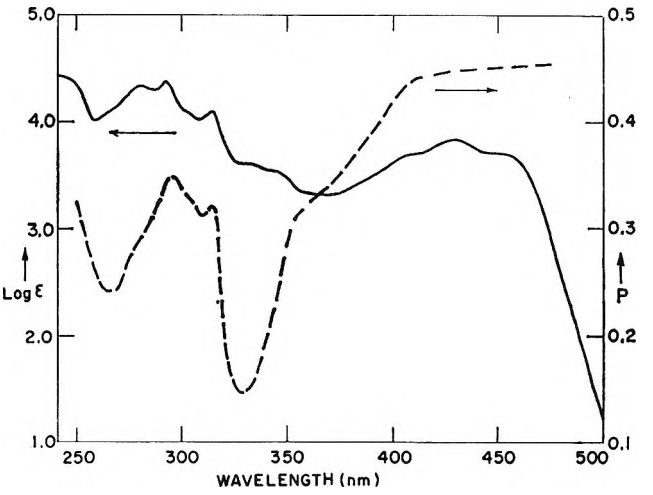

Figure 2. Absorption spectrum of I in hexane, ——, and fluorescence excitation polarization spectrum of I in EPA glass (−196°), - - -.

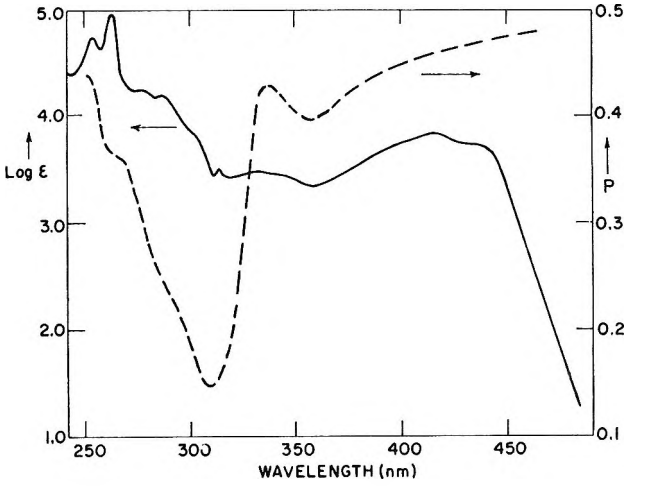

Figure 3. Absorption spectrum of II in hexane, —, and fluorescence excitation polarization spectrum of II in EPA glass (−196°), - - - -.

where A, B', and C are constants characteristic of the solute and L_0 is the weighted mean wavelength. Frequency shifts of several absorption bands of I and II measured in some 23 polar and nonpolar solvents were fitted to eq 3 by the method of least squares. Calculated values of the constants ($AL_0 + B'$) and C are given in Table I. A plot of observed (ν_A^{obsd}) *vs.* calculated (ν_A^{calcd}) frequencies for the long wavelength absorption band of quinone I is shown in Figure 4. The root-mean-square deviation between observed and calculated frequencies is 60 cm^{-1}, which is close to the experimental uncertainty involved in the measurement of absorption frequencies in this work. The constant C may be equated with the ground (μ_g) and excited

(27) F. Perrin, *Ann. Phys.*, 12, 169 (1929).
(28) E. G. McRae, *J. Phys. Chem.*, 61, 562 (1957).

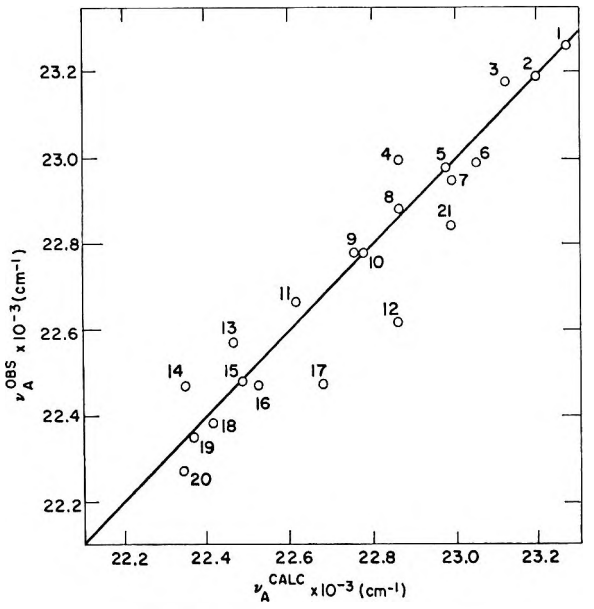

Figure 4. Plot of ν_A^{obsd} *vs.* ν_A^{calcd} for the long wavelength absorption of I in several solvents: 1, hexane; 2, cyclohexane; 3, diethyl ether; 4, acetone; 5, carbon tetrachloride; 6, dioxane; 7, ethyl acetate; 8, acetonitrile; 9, ethyl bromide; 10, 1-bromohexane; 11, dimethylformamide; 12, benzene; 13, dimethyl sulfoxide; 14, acetophenone; 15, pyridine; 16, ethyl iodide; 17, 1,2-dichloroethane; 18, *o*-dichlorobenzene; 19, benzonitrile; 20, benzaldehyde; 21, methanol; 22, 1-chloronaphthalene; 23, chloroform.

state (μ_e) dipole moments and the solvent cavity radius (a) *via* the formula[28]

$$C = \frac{2}{hc}\frac{\mu_g(\mu_g - \mu_e)}{a^3} \qquad (4)$$

Any calculation of the product $\mu_g(\mu_g - \mu_e)$ is extremely sensitive to the choice of the cavity radius a. In view of the difficulty in estimating this radius for nonspherical molecules as investigated here, the calculation was not carred out.

HMO Calculations. Solution of the secular determinants for quinones I and II leads to 23 one-electron energy levels shown in Table II, of which the lowest 12 are doubly occupied in the ground state. The energies (E) of the molecular orbitals are given in the form[25]

$$\frac{E - \alpha}{\beta} = x \qquad (5)$$

where α is the Coulomb integral of the carbon 2p orbital, β the resonance integral of the C–C bond, and x is a coefficient.

Table I: Calculated Values of $(AL_0 + B')$ and C

Absorption wavelength in hexane, nm	$(AL_0 + B')$, cm^{-1}	C, cm^{-1}
	Quinone I	
429	9,800	−715
315	7,020	~0
293	6,400	~0
280	12,400	−875
	Quinone II	
417	8,500	−700
261	9,540	~0

Table II: Calculated Molecular Orbital Energies (β Units)

Quinone I	Quinone II	Orbital designation
−2.394	−2.362	m + 11
−2.225	−2.237	m + 10
−1.805	−1.887	m + 9
−1.580	−1.508	m + 8
−1.341	−1.326	m + 7
−1.213	−1.224	m + 6
−1.073	−1.165	m + 5
−0.991	−0.898	m + 4
−0.751	−0.730	m + 3
−0.576	−0.606	m + 2
−0.045	−0.046	m + 1
0.594	0.624	m
0.913	0.805	m − 1
0.985	0.985	m − 2
1.036	1.037	m − 3
1.076	1.231	m − 4
1.417	1.266	m − 5
1.542	1.620	m − 6
1.765	1.756	m − 7
1.853	1.884	m − 8
2.241	2.185	m − 9
2.308	2.324	m − 10
2.865	2.872	m − 11

In the first-order approximation[29] the calculation of the moments for the corresponding transitions reduces to the summation shown in eq 6

$$Q_{mn} = \sum c_{mj} c_{nj} r_j \qquad (6)$$

where c_{mj} and c_{nj} are the coefficients of atomic orbitals at atom j in the final and initial molecular orbitals m and n, r_j is the position vector for atom j, and the summation is taken over all atoms in the molecule. The direction of the moments for the four lowest transitions in I and II, as calculated by eq 6, are shown in Figure 5. Molecules I and II have the molecular plane as their only symmetry element; however, for purposes of comparison the coordinate system adopted by Drott and Dearman for anthraquinone[10] was used in this work.

π-Electron density at a given atom j is given by eq 7

$$P_j = \sum n_i (C_{ij})^2 \qquad (7)$$

(29) L. Salem, "The Molecular Orbital Theory of Conjugated Systems," W. A. Benjamin, New York, N. Y., 1966, Chapter 7.

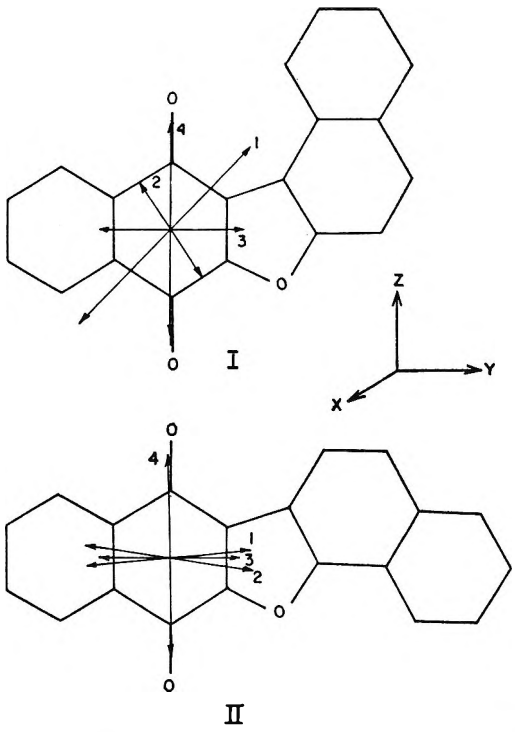

Figure 5. Transition moment vectors calculated using Hückel molecular orbital theory. Numbers refer to transitions discussed in the text.

where n_i is the number of electrons in each molecular ψ_i and C_{ij} is the coefficient of atomic orbital ϕ_j in the ith molecular orbital. Ground-state π-electron densities calculated in this manner are shown in Figure 6, together with changes in electron density occurring at each atom in the lowest energy singlet–singlet transition (values shown in parentheses). Using the calculated electron density changes and coordinates obtained from molecular models, the dipole moment change ($\mu_g - \mu_e$) associated with the long wavelength absorption band were calculated to be -17.3 and -22.4 D for I and II, respectively. The magnitude and direction of the dipole moment changes are also shown in Figure 6. Vectorial addition of σ-bond moments[30] and π moments obtained from ground-state electron densities leads to estimates of 1.4 and 1.9 D for the ground-state dipole moments (μ_g) of I and II, respectively. The product $\mu_g(\mu_g - \mu_e)$ (eq 4) is then -24.2 and -42.6 D^2 for I and II, respectively. Since electron densities as calculated from one-electron wave function are expected to be less reliable for higher energy transitions,[31] the dipole moment changes were only calculated for the lowest transition.

Discussion

The absorption spectra of the isomeric furanquinones I and II show some similarity to each other and to the spectra of p-quinones in general.[6] Four main regions of absorption are identifiable, according to energy and intensity, in the spectra shown in Figure 2 and 3: (a)

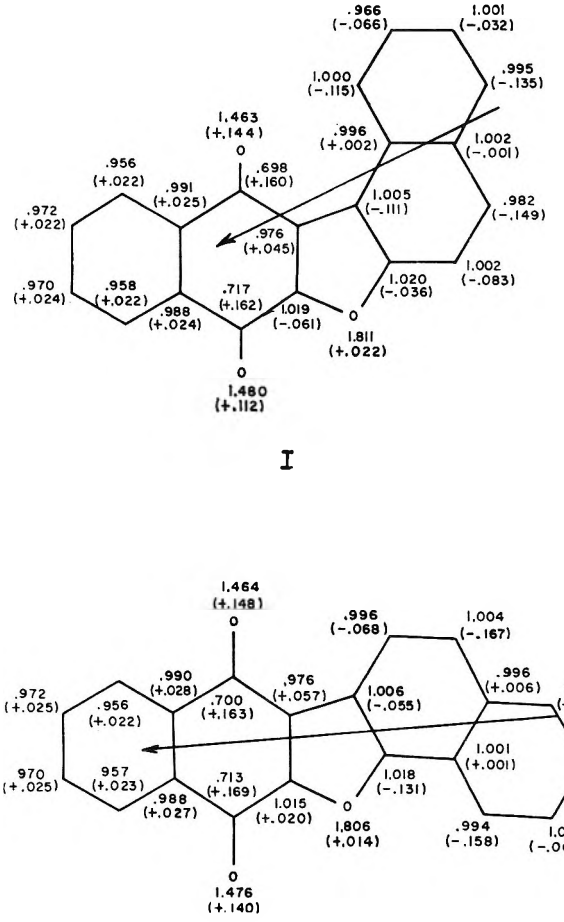

Figure 6. π-Electron density distributions calculated using Hückel molecular orbital theory. Electron density changes for the lowest energy $\pi-\pi^*$ transition shown in parentheses. Arrows depict magnitude and direction of dipole moment changes.

a broad band ($\epsilon \sim 6 \times 10^3$) with maxima in hexane at 429 and 417 nm for I and II, respectively; (b) a slightly weaker absorption ($\epsilon \sim 3 \times 10^3$) with a maximum near 335 nm; (c) a multiple structured absorption ($\epsilon \sim 10^4$) between 270 and 320 nm which possibly contains more than one electronic transition; and (d) a stronger absorption ($\epsilon \sim 10^4$ to 10^5) lying below 270 nm.

The long wavelength absorption (region a) contains a vibrational frequency of approximately 1100 cm^{-1} which is tentatively associated with the furan COC stretching vibration.[32] Polar solvents induce a red shift in the band, with a loss in structure, which with the medium intensity of the band is consistent with a $\pi-\pi^*$ assignment to the transition. As no weak carbonyl n–π^* absorption was observed in the spectra, it is

(30) R. A. W. Hill and L. E. Sutton, *J. Chem. Soc.*, 746 (1949).

(31) R. S. Becker, "Theory and Interpretation of Fluorescence and Phosphorescence," Wiley-Interscience, New York, N. Y., 1969, Chapter 2.

(32) L. J. Bellamy, "The Infra-Red Spectra of Complex Molecules," 2nd ed, Methuen, London, 1958.

expected that the local symmetry forbidden transition is buried beneath this $\pi-\pi^*$ absorption band. The solvent-induced frequency shifts of the transition in absorption suggest a significant increase in dipole moment on exciting these molecules to their lowest excited singlet state. The dipole–dipole contribution to the solvent-induced shifts in absorption, eq 3, is comparable to those observed for the charge-transfer absorption bands of amino- and hydroxy-substituted quinones.[33] The intramolecular charge-transfer nature of this transition is further confirmed by the molecular orbital calculations of the change in π-electron density distribution on going from the ground to first excited singlet state (Figure 6). It is seen that in general there is a shift in π-electron density from various carbon atoms in the heterocyclic side of the molecule to the quinoid carbonyl groups. The magnitude of this loss in density from the ring carbon atoms in I is in agreement with the bathochromic shifts observed when electron donating substituents are attached to these positions.[21] The dipole moment changes ($\mu_g - \mu_e$) for this transition, of -17.3 and -22.4 D for I and II, respectively, are of similar magnitude to the dipole moment changes reported for other intramolecular charge-transfer systems.[34] Though no attempt was made to calculate the dipole moment change for this transition from the solvent shift data (eq 4), due to the inherent errors in calculating the cavity radius for nonspherical molecules, substitution of the calculated values of μ_g and ($\mu_g - \mu_e$) in eq 4 does provide an estimate of this radius. Values of 7.0 and 8.5 Å were obtained for I and II, respectively, which are in fair agreement with the respective values of 6 and 7 Å estimated from molecular models. In this case it would appear that the calculated dipole moment changes are consistent with the observed solvent-induced frequency shifts of the transition. Hückel MO theory also predicts a shift of transition 1 (m $\rightarrow$ m + 1) to higher energies on going from molecule I to II which is in agreement with the observations. Similar shifts in the long wavelength $\pi-\pi^*$ transitions of isomeric heterocyclic molecules have been attributed to variations in the degree of charge polarization (charge transfer) in the isomers.[35] This interpretation is in qualitative agreement with our observations in the furanquinones where the long wavelength transition in II involves a greater degree of polarization than in I. In terms of the weakly interacting chromophore model of quinones[3] this transition is then assigned as benzenoid having its origin in the electronic states of the heterocyclic portion of the furanquinone. The degree of polarization (P) of this transition is close to the theoretical limit of 0.5 for a transition moment parallel to the emission oscillator. This is expected for the longest wavelength $\pi-\pi^*$ singlet–singlet transition in molecules of low symmetry where the fluorescence emission is also $\pi-\pi^*$. Though the absolute direction of polarization cannot be deduced from the polarization spectra, the molecular orbital calculations predict that the transition has both Y and Z polarized components in I and is predominantly Y polarized in II (Figure 5). The long axis polarization of this transition is analogous to the direction of polarization of the intramolecular charge-transfer transition in substituted quinones.[36]

The solvent-induced red shift of the absorption band at 335 nm (region b), though not analyzed in terms of the McRae equation due to poor resolution of the maxima in polar solvents, allows a $\pi-\pi^*$ assignment to this transition in both molecules. Absorption bands of similar intensity and energy are also observed in the spectra of simple p-quinones containing a single benzene ring fused to the quinoid nucleus.[3] The polarization (P) measured for this band predicts polarization angles of 45 and 19° in I and II, respectively. Using the calculated moment direction for transition 1, the 335-nm transition is Y polarized in II and by analogy also Y polarized in I rather than Z polarized. The analogous absorption band in anthraquinone is also Y polarized.[10] The molecular orbital calculations predict transition 2 (m $-$ 1 $\rightarrow$ m + 1) to have a higher energy in I than II and to have both Y- and Z-polarized components in I and be Y polarized in II (Figure 5). This appears inconsistent with the spectral properties of the 353-nm absorption discussed above. The characteristics of this absorption band are in fact more consistent with the calculated energy and direction of polarization of transition 3 (m $-$ 2 $\rightarrow$ m + 1) which is predicted to have similar intensity and energy and Y polarization in both quinone I and II. Thus, either the molecular orbital calculations predicts an incorrect order energetically for transitions 2 and 3 or transition 2 is not obvious in the spectra of these quinones. Some decrease in the degree of polarization is observed in the region of 400 nm in the spectra of both I and II which might indicate an underlying transition in this region. The molecular orbital calculations also predict that the m $-$ 2 orbital in both molecules is localized on the naphthoquinone portion of the molecule which is further indicative of the applicability of a weakly interacting chromophore model to these quinones.

Complexities in the spectra of I and II below 300 nm make identification of the transitions below this wavelength more difficult. Solvent shifts and intensities of the absorption maxima are again consistent with $\pi-\pi^*$ assignments for the transition in both molecules. The analysis of the solvent shift data according to McRae's equation for the maxima in the region 280 to 315 nm (region c) in the spectrum of I indicates two overlapping

(33) Z. Yoshida and F. Takobayashi, *Tetrahedron*, **24**, 933 (1968).
(34) P. Suppan, *J. Mol. Spectrosc.*, **30**, 17 (1939).
(35) G. R. Clemo and D. G. I. Felton, *J. Chem. Soc.*, 1658 (1952).
(36) N. V. Platenova, K. R. Popov, and L. V. Smirnov, *Opt. Spektrosk.*, **26**, 197 (1969).

transitions. The first of these transitions with a maximum at 280 nm in hexane involves an increase in the dipole moment in the excited state as indicated by the dipole–dipole contribution to the solvent shift (Table I). However no increase in dipole moment is indicated by the solvent shift data for the 293-, 303-(shoulder), and 315-nm maxima, and they are therefore assigned to a second transition. The vibrational spacing for the latter transition corresponds to a frequency of approximately 1200 cm^{-1}. The polarization of the spectrum in this region is consistent with this assignment, the degree of polarization of the maximum at 280 nm being lower than that for the other maxima. The absolute direction of polarization for these transitions cannot be deduced, though a value of 28° is obtained for θ from the degree of polarization of the 293-nm band, this angle can only be approximate due to the strong overlap of transitions in this region. With transition 1 having both Y- and Z-polarized components in this molecule, the degree of polarization for this band would indicate either predominantly Y or predominantly Z polarization for these transitions. The maxima at 277 and 285 nm in the spectrum of II are also assigned to one transition while the weaker bands at 300 (shoulder) and 313 nm in the same spectrum are assigned to another. The rapidly changing degree of polarization in this region of the spectrum hinders any deduction of the direction of polarization of these transitions, though the low polarization P for the region near 300 nm does indicate both Y- and Z-polarized components for the weaker transition. In the absence of further evidence to the contrary the absorption at 280 nm in I and at 277 and 285 nm in II are tentatively identified with transition 4 ($m - 3 \rightarrow m + 1$). Hückel MO theory predicts this transition to have similar intensity and energy and Z polarization in both molecules. The analogous transition in other p-quinones has been assigned as quinoid.[3,4] Identification of the other transition in this region with either transition 2 or higher transitions is speculative due to the possibility of an incorrect ordering of transition energies as calculated by the Hückel MO theory used in this work.

The transition(s) in the absorption region below 270 nm (region d) are again identified as π–π^* in both I and II. The transition in II is red shifted and intensified with respect to that in I. The degree of polarization in this wavelength region is positive and indicates the transition moment to be nearly parallel with the emission oscillators in both molecules. No attempt was made to assign the transition to a calculated transition for reasons mentioned above.

In conclusion, transition moment directions calculated by simple MO theory, for the low-lying singlet–singlet π–π^* transitions in these quinones are in fair agreement with experimental observations. Both absorption spectra and theory provide some support for a weakly interacting chromophore model for these quinones. The longest wavelength singlet–singlet π–π^* transition in these molecules is shown to involve significant intramolecular charge transfer. Further, the latter observation is in accord with the significant polar solvent-induced frequency shifts of the fluorescence emission of I and II.[37] The relative position and nature of the low-lying singlet and triplet states of these furanquinones have been ascertained from their fluorescence and phosphorescence spectra and will be reported shortly.[37]

Acknowledgments. The authors wish to thank Dr. A. R. Monahan, Dr. J. B. Flannery, Jr., and Dr. G. E. Johnson for stimulating discussions on this work, A. VanLaeken for assistance in the synthesis of these compounds, and A. Wilson for computer programming.

(37) M. S. Walker, R. L. Miller, and J. E. Kuder, to be published.

Mass Spectrometric Determination of the Dissociation Energies of the Molecules Ho_2, HoAg, and HoAu[1]

by D. L. Cocke and K. A. Gingerich

Department of Chemistry, Texas A & M University, College Station, Texas 77843 *(Received April 22, 1971)*

Publication costs borne completely by The Journal of Physical Chemistry

The equilibria involving gaseous species over the Ho–Ag system (series I) and over the Ho–Al–Au system (series II) have been investigated using the combined Knudsen effusion and mass spectrometric techniques. The third law enthalpies, $\Delta H_0°$, in kilocalories per mole, of the reactions (1) Ho(g) + Ag_2(g) = HoAg(g) + Ag(g), (2) HoAg(g) + Ho(g) = Ho_2(g) + Ag(g), (3) HoAg(g) = Ho(g) + Ag(g), (4) Ho_2(g) = 2Ho(g), (5) Ho(l) + Ho(g) = Ho_2(g) for series I, and (6) HoAu(g) + Al(g) = Ho(g) + AlAu(g) for series II have been evaluated as 8.5 ± 0.4, 8.9 ± 0.5, 28.7 ± 1.2, 19.0 ± 1.1, 56.3 ± 0.6, and 17.6 ± 0.4, respectively. Second law values of $\Delta H_0°$ corresponding to reactions 1 and 6 are 13.7 ± 3.3 and 18.4 ± 4.8 kcal mol^{-1}, respectively. The dissociation energies, $D_0°$, of the molecules, Ho_2, HoAg, and HoAu have been obtained from these enthalpies as 19.0 ± 4, 28.6 ± 4, and 59.7 ± 3 kcal mol^{-1}, respectively. The standard heats of formation, $\Delta H_f°_{298}$ of Ho_2, HoAg, and HoAu have been derived as 124 ± 4, 111 ± 4, and 99.3 ± 3 kcal mol^{-1}, respectively. The Pauling model of a polar bond is assessed with the experimental values of the dissociation energies of Ho_2, HoAg, and HoAu.

Introduction

The recent interest in the gaseous diatomic metals and intermetallic compounds is illustrated by several reviews.[2,3] The applicability of the Pauling model of a polar bond[4] to gaseous diatomic intermetallic compounds has been noted previously.[2b,5] The Pauling model has been confirmed to hold for compounds between metals of substantially different electronegativities[6,7] and has been used to predict bond energies of previously unknown diatomic intermetallic compounds.[6-8]

The Pauling model requires the dissociation energies of symmetric diatomic metals for the estimation of the bond energies of the corresponding heterodiatomic molecules. The lack of knowledge of the dissociation energies of many homonuclear diatomic transition metals restricts the applicability of the Pauling model.

The present investigation of the dissociation energies of Ho_2, HoAg, and HoAu permits the extention of the Pauling model to holmium compounds and allows the model to be tested with the molecules HoAg and HoAu. In addition, this investigation should contribute to the understanding of bonding between metals.

Experimental Section

The mass spectrometer and experimental procedures used for this work have been described previously.[9] This paper describes essentially two independent experiments which will be referred to as series I and series II. Series I is the vaporization study of an initial 3.4:1 atomic ratio holmium–silver system over the temperature range from 1582 to 1763°K, for which a single chamber tantalum Knudsen cell was used. Series II is the vaporization of an initial 1:1:1 atomic ratio Ho–Au–Al system from a molybdenum Knudsen cell over a temperature range from 1851 to 1984°K.

Temperatures for series I and II were measured with a calibrated Leeds and Northrup optical pyrometer *via* a 0.040-in. diameter by 0.125-in. deep hole in the bottom of the Knudsen cell. Measured temperatures were corrected for the effective emissivity of the cylindrical cavity and target material as described by Williams.[10] The effective emissivities for the tantalum and molybdenum targets were taken as 0.94 and 0.89, respectively. Measured temperatures were corrected for the absorbed target brightness by the viewing window and the deflecting prism.

The ions were produced with ionizing electrons and electron emission currents of 18 eV and 1 mA, respec-

(1) Work performed as part of the Ph.D. degree requirement by D. L. Cocke.

(2) (a) B. Siegel, *Quart. Rev., Chem. Soc.*, **19**, 77 (1965); (b) J. Drowart in "Phase Stability in Metals and Alloys," P. S. Rudman, J. Stringer, and R. I. Jaffee, Ed., McGraw-Hill, New York, N. Y., 1967, pp 305–317.

(3) K. A. Gingerich, *J. Cryst. Growth*, **9**, 31 (1971).

(4) L. Pauling, "The Nature of the Chemical Bond," 3rd ed, Cornell University Press, Ithaca, N. Y., 1960.

(5) M. Ackerman, F. E. Stafford, and G. Verhaegen, *J. Chem. Phys.*, **36**, 1560 (1962).

(6) G. D. Blue and K. A. Gingerich, presented at the 16th Annual Conference on Mass Spectrometry and Allied Topics, Pittsburgh, Pa., May 1968; details to be published.

(7) K. A. Gingerich and H. C. Finkbeiner, *J. Chem. Phys.*, **52**, 2956 (1970).

(8) K. A. Gingerich and H. C. Finkbeiner, *J. Chem. Soc. D*, **16**, 901 (1969).

(9) K. A. Gingerich, *J. Chem. Phys.*, **49**, 14 (1968).

(10) C. S. Williams, *J. Opt. Soc. Amer.*, **51**, 564 (1961).

tively, for series I and 20 eV and 5 mA, respectively, for series II. The acceleration voltage used was 4.5 kV; the voltage at the entrance of the shield of the electron multiplier was 1.9 kV.

For series I, an ion source was used which employed magnetic focusing of the electron beam to increase the sensitivity. A conventional electron bombardment ion source was used for series II.[9] Identification of the ions was accomplished by their mass to charge ratio, shutterability, and ionization efficiency curves, and in addition, for series I, by their isotopic intensity distribution. The ions detected from the holmium–silver system at 1654°K were Ho^+, Ag^+, Ag_2^+, $HoAg^+$, and Ho_2^+, in decreasing order of intensity. The ions detected over the holmium–gold–aluminum system at 1873°K were Al^+, Ho^+, Au^+, $AlAu^+$, and $HoAu^+$ in decreasing order of intensity. For series I appearance potentials were determined for Ho^+, Ag_2^+, and $HoAg^+$ by the extrapolated voltage difference method of Warren,[11] using that of Ag^+ as the reference[12] and are given in Table I with the estimated accuracies. The

Table I: Experimental and Estimated Parameters

Ion	Appearance potential, eV	Ionization cross section, σ_i	Relative multiplier gains, γ_i/γ_{Ag}	Intensity correction factor, E_i	Calibration constant k_i, atm/A K
		Series I			
Ho	5.7 ± 0.5	8.62[b]	0.93	1.00	0.128
Ag	7.57[a]	5.44[b]	1.00	1.00	0.190
Ag_2	6.4 ± 0.7	8.16	0.90	1.00	0.141
HoAg	5.7 ± 0.6	10.54	0.93	1.00	0.105
Ho_2	6.0 ± 1.0	12.93	0.84	1.00	0.095
		Series II			
Al	6.6 ± 0.6	5.43[b]	1.59	1.08	
Ho	5.8 ± 0.2	8.62[b]	0.93	1.07	
Au	9.22[a]	6.46[b]	0.75	1.46	
AlAu	7.8 ± 0.3	8.92	0.67	1.00	
HoAu	6.2 ± 0.5	11.31	0.81	1.00	

[a] Reference 12. [b] Reference 15.

relative large error terms for series I ions is attributed to the irregular ionization efficiency curves obtained with the temporary magnetic focusing ion source that was used. The appearance potential for Ho_2^+ was estimated as 6.0 ± 1.0 eV from the rather poor ionization efficiency curve obtained due to the small intensities involved. Appearance potentials for series II ions given in Table I were also determined by the Warren method[11] with that of Au^+ as the reference.[12] For both series I and II, the appearance potentials suggest that all ions are formed by direct ionization of the corresponding neutral atoms or molecules and not by fragmentation. However, as evidenced by the ionization efficiency curve of Ho_2^+ a possible fragmentation contribution of less than 10% was neglected, but was considered in the error estimates.

The ion currents presented below in Tables IV–VII, are relative ion currents because they represent the observed ion currents after amplification with an electron multiplier and recording with a vibrating reed electrometer. The signal-to-noise ratio was larger than 2 for the smallest relative ion currents reported (*e.g.*, for the $I(Ho_2^+)$ values in Table V). The corresponding error in the values reported was less than 30%. As the signal-to-noise ratio increased in proportion with the increasing relative ion current, the error in the measured values decreased to less than 2% (*e.g.*, for the $I(Ho^+)$ values in Table VII below).

For the series I experiment, two methods of pressure calibration were used. The first method was by means of measured intensities of $^{109}Ag^+$ at three temperatures between 1034 and 1061°K, prior to the reaction of the silver with the holmium. In going to the next temperature, 1076°K, a sudden decrease of the Ag^+ intensity occurred. At this moment, apparently the liquid eutectic was formed. The calibration constant, k_{Ag}, was calculated from the ion intensities and known silver vapor pressures[13] for the measurements prior to the formation of the eutectic. An average value for k_{Ag} of 0.190 atm/A K was obtained and used in all subsequent calculations for series I. The k_i values for species i are given in Table I.

The other calibration procedure used to obtain k_{Ag} was from evaluation of the equilibrium $Ag_2(g) = 2Ag(g)$ with a dissociation energy, $D_0°$ of 37.6 ± 2.2 kcal mol^{-1} [2b] over the temperature range from 1582 to 1760°K as described by Grimley.[14] The ion currents used and k_{Ag} values obtained in this calibration are given in Table II. An average calibration constant of 0.188 atm/A K was obtained. Although this value is in close agreement with the k_{Ag} obtained in the other calibration procedure, the observed variation of the calibration constant k_{Ag} as seen in Table II indicates a changing sensitivity. The sensitivity is higher for the first half of the data sets evaluated, giving an average k_{Ag} of 0.139 atm/A K. For the second half, an average k_{Ag} of 0.237 atm/A K is obtained. This observation indicates a decrease in sensitivity of the instrument between the first and second part of the investigation.

As stated previously, the k_{Ag} value of 0.190 atm/A K was used for calculations of absolute pressures in series I. Using this calibration constant and the ion intensities for Ag^+ and Ag_2^+ shown in Table II, the $D_0°$ of Ag_2 was calculated as 37.5 ± 1.0 kcal mol^{-1}, which compares well with the literature value[2b] of

(11) J. A. Warren, *Nature (London)*, **165**, 810 (1950).

(12) C. E. Moore, *Nat. Bur. Stand. (U. S.), Circ.*, **467**, 48, 186 (1958).

(13) R. Hultgren, R. L. Orr, and K. K. Kelley, "Supplement to Metals and Alloys," University of California, Berkeley, Calif., Gold (1969), Aluminum (1968), Silver (1968), and Holmium (1966).

(14) R. T. Grimley in "Characterization of High-Temperature Vapors," J. L. Margrave, Ed., Wiley, New York, N. Y., 1967, pp 195–243.

Table II: Ion Intensities Used in the Calculation of the Calibration Constant k_{Ag} from the Reaction $Ag_2(g) = 2Ag(g)$

T, °K	Relative ion currents, A[a] $I(Ag^+)$	$I(Ag_2^+)$	k_{Ag}, atm/A K
	Part I[b]		
1582	6.27×10^{-8}	3.68×10^{-12}	1.61×10^{-1}
1597	7.73×10^{-8}	4.50×10^{-12}	1.46×10^{-1}
1618	1.09×10^{-7}	7.10×10^{-12}	1.33×10^{-1}
1654	1.54×10^{-7}	1.18×10^{-11}	1.42×10^{-1}
1680	2.34×10^{-7}	1.86×10^{-11}	1.15×10^{-1}
	Part II[c]		
1648	1.25×10^{-7}	1.04×10^{-11}	1.83×10^{-1}
1683	1.29×10^{-7}	9.75×10^{-12}	2.04×10^{-1}
1717	1.36×10^{-7}	1.30×10^{-11}	3.03×10^{-1}
1734	1.49×10^{-7}	1.09×10^{-11}	2.35×10^{-1}
1760	1.32×10^{-7}	8.13×10^{-12}	2.61×10^{-1}
		Av	1.88×10^{-1}

[a] Ion intensities corrected for isotopic distribution. [b] Average $k_{Ag} = 0.139$ atm/A K. [c] Average $k_{Ag} = 0.237$ atm/A K.

37.6 ± 2.2 kcal mol^{-1}. This supports the assumption of unit activity for silver in the calibration procedure using known silver vapor pressures.

Absolute pressures, P_i, were obtained in series I from the measured ion currents, I_i, for each species i by the relations $P_i = k_i I_i T_i$ and $k_i = k_{Ag}\sigma_{Ag}\gamma_{Ag}E_i/\sigma_i\gamma_i$ where σ_i is the relative maximum ionization cross section, γ_i is the relative multiplier gain, I_i has been corrected for isotopic fractional abundance of the species under consideration, and k_i is the pressure calibration constant. The empirical factor, E_i, which is given in Table I, for each ion, is needed to correct the ion intensities measured with an electron voltage that is less than that at the maximum of the ionization efficiency curve. E_i is given by the relation $E_i = I_m/I_i$ where I_m is the ion intensity at the maximum of the ionization efficiency curve and I_i is the intensity at the particular electron energy used. E_i for HoAg and Ho_2 were not measured, but were assumed not to be different from E_{Ho} and E_{Ag}. From the observed ionization efficiency curves for series II ions E_i values were measured and are also given in Table I.

Atomic ionization cross sections were taken directly from Mann[15] while the molecular ionization cross sections were calculated by taking 0.75 of the sum of Mann's atomic cross sections. For series I, the multiplier gains for Ho and Ag were measured as 1.25×10^5 and 2.42×10^5, respectively, using a Faraday cup. Multiplier gains for Ag_2, Ho_2, and HoAg were estimated as $0.9\gamma_{Ag}$, $0.9\gamma_{Ho}$, and $1.0\gamma_{Ho}$, respectively. For series II, the relative multiplier gains to Ag, which were measured in other experiments under similar conditions for Al, AlAu, and HoAu, are given in Table I. The electron multiplier gain for HoAu is taken as $1.08\gamma_{Au}$ in analogy to CeAu.[7]

Results and Discussion

For series I, the third law enthalpies, $\Delta H_0°$, in kilocalories per mole of the reactions

$$Ho(g) + Ag_2(g) = HoAg(g) + Ag(g) \quad (1)$$

$$HoAg(g) + Ho(g) = Ho_2(g) + Ag(g) \quad (2)$$

$$HoAg(g) = Ho(g) + Ag(g) \quad (3)$$

$$Ho_2(g) = 2Ho(g) \quad (4)$$

$$Ho(l) + Ho(g) = Ho_2(g) \quad (5)$$

and for series II of the reaction

$$HoAu(g) + Al(g) = Ho(g) + AlAu(g) \quad (6)$$

were determined and are given in Table III.

Third law enthalpies, $\Delta H_0°$, were calculated using the relation

$$\Delta H_0° = -2.303RT \log K_p - T\Delta[(G_T° - H_0°)/T] \quad (7)$$

where K_p, R, and $-\Delta[(G_T° - H_0°)/T]$ represent the equilibrium constant, the gas constant, and the change of the free energy function for the corresponding reaction.

Second law enthalpies, $\Delta H_T°$, were calculated from the relation

$$\Delta H_T° = -R\mathrm{d} \ln K_p/\mathrm{d}(1/T) \quad (8)$$

and $\Delta H_0°$ values were obtained by using estimated heat content changes, $\Delta(H_T° - H_0°)$, for the corresponding reaction. The second law enthalpies for reactions 1 and 6 were calculated as $\Delta H_{1666}° = 13.5 \pm 3.3$ and $\Delta H_{1876}° = 18.5 \pm 4.8$. The corresponding $\Delta H_0°$ values are given in Table III. The second law procedure was found to be unusable for reactions 2 and 4 because of the few data and short temperature range involved.

The application of the second law treatment to reaction 3 was not possible over the 14 data sets shown in Table VI without consideration of the decrease in sensitivity from the first nine to the last five data sets. Using a k_{Ag} of 0.139 atm/A K, the average of the calibration constants, k_{Ag}, calculated for the first part of the experiment and shown in Table II, and using only the first nine data sets shown in Table VII, a $\Delta H_0° = 32.8 \pm 3.4$ kcal mol^{-1} was calculated from the second law method. Correcting the intensities of the last five data sets shown in Table VII to a sensitivity of 0.139 atm/A K and using all 14 data sets a $\Delta H_0° = 26.6 \pm 3.3$ kcal mol^{-1} was calculated from the second law method. These enthalpies determined by use of the second law method compare favorably with the corresponding third law enthalpies of 29.0 ± 0.4 and 29.1 ± 0.8 kcal mol^{-1}, respectively, as well as to the third

(15) J. B. Mann, *J. Chem. Phys.*, **46**, 1646 (1967).

Table III: Summary of Reaction Enthalpies for the Ho–Ag System (Series I) and the Ho–Au–Al System (Series II)

Reaction	Method	$\Delta H_0°$(exptl), kcal mol^{-1}		$\Delta H_0°$ (selected), kcal mol^{-1}	$D_0°$(AB), kcal mol^{-1}	$D_0°$(AB), kJ mol^{-1}	Molecule AB
			Series I				
$Ho(g) + Ag_2(g) = HoAg(g) + Ag(g)$	3rd law	(8.8)[b]	8.5 ± 0.4[c]	8.6 ± 2			
	2nd law		13.7 ± 3.3	13.7 ± 7	28.6 ± 4[d]	122 ± 17	HoAg
$HoAg(g) + Ho(g) = Ho_2(g) + Ag(g)$	3rd law	(9.9)[b]	8.9 ± 0.5[c]	9.2 ± 3	19.4 ± 5[e]	81.2 ± 21	Ho_2
$HoAg(g) = Ho(g) + Ag(g)$	3rd law		28.7 ± 1.2[c]	28.7 ± 5	28.7 ± 5	120 ± 21	HoAg
$Ho_2(g) = 2Ho(g)$	3rd law		19.0 ± 1.1[c]	19.0 ± 5	19.0 ± 5	79.5 ± 21	Ho_2
$Ho(g) + Ho(l) = Ho_2(g)$[a]	3rd law		56.3 ± 0.6	56.3 ± 7	16.0 ± 7[f]	66.9 ± 29	Ho_2
			Series II				
$Ho(g) + AlAu(g) = HoAu(g) + Al(g)$	3rd law	(15.8)[b]	17.6 ± 0.4	17.0 ± 2	59.7 ± 3[g]	250 ± 13	HoAu
	2nd law		18.4 ± 4.8	18.4 ± 6			

[a] Data taken prior to series I experiment [b] Assuming relative multiplier gains and ionization cross section cancel. [c] Using calibration constants, k_i. [d] $D_0°(Ag_2) = 37.6 \pm 2.2$ kcal mol^{-1} used, ref 2. [e] $D_0°$(HoAg) = 28.6 kcal mol^{-1} used (this investigation). [f] $\Delta H_{vap,0} = 72.3 \pm 0.3$ kcal mol^{-1} used, ref 13. [g] $D_0°$(AlAu) = 77.0 ± 1.0 kcal mol^{-1} used, ref 18.

Table IV: Third Law Enthalpies for the Reaction[a] $Ho(g) + Ag_2(g) = HoAg(g) + Ag(g)$

T, °K	Relative ion currents, A[b,c] $I(Ho^+)$	$I(Ag_2^+)$	$I(HoAg^+)$	$I(Ag^+)$	$-\log K_p$	$-\Delta[(G_T° - H_0°)/T]$, cal mol^{-1} K^{-1}	$\Delta H_0°$, kcal mol^{-1}
1582	7.05×10^{-7}	3.68×10^{-12}	2.84×10^{-12}	6.27×10^{-8}	1.163	0.19	8.7
1597	7.82×10^{-7}	4.50×10^{-12}	3.31×10^{-12}	7.73×10^{-8}	1.138	0.19	8.6
1618	9.90×10^{-7}	7.10×10^{-12}	4.15×10^{-12}	1.09×10^{-7}	1.191	0.18	9.1
1654	1.24×10^{-6}	1.18×10^{-11}	6.37×10^{-12}	1.54×10^{-7}	1.174	0.18	9.2
1680	1.52×10^{-6}	1.86×10^{-11}	8.78×10^{-12}	2.34×10^{-7}	1.139	0.18	9.1
1648	7.70×10^{-7}	1.04×10^{-11}	4.11×10^{-12}	1.23×10^{-7}	1.200	0.18	9.3
1683	6.23×10^{-7}	9.75×10^{-12}	3.66×10^{-12}	1.27×10^{-7}	1.116	0.18	8.9
1717	4.94×10^{-7}	1.30×10^{-11}	4.07×10^{-12}	1.36×10^{-7}	1.065	0.18	8.7
1734	4.60×10^{-7}	1.09×10^{-11}	3.29×10^{-12}	1.49×10^{-7}	1.010	0.18	8.3
1760	3.66×10^{-7}	8.13×10^{-12}	2.40×10^{-12}	1.30×10^{-7}	0.979	0.18	8.2
						Av	8.8 ± 0.4

[a] Assumed relative multiplier gains and ionization cross sections cancel. [b] Ion intensities corrected for isotopic distribution. [c] $p_i = 0.190 I_i T_i \sigma_{Ag} \gamma_{Ag} / \sigma_i \gamma_i$ in atmospheres.

law enthalpy $\Delta H_0° = 28.7 \pm 1.2$ kcal mol^{-1} obtained, using a $k_{Ag} = 0.190$ atm/A K and shown in Table III.

The equilibrium constants K_p for the pressure independent reactions 1, 2, and 6 were calculated from measured ion currents of the products I(C) and I(D) and reactants I(A) and I(B) by the relation $K_p = I(C)I(D)/I(A)I(B)$, where it is assumed that the ionization cross sections and relative multiplier gains of reactant and product ions cancel. The measured ion intensities corrected for isotopic abundance distribution, logarithms of the equilibrium constants, free energy function changes along with the third law enthalpies for reactions 1, 2, and 6 are given in Tables IV, V, and VI, respectively. The averages of these third law enthalpies also are given in parentheses in Table III for purpose of comparison.

Use of the calibration constants, k_i, given in Table I for series I allowed the partial pressures of the reactant and product species of reactions 1, 2, 3, and 4 to be determined. These partial pressures are given by the formulas shown in Tables IV, V, VII, and V, respectively. The corresponding third law enthalpies, where k_i values were used, are shown in Table III, for reactions 1 and 2 and in Tables VII and VIII for reactions 3 and 4, respectively.

The equilibrium constant K_p of reaction 6 was also calculated with the relative multiplier gains and ionization cross sections considered. Reaction 6 is a pressure-independent reaction of the type A + B = C + D for which the equilibrium constant K_p was determined from the relation $K_p = I(C)I(D)\sigma(A)\gamma(A)\sigma(B)\gamma(B)/I(A)I(B)\sigma(C)\gamma(C)\sigma(D)\gamma(D)$. The third law enthalpy, $\Delta H_0°$, of reaction 6 obtained from the resulting equilibrium constant is given in Table III.

Data for reaction 5 were obtained near the end of an experiment of the vaporization of a holmium–silver system in which only a relatively small amount of silver was present. This experiment was performed prior to

Table V: Third Law Enthalpies for the Reaction[a] HoAg(g) + Ho(g) = Ho_2(g) + Ag(g)

T, °K	Relative ion current, A[b,c] I(HoAg$^+$)	I(Ho$^+$)	I(Ho_2^+)	I(Ag)	−log K_p	$-\Delta[(G_T^\circ - H_0^\circ)/T]$, cal mol^{-1} K^{-1}	ΔH_0°, kcal mol^{-1}
1582	2.84×10^{-12}	7.05×10^{-7}	1.74×10^{-13}	6.27×10^{-8}	2.264	4.50	9.3
1618	4.15×10^{-12}	9.90×10^{-7}	1.98×10^{-13}	1.09×10^{-7}	2.280	4.51	9.6
1654	6.47×10^{-12}	1.24×10^{-6}	2.28×10^{-13}	1.54×10^{-7}	2.359	4.51	10.4
1680	8.78×10^{-12}	1.52×10^{-6}	2.76×10^{-13}	2.34×10^{-7}	2.315	4.51	10.2
						Av	9.9 ± 0.5

[a] Assumed relative multiplier gains and ionization cross sections cancel. [b] Ion intensities corrected for isotopic distribution. [c] $p_i = 0.190 I_i T_i \sigma_{Ag}\gamma_{Ag}/\sigma_i\gamma_i$ in atmospheres.

Table VI: Third Law Enthalpies for the Reaction[a] Ho(g) + AlAu(g) = HoAu(g) + Al(g)

T, °K	Relative ion currents, A[b] I(Ho$^+$)	I(AlAu$^+$)	I(HoAu$^+$)	I(Al$^+$)	−log K_p	$-\Delta[(G_T^\circ - H_0^\circ)/T]$, cal mol^{-1} K^{-1}	ΔH_0°, kcal mol^{-1}
1851	5.06×10^{-9}	5.91×10^{-11}	3.84×10^{-13}	1.66×10^{-8}	1.667	0.83	15.7
1778	2.48×10^{-9}	2.38×10^{-11}	1.71×10^{-13}	6.32×10^{-9}	1.733	0.84	15.6
1805	3.10×10^{-9}	3.63×10^{-11}	2.58×10^{-13}	7.77×10^{-9}	1.745	0.83	15.9
1873	3.33×10^{-9}	5.70×10^{-11}	5.34×10^{-13}	7.59×10^{-9}	1.666	0.84	15.9
1918	3.40×10^{-9}	7.04×10^{-11}	8.40×10^{-13}	5.64×10^{-9}	1.699	0.85	16.6
1944	2.16×10^{-9}	1.02×10^{-10}	1.81×10^{-12}	3.29×10^{-9}	1.564	0.85	15.6
1984	2.52×10^{-9}	8.49×10^{-11}	2.95×10^{-12}	2.43×10^{-9}	1.471	0.85	15.0
						Av	15.8 ± 0.5

[a] Assumed relative multiplier gains and ionization cross sections cancel. [b] Ion intensities corrected for isotopic distribution.

Table VII: Third Law Enthalpies for the Reaction HoAg(g) = Ho(g) + Ag(g)

T, °K	Relative ion currents, A[a,b] I(HoAg$^+$)	I(Ho$^+$)	I(Ag$^+$)	log K_p	$-\Delta[(G_T^\circ - H_0^\circ)/T]$, cal mol^{-1} K^{-1}	ΔH_0°, kcal mol^{-1}
1485	3.68×10^{-13}	2.63×10^{-7}	1.41×10^{-8}	0.540	21.54	28.3
1516	8.14×10^{-13}	4.24×10^{-7}	2.61×10^{-8}	0.679	21.56	28.0
1511	6.97×10^{-13}	3.75×10^{-7}	2.47×10^{-8}	0.676	21.57	28.0
1543	1.69×10^{-12}	5.83×10^{-7}	4.58×10^{-8}	0.752	21.58	28.0
1582	2.84×10^{-12}	7.05×10^{-7}	6.27×10^{-8}	0.756	21.60	28.7
1597	3.31×10^{-12}	7.82×10^{-7}	7.73×10^{-8}	0.830	21.62	28.4
1618	4.15×10^{-12}	9.90×10^{-7}	1.09×10^{-7}	0.989	21.63	27.7
1654	6.37×10^{-12}	1.24×10^{-6}	1.54×10^{-7}	1.060	21.66	27.8
1680	8.78×10^{-12}	1.52×10^{-6}	2.34×10^{-7}	1.198	21.69	27.2
1648	4.11×10^{-12}	7.70×10^{-7}	1.23×10^{-7}	0.944	21.66	28.6
1683	3.66×10^{-12}	6.23×10^{-7}	1.27×10^{-7}	0.926	21.69	29.4
1717	4.07×10^{-12}	4.94×10^{-7}	1.36×10^{-7}	0.817	21.72	30.9
1734	3.29×10^{-12}	4.60×10^{-7}	1.49×10^{-7}	0.923	21.73	30.4
1760	2.40×10^{-12}	3.66×10^{-7}	1.30×10^{-7}	0.907	21.74	31.0
					Av	28.7 ± 1.2

[a] $P_i = 0.190 I_i T_i \sigma_{Ag}\gamma_{Ag}/\sigma_i\gamma_i$ in atmosphere. [b] Ion intensities corrected for isotopic distribution.

series I and under the same experimental conditions. The Ho_2^+ ion was first observed and several ion intensity measurements were taken on the Ho^+, Ag^+, $HoAg^+$, and Ho_2^+ species over the temperature range from 1718 to 1763°K, where, for example, at 1743°K, the relative ion intensities were 2.43×10^{-6}, 1.36×10^{-8}, 1.05×10^{-12}, and 5.13×10^{-13} A, respectively. These data allowed evaluation of the third law enthalpy, ΔH_0°, of the pressure-independent reaction 5 where the relative multiplier gains and ionization cross sections were considered, along with the assumption that the liquid holmium was at unit activity. These results

Table VIII: Third Law Enthalpies for the Reaction[a] $Ho_2(g) = 2Ho(g)$

T, °K	log K_p	$-\Delta[(G_T^\circ - H_0^\circ)/T]$, cal mol^{-1} K^{-1}	ΔH_0°, kcal mol^{-1}
1582	2.890	26.10	20.4
1618	3.139	26.14	19.1
1654	3.283	26.17	18.4
1683	3.383	26.20	18.0
		Av	19.0 ± 1.1

[a] Relative ion currents used are given in Table V.

are shown in Table IX. Due to a reaction of holmium vapor with the thermocouple used, it was necessary to estimate the temperatures for the three data points for reaction 5. The temperatures were estimated from the tungsten coil heater power supply setting and are estimated to be correct within ±60°K.

parameters given by Cheetham and Barrow.[16] Free energy functions for Ho_2, HoAg, and HoAu were calculated from estimated molecular parameters. For Ho_2, HoAg, and HoAu, the equilibrium separation, r_e, of the atoms was obtained as 3.04, 2.68, and 2.64 Å, respectively, by the sum of the Pauling metallic radii,[4] for the atoms, and were subsequently corrected in proportion to the spectroscopically observed bond shortening in Au_2 and AlAu.[16] The vibrational frequencies, ω_e, were calculated at 135.2 cm^{-1} for Ho_2, 203.2 cm^{-1} for HoAg, and 217.0 cm^{-1} for HoAu by use of the Guggenheimer relation.[17] Here, the polar bond version was used for HoAg and HoAu. The z values were assumed as 5, 3, and 7, for Ho, Ag, and Au, respectively. In addition, an electronic contribution to the free energy functions for Ho_2, HoAg, and HoAu was taken as 3 cal mol^{-1} K^{-1}. The calculated and estimated free energy functions are listed in Table X.

The uncertainties given in Tables IV–IX, for the average third law enthalpies, ΔH_0°, for reactions 1–6

Table IX: Third Law Enthalpies for the Reaction[a] $Ho(g) + Ho(l) = Ho_2(g)$

T, °K	Relative ion current, A[b] $I(Ho^+)$	Relative ion current, A[b] $I(Ho_2^+)$	$-\log K_p$	$-\Delta[(G_T^\circ - H_0^\circ)/T]$, cal mol^{-1} K^{-1}	ΔH_0°, kcal mol^{-1}
1718	1.98×10^{-6}	3.06×10^{-13}	6.941	0.89	56.1
1743	2.43×10^{-6}	5.13×10^{-13}	6.805	0.85	55.8
1763	2.79×10^{-6}	4.89×10^{-13}	6.886	0.79	56.9
				Av	56.3 ± 0.6

[a] Relative multiplier gains and ionization cross sections included. [b] Ion intensities corrected for isotopic distribution.

Table X: Free Energy Functions $-(G_T^\circ - H_0^\circ)/T$ in cal mol^{-1} K^{-1} for HoAg(g), $Ag_2(g)$, $Ho_2(g)$, AlAu(g), and HoAu(g)

T, °K	HoAg(g)	$Ag_2(g)$	$Ho_2(g)$	AlAu(g)	HoAu(g)
298	58.88	53.24	59.56	52.25	60.22
1400	72.02	66.42	72.92	65.03	73.32
1500	72.62	67.02	73.53	65.62	73.92
1600	73.19	67.59	74.10	66.18	74.49
1700	73.72	68.12	74.63	66.71	75.02
1800	74.22	68.62	75.14	67.20	75.52
1900	74.69	69.10	75.61	67.67	76.00
2000	75.15	69.55	76.06	68.12	76.45

Free energy functions, $-(G_T^\circ - H_0^\circ)/T$, used in the calculation of the third law enthalpies were taken from the literature where available or calculated by means of statistical thermodynamics, using the rigid-rotator, harmonic oscillator approximation, from known or estimated molecular parameters. For Ho, Al, Ag, and Au, the necessary free energy functions were taken from Hultgren, *et al.*[13] For Ag_2 and AlAu, the free energy functions were calculated from molecular

are standard deviations. The uncertainties given for the selected ΔH_0° values and for D_0°(AB) in Table III represent an inclusion of the estimated errors in the intensities, temperature measurements, the free energy functions, the relative multiplier gains, and the ionization cross sections used. Also included where necessary were the estimated uncertainties in the dissociation energies of Ag_2, HoAg, and AlAu, as well as the uncertainty in the heat of vaporization, $\Delta H_{vap,0}$, of holmium.

The average third law enthalpies taken as best for reactions 1 and 2 are 8.5 ± 0.4 and 8.9 ± 0.5 kcal mol^{-1}, where the calibration constants, k_i, were used in their calculation. For reaction 6, the best average third law enthalpy is taken as 17.6 ± 0.4 kcal mol^{-1} where ionization cross sections and relative multiplier gains were included. These enthalpies are given in Table III in the column labeled ΔH_0°(exptl). Giving these values a weight factor of two and combining them with the

(16) C. J. Cheetham and R. F. Barrow in "Advances in High Temperature Chemistry," Vol. I, L. Eyring, Ed., Academic Press, New York, N. Y., 1967, pp 7–41.

(17) K. M. Guggenheimer, *Proc. Phys. Soc.*, **58**, 456 (1946).

third law enthalpies given in parantheses in Table III, the weighted third law averages for reactions 1, 2, and 6 are obtained as 8.6 ± 2, 9.2 ± 3, and 17.0 ± 2 kcal mol^{-1}, respectively.

The weighted third law enthalpies for reactions 1 and 6 compare favorably with the enthalpies, $\Delta H_0°$, of 13.7 ± 7 and 18.4 ± 6 kcal mol^{-1} obtained by the second law method. Considering both the weighted third law enthalpies and the enthalpies obtained from the second law procedure and giving predominant weight to the third law values, final selected values for the enthalpies, $\Delta H_0°$, of reactions 1 and 6 are given as 9.0 ± 2 and 17.3 ± 2 kcal mol^{-1}, respectively. Combining these values with the literature values for the dissociation energies $D_0°(Ag_2)$ = 37.6 ± 2.2 kcal mol^{-1} [2] and $D_0°$(AlAu) = 77.0 ± 1 kcal mol^{-1} [18] yields dissociation energies $D_0°$(HoAg) and $D_0°$(HoAu) of 28.6 ± 4 and 59.7 ± 3 kcal mol^{-1}, respectively.

The dissociation energy $D_0°$(HoAg) 28.6 ± 4 kcal mol^{-1} obtained from reaction 1 agrees well with the $D_0°$(HoAg) = 28.7 ± 1.2 kcal mol^{-1}, obtained directly from reaction 3, shown in Table VII and also with the corresponding values obtained from the second law method mentioned previously. Judging all data, a final value of $D_0°$(HoAg) = 28.6 ± 4 kcal mol^{-1} or 119.7 ± 17 kJ mol^{-1} is selected.

Combining the final selected enthalpy, $\Delta H_0°$, of reaction 2 with the dissociation energy, $D_0°$(HoAg) = 28.6 ± 4 kcal mol^{-1}, yields a dissociation energy, $D_0°(Ho_2)$, of 19.4 ± 5 kcal mol^{-1}. This value is in agreement with the $D_0°$ = 19.0 ± 1.1 kcal mol^{-1} given in Table VIII and calculated directly from reaction 4.

Evaluation of reaction 5 with inclusion of the ionization cross sections and relative multiplier gains and assuming that the condensed holmium is at unit activity yields a third law enthalpy, $\Delta H_0°$, of 56.3 ± 0.6 kcal mol^{-1}. In view of the fact that a small amount of silver was present which would assure an activity of less than unity for holmium, and with the uncertainty in the temperature, a value of 56.3 ± 7 kcal mol^{-1} is chosen. Combining this with the heat of vaporization, $\Delta H_{vap,0}$ = 72.3 ± 0.3 kcal mol^{-1} of holmium yields a dissociation energy $D_0°(Ho_2)$ of 16.0 ± 7 kcal mol^{-1}. This value is somewhat less than the $D_0°(Ho_2)$ value obtained from the other reactions. However, holmium is at less than unit activity and, if this activity were known, a value of the $\Delta H_0°$ of reaction 5 less than 56.3 kcal mol^{-1} would result. A larger value for $D_0°(Ho_2)$ would consequently result, which would more closely approach the previously obtained values. Thus, irrespective of the large uncertainty in the temperature, this value compares well with those determined by reactions 2 and 4. Considering reactions 2, 4, and 5 a weighted average of 19.0 ± 4 kcal mol^{-1} or 79.5 ± 17 kJ mol^{-1} is chosen for $D_0°(Ho_2)$.

Using the dissociation energies $D_{298}°(Ho_2)$, $D_{298}°$(HoAg), and $D_{298}°$(HoAu) of 19.5 ± 4, 29.1 ± 4, and 60.3 ± 3 kcal mol^{-1}, respectively, and the standard heat of sublimation of holmium, $\Delta H_v°_{298}$ = 71.9 ± 0.3 kcal mol^{-1} [13] of silver, $\Delta H_v°_{298}$ = 67.9 ± 0.2 kcal mol^{-1} [13] and of gold, $\Delta H_v°_{298}$ = 87.7 ± 0.2 kcal mol^{-1},[19] the standard heats of formation $\Delta H_f°_{298}(Ho_2)$, $\Delta H_f°_{298}$(HoAg), and $\Delta H_f°_{298}$(HoAu) were obtained as 124 ± 4 kcal mol^{-1} (519 ± 17 kJ mol^{-1}), 111 ± 4 kcal mol^{-1} (464 ± 17 kJ mol^{-1}), and 99.3 ± 3 kcal mol^{-1} (415 ± 13 kJ mol^{-1}), respectively.

The dissociation energy of the holmium dimer, $D_0°(Ho_2)$ = 19.0 ± 4 kcal mol^{-1}, determined in this investigation allows the Pauling model of a polar bond[4] to be further applied and tested with the experimentally determined dissociation energies $D_0°$ of HoAg and HoAu. The arithmetic mean version of the Pauling model, $D(AB) = 0.5[D(AA) + D(BB)] + 23[\chi(A) - \chi(B)]^2$ which relates the bond energy of an asymmetric diatomic molecule $D(AB)$ in kilocalories per mole to a covalent and ionic contribution to the bonding has previously worked well in interpreting the high metal–metal bond energies of gaseous rare earth aurides.[7]

Applying this model to the HoAu molecule and taking the electronegativity χ(Ho) = 1.3, instead of Pauling's value[4] and χ(Au) = 2.4, a value for $D_0°$(HoAu) = 63.6 kcal mol^{-1} is calculated. Here, the $D_0°(Au_2)$ was taken as 53 kcal mol^{-1}.[3] The value predicted by the Pauling model is in fair agreement with the experimentally determined value of 59.7 ± 3 kcal mol^{-1}. The Pauling model of a polar bond is of value in interpreting the rather high stability of the HoAu molecule and indicates a substantial ionic contribution to the bonding as suggested by the large electronegativity difference between gold and holmium.

The Pauling model has been shown to be applicable to intermetallic compounds containing silver and the group IIIA metals Al, Ga, and In.[6] However, application of the Pauling model to HoAg does not show the same success. Using χ(Ag) as 1.9, χ(Ho) as 1.3, and the dissociation energy $D_0°(Ag_2)$ = 37.6 kcal mol^{-1}, a value for the dissociation energy of HoAg is calculated as 36.6 kcal mol^{-1}. This value is 8 kcal mol^{-1} larger than the experimental value of 28.6 kcal mol^{-1}. If the average of the dissociation energies $D_0°(Ag_2)$ and $D_0°(Ho_2)$ is taken, a value of 28.8 kcal mol^{-1} is obtained which is in close agreement to the experimental value. In the case of the HoAg molecule, the Pauling model overemphasizes the ionic contribution to the bonding.

Acknowledgment. The authors wish to thank the National Science Foundation for support of this work under Grant GP-12442.

(18) G. D. Blue and K. A. Gingerich, to be published.

(19) Standard Reference Material 745, Gold, National Bureau of Standards, 1969.

The Reactions of Organic Radicals Formed by Some "Fenton-Like" Reagents[1]

by Gideon Czapski,*

Radiation Research Laboratories and Department of Chemistry, Mellon Institute of Science, Carnegie-Mellon University, Pittsburgh, Pennsylvania 15213

A. Samuni, and D. Meisel

Department of Physical Chemistry, The Hebrew University, Jerusalem, Israel *(Received March 17, 1971)*

Publication costs assisted by Carnegie-Mellon University and the U. S. Atomic Energy Commission

The reactions of Fe^{2+}, Cr^{2+}, V^{4+}, and Ti^{3+} with H_2O_2 in the presence of 2-propanol were studied using the esr flow technique. It was shown that all these "Fenton-like" reagents form OH radicals which can react with the 2-propanol. From studies of the esr intensities of the alcohol radical as a function of H_2O_2, Ti^{3+}, and that of added Ti^{4+}, Fe^{3+}, and Cr^{3+} it is concluded that these ions react faster with $(CH_3)\dot{C}OH$ than with $\dot{C}H_2CHOHCH_3$. The reaction of the alcohol radicals with H_2O_2 was also studied by radiolysis experiments. The unusual kinetics and properties of "Fenton-like reagent" and OH and R radicals generated by these reagents previously reported is shown to be due to wrong kinetic assumptions.

Introduction

The reactions of many organic radicals have been studied with the use of Fenton and "Fenton-like" reagents (V^{4+}, Ti^{3+}, Cr^{2+} with H_2O_2). The addition of organic substrates to these reagents produced secondary radicals, which could be followed either spectrophotometrically, through chemical analysis or by use of esr technique. These measurements have to be made right after the rapid mixing.[2-5]

In these systems, the primary radicals are formed through the reduction of H_2O_2 by the metal ion

$$M^{n+} + H_2O_2 \xrightarrow{k_1} M^{(n+1)+} + OH^- + OH \qquad (1)$$

In the case of titanium, reaction 1 is followed by a relatively rapid formation[6] of peroxy complexes from H_2O_2 and the oxidized metal ion

$$Ti^{4+} + H_2O_2 \underset{k_{-2}}{\overset{k_2}{\rightleftharpoons}} (Ti^{4+}\text{–}H_2O_2) \qquad (2)$$

The OH radical may then react with the peroxytitanium complex producing two different paramagnetic species, usually denoted as S_1 and S_2

$$OH + (Ti^{4+}\text{–}H_2O_2) \longrightarrow S_1, S_2 \qquad (3)$$

(S_1 and S_2 may be formed from two different complexes of Ti^{4+} with H_2O_2 differing in the ligands or degrees of hydrolysis.) In the presence of an excess of H_2O_2, the OH radicals react with H_2O_2 to yield HO_2 radicals which might, in turn, react also with $(Ti^{4+}\text{–}H_2O_2)$ complexes[7]

$$OH + H_2O_2 \xrightarrow{k_4} H_2O + HO_2 \qquad (4)$$

$$HO_2 + HO_2 \xrightarrow{k_5} H_2O_2 + O_2 \qquad (5)$$

$$HO_2 + (Ti^{4+}\text{–}H_2O_2) \xrightarrow{k_6} S_1, S_2 \qquad (6)$$

The inclusion of an organic substrate (denoted RH) with the H_2O_2 leads to the formation of secondary radicals

$$RH + OH \xrightarrow{k_7} H_2O + R \qquad (7)$$

These secondary radicals may decay by self-recombination

$$R + R \xrightarrow{k_8} \text{nonradical products} \qquad (8)$$

Merz and Waters[2a] investigated the $Fe^{2+} + H_2O_2 +$ RH system. They found that the consumption ratio $\Delta[H_2O_2]/\Delta[RH]$ depends on the ratio $[Fe^{2+}]/[RH]$. They concluded that H_2O_2 oxidizes the organic radical, forming a new OH radical according to

$$R + H_2O_2 \xrightarrow{k_9} OH + \text{nonradical products} \qquad (9)$$

Norman and West[2b] used a flow system to study the same reaction by means of esr spectroscopy. They investigated, amongst other reactions, the esr spectra of the two radicals, $(CH_3)_2\dot{C}OH$ and $\dot{C}H_2CHOHCH_3$, denoted R_1 and R_2, respectively, produced upon adding 2-propanol as a substrate. They studied the dependence of the signals intensity of R_1 and R_2 on the concentrations of the reactants, the flow rates, and the order of introducing the various reactants into a double mixing chamber.

(1) Supported in part by the U. S. Atomic Energy Commission.

(2) (a) J. H. Merz and W. A. Waters, *J. Chem. Soc.*, 515 (1949); (b) R. O. C. Norman and P. R. West, *J. Chem. Soc. B*, 389 (1969).

(3) R. E. James and F. Sicilio, *J. Phys. Chem.*, **74**, 1166 (1970).

(4) R. E. James and F. Sicilio, *ibid.*, **74**, 2294 (1970).

(5) E. L. Lewis and F. Sicilio, *ibid.*, **73**, 2590 (1969).

(6) M. Orhanovic and R. Wilkins, *J. Amer. Chem. Soc.*, **89**, 278 (1967).

(7) G. Czapski, H. Levanon, and A. Samuni, *Israel J. Chem.*, **7**, 375 (1969).

Norman and West[2b] reported that the total concentration of the organic radicals ($R_1 + R_2$) is unchanged when excess of H_2O_2 is added, showing that the OH radicals produced in reaction 9 are scavenged by RH, thus perpetuating the formation of R radicals. This conclusion contradicts that of James and Sicilio[3] who used the same technique. The latter concluded that reaction 9 does exist, but the "OH" radicals formed are unreactive towards organic substrates. The conclusion was that a cyclic reaction sequence is not perpetuated by a radical + H_2O_2 reaction, since such an assumption is not in accord with the disappearance of R_1 and R_2, at high $[H_2O_2]$. Moreover, on measuring the consumption ratio $\Delta[RH]/\Delta[H_2O_2]$ they obtained a maximum of 0.5, a result which supports the exclusion of a chain reaction.

Another discrepancy is revealed upon comparing the values of the recombination rate constants (k_8) for various organic radicals formed by radiation[8-11] with those produced by "Fenton-like" reagents.[12-14]

Finally, the assumption that the secondary organic radicals are formed through reaction with a complexed OH radical, rather than by direct action of free OH with the organic molecules, is supported by some workers[12-14] but turned down by others.[2]

In the present study, we tried to elucidate the differences in the experimental results and the various interpretations which have been reported in the literature, and also to introduce new "Fenton-like" reagents.

Experimental Section

Reagents. The following reagents were used without further purification: 30% hydrogen peroxide (Merck), 2-propanol and ethanol (Frutarom Laboratory Chemicals), cerous sulfate and ceric ammonium sulfate (Puriss. Fluka), 70% perchloric acid (Merck), hydroquinone (Puriss. Fluka), and ferrous ammonium sulfate and thorium nitrate (B.D.H.), all of analytical grade.

Vanadium(IV) sulfate (Purum. Fluka), titanous sulfate solution 15% (technical, B.D.H.); titanium(IV) perchlorate was prepared as described previously.[15]

Chromium(II) perchlorate was prepared by dissolving chromium in $HClO_4$ under N_2.

Analytical Methods. Ceric perchlorate solutions were standardized spectrophotometrically in 0.8 *N* H_2SO_4, taking $\epsilon_{320} = 5580\ M^{-1}\ cm^{-1}$.[16] Hydrogen peroxide was determined either by titration with a standard solution of permanganate for flow experiments, or spectrophotometrically using the Ghormley method[17] for radiation experiments. All titanium and vanadium salts were determined spectrophotometrically as peroxy complexes after treating them with an excess of H_2O_2, taking $\epsilon_{412} = 652\ M^{-1}\ cm^{-1}$[18] and $\epsilon_{404} = 198\ M^{-1}\ cm^{-1}$[19] for peroxytitanium(IV) and peroxyvanadium(V), respectively. Chromium solutions were treated with an excess of H_2O_2 and NaOH and were determined spectrophotometrically as chromate.

Acidities were adjusted with perchloric acid. The water used was either singly or triply distilled (no difference was observed in the results when triply distilled water was replaced by singly distilled water). In radiation experiments, only triply distilled water was used. All experiments were carried out at room temperature. Spectrophotometric determinations were done with a Beckman DB-G grating spectrophotometer.

Esr Experiments. Esr spectra were recorded on a Varian X-band 4502 spectrometer. The solutions (which had been deaerated by bubbling N_2 for 15 min) were flown through a Varian-4549-liquid-flow-mixing-cell with a "dead volume" of 0.15 cc between mixing point and the center of the observation in the cell by means of a gas pressure. The flow rate was 370 cc/min unless otherwise stated. Relative intensities of the esr signal were calibrated with a solution of $VOSO_4$ without removing the cell in order to eliminate misalignment problems when comparing VO^{2+} with the radicals.

Radiation Sources. A Cs^{137} source (M Gammator, Radiation Machinery Corp.), at dose rates of approximately 1.2×10^{17} eV g^{-1} min^{-1}, was used. Total doses delivered to the solutions were 1.2×10^{17} to 1.1×10^{18} eV g^{-1}. Dosimetry was done with the Fricke dosimeter taking $G(Fe^{3+}) = 15.6$. Solutions were deaerated in 10-ml syringes by bubbling ultrapure argon for at least 10 min.

Results and Discussion

1. The Effect of $[H_2O_2]$ on $[\dot{R}]$. Esr spectra of R_1 and R_2 have been recorded after mixing solutions of Ti^{3+} with that of H_2O_2 + 2-propanol at pH = 1 and flowing the reaction mixture through the esr cavity. This experiment was repeated varying the H_2O_2 concentration, but keeping $[H_2O_2]$ = [2-propanol].

In Figure 1a, the relative intensities of R_1 and R_2 signals were plotted as a function of $[H_2O_2]$.

Since the ratio of $k_7/k_4 = 30$[20] and the concentration ratio $[H_2O_2]/[RH] = 1.0$, the extent of reaction 4 and of

(8) A. M. Simic, P. Neta, and E. Hayon, *J. Phys. Chem.*, **73**, 3794 (1969).

(9) L. M. Dorfman and I. A. Taub, *J. Amer. Chem. Soc.*, **85**, 2370 (1963).

(10) I. A. Taub and L. M. Dorfman, *ibid.*, **84**, 4053 (1962).

(11) R. W. Fessenden and R. H. Schuler, *J. Chem. Phys.*, **39**, 2147 (1963).

(12) T. Shiga, *J. Phys. Chem.*, **69**, 3805 (1965).

(13) T. Shiga, A. Boukhous, and P. Douzou, "Recent Developments of Magnetic Resonance in Biological Systems," S. Fujiwara and L. H. Piette, Ed., Hirokawa Publishing Co., Tokyo, 1968, p 146.

(14) Y. S. Chiang, J. Craddock, D. Mickevich, and J. Turkewich, *J. Phys. Chem.*, **70**, 3509 (1966).

(15) V. Krishnan and C. C. Patel, *Chem. Ind. (London)*, 321 (1961).

(16) A. I. Medalia and B. J. Byrne, *Anal. Chem.*, **38**, 453 (1951).

(17) T. A. Ghormley, *J. Phys. Chem.*, **56**, 575 (1952).

(18) C. C. Patel and V. Krishnan, *J. Sci. Ind. Res.*, **20B**, 604 (1961).

(19) G. A. Dean, *Can. J. Chem.*, **39**, 1174 (1961).

(20) M. Anbar and P. Neta, *Int. J. Appl. Radiat. Isotopes*, **18**, 493 (1967).

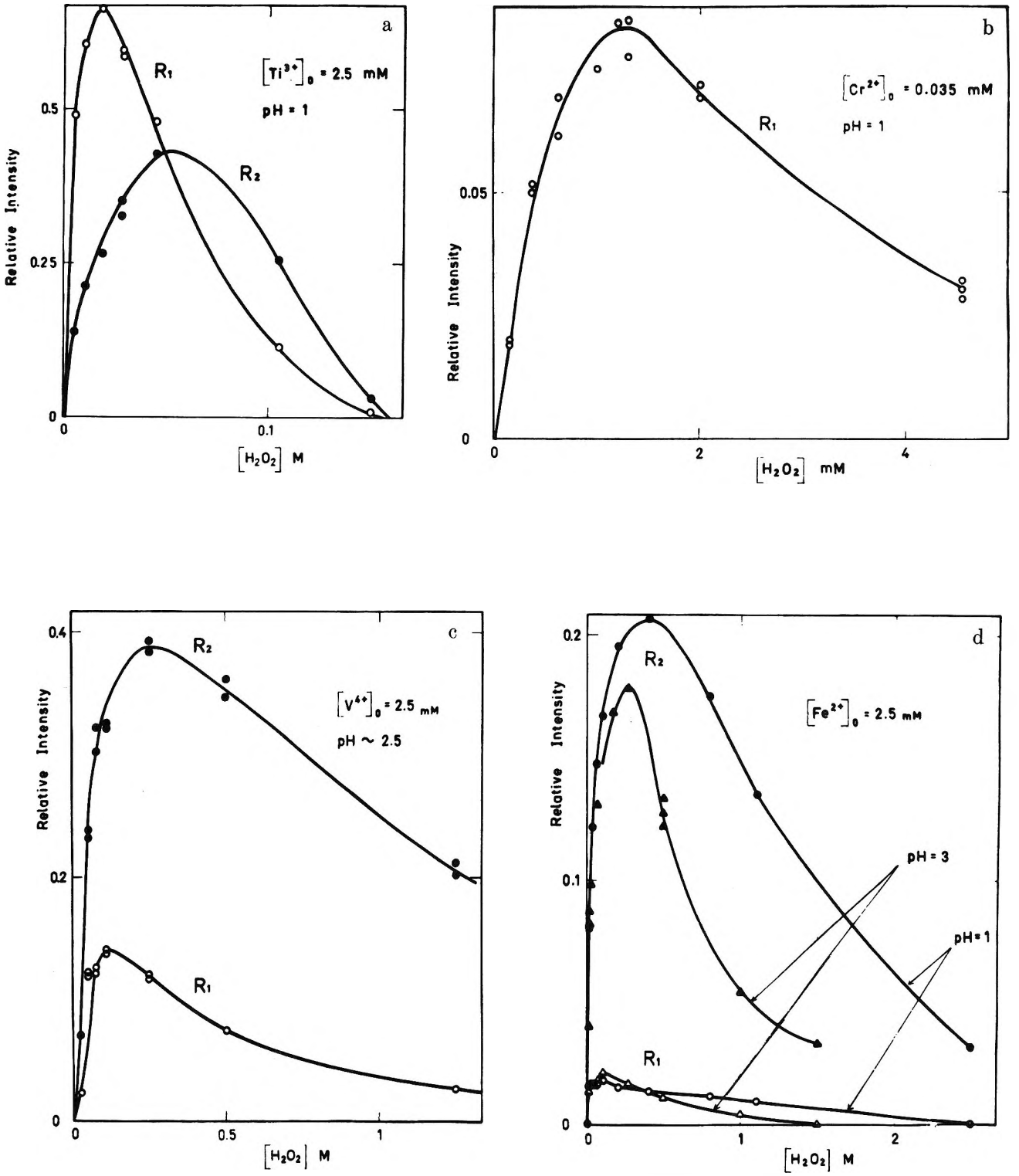

Figure 1. Intensities of esr signals of R_1 and R_2 formed on mixing various metal ions with H_2O_2 + 2-propanol at various concentrations where $[H_2O_2]$ = [2-propanol], $R_1 = (CH_3)_2\dot{C}OH$, $R_2 = CH_3CHOH\dot{C}H_2$.

the consecutive reactions 5 and 6 as compared to 7 are negligible. It can be seen from Figure 1 that on increasing $[H_2O_2]$, the concentrations of R_1 and R_2 first increase then reach a maximum and finally decrease. These results agree with that of James and Sicilio,[3] but not with earlier findings.[2b] The *general shape* of the curves given in Figure 1 are in accord with a mechanism consisting of reactions 1, 7, and 8. The inclining part of the curves in Figure 1 may be amplified by the competition between reaction 7 and 10 (if $k_{10} > 10^9\ M^{-1}$ sec^{-1})

$$Ti^{3+} + OH \longrightarrow Ti^{4+} + OH^- \qquad (10)$$

The declining part in these curves is due to the fact

that at high enough $[H_2O_2]$ most (and finally all) of reaction 1 and consequently reaction 7 are over before the solution reaches the cavity.

Before further analyzing these curves we will discuss the factors determining the concentrations of R in the cavity. In most experiments the solutes concentrations used were such that $k_7[RH] \gg k_4[H_2O_2]$, $k_3[Ti^{4+}-H_2O_2]$, $k_{10}[Ti^{3+}]$; therefore, the only relevant reactions are 1, 7–9. In this mechanism the propagation rate of reactions 7 and 9 are equal under steady-state conditions; hence, $k_7[RH][OH]_{ss} = k_9[H_2O_2][R]_{ss}$. A reasonable assumption would be $k_9 \ll k_7$[21] thus $[OH]_{ss} \ll [R]_{ss}$ and the only termination to be considered is reaction 8. Through making the steady-state approximation for R and OH radicals we get

$$[R]_{ss} = \left(\frac{k_1[M^{n+}][H_2O_2]}{2k_8}\right)^{1/2} \quad (I)$$

When taking $[H_2O_2]_0 > [M^{n+}]_0$, eq I takes the form

$$[R]_{ss} = \left(\frac{k_1[M^{n+}]_0[H_2O_2]_0 e^{-k_1\cdot[H_2O_2]_0\cdot t}}{2k_8}\right)^{1/2} \quad (II)$$

where $[M^{n+}]_0$ is the initial concentration of the metal ion. To verify eq II we measured R_{ss} under identical conditions varying only $[Ti^{3+}]_0$. The linear dependence of R_{ss} on $[Ti^{3+}]_0^{1/2}$ predicted by eq II is displayed in Figure 2. Knowing k_1, $[Ti^{3+}]_0$, $[H_2O_2]_0$, and t and measuring $[R]_{ss}$ we could roughly estimate from the slope of the line in Figure 2 the value of $k_8 \simeq 10^9\ M^{-1}$ sec^{-1} which is of the same order of magnitude as found in pulse radiolysis studies.[8]

James and Sicilio stress that under their experimental conditions almost all of the Ti^{3+} ions have been converted into Ti^{4+} before reaching the observation cell.[3] Taking the value of about 500 M^{-1} sec^{-1} for k_1[22,23] one gets $\tau_{1/2}$ as 14 and 69 msec for 0.1 and 0.02 M H_2O_2, respectively, which are the concentrations used in their study[3] and in that of Norman and West's.[2b] Under the above-mentioned experimental conditions and taking t as the time elapsed between mixing and the observation point (10–100 Msec) the residual concentration of Ti^{3+} ions reaching the cavity is higher than 0.001 M. The fact that R is observable is due to the incompletion of reaction 1 and R_{ss} is given in eq II. If reaction 1 was complete near the mixing point R_{ss} would be given by

$$[R] = \frac{[Ti^{3+}]_0}{1 + 2k_8[Ti^{3+}]_0 t} \quad (III)$$

Introducing the approximate values of $[Ti^{3+}]_0$, t, and $k_8 \simeq 2 \times 10^9\ M^{-1}$ sec^{-1} we find that [R] would be in these experiments[2b,3] smaller than 10^{-8} M and no R would be detectable.

We conclude that in all of these experiments[2b,3] the primary reaction 1 takes place inside the cavity, and hence all the kinetic conclusions deduced are doubtful.

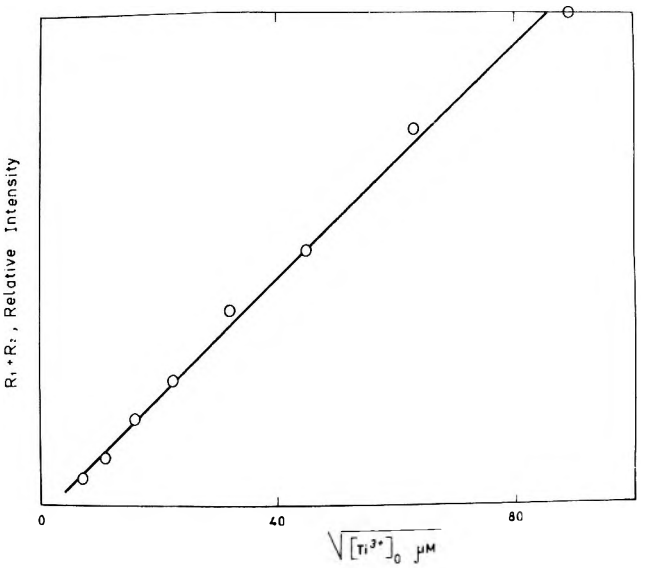

Figure 2. The dependence of the relative intensity of the esr signal of R, (R = R_1 + R_2) obtained on mixing at pH 1, Ti^{3+} with 0.1 M H_2O_2 + 0.1 N 2-propanol on $([Ti^{3+}]_0)^{1/2}$.

A similar criticism only on Sicilio's results[3] was very recently published.[24] The marked discrepancy in the values of k_8 obtained by using the flow technique[3,13] and pulse radiolysis technique[8] seems to be due to the wrong assumptions made. On differentiating eq II with respect to $[H_2O_2]$ and denoting $[H_2O_2]_{max}$ the H_2O_2 concentration for which $[R]_{ss}$ should reach its maximum, then

$$[H_2O_2]_{max} = \frac{1}{k_1 t} \quad (IV)$$

For the curve shown in Figure 1a the value of $[H_2O_2]_{max}$ can be calculated from eq IV. In this experiment t = 30 msec and $[Ti^{3+}]_0$ = 2.5 mM. $k_1 \sim$ 500–1000 M^{-1} sec^{-1},[23] $[H_2O_2]_{max}$ thus calculated equals 0.06 M. The experimental value is somewhat lower.

Considering expression II, one would expect $[H_2O_2]_{max}$ to be equal for both R_1 and R_2. Yet, as it can be seen in Figure 1, $[R_1]_{ss}$ reaches its maximal value at lower $[H_2O_2]$ than $[R_2]_{ss}$ does. In addition the ratio R_1/R_2 is smaller than predicted by the mechanism consisting of reactions 1, 7, and 8 (the ratio should be ~6.3).

These results can be attributed[2b] to a reaction of R_1 with Ti^{4+} or with H_2O_2[2,25] which will be discussed later.

The observation of R in the esr cavity when Ti^{3+} is replaced with other cations such as Cr^{2+}, V^{4+}, and Fe^{2+} is also possible only as long as reaction 1 is not com-

(21) W. A. Seddon and A. O. Allen, *J. Phys. Chem.*, **71**, 1914 (1967).
(22) R. E. Florin, F. Sicilio, and L. A. Wall, *ibid.*, **72**, 3154 (1968).
(23) G. Czapski, A. Samuni, and D. Meisel, submitted for publication in *J. Chem. Soc.*
(24) C. E. Burchill, *J. Phys. Chem.*, **75**, 167 (1971).
(25) C. E. Burchill and I. S. Ginns, *Can. J. Chem.*, **48**, 1232 (1970).

Table I: Values of $[H_2O_2]_{max}$ and k_1 at Various "Fenton-Like" Reagents

M^{n+}	$k_{M^{n+}+H_2O_2}$, M^{-1} sec^{-1}	Reference	pH	$[H_2O_2]_{max}$, M[a]	$k_1 \times [H_2O_2]_{max}$, sec^{-1}
Ti^{3+}	800–1800	22			
				$\sim 4 \times 10^{-2}$	
	500	23	1		~ 20
Fe^{2+}	55	26	1	$\sim 4 \times 10^{-1}$	~ 22
	65	26	3	$\sim 2.5 \times 10^{-1}$	~ 16
V^{4+}	~ 80	23	2.5	$\sim 2.5 \times 10^{-1}$	~ 20
Cr^{2+}[b]	17,000[c]	23	1	$\sim 1.2 \times 10^{-3}$[b]	~ 20

[a] $[H_2O_2]_{max}$ is the H_2O_2 concentration at which $[R]_{ss} = [R_1]_{ss} + [R_2]_{ss}$ reaches its maximal value. [b] In the case of Cr^{2+}, no esr signal due to R_2 radical was detected. [c] This value was estimated from the assumed constancy of $k_1[H_2O_2]_{max}$.

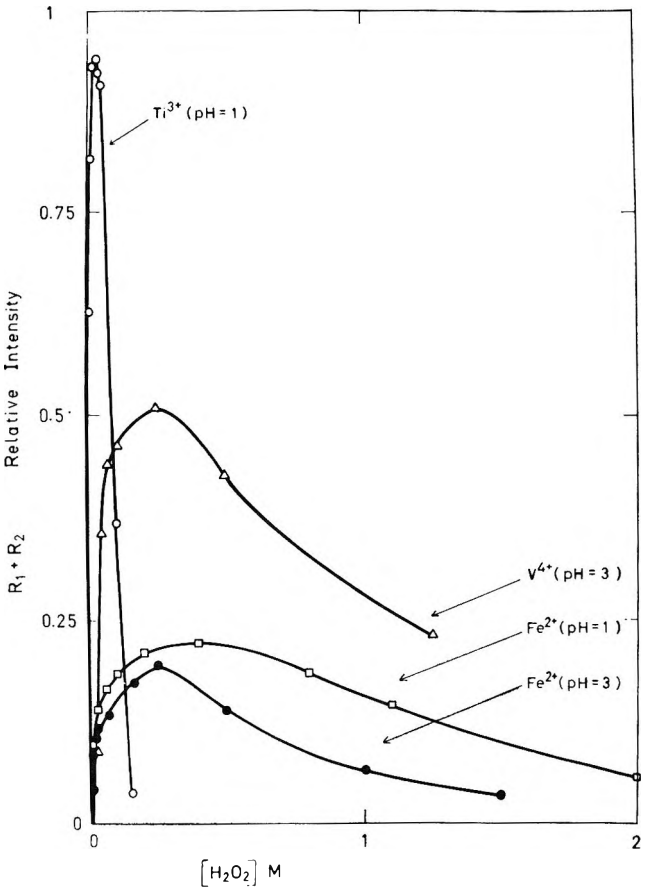

Figure 3. The relative intensities of the esr signals of R = $R_1 + R_2$ formed on mixing various metal ions with various concentrations of H_2O_2 + 2-propanol, where $[H_2O_2]$ = [2-propanol], $[M^{n+}]_0 = 2.5$ mM.

pleted immediately after mixing, but proceeds in the observation cell.

For these cations, having different values of k_1 we expect to find similar curves of [R] *vs.* $[H_2O_2]$ as given for Ti^{3+} in Figure 1a. Assuming a simple mechanism (reactions 1, 7, and 8) the only difference expected is that $[H_2O_2]_{max}$ would be different and proportional to $1/k_1$. We repeated these experiments with Fe^{2+}, Cr^{2+}, and V^{4+} ions.

The results are summarized in Figures 1 and 3 and in Table I[26] where it can be seen that the esr signals of R = $[R_1] + [R_2]$ reach their maximum at lower $[H_2O_2]$ the higher the rate constant of the primary reaction (reaction 1) is.

The results as given in Figures 1–3 and Table I indicate that the mechanism of reactions 1, 7, and 8 is not sufficient to explain all of the results and that other reactions of the radical such as with H_2O_2 and/or the oxidized metal ion should be considered.

2. Radiation-Induced Reduction of H_2O_2. The effect of initial $[H_2O_2]$ on the γ-radiation-induced reduction of H_2O_2, at constant ratio of [2-propanol]/$[H_2O_2]$ = 50 was investigated in deaerated solutions at pH 0.5 and in neutral solutions. Initial H_2O_2 concentrations ($[H_2O_2]_0$) ranged between 10^{-4} and 5×10^{-2} M. $G(-H_2O_2)$ was determined from dose–rate curves, each of which was composed of at least four points. Dose–rate curves tended to bend towards lower G values with increasing the dose delivered to the solution since we allowed maximum of 10% decomposition of the initial H_2O_2 concentration; nevertheless, initial G values were taken from the initial slopes.

The primary act of ionizing radiation on aqueous solutions is to produce H, OH, and e_{aq}^- radicals

$$H_2O \rightsquigarrow H, OH, e_{aq}^-, H_2O_2, H_2O$$

In the absence of a chain reaction (through 9 as chain-initiating step) the "radical products" will react with the solutes through reactions 4, 7, and 11–14.

$$e_{aq}^- + H_2O_2 \longrightarrow OH^- + OH \quad (11)$$

$$e_{aq}^- + H^+ \longrightarrow H \quad (12)$$

$$H + RH \longrightarrow R + H_2 \quad (13)$$

$$H + H_2O_2 \longrightarrow H_2O + OH \quad (14)$$

If the reaction mechanism is a nonchain mechanism, including reactions 4, 5, 7, 8, 11–14, but excluding 9, we can estimate $G(-H_2O_2)$. As [2-propanol] =

(26) C. F. Wells and M. A. Salam, *J. Chem. Soc. A*, 24 (1968).

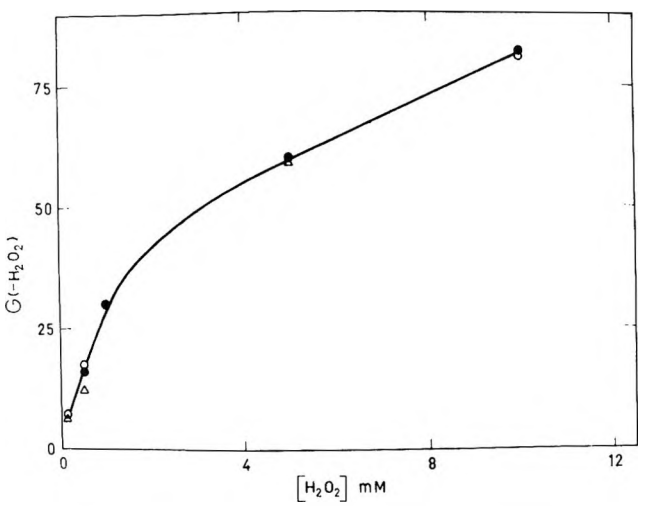

Figure 4. The effect of H_2O_2 concentration on $G(-H_2O_2)$. $[RH]/[H_2O_2] = 50$ for the all experiments: △, pH 1, no Ti^{4+}; ⊕, natural pH, no Ti^{4+}; ●, pH 1, $[H_2O_2]/[Ti^{4+}] = 10$.

$50[H_2O_2]$ reactions 4 and 14 are of negligible contribution as compared to 7 and 13; therefore, the upper limit of $G(-H_2O_2)$ is given as

$$G(-H_2O_2) = G_{e_{aq}^-} \Big/ \left(1 + \frac{k_{12}[H^+]}{k_{11}[H_2O_2]}\right) - G_{H_2O_2} \leq 2.2 \quad \text{(V)}$$

The results shown in Figure 4 are in conflict with this mechanism. The experimental values of $G(-H_2O_2)$ exceed by much the predicted values from eq V; the pH independence of $G(-H_2O_2)$ is also in disagreement with eq V. These results suggest strongly a chain mechanism by including reaction 9. This conclusion is in good accordance with that of Allen, *et al.*,[21] who studied the ethanol–H_2O_2 system. If R radicals produced by Fenton reagents and through ionizing radiation are the same, these results rule out the suggestion[3] of a "nonreactive" OH radical[3] formed in reaction 9. Assuming a chain process (reactions 7 and 9), the consumption ratio Δ[2-propanol]/$\Delta[H_2O_2]$ should approach a value of 1, but this prediction contradicts the results of James and Sicilio.[3] It is easy to see that under their[3] experimental conditions, *i.e.*, $[H_2O_2] = [Ti^{3+}] = 5$ mM, reaction 9 is negligible compared to reaction 8. Even if one takes their low unreasonable values of $k_9 = 4 \times 10^2\ M^{-1}\ \text{sec}^{-1}$ and $k_8 = 1.6 \times 10^7\ M^{-1}\ \text{sec}^{-1}$, the term $k_9[R][H_2O_2]$ in the rate equation for R will be comparable to the term $k_8[R]^2$ only at $[R] < 10^{-6}\ M$ which is not the case under the above-mentioned experimental conditions, where roughly $[R]_{ss} \simeq 10^{-5}\ M$ as given by eq II. In such a case R radicals decay mainly through reaction 8 and since products analysis usually rules out dimerization of radicals, the assumption of disproportionation may well fit the observed consumption ratio $\Delta[H_2O_2]/\Delta$[2-propanol] = 2.[3] Another possibility proposed by the same authors[3] is that R_1 and R_2 formed by the $Ti^{3+} + H_2O_2$ reagent are complexed with the metal ions, thus providing complexed OH radicals as products of reaction 9. We measured $G(-H_2O_2)$ in the presence of Ti^{4+} where $[RH]/[H_2O_2]/[Ti^{4+}] = 500:10:1$. It was found that $G(-H_2O_2)$ is unaffected by Ti^{4+} at comparable concentrations as in the flow experiments.[3] We reject this suggestion on the ground of these results and those coming in section 3. Very recently, Burchill and Ginns[25] studied the γ radiation of H_2O_2 + 2-propanol system reported the occurrence of a chain process. They proposed a mechanism which predicts a linear dependence of $G(-H_2O_2)$ on [RH] and no dependence on $[H_2O_2]$. According to their proposal R_2 decays either by reaction 8 or by a reaction with RH yielding R_1, while R_1 decays only through reaction 9 giving OH radical. Such a mechanism predicts an increase in $[R_1]$ on account of $[R_2]$ with the increase of RH concentration. We checked this hypothesis using esr technique, producing the radicals by $Ti^{3+} + H_2O_2$ system, changing [RH] and keeping all other factors constant. Results are summarized in Table II.

Table II: The Effect of [RH] on R_1 and R_2[a]

[RH], mM	R_1, relative intensity	R_2, relative intensity	$[R_1]/[R_2]$
29	41.0	17.7	2.3
60	38.0	18.0	2.1
120	41.2	18.3	2.2
240	39.0	18.3	2.1
480	36.0	16.9	2.2
1450	33.4	12.9	2.6

[a] $[Ti^{3+}]_0 = 2.5 \times 10^{-3}\ M$, $[H_2O_2]_0 = 2.5 \times 10^{-2}\ M$, $[HClO_4] = 0.1\ M$.

Practically no change was observed in the relative concentration of R_1 and R_2 by a 50-fold increase in [RH]. These results seem to contradict the above-mentioned mechanism.[25]

If one makes the comparison between Burchill's results with those given in Table II more carefully, the difference of two orders of magnitude of the steady-state concentration of the radicals should be considered.

Burchill's mechanism is given by the reactions

$$OH + RH \longrightarrow R_1 \quad (15)$$

$$OH + RH \longrightarrow R_2 \quad (16)$$

$$R_1 + H_2O_2 \longrightarrow OH \quad (17)$$

$$R_2 + RH \longrightarrow R_1 \quad (18)$$

$$R_2 + R_2 \longrightarrow \text{nonradical products} \quad (19)$$

ignoring the reactions

$$R_2 + H_2O_2 \longrightarrow OH \quad (20)$$

$$R_1 + RH \longrightarrow R_2 \quad (21)$$

$$R_1 + R_1 \longrightarrow \text{nonradical products} \quad (22)$$

(where RH = $CH_3CHOHCH_3$, R_1 = $(CH_3)_2\dot{C}OH$, R_2 = $\dot{C}H_2CHOHCH_3$). The justification of neglecting the last three reactions depends on both the values of the various rate constants as well as on H_2O_2, RH, R_1, and R_2 concentrations. Reaction 21 can be omitted on the grounds of thermodynamic reasons, $k_{20} \ll k_{17}$, as it was shown in several reactions, that α radicals are very much more reactive than β radicals.[2,27] $k_{22} \sim k_{19} \sim 2 \times 10^9\ M^{-1}\ \text{sec}^{-1}$,[8] $k_{18} = 53\ M^{-1}\ \text{sec}^{-1}$,[25] and $k_{17} \sim 4 \times 10^4\ M^{-1}\ \text{sec}^{-1}$ for methanol[28] (but was estimated to be higher for 2-propanol up to $5 \times 10^5\ M^{-1}\ \text{sec}^{-1}$ [29]), from the values of these rate constants and from the approximate concentrations of R_1 which is $\sim 10^{-8}\ M$ in Burchill's study and $\sim 10^{-6}\ M$ in our experiments, we will reanalyze the apparent discrepancy. In our experiments k_{18}[2-propanol]/2 $\times$ $k_{19}[R_2] \ll 0.1$; therefore, we may neglect reaction 18 as compared to 19 where in Burchill's experiments reaction 18 has a considerable contribution; this explains why $[R_1]/[R_2]$ is independent of 2-propanol (Table II).

In the flow experiments the chain reaction depends on $[H_2O_2]$; at the low $[H_2O_2]$ the chain length must be very short.

Our results thus agree with those of Burchill and from these results we can put an upper limit for k_{18}, namely, $<10^3\ M^{-1}\ \text{sec}^{-1}$.

The inclusion of a chain process can explain why $[R_1]$ and $[R_2]$ in the same system reach their maxima at different values of $[H_2O_2]$ (Figure 1), as increasing $[H_2O_2]$ will increase the chain length and, therefore, more R_2 radicals will be formed on account of R_1 and $[R_1]_{max}$ will be shifted towards lower $[H_2O_2]$, than expected from the simple mechanism which led to eq II, while $[R_2]_{max}$ will be shifted towards higher $[H_2O_2]$.

3. Radicals Formed by Various "Fenton-Like" Reagents. To determine whether other metal ions produce the same secondary radicals in their reactions with H_2O_2 in the presence of substrates, we mixed solutions of M^{n+} ions (where M^{n+} = V^{4+}, Fe^{2+}, Ti^{3+}, and Cr^{2+}) with H_2O_2 in the presence of (Ti^{4+}–H_2O_2) (Figure 5a), hydroquinone (Figure 5b), Th^{4+} (Figure 5c), ethanol (Figure 6b), and 2-propanol (Figure 6a).

By comparing the esr spectra we conclude that the secondary radicals, namely, S_1, S_2, semiquinone radical,[30] (Th^{4+}–HO_2) radicals,[31] the 2-propanol and ethanol radicals are produced in all these systems and have the same esr spectra independently of the system by which they were produced.

Secondary radicals may be generated through the reactions of HO_2 with various scavengers. To check whether HO_2 is the primary radical formed in these systems we mixed 0.1 mM $Ce(ClO_4)_4$ with 0.01 M H_2O_2 at pH 1, and studied the esr spectrum of the HO_2 radical formed and its dependence on the addition of 2-propanol to the reaction mixture. Neither an appearance of an esr signal due to R radicals nor a decrease in the HO_2 signal's intensity were observed up to 1 M alcohol concentration. These results exclude a reaction between HO_2 radicals and RH. Hence an appearance of R radicals in all M^{n+} + H_2O_2 + 2-propanol systems would indicate that OH radicals rather than HO_2 radicals are the primary species in the reaction mixture.

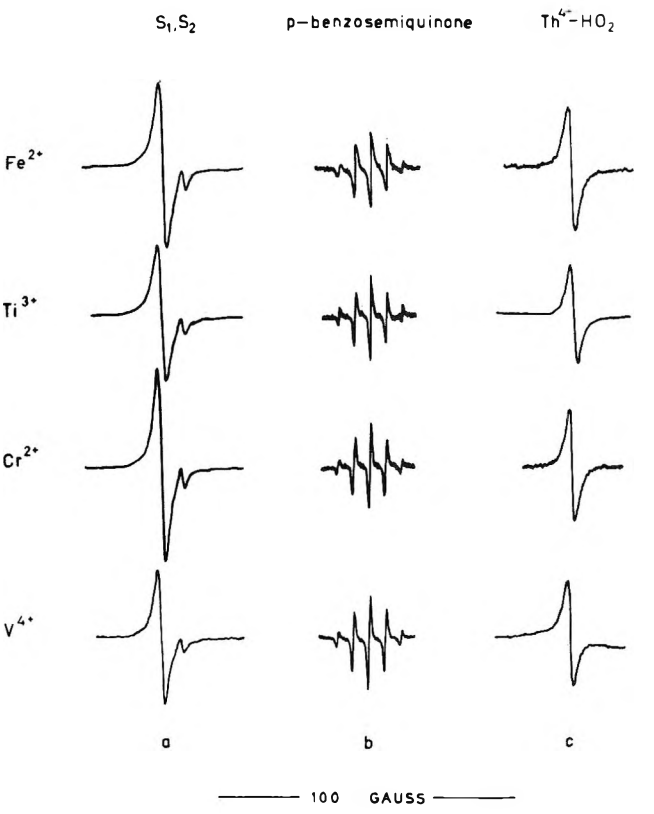

Figure 5. The esr spectra obtained on mixing various metal ions ($\sim$1 mM) with 0.5 M H_2O_2 at the presence of: (a) 0.01 M Ti^{4+}–H_2O_2 at pH 1; (b) 0.1 M p-hydroquinone in the metal ion vessel at pH 3 mixed with H_2O_2 at pH 6.5 in phosphate buffers; (c) 4 mM Th^{4+} at pH 1.

In the case of Cr^{2+}, the signal of R_2 was undetectable both with 2-propanol and in ethanol (Figure 1b). We ascribe this to the low concentration of the radicals due to the low value of $[M^{n+}]_0$ ($[Cr^{2+}]_0 = 35\ \mu M$). In such a case and in the absence of a chain process, $[R_1] > [R_2]$ since $k_{15}/k_{16} \sim 6$,[25] thus leaving R_2 signal below the noise level.

On the other hand, in the case of Fe^{2+} ion, R_1 was observed only in minute amounts as has already been reported[12] and was attributed to a reaction between Fe^{3+} and R_1.[2]

(27) G. E. Adams and R. L. Wilson, *Trans. Faraday Soc.*, 65, 2981 (1969).

(28) C. E. Burchill and I. S. Ginns, *Can. J. Chem.*, 48, 2628 (1970).

(29) C. E. Burchill, private communications.

(30) I. Yamazaki and L. H. Piette, *J. Amer. Chem. Soc.*, 87, 986 (1965).

(31) A. Samuni and G. Czapski, *J. Phys. Chem.*, 74, 4592 (1970).

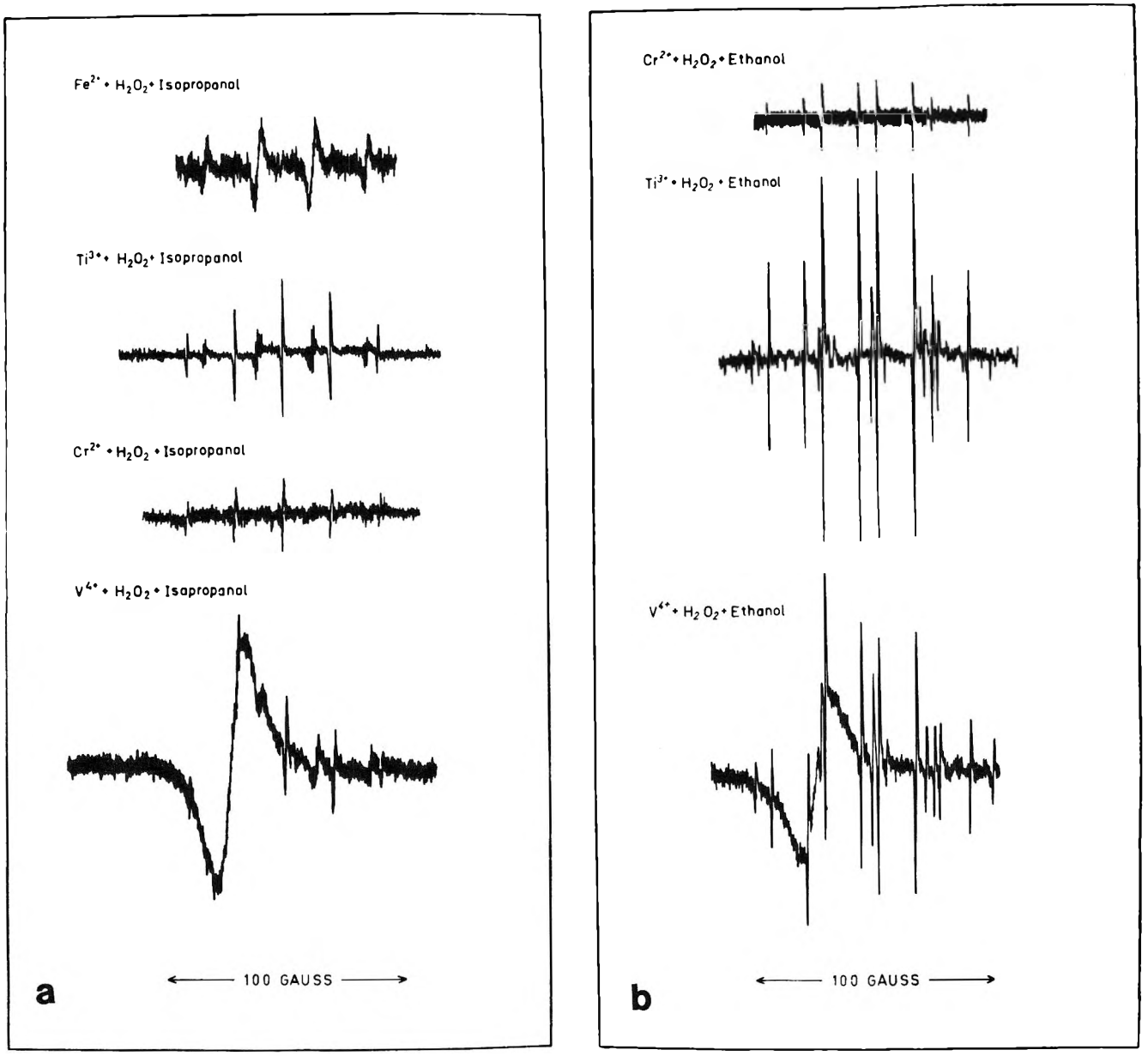

Figure 6. The esr spectra obtained on adding either 0.1 *M* ethanol or 0.1 *M* 2-propanol to the reaction mixtures of M^{n+} ions with H_2O_2.

It might be noted that the spectra of R_1 and R_2 in the vanadium system are superimposed on one of the V^{4+} octet[32] lines in spite of the high H_2O_2 concentration (1 *M*) used in that case.

Upon comparing the spectra of 2-propanol and ethanol radicals produced by all these "Fenton-like" reagents it appears that the same radicals are produced by all of them, and they are identical with the radicals produced during photolysis[33] and radiolysis[34] in the absence of metal ions.

These results exclude the assumption of some coordination between the organic radical[3] and the metal ion. Moreover interaction of R with vanadium ion would lead to an additional esr splitting spectrum of eight lines due to the coupling of the unpaired electron with the nuclear magnetic moment of the ^{51}V.[35,36]

4. The Effect of $M^{(n+1)+}$ Ions on R_1 and R_2. It is seen in Figure 1 that $[R_1]/[R_2]$, $[R_1]_{max}$, and $[R_2]_{max}$, have different values when these radicals are formed by the various $M^{n+} + H_2O_2 +$ 2-propanol systems.

This behavior was observed previously, but the suggested explanations were controversial.[2,12,13]

Shiga, *et al.*,[12,13] claimed that the $Fe^{2+} + H_2O_2$ system possesses a different character as an oxidant, in the sense that OH is not involved in Fenton's reagent.

(32) R. N. Rogers and G. E. Pake, *J. Chem. Phys.*, **33**, 1107 (1961).

(33) R. Livingston and H. Zeldes, (a) *J. Amer. Chem. Soc.*, **88**, 4333 (1966); (b) *J. Chem. Phys.*, **44**, 1245 (1966).

(34) R. W. Fessenden and K. Eiben, to be published.

(35) O. R. Eaton, *Inorg. Chem.*, **3**, 1268 (1964).

(36) R. W. Brandon and C. S. Elliot, *Tetrahedron Lett.*, **44**, 4375 (1967).

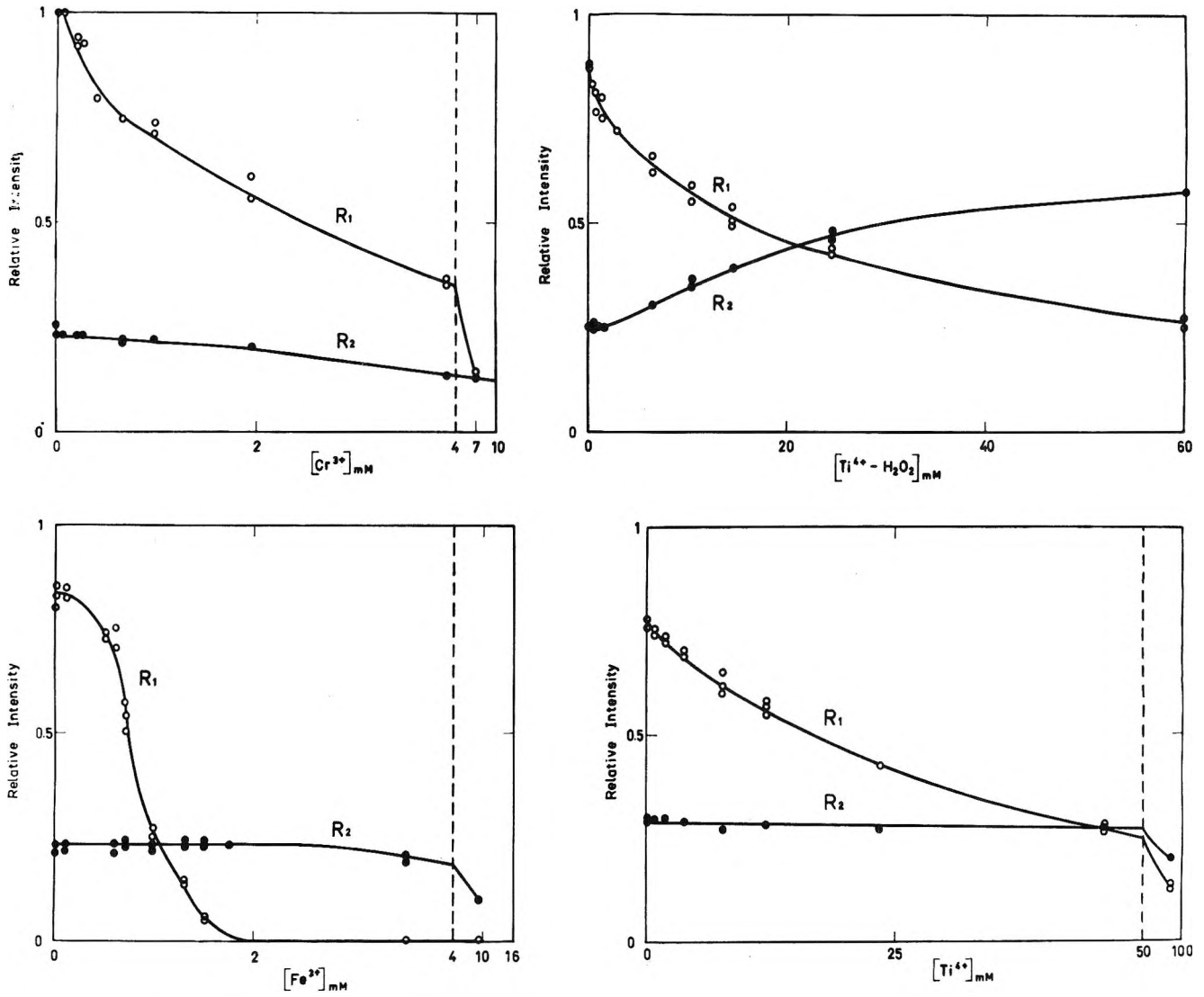

Figure 7. The dependence of the relative intensities of the esr signals of R_1 and R_2 observed on mixing Ti^{3+}, 6 mM, + H_2O_2, 30 mM, + 2-propanol, 0.5 M, at pH 1, on the concentration of various metal ions.

They assumed that an "OH-like" species is formed by the Fenton reagent and thus ascribed the H abstraction in the β position of 2-propanol, to the different character of the primary species formed. (The OH in the $Ti^{3+} + H_2O_2$ reagent and the "OH-like radical" in the Fenton reagent.) Norman and West,[2b] on the other hand, attributed the difference in $[R_1]/[R_2]$, obtained in $Ti^{3+} + H_2O_2$ and $Fe^{2+} + H_2O_2$ to the reaction of R_1 with Ti^{4+} and Fe^{3+}, respectively. We repeated Norman and West's[2b] experiment, using a simple mixing cell (since reaction 1 is incomplete in the cavity, the use of a double cell has no advantage), extending it in order to study the effect of $M^{(n+1)+}$ ions on $[R_1]$ and $[R_2]$.

In our experiments titanium(III) ions were mixed with H_2O_2 + 2-propanol at pH 1 and various amounts of $M^{(n+1)+}$ ions were added either to the Ti^{3+} or to the H_2O_2 solutions. The reaction mixture passed through the esr cavity (at 2 cc/sec flow rate), and the esr spectra of R_1 and R_2 were recorded.

The results are summarized in Figure 7, for $M^{(n+1)+}$ = Fe^{3+}, Ti^{4+}, and Cr^{3+}, demonstrating that $[R_1]$ decreased on the addition of all these metal ions.

This proves that $M^{(n+1)+}$ ions do react with R_1, probably oxidizing it

$$R_1 + M^{(n+1)+} \longrightarrow M^{n+} + \text{nonradical products} \quad (23)$$

On the other hand, R_2 reacts with $M^{(n+1)+}$ much slower. It is also seen that the effectiveness of reaction 23 increases markedly from Ti^{4+} through Cr^{3+} to Fe^{3+}.

These results are in fair agreement with previous suggestions,[3] ruling out Shiga's explanations,[13] since *all* the $M^{n+} + H_2O_2$ systems behave similarly, in the sense that $[R_1] \rightarrow 0$ as $[M^{(n+1)+}]$ increases.

To find out whether (Ti^{4+}–H_2O_2) reacts with the R_1, we investigated the influence of the addition of peroxytitanium(IV) ions to the reaction mixture and the results are shown in Figure 7.

In this case $[R_1]$ decreases on the addition of the peroxy metal ion, while $[R_2]$ increases on its account, leaving $[R] = [R_1] + [R_2]$ nearly constant. A possible

explanation for this observation might be the assumption of a formation of an OH radical through the reaction

$$R_1 + Ti^{4+}\text{–}H_2O_2 \longrightarrow$$

$$Ti^{4+} + OH^- + OH + \longrightarrow \text{products} \quad (24)$$

which in turn reacts again in reactions 15 and 16.

This case is similar to the reduction of H_2O_2 by R_1 through reaction 17, thus perpetuating a chain process and increasing $[R_2]$ on account of $[R_1]$.

The full description of the behavior of the systems as described in Figures 1, 3, and 7 depends on the concentrations of the reagents used (H_2O_2, M^{n+}, RH), as well as on the impurity $[M^{(n+1)}]$ and the rate constant k_1 and all rate constants from k_{15} up to k_{24}.

As for the various "Fenton-like reagents," k_1 and k_{23} have different values one does not expect a unique dependence of R_1 and R_2 on $[H_2O_2]$ in these systems, as shown in Figures 1, 3, and 7. The different values of $[R_1]/[R_2]$ and the different values of $[H_2O_2]$ at which R_1 and R_2 reach their maximum are expected for these reagents as long as the mechanism is including reactions 17–23.

We can indicate the effects of reactions 17, 18, and 23 on the behavior of these systems.

(1) Reaction 18 will not affect the value of $[H_2O_2]_{max}$ for both R_1 and R_2, but the greater the extent of reaction 18 the greater $[R_1]/[R_2]$ will be.

(2) Reaction 17 will affect both $[R_1]/[R_2]$ and the peroxide concentrations at which $[R_1]$ and $[R_2]$ will reach their maxima. The greater the contribution of eaction 17 will be, the ratio $[R_1]/[R_2]$ will decrease and $[R_1]$ will reach its maximum at lower $[H_2O_2]$ while $[R_2]$ at higher $[H_2O_2]$.

(3) Reaction 23 will decrease $[R]_1/[R_2]$ and $[R_1]$ and $[R_2]$ will reach their maxima at higher $[H_2O_2]$, although this last effect depends also on $[M^{(n+1)}]_0$.

Our results as shown in Figures 1 and 7 indicate the importance of reaction 23 and possibly 17 for the different "Fenton-like" reagents.

Conclusion

The above-mentioned observations may be summarized as follows. (i) Cr^{2+}, Ti^{3+}, Fe^{2+}, and V^{4+} in their reaction with hydrogen peroxide yield OH radicals which in turn may react with various scavengers to form secondary radicals. (ii) Neither the organic radicals nor the OH radicals formed by these "Fenton-like" reagents are complexed with the metal ions. (iii) The organic radical (α-2-propanol radical) reduces hydrogen peroxide. The OH formed in this reaction perpetuates a chain process. (iv) α radicals (α-2-propanol radical) are much more reactive as reductants of metal cations and of H_2O_2 than β radicals. (v) The contradictory results obtained in former studies[2,3] stem from the fact that the primary reaction ($M^{n+} + H_2O_2 \rightarrow M^{(n+1)+}$) is proceeding inside the observation cell under their experimental conditions in contrast to what they have assumed. Unless this happens neither R_1 nor R_2 radicals would have been observed by flow-esr technique.

Acknowledgment. We gratefully acknowledge the support of this research by the U. S. Atomic Energy Commission under Contracts AT(30-1)-3753 and AT-(30-1)-2310.

Simultaneous Electrochemical-Electron Spin Resonance Measurements.

I. Cell Design and Preliminary Results

by Ira B. Goldberg and Allen J. Bard*

Department of Chemistry, The University of Texas at Austin, Austin, Texas 78712 *(Received May 5, 1971)*

Publication costs assisted by the Robert A. Welch Foundation

A cell was designed which allows precise control of electrochemical variables during *intra muros* electrogeneration of radical species in the cavity of an esr spectrometer. The advantages of simultaneous electrochemical-esr (SEESR) experiments are discussed, and results of potential step, current step, and cyclic voltammetric experiments on dimethylformamide solutions of anthraquinone, azobenzene, and nitrobenzene are described. Applications to the detection of short-lived electrogenerated radicals using signal-averaging techniques, to the measurement of the kinetics of reactions of electrogenerated radicals, and to the observation of secondary radicals are also discussed.

Introduction

Electrochemical generation of radicals and their detection by electron spin resonance (esr) spectroscopy has been used routinely for the last 10 years. Adams[1] and Kastening[2] have reviewed the most recent developments in this area, and several books[3] provide descriptions of the conventional apparatus required for these experiments. Recently other spectroscopic measurements have been combined with electrochemical experiments such as optical spectroscopy using optically transparent electrodes.[4] Combining electrochemistry with spectroscopy allows more confident identification of intermediates and products and enables the elucidation of mechanisms and the evaluation of kinetic parameters. When spectroscopic-electrochemical methods are combined, careful control of the electrochemical parameters is necessary to ensure that only the desired process is occurring in the zone of detection of the spectrometer. This is difficult to achieve when esr spectroscopy and electrochemistry are combined because of the high resistance of the thin cell[5,6] which must be used when radicals are generated in the microwave cavity. As a result, electrochemical generation in esr spectroscopy has been used primarily as a purely qualitative technique. Most precise esr measurements of the electrochemical behavior of systems has been carried out by generating the radicals away from the microwave cavity and then allowing some of the solution to flow into the cavity at a known rate.[7-9] Here the problems of cell resistance are avoided since an efficient electrochemical cell may be used.

Several kinetic measurements have been carried out by generating the radical inside of the microwave cavity. The behavior of the nitrobenzene anion radicals in aqueous solution was studied by Koopman and Gerischer.[10] In this case because the specific resistance of the solution was sufficiently low, the electrochemical behavior could be controlled. Hirasawa, *et al.*,[11] were able to obtain spectra and kinetic curves of radicals in nonaqueous systems by using a constant current passed through a solution which was flowing rapidly through the cell in the microwave cavity. To minimize electrical resistance, two parallel electrodes were placed in the cell. By using a computer of average transients either esr spectra or signal intensity–time curves could be recorded. Because of the flowing solution, the current distribution along the electrode was not uniform so that kinetic parameters could not be determined. Moreover, no controlled potential experiments were reported.

There have been few discussions of the dynamics of radical generation in conventional electrochemical-esr cells. Usually electrolysis inside of the microwave

(1) R. N. Adams, *J. Electroanal. Chem.*, **8**, 151 (1964).

(2) B. Kastening, *Chem. Ing. Tech.*, **42**, 190 (1970).

(3) C. P. Poole, "Electron Spin Resonance," Interscience, New York, N. Y., 1967, pp 624–633; R. S. Alger, "Electron Paramagnetic Resonance," Interscience, New York, N. Y., 1968, pp 267–272.

(4) See, *e.g.*, G. C. Grant and T. Kuwana, *J. Electroanal. Chem.*, **24**, 211 (1970), and references therein.

(5) D. H. Geske and A. H. Maki, *J. Amer. Chem. Soc.*, **82**, 2761 (1960).

(6) L. H. Piette, P. Ludwig, and R. N. Adams, *Anal. Chem.*, **34**, 916 (1962).

(7) B. Kastening, *Ber. Bunsenges. Phys. Chem.*, **72**, 20 (1968); B. Kastening and S. Vavricka, *ibid.*, **72**, 27 (1968); B. Kastening, *Collect. Czech. Chem. Commun.*, **30**, 4033 (1965); B. Kastening, *Z. Anal. Chem.*, **224**, 196 (1967).

(8) K. Umemoto, *Bull. Chem. Soc. Jap.*, **40**, 1058 (1966).

(9) D. Kolb, W. Wirths, and H. Gerischer, *Ber. Bunsenges. Phys. Chem.*, **73**, 148 (1969).

(10) R. Koopman and H. Gerischer, *ibid.*, **70**, 118 (1966); R. Koopman, *ibid.*, **70**, 121 (1966); R. Koopman and H. Gerischer, *ibid.*, **70**, 127 (1966).

(11) R. Hirasawa, T. Mukaibo, H. Hasegawa, N. Odan, and T. Maruyama, *J. Phys. Chem.*, **72**, 2511 (1968); R. Hirasawa, T. Mukaibo, H. Hasegawa, Y. Kanada, and T. Maruyama, *Rev. Sci. Instrum.*, **39**, 935 (1968).

cavity is carried out with a static solution where an essentially constant current is used. In the typical commercial electrochemical-esr cells[12] the cell resistance is about 1500 Ω/cm of cell length in 0.1 *M* aqueous potassium chloride, and 5000 Ω/cm in 0.1 *M* TBAI–DMF based on a value of about 250 Ω·cm for the specific resistance of 0.1 *M* TBAI–DMF. In ethereal solutions the cell resistance may exceed 100,000 Ω/cm. With a current of only 100 μA, the voltage drop along the electrode would be as high as 0.5 V/cm in DMF solutions. Thus, it is possible for more than one process to occur simultaneously at the electrode. Furthermore, it is not meaningful to attempt a controlled potential experiment, especially in this cell when the reference electrode is above the working electrode. The potentiostat would control only that portion of the working electrode closest to the reference electrode, and the potential would still vary along the rest of the length of the working electrode. Furthermore, there is a large uncompensated resistance (resistance between the working and reference electrode in the current path) so that a small change of current causes a large change in the regulated cell potential.

Dohrmann and Vetter[13] attempted to calculate the minimum lifetime of a radical which could be detected when generated in a conventional electrochemical-esr cell. They suggested that a rapid flow of solution through the cell and a small electrode placed at the center of the cavity would give the greatest signal for a rapidly decaying radical, if the potential of the electrode could be maintained on the plateau of the electrochemical wave of the radical formation. They estimated that if a current density of 0.1 A/cm^2 could be maintained by rapid flow of solution, then a radical with a lifetime of about 10^{-5} sec could be observed.

The purpose of this paper is (1) to present a cell in which the esr signal may be recorded while any of a variety of electrochemical experiments are carried out, *i.e.*, the cell potential may be controlled accurately so that the esr signal or a spectrum which corresponds to that potential, is obtained; (2) to study the behavior of stable radicals formed electrochemically by constant current, at constant potential, and during cyclic linear sweep voltammetry to find the upper and lower limits of time during which radicals can be studied; and (3) to explain briefly the dynamics of conventional internal generation and to contrast this method with the method presented here.

Experimental Section

Chemicals. Dimethylformamide (DMF), obtained from Baker Chemical Co., was purified by distillation at 15 mm from cupric sulfate onto molecular sieves three times. The solvent was then stored under helium atmosphere. The purity was checked periodically by voltammetry on a blank sample. The 9,10-anthraquinone (99.5% pure), obtained from Matheson Coleman and Bell, was used without purification. Azobenzene, obtained from Eastman, was recrystallized twice from 95% ethanol. The purified nitrobenzene, obtained from Baker, was dried by passing directly through an alumina column. Tetrabutylammonium iodide (TBAI) and tetrabutylammonium perchlorate (TBAP) were obtained from Southwestern Analytical Chemicals polarographic grade and were used as received, except that TBAP was dried under vacuum at 145° for 24 hr and stored over Drierite.

Instrumentation. Electron spin resonance measurements were conducted with a Varian V-4502 spectrometer equipped with a 9-in. magnet, 100-kHz field modulation, dual cavity, and a low noise-high power klystron. Electrochemical measurements were carried out in either of two ways. Cyclic chronopotentiometry, cyclic voltammetry, and controlled potential generation were done with a Princeton Applied Research Model 170 electrochemical instrument. Constant current pulses were applied either with the above instrument or by using a Tektronix Pulse Generator, Model 162, and a dropping resistor. In this case, the cell potential was monitored by connecting the reference electrode to a follower constructed with a Philbrick P65 operational amplifier. Simultaneous esr and electrochemical data were recorded with a dual-channel chart recorder. When necessary, a Nuclear Data Enhancetron 1024 was used for signal averaging. A block diagram of the apparatus set up for signal averaging is shown in Figure 1.

Cell Design. The design of the cell for simultaneous esr and electrochemical measurements is extremely critical. For a rectangular microwave cavity, it is necessary that the cell be fairly thin (about 0.05 cm for aqueous solution, 0.1 cm for materials with dielectric constants in the order of 40, and 0.2 cm for solvents with dielectric constants between 6 and 12). Since a low electrolyte resistance even in most aqueous systems is, therefore, nearly impossible, it is important to optimize the electrochemical behavior of the cell, bearing in mind the considerations of maximum esr response.

A diagram of the complete cell assembly is shown in Figure 2. Since DMF, with a dielectric constant of about 37, was used in these experiments, a cell thickness of 0.1 cm was chosen. The walls were constructed of 0.1-cm optical Pyrex. Two tungsten rods (0.075 cm diameter) were placed along the edges of the cell, with a U-shaped rod at the bottom of the cell to hold the long rods parallel. These rods served as the counterelectrode and must be kept as parallel as possible to ensure a uniform current density through the solution. The working electrode was made from a piece of platinum

(12) For example, Varian V-4556 or E-246 (cell dimensions 4 × 0.9 × 0.05 cm), Brucker BER-400 2E, or Jeolco JES-EL10.

(13) J. K. Dohrmann and K. J. Vetter, *J. Electroanal. Chem.*, **20**, 23 (1969).

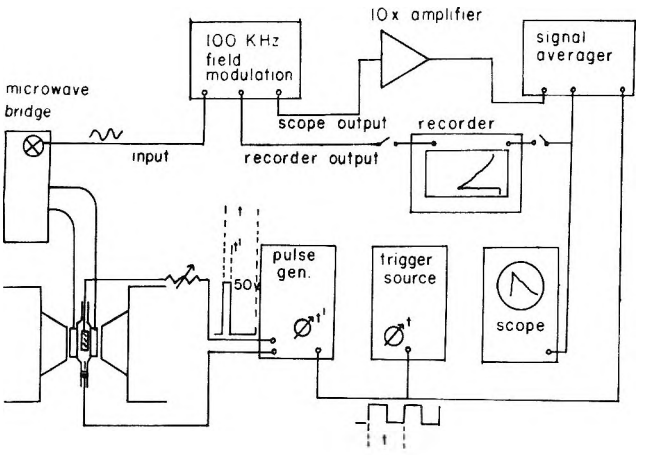

Figure 1. Block diagram of the esr apparatus used in pulse electrolysis experiments with signal averaging.

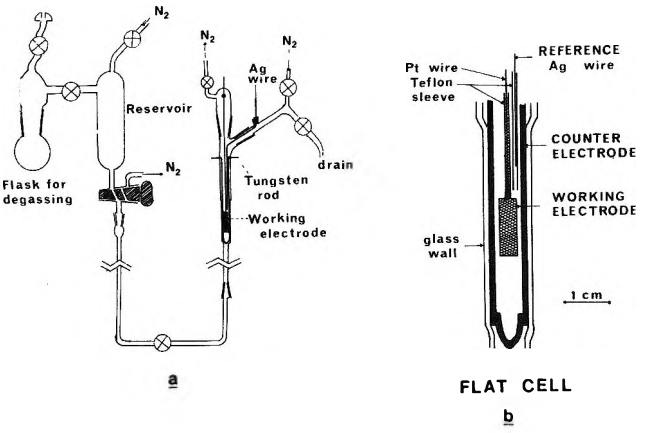

Figure 2. (a) Electrochemical cell and reservoir assembly. (b) Detail of flat cell portion of cell.

mesh, with a grid of 1 mm. Various widths between 0.2 and 0.4 cm, and lengths between 0.5 and 1.5 cm were used. A length of 0.025-cm diameter platinum wire was spot-welded to the mesh, and the wire was passed through a length of 0.038-cm i.d. Teflon tubing which was filled with epoxy. This prevented the long lead to the working electrode from being exposed to the solution. Contact to the electrochemical source was made above the solution level—the stopcock near this connection (Figure 2a) allows the whole cell to be flushed with nitrogen, but when closed, positive pressure keeps the solution level below the connection.

For the reference electrode, a length of 0.012-cm diameter silver wire was passed through a length of 0.038-cm i.d. Teflon tubing until the edge of the silver was 3–5 mm above the end of the Teflon. The Teflon sheath which filled with solution was fixed in place as shown.

Great pains were taken in the assembly of the cell to prevent slow leaks or solution movement within the cell. If one considers a small amount of radical at the region of maximum sensitivity, then to decrease the signal to one-half of the maximum value, the radical need only move about 5 mm in either direction. This would correspond to a loss of only 30 μl of solution. Thus, if a signal which decays by less than 5% within 30 sec is desired, a maximum rate of flow out of the cell would be about 1.0 μl/sec (4 ml/hr).

One consideration to be made in using this cell is the size of the working electrode. If it is desired to study fast kinetics, a long electrode which fills the cavity is desirable to obtain the maximum amount of radical. On the other hand, this should be kept as narrow as possible, since there will be solution resistance between the edge and the center of the electrode. If it is desired to follow chronopotentiometric or cyclic voltammetric experiments, a shorter and wider electrode will be useful since the current passed will be smaller and less uncompensated cell resistance will result. For any specific application, there must be a compromise between maximum electrode area and minimizing the resistive drop. The sensitivity along the length of the cavity parallel to the electrode follows an expression of the form $\cos^2(2\pi x/l)$, where l is the length of the cavity (2.3 cm) and x is the distance measured from the center of the cavity. If the electrode is centered in the cavity, then an electrode 11 mm long will allow a signal of 82% of the theoretical maximum while an electrode 6 mm long will give 50% of the theoretical maximum signal.

Procedure. Each solution was prepared under a nitrogen atmosphere. The solution was degassed by the freeze–pump–thaw method in the round-bottom flask attached to the reservoir (Figure 2). Helium was then allowed to enter above the solution. After the cell was assembled in the esr spectrometer, the reservoir was flushed with dry nitrogen, and the solution was transferred to the reservoir. The reservoir was then connected to the cell. Dry nitrogen was used to flush the apparatus, and the solution was allowed to flow into the cell. The experiments were done under a nitrogen atmosphere. For each electrochemical experiment, fresh solution was allowed to enter the cell.

Results and Discussion

A first test of any system which is designed for dual spectroscopic-electrochemical studies involves the investigation of stable systems in order to determine the range of usefulness of the system. If such an apparatus is to be used for kinetic studies, then stable radicals must not be removed from the zone of detection of the spectrometer by either convection or leakage or by chemical reaction with materials inherent in the cell design (*e.g.*, oxygen, products from the auxiliary electrode, etc.). To examine this cell, three substances which produce stable radicals in DMF were selected. The first 9,10-anthraquinone (AQ) exhibits two reversible electron transfer steps in aprotic media.[14]

(14) P. H. Given, M. E. Peover, and J. M. Schoen, *J. Chem. Soc.*, 2764 (1958).

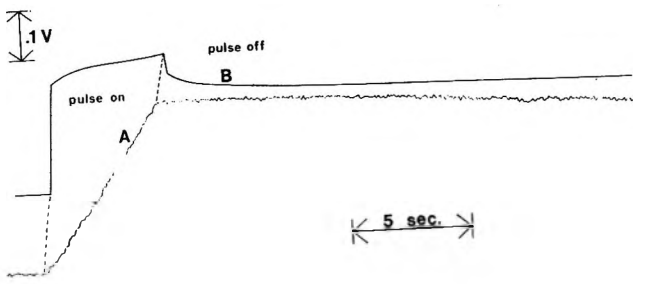

Figure 3. Esr signal (A) and electrode potential (B) during and following a constant current pulse of 200 μA. The solution contained 10.9 $\times$ 10^{-3} M anthraquinone and 0.105 M TBAI in DMF.

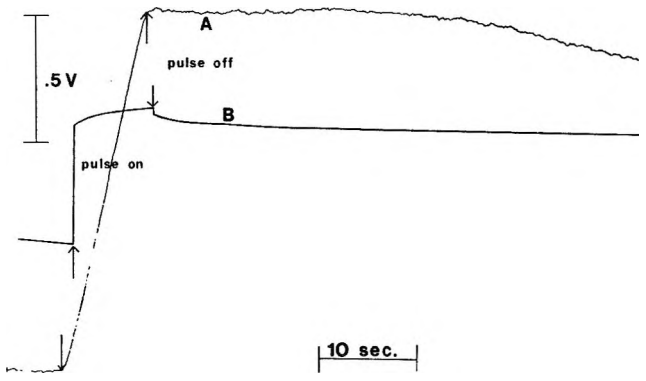

Figure 4. Esr signal (A) and electrode potential (B) during and following a constant current pulse of 200 μA. The solution contained 7.63 $\times$ 10^{-3} M nitrobenzene and 0.106 M TBAI in DMF.

Both the anion radical and the dianion are stable in DMF for at least several minutes. Nitrobenzene (NB) shows a reversible one-electron wave.[15] The second wave which is irreversible begins near the cathodic limit of 0.1 M TBAI–DMF and merges with background. The third substance, azobenzene (AB), also exhibits two one-electron reduction waves in DMF.[16] The radical anion is stable only for several seconds, but the dianion is rapidly protonated by the solvent to form hydrazobenzene.

Current Steps (Chronopotentiometry). Figures 3 and 4 show low current pulses applied to solutions of AQ and NB. Both the esr signal and the cell potential are recorded simultaneously. In both cases a stable signal is observed for 20 to 30 sec after the generation was terminated. The cell potential also remains nearly constant after the current is switched off. When the current is stopped, a small, rapid decrease of the cell potential is observed which arises from the small uncompensated cell resistance between the working and reference electrodes. With a current of 200 μA, this voltage change is between 20 and 40 mV (depending upon the exact position of the reference electrode) which corresponds to an uncompensated resistance of 100 to 200 Ω in this system.

Transition times were measured for AQ at applied current of 100, 200, and 500 μA. The theory of chronopotentiometry predicts that $i\tau^{1/2}/C$ (where i is the current, C is the concentration, and τ is the transition time) is expected to be constant. A value of 0.075 $\pm$ 0.015 A $sec^{1/2}$ M^{-1} was obtained from measurements at several concentrations. The results of these experiments are given in Table I. The evaluation of the transition time constant allows the establishment of the maximum time which a constant current pulse may be applied without a second process occurring.

Table I: Chronopotentiometric Transition Times for Anthraquinone in 0.1 M TBAI–DMF Solutions[a]

Anthraquinone concn, mM	Current (i), μA	Trans. time (τ), sec	$i\tau^{1/2}/C$, A $sec^{1/2}$ M^{-1}
5.25	100	16.0	0.077
4.59	100	8.6	0.064
4.59	200	3.8	0.085
4.59	500	0.5	0.08
10.90	200	14.6	0.071

[a] Electrode area about 0.2 cm^2.

Short pulses may also be applied to this system. Figure 5 shows a high current (25 mA) for 6.3-msec pulse applied to AQ. Because of the short pulse duration, signal averaging was required to obtain sufficient resolution to show the rising portion of the curve.

Similar experiments with azobenzene did not give a steady esr signal after the generation of radicals (Figure 6); here the signal decayed after the termination of the current pulse with a half-life of about 23 sec. Sadler and Bard[16] found that 1.10 to 1.16 F/mol were required to reduce azobenzene completely to the anion radical by controlled potential coulometry. Upon coulometric oxidation, 70% of the material was recovered. The rapid initial decay found with esr measurements suggests that the anion radical reacts with some species in the solvent–electrolyte system, but larger amounts of the anion radical are stable.

Reversal chronopotentiometry was selected as one of the quantitative tests for studying the electrochemical behavior of the cell. When the product generated with a constant current at an electrode is stable, and semi-infinite linear diffusion conditions exist, the time required to reach a transition upon current reversal, t_r, is related to the forward generation time t_f ($t_f \leq \tau$) by $t_r = t_f/3$.[17] On the other hand, if the same experiment is carried out in a thin layer cell,[18] then $t_r = t_f$.

(15) T. Kitagawa, T. P. Layloff, and R. N. Adams, *Anal. Chem.*, **35**, 1086 (1963).

(16) (a) J. L. Sadler and A. J. Bard, *J. Amer. Chem. Soc.*, **90**, 1979 (1968); (b) G. G. Aylward, J. L. Garnett, and J. H. Sharp, *Anal. Chem.*, **39**, 457 (1967).

Table II: Results of Reversal Chronopotentiometry in 0.10 *M* TBAI–DMF Solutions

	i, μA	Time, forward, (t_f), sec	Time, reverse, (t_r), sec	t_r/t_f	Esr signal at t_f, S_f	Esr signal at t_r, S_r	S_r/S_f
7.68×10^{-3} *M* nitrobenzene	100	33.5	6.5	0.20	7.09	5.67	0.80
	200	10.0	2.2	0.22	5.20	4.20	0.80
	200	9.5	2.1	0.22	8.15	6.35	0.78
4.59×10^{-3} *M* anthraquinone	100	2.95	0.77	0.26	4.36	3.25	0.75
	100	1.42	0.38	0.27	3.22	2.28	0.71
	200	3.96	0.92	0.23	6.75	5.20	0.77

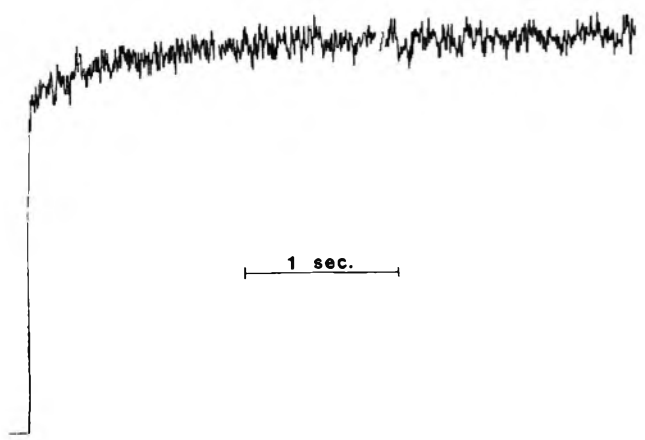

Figure 5. Esr signal (averaged four times) for a constant current pulse of 25 mA for 6.3 msec. The solution contained 4.66×10^{-3} *M* anthraquinone and 0.104 *M* TBAI in DMF.

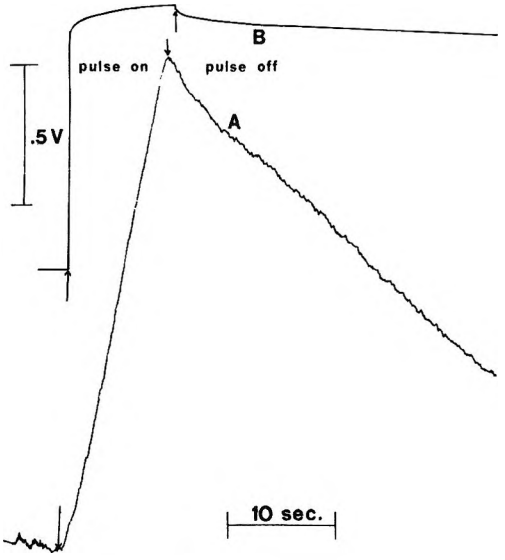

Figure 6. Esr signal (A) and cell potential (B) during and following a constant current pulse of 100 μA. The solution contained 5.50×10^{-3} *M* azobenzene and 0.102 *M* TBAI in DMF.

Figure 7 shows a typical current reversal study, and the results of several such experiments are summarized in Table II. In all cases the t_r/t_f ratio is less than 1:3. Normally, this is taken to indicate instability of the electrogenerated product, because decomposition of the product would decrease the amount available for the reverse electrode process. In this experiment, however, the esr signals at the time that the current is reversed (S_f at t_f), and at the reverse transition time (S_r at t_f) can also be compared. The data on Table II show that in all cases (within ±0.01 units)

$$\frac{t_r}{t_f} = 1 - \frac{S_r}{S_f} \tag{1}$$

Hence, the fraction of radical remaining in solution after the reversal is equal to the fraction of radical which is not reoxidized so that even though $t_r/t_f < 1/3$, no chemical reaction of the product occurs during the time of these measurements. Furthermore, there is no significant curvature of the lines which show the esr signal during the generation and oxidation of the anion radical. (Since both processes are carried out at constant current and 100% current efficiency, a linear rise and decay are expected.) The t_r/t_f ratio of less than one-third probably results from some convection occurring and removing product from the vicinity of the electrode. Double-layer charging may have an effect on these measurements at shorter times, but it is inadequate to explain the deviation from one-third at times greater than about 2 sec.

What occurs at the counterelectrode is an important consideration in using this cell. Figure 2 shows that both the counterelectrode and the working electrode are within the microwave cavity. If radicals were produced at the counterelectrode, then an esr signal from these would result. Radical formation at the counterelectrode was not observed in any of our experiments using TBAI as a supporting electrolyte. During reductions, iodine forms at the counterelectrode. During the oxidation step, iodine near that electrode inside the cavity as well as excess iodine re-

(17) (a) P. Delahay, "New Instrumental Methods in Electrochemistry," Wiley-Interscience, New York, N. Y., 1954; (b) T. Berzins and P. Delahay, *J. Amer. Chem. Soc.*, **75**, 4205 (1953).

(18) A. T. Hubbard and F. C. Anson in "Electroanalytical Chemistry," Vol. 4, A. J. Bard, Ed., Marcel Dekker, New York, N. Y., 1969.

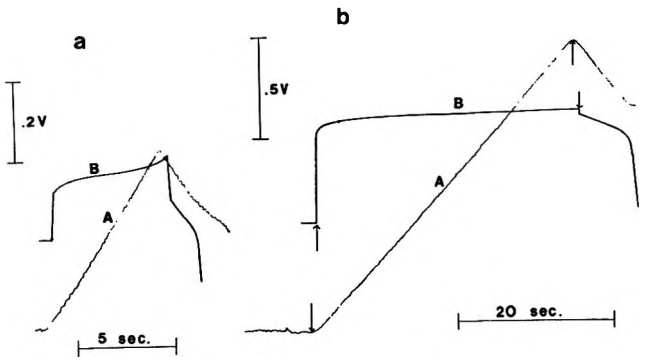

Figure 7. Esr signal (A) and cell potential (B) during reversal chronopotentiometry. (a) 200-μA pulse for 6 sec and reversal. The solution contained 10.9×10^{-3} M anthraquinone and 0.1 M TBAI in DMF. (b) 100-μA pulse for 32 sec and reversal. The solution contained 7.68×10^{-3} M nitrobenzene.

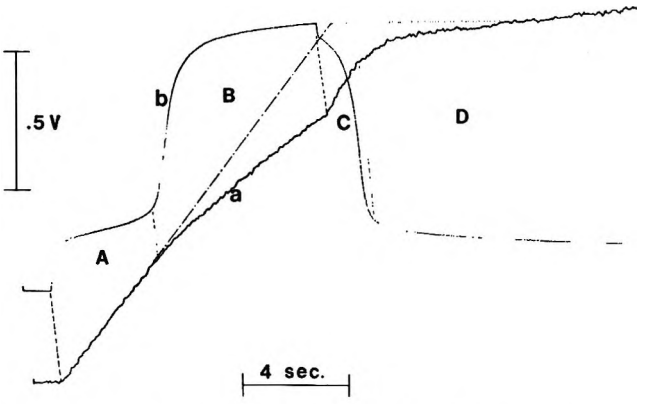

Figure 8. Esr signal (a) and cell potential (b) during and following a constant current pulse of 200 μA. The reduction to the anion and dianion are shown. The solution contained 4.59×10^{-2} M anthraquinone.

maining in solution above the flat cell portion but still in contact with the tungsten counterelectrodes is reduced before radicals are generated. Similar experiments in TBA–perchlorate–DMF solutions, however, where the counterelectrode oxidation products are not as stable as I_3^-, have shown that radicals can be produced at the tungsten nearest the working electrode. In cases when radical formation at the counterelectrode is possible, it may be necessary to add some nonradical producing electroactive substance (esr depolarizer) so that secondary radicals are not generated.

When currents are applied for long periods of time, one must consider the possibility of the products generated at the counterelectrode reacting with the radicals generated at the working electrode. The thickness of the diffusion layer is of the order of $3\sqrt{Dt}$, where D is the diffusion coefficient in square centimeters per second and t is the time of the generation. Since the counterelectrode is about 0.15 cm from the working electrode and assuming D to be 10^{-5} cm^2/sec, then the time required for materials generated at each electrode to diffuse through 0.075 cm when the substances would begin to react is about 60 sec. Convection can reduce this estimated time substantially, however.

When the current is passed for periods greater than the transition time τ, the potential will shift to allow secondary processes to occur. Figure 8 shows a long constant current pulse (with no current reversal) applied to a system containing AQ. For convenience, the figure may be divided into four sections. In section A, the only process which occurs is the reduction of AQ to its anion radical

$$AQ + e^- \longrightarrow AQ^{\cdot-} \qquad (2)$$

at 100% current efficiency and the esr signal shows a linear increase. During the interval section B the processes which occur at the electrode are

$$AQ^{\cdot-} + e^- \longrightarrow AQ^{2-} \qquad (3a)$$

which removes radicals from solution, and

$$AQ + 2e^- \longrightarrow AQ^{2-} \qquad (3b)$$

However, the formation of $AQ^{\cdot-}$ continues in the solution by the reaction

$$AQ^{2-} + AQ \longrightarrow 2AQ^{\cdot-} \qquad (4)$$

Here the esr signal increases at a decreasing rate since the rate of reaction 4 must be slower than the rate of reactions 3a and b. As reactions 3a and b proceed, (3a) becomes more significant with respect to (3b), since the flux of AQ toward the electrode decreases. When the current is stopped (section C), reaction 4 continues, since AQ is still diffusing toward AQ^{2-}, but AQ^{2-} is no longer being produced. Hence, the esr signal increases to a steady value. At the same time a rapid decrease of the cell potential is observed as AQ^{2-} is removed, and the potential becomes determined by the $AQ,AQ^{\cdot-}$ couple.

Section D shows both relatively steady esr signal and cell potential, since all of the AQ^{2-} has now diffused away from the electrode and reacted. The height of the line extrapolated from the initial buildup of radical (section A) to the time that the current is stopped corresponds to the flat portion of the esr signal in region D. This shows that the dianion AQ^{2-} is stable in this environment, and the net yield of $AQ^{\cdot-}$ in the steady-state esr signal is 100%.

Potential Steps. By applying a constant potential to the working electrode, the occurrence of secondary electrode processes are avoided. The results of these experiments show that the first 15–25 sec after a potential on the plateau of the electrochemical wave is applied to the cell, the current decays approximately as $t^{-1/2}$ and the esr signal increases at $t^{1/2}$ as predicted

by theoretical treatments.[17a] However, after this time the current approaches a steady value which is significantly greater than zero while the esr signal slowly increases. The magnitude of the steady-state current, which is probably the result of natural convection, is about 10–20 μA/mM with a 0.44-cm^2 electrode. In continuous constant current generation, as ordinarily employed in *intra muros* electrochemical esr techniques, this magnitude of current can be supported by convection, and secondary processes should not be significant. On several occasions after 2 or 3 min the current begins to oscillate slightly, again probably because of convection.

The potential step method has the advantage of maintaining the electrode at a constant potential, enabling exact control of the electrode process. Moreover, the maximum amount of radical per unit time will be generated by this technique. It is also possible to step to later waves and generate the dianion, dication, or secondary radicals at the electrode and examine their stability in solution.

Cyclic Voltammetry. Cyclic voltammetric studies with simultaneous recording of the esr signal can provide useful information about which electrolytic processes produce radicals and which involve their destruction. The previous current step and potential step experiments showed that the effects of convection become important after 15 to 25 sec, so that for quantitative current–voltage studies, each experiment must be limited to that time duration. If a scan of 1 V and a reversal is desired, the minimum scan rate would be about 20 mV/sec. Slower sweeps can be used for qualitative and semiquantitative studies. Consider qualitatively several representative cyclic voltammograms (Figure 9). The cyclic voltammogram of a system which exhibits a one-electron reduction (eq 5) is shown in Figure 9A. The variation of the esr signal

$$R + e^- \rightleftarrows R^- \qquad (5)$$

(S) with potential shows the following behavior: S increases when reduction begins and the maximum rate of increase of S is at the peak cathodic current (i_{pc}), noted by point a. The signal continues to increase and at point r, the potential sweep is reversed. The signal continues to increase until the current becomes anodic (*i.e.*, the radical is oxidized), denoted by point b. The maximum rate of decrease of the signal occurs near the peak anodic current (i_{pa}) (point c) with a continuous decrease of S as the potential is made more positive.

The current and esr signal as a function of potential for a system in which the radical ion decomposes

$$R^- \xrightarrow{\text{fast}} P \qquad (6)$$

is shown in Figure 9B. Here a buildup of radical is observed as in Figure 9A, but if the rate of decomposition is greater than the rate of electrolysis, the esr signal will

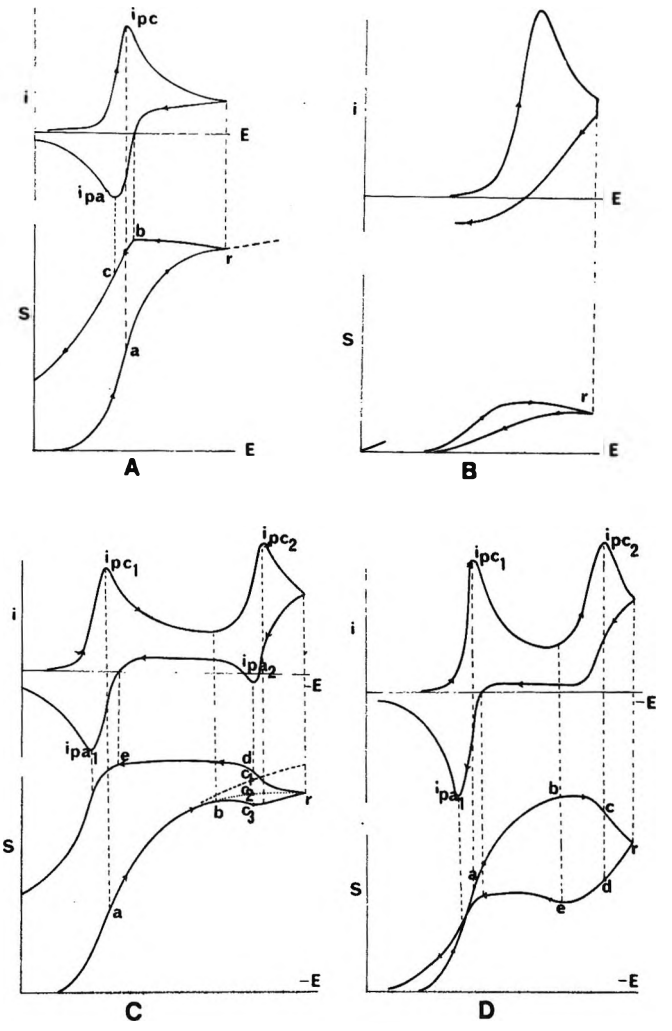

Figure 9. Current (i) and esr signal (S) for cyclic voltammograms representative of several typical electrochemical systems: (A) one-electron transfer and chemically stable and radical product; (B) one-electron transfer and unstable radical product; (C) two one-electron transfer steps with both radical and diamagnetic product stable; (D) two one-electron transfer steps with stable radical and unstable second product.

decrease following reversal. The fact that the radical is unstable is also indicated by the absence of an anodic current peak. Figures 9C and D show cyclic voltammograms for systems which exhibit two waves. The first wave corresponds to generation of a stable radical ion, and the second wave corresponds to the one-electron reduction of the radical anion to a stable dianion (eq 7).

$$R^- + e \rightleftarrows R^{2-} \qquad (7)$$

The current–voltage curve (Figure 9C), where the dianion is stable, shows two reduction waves and, on scan reversal, shows two oxidation waves. In this case S increases as in Figure 9A and will continue to increase until the reduction of the dianion begins (point b). After point b, the trend of S depends on the relative scan rate and diffusion coefficients. If the scan rate is fast, the diffusion layer is very thin, the flux of R coming toward the electrode is large, and S will continue

to increase (line b-c_2) because R^- is produced by reaction of R^{2-} with R (eq 8) more rapidly than it is removed by the reaction in eq 7. This increase

$$R + R^{2-} \longrightarrow 2R^- \quad (8)$$

would be less than the increase that would have been observed had the dianion not been generated (line b-c_1). On the other hand, if the scan rate is slow, so that the diffusion layer is broad, then the flux of R near the electrode is small and a decrease of S is observed (line b-c_3). A minimum would occur at approximately the same potential as the second reduction peak E_{pc2}. After this point the esr signal may again increase, because the rate of the reaction of R^- and R^{2-} becomes greater than that of the reduction of R^- at the electrode. After reversal at point r, when the cell potential again approaches E_{pa2}, S increases rapidly because of the oxidation of R^{2-} to R^- (point d). At point e, S decreases as the current becomes anodic.

A final case which can be considered is one in which the dianion is unstable in solution and decomposes to an electroinactive diamagnetic product Q (eq 9). The

$$R^{2-} \xrightarrow{\text{fast}} Q. \quad (9)$$

current and esr signal are shown as a function of potential in Figure 9D. As before, S increases until point b where the second reduction begins. Now S increases until some potential between b and c where the rate of production of R^- at the electrode is smaller than the rates of reactions given by (7) and (9); at this point, S begins to decrease. The maximum rate of decrease of S will be near point c which corresponds to i_{pc2}. After reversal, S continues to decrease until the potential is again between points d and e. The point at which S begins to increase will depend upon the diffusion layer thickness, and therefore, the scan rate and the rate of decomposition of the dianion. As the potential again becomes more positive, S will follow the same trends as shown in Figures 9A and C.

Several experimental cyclic voltammetric studies with simultaneous recording of the esr signal are shown in Figures 10 and 12. Several typical scans on solutions of NB from 10 to 1 V/sec are shown in Figure 10. The results of cyclic voltammetry on fairly concentrated solutions of NB and AB are given in Table III. The $i_p/v^{1/2}$ values in Table III are not constant as predicted for a simple reversible electrode reaction.[19] There are probably several reasons for this inconsistency. At fast sweep rates, where the currents are high, the uncompensated cell resistance becomes important and the potential sweep departs from linearity.[20] Furthermore, at higher currents the ohmic voltage drop between the center and outside edges of the electrode becomes significant, and the effective electrode area becomes smaller. This resistance between the center and edge of the electrode is about 300 to 400 Ω with the widest electrode used (3.5 mm). On the other hand, at slow scan rates convection becomes a significant factor and higher peak currents result. In general, we find that lower concentrations give better constancy in the value of $i_p/v^{1/2}$ at faster sweep rates.

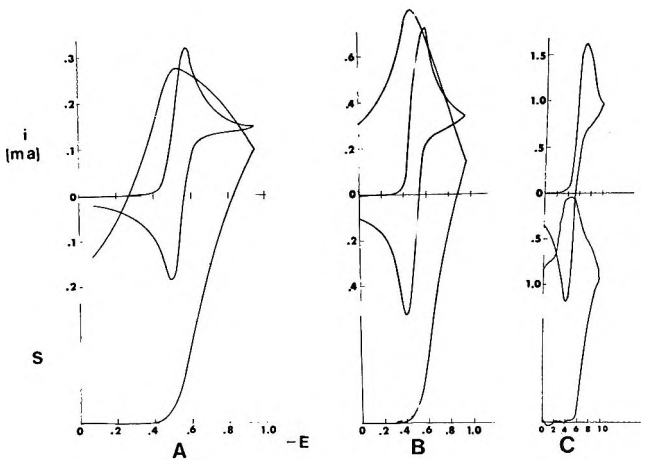

Figure 10. Experimental current (i) and esr signal (S) during cyclic voltammetry in a solution containing 7.68×10^{-3} M nitrobenzene: (A) 10 mV/sec; (B) 100 mV/sec; (C) 1 V/sec.

Table III: Cyclic Voltammetry–Esr Results

v, scan rate, mV/sec	i_{pc},[a] mA	i_{pa},[a] mA	i_{pc}/i_{pa}	S[a]	$i_p/v^{1/2}$
(a) 7.68 mM Nitrobenzene in 0.1 M TBAI-DMF					
5	0.237	0.230	0.97	13.80	3.34
10	0.315	0.308	0.98	11.90	3.15
20	0.410	0.385	0.95	9.54	2.90
50	0.565	0.555	0.98	5.34	2.52
100	0.717	0.717	1.00	3.58	2.26
200	0.910	0.910	1.00	2.23	2.03
500	1.25	1.25	1.00	1.37	1.77
1000	1.60	1.50	1.00	0.98	1.60
(b) 5.50 mM Azobenzene in 0.10 M TBAI-DMF					
5	0.164	0.145	0.88	8.65	2.32
10	0.209	0.185	0.89	5.89	2.09
20	0.270	0.238	0.89	3.10	1.91
50	0.385	0.360	0.93	2.97	1.76
100	0.480	0.460	0.96	1.89	1.54
200	0.642	0.632	0.98	1.26	1.44
500	0.882	0.880	0.99	0.72	1.25
1000	1.18	1.17	0.99	0.54	1.18

[a] i_{pc} is peak current in reduction, i_{pa} reversal peak current, and S = esr signal in arbitrary units.

The variation of esr signal S with sweep rate v and peak current can be derived as follows. The current as a function of potential for a reversible charge transfer is given by eq 10[19]

(19) R. S. Nicholson and I. Shain, *Anal. Chem.*, **36**, 706 (1964).

(20) W. T. DeVries and E. VanDalen, *J. Electroanal. Chem.*, **10**, 183 (1965); R. S. Nicholson, *Anal. Chem.*, **37**, 667 (1965).

$$i = (nF)^{3/2}AC_0(\pi D_0)^{1/2}v^{1/2}\chi\left(\frac{nFvt}{RT}\right)\Big/(RT)^{1/2} \quad (10)$$

where t is the time from the beginning of the sweep, $\chi(nFvt/RT)$ is the "current function"[19] which is a function of the applied potential and the other symbols have their usual meanings. The number of coulombs passed during the potential sweep is

$$Q = \int i\,dt = \frac{(nF)^{3/2}AC_0(\pi D_0)^{1/2}v^{1/2}}{(RT)^{1/2}}\int_0^t \chi\left(\frac{nFvt}{RT}\right)dt \quad (11)$$

Substituting $E = vt$ and $dt = E/v$ into (11) and using the expression for the peak current, i_p

$$i_p = \frac{(nF)^{3/2}AC_0(\pi D_0)^{1/2}v^{1/2}}{RT^{1/2}}\chi_{max} \quad (12)$$

where χ_{max} is the maximum value of the current function yields

$$Q = \left(\frac{i_p}{v}\right)\int_{E=E_1}^{E=E_2}\left[\chi\left(\frac{nFE}{RT}\right)\Big/\chi_{max}\right]dE \quad (13)$$

Because the integral in eq 13 is only a function of the potential range of the sweep, then Q, and hence the esr signal, S, which is proportional to Q, should also be proportional to i_p/v. A plot of S, measured just before the scan reversal, *vs.* i_p/v is shown in Figure 11. A linear relationship exists from sweep rates of 1 V/sec until about 20 mV/sec. At sweep rates below 20 mV/sec, convection again interferes.

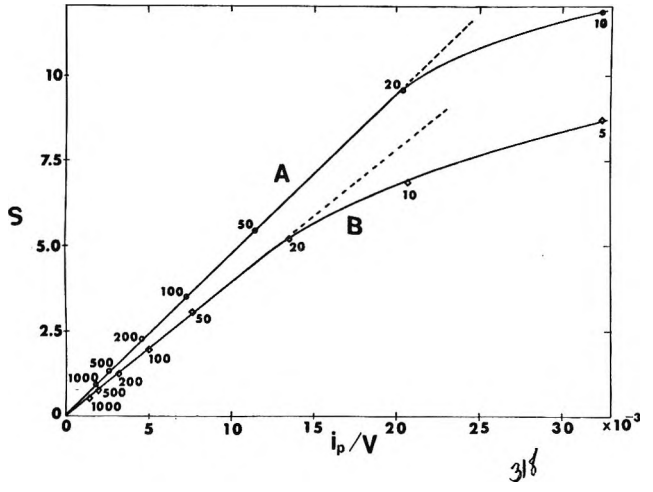

Figure 11. Esr signal (S) *vs.* the peak cathodic current divided by the sweep rate (i_p/v) for solutions of 7.68×10^{-3} M nitrobenzene (A) and 5.50×10^{-3} M azobenzene (B). Value of scan rate (millivolts per second) indicated on figure.

Experimental cyclic voltammograms involving two waves are shown in Figure 12. That of AQ (Figure 12) exhibits two reversible waves, and qualitatively resembles that of Figure 9C. By comparison, the cyclic voltammogram and esr signal of AB shown in Figure 12 is qualitatively similar to that of Figure 9D, except that

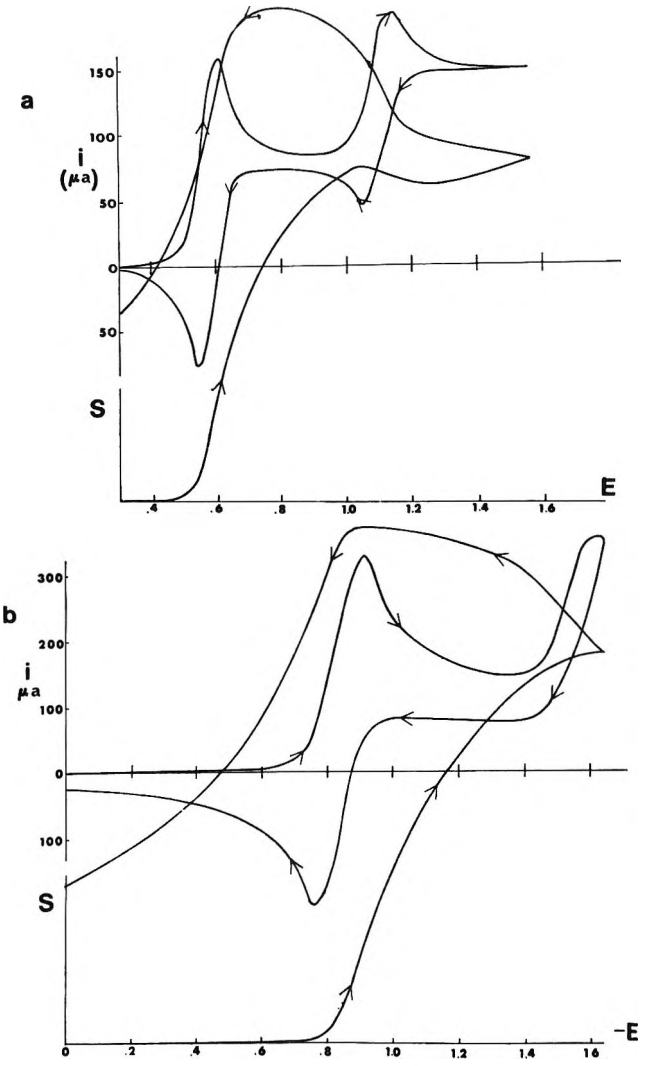

Figure 12. Esr signal (S) and current (i) during cyclic voltammetry: (a) solution of 6.43×10^{-3} M anthraquinone and 0.104 M TBAP in DMF, sweep rate 10 mV/sec; (b) solution of 5.50×10^{-3} M azobenzene and 0.103 M TBAI in DMF, sweep rate 20 mV/sec.

less AB^- was reduced to AB^{2-}, and that S did not decrease as much as in Figure 12.

Conclusions

The cell described is useful for simultaneous electrochemical-esr (SEESR) experiments for times up to about 20 sec. The application of these techniques to the study of the kinetics of decay of electrogenerated radicals requires a theoretical treatment of the expected signal–time behavior for various reaction schemes and reaction orders. A digital simulation[21] treatment of these is being carried out. The application of SEESR techniques to the detection of short-lived electrogenerated radicals, using signal averaging techniques, and to the elucidation of secondary reactions in electrolytic hydrodimerizations is currently under investigation.

(21) S. Feldberg, I. B. Goldberg, and A. J. Bard, unpublished research.

Acknowledgment. The support of the National Science Foundation (GP-6688X) and the Robert Welch Foundation is gratefully acknowledged. We also thank Mr. John Somerville for constructing the esr cell and Mr. Vincent Puglisi and Professor James R. Bolton for helpful advice and suggestions. The esr spectrometer was purchased under a grant from the National Science Foundation (GP-2090).

The Conductance and Association Behavior of Alkali Perchlorates in Water at 25° [1]

by Alessandro D'Aprano

Institute of Physical Chemistry, University of Palermo, Palermo, Italy *(Received June 29, 1970)*

Publication costs borne completely by The Journal of Physical Chemistry

The conductance of the alkali perchlorates at 25° has been measured in water in a concentration range up to 0.06 *M* and the experimental values analyzed by a revised Hsia–Fuoss (1967) conductance equation. Association increases with atomic number; it is negligible for lithium and marginal for sodium. For the other three alkali perchlorates, pair association constants are $K_A(K) = 1.0$, $K_A(Rb) = 1.35$, and $K_A(Cs) = 1.7$.

Introduction

Most previous work on the association of 1:1 electrolytes by conductometric methods was carried out in solvents or solvent mixtures in the range of dielectric constants below 30. In solvents of higher dielectric constant, and especially in water, association is slight and determination of the association constants is therefore difficult. The first estimate for 1:1 salts in water was made by Davies[2] who used the Onsager limiting coefficient plus an empirical term to estimate the conductance Λ_i of the free ions and then calculated the fraction γ of free ions as $\Lambda(obsd)/\Lambda_i$. Based on his "rather tentative values," he concluded that "salts containing a common anion fall, in strength, in the following order: Li > Na > K > Rb > Cs > Tl." More recently, a theoretical derivation[3,4] of the higher terms in the conductance function has been made, which permits a direct calculation of γ from conductance data. This method has been applied to data on the alkali halides in water[5,6] and to salts in mixtures of high dielectric constants.[7-9]

Previous conductometric measurements for alkali metal salts in dioxane–water,[10,11] in ethanol–water[12] mixtures, and in various hydrogen bonded solvents[13,14] have shown that in contrast with direct coulombic interactions, the association of these salts increases as the crystallographic radii of the cations increase. The association sequence found, namely Li < Na < K < Rb < Cs, has been explained by assuming that in hydrogen-bonded solvents, the alkali metal cations are extensively solvated. The same behavior has been postulated by Kay[15] for the association of alkali halides and perchlorates in aqueous solutions.

In order to test this assumption experimentally, the conductance of the alkali perchlorates has been measured in water in a concentration range up to 0.06 *M*, corresponding to the upper limit of applicability of the present theory. Three of the perchlorates (lithium, sodium, and potassium) have already been measured,[16] the curve for potassium perchlorates lies on the limiting

(1) Grateful acknowledgment is made to the "Consiglio Nazionale delle Richerche" for support of this research.

(2) C. W. Davies, *Trans. Faraday Soc.*, **23**, 351 (1927).

(3) R. M. Fuoss and L. Onsager, *J. Phys. Chem.*, **61**, 668 (1957).

(4) R. M. Fuoss and K. L. Hsia, *Proc. Nat. Acad. Sci. U. S.*, **57**, 1550 (1967); **58**, 1818 (1967).

(5) K. L. Hsia and R. M. Fuoss, *J. Amer. Chem. Soc.*, **90**, 3055 (1968).

(6) Y. C. Chiu and R. M. Fuoss, *J. Phys. Chem.*, **72**, 4123 (1968).

(7) A. D'Aprano and R. M. Fuoss, *ibid.*, **72**, 4710 (1968).

(8) A. D'Aprano and R. M. Fuoss, *J. Amer. Chem. Soc.*, **91**, 211 (1969).

(9) A. D'Aprano and R. M. Fuoss, *ibid.*, **91**, 279 (1969).

(10) T. L. Fabry and R. M. Fuoss, *J. Phys. Chem.*, **68**, 971 (1964).

(11) F. Accascina, A. D'Aprano, and R. Triolo, *ibid.*, **71**, 3469 (1967).

(12) R. L. Hawes and R. L. Kay, *ibid.*, **69**, 2420 (1965).

(13) R. L. Kay, *J. Amer. Chem. Soc.*, **82**, 2099 (1960).

(14) G. B. Porfitt and A. L. Smith, *Trans. Faraday Soc.*, **59**, 257 (1963).

(15) R. L. Kay in "Electrolytes," B. Pesce, Ed., Pergamon Press, New York, N. Y., 1962, p 119.

(16) J. H. Jones, *J. Amer. Chem. Soc.*, **67**, 855 (1945).

tangent up to $c \approx 0.015$, while the curves for lithium and sodium perchlorates are visibly curving upward from the tangent at $c \approx 0.005$. This result shows that the potassium salt is relatively more associated than the other two; Monk,[17] using Davies' method,[2] estimated a dissociation constant of 3.0 for potassium perchlorate, which corresponds to an association constant $K_A \approx 0.3$. In order to complete the series of the alkalis, we have measured the conductance of rubidium and cesium perchlorates in water at 25° and also redetermined the conductances of the perchlorates of the first three alkalis. For the latter, our values for limiting conductance agree with those of Jones within 0.1 Λ unit. Association for lithium perchlorate up to 0.06 N is too slight to detect; for sodium, it is marginal. For the other three, the sequence $K_A = 1.0, 1.35, 1.7$ was found, corresponding to increasing association with increasing atomic numbers, K < Rb < Cs.

Experimental Section

The electrical apparatus and the technique used for the conductivity measurements have been described in a previous paper.[18] The erlenmeyer-type cell (k = 7.0897 cm^{-1}) was calibrated[19] using aqueous potassium chloride solutions. The water ($\kappa_0 = 1\text{–}2 \times 10^{-6}$ ohm^{-1} cm^{-1}) was purified as previously described.[20] All the perchlorates (Commercial reagent grade products) were recrystallized four to six times from water–methanol mixtures (1:1 by volume) and dried at 150° in a vacuum oven. The dried salts were kept in a desiccator containing P_2O_5.

Conductance runs were made by the concentration method. All the solutions were prepared by weight and corrected to vacuum conditions. The densities of the solutions were assumed to follow the relationship $d = d_0(1 + \gamma\omega)$ where ω is the electrolyte concentration in equivalents per 1000 g of solution. The constant γ was 0.0625 for $LiClO_4$, 0.0770 for $NaClO_4$, 0.0866 for $KClO_4$, 0.0989 for $RbClO_4$, and 0.0998 for $CsClO_4$.

The experimental results for alkali perchlorates in water at 25° are summarized in Table I[21] where c is the volume concentration (equiv/l.) and Λ is the equivalent conductance. A dielectric constant of 78.35 and a viscosity of 0.8903 cP were used for water at 25°.

Discussion

The experimental data were analyzed by a computer using the conductance equation

$$\Lambda = \gamma[\Lambda_0(1 + \Delta x/x) - \Delta\Lambda_e] \qquad (1)$$

where γ is the ratio of free ion concentration to the stoichiometric one.

The above equation is a revised version of the Hsia–Fuoss (1967) conductance equation[4] with the following main changes. (1) The relaxation term $\Delta x/x$ is the Hsia–Fuoss[4] function in which the variable κa is replaced by $\tau = \beta\kappa/2$, $\beta = \epsilon^2/DkT$; this change[22] corresponds to using the Bjerrum radius $\beta/2$ as the lower limit in the integration instead of the contact distance a. (2) The association constant

$$K_A = (1 - \gamma)/c\gamma^2 f^2$$

is given by the relation

$$K_A = (4\pi N\beta^3/6000)F(b) \qquad b = \beta/a$$

which contains the function

$$F(b) = E_p(b) - (e^b/b)[1 + (1/b)] + 2.435 \qquad (2)$$

derived in 1961 by Fuoss and Onsager[23] and replaces the 1958 equation[24]

$$K_A = (4\pi Na^3/3000)e^b$$

If the data lead to a very small (or slightly negative value!) for the association constant, it is assumed that association is negligible and that K_A may be set equal to zero. The a parameter can in this case not be evaluated, if the Justice modification of the Fuoss–Hsia equation is used. (3) Activity coefficients are computed by[3a]

$$-\ln f = \tau/(1 + \tau)$$

instead of Debye–Hückel limiting equation. (4) The electrophoresis term $\Delta\Lambda_e$, formerly approximated[4] by

$$\Delta\Lambda = [\beta_0 c^{1/2}/(1 + \kappa a)](1 + \Delta x/x)$$

has been replaced by

$$\Delta\Lambda_e = [\beta_0 c^{1/2}/(1 + \tau)]F(\tau)$$

where $F(\tau)$ explicitly gives the effect of interaction between relaxation and velocity fields instead of approximating it by multiplying the limit value $\beta_0 c^{1/2}$ by $(1 + \Delta x/x)$. Its principal effect is to introduce a previously missed term $[-E_2 c \ln c]$ in the electrophoresis.[25] (5) The volume term in volume fraction has been omitted.

The revised conductance eq 1 has been programmed for the electronic computer to find the conductometric parameters (Λ_0, K_A, and $\mathring{a}$). The program is a two-parameter search; given a set of data (c_j, Λ_j), dielectric constant, viscosity, and temperature, it finds the values

(17) C. B. Monk, *J. Amer. Chem. Soc.*, **70**, 3281 (1948).

(18) F. Accascina, A. D'Aprano, and R. M. Fuoss, *ibid.*, **81**, 1058 (1959).

(19) J. E. Lind, Jr., J. J. Zwolenick, and R. M. Fuoss, *ibid.*, **81**, 1557 (1959).

(20) A. D'Aprano, *Ric. Sci.*, **34**(7), 433 (1964).

(21) Table I will appear immediately following this article in the microfilm edition of this volume of the journal. Single copies may be obtained from the Reprint Department, ACS Publications, 1155 Sixteenth Street, N. W., Washington, D. C. 20036. Remit $3.00 for photocopy or $2.00 for microfiche.

(22) J. C. Justice, *J. Chim. Phys. Physicochem. Biol.*, **65**, 353 (1968).

(23) (a) R. M. Fuoss and L. Onsager, *Proc. Nat. Acad. Sci., U. S.*, **47**, 818 (1961), eq 30 and 37; (b) J. F. Skinner and R. M. Fuoss, *J. Amer. Chem. Soc.*, **86**, 3423 (1964), eq 21, 30–36.

(24) R. M. Fuoss, *ibid.*, **80**, 5059 (1958).

(25) P. C. Carman, *J. Phys. Chem.*, **74**, 1653 (1970).

Table II: Derived Conductance Parameter for Alkali Perchlorates in Water at 25°

Electrolytes	Runs	Λ_0	K_A	$\mathring{a}$	σ
$LiClO_4$	1	105.9 ± 0.2	(−0.05 ± 0.07)		0.03
	2	105.9 ± 0.2	(−0.09 ± 0.12)		0.05
	1 + 2	105.9 ± 0.3	(−0.07 ± 0.14)		0.04
$NaClO_4$	3	117.3 ± 0.2	(0.19 ± 0.07)		0.03
	4	117.3 ± 0.3	(0.19 ± 0.09)		0.03
	3 + 4	117.3 ± 0.4	(0.20 ± 0.14)		0.04
$KClO_4$	5	140.71 ± 0.09	0.98 ± 0.03	3.32	0.008
	6	140.74 ± 0.05	0.99 ± 0.01	3.31	0.005
	5 + 6	140.73 ± 0.13	0.98 ± 0.04	3.31	0.009
$RbClO_4$	7	144.20 ± 0.09	1.35 ± 0.03	2.69	0.009
	8	144.21 ± 0.05	1.35 ± 0.02	2.69	0.005
	7 + 8	144.21 ± 0.10	1.35 ± 0.03	2.69	0.007
$CsClO_4$	9	144.5 ± 0.2	1.68 ± 0.09	2.28	0.03
	10	144.55 ± 0.09	1.69 ± 0.09	2.27	0.01
	9 + 10	144.5 ± 0.2	1.69 ± 0.09	2.28	0.02

of Λ_0 and K_A which minimize the sum of the squares of the differences between observed values of Λ and those calculated by eq 1. Then b is obtained by solving the inverse of (2) and the contact distance is given by $a = \beta/b$.

All calculations were made on an Univac 1108 computer. The results are summarized in Table II where Λ_0 is the limiting conductance, K_A the association constant, $\mathring{a}$ the center to center contact distance, and σ the standard deviation.

As it can be seen from the values of the standard deviation σ, the data are reproduced, within the experimental error, by the new conductance equation. From the Λ_0 values obtained with the combined runs of each alkali perchlorate, the average value of 67.2 was calculated for $\Lambda_{0(ClO_4^-)}$ in water (Table III). This result is in agreement with the value $\Lambda_{0(ClO_4^-)} = 67.25$, previously found by Goffredi.[26] Considering the experimental difficulties encountered with the hygroscopic perchlorates the results are better than expected.

As shown in Table II, all the perchlorates considered, except lithium perchlorate with a negative K_A, are slightly associated in water; cesium perchlorate, in spite of its largest cation size, is more associated than the other perchlorates. This result is fully consistent with the order postulated by Kay.[15]

Regarding the negative K_A value found for $LiClO_4$: this result must be considered as merely curve-fitting without any physical significance. In fact, if we put the conductance equation in the form

$$\Lambda = \Lambda_0 - Sc^{1/2}\gamma^{1/2} + Ec\gamma \log c\gamma + Jc\gamma + J_2c^{3/2}\gamma^{3/2} - K_Ac\gamma f^2\Lambda_0$$

K_A results; the empirical coefficient of the $c\gamma f^2\Lambda_0$ term and its numerical value must therefore include any unknown linear terms. Assuming that such terms (not yet found theoretically) are present, then the conductance equation will be

$$\Lambda = \Lambda_0 - Sc^{1/2}\gamma^{1/2} + Ec\gamma \log c\gamma + Jc\gamma + J_2c^{3/2}\gamma^{3/2} - K_Ac\gamma f^2\Lambda_0 + Bc\gamma\Lambda_0 \approx \Lambda_0 - Sc^{1/2} + Ec \log c + J_2c^{3/2} - (J + B\Lambda_0 - K_A\Lambda_0)c$$

and the computer will calculate $(B - K_A)$ as K_A and if $B > K_A$, the resulting K_A will be a negative quantity. The dilemma of a negative K_A value is until now another shortcoming of the present theory and calls for a more detailed treatment including the modification of solvent structure by the ions. Since a negative number obviously can never be an association constant, at this stage it is only possible to conclude that the association of lithium perchlorate is nearly zero in water at 25°.

Furthermore it must be assumed that the unknown positive terms are also present for salts which give positive K values and that the association constants for these salts are actually higher than the values obtained from the present analysis. It must be recognized, therefore, that the probability of eventually revising the

Table III: Limiting Electrolyte and Ion Conductance in Water at 25°

Electrolytes	Λ_0	Λ_0^+	Λ_0^-
$LiClO_4$	105.9	38.7[a]	67.2
$NaClO_4$	117.3	50.1[a]	67.2
$KClO_4$	140.7	73.5[a]	67.2
$RbClO_4$	144.2	77.0[b]	67.2
$CsClO_4$	144.5	77.3[a]	67.2

[a] Data are from R. A. Robinson and R. H. Stokes, "Electrolyte Solution," Academic Press, New York, N. Y., 1959, p 463. (b) Voisinet's corrected value, R. W. Kunze, R. M. Fuoss, and B. B. Owen, *J. Phys. Chem.*, **67**, 1719 (1963).

(26) M. Goffredi and R. Triolo, *Ric. Sci.*, **37**, 1137 (1967).

current values, once it will be known which kind of corrections to make.

In any case, independently of this revision, the association sequence found in the present work for the alkali perchlorates can be explained by taking into account the effect of solvation on ion pairing.[11,27–29] If we consider, in fact, the extreme alkali perchlorates, the following considerations may be made. Sodium, as well as lithium ions, on account of their small radii and high charge densities, strongly orientate the water molecules. Due to the sheath of solvent molecules around the ions, ion pairing almost should not occur for them. The largest cesium cation, on the other hand, is almost unable to orientate the water molecules and must be considered as a bare ion in aqueous solution. Cesium perchlorate should be, therefore, much more associated in water than the other alkali perchlorates.

Acknowledgment. The author wishes to acknowledge the valuable aid of Professor R. M. Fuoss in the present research.

(27) A. D'Aprano and R. M. Fuoss, *J. Phys. Chem.*, **67**, 1704, 1877 (1963).

(28) W. R. Gilkerson and B. Ezell, *J. Amer. Chem. Soc.*, **87**, 3812 (1965); **88**, 3484 (1966).

(29) H. K. Bodenseh and J. B. Ramsey, *J. Phys. Chem.*, **69**, 543 (1965).

Tracer and Mutual Diffusivities in the System Chloroform–Carbon Tetrachloride at 25°

by C. M. Kelly,*[1] G. B. Wirth, and D. K. Anderson

Department of Chemical Engineering, Michigan State University, East Lansing, Michigan 48823
(Received November 12, 1970)

Publication costs borne completely by The Journal of Physical Chemistry

Experimental measurements were made of tracer diffusivities, mutual diffusivities, viscosities, and densities at 25° in the binary liquid system chloroform–carbon tetrachloride. The diffusivities are compared with those predicted by the Hartley–Crank equation for nonideal nonassociated liquid systems. The thermodynamic correction factor in the Hartley–Crank equation undercorrects the mutual diffusivity data. This undercorrection is an unusual result.

Introduction and Theory

A comprehensive model of diffusion must be able to predict both mutual and tracer diffusivities. It should be able to correlate diffusion coefficients to molecular size and shape, to intermolecular interactions, and to temperature and pressure. It must also describe the relationship between tracer and mutual diffusivities.

One moderately successful model is the hydrodynamic model, which treats a diffusing molecule as a particle flowing through a continuous medium. In its earliest form, as set forth by Sutherland[2] and Einstein,[3] it considers the diffusing molecule as a sphere and predicts the diffusivity as a function of temperature, viscosity, and molecular radius. This has been a fairly good approximation for large molecules in dilute solutions.

More recent developments of the hydrodynamic model have differentiated between mutual and tracer diffusion and have included the effects of intermolecular associations, molecular size and shape (as distinct from molecular radius), and solution nonideality.

It has been shown[4] that according to the hydrodynamic model the tracer diffusivity of a component which is not associated in solution should be given by

$$D_i^* = \frac{RT}{\eta\sigma_i} \tag{1}$$

where T is the temperature, η is the viscosity of the solution, R is the gas law constant, and σ_i is the "friction coefficient" of the component, assumed constant. The mutual diffusivity in such a system is related to the tracer diffusivities of the components by

$$D_{AB} = \frac{RT}{\eta}\left[\frac{X_A}{\sigma_B} + \frac{X_B}{\sigma_A}\right]\frac{\partial \ln a}{\partial \ln X} \tag{2}$$

(1) To whom correspondence should be addressed at Department of Chemical Engineering, Villanova University, Villanova, Pa.

(2) W. Sutherland, *Phil. Mag.*, **9**, 784 (1905).

(3) A. Einstein, *Ann. Phys. Chem.*, **17**, 549 (1905).

(4) L. S. Darken, *Trans. Faraday Soc.*, **45**, 801 (1949).

This is the familiar Hartley–Crank equation. It was initially derived[5] for the case of constant volumes. It was later shown that this is not a necessary restriction.[6]

The Hartley–Crank equation has been found to predict mutual diffusivities quite accurately in ideal liquid solutions,[7] where the thermodynamic correction factor is unity. In nonideal systems, however, it has not been so successful. In almost all cases the thermodynamic correction factor has been found to overcorrect. That is, the predicted difference between actual mutual diffusivities and the mutual diffusivities if the solution were ideal is usually too large. In most cases the predicted diffusivities do at least qualitatively agree with experimental results, though. The shape of the predicted graph of mutual diffusivity *vs.* composition is generally verified by measurements.

The present paper presents a binary liquid system, chloroform–carbon tetrachloride, in which the Hartley–Crank equation appears to undercorrect for solution nonideality.

Experimental Section

In this study tracer diffusivities were measured by the microcapillary method. In this method, a Teflon capillary approximately 8 cm in length and 2 mm i.d. is filled with a solution, one of whose components is tagged with ^{14}C. The capillary is immersed in a large volume of a bulk solution of the same chemical composition, but with no tagged molecules. After a 3- to 5-day period, the capillary is removed from the bulk solution, emptied, and counted. The capillary is then filled with the same tagged solution and immediately emptied and counted. The ratio of these two count rates is then compared to a tabulated solution of the associated boundary value problem to determine the diffusivity.

To eliminate convective transfer from the open end of the capillary into the bulk solution (a major source of error in this technique) a porous glass disk covers the open end during the experiment. In this case the boundary condition for diffusion is not a zero concentration at the open end. Rather, the concentration gradient is proportional to the concentration at the end of the capillary. The constant of proportionality involves a resistance term for transfer through the disk, which depends on pore size and structure within the disk. This resistance constant appears in the solution of the boundary value problem. It may be determined experimentally by performing the experiment on a substance whose diffusivity is known. This was done using carbon tetrachloride, with a self-diffusivity of 1.32×10^{-5} cm^2/sec (as suggested by Rathbun and Babb[7]). The absolute precision of this method depends on the accuracy of the calibration procedure, hence upon the reported value of the self-diffusivity of carbon tetrachloride.

The precision of this method was determined by repetitive measurements and comparison with known mutual diffusivities extrapolated to infinite dilution. The precision level to be expected in a given experiment was generally found to be $\pm 2\%$.

Mutual diffusivities were measured by means of a Mach–Zehnder interferometer.[8] Bidlack[9] gives details of construction and operation. This method consists of following diffusion into a pseudo-infinite medium from a free boundary by means of optical interference fringes. The interference fringes represent a plot of refractive index *vs.* location in the diffusion cell, which can be related to concentration *vs.* location. These are photographed at various times during the experiment, and measurements taken from the photographs are compared to a solution of the boundary value problem to determine the diffusivity.

This procedure yields the integral diffusion coefficient over the concentration difference between the two solutions on either side of the interface. In this investigation the refractive indices of the components were such that differences in concentration of the two solutions were generally on the order of 0.01 mole fraction or less. Under these conditions the integral diffusion coefficient obtained from solution of the boundary-value problem should be a good approximation to the differential diffusion coefficient at the average composition. Since the overall change in the diffusion coefficient is approximately 0.7×10^{-5} cm^2/sec, the change in diffusivity during one experimental determination should be on the order of 0.007×10^{-5} cm^2/sec, which is relatively small.

The precision of the method was determined by comparison of experimental determinations of mutual diffusivities to published results in the sucrose–water system.[10] Agreement for this system was within $\pm 0.5\%$. Experimental difficulties in handling the volatile chloroform–carbon tetrachloride system decrease the precision somewhat. Repetitive measurements in this system indicate that a reasonable estimate of the experimental precision is $\pm 1.5\%$.

Viscosities were measured using a Cannon–Fenske capillary viscometer. Repetitive measurements and comparison to various accepted literature values indicate a precision of $\pm 0.5\%$.

All experiments were conducted in a water thermostat with a miximum temperature cycle of $\pm 0.1°$.

Results and Discussion

Experimentally determined values of tracer diffusivi-

(5) G. S. Hartley and K. Crank, *Trans. Faradcy Soc.*, **52**, 781 (1956).
(6) C. S. Caldwell and A. L. Babb, *J. Phys. Chem.*, **60**, 51 (1956).
(7) R. E. Rathbun and A. L. Babb, *ibid.*, **65**, 1072 (1961).
(8) C. S. Caldwell, J. R. Hall, and A. L. Babb, *Rev. Sci. Instrum.*, **28**, 816 (1957).
(9) D. L. Bidlack, Ph.D. Thesis, Michigan State University, 1964.
(10) L. J. Gosting and M. S. Morris, *J. Amer. Chem. Soc.*, **71**, 1998 (1949).

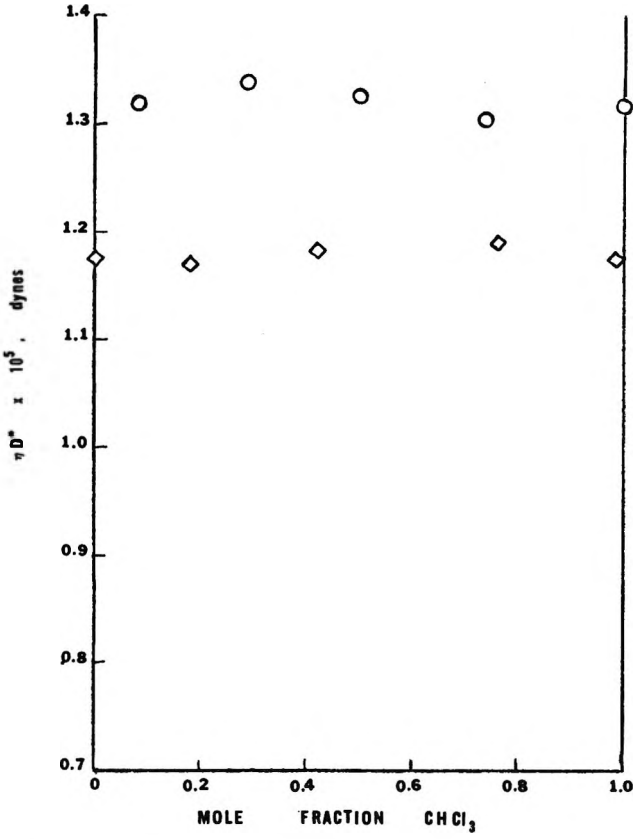

Figure 1. Tracer diffusivity–viscosity product in the system $CHCl_3$–CCl_4 at 25°: ○, ηD_{CHCl_3}; ◊, ηD_{CCl_4}*.

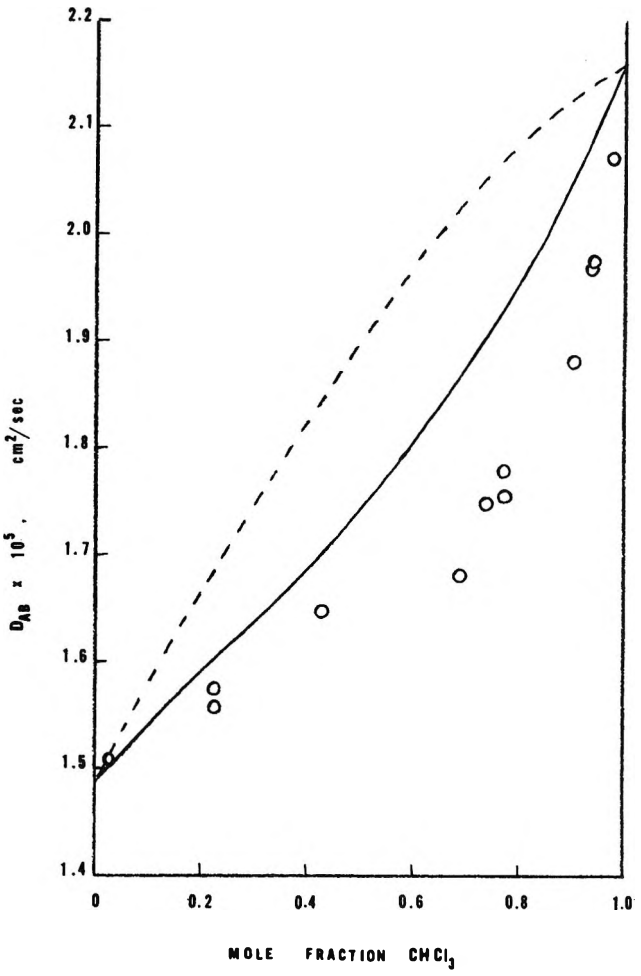

Figure 2. Mutual diffusivity in the system $CHCl_3$–CCl_4 at 25°: – – – –, 4; ———, 5; ○, experimental.

ties, mutual diffusivities, viscosities, and densities at 25° are given in Tables I, II, and III, respectively. The variation, of diffusivity and diffusivity–viscosity product with composition are illustrated in Figures 1 and 2.

Table I: Tracer Diffusivities in the System Chloroform–Carbon Tetrachloride at 25°

X_{CHCl_3}	$D_{CHCl_3}^* \times 10^5$, cm²/sec	$D_{CCl_4}^* \times 10^5$, cm²/sec
0.00	...	1.32
0.08	1.57	...
0.18	...	1.49
0.29	1.82	...
0.42	...	1.73
0.50	2.02	...
0.75	2.23	...
0.76	...	2.04
0.98	...	2.16
1.00	2.44	...

Table II: Mutual Diffusivities in the System Chloroform–Carbon Tetrachloride at 25°

X_{CHCl_4}	$D_{AB} \times 10^5$, cm²/sec
0.027	1.505
0.234	1.557
0.234	1.572
0.431	1.644
0.690	1.680
0.739	1.752
0.774	1.757
0.774	1.779
0.907	1.881
0.942	1.972
0.946	1.976
0.977	2.007

Equation 1 predicts that the product for a nonassociated component is constant at a given temperature. It can be seen from Figure 1 that this product is constant in this system. This is more or less expected, since the outer electron shells of the chlorine atoms do not support hydrogen bonding with the hydrogen of chloroform. Any other intermolecular attractions are likely to be too weak to maintain a stable associated complex.

Furthermore, absence of a temperature effect upon

Table III: Densities and Viscosities in the System Chloroform–Carbon Tetrachloride at 25°

X_{CHCl_3}	η, cP	ρ, g/cm³
0.000	0.889	1.5945
0.112	0.826	1.5744
0.232	0.761	1.5600
0.492	0.661	1.5322
0.845	0.568	1.4955
1.000	0.540	1.4798

the heat of mixing supports the conclusion that this system is not associated.[11]

The Hartley–Crank equation has been modified to explain the usual overcorrection by the thermodynamic factor in terms of simultaneous diffusion of monomers and associated complexes (dimers, trimers, etc.). These have been reasonably successful[12–14] in predicting the direction of the overcorrection. They usually contain an extra parameter (such as the equilibrium constant for the association) which quantitatively removes the overcorrection for reasonable values of the bond strength of the associated complex.

For nonassociated systems such as the present system, however, the Hartley–Crank equation should apply.

If the solution were ideal, the Hartley–Crank equation would have the form

$$D_{AB} = \frac{RT}{\eta}\left[\frac{X_A}{\sigma_B} + \frac{X_B}{\sigma_A}\right] \tag{3}$$

or, after some substitutions and rearrangement

$$D_{AB} = \frac{1}{\eta}[\eta D_B^* X_A + \eta D_A^* X_B] \tag{4}$$

The terms ηD_A^* and ηD_B^* are constant and may be obtained from Figure 1. Equation 4 is plotted in Figure 2 for comparison with the experimental measurements.

The thermodynamic correction factor may be obtained from isothermal vapor–liquid equilibrium data. Hala, *et al.*,[15] have fit published vapor–liquid data for a variety of systems to various descriptive equations (such as Van Laar, Margules, etc.) relating activity coefficients to solution composition.[15] The constants they obtained for the present system from the data of McGlashan, Prue, and Sainsbury[16] were used to calculate thermodynamic correction factors for use in the equation

$$D_{AB} = \frac{1}{\eta}[\eta D_B^* X_A + \eta D_A^* X_B]\frac{\partial \ln a}{\partial \ln X} \tag{5}$$

It may be noted that this system does not deviate too badly from ideality, so that the correction factor is rather small. Equation 5 is also plotted in Figure 2.

Comparing the experimental data to the predictions of eq 4 and 5 shows that the Hartley–Crank equation predicts qualitatively the shape of the D_{AB} *vs.* mole fraction curve. It does not, however, correct properly for solution nonideality. In fact it undercorrects, which is unusual.

In the past, such deviations have often been attributed to intermolecular associations, but this cannot be the case here. It is possible that the vapor–liquid equilibrium data are in error, since small errors in this sort of data are amplified when determining activity coefficients. This seems somewhat unlikely, for the experimental data fit both Van Laar and three-term Margules equations very well.

It is hoped that further refinements in diffusional models and theory will explain the undercorrection in this system. At present, however, the most probable reason is a slight error in determining solution nonideality (*i.e.*, obtaining activity coefficients from vapor–liquid equilibrium data).

Although the Hartley–Crank equation is ordinarily at least qualitatively applicable to nonideal solutions, care must be taken in applying it predictively. In this system at least, there are some anomalous effects which are as yet unexplained. Perhaps future experimental or theoretical work will help to clarify this situation.

Appendix. Nomenclature

a	activity
D^*	tracer diffusivity, cm²/sec
D_{AB}	mutual diffusivity, cm²/sec
R	gas law constant
T	temperature
X	mole fraction
η	viscosity, cP
ρ	density, g/cm³
σ	friction factor, cm/g-mol

subscript A refers to component A
subscript B refers to component B
subscript i refers to component i

(11) J. H. Hildebrand and R. L. Scott, "The Solubility of Nonelectrolytes," 3rd ed, Reinhold, New York, N. Y., 1950.

(12) P. C. Carman, *J. Phys. Chem.*, **71**, 2565 (1967).

(13) D. K. Anderson and A. L. Babb, *ibid.*, **66**, 1281 (1962).

(14) D. K. Anderson and A. L. Babb, *ibid.*, **66**, 899 (1962).

(15) E. Hala, I. Wichterle, J. Polák, and T. Boublik, "Vapor-Liquid Equilibrium Data at Normal Pressures," Pergamon Press, Elmsford, N. Y., and Oxford, 1968.

(16) M. L. McGlashan, J. E. Prue, and J. E. J. Sainsbury, *Trans. Faraday Soc.*, **50**, 1284 (1954).

Transfer Diffusion. I. Theoretical

by I. Ruff* and V. J. Friedrich

Institute of Inorganic and Analytical Chemistry, L. Eötvös University, Budapest, Hungary *(Received January 18, 1971)*

Publication costs borne completely by The Journal of Physical Chemistry

In a system in which AX diffuses in the presence of A, transfer diffusion has been defined as the apparent diffusion due to the jump of X from an A it was bound to, to another, free A. This process results in the displacement of AX without translating A's. Theoretical equations have been given for such types of transport phenomena, particularly for isothermal diffusion, electric conduction, and thermal diffusion. The correlations obtained are suitable to calculate the second-order rate constant of the exchange reaction $AX + A^* \rightleftharpoons A + A^*X$. The conditions of the application of this effect for kinetic measurements of very fast processes are discussed in various cases. It is shown that the diffusion limit is also affected by transfer diffusion and results in a concentration dependence of the diffusion limit.

1. Introduction

In previous communications[1] a new method has been suggested for the investigation of very fast exchange reactions which is based on the measurement of the diffusion coefficient apparently increased by the exchange reaction in a system where both reactants are present and—at least—one of those diffuses according to a concentration gradient. Some aspects about this phenomenon in electron or proton transfer reactions have been discussed theoretically by Levich,[2] Dahms,[3] and Wyatt,[4] but they considered only special cases with respect to either the type of transport or the type of reaction.

The methods, applied so far for the determination of the rate of exchange reactions, were isotopic exchange and nmr line broadening techniques. The upper limit of the first one is related to the time consumed for mixing the reactants and for separating them, while that of the latter one corresponds to the ratio of the time of interaction of the electromagnetic quantum with the species and the lifetime of that species in the initial or product state. These technical and principal restrictions caused the upper limit to be about 10^7 and—in successful cases—10^9 M^{-1} sec^{-1} for the second-order rate constant, respectively.

It will be shown below that the transfer diffusion method, as we intend to call it further, gives the possibility to determine the rate of the exchange reactions within about one order of magnitude below the diffusion limit. Thus, it has a significant importance in investigating the processes which proved to be too fast for the methods known so far.

The purpose of the studies to be published in the series, started with the present paper, is to show the applicability of the effect of transfer diffusion for kinetic investigations of exchange reactions near the diffusion limit and to gain some information about the mechanism of these very fast processes. The theoretical discussion given here serves partly as a basis for the experimental parts; nevertheless, in many points of view, it gives the first detailed description of the phenomenon itself.

2. General Theory

Let us consider an exchange reaction in which A and A* are chemically identical particles and X is an atom, radical, ion, electron, or an energy quantum that can transfer between them

$$AX + A^* \rightleftharpoons A + A^*X \qquad (1)$$

where the asterisks serve only for distinguishing between the two sides of eq 1; they do not mean, however, any physical or chemical differences except that A is *another* particle in the space than A*.

Let a system consist of several AX's and A's which can equally be a mixture of the gases or their solution in either liquid or solid state. If the gradient in their chemical potential is not zero all over the space considered, they would move according to this gradient. In course of their translation two processes are in operation: (i) the conventional migration of the species, and (ii) the exchange reaction which causes an apparent displacement of, say, A by every effective collision with AX that results in the transfer of X, since, after such a collision, A can continue its movement from the point at which the species AX has situated.

It is again due to the gradient in the chemical potential that the jump of X is favored in the direction of the gradient; thus, in addition to the conventional transport, the exchange reaction *increases* the flux of AX.

As some simple examples, the effect of the exchange

(1) (a) I. Ruff, *Electrochim. Acta*, **15**, 1059 (1970); (b) I. Ruff and I. Körösi-Ódor, *Inorg. Chem.*, **9**, 186 (1970).

(2) V. G. Levich, *Advan. Electrochem. Electrochem. Eng.*, **4**, 314 (1966).

(3) H. Dahms, *J. Phys. Chem.*, **72**, 362 (1968).

(4) P. A. H. Wyatt, 1st Interam. Conference on Radiochemistry, Montevido, 1963.

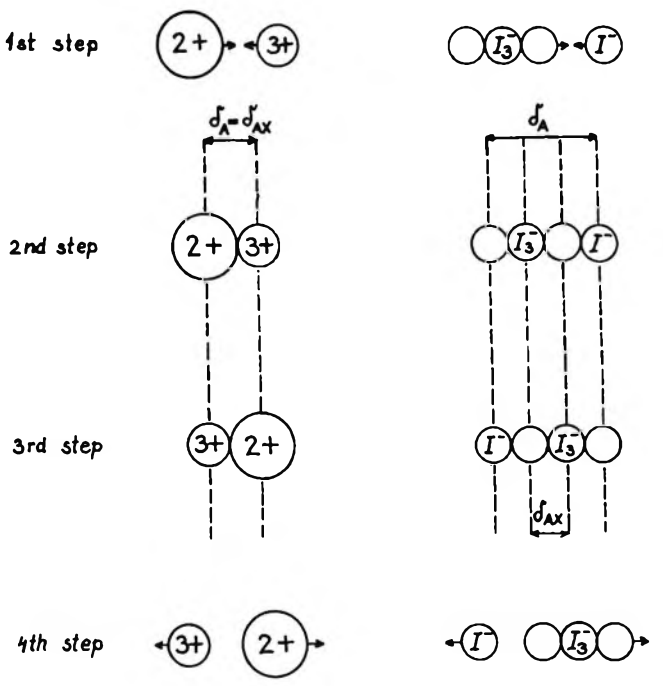

Figure 1.

reactions of iron(II) with iron(III) and iodide with triiodide is shown schematically in Figure 1. In the iron(II)–iron(III) exchange A corresponds to iron(III) and X stands for the electron, while in the other reaction A is the iodide ion and X is I_2. In Figure 1, four steps of the collision process are shown: (1) the approach of the reactants, (2) the moment of collision before X is transferred, (3) that after the transfer, and (4) the separating products. It can be seen that the distances δ_A and δ_{AX} which should not be moved along by A and AX, respectively, are always the distance between the mass centers of the initial and final A or AX. They can be incidentally equal to each other, if X is a pointlike particle as it is in electron exchange reactions; however, in general, their length is different. In general, the directions of the jumps do not lie in the same line, but they are always parallel, since the mass center of the activated complex, as a whole, does not change.

To formulate the effect of the exchange reaction increasing the transport, the quantities involved should be defined. For the chemical potentials we have

$$\mu_A = H_A - TS_A + RT \ln c_A + z_A FE + \text{m.t.} \quad (2)$$

and

$$\mu_{AX} = H_{AX} - TS_{AX} + RT \ln c_{AX} + z_{AX} FE + \text{m.t.} \quad (3)$$

where H = enthalpy of formation, S = entropy of formation, T = temperature in °K, R = universal gas constant, c = concentration (supposing ideal behavior), z = electric charge in atomic units, F = Faraday constant, E = electric potential, and the abbreviation m.t. stands for "more terms" which influence the chemical potential in particular cases not considered here, *e.g.*, pressure, magnetic field, *etc.* Some of the quantities listed above as T, c, E, can depend on the position coordinates x, y, and z, but this will not be marked separately.

It seems to be useful for the sake of simplicity to exclude the conditions, when the directions of the two gradients are not parallel at any point of the system. This restriction involves that along any surface where μ_A is constant, μ_{AX} is also constant. The parallelism of the gradients does not mean any additional restriction except with respect to the concentration gradients, since any gradient in the intensive parameters (T, E, etc.) gives evidently parallel gradients in the chemical potential of both reactants.

Let us define the flux of X, disregarding whether it is carried along by the migration of an AX or it jumps from an AX to an A, over a surface where the chemical potentials are constant. Thus

$$\frac{dn_X}{dt} = -\rho_{AX} \text{ grad } \mu_{AX} + v_f - v_b \quad (4)$$

where n_X is the moles crossing a unit area of this surface, ρ_{AX} is the general transport coefficient, and the v's are the rates of the exchange reaction between the layers of the two sides of the surface in forward (positive flux) and backward (negative flux) directions.

Consider an elementary area of the surface mentioned above with an AXA activated complex whose axis δ_{AX} crosses the surface with an angle φ. Introducing the local coordinate λ which is perpendicular to the plane of the elementary surface area and its direction points to that of the positive flux of AX, for the chemical potentials at the points of the mass centers of the *initial* AX and A one has

$$\mu_A = \mu_{A,s} + \int_0^{\delta_A' \sin \varphi} \text{grad } \mu_A d\lambda \quad (5)$$

and

$$\mu_{AX} = \mu_{AX,s} - \int_0^{(\delta_{AX} - \delta_{AX}') \sin \varphi} \text{grad } \mu_{AX} d\lambda \quad (6)$$

where $\mu_{A,s}$ and $\mu_{AX,s}$ are the chemical potentials at the surface (constant all over it) and for the meaning of the distances δ_A' and δ_{AX}' we refer to Figure 2.

On the other hand, the chemical potentials at the points of the mass centers of the *final* states, marked by parentheses in Figure 2, are

$$\mu_{(A)} = \mu_{A,s} - \int_0^{(\delta_A - \delta_A') \sin \varphi} \text{grad } \mu_A d\lambda \quad (7)$$

and

$$\mu_{(AX)} = \mu_{AX,s} + \int_0^{\delta_{AX}' \sin \varphi} \text{grad } \mu_{AX} d\lambda \quad (8)$$

The rate of a chemical reaction, in general, can be

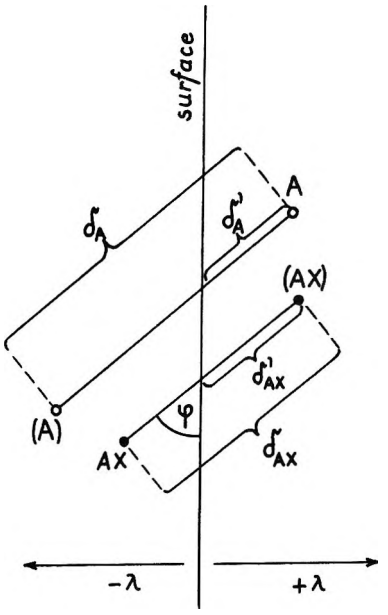

Figure 2.

given as the product of the concentration of the activated complex and the frequency factor Z of its decomposition to the products.

Using the well-known correlation of the thermodynamics

$$G^{\pm} - G_1 - G_2 = -RT \ln \frac{c^{\pm}}{c_1 c_2} \tag{9}$$

one obtains

$$v = Zc^{\pm} = Z \exp\left(-\frac{G^{\pm} - \mu_1 - \mu_2}{RT}\right) \tag{10}$$

where $G^{\pm}$ is the free energy of the activated complex and G_1 and G_2 are those of the reactants.

In this way, the chemical potential of the activated complex for the case under discussion should consist of three parts: (i) the sum of the chemical potential of the reactants in a system in which there is no gradient and their value is equal to that of $\mu_{A,s}$ and $\mu_{AX,s}$; (ii) the increase in the chemical potential $\Delta\mu_s{}^{\pm}$ due to the interactions between the reactants that is characteristic to the particular reaction, but independent of the gradients; and (iii) the effect of the gradients on the activated complex.

The determination of this latter quantity needs some approximation. If the gradients were zero, the structure of the activated complex would correspond to that X would be at the half of its pathway between the initial and final states; *i.e.*, one-half of the particles AX which gained the necessary free energy of activation are still in their initial position and one-half of them already transferred. The same is valid for A. If, however, the gradients have finite values, the potential barrier to be overcome by X is more or less distorted, its maximum is not in the middle of the pathway of X, and so the activated complex is asymmetric. The less the gradients, the less this asymmetry. Thus, if the gradients are small enough in comparison to the interaction listed under ii, the change in the chemical potential of the activated complex due to the gradients can be approximated by the arithmetic mean of those of the initial and final states

$$\mu_{AXA} = \mu_{A,s} + \mu_{AX,s} + \Delta\mu_s{}^{\pm} + \frac{1}{2}\left[\int_0^{\delta_{A'}\sin\varphi} \text{grad}\,\mu_A d\lambda + \int_0^{\delta_{AX'}\sin\varphi} \text{grad}\,\mu_{AX} d\lambda - \int_0^{(\delta_A-\delta_{A'})\sin\varphi} \text{grad}\,\mu_A d\lambda - \int_0^{(\delta_{AX}-\delta_{AX'})\sin\varphi} \text{grad}\,\mu_{AX} d\lambda\right] \tag{11}$$

According to eq 10, we have

$$v_f = Z \exp\left(-\frac{G_{AXA} - \mu_A - \mu_{AX}}{RT}\right) \tag{12}$$

and

$$v_b = Z \exp\left(-\frac{G_{AXA} - \mu_{(A)} - \mu_{(AX)}}{RT}\right) \tag{13}$$

Substituting eq 5–8 and 11 and 12 into eq 13 and 14, one obtains from eq 4

$$\frac{dn_X}{dt} = -\rho_{AX} \text{grad}\,\mu_{AX} - 2v\int_0^{\pi/2}\int_0^{\delta_{AX}\sin\varphi} \sinh\left[\frac{1}{2RT} \times \left(\int_0^{\delta_{AX'}\sin\varphi} \text{grad}\,\mu_{AX} d\lambda + \int_0^{(\delta_{AX}-\delta_{AX'})\sin\varphi} \text{grad}\,\mu_{AX} d\lambda - \int_0^{\delta_{A'}\sin\varphi} \text{grad}\,\mu_A d\lambda - \int_0^{(\delta_A-\delta_{A'})\sin\varphi} \text{grad}\,\mu_A d\lambda\right)\right] d\lambda d\varphi \tag{14}$$

where v is the same as in eq 10, but with μ_1 and μ_2 equal to $\mu_{A,s}$ and $\mu_{AX,s}$, respectively. Integration over φ takes into account that any case from δ_{AX} parallel to the surface to δ_{AX} perpendicular to that can equally influence the flux, while the second integration over λ from zero to $\delta_{AX}\sin\varphi$ accounts for the fact that all positions of the activated complex affect the flux, if δ_{AX} crosses the surface or—at least—reaches it by one of the ends. (It is mentioned, however, that integration over λ—between 0 and $\delta_A \sin\varphi$—must not be done, since displacement of the mass center of A along δ_A does not directly influence the flux of X.)

The integrations of eq 14 can be performed, if the function of the gradients with respect to the position coordinates—and so to λ—is known. For the most of the practical cases the approximation grad μ_A = constant and grad μ_{AX} = constant, within the ranges the integration is done, seems to be satisfactory. Hence

$$\frac{dn_X}{dt} = -\left\{\rho_{AX} + \frac{v\delta_{AX}^2\pi}{4RT} \times \left[1 - \frac{\delta_A}{\delta_{AX}} \frac{\text{grad } \mu_A}{\text{grad } \mu_{AX}}\right]\right\} \text{grad } \mu_{AX} \quad (15)$$

It is seen that the term involving v in this equation *depends on the particular structure of the activated complex and on the gradients in the chemical potential of the reactants, i.e., on the experimental conditions.* The latter can certainly be varied so as to get effect in addition to ρ_{AX} on the basic transport process, and in this way

$$v = kc_{A,s}c_{AX,s} \quad (16)$$

can be determined, if the δ's can be calculated from other sources. The main restriction that still remains in the experimental application is that the term including v (*i.e.*, "transfer diffusion term") *should exceed* the error in ρ_{AX}. These errors result in a lower limit in k. Nevertheless, an experimental method can be suggested on the basis of the correlation in eq 15 by measuring the increase in the transport due to exchange reactions fast enough.

Equation 15 becomes less complicated in particular cases, when the concrete form of the gradients in the chemical potentials are substituted and, *e.g.*, the δ's are equal. These examples will be discussed below.

3. Special Cases

A. Isothermal Diffusion. For isothermal diffusion, one has

$$\text{grad } \mu = \frac{RT}{c} \text{ grad } c \quad (17)$$

and hence the flux in eq 15 can be rewritten as

$$\frac{dn_X}{dt} = -\left\{D_{AX} + \frac{k\delta_{AX}^2\pi}{4}\left[c_{A,s} - c_{AX,s}\frac{\delta_A}{\delta_{AX}}\frac{\text{grad } c_A}{\text{grad } c_{AX}}\right]\right\} \text{grad } c_{AX} \quad (18)$$

if the diffusion coefficient

$$D = \frac{RT}{c}\rho \quad (19)$$

is introduced.

Let us simplify eq 18 according to the following conditions.

Case 1. If the diffusion is linear, say, in the direction x

$$\text{grad } c = \frac{dc}{dx} \quad (20)$$

Let the concentration c_A be constant all over the space. Thus

$$\frac{dn_X}{dt} = -\left(D_{AX} + \frac{k\delta_{AX}^2\pi}{4}c_A\right)\frac{dc_{AX}}{dx} \quad (21)$$

In this case the transfer diffusion term becomes independent of x, and so a normal diffusion is observed in the presence of A too. Thus D_{AX} should be determined in the absence of A, while in its presence the enhanced diffusion constant D_{AX}' can be obtained, since

$$D_{AX}' = D_{AX} + \frac{k\delta_{AX}^2\pi}{4}c_A \quad (22)$$

The difference $D_{AX}' - D_{AX}$ serves for the calculation of k, if δ_{AX} is known, *e.g.*, from crystallographic data on A and AX, or—reversed—δ_{AX} can be calculated, if k is known from an independent source. An experimentally determined value of δ_{AX} is of importance to the mechanism of the exchange reaction.

To observe any difference between D_{AX} and D_{AX}', the second term in eq 22 must exceed twice the errors in those, ΔD_{AX}, hence

$$k \geqslant \frac{8\Delta D_{AX}}{c_A\pi\delta_{AX}^2} \quad (23)$$

Because the order of magnitude of ΔD_{AX} is about 10^{-8} cm^2 sec^{-1} and that of δ_{AX}^2 is 10^{-15} cm^2, k must be about $5 \times 10^7/c_A\ M^{-1}$ sec^{-1} or larger. The lower limit of the observation of the effect of transfer diffusion is quite high, but often just this region of fast exchange reactions cannot be studied by other methods.

Case 2. Consider again a linear diffusion, but let the reaction be electron exchange ($\delta_{AX} = \delta_A$) with the initial conditions

$$\begin{aligned} c_{AX} &= c^\circ \text{ and } c_A = 0, \text{ if } x < 0 \\ c_{AX} &= 0 \text{ and } c_A = c^\circ, \text{ if } x > 0 \\ c_{AX} &= c_A = c^\circ/2, \text{ if } x = 0 \end{aligned} \quad (24)$$

This is a case of "counterdiffusion," when AX diffuses into a space there was only A at the beginning and *vice versa*. Thus, for the flux across a plane at a certain x one has

$$\frac{dn_X}{dt} = -\left[D_{AX} + \frac{k\delta_{AX}^2\pi}{4} \times \left(c_{A,x} - c_{AX,x}\frac{\frac{dc_A}{dx}}{\frac{dc_{AX}}{dx}}\right)\right]\frac{dc_{AX}}{dx} \quad (25)$$

This is the particular equation Dahms obtained[3] for "electronic conduction in solution" due to concentration gradients.

Because the term in the brackets of eq 25 depends on x, the diffusion experiment performed in the presence of A should be evaluated from point to point along x

by a suitable iteration procedure. In this case, both D_{AX} and D_A must be determined in the absence of A and AX, respectively. If, however, D_A is incidentally equal to D_{AX} or sufficiently near to it, a relation similar to that in eq 22 can be obtained except that the sum $c_A + c_{AX}$ appears instead of c_A. (It is to be noticed that here the gradients are of opposite directions.)

If the latter simplification is valid, an indirect method seems to be applicable also: any parameter that depends on the diffusion coefficient can be investigated as a function of the sum of the concentrations, and there should be a deviation from the usual dependence of that parameter on concentration due to the transfer diffusion term, if it is high enough. Namely, voltametric limiting or peak currents vary usually as linear functions of the concentration of the electroactive species; transfer diffusion, however, would result in a deviation upwards from this linearity according to the diffusion coefficient which depends itself on the concentration. The "counterdiffusion" would be developed in the vicinity of the electrode by the electrochemical reaction itself.

B. Electric Conductivity. Assuming that no concentration gradient is caused by an alternating current of sufficient frequency and the system is otherwise homogeneous, the gradient in the chemical potential becomes

$$\text{grad } \mu = zF \text{ grad } E \tag{26}$$

Since the flux times z gives the current density, and the total current density is the sum of that for A and AX, we have

$$i = -\frac{F^2}{RT}\left[D_A c_A z_A^2 + D_{AX} c_{AX} z_{AX}^2 + \frac{k\delta_{AX}^2\pi}{4} c_A c_{AX} z_{AX}^2\left(1 - \frac{z_A}{z_{AX}}\frac{\delta_A}{\delta_{AX}}\right) + \frac{k\delta_A^2\pi}{4} c_A c_{AX} z_A^2\left(1 - \frac{\delta_{AX} z_{AX}}{\delta_A z_A}\right)\right] \text{grad } E \tag{27}$$

It is seen that the increase of the conductivity, when both reactants are present, in comparison to the sum of their own conductivity measured in the absence of the other reactant, is caused by transfer diffusion. Taking into account that the terms in the brackets are in the order of magnitude of one, the reaction must be again as fast as given in eq 23 to exhibit any unusual behavior. This is why no effect could be observed by Wyatt[4] in the conductivity of the systems $Fe^{2+} + Fe^{3+}$, hexacyanoferrate(II) and -(III), and $MnO_4^{2-} + MnO_4^-$, since the second-order rate constants for these exchanges are about 1, 10^3, and 10^2 M^{-1} sec^{-1}, respectively.

Equation 27 does not include the conductivity due to the other ions certainly present as counterions B^{z_B-} of the electrolytes $A_{z_B}^{z_A+}B_{z_A}^{z_B-}$ and $AX_{z_B}^{z_{AX}+}{}_{z}B_{AX}^{z_B-}$. If these counterions diffuse much slower than those giving the transfer diffusion, eq 27 still remains valid. If not, the weight average of the conductivity of the cations and anions with respect to the transference numbers should be introduced in the well-known way as it has to be done for electrolytes. An unsuccessful choice of the counterions (when they diffuse much faster than those responsible for the transfer diffusion) can depress the whole effect expected. To avoid this complication, counterions of small mobility should be chosen, if possible.

C. Thermal Diffusion. The result of the temperature gradient is, in general, a gradient in concentration; thus grad μ should be transformed with respect to these two parameters

$$\text{grad } \mu = (R \ln c - S) \text{ grad } T + (RT/c) \text{ grad c} \tag{28}$$

By introducing eq 28 into eq 16, both the flux of AX and A can be obtained. Combining these two equations in order to eliminate the concentration gradient of A, one gets a relation between concentration gradient and temperature gradient for the stationary case, when the fluxes of both species are zero

$$\frac{\text{d ln } c_{AX}}{\text{d ln } T} = \frac{D_A'(R \ln c_{AX} - S_{AX})}{RD_A'D_{AX}' - \kappa^2 c_A c_{AX} Q_A Q_{AX}} \times \left(D_{AX}'' + D_A'' c_A \frac{D_{AX}'' - D_{AX}'}{D_A'}\right) \tag{29}$$

where

$$Q_A = \frac{\delta_A}{\delta_{AX}} \tag{30}$$

$$D_A'' = D_A + \kappa c_{AX}(1 - Q_A Y_{AX}) \tag{31}$$

$$\kappa = \frac{k\delta_{AX}^2}{4} \tag{32}$$

$$Y_A = \frac{R \ln c_A - S_A}{R \ln c_{AX} - S_{AX}} \tag{33}$$

and Q_{AX}, D_{AX}'', and Y_{AX} are similar quantities with the labels exchanged.

The right-hand side of eq 29 is the Soret coefficient in its extended form due to the transfer diffusion. If no transfer diffusion exists, it is

$$\frac{\text{d ln } c_{AX}}{\text{d ln } T} = \ln c_{AX} - \frac{S_{AX}}{R} \tag{34}$$

Thermodiffusion also seems suitable to determine the effect under discussion, although the complicated feature of eq 29 with respect to the parameters depending on the individual behavior of the system does not allow any general conclusion in addition to that the effect appears in this case too.

4. Effect on the Diffusion Limit

Smoluchowski[5] treated the problem of the diffusion limit of chemical reactions by the "sink model" cal-

(5) M. V. Smoluchowski, *Z. Phys. Chem.* (*Leipzig*), **92**, 129 (1917).

culating the flux of the reaction partners B over the surface of the sphere of radius δ around one of the other reactants A. δ is the sum of the radii of A and B. Summation over all A gives the number of collisions in unit time. If every collision is effective in resulting in the products, *i.e.*, the free energy of activation is very small in relation to RT, the rate constant of the reaction proceeding as fast as possible is

$$k_1 = 4\pi N_A \delta (D_A + D_B) \times 10^{-3} \quad (35)$$

in M^{-1} sec^{-1} units. Here N_A is the Avogadro number.

Though several modifications in the treatment have been made (see ref 6 and the references therein), Smoluchowski's result proved to be correct. Transforming eq 35 for the reaction in eq 1, if no transfer diffusion operates, one gets a similar relationship to that in eq 35 with B replaced by AX. This equation holds only when the effectivity of the collision is equal at every point of the spherical A and AX. If not, the sensitivity of the collision to its direction would appear as a configurational entropy of activation and so the free energy of activation would not be negligibly small. Including this latter case, Noyes[7] deduced the relation

$$k = k_1/(1 + k_1/k_2) \quad (36)$$

where k is the rate constant that can be observed as a resultant one, if both diffusion and activation control the reaction, and k_2 is the rate constant for the purely activation controlled reaction.

When transfer diffusion influences the diffusion, it should enhance the value of the diffusion limit as well. To obtain the correlation for such a case, let us follow Smoluchowski's deduction. Consider a spherical surface with a radius δ around the center of an A and define the flux in eq 18 for that surface. Every AX crossing this surface "sinks" into the sphere, *i.e.*, $c_{AX,s} = 0$. On the other hand, nothing happens to an A, if it comes close to the one in the center of the sphere; thus grad $c_A = 0$. Hence the flux is given by eq 21, while for the reversed case—the flux of A across a similar sphere around an AX—is described by an equation identical with eq 21, but with the subscripts exchanged. For the diffusion limit one obtains in this way

$$k_1' = k_1 + a(c_A\delta_{AX}^2 + c_{AX}\delta_A^2)k \quad (37)$$

where

$$a = \pi^2 N_A \delta \times 10^{-3} \quad (38)$$

Substituting k_1' instead of k_1 into eq 36 it is altered to

$$(c_A\delta_{AX}^2 + c_{AX}\delta_A^2)ak^2 + [k_1 + k_2 - a(c_A\delta_{AX}^2 + c_{AX}\delta_A^2)k_2]k - k_1k_2 = 0 \quad (39)$$

which can be easily solved with respect to k.

The important feature of k is that it slightly *depends on the concentrations, if it is close to the diffusion limit* and this is just the case, when transfer diffusion can be observed at all. This subsidiary dependence of the transfer diffusion terms written in the previous sections should be always accounted for.

It leads, however, *to a more general consequence in reaction kinetics*, too. Let us formulate a chemical reaction of finite net free energy change as

$$AX + B \xrightarrow[k_{AXB}]{} BX + A \quad (40)$$

If at least one of the exchanges AX + A or BX + B is fast enough to approach the diffusion limit of the exchange, the rate of the reaction in eq 40 would be increased also due to the transfer diffusion term appearing in it like in eq 37. This would affect k_{AXB} even if the cross reaction is slow, since the resultant rate constant is the product of the diffusion limit and $\exp(-(\Delta F^*/RT))$ (see eq 36, if $k_2 \ll k_1$). Thus, when the fast exchange is, *e.g.*, that between A and AX, one has

$$k_{AXB} = (k_{1,AXB} + ac_{AX}\delta_{AX}^2 k) \exp\left(-\frac{\Delta F^*}{RT}\right) \quad (41)$$

if the free energy of activation dominates. Owing to the dependence of k_{AXB} on c_{AX}, the order of reaction for AX would not be 1, but, apparently, somewhat higher.

Some other cases—both exchanges are close to their diffusion limit, the cross reaction still slow, etc.—can be discussed similarly. The very important conclusion is that *transfer diffusion should be accounted for in almost every case, when diffusion limit is approached in sufficiently high concentration of the reactants in either the exchange reaction of one of the reactants or the cross reaction itself.*

(6) E. Pitts, *Trans. Faraday Soc.*, 65, 2372 (1969).
(7) R. M. Noyes, *J. Chem. Phys.*, 22, 1349 (1954).

Transfer Diffusion. II. Kinetics of Electron Exchange Reaction between Ferrocene and Ferricinium Ion in Alcohols

by I. Ruff,* V. J. Friedrich, K. Demeter, and K. Csillag

Institute of Inorganic and Analytical Chemistry, L. Eötvös University, Budapest, Hungary *(Received January 18, 1971)*

Publication costs borne completely by The Journal of Physical Chemistry

The rate of the electron exchange reaction between ferrocene and ferricinium ion has been determined by direct measurement of the diffusion coefficient of the ferricinium ions, increased due to transfer diffusion, in methanol, ethanol, and 1-propanol as solvents. The rate proved to be close to the diffusion limit near room temperature. The data are in good agreement with the isotopic exchange measurements at around −70° in methanol.

1. Introduction

In the previous part of this series, transfer diffusion has been theoretically discussed in detail.[1] The physical background of this phenomenon is that the movement of a species due to its concentration gradient does not take place only by its migration, but in addition to this an apparent translation occurs owing to an exchange reaction, if the other reactant of this exchange is present. In the case under discussion, this means, *e.g.*, for ferricinium ion, that it gains the path of the iron-to-iron distance which should not be really moved along, when it collides with a ferrocene molecule and they exchange the electron. After the exchange, the newly formed ferricinium ion continues its translation from the point at which the ferrocene is situated. The apparent diffusion coefficient D_{AX}' involves in this way the true diffusion coefficient D_{AX} and a term corresponding to the electronic jump

$$D_{AX}' = D_{AX} + k\delta^2\frac{\pi}{4}\left(c_A - c_{AX}\frac{\frac{dc_A}{dx}}{\frac{dc_{AX}}{dx}}\right) \quad (1)$$

where k is the second-order rate constant of the exchange reaction, δ is the distance between the center of the reactants in the activated complex, c_A and c_{AX} are the concentration of the reactants at a distance x (supposing linear diffusion). The equation is formulated in a general way for any exchange reaction

$$AX + A \rightleftharpoons A + AX \quad (2)$$

where X is the pointlike particle exchanged. In the present case A should stand for ferrocene, AX for ferricinium, and X for the electron deficiency (hole) on the ferricinium ion, since the process has been followed by the diffusion measurement of the ferricinium ion.

The determination of k can thus rely on the difference between D_{AX}' and D_{AX}, if the second term in eq 1 exceeds the errors in measuring these two quantities in the presence and absence of ferrocene, respectively, for the saturation of alcohols with ferrocene does not allow higher concentration than 0.05 M, and the true diffusion coefficient of ferricinium proved to be about 10^{-5} cm^2 sec^{-1} with a standard deviation of about 3% in the best case; the lower limit of observing any difference between the two diffusion coefficients gives

$$k \geqq 1.5 \times 10^9\ M^{-1}\ \text{sec}^{-1} \quad (3)$$

in methanol. In ethanol and propanol it is somewhat lower due to the lower true diffusion coefficients: about 6×10^8 and 4×10^8, respectively. There was still some hope to get useful results, since in methanol the extrapolation of Stranks' isotopic exchange measurements[2] at −75, −70, and −65° to room temperature supported values high enough to fulfill eq 3.

Concerning the general aspects of the knowledge of chemical exchange processes as fast as these figures, it is almost evident how useful a kinetic method can be giving comparable data for reactions which have been known as immeasurably fast ones so far. Thus the purpose of the present paper is to show the applicability of the transfer diffusion in the case of this particular reaction.

2. Experimental Section

Materials. Ferrocene was purchased from the Koch-Licht Laboratories. It was purified by resublimation at 101°. All the other chemicals were of analytical grade.

Stock Solutions. $HClO_4$ (1 M) solutions have been obtained by diluting concentrated perchloric acid by the solvents used; 100 ml of the ferricinium solutions usually contained 5 ml from this stock solution, so the water content was sufficiently low.

(1) I. Ruff and V. J. Friedrich, *J. Phys. Chem.*, **75**, 3297 (1971).
(2) D. R. Stranks, *Discuss. Faraday Soc.*, **29**, 73 (1960).

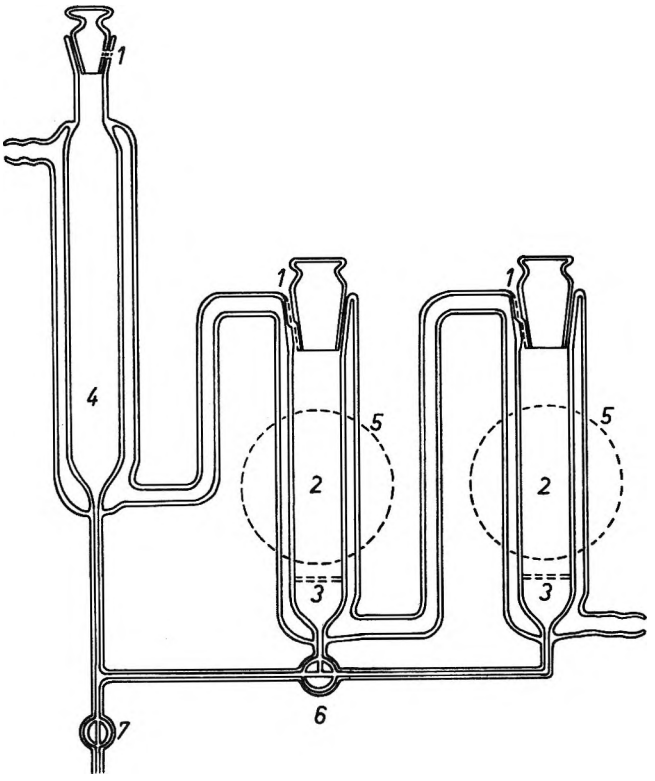

Figure 1. Apparatus for photographic measurement of diffusion coefficients.

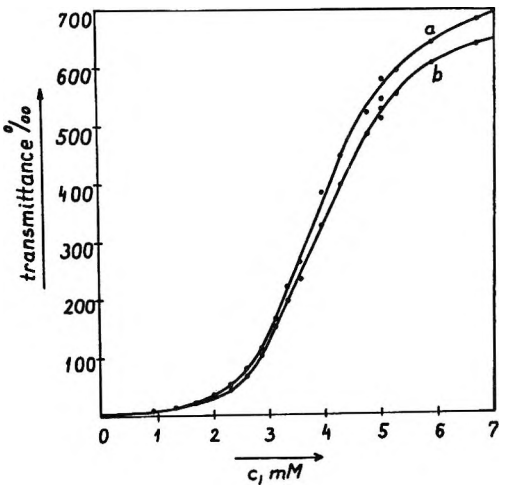

Figure 2. Calibration curve for ferricinium.

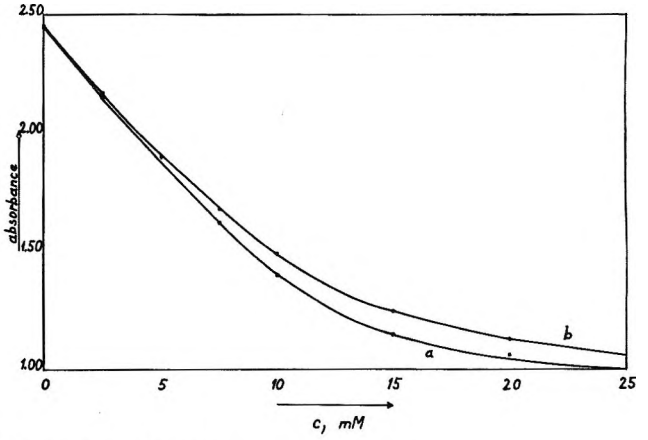

Figure 3. Calibration curve for ferrocene.

The ferrocene solution was 0.05 M in methanol and 1-propanol and 0.04 M in ethanol.

Ferricinium perchlorate solution was always freshly prepared by oxidation of 5 ml of ferrocene solution and 2.5 ml of 1 M perchloric acid by PbO_2. After filtration this was diluted to 50 ml.

Apparatus. Diffusion coefficient has been measured in a glass apparatus shown in Figure 1. Photographic evaluation has been used. Filter 3 (Schott GmbH. Type G4) permitted the sufficiently slow flow of the solution from tube 4 to tube 2 (flow rate 5–10 ml/hr). All three of the tubes could be thermostated. After filling tube 4 with the solution of higher density which was usually the ferricinium solution when measuring D_{AX} or D_{AX}', while it was the ferrocene solution for the determination of D_A, the solution was pressed through filter 3 by a rubber ball applied to the end of tube 4 that eliminated the bubbles under the filters. The solution above the filters was then removed and replaced by the one into which the diffusion of the lower solution was wanted to proceed. After a period of thermostating, diffusion was started by opening stopcock 6. The communication of the air was enabled by the hole and slotted grindings 1 which could be closed by turning the stoppers. When the interface of the two solutions reached the middle of the illuminated tube, the stopcock was closed. The mercury lamp of a Pulfrich-type photometer served behind the tubes 2 to give the two illuminated circles 5, while the camera (Zeiss, Type Exacta Varex) was fixed in front of them. ORWO NP 15 film was used. If the blue solution of ferricinium was to be photographed, a red filter, eliminating the yellow color of ferrocene (also present in the case of the measurements of D'), was applied. When ferrocene diffusion was measured, a violet filter gave better contrasts.

The advantage of this method is that the diffusion can be followed by snaps taken at different time intervals, and it gives the possibility to start the diffusion from a very sharp interface; usually no convection could be seen, which was proved by the fact that the diffusion coefficient was really independent of the time of diffusion.

Evaluation. The calibration curve (transmittance of the film *vs.* concentration) had to be measured for both tubes, since there was some difference in the intensity of the light. For ferricinium and ferrocene solutions they are shown in Figures 2 and 3, respectively. Transmittance was determined by a Zeiss microphotometer by which it could be measured in each 0.1 mm of the film, which corresponded to 3.3 mm in the diffusion column.

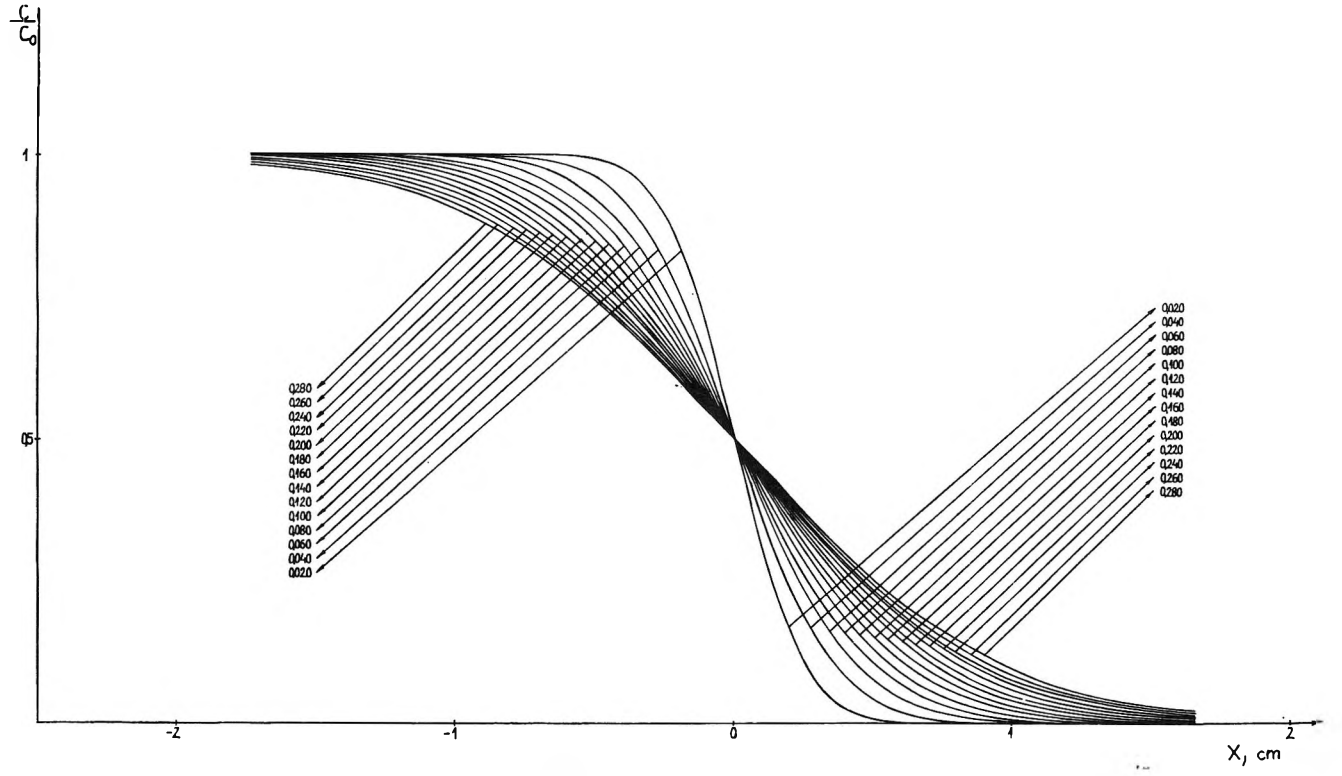

Figure 4. Calculated concentration distribution along the diffusion tube.

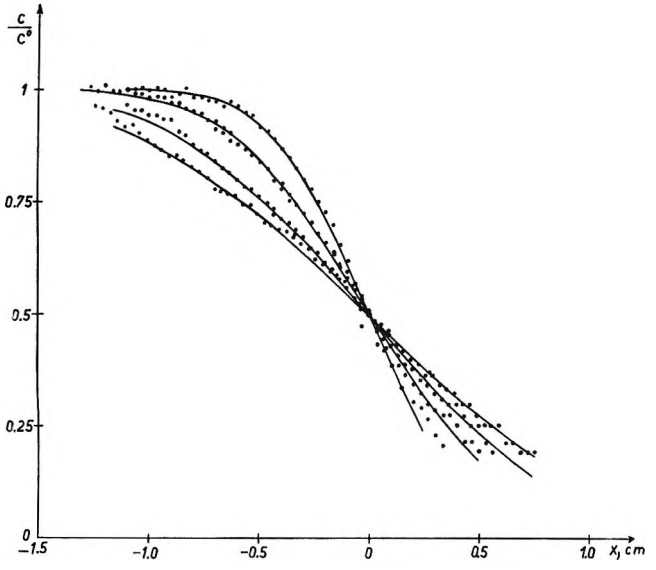

Figure 5. Distribution of ferricinium in methanol at 25° in different times of diffusion (1:03, 2:00, 4:02, and 6:00 hr in the order of decreasing slopes).

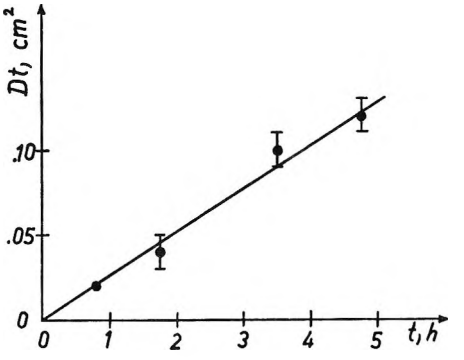

Figure 6. Dependence of Dt on the time.

The slit width was 0.04 mm, so the transmittance could be measured within practically pointlike distances.

Using the calibration curves, the concentration could be determined as a function of the height of the column. The plot c/c_0, where c_0 is the initial concentration of the species, *vs.* the linear coordinate x was fitted to a family of calculated curves (Figure 4), each curve corresponding to a certain value of Dt. These Dt values were then plotted *vs.* the time t that should be theoretically a linear function of t and cross the origin. If this intercept was really obtained, it proved the interface to have been sharp enough at $t = 0$. In some runs the intercept on the time axis was at negative values that meant a convection resulting in a diffusionlike concentration distribution when starting the diffusion. If the linearity still remained, diffusion coefficients were calculated by taking into account this additional apparent time as if diffusion had started earlier. In Figures 5–10 some typical plots are shown to demonstrate these cases (Figures 6, 8, and 10 belong to Figures 5, 7, and 9, respectively).

Calculation of D_{AX}' differed somewhat from that described above. Considering that it may depend on x owing to it involves the ratio of the concentration gradient (see eq 1), the graphical evaluation gave only a starting value to an iteration procedure as follows.

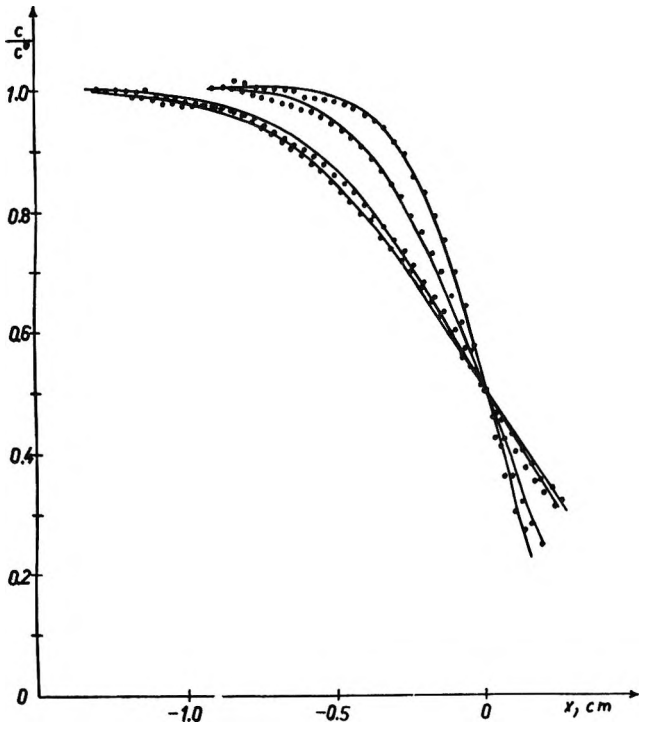

Figure 7. Distribution of ferricinium in ethanol at 35° in different times of diffusion (1:00, 3:30, and 5:00 hr in the order of decreasing slopes).

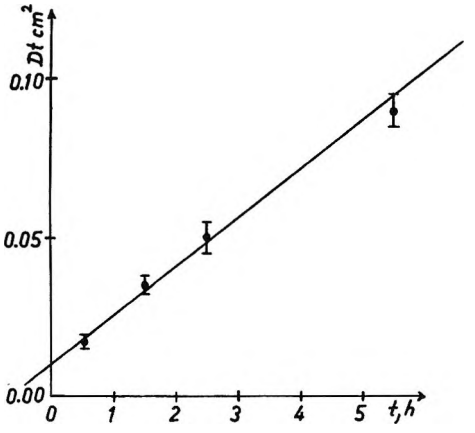

Figure 8. Dependence of Dt on the time.

If the condition $c_A + c_{AX} = c^\circ = c_A^\circ + c_{AX}^\circ$ is satisfied (where c_A° and c_{AX}° are the initial concentration of the reactants) which includes the assumption $D_A = D_{AX}$, the ratio of the gradients in equal to -1, *i.e.*

$$D_{AX}' = D_{AX} + k\delta^2 \frac{\pi}{4} c^\circ$$

This can be taken as a first approach for calculating $k\delta^2$. Using this value and its 75 and 125%, one can compute three theoretical curves for c/c° as a function of x. In doing this, the concentration gradients were calculated in the first iteration step as if no transfer

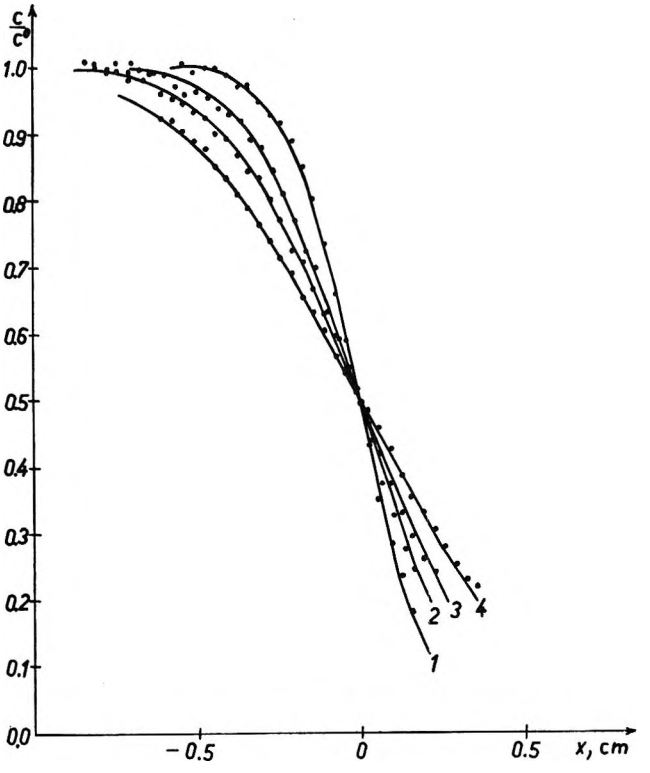

Figure 9. Distribution of ferricinum in 1-propanol at 35° in different times of diffusion (0:32, 1:30, 2:32, and 5:30 hr in order of decreasing slopes).

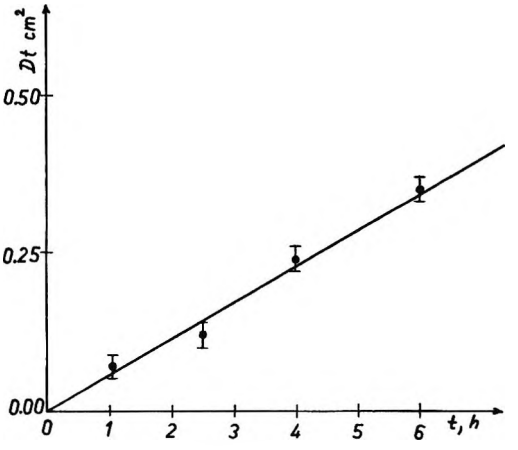

Figure 10. Dependence of Dt on the time.

diffusion occurred; in this way a better approach of D_{AX}' at a certain x could be obtained, then the gradients were corrected by the new value of D_{AX}' and the procedure was repeated until the same value of D_{AX}' was twice obtained within 0.1 relative per cent. These curves were fitted again to the experimental points of the c/c° *vs.* x plot and the real $k\delta^2$ was chosen by the best fit. The iteration was usually very short, within two steps the correct value was reached, and thus no appreciable influence of the ratio of concentration gradients could be obtained.

3. Results and Discussion

For ferricinium perchlorate the diffusion coefficients measured are summarized in Table I. It is seen that the errors range from 3 to 15% which can be considered as a satisfactory precision, since in the presence of ferrocene the increase in the diffusion coefficient is in general three times this error or more.

Table I: Diffusion Coefficients of Ferricinium Perchlorate in the Presence and Absence of Ferrocene at Different Temperatures

t, °C	[$HClO_4$], mM	Lower soln: [Fe(III)], mM	Lower soln: [Fe(II)], mM	Upper soln [Fe(II)], mM	$\bar{D} \times 10^6$, cm² sec⁻¹
			In Methanol		
12.5	50	5	0	0	9.17 ± 0.87
	50	5	45	50	12.0 ± 1.4
20.0	100	10	0	0	10.3 ± 0.5
	50	5	0	0	
	50	5	40	45	12.8 ± 0.2
25.0	100	10	0	0	
	50	10	0	0	12.6 ± 0.1
	50	5	0	0	
	100	10	35	45	16.8 ± 0.5
	50	10	40	47.5	16.4 ± 0.6
	50	5	42.5	47.5	
	10	4.4	45.6	50	16.0 ± 0.9
35.0	50	5	0	0	15.4 ± 1.7
	50	5	45	50	20.1 ± 1.0
			In Ethanol		
12.5	50	4	0	0	4.47 ± *0.30*[a]
	50	4	36	40	5.24 ± *0.40*
20.0	50	4	0	0	4.66 ± *0.08*
	50	4	36	40	6.98 ± 0.58
25.0	50	4	0	0	4.28 ± *0.50*
	50	4	36	40	7.33 ± 1.0
35.0	50	4	0	0	4.33 ± 0.56
	50	4	36	40	5.91 ± 0.22
			In 1-Propanol		
12.5	50	5	0	0	0.94 ± 0.20
	50	5	45	50	1.24 ± *0.15*
20.0	50	5	0	0	1.63 ± 0.02
	50	5	45	50	2.58 ± 0.21
25.0	50	5	0	0	2.08 ± 0.06
	50	5	45	50	3.64 ± 0.09
35.0	50	5	0	0	2.73 ± 0.02
	50	5	45	50	3.89 ± 0.09

[a] The errors printed in *italics* do not arise from the scattering of the diffusion coefficients corresponding to different diffusion times, but to the uncertainty of the intercept of the line Dt *vs.* t.

To exclude the possibility that the increase in the diffusion constant in the presence of ferrocene is due to some other effect of changing the solvent structure, it would be preferred to repeat the measurements by using a system identical with that of ferrocene and ferricinium but slow enough to give no transfer diffusion effect. Unfortunately such a system is not available, since the exchange processes of other metallocenes which would meet the requirements have not been studied. The only test one can do is to measure the viscosity of the ferrocene solutions. If viscosity remains the same when adding ferrocene, the increase in the diffusion constant is by all means due to transfer diffusion. In some viscosity measurements at 25°, exactly this was observed: 0.550, 0.655, and 1.95 cP was measured for pure methanol, ethanol, and 1-propanol, while the values for the solutions were 0.558, 0.652, and 1.89, respectively.

The temperature dependence of the true diffusion coefficient was calculated by least-squares method and resulted in +4.55 ± 0.06, −0.25 ± 0.5, and +8.22 ± 0.08 kcal/mol for the energy of activation in methanol, ethanol, and 1-propanol, respectively. In Table II, the diffusion coefficients of ferrocene are shown. The values of the energy of activation are 6.05 ± 0.07, 0.88 ± 0.04, and 2.81 ± 0.04 kcal/mol, respectively. The unusual behavior of the temperature dependence in ethanol is significant; its reason, however, is out of interest in the present work. (It should still be noticed that the solubility of ferrocene is somewhat less in ethanol which also shows an unusual behavior.)

Table II: Diffusion Coefficients of Ferrocene

t, °C	[Fe(II)], mM	$\bar{D}_A \times 10^6$, cm² sec⁻¹
	In Methanol	
15.0	50	15.3 ± 0.7
20.0	50	16.7 ± 2.4
25.0	50	23.5 ± *2.0*
35.0	50	29.5 ± 3.5
	In Ethanol	
15.0	40	11.0 ± 0.8
20.0	40	10.4 ± 0.7
35.0	40	12.2 ± 0.8
	In 1-Propanol	
15.0	50	6.48 ± 0.19
20.0	50	7.45 ± 0.38
25.0	50	8.61 ± 0.41
35.0	50	9.00 ± 0.41

From these data both the diffusion limit and the second-order rate constant of the reaction can be calculated. For the first quantity Smoluchowski's equation[3] was used

$$k_1' = 4\pi N_A \delta (D_A'' + D_{AX}'')/1000 \quad (4)$$

where N_A is the Avogadro number, and

$$D_{AX}'' = D_{AX} + \frac{k\delta^2\pi}{4} c_A \quad (5)$$

D_A'' is a similar apparent diffusion coefficient as D_{AX}''

(3) M. V. Smoluchowski, *Z. Phys. Chem. (Leipzig)*, **92**, 129 (1917).

in eq 5, but with the labels exchanged (cf. eq 38 in ref 1).

In Table III the values of the diffusion limit are compared to the second-order rate constants measured. According to that the errors should always be additional quantities in both cases; while either the sum or the difference of the diffusion coefficients appear in k_1' or k, respectively, the relative error is higher for the latter one. Thus, it can be concluded that the reaction takes place with a rate equal or very close to the diffusion limit.

Table III: Comparison of the Diffusion Limit and the Rate Constant Measured for the Ferrocene–Ferricinium Exchange

t, °C	$k_1' \times 10^{-9}$, M^{-1} sec^{-1}	$k^d \times 10^9$, M^{-1} sec^{-1}	$[H]^+$, mM
	In Methanol		
−75	0.19 ± 0.04[b]	0.000087 ± 0.000022[a]	?
−70	0.25 ± 0.04[b]	0.00017 ± 0.00004[a]	?
−65	0.35 ± 0.04[b]	0.00035 ± 0.00018[a]	?
12.5	12.5 ± 1.4[b]	14 ± 11	50
20	15.8 ± 1.3	13 ± 4	50
25	20.3 ± 1.3	18 ± 3	10
25	20.3 ± 1.3	20 ± 3	50
25	20.3 ± 1.3	23 ± 3	100
35	27.1 ± 1.4	19 ± 14	50
	In Ethanol		
12.5	8.9 ± 0.8[b]	5 ± 3	50
20	8.4 ± 1.0	15 ± 4	50
25	10.1 ± 1.1[c]	19 ± 10	50
35	8.8 ± 0.6	10 ± 5	50
	In 1-Propanol		
12.5	4.8 ± 0.2[b]	≦3.3	50
20	5.4 ± 0.3	4.8 ± 1.2	50
25	6.6 ± 0.3	7.9 ± 0.8	50
35	6.9 ± 0.3	5.9 ± 0.6	50

[a] See ref 2. [b] Extrapolated values. [c] Interpolated values. [d] Calculated with δ = 7.08 Å (see ref 2).

It seems to be important to note that, on one hand, low true diffusion coefficients favor the application of the transfer diffusion method (see eq 1); on the other hand, the lower the diffusion coefficients the lower the diffusion limit. Thus, the range in k that could be studied at all can be quite small due to a *methodical* lower limit and an objective upper one. This range in the cases under discussion is about one order of magnitude below the diffusion-controlled rate.

Though the extrapolation of the diffusion coefficients to low temperature is somewhat uncertain, Stranks' data for the rate constant in methanol are significantly less than the corresponding diffusion limit. In this way the enthalpy and entropy of activation can also be calculated with satisfactory precision using Noyes' equation[4] for the resultant rate k, when both diffusion and activation control is in operation

$$k = k_1'/(1 + k_1'/k_2) \tag{6}$$

where k_2 is the rate constant of the activation controlled reaction. Substituting the temperature dependence of k_2 according to Eyring, one has

$$\frac{\Delta F^{\pm}}{T} = R \ln \frac{\mathbf{k}T}{h}\left(\frac{1}{k} - \frac{k}{k_1'}\right) \tag{7}$$

where $\mathbf{k}$ and h are the Boltzmann and Planck constants, respectively.

Otherwise, when k_2 is written in the form $k_2 = Z \exp(-\Delta F^*/RT)$ where Z is the number of collisions in unit time that can be taken as equal to the diffusion limit, the following equation can be obtained

$$\frac{\Delta F^*}{T} = R \ln \left(\frac{k_1'}{k} - 1\right) \tag{8}$$

The term at the left-hand side of eq 7 and 8 was calculated as a linear function of $1/T$ by a least-squares program. The activation parameters obtained are $\Delta H^{\pm}$ = 14.8 ± 1.4 and ΔH^x = 8.8 ± 1.6 kcal/mol, $\Delta S^{\pm}$ = 44 ± 6 and ΔS^x = 33 ± 9 eu in methanol.

It is to be noted that these values are very sensitive to the low temperature data of Stranks, while those measured by us do not influence their absolute value too much, but their errors. This is due to that the Arrhenius plot cannot sweep in the large range Strank's data would allow, but it must cross the range given by our points. Since the temperature range covered is quite large, the activation parameters can be given with a much smaller scattering than one would expect from the uncertainty of the rate constants. This is why no enthalpy and entropy of activation can be given for the reaction in ethanol and 1-propanol which solvents were not studied at low temperatures. The thermodynamic parameters of the reaction seem, however, unreasonable, since one would expect values near zero for both the enthalpy and entropy of activation. This is due to that, on one hand, probably the structure of the complexes is the same in the oxidized and reduced form and, on the other hand, ferrocene is an uncharged molecule; thus neither Franck–Condon restriction nor Coulombic repulsion would appear. Some recent electrochemical measurements[5] at low temperature support this expectation being in contradication with Stranks' data.

The main conclusion—in addition to the proof of the existence of the transfer diffusion—is that the electron transfer reaction takes place through an activated complex in which the reactants are as close to each other as possible. This follows from the agreement of the diffusion limit with the rate constants measured near room temperature, for the diffusion limit is proportional to δ while the transfer diffusion term in eq 1 de-

(4) R. M. Noyes, *Progr. React. Kinet.*, 1, 129 (1961).

(5) I. Ruff, M. Zimonyi, and G. Farsang, to be published.

pends on δ^2. The use of a smaller δ, if reasonable at all, would result in that the diffusion limit is smaller than the rate observed. In this way, very important information about the mechanism of the reaction, namely the distance of the reactants in the activated complex, can be tested.

Acknowledgment. One of the authors (V. J. F.) is very grateful to the Hungarian Academy of Sciences for the Graduate Fellowship awarded to him. The authors are very indebted to Dr. B. Rozsondai, who called their attention to the photographic method of the measurement of the diffusion coefficient.

The Charge Density on the Phosphoryl Oxygen in a Series of Phosphate Esters; Tributyl Phosphate, a Monocyclic Phosphate, and a Bicyclic Phosphate Ester[1]

by A. L. Mixon and W. R. Gilkerson*

Department of Chemistry, University of South Carolina, Columbia, South Carolina 29208 *(Received April 1, 1971)*

Publication costs borne completely by The Journal of Physical Chemistry

The effects of adding a series of phosphate esters on the conductances of dilute solutions of piperidinium, *N*-methylpiperidinium, and *N*-ethylpiperidinium picrates in chlorobenzene at 25° have been measured. Cation–ligand association constants, K_L, have been calculated for the *N*-methyl- and *N*-ethylpiperidinium cations with tributyl phosphate, *n*-octyl trimethylene phosphate, and 1-oxo-4-ethyl-2,6,7-trioxa-1-phosphabicyclo[2.2.2]octane. The ratio of the cation–ligand association constant for the *N*-ethyl cation, $K_L(Et)$, to that for the *N*-methyl derivative, $K_L(Me)$, has been used as a probe of the electron density on the phosphoryl oxygen atoms in the esters. These results are compared with phosphoryl oxygen stretching frequencies, ν_{PO}, and with calculated (Hückel–MO) values of charge densities.

Introduction

Bicyclic phosphate esters have been found[2] to be poor extractants, compared to acyclic esters, for lanthanide metal ions. The same report contained the observation that these bicyclic esters had abnormally high phosphoryl oxygen stretching frequencies. Burger[3] reported a linear relation between extractant ability and the phosphoryl oxygen stretching frequency, ν_{PO}: the lower the frequency, the better the extractant. Wagner[4] carried out LCAO–MO calculations for a number of acyclic phosphoryl compounds and found an excellent correlation between the calculated phosphoryl PO π-bond orders and experimental values of phosphoryl oxygen stretching frequencies. The calculated values of the net charges on the phosphoryl oxygen also show excellent correlation with ν_{PO}. Presumably the extractant ability of a phosphoryl derivative is greater the greater the negative charge on the phosphoryl oxygen, and the larger the π-bond order of the phosphoryl bond, the smaller the net negative charge on oxygen and the larger the phosphoryl oxygen stretching frequency.

Recent Hückel–MO calculations by Collin[5] indicate that the net negative charge on the phosphoryl oxygen decreases in the order ethylene phosphate anion > trimethylene phosphate anion > diethyl phosphate anion. Calculated values of the positive charge on phosphorus decrease more markedly in the same order. Boyd[6] reported extended Hückel–MO calculations of both net charges on atoms and bond orders. Boyd's calculations indicate that net negative charge on the phosphoryl oxygen decreases in the order trimethyl phosphate > methyl ethylene phosphate. This is the reverse of the order given by Collin for the diester anions.

The theoretical studies of both Collin and Boyd were concerned principally with the influence of the geo-

(1) This work has been supported in part by Grant GP 6949 from the National Science Foundation.

(2) S. G. Goodman and J. G. Verkade, *Inorg. Chem.*, 5, 491 (1966).

(3) (a) L. L. Burger, *J. Phys. Chem.*, 62, 590 (1958); (b) J. L. Burdett and L. L. Burger, *Can. J. Chem.*, 44, 111 (1966).

(4) E. L. Wagner, *J. Amer. Chem. Soc.*, 85, 161 (1963).

(5) R. L. Collin, *ibid.*, 88, 3281 (1966).

(6) D. B. Boyd, *ibid.*, 91, 1200 (1969).

metrical constraints imposed by the presence of $-(CH_2)_n-$ bridges between two of the alkoxyl oxygens on the stability of the esters. The two studies are in agreement regarding the effect of the presence of rings on the positive charge on phosphorus but not on the effect on the negative charge on the phosphoryl oxygen.

We believe that we have an experimental tool wherewith we can determine which in a series of phosphate esters has the greater negative charge on the phosphoryl oxygen atom and which has the least. We have found[7,8] that the cation–ligand association constants, K_L (eq 1), for a series of ligands with piperidinium

$$BH^+ + L \rightleftharpoons BH^+,L$$
$$K_L = [BH^+,L]/[BH^+][L] \quad (1)$$

($PipH^+$), 1-methylpiperidinium ($MePipH^+$), and 1-ethylpiperidinium ($EtPipH^+$) cations fell into two distinct classes: the first group, consisting of the free piperidines themselves, 2,6-dimethylpyridine (lut), and triphenylphosphine all had K_L values which decreased in the expected order $PipH^+ > MePipH^+ > EtPipH^+$, while the second group, consisting of triphenylphosphine oxide (Ph_3PO) and tetrahydrofuran, had K_L values which decreased in the order $PipH^+ > EtPipH^+ > MePipH^+$. We attributed the reversal of the order for ethyl- and methylpiperidinium cations with the second group of ligands to the presence of more than one lone pair of electrons on the oxygen atom. With one pair of electrons involved in the interaction with the $\equiv NH^+$ group, the other pair are available for interaction with a terminal CH proton on the end of the ethyl substituent on the cation, (**1**).

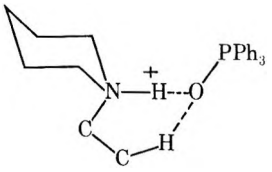

1

We propose that the ratio $K_L(Et)/K_L(Me)$, where $K_L(R)$ represents the K_L value for the *N*-alkylpiperidinium cation, may be used as a probe for relative electron density on a coordinating atom in a series of ligands of not too different structure. We report here application of these ideas to the problem of the electron density on the phosphoryl oxygen in a series of trialkyl phosphate esters, tributyl phosphate (**2**), *n*-octyl trimethylene phosphate (**3**), and 1-oxo-4-ethyl-2,6,7-trioxa-1-phosphabicyclo[2.2.2]octane (**4**). These were chosen because of their stability, ease of preparation, and availability of other physical properties such as dipole moments and infrared spectra. The dipole moment of compound **3** has been determined in the course of this work.

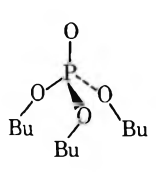

2

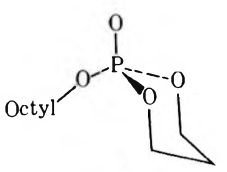

3

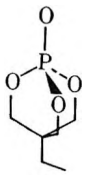

4

Experimental Section

Chlorobenzene (PhCl) was purified as before.[9] Benzene (Baker and Adamson, reagent grade) was passed through alumina (Alcoa, grade F-20), kept for 1 day over sodium ribbon and then distilled from the sodium ribbon on a 38-cm column packed with glass helices. A middle cut was taken. Piperidinium picrate (PipHPi), *N*-methylpiperidinium picrate (MePipHPi), and *N*-ethylpiperidinium picrate (EtPipHPi) were prepared as described previously.[7] Tri-*n*-butyl phosphate, **2** (Eastman Organic Chemicals, White Label), was distilled under vacuum using a Hickman molecular still; the bath temperature was maintained at 75°. *n*-Octyl trimethylene phosphate, **3** (MCP), was supplied by Dr. T. H. Siddal, III, of the Savannah River Laboratory, E. I. duPont de Nemours and Co. This phosphate was purified by distillation at 148° (2 mm). A middle fraction was taken. The density of **3** was found to be 1.072 g/ml at 25°, and the refractive index at 25° (Na D line) is 1.4480. 1-Oxo-4-ethyl-2,6,7-trioxa-1-phosphabicyclo[2.2.2]octane, **4**, the bicyclophosphate (BCP), was also supplied by Dr. T. H. Siddal, III. Before each use it was recrystallized once from ethanol, mp 209–210° (lit.[10] mp 207°). Precision conductance measurements were carried out at 25.00° using bridge, constant temperature oil bath, and Kraus erlenmeyer conductance cells previously described.[9] A Balsbaugh Laboratories Type 100T3 cell with nickel electrodes was used for measurements of dielectric capacitance. The air capacity of this cell is 104.9 pF. The capacitance measurements were made using a General Radio Type 716-C capacitance bridge and 716-P-4 guard circuit. The oscillator, operated at 100 kHz, was a General Radio Type 1330-A, and the detector was a General Radio Type 1231-B amplifier and null detector. Density measurements were made using a Lipkin pycnometer. Refractive indices were measured on a Bausch and Lomb Abbe-SL refractometer.

The dielectric constant of chlorobenzene is 5.621.[11] The viscosity of chlorobenzene is 0.752 cP[12] and the density is 1.011 g/cc.[9] All the foregoing physical constants are for 25.0°. All concentrations are expressed in units of moles per liter.

(7) A. L. Mixon and W. R. Gilkerson, *J. Amer. Chem. Soc.*, **89**, 6410 (1967).

(8) W. R. Gilkerson and A. L. Mixon, *ibid.*, **89**, 6415 (1967).

(9) E. R. Ralph, III, and W. R. Gilkerson, *ibid.*, **86**, 4783 (1964).

(10) O. Neunhoeffer and W. Maiwold, *Chem. Ber.*, **95**, 108 (1962).

(11) A. A. Maryott and E. A. Smith, *Nat. Bur. Stand. (U. S.), Circ.*, **514**, 1 (1951).

(12) R. L. McIntosh, D. J. Mead, and R. M. Fuoss, *J. Amer. Chem. Soc.*, **62**, 506 (1940).

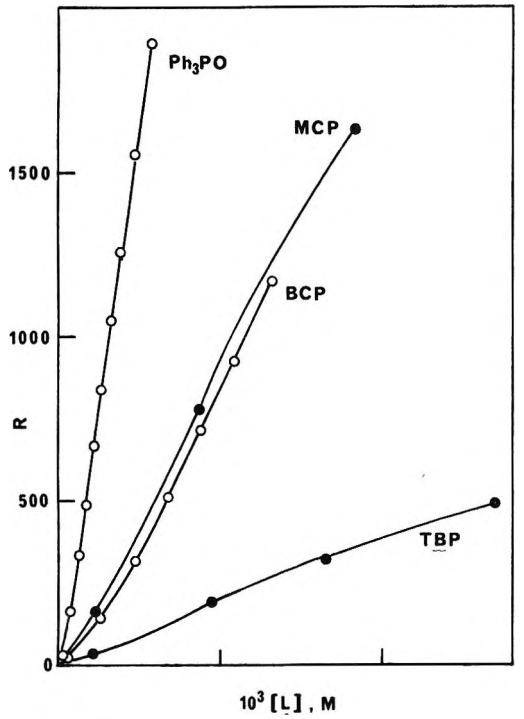

Figure 1. Conductance ratios, R, for PipHPi in chlorobenzene at 25° with Ph_3PO, TBP, MCP, and BCP as addends.

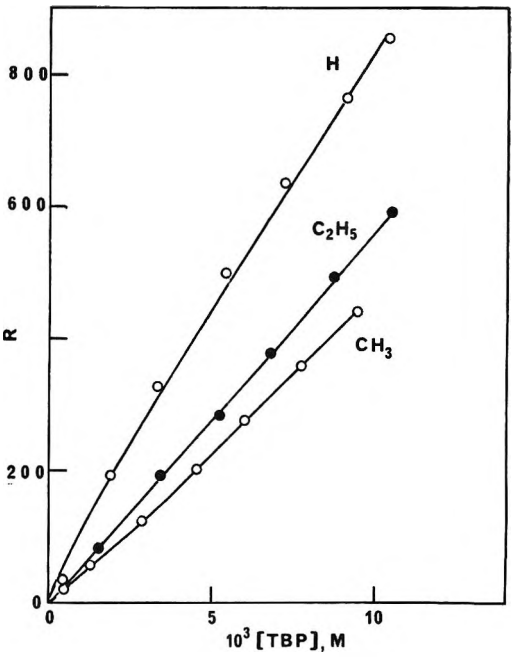

Figure 2. Conductance ratios, R, for piperidinium picrate (H), N-methylpiperidinium picrate (CH_3), and N-ethylpiperidinium picrate (C_2H_5) with tributyl phosphate as addend in chlorobenzene at 25°.

Results

We define a quantity, $R \equiv (g/g_0)^2$, where g is the conductance of the salt solution at a ligand concentration [L], and g_0 is that in the absence of ligand. Figure 1 shows values of R for PipHPi plotted *vs.* [L] for the phosphate ligands TBP (0.229 mM in salt), MCP (0.231 mM in salt), and BCP (0.240 mM in salt) as well as values already obtained[7] for Ph_3PO (0.244 mM in salt). The curves for the three phosphates are distinctly S-shaped, and close inspection of the curve for the phosphine oxide shows that it too is sigmoid. If a 1:1 cation–ligand complex is the only complex forming in a salt–ligand system, eq 1, then it has been shown[9,13] that R is related to the ligand concentration by

$$R = 1 + K_L[L] \qquad (2)$$

Obviously more complex interactions are occurring in these systems. We will not attempt to analyze these results to extract equilibrium constants but will discuss them qualitatively in the following section.

Figure 2 shows the values of R for the salts PipHPi (0.229 mM), MePipHPi (0.309 mM), and EtPipHPi (0.306 mM) with tributyl phosphate (TBP) as ligand. The curvature upward in these graphs for the N-methyl- and N-ethylpiperidinium picrates indicates[13] that a second ligand molecule is adding on to the cation–ligand complex, eq 3

$$BH^+,L + L \rightleftharpoons BH^+,L_2$$

$$K_{2L} = [BH^+,L_2]/[BH^+,L][L] \qquad (3)$$

In such a case R is related to the ligand concentration by

$$R = 1 + K_L[L] + K_LK_{2L}[L]^2 \qquad (4)$$

We may then plot $(R - 1)/[L]$ *vs.* [L]. The intercept at [L] = 0 is K_L and the slope is K_LK_{2L}. Values of K_L so obtained appear in Table I. The slopes were so small and/or uncertain that we do not report here any values of K_{2L}.

Values of K_L for the methyl- and ethylpiperidinium

Table I: Ligand Association with Methylpiperidinium and Ethylpiperidinium Cations in PhCl at 25°

	Ligands			
	Ph_3PO	TBP	MCP	BCP
10^{-3} K_L(Me), M^{-1}	150[a]	44	125	110
K_L(Et)/K_L(Me)	1.86[a]	1.27	1.14	1.12
ν_{PO}, cm^{-1}	1200[b]	1260[c]	1300[d]	1325[c]
μ, D	4.37[e]	3.07[f]	5.5[g]	7.10[h]

[a] Reference 7. [b] Reference 4. [c] References 2 and 3. [d] Obtained in this laboratory. The ir spectrum was obtained using a neat sample in a KBr cell on a Perkin-Elmer 337 spectrophotometer. [e] G. M. Phillips, J. S. Hunter, and L. E. Sutton, *J. Chem. Soc.*, 146 (1945). [f] G. K. Estok and W. W. Wendlandt, *J. Amer. Chem. Soc.*, 77, 4767 (1955). [g] This work. [h] T. L. Brown, J. S. Verkade, and T. S. Piper, *J. Phys. Chem.*, 65, 2051 (1961). The dipole moment given is for the 4-methyl derivative rather than BCP which is the 4-ethyl derivative. The difference is expected to be negligible.

(13) J. B. Ezell and W. R. Gilkerson, *J. Phys. Chem.*, 72, 144 (1968).

cations for both the monocyclic phosphate, **3** (MCP), as ligand and the bicyclic phosphate, **4** (BCP), as ligand were obtained as described above and are listed in Table I. Also listed in Table I are values of K_L for methyl- and ethylpiperidinium cations with triphenylphosphine oxide, Ph_3PO previously reported.[7]

The dielectric constants of solutions of the monocyclic phosphate in benzene at 25° are related to the mole fraction of solute, x, by the empirical equation, $\epsilon = \epsilon_0 + 42.1x$. The dielectric constant of pure benzene ϵ_0 was taken as[11] 2.274. The dipole moment of MCP was calculated using the method of Hedestrand.[14] In this method, the density is taken to be a linear function of the mole fraction of solute, $\rho = \rho_1 + bx_2$. If the volumes of solute and solvent are additive the value of b can be shown to be given by $b = (M_2 - \rho_1 \bar{V}_2^\circ)/\bar{V}_1^\circ$, where M_2 is the molecular weight of solute, and $\bar{V}_1^\circ$ is the molar volume of pure component i. It was assumed that the molar distortion polarization of the solute at infinite dilution is equal to that of the pure solute, *i.e.*, the molar refraction of MCP. This last should not be a critical assumption since this contribution is only 10% of the total molar polarization. We calculated the dipole moment of MCP to be 5.52 D.

Discussion

The effects of added Ph_3PO and the phosphate esters on the conductance of PipHPi are more complex than we had previously believed.[7] We believe the sigmoid shapes of the R *vs.* [L] curves to be due to the combined effects of the following reaction, in addition to eq 1 and 3

$$\text{PipHPi} + \text{L} \rightleftarrows \text{PipH}^+,\text{L},\text{Pi}^- \qquad (5)$$

$$K_2 = \frac{[\text{PipH}^+,\text{L},\text{Pi}^-]}{[\text{PipHPi}][\text{L}]}$$

where $\text{PipH}^+,\text{L},\text{Pi}^-$ represents a complex between ligand and the ion pair **5**. The ligands Ph_3PO and the

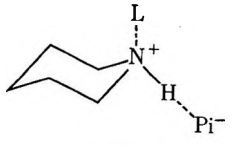

5

phosphate esters are interacting through the phosphoryl oxygen, which is sterically most favorably situated to add to the cation in the ion pair as shown. These are not the only equilibria involved, however. We are able to fit these data using one set of parameters K_L, K_2, and K_{2L} in the low [L] region but need to adopt another set in the high [L] region. One set will not allow a fit over the entire concentration region. It is not necessary for the main purpose of the present study to have values of K_L for the piperidinium ion with these ligands, so we leave that topic.

We shall be concerned in the main with the values of K_L(Me) for the *N*-methylpiperidinium cation and K_L(Et) for the *N*-ethylpiperidinium cation with the ligands Ph_3PO, TBP, MCP, and BCP. We had previously found[15] that with Bu_3NH^+ as the cation, K_L generally increased in magnitude as the dipole moment of the ligand increased. Here with the phosphate esters, K_L(Me) values increase and then decrease as the dipole moments increase (Table I). The ratios $K_L(\text{Et})/K_L(\text{Me})$ decrease as the moments increase.

We believe the manner in which K_L(Me) and K_L(Et) change from ester to ester to be the result of two opposing effects. The first is a decreasing electron density on the phosphoryl oxygen as L changes from TBP to MCP to BCP (this will be discussed more fully below), and the second is the increase in dipole moments of the ligands in the order TBP < MCP < BCP as first two and then all three alkoxy groups are constrained to a conformation in which the ROP group dipoles have their negative ends roughly pointed in the same direction as the phosphoryl oxygen. The ROP group moments contribute proportionally much more to the total molecular dipole moments of the phosphate esters MCP and BCP than to the electrostatic potential energy of interaction between the positive charge on the cation and the various group dipoles in the ester ligands. Our view of the cation–ligand complexes places the $\equiv N^+H$ group from the cation along the phosphoryl oxygen-to-phosphorus axis. The center of the phosphoryl group moment then is closest to the site of positive charge on the cation, with the alkoxy dipoles further removed from the cation charge. Since ion–dipole interaction energy falls off as the inverse square of the separation distance, the alkoxy dipoles make a proportionally smaller contribution to the potential energy of the cation–ligand complexes in the case of MCP and BCP than to the total molecular dipole moments of these two ligands.

The decrease in $K_L(\text{Et})/K_L(\text{Me})$ as L is varied from Ph_3PO to TBP to MCP to BCP we interpret as indicating a decrease in net negative charge on the phosphoryl oxygen in the order Ph_3PO > TBP > MCP > BCP. Note that the values of ν_{PO}, the phosphoryl oxygen stretching frequency, included in Table I, increase in the same order. Such increases in ν_{PO} have been correlated elsewhere[4] with decreasing negative charge on the phosphoryl oxygen.

The relative negative charges on the phosphoryl oxygens in this series of phosphate esters, TBP, MCP, and BCP, are in an order similar to that found in Boyd's calculations (trimethyl phosphate greater than methyl ethylene phosphate) and are inverted when compared to the order calculated by Collin for phos-

(14) G. Hedestrand, *Z. Phys. Chem.* (*Leipzig*), B2, 428 (1929).

(15) W. R. Gilkerson and J. B. Ezell, *J. Amer. Chem. Soc.*, 89, 808 (1967).

phate diester anions. The comparisons between our experimental results and the results of both sets of calculations are not as direct as we should like.

The theoretical calculations of Collin and of Boyd were carried out with model compounds which are not the same as any in our series but several in each set bear a strong resemblance to ones in our present set. We conclude from our experimental results that Boyd's set of calculations[6] is more valid than the other with the regard to the net charge on the phosphoryl oxygen.

We are more satisfied that our previous explanation[8] of the inversion of the values of K_I, for the methyl- and ethylpiperidinium cations in the case of the oxygen-containing ligands is a correct one in view of the excellent correlation of the values of the ratios $K_L(Et)/K_L(Me)$ and ν_{PO}.

Intermolecular Hydrogen Bonding. I. Effects on the Physical Properties of Tetramethylurea–Water Mixtures[1]

by K. R. Lindfors,* S. H. Opperman, M. E. Glover, and J. D. Seese

Department of Chemistry, Central Michigan University, Mt. Pleasant, Michigan 48858 *(Received March 31, 1971)*

Publication costs assisted by Central Michigan University

Vapor pressures, viscosities, densities, surface tensions, heat of mixing, and molar refractivities of water–tetramethylurea mixtures were measured at temperatures from 25 to 85°. The data show that the tri- to pentahydrates are the most stable water–tetramethylurea species formed.

Introduction

Recently there has been considerable interest in the interactions in hydrogen bonded binary mixtures.[2,3] The powerful interactions which occur between a protic and a dipolar–aprotic liquid produce marked changes in many chemical[3b] and physical[4] properties.

Tetramethylurea (TMU) and water form such a binary pair which has not been extensively studied. We report here studies on the TMU–water system using classical physical-chemical techniques. The effects of the TMU–water hydrogen bonds on density, viscosity, surface tension, vapor pressure, refractive index, and heat of mixing of these solutions were measured. The main purpose of the investigation was to determine the most prominent TMU–water complex species present in solution at various temperatures.

When TMU and water are mixed, some of the hydrogen bonds between the water molecules are broken. New hydrogen bonds form between the water molecules and the TMU molecules. Thus the deviations in properties of the TMU–water mixtures from a linear interpolation between the properties of the pure components result not only from the formation of TMU–water complexes but also from the disruption of the water structure. However, large deviations in physical properties are strong evidence for the existence of interactions. The presence of a hydrogen bond donor, the water, and of possible acceptors, the oxygen and nitrogens of the TMU, suggest that at least a major part of these interactions will be hydrogen-bond in nature.

The chemical and physical properties of TMU have been reviewed in considerable detail previously.[5] It is a clear, polar, aprotic liquid which is miscible in all proportions with water and all common organic solvents. TMU has been suggested as a useful reaction medium. In its solvent properties, it resembles pyridine and dimethylformamide except that it has a higher boiling point (176.5° (760 Torr)).[6] It is an important medium for aryl deaminations[7] and is the solvent of choice for higher temperature Ullmann reactions.[5] TMU also increases the rate of alkylation reactions.[5]

(1) Work supported in part by The Ott Chemical Co., Muskegon, Mich.

(2) A. K. Covington and P. Jones, Ed., "Hydrogen-Bonded Solvent Systems," Proceedings of a Symposium on Equilibrium and Reaction Kinetics in Hydrogen-Bonded Solvent Systems, University of Newcastle upon Tyne, Jan 10–12, 1968, Taylor and Francis Ltd., London, 1968.

(3) (a) J. F. Coetzee and C. D. Ritchie, "Solute–Solvent Interactions," Marcel Dekker, New York, N. Y., 1969; (b) A. J. Parker, *Chem. Rev.*, **69**, 1 (1969).

(4) G. C. Pimentel and A. L. McClellan, "The Hydrogen Bond," W. H. Freeman and Co., San Francisco, Calif., 1960.

(5) A. Lüttringhaus and A. W. Dirksen, *Angew. Chem. Int. Ed. Engl.*, **3**, 260 (1964).

(6) W. Mischler and C. Escherich, *Chem. Ber.*, **12**, 1162 (1879).

(7) K. G. Rutherford and W. Redmond, *Org. Syn.*, **43**, 12 (1963).

Experimental Section

The TMU was obtained from the Ott Chemical Co., Muskegon, Mich. It was purified by the following procedure. Ten per cent by volume of dry benzene was added to the TMU. After stirring, the benzene was distilled off at atmospheric pressure. The dissolved water and dimethylamine codistill with the benzene. The remainder was vacuum distilled. The fraction boiling at 62–64° at 13 Torr was collected and stored in glass-stoppered flasks in the dark.

The formation of hydrogen-bonded complexes can be inferred by a number of different experimental methods.[4] We report here the measurements of several intensive physical properties at temperatures from 25 to 80° made on TMU–water mixtures ranging in mole fraction from 0 to 1. Systematic deviations of experimental values from calculated ones are evidence of association.

Vapor pressures of TMU-water mixtures were measured in a greaseless vacuum apparatus similar in design to the one described by Christian, *et al.*[8,9] The entire apparatus was immersed in a constant temperature water bath at 45.00 ± 0.02° and the pressures were measured manometrically. Samples were introduced through the mercury seal, using a syringe with a blunted needle. The amounts added were determined by weight.

Densities were measured pycnometrically at 25, 45, and 80° in baths regulated to ±0.02°. The pycnometers were calibrated with water and the calibrations were checked several times at each temperature.[10]

Viscosities were determined using a standard Ostwald viscometer in the same regulated baths as above. Water was used to calibrate the viscometer at the various temperatures.[11]

Surface tensions were measured using the capillary rise technique. Measurements were done in the above baths. The liquid levels were read with a cathetometer. Water was used for the calibrations.[12]

The refractive index measurements of the solutions were made with an Abbe refractometer through which water from the 25° bath was circulated.

The heat of mixing determinations were made in a calorimeter of our own design. It consisted of a small Dewar flask fitted with a stirrer, heater, and thermistor. The thermistor made up the fourth leg of a Wheatstone bridge. The bridge balance was monitored on a variable sensitivity recorder. As can be shown, for small temperature changes, the signal to the recorder is directly proportional to the temperature change from the balance condition. A weighed amount of TMU or water was placed in the Dewar and the bridge was balanced. Weighed portions of the other ingredient, adjusted to the same temperature, were then added. The change in bridge output was noted. After each addition, a known amount of electrical energy was added and the pen shift was again noted. In this way the heat of mixing was determined over the entire concentration range.

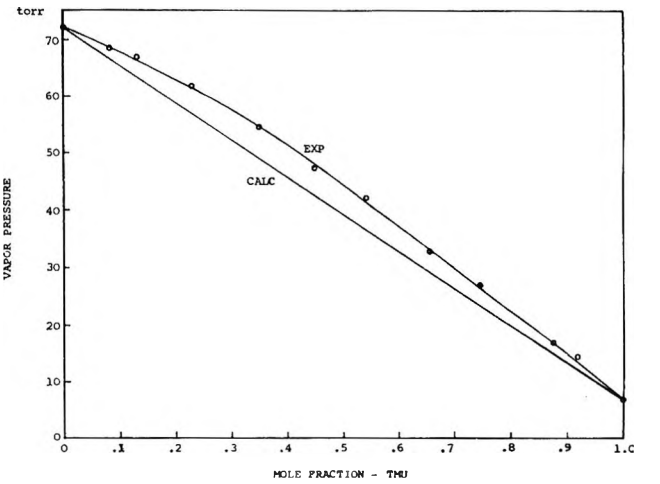

Figure 1. Vapor pressures of TMU–water mixtures at 45°.

Results and Discussion

Figure 1 shows a plot of the observed vapor pressures of water–TMU mixtures at 45°. As can be seen, the deviations from Raoult's law are small but always positive. Apparently the change from water–water hydrogen bonding to water–TMU association produces little change in the vapor pressures of such mixtures. However, apparent agreement with Raoult's law is not necessarily indicative of ideality. Many systems are known where a cancellation of effects leads to apparent ideality whereas association is known to occur.[13] The pyridine–ethanol system is an example.[14]

The densities of TMU–water mixtures show marked deviations from additivity at the three temperatures studied, 25, 45, and 80°. At the two lower temperatures, the densities go through a maximum near mole fraction of 0.2 indicating a $TMU \cdot (H_2O)_n$ complex where n is between 3 and 6. At 80° the densities no longer show this maximum and in fact show a negative deviation from linearity. The densities for pure TMU were 0.9622, 0.9458, and 0.9131 g/ml at 25, 45, and 80°, respectively. Figure 2 is a plot of Δd *vs.* X_T where $\Delta d = d(\text{exptl}) - d(\text{calcd})$ and X_T is the mole fraction of TMU.

$$d_{\text{calcd}} = X_T d_T^0 + X_w d_w^0$$

where d_T^0 and d_w^0 are the densities of pure TMU and

(8) S. D. Christian, H. E. Affsprung, and C. Lin, *J. Chem. Educ.*, **40**, 323 (1963).

(9) A. A. Taha, R. D. Grigsby, J. R. Johnsor., S. D. Christian, and H. E. Affsprung, *ibid.*, **43**, 432 (1966).

(10) R. C. Weast, Ed., "Handbook of Chemistry and Physics," 49th ed, The Chemical Rubber Co., Cleveland, Ohio, 1969, p F5.

(11) See ref 10, p F45.

(12) See ref 10, p F30.

(13) G. C. Pimentel and A. L. McClellan, "The Hydrogen Bond," W. H. Freeman and Co., San Francisco, Calif., 1960, p 38.

(14) A. Blackburn and J. J. Kipling, *Nature*, **171**, 174 (1953).

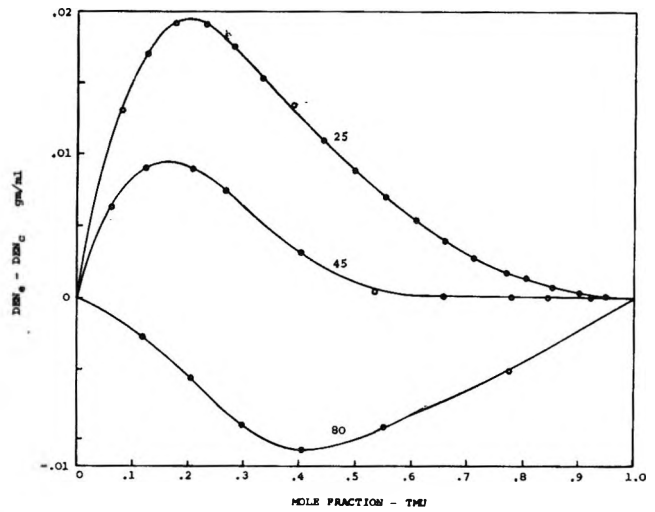

Figure 2. The differences between experimental and calculated densities for TMU–water mixtures at 25, 45, and 80°.

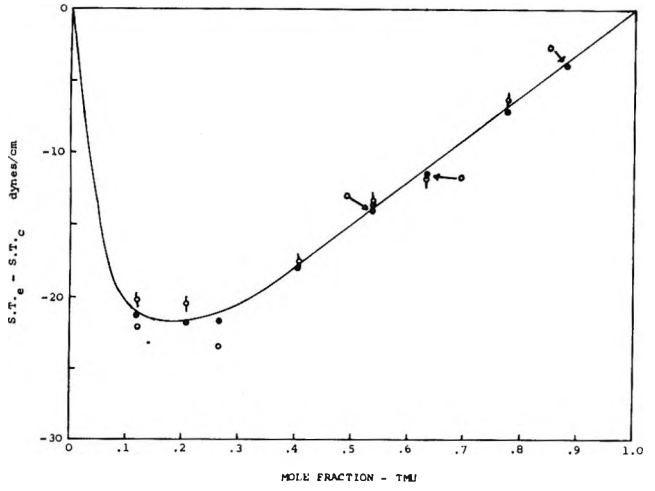

Figure 3. The differences between experimental and calculated surface tensions for TMU–water mixtures: ○, 25°; ●, 45°; ◊, 80°.

pure water, respectively. This plot more clearly shows the positive and negative deviations.

The formation of hydrogen bonds leads to an increase in density and *vice versa*. Since both the formation and rupturing of hydrogen bonds is occurring in this system, the complex results are not unexpected.

For the three temperatures, the differences between calculated and experimental values of surface tension fell along the same curve, as is shown in Figure 3.

$$\gamma_{\text{calcd}} = X_T\gamma_T^0 + X_w\gamma_w^0$$

The values of surface tension observed for pure TMU at the three temperatures were 34.60, 31.64, and 28.30 dyn/cm. The surface tension of binary mixtures has been used to determine the form of hydrated species.[15] The fairly sharp break in Figure 3 near a mole fraction of TMU of 0.16 supports a hydrate with the formula $TMU \cdot 5H_2O$.

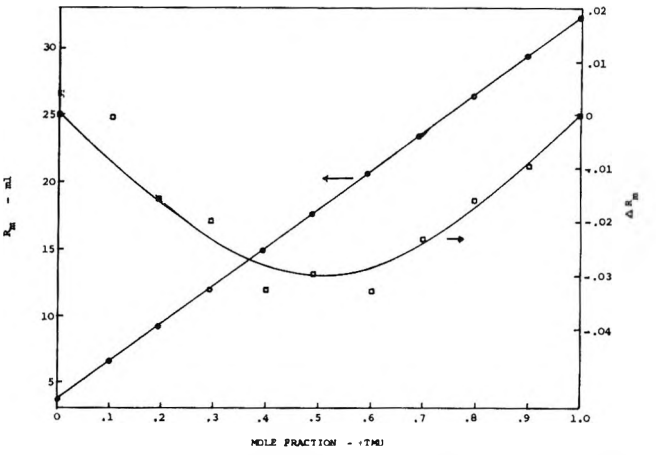

Figure 4. Molar refractions and their deviations from linearity for TMU–water mixtures at 25°.

The molar refractions and the differences between experimental and calculated molar refractions at 25° are shown in Figure 4.

$$R_m = \frac{n^2 - 1}{n^2 + 2}\frac{(X_T M_T + X_w M_w)}{d}$$

$$R_m \text{ (calcd)} = \frac{n^2_T - 1}{n^2_T + 2}\frac{X_T M_T}{d_T} + \frac{n^2_w - 1}{n^2_w + 2}\frac{X_w M_w}{d_w}$$

where n, n_T, and n_w are the refractive indices of the solution, of pure TMU, and of pure water; M_T and M_w are the appropriate molecular weights; and d, d_T, and d_w are the densities of the solutions, pure TMU, and pure water. The experimental molar refraction data lie on a very nearly linear curve. There are, however, systematic deviations as can be seen from the ΔR_m plot. These deviations are small and go through an extreme near 0.5 mole fraction TMU.

The heat of mixing data for the TMU–water system are shown in Figure 5. The heat evolved per mole of TMU passes through a minimum of −13.7 kcal/mol at mole fraction TMU of 0.07. Since there can be many contributions to the heat of mixing, the location of this maximum is not necessarily indicative of the form of the complex.

The fluidities (the reciprocals of the viscosities) at the various temperatures of the solutions all pass through minima near mole fraction TMU of 0.15. Figure 6 shows the difference between experimental and calculated fluidities. The calculated values were computed using the Kendall[16] equation

$$\log \varphi = X_T \log \varphi_T + X_w \log \varphi_w$$

Large deviations from the Kendall equation are seen to occur at all three temperatures. The measured values

(15) P. Dunn and J. B. Polya, *Recl. Trav. Chim.*, **69**, 1297 (1950).
(16) J. Kendall and K. P. Monroe, *J. Amer. Chem. Soc.*, **39**, 1787 (1917).

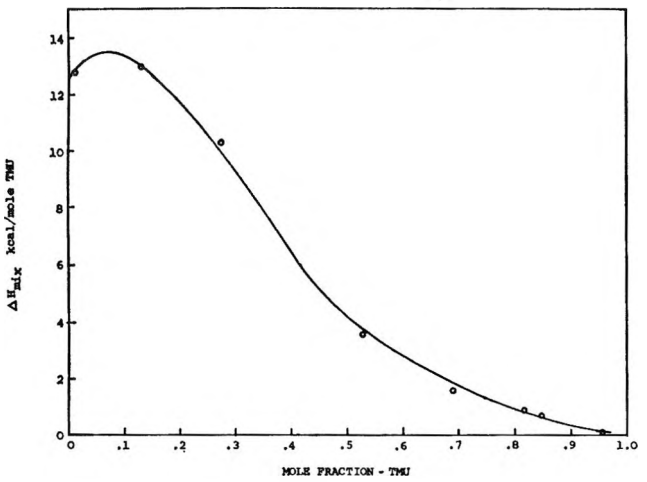

Figure 5. The heat of mixing per mole of TMU for TMU and water.

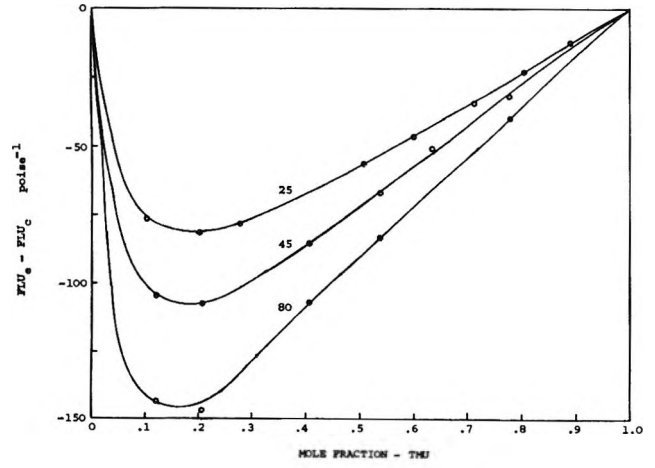

Figure 6. The differences in fluidities of TMU–water mixtures at 25, 45, and 80° from those predicted by the Kendall equation.

of fluidity for pure TMU at the three temperatures were 73.7, 101.6, and 161.3 P^{-1}.

The fluidity is a reliable and sensitive probe of association. The formation of complexes, either strong or weak, leads to large deviations from the Kendall equation.[17,18] Schott[18] has argued that fluidity is the preferred method in that the deviations from ideality are much larger than for other techniques. In Figure 6 the fluidity data indicate that the tri- to pentahydrate is the major complex formed between TMU and water.

In Table I are listed the compositions of maximum deviations, values of the properties, and the percentage

Table I: Deviations in Physical Properties of TMU–Water and DMSO–Water Mixtures from Ideality

	TMU–water		DMSO–water	
Property	X_T	% dev	X_{DMSO}	% dev
γ	0.175	61		
R_m	0.50	0.17	0.51	0.7
φ_{25}	0.19	810	0.23	203
d^{25}_4	0.19	19	0.30	5.6
ΔH_{mix}	0.07			
V_p	0.35	11		

deviations in the various properties for TMU–water mixtures.

$$\text{dev} = 100|\text{exptl} - \text{calcd}|/\text{exptl}$$

For comparison, dimethyl sulfoxide–water mixture properties are also included. Dimethyl sulfoxide is known to hydrogen bond with water to form a trihydrate.

From the large systematic differences between the experimental and calculated values for the physical properties of TMU–water mixtures, the existence of strong interactions can be inferred. These are most likely hydrogen-bonding in nature. Infrared and nuclear magnetic resonance studies (to be published) also support the existence of hydrogen bonds in this system.

To assign a formula to the TMU–water complex unambiguously on the basis of these data is impossible. In fact, there may well be more than a single complex present. Since many types of interactions exist in these solutions, such as dipole–dipole, the maximum deviations of experiment and calculations should not all occur at the same composition. The most stable complex appears, however, to be between the tri- and pentahydrate.

Acknowledgments. The authors whish to thank Dr. D. X. West and Dr. Paul D. Cratin for many helpful discussions, the Numerical Analysis Laboratory of Central Michigan University for computer time, Mrs. A. Fallon for computer assistance, and the Faculty Research and Creative Endeavor Committee for partial financial support. We also thank The Ott Chemical Co. for the gift of the TMU and for partial financial support of this project.

(17) S. Glasstone, "Textbook of Physical Chemistry," 2nd ed, Van Nostrand, New York, N. Y., 1951, p 500.
(18) H. Schott, *J. Pharm. Sci.*, **58**, 946 (1969).

Salt-Induced Critical-Type Transitions in Aqueous Solution. Heats of Dilution of the Lithium and Sodium Halides

by Fred Vaslow

Chemistry Division, Oak Ridge National Laboratory,[1] Oak Ridge, Tennessee 37830 *(Received December 7, 1970)*

Publication costs assisted by the Oak Ridge National Laboratory

Measurements have been made of the differential heats of dilution of LiCl, LiBr, LiI, NaCl, NaBr, and NaI in aqueous solution at 25°. The initial solutions between 1.5 and 1.0 *m* were diluted with 10 to 18 successive increments of water, each about 4% of the total volume with a similar amount of solution removed after the dilution. With the possible exception of some preliminary runs each of the 16 curves obtained showed an apparently anomalous region, close to or within that previously reported in volume measurements. The consistency of form of the dilution curves together with the consistency with the effects found in the volume curves suggests that a significant physical phenomenon is being studied although some problems and questions remain.

Introduction

In an earlier paper[2] it was found that for most of the Na^+ and Li^+, Cl^-, Br^-, and I^- salt solutions, the curves of $\Delta\phi_v/\Delta\sqrt{c}$ as a function of $\sqrt{c}$ appeared to be discontinuous in a form suggesting a λ-shaped region for the integral curve. ϕ_v is the apparent molal volume of the salt, c is the molar concentration, and the Δ refers to the differences of successive measured values of ϕ_v and of $\sqrt{c}$. The discontinuities were extremely small with the deviations of $\Delta\phi_v/\Delta\sqrt{c}$ from a smooth curve being related to density differences of the order of 1 ppm.

While the effect for LiI solutions was quite erratic, in general the effect was consistent, reproducible, and substantially larger than the uncertainty of the measurement. Consequently, the evidence for a physically significant anomaly was considered to be substantial although clearly more information was needed before any definite conclusion could be reached.

The present paper is an extension of the earlier work to a different type of measurement, *i.e.*, heats of dilution, in order to examine the significance of the apparent anomalies further. The relative precision possible with the heat measurements is much lower than for density measurements; however, the value of $\Delta\phi_H$ (change in apparent molal heat content) is directly given by each experiment rather than as the difference of two experimental values. Consequently, a much lower level of precision is acceptable for the heat measurements although to some extent the advantage of measuring $\Delta\phi_H$ directly is lost because of the very large values of $\Delta\phi_H/\Delta\sqrt{m}$ and its change with concentration, relative to the corresponding volume quantities. These large values of $\Delta\phi_H/\Delta\sqrt{m}$ and its variation make very short $\Delta\phi_H$ chords necessary in order to obtain sufficient resolution and thus some of the possible precision is lost.

As in the volume measurements,[2] the primary purpose of these experiments is one of obtaining a high precision for each point, relative to adjacent points, rather than high absolute precision. By designing the experiment for a differential type of measurement, a significant increase in the relative precision can be obtained over that where each point is measured in a separate calorimetric experiment. The conditions are not optimum for high absolute precision and a small overall loss in precision is possible.

With the exception of the work of Young and Machin[3] on NaCl solutions, there is apparently no work in the literature on $\Delta\phi_H/\Delta\sqrt{m}$ at moderate concentrations having both sufficient precision and detail to be applied to the present purpose. The work of Young and Machin has both sufficient precision and sufficiently short chords to be applicable. However, even here there are only a relatively few and isolated points while a continuous set of closely spaced points is necessary for the present work. All measurements of this work are at 25°.

Experimental Section

The calorimeter is basically similar to one used previously[4] and also to the calorimeters used by Young and coworkers.[3,5] The 600-cm³ dewar has thin inner walls with the top part unsilvered and the outer wall exposed to the thermostat liquid. The pipets of 20 and 40 cm³ capacity were similar to those used by Young and

(1) Research sponsored by the U. S. Atomic Energy Commission under contract with Union Carbide Corp.

(2) F. Vaslow, *J. Phys. Chem.*, **73**, 3745 (1969).

(3) T. F. Young and J. S. Machin, *J. Amer. Chem. Soc.*, **58**, 2254 (1936).

(4) G. E. Boyd and F. Vaslow, *J. Chem. Eng. Data*, **7**, 237 (1962); G. E. Boyd, F. Vaslow, and S. Lindenbaum, *J. Phys. Chem.*, **71**, 2214 (1967).

(5) T. F. Young and M. B. Smith, *ibid.*, **58**, 716 (1954).

Smith[5] but were of gold-plated copper rather than tantalum. The pipet mounting was fitted with a copper ground joint fitting into the lid with the lid opening surrounded by a chimney as for the other calorimeter openings. The mounting also had a radiation shield about 10 cm above the lid but below the external water level. Using this device pipets could be removed and changed with a minimum disturbance of the calorimeter. The heater, propellers, and general configuration are similar to those used by Young and Machin.[3]

The temperature-measuring circuit consisted of two 2000-ohm thermistors a short distance apart in a single glass probe and connected as opposite sides of a Wheatstone bridge.[4] With a given current in any thermistor the sensitivity is about twice that of a single thermistor, and for the small temperature changes used, the nonlinearities were negligible. The other arms of the bridge were a 4- and a 6-dial resistance box. In any measurement only the lowest three dials of the 6-dial box (smallest step 0.01 ohm) were moved and these were calibrated to 0.0001 ohm. A Keithley 150 B amplifier and a recorder were used to interpolate resistance changes to 0.001 ohm, corresponding to about 5×10^{-6} deg. With 0.1 mA in each thermistor the amplifier was set so that 0.001 ohm corresponded to about 1 mm on the chart which could be easily determined in the normal noise level.

The calorimeter was calibrated with a 200-ohm electric heater using a constant current source and measuring the voltage across the heater directly with a Fluke 8300 digital voltmeter while the current was determined from the potential across a 100-ohm standard resistor. The Monsanto 100A quartz crystal timer was activated with a rotary leaf switch in parallel with the heater current switch.

The calorimeter was finally checked by comparing the heats of dilution for NaCl solutions of Young[3] and Machin with those obtained presently. The results shown in Figure 1 are within 0.3% at the higher concentration and 1% at the lower concentration which is regarded as satisfactory.

The LiCl and LiBr were the same materials previously used in the density measurements. The LiI was prepared from reagent grade Li_2CO_3 and freshly distilled HI, and the solution obtained after boiling and final neutralization with LiOH was used as a stock solution without crystallizing or drying. The NaCl used was commercial reagent grade although the samples used for the first three NaCl (preliminary) runs were from previously opened laboratory bottles which might have been of questionable purity. In any case, these bottles indicated an assay of 99.5% compared with 99.9% for the fresh bottle used for the last three runs.

The initial salt solutions were prepared gravimetrically and analyses of the initial and final solutions were

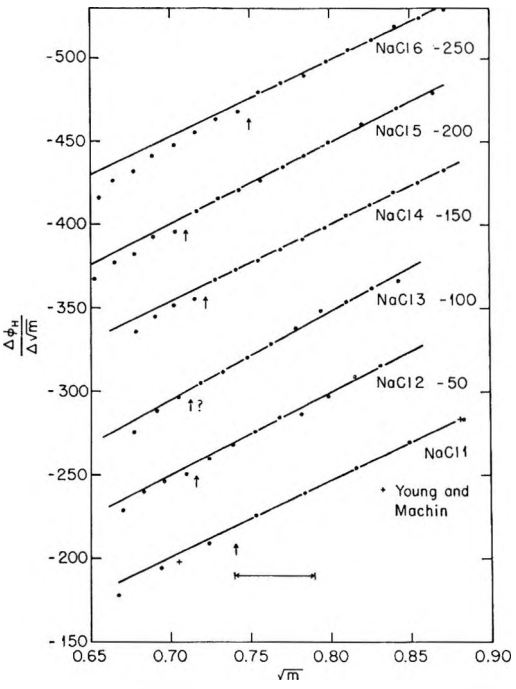

Figure 1. $\Delta\phi_H/\Delta\sqrt{m}$ for NaCl: +, Young and Machin.[3]

made either by weighing dried residues or by density using previously published values.[2,6]

For each run about 550 cm³ of the salt solution was weighed into the calorimeter with a weight buret. For each dilution 20 cm³ of water was weighed into the pipet and the pipet was placed into the calorimeter for 1 hr before opening, with a final drift rate of less than 2×10^{-4} deg/hr. The drift rate generally became linear within 2 min after opening the pipet and was usually followed for 10 min.

Two electrical calibrations were made for each dilution, each of 20-sec duration (reading to 0.001 sec) and about 3.0 cal corresponding to a 1.1 ohms change on the balancing resistor. The average difference between the two calibrations for a dilution was 0.12% (*i.e.*, 0.0036 cal) and, on normalizing all the calibrations for a given run, by dividing by the weight of water at each point, the average deviations from the means were about 0.07%.

After the calibrations the pipets were closed and removed and replaced with a fresh pipet containing water. The amount removed was determined by weighing and between 10 and 20 dilutions were made in each run. Solution concentrations during the run were calculated from the initial quantities and the material balance; however, analysis of the final solutions agreed with the calculated values to 0.2% or better.

The estimated error is based on a precision in reading the chart of ±1 mm or ±0.0025 cal. In addition, the heat of the pipet opening ranged between 0.0125 and 0.0175 cal or 0.015 ± 0.0025 cal. The combined un-

(6) F. Vaslow, *J. Phys. Chem.*, **70**, 2286 (1966).

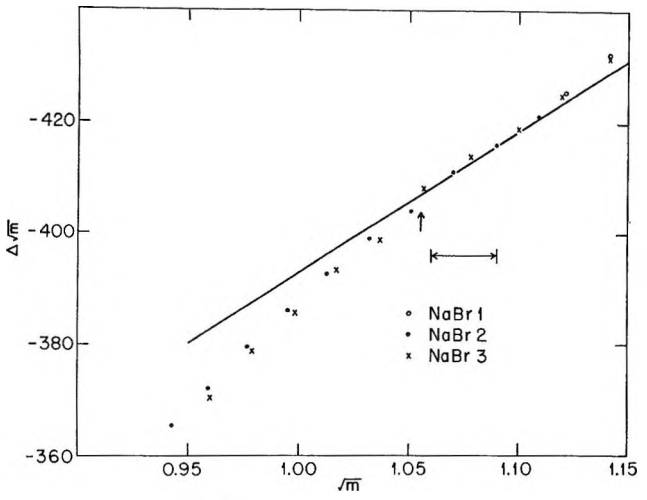

Figure 2. $\Delta\phi_H/\Delta\sqrt{m}$ for NaBr.

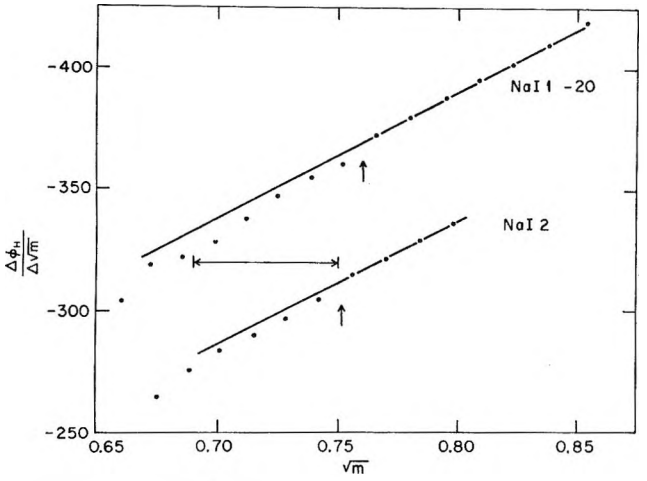

Figure 3. $\Delta\phi_H/\Delta\sqrt{m}$ for NaI.

certainty was taken as ±0.0040 cal or about ±1.5 mm on the chart reading. Other nonsystematic errors were probably contributed by an occasional very high electronic noise level in the laboratory, some sharp fluctuations in room temperature, and inefficient stirring when there were large differences in density between the calorimeter solution and pure water in the pipet.

The heats of dilution range from about ±7 cal (+ for Li, − for Na) to about ±0.3 cal, so that the estimated uncertainties in the heat evolution were of the order of less than 0.1% at the highest concentration to 1% at the lowest concentration.

Results

Each measured heat value $\Delta\phi_H$ on a per mole salt basis divided by the value of $\Delta\sqrt{m}$ (the change in root molality of the dilution) is the average value of the slope for the variation of the apparent molal heat content with $\sqrt{m}$, over the interval. These average values are plotted as points at the center of the interval with $\sqrt{m}$ as the abscissa and are shown in Figures 1 to 6 for salts NaCl, NaBr, NaI, LiCl, LiBr, and LiI, respectively. With the exception of the NaBr curves the different runs are shown displaced from one another rather than superimposed. Shown on the NaCl-1 curve are the two points from Young and Machin[3] which overlap the present work.

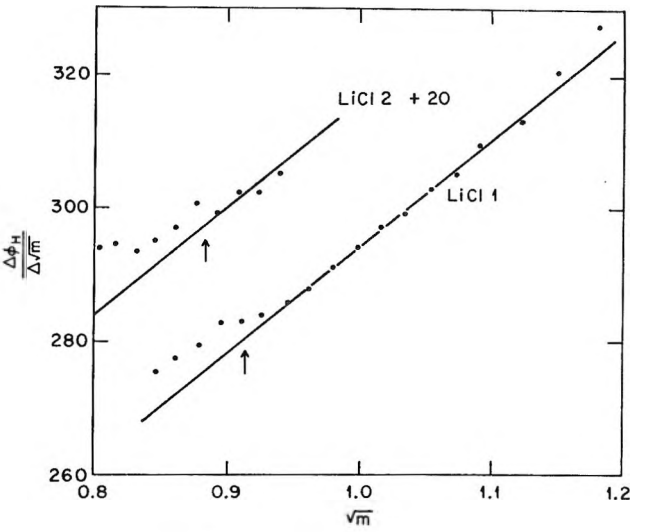

Figure 4. $\Delta\phi_H/\Delta\sqrt{m}$ for LiCl.

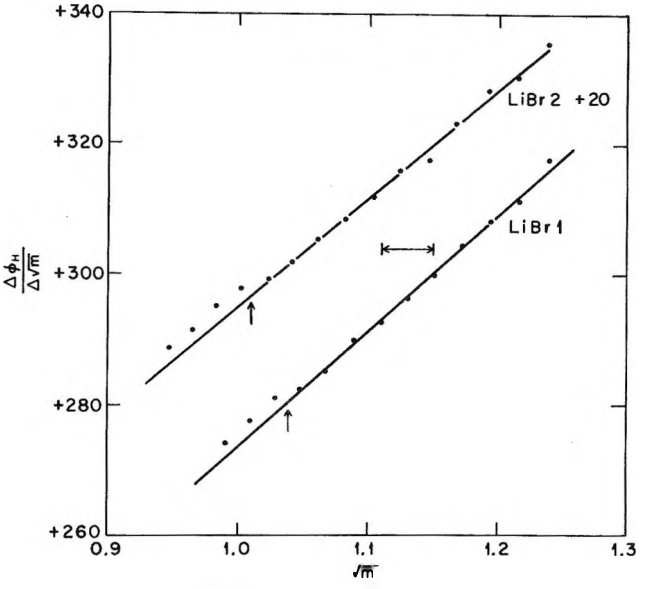

Figure 5. $\Delta\phi_H/\Delta\sqrt{m}$ for LiBr.

The lines drawn through the points and the vertical arrows indicate what appears to be a discontinuity or displacement of one part of each curve relative to another. The horizontal arrows indicate the position of a chord in the volume measurements where an anomaly appeared to exist. It should be noted that the ordinates for the Na salt curves are negative so that the displacements shown have the same sign for both the Li and Na curves and also that NaCl-1, -2, and -3 are considered as preliminary curves with less weight than the later three curves. Also in NaCl-1, 40-cm³ dilutions were used and the resolution is lower than that of

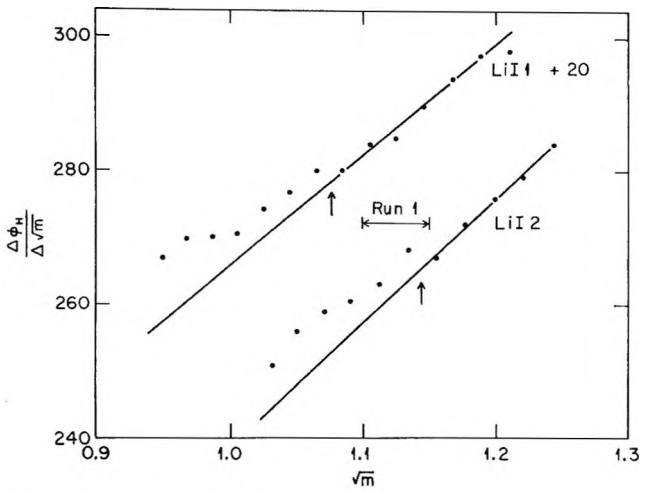

Figure 6. $\Delta\phi_H/\Delta\sqrt{m}$ for LiI.

the other curves. Comparisons of the data with previous work are limited to the two points of Young and Machin where the agreement is excellent. Data calculated from integral heats of dilution of LiCl[7] are also in agreement but only very crude estimates can be obtained from the integral heats.

The curves shown in Figures 1 through 6 are short segments of the extended concentration range curves such as that shown by Young and Machin for NaCl or that can be calculated from integral data for LiCl. These extended curves are rather close to parabolas with a theoretical zero intercept of +459[8] for all the curves and a minimum of about +260 at $\sqrt{m} = 0.7$ for LiCl and −400 at $\sqrt{m} = 1.4$ for NaCl. The other salts are similar with the bromides and iodides being successively more negative.

For NaCl-1 eight more points were determined not shown in Figure 1, going up to 1.2 m and conforming closely to the Young and Machin interpolated curve. Complete detailed results of the heat measurements are available on microfilm.[9]

Discussion

As in the earlier papers of this series,[2,6,10] the major problem of the discussion is a consideration of whether the anomalous behavior suggested is real and physically significant or a matter of artifact and random experimental variations. There are variations in the magnitude and position of the effect for a given salt and also some deviations of the points from a smooth curve are ascribed to physical effect, while others of a comparable magnitude are ascribed to error. Consequently, no claim of proof of the effect can be considered yet; nevertheless, simple statistical arguments concerning the consistency and form of the curves will be given, suggesting at least a strong probability that the existence of anomalies is a valid interpretation of the data.

In order to test whether the division of the curves indicated by Figures 1 through 6 is statistically justified, polynomials from the second to the fifth degree have been fitted by least-squares procedure to the complete curves and linear and quadratic expressions to each of the separate segments. For the least-squares procedure, points based on temperature changes equivalent to 0.5 ohm or larger have been weighted unity and points with smaller temperature changes are weighted in proportion to 0.5. All of the points for the Li^+ salts are correspondingly given unit weights while the Na^+ points range from unity at about $\sqrt{m} = 0.85$ down to 0.3 at the lowest concentrations.

The optimum total number of parameters in either the one- or two-segment fits has been determined by minimizing the expression $\Sigma(y_0 - y)^2/(n - p)$, *i.e.*, the Gauss criterion,[6,11] where y_0 is the calculated $\Delta\phi_H/\Delta\sqrt{m}$, y is the observed value, n is the total number of points, and p is the total number of parameters which for the two-segment fits is the sum of the parameters for each segment. The results of this analysis are shown in Table I for the minimum value of the Gauss criterion for either method of fitting.

Table I: Sums of Squares of Deviations for Various Fits of Curves

Run	No. of points	No. of parameters	1-Section $\Sigma(y_0 - y)^2$	2-Section $\Sigma(y_c - y)^2$	Quadr. $\Sigma(y_0 - y)^2$
NaCl-1	18	6	5.6	8.1	17.2
NaCl-4	15	5	7.3	3.0	9.4
NaCl-5	15	5	12.0	9.4	12.7
NaCl-6	18	5	13.9	15.6	23.3
NaBr-2	13	5	7.2	5.9	7.6
NaBr-3	10	5	0.98	0.89	1.16
NaI-1	15	5	9.8	3.9	10.4
NaI-2	10	5	2.7	2.3	4.7
LiCl-1	18	6	8.5	5.6	10.3
LiBr-1	13	5	4.9	3.6	5.6
LiBr-2	14	5	4.9	3.2	5.8
LiI-1	14	5	12.8	10.3	14.5
LiI-2	11	4	9.3	4.5	12.4

The table shows the number of points for each experiment, the number of parameters for the best fit, and the sum of the squares of the deviations for the one- and two-section fits with minimum Gauss parameter and also, for comparison, the quadratic fit of the full curve. The LiCl-2 curve was omitted since it has

(7) E. Lange and F. Dürr, *Z. Phys. Chem.*, 121, 361 (1926).

(8) G. N. Lewis and M. Randall, "Thermodynamics," revised by K. S. Pitzer and L. Brewer, McGraw-Hill, New York, N. Y., 1961.

(9) Complete tables of the experimental heat measurements will appear immediately following this article in the microfilm edition of this volume of the Journal. Single copies may be obtained from the Reprint Department, ACS Publications, 1155 Sixteenth St., N.W., Washington, D. C. 20036. Remit check or money order for $4.00 for photocopy or $2.00 for microfiche.

(10) F. Vaslow, *J. Phys. Chem.*, 71, 4585 (1967).

(11) A. G. Worthing and J. Geffner, "Treatment of Experimental Data," Wiley, New York, N. Y., 1943.

apparently only one point of the upper part of the curve and although two of the preliminary NaCl curves were omitted, NaCl-1 was included since it covers a considerably larger concentration range than any other NaCl curve. The distribution of the points between the segments and the type of expression for each segment are fairly obvious from the figures and the total number of parameters.

It is seen that of the 13 curves, in 11 of them the two-segment fit is the better one and in some cases markedly so. Of the two exceptions, that for NaCl-1 clearly justified a six-parameter fit indicative of complex behavior and also the longer chords tend to smooth the presumed discontinuity. NaCl-6 does have the same appearance as the other curves and aside from the large error level there is no apparent reason why it has given different results.

Another type of test can be applied by considering just the upper segment of any curve and the deviation from this curve of the point at the left of the discontinuity. With the exception of NaCl-1, which required a quadratic expression, these upper portions are all linear for the Na salts and the deviations from these lines at the discontinuity can be compared with the standard deviations in the curves. For NaCl-6 the deviation at the jump is 4.9 times the standard deviation and for the other Na salts the ratios range from 3 to 6.

These consistently large ratios are clearly outside of any normal behavior and again indicate the probability of some sort of transition. Since the long-range behavior of the NaCl curves is known to be close to a parabola,[3] the linear sections in themselves are anomalous and appear to represent a small upward inflection of the curves.

The possibility of experimental artifact would not appear to be strong since the direction of the jump is the same for curves involving both *endo-* or *exo*thermic processes and the jump occurs over a variety of concentrations for the different salts.

The results obtained here can also be compared with the previous results from density measurements and this comparison is given in Table II. The table gives the centers of the chords where the transition occurred except for LiCl where the start of the diffuse region is given and for LiI the highest value found is given. Although there are some significant variations, the agreement is generally very good and highly consistent.

Table II: Transition Centers in Volume and Heat Curves

Salt	V, $c^{1/2}$	H, $m^{1/2}$
LiCl	0.9	0.9
LiBr	1.14	1.05
LiI	1.12	1.14
NaCl	0.75	0.73
NaBr	1.07, 1.05[a]	1.05
NaI	0.72	0.75

[a] W. Geffken, A. Kruis, and L. Solana, *Z. Phys. Chem.*, **B35**, 317 (1935).

It was mentioned earlier[2] that if a critical type of transition does occur, the variations might not be unexpected. The heats of the reactions are determined largely within 2 min and this time may be too short for equilibrium if there is a transition.

It should be noted that even for a fixed transition point and transition magnitude, the experimental chords spanning the transition point will show variations depending on the length and position of the chords with respect to the fixed point.

It is impossible to know whether the above explanation is satisfactory or not and consequently there must remain fundamental questions as to the nature of the effects. The effects are also small and difficult to measure, adding to the difficulty of interpretation. In spite of these serious defects, the high degree of consistency of form of these effects and the substantial statistical evidence do indicate a strong probability that a physical transition does occur.

Phase Transitions in Water Adsorbed on Silica Surfaces

by Myron N. Plooster*[1] and Sonia N. Gitlin

National Center for Atmospheric Research, Boulder, Colorado 80302 *(Received October 26, 1970)*

Publication costs assisted by the National Center for Atmospheric Research

Heat capacities of water adsorbed on two nonporous silica powders, which have different water adsorption properties, have been measured calorimetrically. For samples with adsorbed water films up to at least 5 to 7.5 nm in thickness, the adsorbed films undergo a phase transition characterized by a broad maximum in heat capacity which lies entirely below 0°. The temperature and amplitude of the maximum increase with increasing film thickness. Samples with higher water content exhibit a second sharp heat capacity peak at 0°. Heats of transition lie below those for the ice–water transition. The suppression of the transition temperature cannot be described by capillarity theories depending on contact angles. The data are interpreted in terms of an alteration in structure and properties of the adsorbed water by the silica surface, an effect whose magnitude decreases with increasing distance from the surface. The strength of the interaction and the distance to which it extends from the surface increase with an increase in the hydrophilic character of the surface.

Introduction

The structure and properties of physically adsorbed films are usually assumed to approach those of the bulk adsorbate as film thickness increases, with only the first few monolayers being strongly affected by surface forces. The calorimetric study of phase transitions in adsorbed films has proved to be a sensitive tool for investigating the range of interfacial effects. In studies of the nonpolar adsorbates N_2, Ar, and CH_4, adsorbed on rutile, the first one to three monolayers appeared not to exhibit any phase transitions.[2-4] With increasing film thickness, however, broad maxima first appeared in the specific heat of the adsorbed phase at about 10° below the bulk melting point and thereafter rapidly increased in sharpness and approached the bulk melting temperatures. Moreover, the observed heats of transition likewise rapidly approached the heats of fusion of the bulk adsorbates.

For nonpolar adsorbates, the bonding between adjacent layers is almost wholly due to short-range, nondirectional van der Waals' forces. For polar molecules, and especially for those capable of forming strong and directional hydrogen bonds, such as water, it seems probable that ordering effects from a solid surface could propagate through a greater depth of adsorbed film.[5] Direct studies of phase transitions in adsorbed water films to date have been largely confined to work with porous adsorbents, such as porous glass[6] and silica gel.[7]

We present here the results of a calorimetric study of phase transitions in water adsorbed on two nonporous silicas with differing surface properties: Cab-O-Sil, grade M-5, a pyrogenic silica supplied by the Cabot Corp., and Hi-Sil-233, a precipitated silica supplied by PPG Industries, Inc.

Experimental Section

1. Adsorption Measurements. Surface areas of the silicas used here were determined by the BET method, from N_2 adsorption measurements in a standard volumetric adsorption rig. Water adsorption isotherms were obtained gravimetrically using a Worden quartz microbalance connected to a conventional vacuum apparatus.

2. Sample Preparation. The specific surface area of Cab-O-Sil in this work was 190 m^2/g, while that of the Hi-Sil was 133 m^2/g. Assuming a cross-sectional area of 10.5×10^{-20} m^2 for the water molecule, the weights of the statistical monolayer of H_2O, per gram of silica, on these powders are 54 and 38 mg, respectively. Thus, the average depth of surface coverage by water in the multilayer adsorption region can be determined by direct weighing. Samples for calorimetric measurements were prepared by mechanical mixing of bulk water and powder in sealed containers. Sample composition was determined at the end of each run by weighing the sealed calorimeter with the sample, the empty calorimeter, and the silica powder after it was removed from the calorimeter and dried at 110° overnight.

3. Calorimetric Measurements. The calorimeter was of the controlled-heat-flow type, wherein a known temperature difference was maintained between the calorimeter and a surrounding heating element. The calorimeter itself was a thin-walled brass cylinder, 7 mm diameter and 15 mm high, sealed with a tight-fitting

(1) Correspondence should be addressed to Denver Research Institute, Denver, Colo. 80210.

(2) J. A. Morrison, L. E. Drain, and J. S. Dugdale, *Can. J. Chem.*, **30**, 890 (1952).

(3) J. A. Morrison and L. E. Drain, *J. Chem. Phys.*, **19**, 1063 (1951).

(4) K. S. Dennis, E. L. Pace, and C. S. Baughman, *J. Amer. Chem. Soc.*, **75**, 3269 (1953).

(5) J. C. Henniker, *Rev. Mod. Phys.*, **21**, 322 (1949).

(6) G. G. Litvan, *Can. J. Chem.*, **44**, 2617 (1966).

(7) W. A. Patrick and W. A. Kemper, *J. Phys. Chem.*, **42**, 369 (1938).

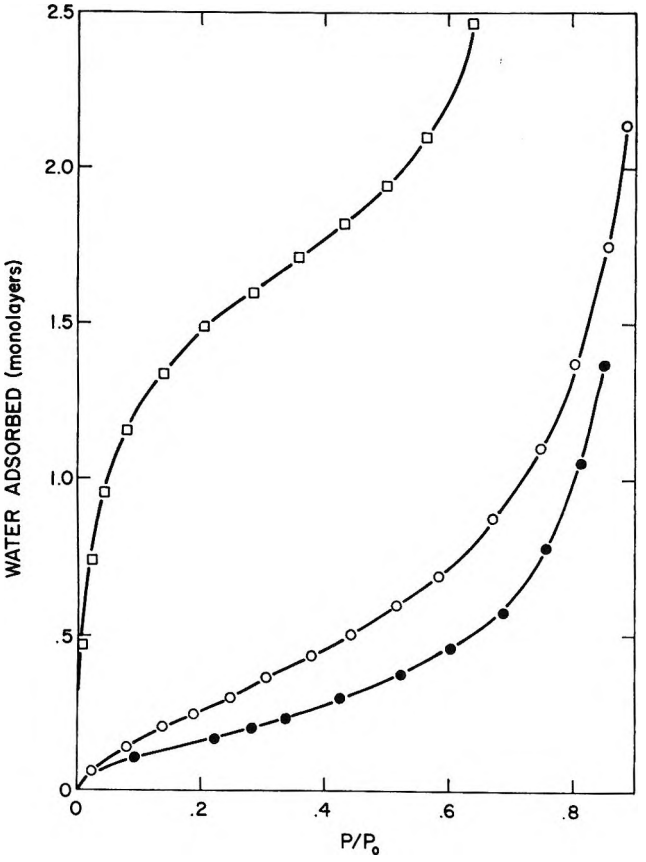

Figure 1. Water adsorption isotherms at 10° on Hi-Sil (□), Cab-O-Sil as received (●), and Cab-O-Sil compacted by slurrying with water and subsequent drying (○). The amount adsorbed is expressed in statistical monolayers, calculated from the BET nitrogen surface area.

plastic cap. The heating element was a copper cylinder 2.5 cm i.d., 2.7 cm o.d., and 25 cm long, evenly wound with nichrome resistance wire. The calorimeter was held at the center of the heating tube in a close-fitting styrofoam holder, and the remaining void spaces in the heating element were also filled with styrofoam. The entire assembly was then mounted in a thick-walled copper cylinder, to minimize longitudinal thermal gradients, and was immersed in a methanol–water cold bath maintained near −50°. The heating rate was controlled by maintaining a constant potential difference between copper–constantan thermocouple junctions in contact with the calorimeter and heater, respectively. The calorimeter temperature was measured with a second thermocouple, referenced to an ice bath. A crystal-controlled time base was used to trigger a printing digital voltmeter at regular time intervals to record the emf of this thermocouple. From the resulting curves of temperature *vs.* time, the heat capacity of the calorimeter and its contents as a function of temperature was derived. The calorimeter was calibrated with aluminum oxide, using the heat capacity data of Ginnings and Furukawa.[8]

The accuracy and reproducibility of the calorimetric

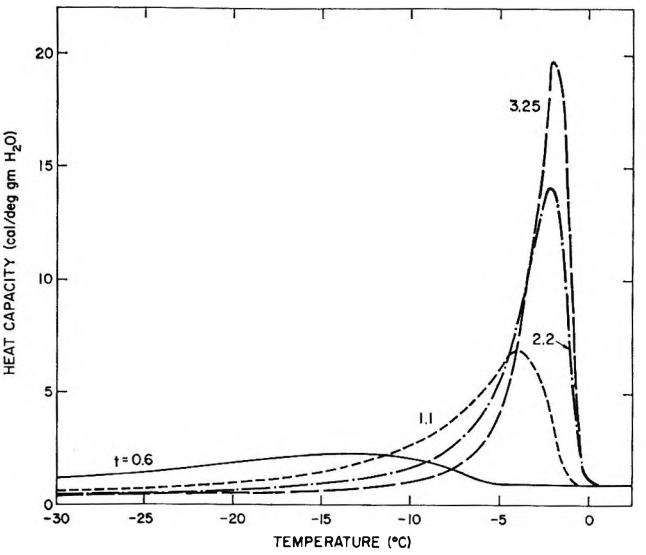

Figure 2. Specific heat of water adsorbed on Cab-O-Sil, *vs.* temperature, for indicated values of adsorbed film thickness t (nm).

data varied inversely with the water content of the sample. The integrated enthalpy change of the calorimeter and its contents was reproducible to ±1% in repeated runs on a given sample. For the samples with lowest water content used here, the heat capacity of the water was about 10% of the total heat capacity, so that the probable error in this parameter was of the order of ±10%. For samples of high water content, errors in calorimetric data and in sample composition combined to give a total probable error of ±3% in heat capacity data. Temperatures were accurate to within ±0.25° at 0°, the error being largely due to long-term drift in the thermocouple amplifier; short-term drift appeared to be less than 0.5 μV, corresponding to a temperature change of about 0.01°.

Results and Discussion

Surface Properties of Silicas. The surface of Hi-Sil-233 is hydrophilic. Hi-Sil is a precipitated silica, and its surface is fully hydroxylated; *i.e.*, every Si surface atom bears a hydroxyl group. The Cab-O-Sil surface, on the other hand, is not fully hydroxylated, and a substantial fraction of the surface is hydrophobic. Hi-Sil exhibits a surface area to water adsorption which is about 1.3 times the N_2 surface area, assuming areas of 10.5 and 16.2 × 10^{-20} m^2 per molecule of H_2O and N_2, respectively. The apparent surface area of Cab-O-Sil for water adsorption is much lower, lying between 0.15 and 0.25 times its N_2 surface area. The lower figure is typical of the low bulk density powder as received from the manufacturer. In some of our experiments, its bulk density was increased (by over a factor of 10) by slurrying the powder in water and

(8) D. C. Ginnings and G. T. Furukawa, *J. Amer. Chem. Soc.*, **75**, 522 (1953).

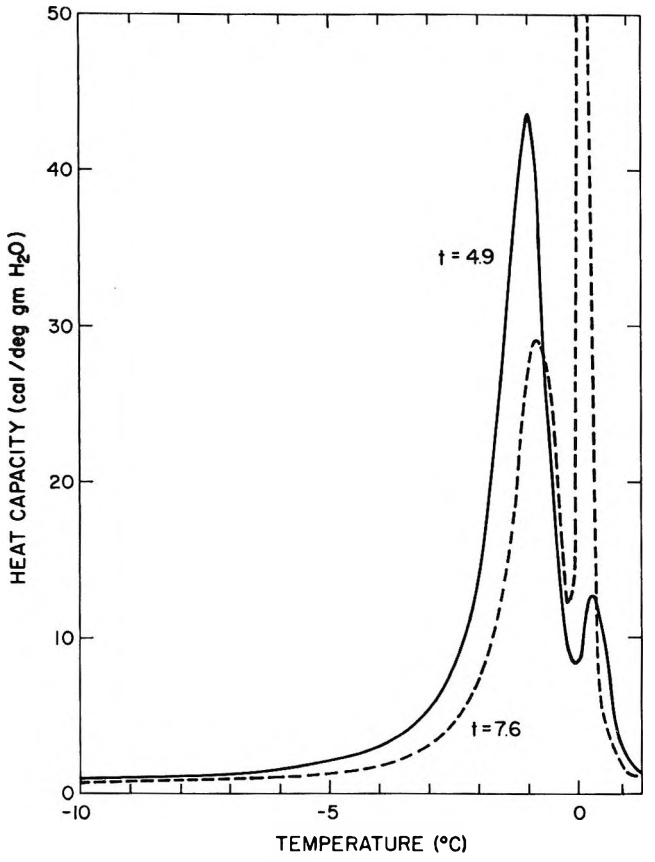

Figure 3. Specific heat of water adsorbed on Cab-O-Sil *vs.* temperature, for high values of adsorbed film thickness t (nm).

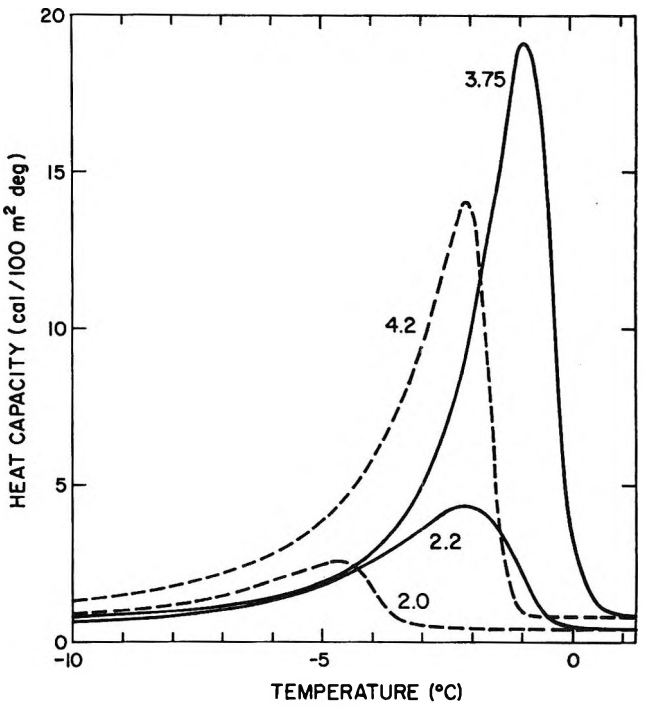

Figure 4. Heat capacities of water adsorbed on Cab-O-Sil (solid curves) and Hi-Sil (dashed curves), per 100 m^2 surface area, *vs.* temperature, for indicated values of adsorbed film thickness t (nm).

subsequently drying it at 110°. This powder is more hydrophilic. Figure 1 shows water adsorption isotherms for Hi-Sil and for both the treated and untreated Cab-O-Sil powders.

From our surface area measurements and the particle densities quoted by the manufacturers (2.2 and 2.0 g cm^{-3} for Cab-O-Sil and Hi-Sil, respectively) the respective average particle radii were found to be 7 and 11 nm. In the following, the quantity of water adsorbed is given in terms of the thickness, t, of the adsorbed layer, calculated by assuming that the particles are spherical and that the water forms a concentric spherical shell of unit density around each particle. This gives a lower limit to the true film thickness, since aggregation of particles will displace some of the adsorbed film to greater distances from their surfaces.

Heat Capacity of Adsorbed Water. The heat capacity *vs.* temperature curves for water adsorbed on both Hi-Sil and Cab-O-Sil were similar. A broad maximum in heat capacity first appeared near −14° for coverages of about two monolayers ($t \approx 0.6$ nm). As coverage increased the maxima increased in amplitude and sharpness. The temperature at the peak also increased, but did not approach 0° in a continuous manner. At film thicknesses near 5 nm for Cab-O-Sil and 7.5 nm for Hi-Sil, the heat capacity peaked near −1° and had fallen to a value near unity at 0°. With addition of still more water, a second very sharp peak was observed at 0°, corresponding to the bulk phase transition. Figure 2 shows heat capacity curves for water adsorbed on Cab-O-Sil for $t \leq 3.25$ nm, while the appearance of the second peak at higher coverages is shown in Figure 3. For both Cab-O-Sil and Hi-Sil, the second heat capacity peak appears at H_2O/SiO_2 mass ratios near 1.8–2. (Interestingly, the appearance of the peak at 0° coincides with the onset of visual evidence of water in the samples. Cab-O-Sil mixed with less than twice its weight of water behaves as a free-flowing powder; only at higher water concentrations does the mixture exhibit gellike properties.)

Hi-Sil appears more effective than Cab-O-Sil in suppressing the amplitude and temperature of the heat capacity maxima. Figure 4 shows two pairs of heat capacity curves for the two silicas, taken at comparable values of t. The heat capacities are expressed in calories per degree per 100 m^2 surface area to correct for the difference in specific area of the two silicas. The lower amplitudes and peak temperatures shown in Figure 4 for water adsorbed on Hi-Sil persist to higher coverages.

Heats of Transition. The observed broad maxima in the heat capacities of water on silica obviously represent diffuse first-order transitions, in the nomenclature of Mayer and Streeter.[9] The second sharp peak, observed at 0° at high water coverages, corresponds

(9) J. E. Mayer and S. F. Streeter, *J. Chem. Phys.*, 7, 1019 (1939).

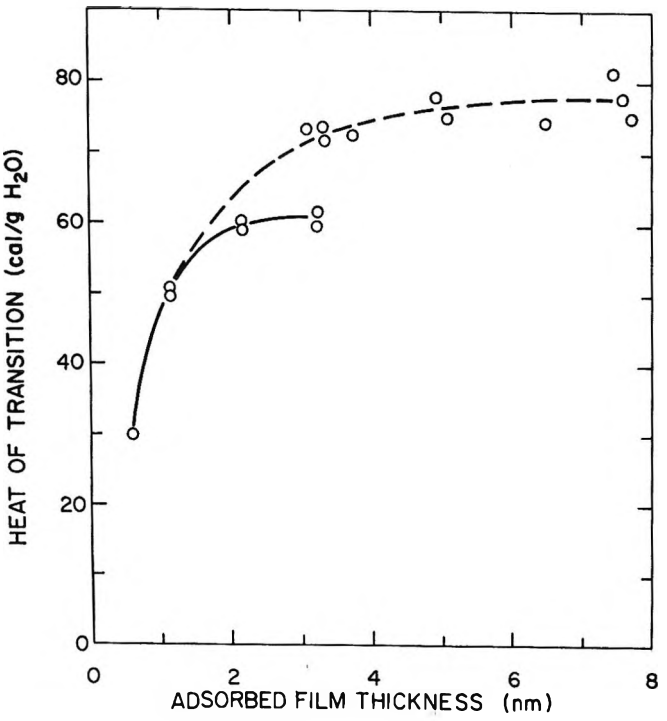

Figure 5. Heats of transition of water adsorbed on Cab-O-Sil *vs.* adsorbed film thickness t; samples prepared from uncompacted powder (solid curve) and from compacted powder (dashed curve).

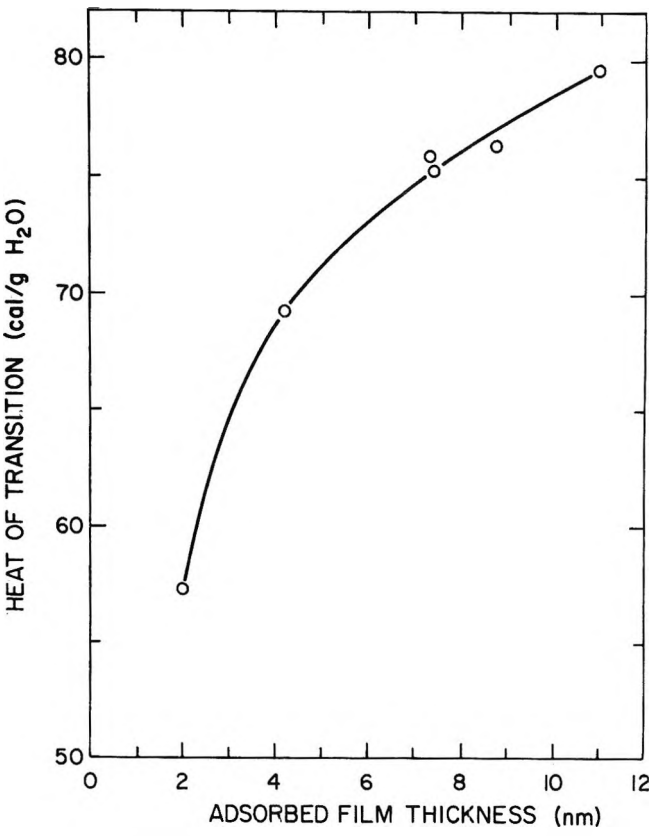

Figure 6. Heats of transition of water absorbed on Hi-Sil *vs.* adsorbed film thickness t (nm).

to the normal first-order transition. The heat of transition for the diffuse transition cannot be determined unambiguously, since we do not know the true heat capacities of the adsorbed films. We have arbitrarily defined a total heat of transition, ΔH_t, as the integral of the total heat capacity of the adsorbed layer between -25 and $+5°$, less the integrated heat capacities of bulk ice between -25 and $0°$ and of liquid water above $0°$. This method probably gives an upper limit to the true heat of transition, since it neglects the fact that the proportion of the high-temperature, disordered phase increases as the sample warms. The error is probably small for high t values, but may be as large as 10 cal g^{-1} at low coverages.

The heats of transition of water on Cab-O-Sil and Hi-Sil are shown in Figures 5 and 6, respectively, plotted as functions of t. In all cases, it is seen that the heats of transition lie well below that for the ice–water transition until the film thickness is large.

The discontinuity in the data for Cab-O-Sil in Figure 5 appears to be due to a change in sample preparation technique. The data at low coverages were obtained using Cab-O-Sil powder as received from the manufacturer, and lie along the solid curve in Figure 5. The data at high t values were taken using powder whose bulk density was increased by slurrying with water and subsequent drying, as described above. These points lie on the dashed curve in Figure 5. The scatter in these points reflects variations in sample properties; the internal consistency of the data obtained using the powders in their original state is shown by the points along the solid curve in Figure 5 and by all the data obtained on H-Sil samples.

Interpretation of Results. Our data show that silica powders suppress the temperature and heat of transition of water adsorbed thereupon, that this effect persists to distances of the order of 20 molecular diameters from the particle surfaces, and that the magnitude of the effect varies with the hydrophilic character of the surfaces and with the bulk density of the powders.

The dependence on surface properties is easily understood. The Hi-Sil surface, which is fully hydroxylated, affords opportunity for each adsorbing H_2O molecule to form multiple hydrogen bonds to surface silanol groups. Since hydrogen bonds to water molecules are highly directional, the position and orientation of the molecules in the first monolayer will be strongly determined by the silica surface. This layer will then also influence the structure of the next layer, and one can visualize a surface-dependent structure persisting to a considerable distance from the surface itself. The Cab-O-Sil surface, on the other hand, is not fully hydroxylated, and contains numerous isolated silanol groups. Water molecules adsorbed on these sites retain a greater degree of freedom. The structuring influence of the surface in this case would be expected to be less pronounced, an expectation which is borne out by the data.

All our results are consistent with a simple model in which the transition temperature of each layer of adsorbed water is a function only of its distance from a silica surface. Layers close to a surface become disordered (in the sense of melting) at the lowest temperature, and as temperature increases the phase boundary moves radially outward. The specific enthalpy of transition also increases, approaching the bulk value, with increasing distance from the particle surface. Each particle can thus be considered as the center of a sphere of influence, the magnitude of the influence decreasing with increasing radius.

The behavior of water adsorbed on Cab-O-Sil powders of different bulk densities follows from this model. In the low density state in which Cab-O-Sil is supplied, the individual particles are sintered together to form very open, chainlike aggregates with large void spaces between chains. The result of powder compaction is to reduce the effective volume of each particle's sphere of influence due to the intrusion of neighboring particles. At the higher water coverages used in this work (where the volume of the adsorbed water considerably exceeds the volume of the silica particles themselves) compaction of the powder displaces some of the water to a greater distance from the particle surfaces, where the influence of the surface will be smaller. Figure 7 shows specific heat curves for two samples, one using the low-density Cab-O-Sil powder and the other using compacted powder. For both these samples, the water/silica mass ratio was near unity. The two curves are practically coincident below -6 and above 0°. Between -6 and $-2°$, the heat capacity curve for water on the compacted powder lies below the other curve, reflecting the decreased volume available for adsorption near the particles. This water is displaced to regions farther from the particles, where its transition temperature and heat of transition are higher, thus giving rise to the higher heat capacity peak above $-2°$.

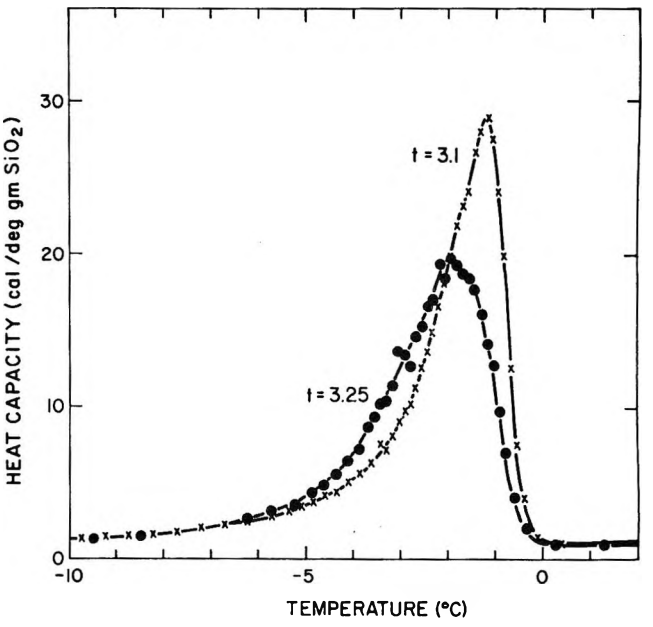

Figure 7. Comparison of heat capacity curves for water adsorbed on uncompacted Cab-O-Sil (●) and a compacted powder (×).

These results cannot be interpreted in terms of a capillary freezing process, characterized by a contact angle between phase boundary and substrate, in the pores between powder particles. In such a process, if the transition temperature is depressed by the pore walls, it should continue to decrease as the particles comprising the walls move closer together. The dependence of transition temperature on powder density observed here is precisely the opposite.

Acknowledgment. The authors acknowledge the contribution of C. L. Frush and C. M. Wyman in the design and construction of the calorimeter and in gathering the experimental data. The National Center for Atmospheric Research is sponsored by the National Science Foundation.

Location of Univalent Cations in Synthetic Zeolites of the Y and X Type with Varying Silicon to Aluminum Ratio. I. Hydrated Potassium Exchanged Forms

by W. J. Mortier* and H. J. Bosmans

Laboratorium voor Oppervlaktescheikunde, De Croylaan 42, 3030 Heverlee, Belgium *(Received May 4, 1971)*

Publication costs borne completely by The Journal of Physical Chemistry

The structure of four potassium-exchanged synthetic X and Y zeolite powders, with varying Si:Al ratio (2.98, 2.51, 1.75, and 1.22), were studied using X-ray diffraction. The main purpose of the study was the location of the exchangeable cations and the occupancy of the different sites in the hydrated state. The total population of the sites I and I′ was about one-fourth of the exchangeable cations and the occupancy of site I′ decreased with increasing Al content, while the population of the sites I and II accordingly increased. A fraction of the cations could not be located. Liquid scattering functions were used in order to take in account the unlocated scattering matter (water molecules and some cations). A comprehensive discussion on the cation distribution is given, including the discussion of a possible site III′ in the large cage, formed by two O_1 and two O_4 oxygens.

Introduction

Much research has been performed on zeolites, particularly on faujasites, attempting to explain the interesting properties of these minerals, in the field of ion exchange, molecular sieve properties, catalysis, etc. An interpretation of their properties relies to a large extent on a precise description of structural features such as framework parameters, size of apertures and cages, cation location and occupancy of sites, and even the location of water molecules.

The structure of faujasite (Figure 1) was first described by Bergerhoff, Baur, and Nowacki.[1] They studied a natural hydrated crystal with a Si:Al ratio of about 2.3 saturated mainly with Na^+ and Ca^{2+} ions. Since then, several structure determinations were made on natural faujasites, and also on the synthetic isotypes, the molecular sieves Linde X (Si:Al $\simeq$ 1.25) and Y (Si:Al between 2.2 and 3) zeolites, exchanged with univalent, divalent, or trivalent cations. Only a few studies on natural or synthetic faujasites in the hydrated form and exchanged with univalent cations are present in the literature. Broussard and Shoemaker[2] studied a synthetic NaX powder, whereas Baur[3] reinvestigated the structure of the previously mentioned faujasite crystal in order to locate better the cations and the water molecules. The composition of this sample was close to that of synthetic Y. Data of hydrated Y saturated with monovalent ions are not available. Recently, Olson[4] investigated a hydrated synthetic NaX monocrystal. These four samples represent two different Si:Al ratios. Although they have the same framework structure, they show a difference in cation location.

Therefore it seemed important to us to study systematically the cation location and the occupancy of the different cation sites on a series of synthetic faujasite samples with varying Si:Al ratio, saturated with univalent cations. Potassium exchanged faujasites were preferred over sodium faujasites, since more accurate occupancy factors could be expected for the material containing the higher atomic number cation. Sodium faujasites can be converted into the pure potassium form.[5]

Experimental Section

Four synthetic Na faujasites with a chemical composition ranging from the extreme Y to extreme X type were kindly supplied by the Linde Co. Chemical analysis of these samples in the Na form, and equilibrated to a constant weight in a 32% water-saturated atmosphere ($CaCl_2$ solution) at room temperature, is given in Table I. The analytical methods followed were mainly those described by Voinovitch, *et al.*[6] One of the samples was analyzed a second time because of its less reliable results. By comparison, an error estimate of the analyses can be made. The structural formulas are given in Table II together with the calculated Si:Al and water:cation ratios. The name indicated

(1) G. Bergerhoff, W. H. Baur, and W. Nowacki, *Neues Jahrb. Mineral., Monatsh.*, 193 (1958).

(2) L. Broussard and D. P. Shoemaker, *J. Amer. Chem. Soc.*, **82**, 1041 (1960).

(3) W. H. Baur, *Amer. Mineral.*, **49**, 697 (1964).

(4) D. H. Olson, *J. Phys. Chem.*, **74**, 2758 (1970).

(5) H. S. Sherry, *ibid.*, **70**, 1158 (1966).

(6) I. A. Voinovitch, J. Debras-Guédon, and J. Louvrier, "L'Analyse des Silicates," Hermann, Paris, 1962.

Table I: Chemical Analysis of the Original Samples

	Two analyses Sample KF 48.2		Sample KF 54.7	Sample KF 69.8	Sample KF 86.5
H_2O grav	24.93	25.06	25.42	25.15	25.58
SiO_2 grav[a]	48.56	48.86	45.97	40.42	33.61
SiO_2 color.[a]	0.78	0.75	2.29	1.87	1.34
Al_2O_3 grav[a]	13.91	14.06	16.24	20.39	24.23
Fe_2O_3 color.[a]	0.22	0.18	0.13	0.14	0.04
CaO titr[b,c]	0.72	0.48	0.62	0.61	0.67
K_2O fl phot[b]	0.03	0.06	0.06	0.26	0.17
Na_2O fl phot[b]	10.38	9.67	9.00	11.25	14.00
Total	99.53%	99.12%	99.73%	100.09%	99.64%

[a] After fusion with a Na_2CO_3–K_2CO_3 mixture. [b] After dissolution with a HF–H_2SO_4 solution. [c] The sum (CaO + MgO) was titrated with EDTA and calculated as CaO.

Table II: Chemical Composition of the Original Samples

Sample	Structural formula of the original Na samples	Si:Al ratio	H_2O:Na ratio	a_0 value of the K sample, Å
F 48.2	$Na_{48.2}Al_{48.2}Si_{143.8}O_{384}\cdot 243H_2O$	2.98	5.04	24.692 (4)
F 54.7	$Na_{54.7}Al_{54.7}Si_{137.3}O_{384}\cdot 241H_2O$	2.51	4.41	24.731 (2)
F 69.8	$Na_{69.8}Al_{69.8}Si_{122.2}O_{384}\cdot 247H_2O$	1.75	3.54	24.920 (2)
F 86.5	$Na_{86.5}Al_{86.5}Si_{105.5}O_{384}\cdot 258H_2O$	1.22	2.98	25.116 (2)

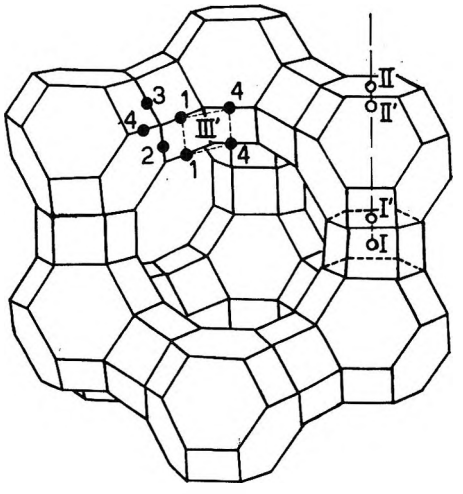

Figure 1. Faujasite framework and cation site indication.

in that table and used throughout the text includes the number of cations per unit cell. F 54.7 and F 86.5 are the conventional Y and X samples, respectively. A 5-g sample of each was stirred during 24 hr in 200 ml of a 2 *M* KCl solution and, after centrifugation, again twice for 24 hr in 200 ml of a 1 *M* KCl solution. The excess of salt was removed by three subsequent washings with distilled water. Chemical analysis of potassium and sodium by flame photometry after dissolution of the samples with a HF–H_2SO_4 solution gave the following Na_2O/K_2O ratios: 0.014 (KF 48.2), 0.011 (KF 54.7), 0.013 (KF 69.8), and 0.025 (KF 86.5). This means an almost complete saturation of the samples by potassium. The unit cell parameters a_0 for the potassium-saturated samples are also given in Table II. These were obtained by plotting about 20 a_0 values, calculated from the strongest CuKα_1 (λ 1.54050 Å) diffracted peaks, against $\cos^2\theta/\sin\theta$ and by extrapolating to $\theta = 90°$.[7] The diffractometer was carefully adjusted before with a Si powder as standard.

Recording the diagram at high resolution, only a trace of Barrer's P1 zeolite could be identified in three of the samples (F 48.2, F 54.7, and F 69.8). The other diffracted peaks for each sample fitted a cubic cell and the extinctions agreed with the space group *Fd3m* (no. 227) or with the less symmetric space group *Fd*3 (no. 203). We always used *Fd3m*, because lowering of the symmetry increases the number of atomic parameters, which seemed to us less favorable, taking into account that the information was obtained from powder diagrams.

The peak intensities were estimated from the weights of paper cuts, made in tracing paper. Unobserved intensities were taken as $I_{min}/2$. It was found that much better agreement was obtained by averaging several measurements. The intensities of four recordings were averaged.

With the given slit system, the radiation at 2θ less than 8° partially fell outside the sample holder used (38 mm × 11 mm × 3 mm). The intensity of the first diffracted peak ($2\theta \approx 6°$) was multiplied by a factor taking into account the part of the beam falling

(7) W. Parrish, J. Taylor, and M. Mack, *Advan. X-Ray Anal.*, 7, 66 (1964).

Table III: Hydrated Potassium Faujasites: Atomic Parameters[a]

		KF 48.2	KF 54.7	KF 69.8	KF 86.5
(Si,Al)	x	0.1245 (2)	0.1254 (2)	0.1251 (2)	0.1232 (2)
	y	0.9458 (2)	0.9454 (2)	0.9463 (2)	0.9459 (2)
192 (i)	z	0.0362 (2)	0.0367 (2)	0.0350 (2)	0.0363 (3)
	B, Å^2	1.88 (0.13)	1.86 (0.13)	1.86 (0.12)	2.08 (0.17)
O_1	$x = -y$	0.1089 (11)	0.1089 (9)	0.1084 (9)	0.1076 (15)
	z	0.0	0.0	0.0	0.0
96 (h)	B, Å^2	5.58 (0.51)	4.01 (0.39)	5.16 (0.41)	8.06 (0.71)
O_2	$x = y$	0.2503 (9)	0.2498 (10)	0.2525 (7)	0.2491 (13)
	z	0.1383 (6)	0.1409 (6)	0.1407 (5)	0.1386 (8)
96 (g)	B, Å^2	1.79 (0.37)	3.78 (0.37)	1.78 (0.29)	4.53 (0.50)
O_3	$x = y$	0.1753 (8)	0.1738 (7)	0.1738 (7)	0.1771 (7)
	z	0.9666 (6)	0.9652 (5)	0.9658 (5)	0.9622 (6)
96 (g)	B, Å^2	1.12 (0.34)	0.0 (0.29)	1.77 (0.30)	0.0 (0.36)
O_4	$x = y$	0.1782 (10)	0.1802 (8)	0.1799 (9)	0.1797 (12)
	z	0.3268 (7)	0.3268 (6)	0.3246 (6)	0.3234 (9)
96 (g)	B, Å	3.13 (0.43)	1.84 (0.32)	4.23 (0.39)	5.05 (0.59)
K(I)	$x = y = z$	...	0.0	0.0	0.0
	occupancy	...	0.0834 (48)	0.4391 (309)	0.5572 (357)
16 (c)	B, Å^2	...	10.59 (8.35)	8.71 (1.24)	4.69 (0.95)
K(I′)	$x = y = z$	0.0820 (22)	0.0802 (20)	0.0784 (23)	0.0736 (51)
	occupancy	0.4260 (221)	0.4144 (206)	0.3754 (214)	0.2236 (275)
32 (e)	B, Å^2	3.79 (0.39)	3.82 (0.67)	6.02 (0.85)	6.08 (1.98)
K(II)	$x = y = z$	0.2570 (12)	0.2574 (11)	0.2559 (8)	0.2523 (10)
	occupancy	0.5563 (172)	0.6289 (177)	0.7578 (144)	0.7237 (190
32 (e)	B, Å^2	1.55 (0.65)	2.21 (0.34)	2.09 (0.25)	0.80 (0.33)
H_2O	$x = y = z$	0.3750	0.3750	0.3750	0.3750
	radius (R)	5.7	5.75	5.85	5.7
8 (b)	no. of molecules	227.0	217.0	215.0	232.4
	B, Å	10.0	10.0	10.0	10.0
H_2O	$x = y = z$	0.1250	0.1250	0.1250	0.1250
	radius (R)	2.3	2.3	2.3	2.3
8 (a)	no. of molecules	16.0	24.0	32.0	25.6
	B, Å^2	10.0	10.0	10.0	10.0
K^+	$x = y = z$	0.3750	0.3750	0.3750	0.3750
	radius (R)	5.2	5.1	5.3	5.6
8 (b)	no. of cations	16.77	19.98	26.51	47.27
	B, Å^2	10.0	10.0	10.0	10.0
Final	R_I	0.1992	0.1616	0.1629	0.2030
	R_F	0.1331	0.1150	0.1114	0.1343

[a] The standard deviations are indicated in parentheses.

outside the sample. Up to 128 peaks, going to $N = h^2 + k^2 + l^2 = 396$, *i.e.*, at about $2\theta = 77°$, representing 236 *hkl* values, were measured. Including more peaks would not impart more accuracy because introducing further peaks involves more and more coinciding *hkl* values in the same measured peak. Using a sufficiently thick layer (3 mm) of sample (apparent density 0.64 g cm^{-3}) the X-rays were adsorbed for more than 99.9% even in the least favorable direction. In this way, absorption decreased the intensities of the diffracted beams with the same factor in all directions, and no extinction correction was needed.[8]

Programs for least-squares refinement and Fourier analysis were written especially for this problem. The observed intensities were previously divided by the combined Lorentz polarization geometrical factor $(1 + \cos^2 2\theta)/(\sin^2 \theta \cos \theta)$. For coinciding *hkl* values, the calculated intensity ratios of the former cycle were used for the calculation of the observed intensities, from which the structure factors were derived. In the least-squares program, a block-diagonal approximation was used to solve the matrix of normal equations. The parameters x, y, z, and B for the individual framework atoms were taken in separate blocks. The parameters of the exchangeable cations were taken together in another single block, refining alternatively positional and temperature factors, and positional and occupancy factors, in order to eliminate as well as possible the close correlation of population and temperature factors in the refinement procedure. Sufficient convergence in the least-squares refinement was reached after the use of damping factors[9] and fixing of the scale factor.

(8) B. D. Cullity, "Elements of X-Ray Diffraction," Addison-Wesley, Reading, Mass., 1956, p 188.

(9) G. H. Stout and L. H. Jensen, "X-Ray Structure Determination," Macmillan, New York, N. Y., 1968, p 397.

This also resulted in a good agreement between the occupancy factors of the different sites, as determined from least-squares and Fourier approximation. Indeed, the large number of reflections in faujasite allowed us to use a plot of $\ln(\Sigma_{10}I_o/\Sigma_{10}I_c)$ *vs.* $\sin^2\theta/\lambda^2$, for every ten lines, to have an estimate of the scale and temperature factor correction to be applied. During refinement, this plot was examined every four cycles. In doing so, a sufficient and rapid convergence was achieved, with almost zero shifts of the framework parameters in the last cycles.

To improve the agreement between the calculated and the experimental intensity values for the low order reflections, we applied the method of Simpson and Steinfink[10] introducing the effect of all the water molecules and of the unlocated potassium ions. In fact, no water molecules could be localized because tridimensional Fourier analysis did not show any indication of excess electron density at possible sites, as found, *e.g.*, by Olson.[4] The water in the large cage and also in the sodalite cage was supposed to be distributed randomly throughout a sphere. The centers of the unlocated potassium ions were taken to be located uniformly at the surface of a sphere concentric with the water sphere in the large cage. Inside the sodalite unit, the radius of the water sphere was taken as 2.3 Å. This radius was found to be a reasonable value, also adopted by Simpson and Steinfink.[10] In the large cavities the radii of the water sphere and of the potassium sphere were calculated by systematic trial calculations on the first 20 reflections, to obtain the best agreement. The values of these radii (R) are included in Table III. The distribution of the water molecules between the sodalite cages and the supercages was also fitted to obtain the best agreement. For the spheres an additional temperature factor of 10 Å^2 was adopted. The extent of the water spheres in the large cage and in the sodalite cage includes the cation sites. This means that the occupancy factor obtained by our calculations must be considered as superposed to the relatively less important Fourier background. In fact, at these sites, Olson could indicate some water molecules also.

The F_o synthesis always indicated a large electron density peak at the center of the 12-ring. However, this was believed to be partly an effect of series termination. Indeed, ΔF synthesis indicated that the estimation of the occupancy of the different sites obtained from least-squares refinement was sufficient, and that in the center of the 12-ring, no fixed scattering matter was present.

We used the weighting scheme suggested by Cruickshank, *et al.*,[11] for $|F_c| > |F_o|_{min}$, *i.e.*, $w_i = 1/(2|F_o|_{min} + |F_o| + 2|F_o|^2/|F_o|_{max})$. Otherwise, a zero weight was used.[12] The atomic scattering factors were taken from the International Tables for X-ray crystallography III. The following charges were given to the atoms: Si^{2+}, Al^{2+}, O^-, and for the cations their real charge +1. The residuals were defined as

$$R_F = \sum_{hkl}|k|F_o| - |F_c||/\sum_{hkl}k|F_o|$$

and

$$R_I = \sum_N|kI_o - I_c|/\sum_N kI_o$$

where I_o was the intensity, corrected for the continuously varying factors. For the calculation of the atomic distances and bond angles, the program ORFFE[13] was used.

Results

The parameters describing the structure are given in Table III, together with the residuals. The cation site indication is the one used by Smith[14] (see Figure 1). The sites I are in the center of the hexagonal prism, the sites I′ inside the cuboctahedron at the six-membered ring of oxygen ions belonging to the hexagonal prisms. There are 16 sites I and 32 sites I′ per unit cell. Sites II and II′ share the six-ring of the cuboctahedron facing the large cavity: II′ is inside the cuboctahedron, II is in the large cage. There are 32 of each of these sites per unit cell. Further in the discussion we shall define as sites III′ the four-membered ring formed by two O_1 oxygens and by two O_4 (see Figures 1 and 3).

Table IV gives the atomic distances and bond angles and also the distances from the center of the large cage and of the cuboctahedron to the center of the surrounding atoms. A survey of the population of the different cation sites is presented in Table V. All the electron density on these sites was assigned to potassium ions; otherwise the large variations in occupancy cannot be explained. A list of I_c and I_o values is available on request.

Discussion

The structure of the faujasite lattice obtained in this work is essentially the same as in previous studies. The dimensions of the $(Si,Al)O_4$ tetrahedra correspond to the theoretical values of the T–O and O–O distances, within the experimental error. Assuming the distances Si–O = 1.61 Å, Al–O = 1.75 Å, O_{Si}–O_{Si} = 2.63 Å, and O_{Al}–O_{Al} = 2.86 Å (Smith and Bailey[15]), the interatomic distances are calculated and compared to the experimental mean values in Table VI.

The K–O distances are more variable especially on sites II and I′ (see Table IV). The changes in K–O distances seem to follow the sequence of the framework charges. The values can be compared to the data

(10) H. D. Simpson and H. Steinfink, *Acta Crystallogr., Sect. A*, **26**, 158 (1970).

(11) H. Lipson and W. Cochran, "The Determination of Crystal Structures," G. Bell, London, 1966, p 340.

(12) A. J. Dunning and V. Vand, *Acta Crystallogr., Sect. A*, **25**, 489 (1969).

(13) W. R. Busing, K. O. Martin, and H. A. Levy, ORFFE, Oak Ridge National Laboratory, Oak Ridge, Tenn., 1964.

(14) J. V. Smith, Second International Conference on Molecular Sieve Zeolites at Worcester, Mass., 1970.

(15) J. V. Smith and S. W. Bailey, *Acta Crystallogr.*, **16**, 801 (1963).

Table IV: Hydrated Potassium Faujasites: Interatomic Distances (Å)[a] and Bond Angles (deg)[a]

	KF 48.2	KF 54.7	KF 69.8	KF 86.5
		Tetrahedron		
$T-O_1$	1.665 (23)	1.671 (19)	1.671 (20)	1.670 (32)
$T-O_2$	1.643 (22)	1.673 (29)	1.629 (18)	1.688 (32)
$T-O_3$	1.637 (20)	1.635 (19)	1.666 (18)	1.615 (18)
$T-O_4$	1.686 (24)	1.676 (20)	1.703 (22)	1.726 (30)
Mean	1.658 (11)[b]	1.664 (10)[b]	1.667 (10)[b]	1.675 (14)[b]
$T-O_1-T$	131.6 (1.7)	133.4 (1.4)	132.8 (1.4)	132.5 (2.4)
$T-O_2-T$	147.7 (1.2)	145.3 (1.3)	147.4 (1.0)	144.1 (1.7)
$T-O_3-T$	140.6 (1.0)	143.1 (0.9)	144.7 (0.9)	145.7 (1.1)
$T-O_4-T$	135.3 (1.2)	133.1 (1.1)	136.8 (1.1)	137.3 (1.6)
Mean	138.8 (0.7)[b]	138.7 (0.6)[b]	140.4 (0.6)[b]	139.8 (0.9)[b]
O_1-O_2	2.778 (34)	2.812 (33)	2.760 (28)	2.834 (49)
O_1-O_3	2.756 (27)	2.750 (22)	2.769 (22)	2.681 (32)
O_1-O_4	2.588 (31)	2.592 (26)	2.634 (27)	2.671 (41)
O_2-O_3	2.562 (28)	2.616 (27)	2.656 (23)	2.634 (33)
O_2-O_4	2.776 (30)	2.745 (29)	2.731 (26)	2.754 (41)
O_3-O_4	2.773 (30)	2.778 (25)	2.778 (27)	2.828 (34)
Mean	2.705 (12)[b]	2.716 (11)[b]	2.721 (10)[b]	2.734 (16)[b]
O_1-T-O_2	114.2 (1.0)	114.4 (1.0)	113.5 (0.8)	115.1 (1.4)
O_1-T-O_3	113.2 (1.1)	112.5 (0.9)	112.2 (0.9)	109.3 (1.3)
O_1-T-O_4	101.2 (1.1)	101.5 (0.9)	102.6 (0.9)	103.7 (1.5)
O_2-T-O_3	102.7 (0.9)	104.4 (0.9)	107.4 (0.8)	105.8 (1.0)
O_2-T-O_4	113.0 (0.9)	110.1 (0.8)	110.0 (0.8)	107.6 (1.2)
O_3-T-O_4	113.1 (1.1)	114.1 (0.9)	111.0 (1.0)	115.6 (1.3)
Mean	109.5 (0.4)[b]	109.5 (0.4)[b]	109.5 (0.4)[b]	109.5 (0.6)[b]
		Cations		
$K(I)-O_1$	3.803 (23)	3.809 (22)	3.820 (22)	3.822 (38)
$-O_2$	3.415 (15)	3.485 (15)	3.507 (12)	3.481 (20)
$-O_3$	2.735 (19)	2.801 (17)	2.817 (17)	2.758 (17)
K(I)-K(I′)	3.507 (54)	3.435 (49)	3.384 (57)	3.202 (128)
$K(I')-O_2$	3.193 (58)	3.175 (54)	3.246 (59)	3.055 (131)
$-O_3$	2.859 (56)	2.848 (51)	2.807 (59)	2.798 (129)
K(I′)-K(I′)	3.003 (108)	3.134 (99)	3.285 (114)	3.651 (256)
$K(II)-O_2$	2.940 (33)	2.893 (31)	2.873 (23)	2.858 (32)
$K(II)-O_4$	3.247 (37)	3.199 (33)	3.179 (29)	3.137 (38)
		Framework[c]		
Center cubocta-hedron				
-K(I′)	1.839	1.919	2.011	2.236
$-O_3$	4.287	4.305	4.324	4.488
$-O_2$	4.388	4.382	4.510	4.421
-T	4.938	4.949	4.986	5.020
$-O_4$	5.318	5.351	5.337	5.348
-K(II)	5.645	5.671	5.560	5.538
$-O_1$	6.650	6.571	6.611	6.647
Center large cage				
-K(II)	5.047	5.037	5.141	5.338
$-O_4$	6.974	6.916	6.989	7.057
$-O_2$	7.298	7.259	7.261	7.433
$-O_1$	7.270	7.282	7.349	7.426
-T	7.560	7.558	7.605	7.719

[a] Estimated standard deviations in parentheses. [b] Standard deviation, calculated from $1/n[\sum_n \sigma_i^2]^{1/2}$. [c] Standard deviations were not calculated.

given by Radoslovich[16] for muscovite (K–O = 2.81 Å).

In general, the temperature factors are acceptable. We notice the large temperature factors of some oxygens and of the cations on sites I and I′. For the oxygens, the deformation of the lattice due to Al substitution and the proximity of a cation results in a large temperature factor. A too symmetric space group would have the same effect. The potassium coordinates are cer-

(16) E. W. Radoslovich, *Amer. Mineral.*, **48**, 76 (1963).

Table V: Population of the Different Cation Sites (Cations per Unit Cell)

	KF 48.2	KF 54.7	KF 69.8	KF 86.5
Site I	0.0	1.3	7.0	8.9
Site I′	13.6	13.3	12.0	7.2
Site I + I′	13.6	14.6	19.0	16.1
Site II	17.8	20.0	24.3	23.2
Large cage (unlocalized)	16.8	20.1	26.5	47.2

Table VI

	Samples			
	F 48.2	F 54.7	F 69.8	F 86.5
	T–O distances			
Calcd	1.645	1.649	1.661	1.673
Obsd	1.658	1.664	1.667	1.675
	O–O distances			
Calcd	2.687	2.695	2.714	2.733
Obsd	2.705	2.716	2.721	2.734

tainly influenced by local lattice distortions and by the charge distribution, which also results in a large temperature factor. Moreover, the correlation between temperature and occupancy factors may not be entirely eliminated in the calculation procedure that we followed.

A plot of the population frequency of the different sites against the number of cations per unit cell (Figure 2) reveals an interesting relation between the population of sites I, I′, and II. While for F 48.2 the hexagonal prism (site I) was found empty, for F 86.5 it was filled for more than 50%. The population of site I′, however, varies from almost two cations per cubooctahedron for the F 48.2 to only one in the case of F 86.5. In the same sequence the number of potassium ions in site II changes from two to three per sodalite cage (for the number of ions per unit cell see Table V). The observed variation in the population at site I and I′ is in agreement with the differences between X and Y zeolites mentioned in the Introduction. There was indeed a difference in the ($2Na^+$, Ca^{2+}) content on site I and I′ for the hydrated faujasite crystal investigated by Baur,[3] and the Na^+ content at the same sites for the synthetic X zeolites studied by Broussard, *et al.*,[2] as a powder sample, and by Olson[4] as a monocrystal. Whereas Baur[3] indicated only 50% occupancy at site I′, and zero occupancy of site I, Broussard, *et al.*,[2] found a full occupancy in site I and nothing in site I′. Our results for F 86.5 are in very close agreement with the population frequencies of sites I and I′ determined by Olson,[4] namely nine in site I and eight in site I′.

In the space group *Fd3m*, all T atoms are equal, and only four different oxygens are distinguished. The

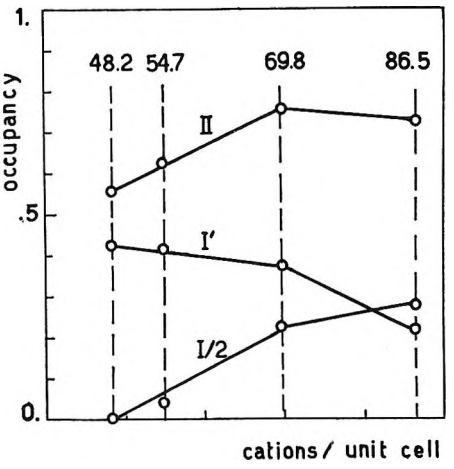

Figure 2. Hydrated K faujasites: occupancy of the cation sites.

substitution of a Si^{4+} by an Al^{3+} results in an excess negative charge. An oxygen, however, shall never share two Al^{3+} tetrahedra, as is described by the cation avoidance rule of Loewenstein.[17] For each Al^{3+} tetrahedron four different oxygens can provide neutralization, which may be interpreted by either partial covalent bonding (Brown, Gibbs, and Ribbe[18]) or ionic bonding (Jones and Taylor[19]) with the exchangeable cations. For the conventional sites (I, I′, and II), only two oxygens, O_2 and O_3, can provide neutralization. In our case, from the above viewpoint, a cation in, *e.g.*, site I′ can never neutralize the Al^{3+} tetrahedra, if there is more than one such tetrahedron in a six-ring. Other oxygens than the O_3 and O_2 must therefore participate in the neutralization of the framework charge. We think that a valuable approximation to the cation location can be made by a statistical distribution of them over the four types of framework oxygens, *i.e.*, one-fourth of the cations located at sites near each oxygen species.

What are the neutralization possibilities for the different types of oxygen ions? The O_1 oxygen ions are accessible for cations only from the large cage. Three O_2 atoms are closest to a cation in site II, and they also participate to the six-ring of site I. The O_3 are closest to the center of symmetry, where they form an octahedral arrangement around site I and also share directly a possible cation at site I′. The O_4 atoms are part of the four-membered ring of the cuboctahedra and of the six-ring around site II. Although a cation in site II does not touch an O_4, their mutual distance is rather short (see Table IV).

Ordering of the Al–Si will have an influence on the distribution of the cations in the zeolitic framework.

(17) N. Loewenstein, *ibid.*, **39**, 93 (1954).

(18) G. E. Brown, G. V. Gibbs, and P. H. Ribbe, *ibid.*, **54**, 1044 (1969).

(19) J. B. Jones and W. H. Taylor, *Acta Crystallogr., Sect. B*, **24**, 1387 (1968).

Dempsey[20] proposed valuable models on that point, where he accepted the zeolite framework as constructed with double sodalite units having a zero dipole moment. Nevertheless for further discussion we prefer to use the number of Al^{3+} ions per unit cell, as obtained from chemical analysis. Statistical data on the Al^{3+} distribution, based on the only assumption of the rule of Loewenstein,[17] are given in Table VII.

Table VII: Distribution of the Al Atoms: Statistical Values[a]

		KF 48.2	KF 54.7	KF 69.8	KF 86.5
		A			
6 MR's					
with 2Al	A_1	16.2	22.7	26.5	9.5
with 3Al	A_2	0.0	0.0	5.8	22.5
		B			
4 MR's					
with 2Al	B	0.0	6.6	21.8	38.5

[a] The numbers are given in number per unit cell. A, number of six-membered rings carrying two aluminum atoms (A_1) or three aluminum atoms (A_2). B, number of four-membered rings of T atoms in the hexagonal prism carrying two aluminum atoms (total number of such four-rings being 48 per unit cell).

On the basis of these considerations we can discuss our results as follows.

1. One-fourth of the cations shall be located at the innermost sites (I and I′) to neutralize the charges transferred by the O_3 oxygens. One-fourth of the exchangeable cations corresponds to the following figures.

	F 48.2	F 54.7	F 69.8	F 86.5
Univalent cations/4	12.1	13.7	17.5	21.6

These figures correspond very closely to the experimental data on the population of sites I plus I′. Only for KF 86.5 this number is slightly lower, but the large number of cations present in the large cage suggests a higher degree of neutralization of the framework charge from the outside (probably site III′). On the other hand, these data are of the same order as the number derived indirectly by the ion-exchange experiments of Sherry,[5] *i.e.*, about 16 cations in the small pore system. However, our results showed a trend to increase with the Al content.

2. Simultaneous occupancy of a sites I and I′ belonging to the same hexagonal prism is probably not allowed. Therefore, the increasing number of cations in site I shall necessarily result in a decrease of the population of site I′. This seems valuable for all samples. Moreover, the occupancy of site I′ seems to be limited to a maximum of two potassium ions per cuboctahedron (50% occupancy). This limit may be due to space requirements and to electrostatic repulsion between the cations in site I′ and possibly also in site II. Figure 2 reveals indeed that a higher population in site II corresponds to a lower population of site I′. However, the electrostatic effect will be reduced by the water molecules in the sodalite cage. Probably, an increasing Al^{3+} content, *i.e.*, higher framework charge, will also be a cause for the increasing number of cations in the hexagonal prism and for the inversion of the population of sites I and I′.

3. Considering that the O_2, and to some extent the O_4, oxygens participate in the neutralization of the AlO_4 tetrahedra, it is likely that more than one-fourth of the cations are located at the sites II. For NaX, Olson[4] showed that only the six-rings with three Al atoms are able to fix a cation. For the Y-type samples, no six-rings with three Al atoms are present (see Table VI), and the available data showed no filling of the sites II with cations (Smith[14]). This could be true for our K samples also. From our present results it is clear that this possibility is not realized. Comparing the values of Table VII, part A, with the numbers of cations found at site II we conclude that in every structure only those sites II are occupied which have the highest charge density, and that at least one-fourth of the cations are at such sites. In our samples KF 48.2 and KF 54.7 this corresponds to the occupancy of six-rings having two aluminum atoms. In zeolite X (F 86.5) this is realized with the six-rings having three aluminum atoms as proposed by Olson[4] and Smith.[14] For the sample KF 69.8 the six-rings with three aluminum atoms do not provide a sufficient number of sites and are supplemented by six-rings with two aluminum atoms.

4. In the large cages no X-ray evidence was found for cations fixed at sites other than sites II. Nevertheless the charge transferred by the atoms O_1, and to some extent by O_4, must be neutralized by cations in the large cavities not located at sites II. Baur[3] presented several arguments in favor of the idea that the water molecules and the unlocated cations in the large cavities form a near-liquid phase similar to an electrolyte solution. In the hydrated state a kind of Stern–Gouy double layer[21] would be formed to neutralize the resulting part of the framework charge. However, we investigated the same samples in the dehydrated state,[22] and there also an important fraction of the cations cannot be located in the samples with the highest lattice charge. In dehydrated samples, the ions must be located close to the oxygen framework, and therefore we considered the possibility of fixed sites along the sequences of four-membered rings of oxygen

(20) E. Dempsey, "Molecular Sieves," Special Publication, Society of Chemical Industry, London, 1968, p 293.

(21) J. Th. G. Overbeeck in "Colloid Science I," H. R. Kruyt, Ed., Elsevier, Amsterdam, 1952, p 129.

(22) W. J. Mortier, H. J. Bosmans, and J. B. Uytterhoeven, to be published.

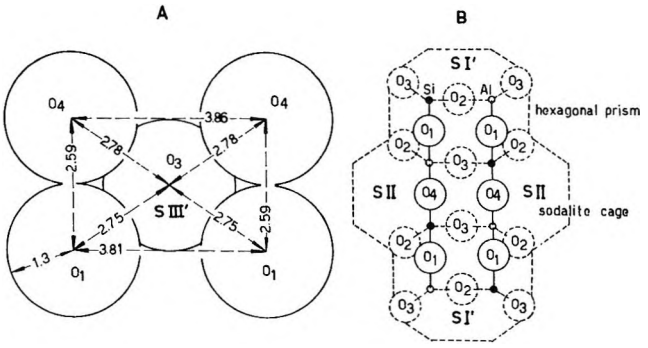

Figure 3. Oxygen arrangement at site III'.

ions in the large cavities. Considering the geometry of the oxygen atoms we defined the sites III', formed by two O_4 and two O_1 oxygens, as possible cation sites (Figure 3). In agreement with Loewenstein's rule, the highest charge density at these sites is realized in the case of a local 1:1 silicon and aluminum ordering. In that case all the oxygen atoms forming these sites are part of an aluminum tetrahedron. Moreover, as soon as a four-ring of T atoms, belonging to the cuboctahedron or to the hexagonal prism, contains two aluminum atoms, the site III' in consideration is highly charged. Indeed, three of the four oxygen atoms (O_4 and O_1) plus the underlying O_3 take then part in an Al^{3+} tetrahedron. The whole framework can be constructed with four-rings of T atoms of the hexagonal prism; 48 of such rings must be considered. The number of these rings containing two aluminum atoms is given in Table VI, line B. When we compare these values to the number of unlocated cations we are inclined to assume that in the samples F 86.5 and F 69.8 an important part of the potassium ions may be fixed to sites III' because of the high local framework charge. In the other cases, a more uniform balancing of charges through the agency of the water dipoles must form a more favorable situation. In this way, the large number of possible arrangements should result in an occupancy too low to be detected.

Acknowledgments. One of us (W. J. M.) is grateful to the "Belgisch Nationaal Fonds voor Wetenschappelijk Onderzoek" for a research grant as "Aspirant," and for a grant for a 3-week stay at the ETH-Zürich. The authors thank Professor J. B. Uytterhoeven for his interest and for helpful comments on the manuscript. We also thank Professor W. M. Meier for much valuable advice on the refinement procedure. The calculations were performed in the calculation center of the Katholieke Universiteit Leuven. We thank J. Paenhyus, who performed the chemical analyses. The gifts of the samples by the Linde Co. are gratefully acknowledged.

Detection of Slow Motions in Solids with Wide-Line Nuclear Magnetic Resonance Spectroscopy[1a]

by Edwin M. Roberts[1b]

3800 Granger Drive, Atlanta, Georgia 30341 *(Received May 6, 1971)*

Publication costs borne completely by The Journal of Physical Chemistry

The possibility is examined of detecting, with conventional nmr spectroscopy, atomic motions too slow to affect the second moment. Such motions are expected to have a noticeable effect on the free decay of transverse magnetization only after times long compared to the inverse line width. A new definition of T_2 is given which is dependent on the long-time behavior of the transverse magnetization. The new definition equates T_2 with θ, the root-mean-square time for which transverse magnetization persists. A discussion is given regarding the qualitative equivalence of this definition and more conventional definitions. Experimental data on $TiH_{1.94}$ confirm that slow atomic motions may be detected by examining the temperature dependence of θ. Spectra were recorded using large amplitude, square-wave magnetic field modulation. It is proved that this method provides an undistorted reproduction of the absorption spectrum.

I. Introduction

It is well known that the gross features of an nmr spectrum are sensitive only to motions of the spins which occur with characteristic frequencies comparable to the rigid lattice line width. For a system which exhibits motional narrowing, a graph of the apparent second moment as a function of temperature shows a

(1) (a) Work performed at The Lockheed-Georgia Co., Marietta, Ga. (b) The author is now affiliated with Dames and Moore, Consulting Engineers, 1314 West Peachtree St., Atlanta, Ga. 30309.

low temperature plateau along which the second moment is constant. In most instances, the second moment falls off sharply and monotonically as higher temperatures are approached until finally a high temperature plateau is reached. The low temperature plateau is sometimes termed the rigid lattice plateau, since in that temperature range there is agreement with the theoretical second moment for a static spin system.

It is understood that within the rigid lattice region the nuclear spins are not static but may possess motions in addition to the usual vibrational motion. These motions are of the same type which cause motional narrowing, but they occur at a rate too slow to affect the gross features of the line shape. They have been detected by Slichter and Ailion[2] and termed by them ultraslow. Their method of detection involves the experiment of adiabatic demagnetization in the rotating frame. Thus, Slichter and Ailion were able to extend the detectable values of the atomic jump time for metallic lithium by about five orders of magnitude. The question whether conventional magnetic resonance spectroscopy can be used to detect motions that are too slow to affect the second moment is to be examined here. The compound used in this work is $TiH_{1.94}$.

II. Transverse Relaxation

A. Conventional Concepts. Attention is restricted here to solids where any existing motion of the spins is slow enough for the adiabatic approximation to be valid. That is, only that part of the line broadening perturbation that commutes with the Zeeman operator is retained in the total Hamiltonian. With this restriction and for sufficiently high temperature, the tranverse magnetization, following a 90° radiofrequency pulse, relaxes along a curve $G(t)$ identifiable with the Fourier transform of the absorption curve $g(\omega)$.[3] The relaxation function $G(t)$ plays an important role in the theory of motional narrowing. An equally valid concept of $G(t)$ is that it is equal to the average of cos $\varphi(t)$ over all nuclei.[3,4] Here, $\varphi(t)$ is the phase deviation. For a system of localized spins $\varphi(t)$ is just ωt, where ω is the deviation from resonant frequency.[3] For a system of spins in thermal motion, ω is a random function in time. In this case, $\varphi(t)$ is the integral of $\omega(t)$ over the time interval $(0,t)$.[4]

A single relaxation time T_2 is often used to describe the decay of transverse magnetization. Several qualitatively equivalent definitions of T_2 have been found useful in practice. Because of the rather large changes in line shape which are usually observed with motional narrowing, the precise definition is not important. One definition of T_2 equates it with the time necessary for a group of spins, initially in phase, to become dephased by 1 radian as a result of their interactions with various local fields. Another useful definition relates T_2 to the time required for transverse magnetization to decay freely to approximately one-half of its initial value. Still another definition relates T_2 to the inverse half-width of the absorption spectrum. The qualitative equivalence of these definitions is well known and need not be proved here.[4]

B. Properties of $g(\omega)$ and $G(t)$. Let σ^2 be the second moment of $g(\omega)$, and let θ^2 be the second moment of $G(t)$. Both $g(\omega)$ and $G(t)$ are assumed to be centered at the origins of their arguments. Then

$$\sigma\theta \geqslant {}^1/_2 \tag{1}$$

In (1), the inequality sign may be dropped after replacing the number $^1/_2$ by a number C which depends on the function $g(\omega)$. In all cases of practical interest, C is of the order of unity. It is well known that σ^2 exists for physically real systems. It will be shown later that θ^2 also exists. Equation 1 shows that σ^2 and θ^2 are intimately and naturally related.

The half-width of $g(\omega)$ at half-maximum is often used as an indication of the average of the absolute value of the local field. This half-width has only qualitative significance. Of more fundamental significance are the various moments of $g(\omega)$. In principle, they may be calculated for any fixed arrangement of spins. The function $g(\omega)$ is uniquely determined by its moments if they all exist and if the resulting moment generating function is covergent. In practice, however, only the first few moments may be calculated *ab initio* or from experimental data. The second moment σ^2 is the most important of the various moments because it is relatively easy to calculate both theoretically and experimentally.[5] Also, the physical significance of σ as a measure of the magnitude of the local field is more readily apparent than that of the other moments.[6]

As will be shown, θ^2 may be computed rather easily from experimental data. It is not readily calculated from theory. Although σ^2 and θ^2 are not generally capable of completely defining $g(\omega)$ and $G(t)$, respectively, their determination is an important first step toward defining the functions $g(\omega)$ and $G(t)$.

C. A New Definition of T_2. The purpose of this discussion is to suggest that θ has the same physical significance as T_2 when the latter is given by any of the three definitions discussed above. As will be shown, θ and T_2 have approximately the same numerical value. Thus, T_2 is redefined as

$$T_2 = \theta \tag{2}$$

From the definition of $G(t)$ as the Fourier transform of $g(\omega)$, it follows that

(2) (a) C. P. Slichter and D. C. Ailion, *Phys. Rev.*, **135**, A1099 (1964); (b) D. C. Ailion and C. P. Slichter, *ibid.*, **137**, A235 (1965).
(3) I. J. Lowe and R. E. Norberg, *ibid.*, **107**, 46 (1957).
(4) P. W. Anderson, *J. Phys. Soc. Jap.*, **9**, 316 (1954).
(5) J. H. Van Vleck, *Phys. Rev.*, **74**, 1168 (1948).
(6) A. G. Redfield, *ibid.*, **98**, 1787 (1955).

$$\theta^2 = \left|\frac{g''(0)}{g(0)}\right| \tag{3}$$

where $g''(0)$ denotes the second derivative of $g(\omega)$ evaluated at $\omega = 0$. It is evident that θ^2 must exist because absorption spectra with undefined or infinite curvature are never observed. From eq 2 and 3, it is evident that T_2 is now defined in terms of the spectrum in the vicinity of the central frequency. This is in contrast to the usual concepts of T_2, which are equivalent to an inverse half-width. Some examples will serve to illustrate that the definition 2 is not in serious disagreement with the older definitions of T_2.

The Gaussian and Lorentzian functions are useful for purposes of discussion. The Gaussian function

$$g(\omega) = (2\pi\sigma^2)^{-1/2} \exp(-\omega^2/2\sigma^2)$$

has the Fourier transform

$$G(t) = \exp(-{}^1/_2\sigma^2t^2)$$

The root-mean-square phase deviation is σt, and the half-width at half-intensity is $\delta = (2 \log 2)^{1/2}\sigma$. Application of eq 3 shows that $\theta^2\sigma^2 = 1$. It is evident that the numerical value of θ is in substantial agreement with older definitions of T_2.

The Lorentzian function

$$g(\omega) = \delta\pi^{-1}(\delta^2 + \omega^2)^{-1}$$

has a Fourier transform

$$G(t) = \exp(-\delta t)$$

In this case, the second moment of $g(\omega)$ does not exist if the range of ω is taken as $(-\infty, \infty)$. Application of eq 3 shows that $\theta^2\delta^2 = 2$. Again, the numerical value of θ is in substantial agreement with the older definitions of T_2.

Aside from being somewhat more general than the previous definitions, the new definition has one distinct advantage. It reflects more accurately the behavior of $G(t)$ for long times. Exceptions to this are found in the above examples and arise whenever one parameter is sufficient to describe completely both $g(\omega)$ and $G(t)$. These exceptions do not detract from the stated advantage, because it is probable that an actual spectrum is neither Gaussian nor Lorentzian.

The higher order moments are even more dependent than θ^2 on the behavior of $G(t)$ at long times. The introduction of the higher order moments is analogous, perhaps equivalent, to the use of several time constants to describe transverse relaxation. Because of the questionable accuracy involved in their calculation and the vagueness of their physical significance, the moments of order greater than 2 will not be considered.

D. Motional Effects. The behavior of $G(t)$ for long times is of importance, because the effect of slow motion is expected to be manifested at the longer times. Consider a system of spins which may experience various magnetic environments. The spins are assumed to sample each magnetic environment for an average time τ. The rigid lattice second moment is denoted by σ^2. There are two distinct situations. If $\sigma\tau < 1$, the spin system dephases according to a stochastic process. As a result of the rapid fluctuations in magnetic environment, the sign of ω will change before the phase deviation can become appreciable. The situation is completely different if $\sigma\tau > 1$, since the spin system is significantly dephased before the average magnetic environment changes. In this case, that of slow motion, the function $G(t)$ has a behavior at early times which is practically the same as that of $G(t)$ for a rigid lattice. Departure from rigid lattice behavior will be evident only for relatively longer times. The spin system is dephased every τ sec so that

$$\frac{1}{T_2} = \frac{1}{T_2'} + \frac{1}{\tau} \tag{4}$$

where T_2' is the transverse relaxation time of a rigidly fixed spin system.[7]

As temperature increases, τ decreases. According to eq 4, $1/T_2$ should increase as temperature increases.[7] Transverse relaxation times based on the usual concepts do not show the behavior predicted by eq 4, because they are not sufficiently influenced by the behavior of $G(t)$ at long times. The definition $T_2 = \theta$ is so influenced. The points brought out in the previous discussion strongly suggest that in the temperature range commonly known as the rigid lattice region, the values of θ should obey the equation

$$\frac{1}{\theta} = \frac{1}{\theta'} + \frac{1}{\tau} \tag{5}$$

where θ' is the value of θ for a rigidly fixed spin system. For rapid motion where $\sigma\tau \ll 1$, it is expected that

$$\frac{1}{\theta} = \sigma^2\tau \tag{6}$$

The experimental results to be presented here on $TiH_{1.94}$ verify these expectations.

III. Experimental Section

A. Apparatus and Sample. A Varian VF-16 wide-

(7) D. S. Schreiber and R. M. Cotts, *Phys. Rev.*, **131**, 1118 (1963). Equation 4 has been derived by Schreiber and Cotts to describe the effect of quadrupole interaction on the lanthanum line width of lanthanum hydride. In their application τ^{-1} is the frequency with which a lanthanum nucleus is visited by diffusing defects. The theory leading to eq 4 is valid so long as the restriction $\tau\tau > 1$ is valid. The prediction that the line width should first increase as temperature increases is substantiated by the lanthanum resonance. The hydrogen line width does not exhibit this property. The difference in behavior between the two resonance lines is due to the fact that the quadrupole interaction is a much more effective mechanism for relaxation than is dipolar coupling. If T_2, in eq 4, could be interpreted in terms of a quantity more sensitive than the line width, the effect might be expected to be enhanced in the case of the hydrogen resonance. It might be mentioned that eq 4 is applicable to slow exchange, between different sites, of spins which obey the Bloch equations.

line spectrometer was used. The detection at the audiofrequency was accomplished with a Princeton Applied Research Model HR-8 lock-in amplifier. The audiomodulation of the magnetic field was derived from a Hewlett-Packard Model 3300A function generator and a Model 467A amplifier. The function generator was phase locked to the internal reference signal of the lock-in amplifier. Field modulation was performed with a square wave applied to the modulation coils. The modulation frequency was 20 Hz. The maximum peak-to-peak modulation amplitude attainable was 50 G. The sample temperature was regulated with a V-4557 variable-temperature accessory adapted for use in the wide-line probe. Frequencies were measured with a Hewlett-Packard Model 5245-L counter.

A sample of commerically obtained titanium hydride was used. Chemical analysis gave a composition of $TiH_{1.94}$ with less than 0.23% impurity by weight. The sample was annealed at 300° to homogenize the distribution of hydrogen. It was in powder form with particles less than 37-μ diameter. It was the same sample used in previous work.[8]

B. Spectra. There are two possibilities for the determination of θ from continuous wave data. With the use of small amplitude of modulation, the derivative of the absorption spectrum may be recorded. The relaxation function may then be obtained by numerical integration. Another numerical integration produces θ^2. Even though the effect of nonzero amplitude of modulation may be taken into account,[8] there was originally a question in the author's mind concerning the accuracy of that correction at large values of time. The reason for this concern was that the peak of absorption is the part of the curve most affected by the modulation. This difficulty could be relieved by using very small amplitude of modulation, but the signal-to-noise ratio in the vicinity of the peak of absorption becomes poor. An alternative scheme of spectral presentation was thought desirable.

The absorption, rather than its derivative, may be obtained by modulating with a large amplitude square wave.[9] This method may be called the absorption method to distinguish it from the derivative method. To the author's knowledge, no proof exists that the method actually produces an unmodified version of the absorption. Experimental proof is presented here that the absorption method and the derivative method yield identical relaxation functions. Therefore, they are equivalent. In this application, the relaxation function is merely a mathematical convenience used to show that the signals obtained by the two methods describe the same distribution. Before presenting the experimental data a few qualitative observations may be made with regard to obtaining the spectrum.

The peak-to-peak amplitude H_m of the modulation field must be large enough to encompass the entire spectrum. A convenient rule is to choose $H_m > 3\Delta H$,

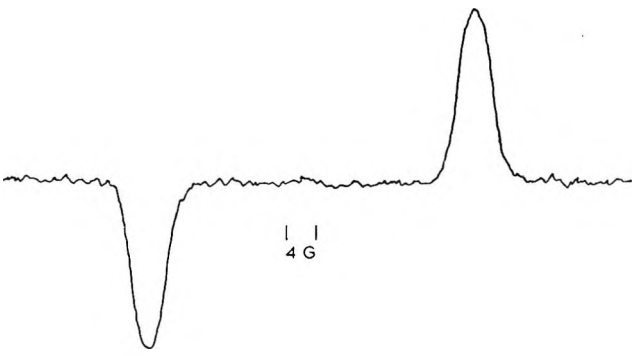

Figure 1. A signal obtained *via* the absorption method. The separation between the two spectra is 45.0 G. The resonant nuclei are protons in NH_4Cl at room temperature.

where ΔH is the line width. The modulation frequency ν_m should be chosen such that nonadiabatic conditions prevail. The recorded signal from NH_4Cl is shown in Figure 1. The signal consists of two spectra separated by H_m and relatively inverted. The occurrence of twin spectra is due to the nature of the lock-in amplifier. This spectra should not be confused with that obtained by high frequency modulation in high resolution nmr spectroscopy.

The titanium hydride $TiH_{1.94}$ was used as a test case. The line width of $TiH_{1.94}$ at room temperature is 13 G. A square-wave modulation field with an amplitude of 45 G and a frequency of 20 Hz was used. The relaxation functions from the two methods are compared in Figure 2. Each point is actually an average of several points. The correction for field modulation was included in the computation of $G(t)$ from the derivative data. In obtaining the derivative data, the modulation amplitude was kept small enough such that the corrective factor,[8] $J_1(bt)/(bt)$, did not vanish for times less than 4×10^{-5} sec. The close agreement between the curves suffices to show that the absorption method produces a signal which is the integral of the signal obtained with the derivative method.

C. Calibrations. The data collected with the derivative method must be corrected for the effect of field modulation. This is particularly important for the present purposes, since the effect of modulation becomes more pronounced for large values of time. The peak-to-peak amplitude of the modulation field was measured by adjusting the resonant frequency of water to coincide with the extremes of the modulated field.

The radiofrequency was 8 Mc. The possibility of saturation was avoided by using a radiofrequency power well below the point where saturation occurred. Spectra were recorded using a scanning speed of 0.083 G/sec. The scanning rate $\gamma\dot{H}_0$ was calibrated by scanning through a narrow resonance line at two different

(8) E. M. Roberts and C. W. Merideth, *Phys. Rev.*, **179**, 381 (1968).
(9) E. R. Andrew, "Nuclear Magnetic Resonance," Cambridge University Press, London, 1955, p 163.

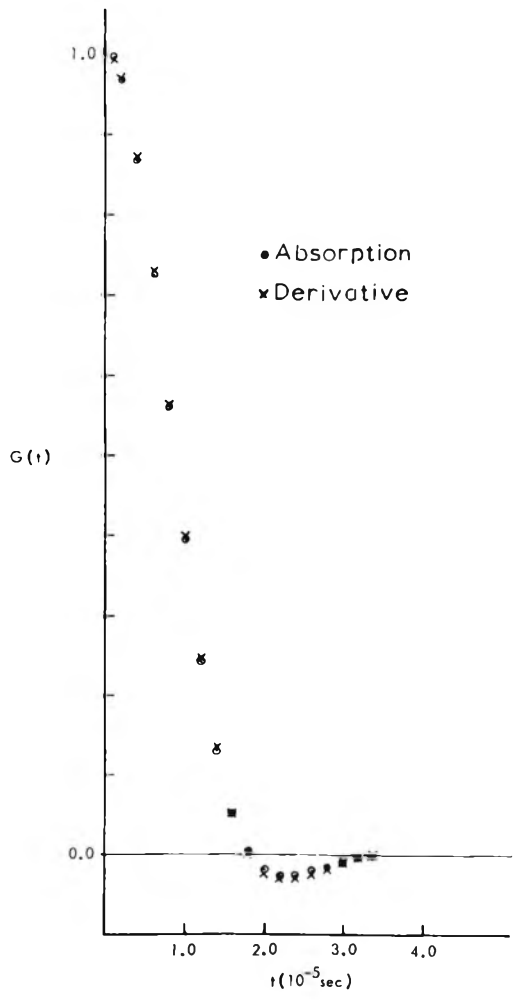

Figure 2. Comparison of Fourier transforms as obtained by the absorption method and derivative method. The data are for $TiH_{1.94}$ at 307°K.

radiofrequencies. The two scans were stored successively in a multi-channel analyzer and then jointly displayed on the recorder. The scanning rate is the frequency separation multiplied by the channel separation divided by the channel advance rate.

The sample was sealed in a Pyrex tube 8.5 mm in i.d. A capillary thermocouple well entered the top of the tube through a ring seal. The closed bottom of the capillary was 2 cm from the bottom of the sample tube. This arrangement allowed the temperature to be measured at a point near the center of the receiver coil. A silicone rubber plug molded in place around the thermocouple and fitting tightly in the capillary prevented moisture from condensing in the well. The temperature of the sample was measured by means of a copper–constantan thermocouple having Teflon insulation.

D. Calculations. The absorption method was used to collect data in the rigid lattice region. Derivative spectra were used for calculations in the temperature range corresponding to narrowed spectra.

The curvature $g''(0)$ was calculated by plotting the normalized absorption $g(\omega)$ *vs.* $\omega^2/2$. The points near the origin were fitted to a straight line using the method of least squares. It is important to decide for which interval, about $\omega = 0$, the above plots may be considered safely linear. For this purpose, the absorption may be assumed to have a Gaussian shape. Then, the condition that the ω^2 term predominates is $\omega^2 \ll 4\sigma^2$. The second moment of $TiH_{1.94}$ is approximately 25 G^2. If an interval of 2 G on either side of center is used, a sufficient number of data points may be obtained, and the above inequality will be satisfied. The slope and intercept of this straight line give $g''(0)$ and $g(0)$, respectively. The normalization factor, second moment, and the relaxation function were calculated for each case by numerical integration. Actually, the normalized values of $g(\omega)$ are not needed for the calculation of θ^2. However, the separate values of $g''(0)$ and $g(0)$ are of considerable interest, and for these the normalized values of $g(\omega)$ are needed.

Numerical integration of

$$\theta^2 = \int_0^\infty t^2 G(t)\mathrm{d}t \Big/ \int_0^\infty G(t)\mathrm{d}t \qquad (7)$$

was performed using relaxation functions previously determined for the motionally narrowed spectra.[8] For the three higher temperatures, the relaxation functions do not decay sufficiently before the necessary correction for modulation becomes intolerably large. In these cases, the relaxation functions were extrapolated to longer times using an exponential approximation.

IV. Results

A. Qualitative. Motional narrowing first appears for $TiH_{1.94}$ in the neighborhood of 400°K. The second moment of $g(\omega)$ is constant for temperatures less than 370°K. Between 370 and 400°K is an intermediate range for which $\sigma\tau \approx 1$. The temperature range for which $T < 370$°K will be referred to as the "rigid lattice region" even though the spins may still have a slow thermal motion. The region for $T > 400$°K will be referred to as the "motionally narrowed region."

Absorption spectra were taken at the temperatures 99.2, 195.2, 246.5, 307.2, and 336.2°K. A spectrum at 99.2°K is shown in Figure 3. The signal-to-noise ratio decreases with increasing temperature. According to the general theory of nuclear magnetism, the absorption intensity should be inversely proportional to the absolute temperature when the high temperature approximation is valid. The unnormalized intensity data, plotted in Figure 4, show that the high temperature approximation is valid. The temperature dependence of the spectra due to the Boltzmann distribution of spins over the energy levels is contained in a simple factor which cancels on normalization.

In the motionally narrowed region, the spectra were obtained with the derivative method. For this range of temperatures the absorption method produced spectra with poor signal-to-noise ratios. Signal enhance-

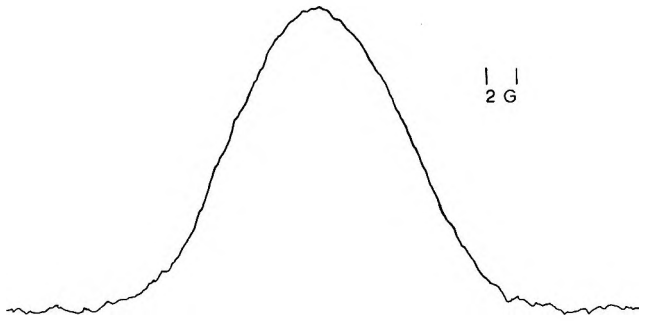

Figure 3. Typical spectrum of $TiH_{1.94}$ at 99°K. The line width at half-maximum is 12.8 G.

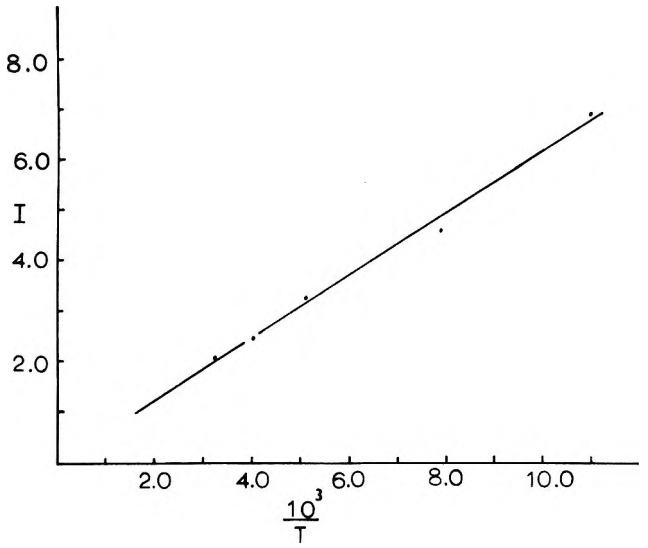

Figure 4. Arbitrary intensity of $TiH_{1.94}$ absorption *vs.* $10^3/T$.

ment with a time-averaging computer would have been necessary for the attainment of accurate results with the absorption method. On the other hand, derivative spectra were available from previous work.[8] Although it is more desirable, from the standpoint of consistency, to use the same method throughout, it was more practical to use the derivative data already available. The spectra were recorded at temperatures 377.2, 400.0, 421.7, 445.2, 464.8, 481.4, 514.2, and 534.2°K.

B. Quantitative. For the rigid lattice region, the values of θ were calculated from the spectral data according to eq 3. For the motionally narrowed region the values of θ were calculated in the manner indicated by eq 7. The results are shown in Figure 5. Also shown in Figure 5 are the values of T_2 defined by $G(T_2) = e^{-1/2}$.[8] The initial increase of θ^{-1} with temperature is in agreement with eq 5.

No less than ten spectra were recorded for each point in the rigid lattice region. The θ values plotted in Figure 5 are averages. The significance of the observed temperature dependence is best tested by considering the calculated values of $g''(0)$, $g(0)$, and σ^2 separately. This was done for the sets of data at 99.2 and 307.2°K. The averages for $g''(0)$, $g(0)$, and σ^2

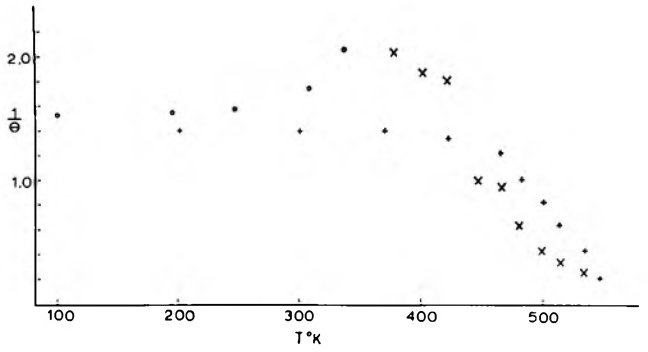

Figure 5. $1/T_2$ *vs.* T for $TiH_{1.94}$. The points marked O and × are those for which $T_2 = \theta$. The former correspond to data obtained with the absorption method; the latter are from the derivative method. The points marked + correspond to the definition $G(T_2) = e^{-1/2}$.

are given in Table I for the two sets of data. The statistical t-test[10] was applied to determine if the averages for the two temperatures are significantly different. The results of that test are shown in Table I. The meaning of t and t_x is that if $t > t_x$, there is a probability greater than $(100 - x)$ per cent that the two sets of data, as described by the given averages, are significantly different. It is evident from the standpoint of curvature and maximum intensity that there is a significant difference between the nmr line shapes at the two temperatures. However, from the standpoint of second moment, there is no significant difference. Of the three parameters, $g''(0)$ is the most sensitive. The average values of $g''(0)$, $g(0)$, and θ are listed in Table II for the points in the rigid lattice region. The indicated precisions are standard deviations.

Table I: A t-Test Comparison of Curvature, Intensity and Second Moment for Temperatures 307.2 and 99.2°K[a]

T	$g''(0)$ (10^{-16} sec^2)	t	t_1
307.2	-0.90 ± 0.16	4.80	2.82
99.2	-1.19 ± 0.08		
T	$g(0)$ (10^{-8} sec)	t	t_1
307.2	2.74 ± 0.04	3.96	2.82
99.2	2.81 ± 0.05		
T	σ^2 (10^{10} sec^{-2})	t	t_{50}
307.2	1.80 ± 0.08	0.367	0.685
99.2	1.81 ± 0.13		

[a] The indicated errors are standard deviations.

If the temperature variation of θ in the rigid lattice region is due to slow thermal motion, eq 5 should be descriptive of that variation. The correlation time τ

(10) W. J. Youden, "Statistical Methods for Chemists," Wiley, New York, N. Y., 1951.

Table II: Average Values of $g''(0)$, $g(0)$, and θ in the Rigid Lattice Region[a]

Temp, °K	$g''(0)$ (10^{-16} sec^2)	$g(0)$ (10^{-16} sec)	θ (10^{-5} sec)
99.2	1.190 ± 0.080	2.814 ± 0.048	0.651 ± 0.040
195.2	1.156 ± 0.09	2.757 ± 0.020	0.648 ± 0.030
246.5	1.108 ± 0.160	2.754 ± 0.029	0.631 ± 0.049
307.2	0.902 ± 0.159	2.740 ± 0.040	0.573 ± 0.060
336.2	0.663 ± 0.061	2.756 ± 0.030	0.489 ± 0.019

[a] The indicated precisions are standard deviations.

in eq 5 and 6 is usually equated to the mean atomic jump time of a diffusion process and should have a temperature dependence according to

$$\tau = \tau' \exp(E/RT) \quad (8)$$

The factor τ' may actually have a temperature dependence, but over a narrow temperature range the variation of τ' ordinarily is obscured by the exponential change. If there are several processes responsible for the changing magnetic environment, $1/\tau$ in eq 5 should be replaced by a sum over the separate terms $1/\tau_i$.

The value of θ for the rigidly fixed system of spins is evidently given closely by the value at 99°K. A log plot of $(1/\theta - 1/\theta')$ *vs.* $10^3/T$ is shown in Figure 6. The line is a least-squares fit of the data. Values for τ' and E are given in Table III. The precisions of these numbers are derived from estimates of the variances, as is usual in a least-squares fit.

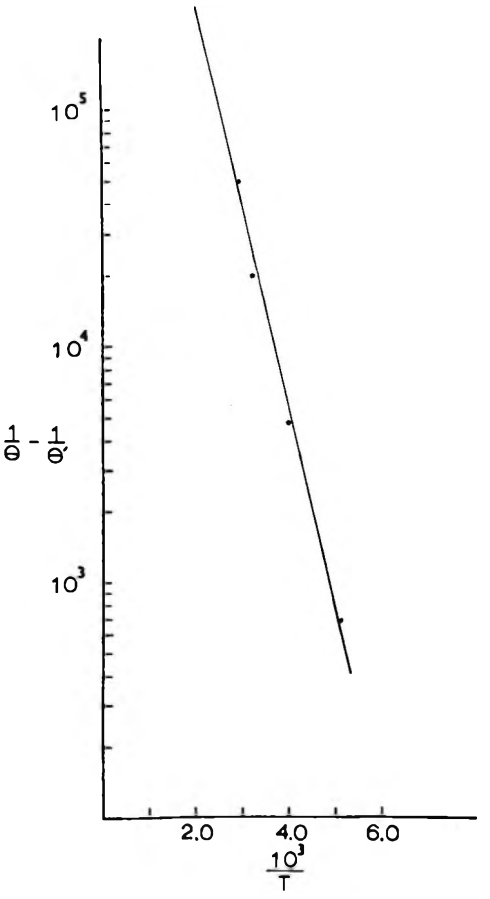

Figure 6. Log plot of $(1/\theta - 1/\theta')$ *vs.* $10^3/T$ for the rigid lattice region. The data are from Table II. A straight line least-squares fit of the points is drawn.

Table III: Values of E and τ' Obtained from Eq 5 and 8 for the Rigid Lattice Region Compared with E and τ' Obtained from Eq 9 and 8 for the Motionally Narrowed Region[a]

	Rigid lattice region	Motionally narrowed region — This paper	Motionally narrowed region — Reference 4
log τ'	−7.1 ± 0.2	−14.6 ± 0.6	−12.9 ± 0.5
E, kcal mol^{-1}	3.8 ± 0.2	18.9 ± 1.2	17.5 ± 1.0

[a] The numbers represent a least-squares fit of the data shown in Figures 6 and 7.

In the motionally narrowed region, the jump time τ was related to θ through the equation

$$1 = {}^1/_2(\tau/\theta'')^2[e^{-2\theta/\tau} - 1 + 2\theta/\tau] \quad (9)$$

where θ'' is the maximum value of θ. Equation 9 incorporates an obvious *ad hoc* adjustment in the equation previously used to relate the jump frequency with transverse relaxation time.[8] The values of $2/\tau$ obtained by solving eq 9 with $\theta'' = 0.5 \times 10^{-5}$ sec are shown in Figure 7. The results for τ' and E are shown in Table III. Compared with these values are the values of τ' and E obtained previously using T_2 defined by $G(T_2) = e^{-1/2}$.[8]

V. Discussion

A. Explanation Based on Motion. It has been found that, in the rigid lattice region, the experimental values of θ are described well by eq 5 with τ given by eq 8. This is very good evidence that a motional effect is responsible for the temperature dependence of θ. For the motionally narrowed region, the values of τ calculated using $T_2 = \theta$ are in good agreement with the values of τ using T_2 defined by $G(T_2) = e^{-1/2}$.

The position of hydrogen within the lattice and the diffusion mechanism in the motionally narrowed region have been studied in titanium hydrides by Stalinsky, *et al.*[11] They find that, in the rigid lattice region, the protons are situated in sites located at the tetrahedral positions around the titanium atoms. In the motionally narrowed region, diffusion proceeds by way of a vacancy mechanism involving empty tetrahedral sites. The octahedral sites appear to play little or no role in the diffusion mechanism. In $TiH_{1.94}$, the fraction of unoccupied tetrahedral sites is small, which implies that the diffusion mechanism involving vacancies two or more sites removed is unlikely. The assump-

(11) B. Stalinsky, C. K. Coogan, and H. S. Gutowsky, *J. Chem. Phys.*, **34**, 1191 (1961).

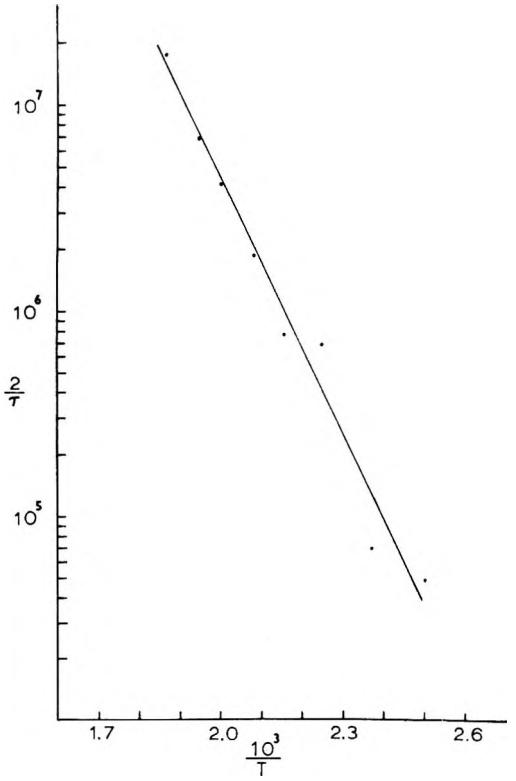

Figure 7. Log plot of $2/\tau$ *vs.* $10^3/T$ for the motionally narrowed region. Equation 9 was used to calculate τ from θ.

tion will be made here that diffusion in $TiH_{1.94}$ occurs by the movement of a proton into an immediately adjacent empty site.

Considerably different activation energies have been found in the present work for the two temperature regions. Evidently, two processes are involved. The simplest explanation of the observations based on two separate processes is as follows. The magnetic behavior of the spins is a collective one, but it is simpler to think in terms of the single spin approximation. The magnetic environment of a given spin may change in either of two ways. First, a spin may move to a neighboring vacancy, if that vacancy already exists. Second, the formation of a vacancy in the neighborhood of the spin is capable of changing the magnetic environment. The second process is much more complicated than the first, and there is no reason to suspect that the two processes have the same activation energy.

The time scale is important in the analysis of the effect of diffusion on relaxation. The time with which τ must be compared is θ'. Here, τ is the mean time of change of magnetic environment, and it must be related to the process causing that change. Suppose first that $\tau < \theta'$. The magnetic environment changes often by both processes before significant dephasing occurs. What is observed in this case is the composite process which has an activation energy equal to the sum of the activation energies of the two processes.[12] On the other hand, if $\tau > \theta'$, what is observed is one process or the other, but not both. In the last statement, the assumption was made that the probability of a simultaneous or near simultaneous occurrence of the two processes is negligible on the time scale for which θ' is small. In this case, the process which affects the magnetic environment occurs with a rate $\tau_1^{-1} + \tau_2^{-1}$ where τ_1 and τ_2 are the correlation times of the two processes.[12] If $\tau_1 \gg \tau_2$, only the second process will be effective as a relaxation mechanism. It seems probable that the activation energy 3.8 kcal/mol, observed for the rigid lattice region, is associated with a jump on an already present vacancy.

Diffusion in a pure metal proceeds by a least three processes. In addition to the two processes discussed above, there is the process of creating extra vacancies within the lattice. The experiment on lithium by Ailion and Slichter detected only one activation energy. The criterion for which their technique may be used to detect atomic motion is $\tau < T_1$. Evidently this criterion ensures that the process which affects the experimental data is the composite one with an activation energy equal to the sum of the separate activation energies.

B. Alternative Explanations. There are alternative mechanisms which might cause changes in the curvature of the absorption $g(\omega)$. Stalinski, *et al.*,[11] observed negative Knight shifts in titanium hydrides of various compositions. These shifts are dependent on concentration and temperature. If the sample were not homogeneous in concentration these shifts could cause changes in line shape. Such changes would by asymmetric. No asymmetry in the line shape is observed, and the values of $g''(0)$ are independent of whether one plots $g(\omega)$ *vs.* ω^2 for $\omega < 0$ or $\omega > 0$. It may be concluded that changes in curvature due to a distribution in Knight shifts are within the experimental error and are not responsible for the results reported here.

The shifts noted above actually may not be Knight shifts. They may be due to demagnetizing fields the magnitudes of which depend on the geometries of the particles in the sample.[13,14] The susceptibility of titanium hydride is dependent on concentration and temperature. The argument of the preceding paragraph may be repeated here to show that a distribution of shifts due to an inhomogeneous distribution of demagnetizing fields is not responsible for changes in curvature of absorption.

(12) In the simplified theory, rates are combined according to the rules of probabilities of independent processes. If both processes occur simultaneously, the overall rate is the product of the two rates. If one or the other but not both occur, then the overall rate is the sum of the rates. In the first case an activation energy exists for the composite process and is equal to the sum of the activation energies. In the second case no composite activation energy exists except when one rate is exceedingly larger than the other.

(13) D. S. Schreiber and L. D. Graham, *J. Chem. Phys.*, **43**, 2573 (1965).

(14) L. E. Drain, *Proc. Phys. Soc.*, **80**, 1380 (1962).

It is believed that the above arguments are effective in ruling out the possibility that either Knight shifts or magnetic susceptibility variations are responsible for the observed temperature dependence of θ'. A further test was applied to strengthen this conclusion. Spectra were taken at 307°K utilizing a radiofrequency of 16 Mc. The value of θ^2 at the frequency 16 Mc was equal to θ^2 at 8 Mc, within experimental precision. If the observed line shape variations were due to Knight shifts and magnetic susceptibility variations, they would be dependent on magnetic field.

One further possibility is that a small nonsecular broadening is present and is most evident in the vicinity of peak absorption. Experiment at room temperature indicates that T_1 is on the order of 0.1 sec. This is long compared to T_2, and it seems unlikely that the effects observed here could be due to T_1 broadening.

VI. Summary

Evidence has been presented which is believed to illustrate conclusively that motion of the spins, too slow to affect the second moment, may be detected by examining the finer features of the line shape. The new definition of T_2, while not drastically different from the older definitions, depends more on the finer features of the line shape than do the older definitions. The fact that the temperature dependence of θ is described by eq 5, in which τ is given by eq 8, strongly indicates that a rate process is involved.

The result of this work is that the range of correlation times, detectable by conventional nuclear magnetic resonance spectroscopy, may be extended by about two orders of magnitude. The upper end of the new range of correlation times is within the range detectable with the method of Slichter and Ailion.[2] The rates which may be detected with the present method may be called "slow" in contrast to the ultraslow rates detected with the method of Slichter and Ailion. The advantages of the method presented here are (1) simplicity in execution, and (2) the need for only conventional nmr apparatus.

The validity of the technique of modulating with very large amplitude followed by phase sensitive detection to produce an undistorted absorption spectrum has been demonstrated. The absorption method has the advantage that θ may be obtained more simply than with any other mode of spectral presentation.

Hydrogen Peroxide Formation upon Oxidation of Oxalic Acid in Presence and Absence of Oxygen and of Manganese (II). I. Manganese(VII), Cerium(IV), Chromium(VI), and Cobalt(III) as Oxidants

by I. M. Kolthoff,* E. J. Meehan, and Masaru Kimura[1]

School of Chemistry, University of Minnesota, Minneapolis, Minnesota 55455 *(Received March 16, 1971)*

Publication costs borne completely by The Journal of Physical Chemistry

In the presence of oxygen and an excess of manganese(II) the amount of hydrogen peroxide formed increases greatly with increasing temperature, increasing concentration of manganese(II), and decreasing rate of addition of permanganate, cerium(IV), or chromium(VI) to an acidified solution of oxalic acid. The three oxidants yield the same results, which indicates that the initial reaction is the formation of a complex manganese(III) oxalate, denoted as $Mn^{III}Ox$. The formation of large amounts of hydrogen peroxide is accounted for by a chain mechanism

$$Mn^{III}Ox \longrightarrow Mn(II) + CO_2 + CO\cdot^-; \quad CO_2\cdot^- + O_2 \longrightarrow O_2CO_2\cdot^-;$$
$$O_2CO_2\cdot^- + Mn(II) + Ox^{2-} + 2H^+ \longrightarrow Mn^{III}Ox + CO_2 + H_2O_2$$

A similar mechanism can be written for the formation of hydrogen peroxide in the decomposition of a solution of $K_3Co^{III}(C_2O_4)_3$ in acid medium, where the initial reaction is $Co^{III}(Ox)_3^{3-} \rightarrow Co(II) + 2Ox^{2-} + CO_2 + CO_2^-$. The effects of various factors on the peroxide formation are reported. In the absence of added manganese(II) the concentration of peroxide formed remains small, and no peroxide is formed with chromium(VI). Mechanisms are presented to account for these facts.

Introduction

It has been known for many years that small amounts of hydrogen peroxide are formed in the titration of oxalic acid with permanganate.[2,3] Hydrogen peroxide is not formed in the absence of oxygen. Since the titer of the oxalic acid is the same in the presence of oxygen as in its absence, the overall reaction leading to the formation of hydrogen peroxide must be

$$H_2C_2O_4 + O_2 \longrightarrow H_2O_2 + 2CO_2 \qquad (1)$$

Deiss[4] assumed the intermediate formation of peroxalic acid which disproportionates into carbon dioxide and hydrogen peroxide. However, Milburn and Taube[5] showed that peroxalic acid is formed only in strongly acid medium.

No systematic studies have been reported in the literature on the quantities of hydrogen peroxide formed under various experimental conditions. We have found that reaction 1 may occur quantitatively if a trace of permanganate or other oxidant is added very slowly to a mixture of oxalic acid, dilute sulfuric acid, and manganese(II). Before presenting the results of our experiments, a brief review is given of the interpretations of the mechanism and kinetics of the reaction between oxalic acid and permanganate.

From the work of Launer, *et al.*,[6] and Noyes, *et al.*,[7] it appears that two overall reactions can be written for the oxidation of oxalate in acid medium with permanganate in the presence of manganese(II)[7b]

$$MnO_4^- + 4Mn^{2+} + 5nC_2O_4^{2-} + 8H^+ \longrightarrow 5Mn(C_2O_4)_n^{3-2n} + 4H_2O \qquad (A)$$

$$2Mn(C_2O_4)_n^{3-2n} \longrightarrow 2Mn^{2+} + (2n-1)C_2O_4^{2-} + 2CO_2 \qquad (B)$$

where n may be 1, 2, or 3. In the absence of manganese(II) no reaction occurs between oxalic acid and permanganate. In the presence of manganese(II) the first steps of reaction A are postulated to be

$$MnO_4^- + MnC_2O_4 \longrightarrow MnO_4^{2-} + MnC_2O_4^+ \qquad (A_1)$$
$$Mn(VI) + Mn(II) \longrightarrow 2Mn(IV) \qquad (A_2)$$
$$Mn(IV) + Mn(II) \longrightarrow 2Mn(III) \qquad (A_3)$$

(1) This investigation was carried out under a grant from the National Science Foundation.

(2) (a) K. Schröder, *Z. Offentl. Chem.*, **16**, 270 (1910); (b) I. M. Kolthoff, *Z. Anal. Chem.*, **64**, 185 (1924).

(3) F. Oberhauser and W. Heusinger, *Ber.*, **61**, 521 (1928).

(4) E. Deiss, *Z. Angew. Chem.*, **39**, 664 (1926).

(5) R. M. Milburn and H. Taube, *J. Amer. Chem. Soc.*, **81**, 3515 (1959).

(6) (a) H. F. Launer, *ibid.*, **54**, 2597 (1932); (b) *ibid.*, **55**, 865 (1933); (c) Launer and D. M. Yost, *ibid.*, **56**, 2571 (1934).

(7) (a) R. M. Noyes, *Trans. N. Y. Acad. Sci.*, **13**, 314 (1951); (b) J. M. Malcolm and R. M. Noyes, *J. Amer. Chem. Soc.*, **74**, 2769 (1952); (c) S. J. Adler and R. M. Noyes, *ibid.*, **77**, 2036 (1955).

Manganese(III) forms various complexes with oxalate. Cartledge and Ericks[8] prepared the yellow $Mn^{III}(C_2O_4)_2^-$ and the red $Mn(C_2O_4)_3^{3-}$ complexes as salts in the solid state. In addition there can be formed a positively charged complex $Mn^{III}C_2O_4^+$ which apparently is cherry-red.[9] None of these complex ions is stable in solution and all decompose into Mn(II) and carbon dioxide, but with different rates, the red trioxalate complex giving the slowest reaction. Adler and Noyes[7c] found that the rate at which permanganate is reduced to manganese(III) and -(II) in a solution containing a large excess of oxalate is exactly equal to the rate at which the manganese(III) would form manganese(II) in the absence of permanganate. This is accounted for by the rapid formation of manganese(III) oxalate by the overall reaction

$$MnO_4^- + Mn^{2+} + (2n + 3/2)C_2O_4^{2-} + 8H^+ \longrightarrow 2Mn(III)(C_2O_4)_n^{3-2n} + 3CO_2 + 4H_2O$$

Launer,[6] Noyes,[7] and other authors agree that in the decomposition of manganese(III) oxalate a free radical $CO_2\cdot^-$ is formed

$$Mn^{III}(C_2O_4)_n^{3-2n} \longrightarrow Mn^{2+} + (n-1)C_2O_4^{2-} + CO_2 + CO_2\cdot^- \quad (B_1)$$

$$Mn^{III}(C_2O_4)_n^{3-2n} + CO_2\cdot^- \longrightarrow Mn^{2+} + nC_2O_4^{2-} + CO_2 \quad (B_2)$$

Dependent on the pH, oxalate concentration, and temperature, part of the manganese(II) is present as Mn^{2+} and part as a complex with oxalate. The formation of hydrogen peroxide was accounted for by Launer and Yost[6c] by the reactions

$$CO_2\cdot^- + O_2 \longrightarrow O_2CO_2\cdot^- \quad (C_1)$$

$$O_2CO_2\cdot^- + Mn(II) + 2H^+ \longrightarrow Mn(III) + H_2O_2 + CO_2 \quad (C_2)$$

For the sake of convenience we have written Mn(III) instead of $Mn^{III}(C_2O_4)_n^{3-2n}$. Reaction C_1 is expected to be very rapid.

Experimental Section

Chemicals. All chemicals used were of reagent grade. Baker's Analyzed CP manganous sulfate contained a trace of metallic impurity which gave a polarographic reduction wave; the species which causes it has not been identified. After two recrystallizations this wave had disappeared; the purified salt was used in all experiments. Air, pure oxygen, and mixtures of air and nitrogen served as sources of oxygen of different pressure. Tank nitrogen used for experiments in the absence of oxygen was passed over copper heated at 200°; the results were the same as those obtained without purification. A few experiments have been carried out on the formation of hydrogen peroxide in the decomposition of the cobalt(III) oxalate complex in acidified solutions. The green salt $K_3Co^{III}(C_2O_4)_3$ was prepared following the directions of Sörensen.[10]

Technique. Experiments in which the oxidant was added dropwise at a uniform rate over various periods of time were carried out in a gas stream, stirring of the solution sometimes being enhanced by a magnetic stirrer. When experiments were made in the absence of oxygen, the solution of oxidant being added was continually bubbled with nitrogen which was presaturated with water. Unless stated otherwise, experiments were carried out at room temperature.

Analysis. Hydrogen peroxide formed was determined iodometrically in the presence of some molybdate as catalyst[11] or polarographically. In several instances both methods were used in the analysis of a given sample and the same results were obtained. When the peroxide content was less than 5×10^{-4} *M*, the iodine formed was titrated amperometrically. At higher peroxide concentrations, the end point was found visually using starch as indicator.

The sum of hydrogen peroxide and residual oxalic acid was determined by titration with permanganate at 50°. Blank experiments with mixtures of hydrogen peroxide and oxalic acid solutions, containing the same constituents as the initial reaction mixtures, showed that the method of analysis yields reliable results. For the sake of brevity, concentrations are expressed in terms of the final reaction mixture, after addition of oxidant.

Results

Experiments without Added Manganese(II) Sulfate. Permanganate as Oxidant. A slow titration of 0.05 *M* oxalic acid in 0.5 *M* sulfuric acid was carried out at 25° with 0.1 *N* permanganate. After addition of 50 equiv % of oxidant in 10 min (*i.e.*, 0.01 *M* permanganate) the hydrogen peroxide content was 2×10^{-4} *M*. Upon further addition of only 1 equiv % of oxidant (2×10^{-4} *M*) in 1 hr the hydrogen peroxide content was 8.5×10^{-4} *M*, and upon further addition of 1 equiv % of permanganate in 4 hr [H_2O_2] was 15×10^{-4} *M*. In other experiments in the dark at 25° permanganate was added alsowly to 0.05 *M* oxalic acid in 0.1 *M* sulfuric acid. After addition of 13 equiv % permanganate in 1 hr [H_2O_2] was 0.14×10^{-4} *M*, after addition of 22% in 2 hr 0.4×10^{-4} *M*. However, when the initial reaction mixture was also 0.1 *M* in manganese(II) sulfate, the hydrogen peroxide content after addition of 13 equiv % permanganate in 1 hr was 5.0×10^{-3} *M*. The above and similar experiments (*vida infra*) with different initial concentrations of oxalic acid indicated

(8) G. H. Cartledge and N. P. Ericks, *J. Amer. Chem. Soc.*, **58**, 2061, 2065 (1936).

(9) H. Taube, *ibid.*, **69**, 1418 (1947).

(10) S. P. L. Sörensen, *Z. Anorg. Allg. Chem.*, **11**, 1 (1896).

(11) I. M. Kolthoff and R. Belcher, "Volumetric Analysis," Vol. III, Interscience, New York, N. Y., 1957, p 283.

that presence of manganese(II) and very slow addition of permanganate favor peroxide formation.

Addition of permanganate to a mixture of oxalic acid and hydrogen peroxide in the absence of added manganese(II) yielded results showing that hydrogen peroxide reacts faster than oxalic acid with the oxidant.

Ceric Sulfate as Oxidant. A large number of experiments was carried out in an oxygen stream in which cerium(IV) was used as oxidant. In all instances traces of hydrogen peroxide were formed. With initial concentrations of oxalic acid varying between 0.05 and 0.005 M the hydrogen peroxide concentration at various stages of the titration (slow, rapid, 25°, 50°) varied between 0.1 and 1.5×10^{-4} M. At 75° addition of 0.2 equiv % of oxidant to 0.05 M oxalic acid in an oxygen stream yielded peroxide concentrations of 3×10^{-4} and 6×10^{-4} M with addition times of 5 min and 1 hr, respectively. Again it was found that in the absence of added manganese(II) hydrogen peroxide reacts much faster with the oxidant than oxalic acid does.

Chromium(VI) as Oxidant. With potassium dichromate as oxidant no hydrogen peroxide formation was ever observed (absence of manganese(II)) even at 75° in an oxygen atmosphere.

Experiments in the Presence of Manganese(II) Sulfate. Permanganate as Oxidizing Agent. Absence of Oxygen. A large number of experiments were carried out in a nitrogen atmosphere, in which 0.1, 1, 2, and 10 equiv % of permanganate was added in 1, 2, 3, and 4 hr, respectively, and at temperatures of 25, 50, and 75°. The initial solutions were 0.02, 0.01, or 0.001 M in oxalic acid, and 0.1 M in sulfuric acid and 0.1 M in manganous sulfate. Under no conditions was peroxide formed and the amount of oxalic acid decomposed was equivalent to the amount of permanganate added. Experiments were carried out with solutions 0.005 M in oxalic acid and in hydrogen peroxide and 0.1 M in sulfuric acid and in manganese(II). After 4 hr at 25° no reaction between oxalic acid and peroxide was observed; at 50° after 4 hr 2 to 3% peroxide and oxalic acid had reacted. At 75° the reaction was more pronounced; after 2 hr 16% had reacted and after 4 hr 35 to 38%.

Experiments were also carried out at 50° in nitrogen in which to the above reaction mixture (0.005 M in oxalic acid and in peroxide) 2 and 10% equiv % of permanganate, respectively, were added in 4 hr. In both instances 20% of oxalic acid and 20% of hydrogen peroxide had reacted, indicating that slow addition of permanganate at 50° induces the reaction between oxalic acid and peroxide in the presence of manganous sulfate.

Presence of Oxygen. Temperature 25°. Effects of Time of Addition of Various Amounts of Mn(VII) and of Concentration of Oxalic Acid. In Table I are reported results obtained with an initial concentration of oxalic acid of 0.01 M. The same results were found in the dark and in daylight.

Table I[a]

$KMnO_4$ added, equiv %	Addition time of $KMnO_4$, hr: 0.1	0.5	1	2	4
	$[H_2O_2]$ formed $\times 10^4$ M				
60		15		26	32
30				34	
10		23			50
5		21		37	44
1	6.0	11.0	17.4	24	29
0.5	1.6	8.5		17	
0.1		1.9		6.0	10.0
0	0	0	0	0	0 (after 8 hr)

[a] Solution 0.01 M in oxalic acid, 0.1 M in sulfuric acid, and 0.1 M in $MnSO_4$; O_2 saturated; 25°.

From Table I it is seen that the rate of addition of permanganate has a large effect upon the amount of peroxide formed. In all instances the final concentration of oxalic acid was determined. When 5 equiv % or less permanganate was added, the molar concentration of hydrogen peroxide formed was found almost equal to the concentration of oxalic acid which had disappeared, taking into account the effect of permanganate added; *i.e.*, equivalents of peroxide formed equals equivalents of oxalic acid disappeared minus equivalents of permanganate added. Actually in most experiments it was found that 1 to 2% less peroxide was formed than oxalic acid which had disappeared. Similar results as in Table I were found when the initial concentration of oxalic acid was 0.05 and 0.001 M. Results obtained at the latter concentration are listed in Table II.

Table II[a]

$KMnO_4$ added, equiv %	Addition time of $KMnO_4$, hr: 0.5	1	2	4
	$[H_2O_2]$ formed $\times 10^4$ M			
50	4	5	5	5
20	7.5	7.5	7.5	7.5
10		9.0		9.6
5	8.6	9.0		9.0
2	6.6	9.6		9.5
0.5	3.6	5.6	6.6	8.6
0.2	2.4		4.1	6.4
0				0

[a] Conditions as in Table I; except 0.001 M oxalic acid (instead of 0.01 M).

Again it is clear that the amount of hydrogen peroxide formed increases with decreasing rate of addition of permanganate. When 2 equiv % permanganate was added in 4 hr, practically all oxalic acid had yielded an equimolar amount of peroxide. This corresponds to the overall reaction 1, in which the decomposition of

nearly 0.001 M oxalic acid in the presence of oxygen is induced by the addition of only 8×10^{-6} M permanganate. When more permanganate, *e.g.*, only 5 equiv %, was added, most of the oxalic acid had reacted with oxygen (eq 1), no oxalic acid being left after 4 hr. In the experiments in Tables I and II a slow stream of oxygen was passed through during the addition of permanganate. The experiments were repeated with additional stirring with a magnetic stirrer; the same results were obtained.

Effect of Concentration of Manganese(II) Sulfate. This effect is quite large. Experimental conditions were the same as in Table I; the same results were obtained in both light and dark. When 1 equiv % of permanganate was added in 2 hr, the percentages of oxalic acid having reacted to yield hydrogen peroxide were 0.5, 12, and 25 at manganese(II) concentrations of 0, 0.01, and 0.1 M respectively. With an addition time of 4 hr the percentages were 0.5, 15, and 30.

Effect of Initial Presence of Hydrogen Peroxide. Experimental conditions were the same as in Table I, except that the original reaction mixture also contained 1, 2, 5, 10, and 20 mol % (referred to oxalic acid concentration), respectively, of hydrogen peroxide; the amount of permanganate added varied between 1 and 0.05 equiv %. No effect of the initial concentration of peroxide upon the amount of peroxide formed was observed.

Effect of Concentration and Kind of Acid. The effect of the concentration of sulfuric acid was investigated in a solution of the composition given in Table I. For the sake of brevity only results are given after addition of 1 equiv % of permanganate in 4 hr. The molar concentrations of hydrogen peroxide were 2.0×10^{-3} in 0.01 M, 2.9×10^{-3} in 0.1 M, and 3.4×10^{-3} in 1 M sulfuric acid. With hydrochloric instead of sulfuric acid and 0.1 M manganese(II) chloride instead of sulfate the peroxide concentration in 0.2 M acid was 3.0×10^{-3} M. With 0.1 M phosphoric acid and 0.1 M manganese(II) sulfate the peroxide content was 1.9×10^{-3} M and with 0.5 M phosphoric acid 2.8×10^{-3} M. When no acid was added (the initial reaction mixture was 0.01 M in oxalic acid) the hydrogen peroxide concentration was 1.7×10^{-3} M, either in the presence of 0.1 M manganese(II) sulfate or chloride. It may be noted that in the absence of added acid the peroxide concentration was the same as in the presence of 0.1 M phosphoric acid. Perchloric acid had the same effect as hydrochloric acid. The effect of a neutral salt, sodium perchlorate, was determined in a solution of the composition given in Table I. The concentrations of peroxide formed after addition of 1 equiv % permanganate were 2.5, 2.1, and 1.8×10^{-3} M after 2 hr in the presence of 0, 0.5, and 1 M salt and 2.9, 2.4, and 2.2×10^{-3} after 4 hr addition.

Effect of Temperature and Other Variables at Higher Temperatures. The effect of temperature on hydrogen peroxide formation is large. Examples are given in Table III.

Table III[a]

Temp, °C	Time of addition, hr: 0.1	1	4
	$[H_2O_2] \times 10^4$ M		
0		1.3	3.2
25	6	17	29
50	16	47	65
75	27	86	90

[a] Composition as in Table I. Results in dark the same as in daylight; 1 equiv % of permanganate added. Oxygen, washed through water at the listed temperature, passed through reaction vessel.

As in all previous experiments the residual oxalic acid was determined. Corrected for the amount of permanganate added the concentration of oxalic acid corresponding to that which had disappeared was 0.5 to 1.5×10^{-4} M greater than peroxide formed, except in the 4-hr experiment at 75° when practically all oxalic acid had disappeared. Apparently some hydrogen peroxide decomposed at this high temperature, as the concentration of peroxide formed should be 97×10^{-4} M, as compared to 90×10^{-4} M found.

The effect of concentration of sulfuric acid on peroxide formation was found to be much larger at higher temperatures than at room temperature. For example, using a reaction mixture and conditions as in Table III, but at varying sulfuric acid concentrations, the peroxide concentration after addition of 1 equiv % of permanganate in 1 hr at 50° was 1.3, 4.7, and 5.4×10^{-3} M at initial concentrations of acid of 0.01, 0.1, and 1.0 M, respectively. When carried out at 75°, the corresponding peroxide concentrations were 2.9, 8.6, and 6.5×10^{-3} M as compared to 1.1, 1.7, and 2.1×10^{-3} M at 25°. In these experiments the concentration of oxalic acid disappeared was 1 to 2×10^{-4} M greater than the concentration of peroxide formed. In the above and the following series of experiments additional stirring with a magnetic stirrer had no effect on the results. The effect of concentration of manganous sulfate was determined at 50°. The composition of the reaction mixture and experimental conditions were the same as in Table I, except that 0.5 equiv % of permanganate was added in 4 hr at 50°. At initial concentrations of manganous sulfate of 0.01, 0.05, 0.1, 0.25, and 0.50 M the concentrations of peroxide formed were 3.4, 5.5, 6.7, 6.8, and 6.9×10^{-3} M, respectively. Within the experimental error the molar concentration of oxalic acid disappeared was equal to that of peroxide formed.

Effect of Oxygen Concentration. At the same composition and under the experimental conditions as in Table I 0.5 equiv % permanganate was added in 4 hr at 50°, while the solution was bubbled with either oxygen or air or a mixture of four parts of nitrogen and one

part of air. The concentrations of peroxide formed were 6.7 (O_2), 5.1 (air), and 1.1 $\times 10^{-3}$ M, respectively. Again the number of moles of peroxide formed was equal to that of oxalic acid which had disappeared.

Cerium(IV) Sulfate or Chromium(VI) as Oxidizing Agents. Many of the experiments reported in the preceding section at a manganous sulfate concentration of 0.1 M were repeated using cerium(IV) or chromium(VI) as oxidants. The results were the same as those obtained with permanganate.

Decomposition of Solutions of $K_3Co^{III}(C_2O_4)_3$. Dark green solutions of this salt are unstable, 1 mol of cobalt(III) oxidizing 0.5 mol of oxalic acid; the resulting solution has a pink color due to cobalt(II). When the initial concentration of the salt was greater than 0.025 M a pink precipitate of cobalt(II) oxalate was formed. Upon decomposition in 0.1 M sulfuric acid in the presence of manganese(II) and oxygen, hydrogen peroxide was formed, the results being the same in light and dark. In all instances the amount of peroxide formed was equimolar to the amount of oxalic acid oxidized. No peroxide was formed in the absence of oxygen. Most of the experiments were carried out at 50°, the solutions being 0.1 M in sulfuric acid. Under these conditions and in the absence of oxygen the salt in the solution had decomposed completely in about 3 hr; in the presence of oxygen the decomposition rate was considerably smaller. A few results on the effect of concentration of cobalt(III) salt, of manganese(II), and of time of standing on the formation of hydrogen peroxide are reported in Table IV.

Again presence of manganese(II) promotes the formation of peroxide. On the other hand, in the absence of manganese(II) the concentrations of peroxide formed were much greater than with permanganate or cerium(IV) as oxidants. The amounts of peroxide formed after the complete decomposition of the complex in the absence of manganese(II) were the same at 25 and at 50°, the rate of decomposition of the salt at 25° being about one-fortieth as large as at 50°.

Table IV: Peroxide Formation in Decomposition of Solutions of $K_3Co(C_2O_4)_3$ at 50°[a]

Concentration Co(III) salt, M	$[MnSO_4]$, M	Time of standing, hr	$[H_2O_2]$ $\times 10^3$, M
0.011	0	0.2	0.75
0.011	0	4	1.5
0.011[b]	0	4	2.2[b]
0.011	0.04	4	8.2
0.02	0	4 to 10	2.5[c]
0.02	0.01	4 to 8	10.3[c]

[a] Solution 0.1 M in sulfuric acid. Air passed through. [b] Oxygen passed through. [c] Pink precipitate formed after 2 hr; after complete decomposition solution was barely pinkish.

Discussion

In the Introduction it has been mentioned that manganese(III) can form three complexes with oxalate. We will use the notation $Mn^{III}Ox$ for these complexes. Manganese(II) also can form one or more complexes with oxalate, and we use the symbol Mn(II) for all forms of manganese(II). As with $Mn^{III}Ox$, equilibria are dependent on concentrations of manganese, oxalate, and acid and on temperature.

In the presence of sufficient Mn(II) the amount of hydrogen peroxide formed was the same, irrespective whether small amounts of permanganate, cerium(IV), or chromium(VI) were used as oxidants. Therefore in all instances the initial reaction (for simplicity not balanced) must be the following

$$\text{Mn(VII) or Ce(IV) or Cr(VI)} + \text{Mn(II)} + Ox^{2-} \longrightarrow Mn^{III}Ox \quad (2)$$

Since the concentration of peroxide formed is many times greater than corresponds to the concentration of oxidant added, a chain reaction must occur in the presence of oxygen

$$Mn^{III}Ox \longrightarrow \text{Mn(II)} + CO_2 + CO_2\cdot^- \quad \text{[measurable rate]} \quad (B_1)$$

$$CO_2\cdot^- + O_2 \longrightarrow O_2CO_2\cdot^- \quad \text{[very fast]} \quad (C_1)$$

$$O_2CO_2\cdot^- + \text{Mn(II)} + 2H^+ \longrightarrow H_2O_2 + CO_2 + Mn^{III}Ox \quad \text{[fast]} \quad (C_2)$$

Reactions B_1, C_1, and C_2 constitute a chain reaction in which eq 2 is the initiating reaction. The most probable termination reaction is

$$CO_2\cdot^- + Mn^{III}Ox \longrightarrow CO_2 + \text{Mn(II)} \quad \text{[fast]} \quad (3)$$

The amount of peroxide formed increases very much with decreasing rate of addition of oxidant. The reason is that there is competition between reactions C_1 and 3. The instantaneous concentration of $Mn^{III}Ox$ becomes smaller with slower addition of oxidant thus favoring reactions C_1 and C_2 over 3.

Quantitatively, the sequence of reactions 2, B_1, C_1, C_2, and 3, with any of the oxidants listed in reaction 2, leads to the following predicted kinetics. In the following, O represents Mn(VII), Ce(IV), or Cr(VI). In the initial presence of Mn(II), considering the small amount of O added, [Mn(II)] remains constant. Similarly $[O_2]$ and $[Ox^{2-}]$ are constant. The concentrations of these three substances are not included in the rate expressions, but are understood to be included in the appropriate rate constants. When c_0 moles of O per liter of final solution is added continuously over the interval τ sec, we have for time t up to τ

$$\frac{d[O]}{dt} = \frac{c_0}{\tau} - k_2[O] \quad (I)$$

$$[O] = \frac{c_0}{\tau}(1 - e^{-k_2 t}) \quad (II)$$

With all the oxidants k_2 is relatively large, and for the values of t and τ used in the present work (II) reduces to (III)

$$[O] = \frac{c_0}{k_2 \tau} \quad (III)$$

The rate of formation of hydrogen peroxide is given by (IV)

$$\frac{d[H_2O_2]}{dt} = k_{c_2}[O_2CO_2]\cdot^- \quad (IV)$$

The assumption of steady states for $Mn^{III}Ox$, $OCO_2\cdot^-$, and $CO_2\cdot^-$ leads to (V)

$$k_{c_2}[O_2CO_2\cdot^-] = -\frac{k_2[O]}{4} + \frac{1}{4}\sqrt{k_2^2[O]^2 + \kappa k_2[O]} \quad (V)$$

where $\kappa = 8k_{B_1}k_{c_1}/k_3$. Substituting (III) and integrating to $t = \tau$ gives the result

$$[H_2O_2] = -\frac{c_0}{4} + \frac{1}{4}\sqrt{c_0^2 + \kappa c_0 \tau} \quad (VI)$$

The value of k_2 does not appear in eq VI. Therefore the amount of peroxide formed should be independent of the oxidant, as is observed. Figure 1, which is based on the data of Table I with Mn(VII) as oxidant, is a plot of $\{[H_2O_2] + c_0/4\}^2$ *vs.* τ. In Table I, 1 equiv % of Mn(VII) corresponds to 2×10^{-5} M. The plots should be straight lines with slopes proportional to c_0. (Under most of the conditions of Table I, c_0 is so small with respect to $[H_2O_2]$ that $[H_2O_2]$ is proportional to $\tau^{1/2}$.) The agreement with eq VI is satisfactory for the smallest values of c_0, the value of κ being 3.4, 4.0, and 4.1×10^{-5} (t in sec) for $c_0 = 2 \times 10^{-6}$, 1×10^{-5}, and 2×10^{-5} M, respectively. At $c_0 = 1 \times 10^{-4}$ M, the dependence on τ is of the same form as at smaller c_0, but κ is only 2×10^{-5}. The sequence of reactions 2, ...3 cannot account for a maximum formation of peroxide at an intermediate c_0 (*cf.* Table I). Equation VI does not hold at the higher rates of addition (higher values of c_0), undoubtedly as a result of the reaction of Mn(III) with hydrogen peroxide. A quantitative interpretation of the effects of Mn(II), H^+, and $H_2C_2O_4$ is not possible, as the equilibria determining the concentrations of various forms of Mn(III) and Mn(II) are not known. Also, it is not known how temperature affects the equilibria between the various Mn(III) and Mn(II) complexes. The hydrogen ion concentration also affects these equilibria. The large increase in peroxide formation with increasing temperature probably must be accounted for by the increase in the rate of decomposition of $Mn^{III}Ox$ (reaction B),

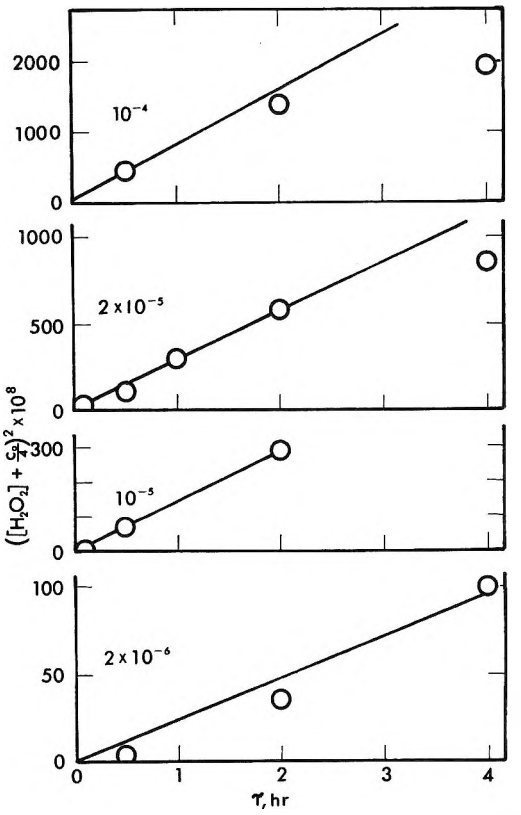

Figure 1. Plot of $([H_2O_2] + c_0/4)^2$ *vs.* τ (*cf.* eq VI, Table I) for indicated values of c_0.

although the rates of the other reactions also increase. It is interesting to note that, according to Launer,[6a] increase of ionic strength greatly increases the rate of decomposition of $Mn^{III}Ox$, while in the present work we found a slight decrease in the amount of peroxide formed with increasing ionic strength. Launer carried out most of his experiments at a pH of the order of 5, while in our work the pH was of the order of 1. Also, Launer used a large excess of oxalate over manganese, resulting in the formation of $Mn^{III}(C_2O_4)_3^{3-}$, while in many of our experiments conditions were favorable for the formation of $Mn^{III}(C_2O_4)_2^-$ and $Mn^{III}(C_2O_4)^+$, the rates of decomposition of the lower oxalate complexes being much greater than that of the trioxalate (Taube[9] and Adler and Noyes[7c]).

In the absence of manganese(II) in the reaction mixture the amounts of peroxide formed on titration with permanganate or cerium(IV) sulfate are found to be very small. With the latter oxidant no manganese is present during the titration. The formation of peroxide in the presence of oxygen is accounted for by the following reactions

$$C_2O_4^{2-} + Ce(IV) \longrightarrow Ce(III) + CO_2 + CO_2\cdot^- \quad (4)$$

$$CO_2\cdot^- + O_2 \longrightarrow O_2CO_2\cdot^- \quad (C_1)$$

$$O_2CO_2\cdot^- + H^+ \longrightarrow HO_2\cdot + CO_2 \quad (5)$$

$$2HO_2\cdot \longrightarrow H_2O_2 + O_2\cdot \quad (6)$$

The reason why the concentration of peroxide remains so small during the titration is that hydrogen peroxide reacts much more rapidly with cerium(IV) than oxalic acid does.

With permanganate as oxidant manganese(II) and -(III) are formed during the titration. When the titration is carried out very slowly, the amount of peroxide formed increases in the latter stages of the titration. It is of interest to note that with dichromate as oxidizing agent (absence of Mn(II)) not a trace of peroxide is formed. Apparently, no $CO_2\cdot^-$ free radical is formed, which can be explained by the following reaction mechanism

$$C_2O_4^{2-} + Cr(VI) \longrightarrow 2CO_2 + Cr(IV)$$
$$Cr(IV) + Cr(VI) \longrightarrow 2Cr(V)$$
$$2Cr(V) + 2C_2O_4^{2-} \longrightarrow 4CO_2 + 2Cr(III)$$

In the beginning of the section on experimental results it was shown that in the presence of excess manganese(II) and absence of oxygen small amounts of permanganate induce the oxidation of oxalic acid by hydrogen peroxide in a nitrogen atmosphere. The $Mn^{III}Ox$ formed yields $CO_2\cdot^-$ which can react with hydrogen peroxide by a chain reaction mechanism

$$CO_2\cdot^- + H_2O_2 \longrightarrow CO_2 + OH^- + OH\cdot$$
$$OH\cdot + Mn^{II}Ox \longrightarrow Mn^{III}Ox + OH^-$$

followed by (B_1).

In the absence of added manganese(II) the amount of hydrogen peroxide formed is much greater with $K_3Co^{III}(C_2O_4)_3$ as oxidizing agent than with permanganate or cerium(IV). The primary reaction again yields $CO_2\cdot^-$, which apparently is not oxidized by the cobalt(III) or only very slowly as compared to its reaction with oxygen to form $HO_2\cdot$ which in turn disporportionates into peroxide and oxygen (eq 5 and 6). The favorable effect of added manganese (Table IV) upon the formation of peroxide must be attributed to the occurrence of reaction C_2, considering that upon decomposition of 1 mol of $K_3Co^{III}(C_2O_4)_3$ 2 mol of uncomplexed oxalate is formed.

In subsequent papers the hydrogen peroxide formation with oxygen as oxidant and the effect of retarders will be discussed.

Photochemically Induced Isotopic Exchange between Iodobenzene and Molecular Iodine

by A. Levy,* D. Meyerstein,

Nuclear Research Centre-Negev, Israel

and M. Ottolenghi

Department of Physical Chemistry, The Hebrew University, Jerusalem, Israel *(Received March 8, 1971)*

Publication costs borne completely by The Journal of Physical Chemistry

The photochemical isotopic exchange between iodobenzene and radioactive molecular iodine ($I^{131}I$) was studied in methylcyclohexane solutions. The limiting exchange yields, ϕ_{EX}^0, measured at several excitation wavelengths in the uv range were found to be identical with the corresponding deiodination limiting yields, ϕ_{DE}^0. This observation and a study of the effects of dissolved oxygen and iodine concentrations suggest that the exchange is initiated by photocleavage of iodobenzene to phenyl (Ph·) and iodine radicals, with O_2 and I_2 competing in the scavenging of Ph· ($k_{I_2+Ph\cdot}/k_{O_2+Ph\cdot} = 2.1 \pm 0.5$). The photocleavage of iodobenzene was found to be wavelength dependent in the near-uv range (*e.g.*, 334 and 365 nm), where part of the absorption leads directly to the iodobenzene triplet. It is suggested that dissociation takes place from the lowest excited singlet, but practically not from the triplet state. It is shown that iodine atoms, produced by selective excitation in the visible range, do not exchange with iodobenzene. Neither does excitation of the charge-transfer (CT) complex between iodobenzene and iodine lead to exchange or deiodination.

Introduction

The isotopic exchange process $AI + I^*I \rightarrow AI^* + I_2$ where A is aliphatic, olefinic, or aromatic, can be induced by thermal, radiation-, or photochemical activation.[1-8] The mechanisms of the thermal[3] and radiation[4,5] induced exchange in aromatic iodides have been recently investigated and discussed. However, only partial and controversial information appears to be available concerning the corresponding photochemical exchange process. Such a process, first reported by Noyes,[6] was later studied by Anbar and Rein[7] who suggested the step $ArI + I\cdot^* \rightarrow ArI^* + I\cdot$ as the major exchange path. This conclusion appears to be inconsistent with observations (see ref 5 and later in this work) indicating that iodine atoms are unreactive with iodoaromatics.

In an attempt to elucidate the mechanism of the photochemical exchange, we have recently investigated the $PhI-I^{131}I$ system using monochromatic excitation at 365, 334, and 313 nm.[8] The observed yields were found to be wavelength dependent but, under the corresponding experimental conditions ($[I_2] > 10^{-3}\ M$), they were not significantly affected by deaeration. Such observations induced us at the time to reject the dissociation $PhI \xrightarrow{h\nu} Ph\cdot + I\cdot$ as the step initiating the exchange process, favoring a mechanism involving an excited state of the $PhI\cdot I^{131}I$ CT complex. This was supported by the wavelength dependence of the iodobenzene exchange yields, in contrast to those of the corresponding deiodination process which were assumed to be wavelength independent. Very recently we have reexamined these conclusions in view of new experiments showing an oxygen effect on the exchange yields, detectable at low iodine concentrations. In the present work these new data are reported accompanied by a careful reinvestigation of the effects of wavelength, as well as those of oxygen and iodine, on the photodeiodination of iodobenzene. It will be shown that all observations lead to the formulation of a new reaction scheme for the photoexchange of iodine in iodoaromatics, involving phenyl radicals. The clarification of the photochemical exchange mechanism bears also on practical applications, such as the development of "clean" labeling techniques for aromatic iodides, free from by-products such as those associated with thermal or radiation-chemical methods.

Experimental Section

Materials. Iodobenzene (Aldrich Chemical Co.) was purified by vacuum distillation in an atmosphere of dry nitrogen. Light absorption at 365 nm was used for

(1) R. M. Noyes and D. J. Sibbett, *J. Amer. Chem. Soc.*, **75**, 767 (1953).

(2) R. K. Sharma and N. Kharasch, *Angew. Chem., Int. Ed. Engl.*, **7**, 36 (1968).

(3) M. Nakashima, C. Y. Mok, and R. M. Noyes, *J. Amer. Chem. Soc.*, **91**, 7635 (1969).

(4) A. Appleby, J. C. Charlton, and R. E. Spillett, *Chem. Commun.*, 958 (1967).

(5) R. Riess and H. Elias, *J. Phys. Chem.*, **74**, 1014 (1970).

(6) R. M. Noyes, *J. Amer. Chem. Soc.*, **70**, 2614 (1948).

(7) M. Anbar and R. Rein, *Chem. Ind. (London)*, 1524 (1963).

(8) A. Levy, D. Meyerstein, and M. Ottolenghi, *J. Amer. Chem. Soc.*, **92**, 418 (1970).

checking the purity of iodobenzene solutions in methylcyclohexane (ϵ_{PhI} at 365 nm, 0.13 ± 0.01). Iodine, resublimed (Fisher Scientific Co.), and methylcyclohexane (Matheson spectroquality) were used with no further purification.

Allyl iodide, used as a monitor of iodine atoms, was purified by the method described by Sibbett and Noyes.[9]

Iodine-131 carrier-free, in a basic aqueous iodide solution containing no reducing agents, was produced at the Nuclear Research Centre, Negev, by dry distillation of reactor-irradiated TeO_2. Special care (using triply distilled water) was taken to ensure that the solution was free from organic impurities.

Light Source and Actinometry. Excitation wavelengths were selected from a medium pressure mercury arc by means of interference (Baird-Atomic Inc. λ 254, 313, and 334 nm). Corning glass (λ 365 nm with 0–52 and 7–37, and λ > 520 nm with 3–69) or Pyrex glass (λ > 285 nm) filters.

Actinometry in the uv range was performed using an uranyl oxalate actinometer. The rate of iodine atoms production by irradiation of iodine solutions in the visible range was evaluated using allyl iodide (0.1 *M*) as a selective iodine atom scavenger.[10]

Procedure. Solutions of radioactive iodine were prepared by shaking a 3-ml I_2–methylcyclohexane solution for 5–10 min with about 1 ml of aqueous iodide-131 solution, to which 0.2 ml of 0.1 *M* H_2SO_4 and 0.1 ml of 0.01 *M* KIO_3 were previously added. The organic layer was separated and used for exchange experiments within 2 days. For each irradiation a sample of 0.5–1.5 mCi, or 0.5–1.5 μCi in the low activity samples, was employed. Solutions were deaerated by consecutive freeze and thaw cycles on a vacuum line. Oxygen concentrations were controlled by shaking the solution under the appropriate pressure of air. The exact amounts of dissolved oxygen were determined using gas-liquid chromatography on an 8-ft 13X molecular sieve column at 100°. At 23°, under a partial air pressure of 720 mm, the value of 3.4×10^{-3} *M* was obtained. After the irradiations, always carried out at room temperature, 24 ± 1°, a known volume of the reaction mixture was shaken thoroughly for 10 min with a basic aqueous thiosulfate solution (0.1 *M* NaOH and 0.1 *M* $Na_2S_2O_3$). A part of the organic layer was then separated and counted in an ionization chamber (Mediac dose calibrator, Nuclear–Chicago) or in a well-type NaI(Tl) 2-in. crystal for the low activity samples. A blank, nonirradiated, sample was submitted to the same treatment, to account for thermal exchange. When low activity samples were used, iodine concentrations were determined spectrophotometrically before and after each irradiation. Exchange yields at 365 nm were found to be considerably affected by impurities, probably because of the very weak absorption of iodobenzene in this spectral range. This is apparently the reason for the somewhat higher exchange yields reported previously at 365 nm.[8]

Deiodination yields were determined by measuring the optical density of the iodine photoproduct at 520 nm (ϵ_{I_2} 910), using a Hilger (Uvispek H 700) spectrophotometer.

Treatment of Data. The rate of exchange, R_{EX}, was calculated by applying McKay's equation[11] to our experimental conditions in which $[PhI] \gg [I_2]$, leading to

$$R_{EX} = \frac{2[\bar{I}_2] \ln\left(\frac{1}{1-F}\right)}{t} \quad (1)$$

where F is the exchange fraction and $[\bar{I}_2]$ is the average molar iodine concentration during the irradiation time t. This equation was used since the maximum increase in iodine concentration during a run was only 10%, while the change in iodobenzene concentration was of course negligible. Under these conditions, computation according to the method of Luehr, *et al.*,[12] which takes into account changes in the concentration of the reactants, does not give any improvement relative to the range of our experimental accuracy. The exchange quantum yield, Φ_{EX}, was determined by means of the expression

$$\phi_{EX} = \frac{R_{EX}}{I_0 \alpha_x} \quad (2)$$

where I_0 is the intensity of light reaching the reaction cell (einstein/second, liter) and α_x is the light fraction absorbed by the photoactive species x, *e.g.*, identifying x with iodobenzene, we obtain $\alpha_{PhI} = D_{PhI}(\alpha_T/D_T)$ where D_T and α_T are, respectively, the total optical density and the total light fraction absorbed. The corresponding expression for the deiodination process is

$$\phi_{DE} = \frac{R_{DE}}{I_0 \alpha_x} = \frac{2\Delta[I_2]}{t(I_0 \alpha_x)} \quad (3)$$

where $\Delta[I_2]$ is the increment in the iodine concentration at time t.

Results and Discussion

1. Excitation within the Visible I_2 Band. In order to check the role of iodine atoms produced as the only reactive radicals in the PhI–$I^{131}I$ system, we have submitted deaerated iodobenzene–$I^{131}I$ solutions in methylcyclohexane to visible light excitation. A 3–69 Corning glass filter was employed to transmit light above 520 nm, in the range of the iodine absorption

(9) D. J. Sibbett and R. M. Noyes, *J. Amer. Chem. Soc.*, **75**, 761 (1953).

(10) (a) F. W. Lampe and R. M. Noyes, *ibid.*, **76**, 2140 (1954); (b) J. Zimmerman and R. M. Noyes, *J. Chem. Phys.*, **18**, 658 (1950).

(11) See A. C. Wahl and N. A. Bonner, "Radioactivity Applied to Chemistry," Wiley, New York, N. Y., 1951, p 7.

(12) C. P. Luehr, G. E. Challenger, and B. J. Masters, *J. Amer. Chem. Soc.*, **78**, 1314 (1956).

band. The iodobenzene concentration was 0.1 M and that of the iodine carrier was varied in the 7×10^{-5} to 8×10^{-4} M range. Under these conditions light is exclusively absorbed by molecular iodine leading to iodine atoms. No photochemically induced pickup of radioactive iodine by iodobenzene could be detected, even after prolonged irradiations. From the yields of iodine atoms production, estimated by means of the allyl iodide technique,[10] an upper limit of $\phi_{EX} < 10^{-5}$ was determined for the exchange induced by excitation within the visible I_2 band. We may therefore conclude that iodine atoms as such do not play a detectable role in the photochemical process. This conclusion, in agreement with a previous suggestion of Riess and Elias,[5] rules out the exchange process ($ArI + {}^{131}I\cdot \rightarrow Ar^{131}I + I\cdot$) suggested by Anbar and Rein[7] for alcoholic solutions. An alternative path: $ArI\cdot I^{131}I + I\cdot \rightarrow Ar^{131}I\cdot I_2 + I\cdot$, involving a reaction between an iodine atom and an iodobenzene–iodine CT complex, is also ruled out in our systems by the present experimental data. Such a mechanism has been recently proposed by Milligan and coworkers to account for the closely related photochemical interchange of halogens between haloaromatics and halogen molecules in solution.[13]

2. Exchange and Deiodination Induced by Uv Irradiation. As previously reported[2,6,8] uv irradiation of iodobenzene–iodine systems leads to a substantial exchange of iodine. As expected from a simple exchange process, the radioactivity of the aromatic material was found to be proportional to the initial iodine radioactivity. The exchange rate exhibited the characteristic exponential dependence on the irradiation time, and the equilibrium value $[PhI^*]_\infty$ (*i.e.*, the maximum radioactivity obtainable in iodobenzene) was found to be consistent with the expected value

$$[PhI^*]_\infty = [II^*]_0 \frac{[PhI]}{[PhI] + 2[II]} \qquad (4)$$

where $[II^*]_0$ is the initial concentration of radioactive iodine.

Using a Pyrex glass filter, transmitting above 285 nm, photochemical experiments were carried out in 3.0×10^{-2} M iodobenzene–methylcyclohexane solutions in the presence of 1.1×10^{-4} to 4.4×10^{-4} M molecular iodine. Under such experimental conditions the principal uv mercury lines absorbed by the solutions are those at 303 and 313 nm with only a small contribution (~20%) from the 334-nm line and a negligible one (less than 2%) from that at 365 nm. The irradiated solutions were tested for both exchange and deiodination, as functions of oxygen and iodine concentrations. Exchange yields, unaffected by $[O_2]$ at relatively high iodine concentrations, were found to be markedly affected by either $[O_2]$ or $[I_2]$, when both values fell within the proper 8×10^{-5} to 8×10^{-4} M range. Explicitly, R_{EX} increases with increasing $[I_2]$ but is lowered by dissolved oxygen (see Figure 1). As to deiodination rates, R_{DE}, they were found to exhibit oxygen and iodine concentrations effects, opposite to those of R_{EX} (Figure 2). Such observations, indicating that exchange and deiodination are essentially two competing processes, suggest the validity of the simple scheme

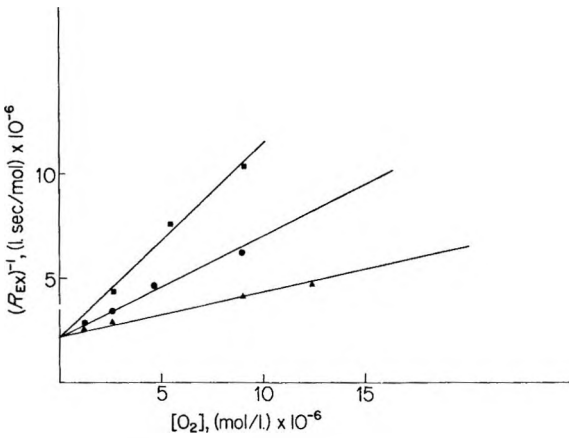

Figure 1. Reciprocal exchange rates $(R_{EX})^{-1}$ as function of the oxygen concentration in 0.03 M solutions of PhI in methylcyclohexane: ■, $[I_2] = 1.1 \times 10^{-4}$ M; ●, $[I_2] = 2.3 \times 10^{-4}$ M; ▲, $[I_2] = 4.4 \times 10^{-4}$ M. Excitation was polychromatic as described in the text.

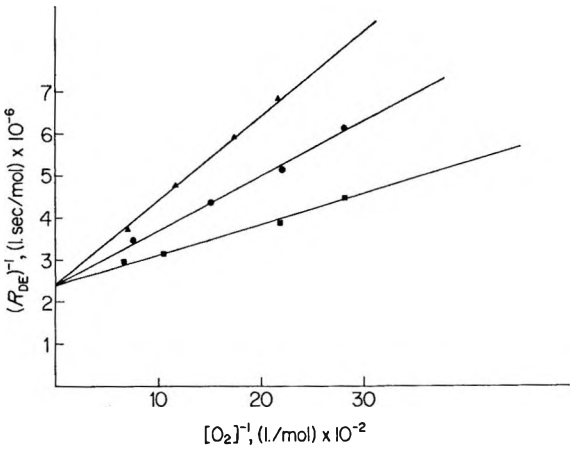

Figure 2. Reciprocal rates of deiodination $(R_{DE})^{-1}$ plotted *vs.* $[O_2]^{-1}$ in 0.03 M solutions of PhI in methylcyclohexane: ■, $[I_2] = 1.2 \times 10^{-4}$ M; ●, $[I_2] = 2.5 \times 10^{-4}$ M; ▲, $[I_2] = 3.3 \times 10^{-4}$ M. Excitation was polychromatic as described in the text.

$$PhI \xrightarrow{h\nu} Ph\cdot + I\cdot \qquad (5)$$

$$Ph\cdot + O_2 \xrightarrow{k_2} \text{oxidation products (deiodination)} \qquad (6)$$

$$Ph\cdot + I_2 \xrightarrow{k_3} PhI + I\cdot \text{ (exchange)} \qquad (7)$$

to account for the effects of oxygen and iodine. The scheme leads to the expressions

(13) J. T. Echols, V. T. C. Chuang, C. S. Parrish, J. E. Rose, and B. Milligan, *J. Amer. Chem. Soc.*, **89**, 4081 (1967).

$$R_{DE} = R_{DE}^0 \frac{k_2[O_2]}{k_2[O_2] + k_3[I_2]} \quad (8)$$

$$R_{EX} = R_{EX}^0 \frac{k_3[I_2]}{k_3[I_2] + k_2[O_2]} \quad (9)$$

where R_{DE}^0 is the deiodination rate when $[O_2] \gg [I_2]$ and R_{EX}^0 is the exchange rate when $[I_2] \gg [O_2]$.

The applicability of these equations to our experimental data is tested in Figure 1 where $1/R_{EX}$ is plotted *vs.* $[O_2]$, and in Figure 2 where $1/R_{DE}$ is plotted against $1/[O_2]$. A linear behavior is obtained in both cases for various iodine concentrations in the 1.1×10^{-4} to 4.4×10^{-4} *M* range. In each figure a common intercept is obtained for lines of different $[I_2]$ values, and the same rate constants ratio, $k_3/k_2 = 2.2 \pm 0.3$, is calculated from each line in either Figure 1 (k_3/k_2 = intercept/slope $[I_2]$) or Figure 2 (k_3/k_2 = slope/intercept $[I_2]$). From the corresponding intercepts, R_{EX}^0 and R_{DE}^0 were calculated leading to the yield ratio: $(\phi_{EX}^0/\phi_{DE}^0) = 1.04 \pm 0.06$. We may thus conclude that the experimental data are in complete agreement with the mechanism consisting of reactions 5–7. The role of iodine as a phenyl radical scavenger, which has been a matter of some controversy,[2,4,14] is now clearly established.

We have previously ruled out any significant role of iodine atoms produced from the photolysis of I_2 in the exchange process. We may still question, however, their role when produced from the photolysis of iodobenzene. This point is relevant to the recent radiation-chemical work of Reiss and Elias in which the reaction

$$PhI^{\pm} + I^{*}\cdot \longrightarrow PhI^{*} + I\cdot$$

(where $PhI^{\pm}$ is an unidentified excited state of iodobenzene) has been suggested as the major exchange step. When photolyzing PhI, both iodine atoms and excited iodobenzene molecules may be present to allow the proposed reaction. However, the kinetic analysis presented above, showing that I_2 and O_2 compete in the scavenging of the same intermediate, is inconsistent with the above step. Also, the mechanism involving $PhI^{\pm}$ will not explain the identity between ϕ_{DE}^0 and ϕ_{EX}^0, and can therefore be rejected in our photochemical system in favor of the scheme of reactions 5–7.

Experiments similar to the above were also performed using monochromatic excitation at 254, 313, 334, and 365 nm. The values obtained for the ratios k_3/k_2 (2.1 ± 0.5) and ϕ_{EX}^0/ϕ_{DE}^0 (1.00 ± 0.06) were practically identical with those reported above for the polychromatic light. However, in the monochromatic cases, absolute values for ϕ_{EX}^0 (and ϕ_{DE}^0) could also be calculated. The values obtained taking α_x as the light fraction absorbed by iodobenzene at each wavelength (see Experimental Section) are presented in Table I. It is of interest to point out that the quantum yields for deiodination of iodobenzene in the above spectral region are currently assumed to be very close to unity.[2,15] Our data for methylcyclohexane solutions at room temperature appear to be in better agreement with the early work of Olaerts and Jungers,[16] who report a maximum value of 0.37 for the quantum yield of the deiodination process.

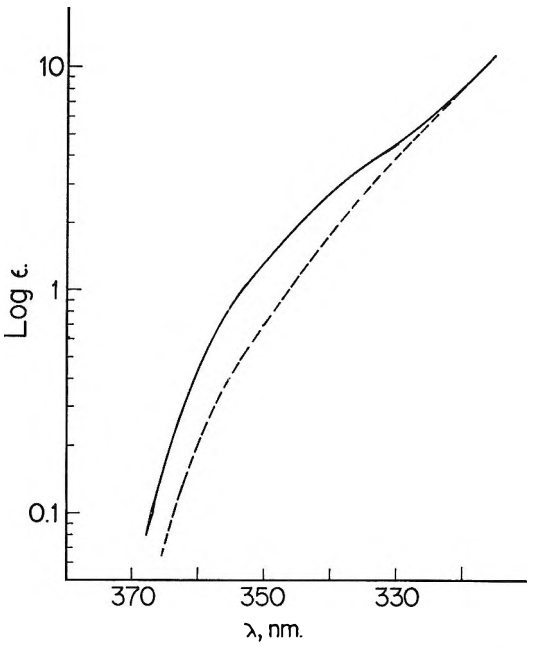

Figure 3. Long wavelength range of iodobenzene absorption in methylcyclohexane, measured at [PhI] = 0.1–1 *M*. Continuous line is experimental spectrum, dotted line is a rough estimate of the separate contribution of the $S_0 \rightarrow S_1$ transition. The difference between the curves is attributed to the direct $S_0 \rightarrow T_1$ absorption (see also ref 16).

Table I: Deiodination and Exchange Quantum Yields for Methylcyclohexane Solutions at Room Temperature (24 ± 1°)

Wavelength, nm	Iodobenzene concentration, mol/l.	Iodine concentration, mol/l.	Φ_{DE}^0	Φ_{EX}^0
254	0.001	$2–6 \times 10^{-4}$	0.39 ± 0.02	0.39 ± 0.02
313	0.03	$2–7 \times 10^{-4}$	0.39 ± 0.02	0.39 ± 0.02
334	0.1–0.5	$1–6 \times 10^{-4}$	0.30 ± 0.02	0.30 ± 0.02
365	0.1–0.5	$1–6 \times 10^{-4}$	0.22 ± 0.02	0.22 ± 0.02

As mentioned above, the identity between ϕ_{DE}^0 and ϕ_{EX}^0 presents the main evidence for the exchange mechanism initiated by the photocleavage of iodobenzene. As shown in Table I, ϕ_{DE}^0 and ϕ_{EX}^0 are independent of $[I_2]$. Recalling that both parameters were calculated

(14) J. F. Garst and R. S. Cole, *Tetrahedron Lett.*, 11, 679 (1963).

(15) See J. G. Calvert and J. N. Pitts, "Photochemistry," Wiley, New York, N. Y., 1967, p 528.

(16) E. Olaerts and J. C. Jungers, *Discuss. Faraday Soc.*, 2, 222 (1947).

assuming that PhI is the photoactive species (*i.e.*, x ≡ PhI), this second observation yields additional evidence in favor of the exchange being initiated by light absorption of iodobenzene. Assuming the alternative mechanism, involving light absorption by the $PhI \cdot I_2$ charge-transfer complex (*i.e.*, x ≡ $PhI \cdot I_2$), the same experimental data will lead to a marked dependence of the exchange yields on $[I_2]$, a fact for which it will be difficult to account reasonably. We therefore attribute all photoprocesses to the excitation of PhI, concluding that the charge-transfer complex is photochemically inactive.

Attention should now be paid to the marked drop in the quantum yields observed upon increasing the excitation wavelengths to 334 and 365 nm. Such effects should be considered in view of the characteristic absorption spectrum of iodobenzene in this region. It has been pointed out by Ferguson and Iredale[17] (see also Figure 3) that concentrated iodobenzene solutions exhibit a distinct shoulder around 350 nm. Their low-temperature phosphorescence experiments strongly suggested that this low-energy band should be attributed to the $S_0 \rightarrow T_1$ transition. A rough estimate gives 0.5 and 0.8 for the intensity ratio $\epsilon_{(S_0 \rightarrow S_1)}/[\epsilon_{(S_0 \rightarrow S_1)} + \epsilon_{(S_0 \rightarrow T_1)}]$ at 365 and 334 nm correspondingly. These two numbers should be compared with the limiting deiodination yields ratios: $[\phi_{DE}^0(365\text{ nm})/\phi_{DE}^0(254\text{ nm})] = 0.56$ and $[\phi_{DE}^0(334\text{ nm})/\phi_{DE}^0(254\text{ nm})] = 0.77$. The same values (see Table I) are obtained for the corresponding limiting exchange yields. Recalling that at 254 nm $\epsilon_{(S_0 \rightarrow S_1)} \gg \epsilon_{(S_0 \rightarrow T_1)}$, the matching within each of the two pairs means that the limiting deiodination or exchange yields are proportional to the population of S_1, and that the lowest triplet state does not undergo a detectable photodissociation at room temperature.

Thus, the photochemistry of iodobenzene in the 250–400-nm range is only due to light absorption within the $S_0 \rightarrow S_1$ band which leads to dissociation into Ph· and I· radicals, with phenyl radicals reacting with both iodine and oxygen. Under our particular experimental conditions we have found no evidence for their reaction with iodobenzene, as recently suggested for aqueous solutions.[18] These results seem to clarify some controversy concerning the mechanism of radiolytically induced exchange in iodoaromatics[4,5] supporting the scheme involving a reaction between I_2 and Ph· as suggested by Appleby, Charlton, and Spillett for aqueous solutions.[4]

Acknowledgment. The authors are indebted to Mr. S. Shrem for his help in carrying out photochemical experiments, to Mr. Y. Kalifa for his skillful technical assistance, and to Mr. Ch. Klein who performed the gas chromatographical determinations.

(17) J. Ferguson and T. Iredale, *J. Chem. Soc.*, 2959 (1953).
(18) B. Cercek and M. Kongshaug, *J. Phys. Chem.*, **74**, 4319 (1970).

Electronic Absorption Spectra and Electron Paramagnetic Resonance of Copper(II)–Amine Complexes

by M. Dale Alexander,* Patricia C. Harrington,[1]

Chemistry Department, New Mexico State University, Las Cruces, New Mexico 88001

and Alan Van Heuvelen

Physics Department, New Mexico State University, Las Cruces, New Mexico 88001 *(Received February 26, 1971)*

Publication costs assisted by the National Science Foundation and the National Institutes of Health

The synthesis and characterization of two new copper(II) complexes, Cu(3,2,3-tet)Cl_2 and Cu(3,2,3-tet)$(NO_3)_2$, where 3,2,3-tet is $NH_2(CH_2)_3NH(CH_2)_2NH(CH_2)_3NH_2$, is reported. The visible absorption spectra of these complexes together with the spectra of the analogous complexes of ethylenediamine and 2,3,2-tet, where 2,3,2-tet is $NH_2(CH_2)_2NH(CH_2)_3NH(CH_2)_2NH_2$, give information pertinent to the ordering of electronic energy levels of copper(II) in amine complexes. The absorption spectral data and epr data when used to calculate covalent bonding parameters for the copper(II) complexes give results which are not satisfactory.

Introduction

Complexes of the new tetradentate ligand 4,7-diaza-1,10-decanediamine, $NH_2(CH_2)_3NH(CH_2)_2NH(CH_2)_3NH_2$(3,2,3-tet), containing cobalt(III) have been prepared recently.[2] This ligand has a much greater tendency to form trans complexes with cobalt(III) and presumably other six coordinate metal ions than two other linear tetramines which have been under investigation: triethylenetetramine (2,2,2-tet) and 3,7-diaza-1,9-nonanediamine (2,3,2-tet). One would predict that 3,2,3-tet would be an ideal ligand to coordinate to copper(II) because of this metal ion's well-known ability to bond strongly to four coplanar donor amine functions. In our laboratories copper(II) complexes of 3,2,3-tet have been prepared and characterized. Epr and visible absorption spectral data for these 3,2,3-tet complexes and analogous complexes containing 2,3,2-tet and ethylenediamine (en) have been obtained (Table I). The visible absorption spectra are interpreted using a ligand field model, and the epr data are used in theories relating covalent bonding with the experimentally measured results. The results in applying these theories to the epr data are not satisfactory.

Experimental Section

Reagents. Reagent grade copper(II) chloride dihydrate, copper(II) nitrate trihydrate and Eastman White Label *N,N'*-bis(2-aminoethyl)-1,3-propanediamine (2,3,2-tet) were used without further purification. 4,7-Diaza-1,10-decanediamine (3,2,3-tet) was prepared by the method of Alexander and Hamilton.[2a] Eastman Practical ethylenediamine was distilled before use.

Preparation of Cu(2,3,2-tet)Cl_2 and Cu(2,3,2-tet)$(NO_3)_2$. The complexes were prepared according to the method of Bosnich, *et al.*[3]

Preparation of Cu(3,2,3-tet)Cl_2 and Cu(3,2,3-tet)$(NO_3)_2$. These complexes were prepared in the same manner as that used for the 2,3,2-tet complexes. *Anal.* Calcd for Cu(3,2,3)Cl_2: C, 26.56; H, 6.14. Found: C, 27.17; H, 6.09. Calcd for Cu(3,2,3)$(NO_3)_2$: C, 31.12, H, 7.19. Found: C, 31.45; H, 7.41.

Preparation of Cu(en)$_2$Cl and Cu(en)$_2(NO_3)_2$. The complexes were prepared by the method of Caglioti, *et al.*[4]

Visible Spectra. Visible spectra were recorded on a Cary Model 14 spectrophotometer. Solid samples were finely ground in Nujol and supported on filter paper. Visible spectra were also recorded for aqueous solutions (0.01 *M*) of each complex.

Elemental Analysis. Carbon and hydrogen analyses were performed by Galbraith Laboratories, Knoxville, Tenn.

Epr Measurements. The epr spectra were taken with a Varian 4502 spectrometer. DPPH was used as a reference line. The magnetic field was measured with a Varian Fieldial magnetic field regulator. A Varian variable temperature accessory was used for the low-temperature studies. Epr spectra were taken of the various copper complexes as chlorides at −160° (0.004 *M* copper in 60% glycerin–40% water frozen solution)

(1) NDEA Predoctoral Fellow.

(2) (a) M. D. Alexander and H. G. Hamilton, Jr., *Inorg. Chem.*, **8**, 2131 (1969); (b) G. R. Brubaker and D. P. Schaefer, *ibid.*, **9**, 2373 (1970).

(3) B. Bosnich, R. D. Gillard, E. D. McKenzie, and G. A. Webb, *J. Chem. Soc., A*, 1331 (1966).

(4) V. Caglioti, C. Furland, G. Dessy, and C. Ibarra, *Gazz. Chim. Ital.*, **92**, 1276 (1962).

Table I: Visible Spectra Data

Compd	λ_{max} (solid), nm	λ_{max} (H_2O), nm	ϵ_{max} (H_2O)
$Cu(en)_2(NO_3)_2$	533	547	57
$Cu(en)_2Cl_2$	550	545	
$Cu(2,3,2\text{-tet})(NO_3)_2$	532	527	66
$Cu(2,3,2\text{-tet})Cl_2$	544	524	
$Cu(3,2,3\text{-tet})(NO_3)_2$	540	535	86
$Cu(3,2,3\text{-tet})Cl_2$	553	538	

and at room temperature (0.01 *M* copper in water). In these solutions the copper complexes exist as $Cu(amine)_4(H_2O)_2^{2+}$. The g values, hyperfine constants, and line widths were evaluated for the three copper complexes by matching a computer calculated spectrum to the observed spectrum. The computer spectrum is for tetragonal symmetry and varies the g values ($g_{||}$ and $g_\perp$), the hyperfine constants (A and B) and the line widths ($\Delta H_{||}$ and $\Delta H_\perp$) to get a least-squares fit to the observed spectrum. The program uses either Gaussian or Lorentzian line shapes. The epr spectra of the frozen solutions along with the calculated spectrum for the $Cu(en)_2$ complex are shown in Figure 1. The computer-calculated parameters are given in Table II.

There was little difference in the epr spectra of the three different copper complexes, $Cu(en)_2(H_2O)_2^{2+}$, $Cu(3,2,3\text{-tet})(H_2O)_2^{2+}$, and $Cu(2,3,2\text{-tet})(H_2O)_2^{2+}$ at $-160°$ and also at room temperature. A careful visual inspection of the three spectra does indicate that the value of g for the 2,3,2-tet complex is slightly less than for the other two complexes. This is also confirmed by the computer evaluation.

It is difficult to assign uncertainties to the values of the epr parameters given in Table II. The complexes undoubtedly have some rhombic distortions, whereas our program assumes tetragonal symmetry. Thus for example the value of $g_\perp$ is probably an average of the values of g_x and g_y. We have estimated the absolute uncertainties for any one of the following complexes: $A(\pm 6 \times 10^{-4}\ cm^{-1})$, $B(\pm 6 \times 10^{-4}\ cm^{-1})$, $g_{||}(\pm 0.01)$, and $g_\perp(\pm 0.01)$. The uncertainties of the parameters for the three complexes relative to each other are somewhat better than this. The lowering of the $g_{||}$ value for the 2,3,2-tet complex as compared with the $(en)_2$ and 3,2,3-tet complexes was observed consistently for several separate runs with complexes in the water–glycerin solvent and also when the complexes were dissolved in methanol.

Results and Discussion

Electronic Spectra. Copper(II) complexes of the formulation $Cu(en)_2X_2$ and $Cu(2,3,2\text{-tet})X_2$ where X is an anionic ligand have been prepared previously.[3,4] In these complexes all amine groups bond to the metal ion in the tetragonal plane. We have prepared analogous 3,2,3-tet complexes of copper(II) using procedures very similar to those employed in the synthesis of the en and 2,3,2-tet complexes. The similarity between the solid-state spectra of corresponding 3,2,3-tet, 2,3,2-tet, and en complexes, as seen in Table I, supports the notion that 3,2,3-tet also functions as a tetradentate ligand coordinating in the tetragonal plane with the anionic ligands coordinating weakly perpendicular to the plane as is the case for the $(en)_2$ and 2,3,2-tet complexes.

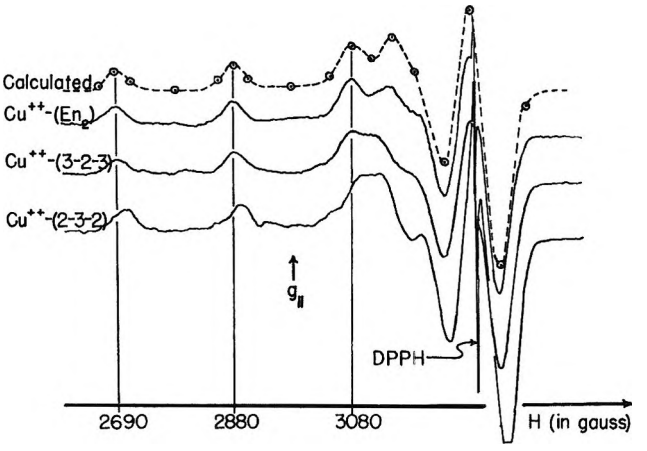

Figure 1. The epr spectra of $Cu(amine)_4(H_2O)_2^{2+}$ complexes taken at 90°K. The top curve (- - - -) is a calculated spectrum which best matched the $Cu(en)_2(H_2O)^{2+}$ epr spectrum.

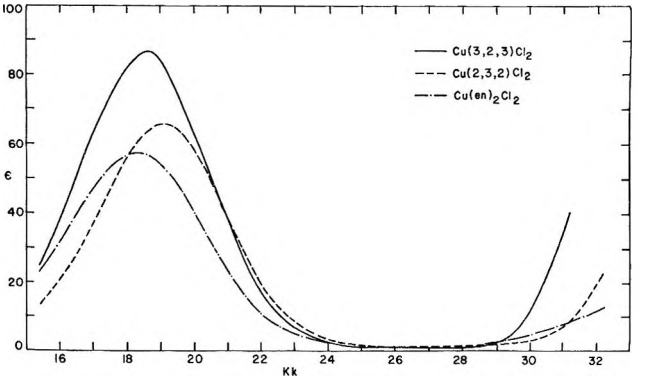

Figure 2. Absorption spectra of aqueous solutions of $Cu(amine)_4(H_2O)_2^{2+}$ complexes.

Aqueous solution spectra of the complexes as chloride salts are shown in Figure 2. In aqueous solution the amines retain their "planar" coordination but the axially coordinated anions are replaced by water molecules. The spectra are similar especially in the shape of the bands. Before examining the spectra in detail consider the ligand field splitting diagram for Cu(II) in Figure 3, which shows the state splitting for various symmetries. The complexes under consideration are of pseudo-D_{4h} symmetry. Procter, Hathaway, and Nicholls[5] have examined the absorption spectra of

(5) I. M. Procter, B. J. Hathaway, and P. Nicholls, *J. Chem. Soc. A*, 1678 (1968).

Table II: Epr Parameters for Cu–Amine Complexes

Complex	$H_{\|\|}$, G[a]	$H_{\perp}$, G[a]	$A \times 10^4$, cm^{-1}	$B \times 10^4$, cm^{-1}	$g_{\|\|}$	$g_{\perp}$
$Cu(en)_2(H_2O)_2^{2+}$	14.1	26.0	−197	−30	2.201	2.040
$Cu(3,2,3\text{-tet})(H_2O)_2^{2+}$	15.8	25.4	−189	−32	2.204	2.038
$Cu(2,3,2\text{-tet})(H_2O)_2^{2+}$	18.7	25.5	−202	−31	2.195	2.045

[a] The spectra were best fit using gaussian line shapes.

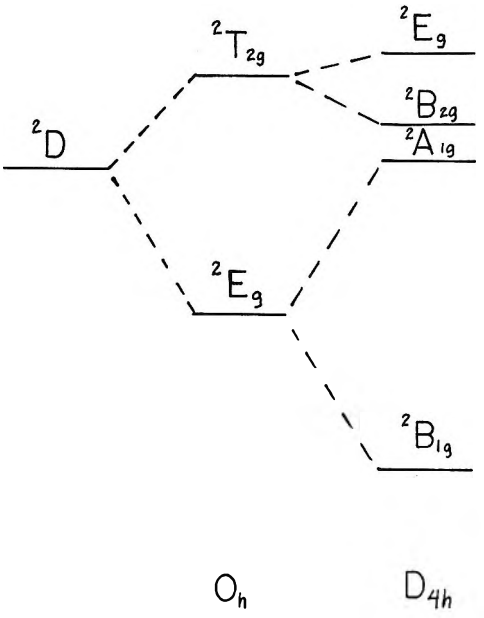

Figure 3. Ligand field splitting of copper(II) in various symmetries.

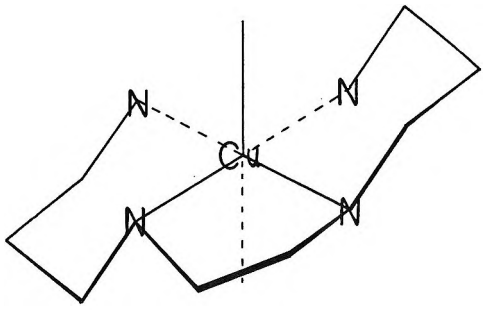

Figure 4. Probable configuration of 3,2,3-tet in copper(II) complexes.

several $Cu(en)_2X_2$ complexes and have concluded that the energies of the ^2E_g, $^2B_{2g}$, and $^2A_{1g}$ states are similar enough so that the single band obtained in the spectrum of each of these complexes is due to all three transitions with the $^2B_{1g} \rightarrow {}^2E_g$ being highest in energy. However, they could not reach any conclusions concerning the relative energies of the $^2B_{2g}$ and $^2A_{1g}$ states. Recently, Smith[6] has developed a theory which works well in explaining the presence of the three d–d transitions in the one band. Furthermore, his theory indicates that the $^2A_{1g}$ state is the lowest in energy of the three excited states. Comparison of the spectra of the $(en)_2$, 2,3,2-tet, and 3,2,3-tet complexes supports this conclusion. The position of the band maximum decreases in the order 2,3,2-tet > 3,2,3-tet > $(en)_2$ indicating a slight decrease in ligand field strength in the amine plane (Dq^{xy}) in the same order. The effect on the relative energies of the states is to first of all decrease the separation between the center of gravity of the $^2E_g + {}^2B_{2g}$ states and the center of gravity of the $^2A_{1g}$ and $^2B_{1g}$ states, and secondly, to decrease the ^2E_g, $^2B_{2g}$ splitting and to a much greater extent the $^2A_{1g}$, $^2B_{1g}$ splitting. Now, if the $^2A_{1g}$ state is higher in energy than the $^2B_{2g}$ the effect of a decreased Dq^{xy} would be to cluster the energies of the ^2E_g, $^2A_{1g}$, and $^2B_{2g}$ states more closely while if the $^2B_{2g}$ state is higher in energy an increase in separation of the energy of the $^2A_{1g}$ state from the ^2E_g and $^2B_{2g}$ states should occur. Thus in the former case a slight decrease in Dq^{xy} should result in a narrowing of the band as well as a shift in the position of the maximum while in the latter case a broadening of the band is predicted. The half-width of the $(en)_2$ band (4900 cm^{-1}) is indeed greater than that of the 2,3,2-tet band (4500 cm^{-1}) and the half-width of the 3,2,3-tet band (4530 cm^{-1}) is nearly the same as that of 2,3,2-tet. Therefore the results are compatible with the $^2A_{1g}$ state being lower in energy than the $^2B_{2g}$ state.

The intensity of the band for the 3,2,3-tet complex is considerably greater than those for the $(en)_2$ and 2,3,2-tet complexes. This is likely a result of a greater deviation from D_{4h} symmetry in the 3,2,3-tet case. Consider the most likely configuration and conformation of 3,2,3-tet in the complex (Figure 4). The six-membered chelate rings are in the preferred chair conformation, the five-membered ring is in the preferred gauche conformation, and the secondary amine functions are in the *RR*(*SS*) configuration. One will note that the trimethylene linkage for one six-membered ring is crowded above the amine plane and that of the other is crowded below the plane. This crowding could be alleviated by raising one primary amine function and lowering the other resulting in a pseudo-tetrahedral distortion. A slight distortion of this type would account for the increased band intensity.[7]

(6) D. W. Smith, *J. Chem. Soc., A*, 1708 (1969).

Epr Spectra. Epr and visible absorption spectra have been used many times to determine covalent bonding parameters for copper(II) ions in various ligand field environments. The epr parameters $g_{||}$, $g_{\perp}$, and A and B and the separation of the d orbitals ($E_{xy} - E_{x^2-y^2} = \Delta E_{xy}$; $E_{xz,yz} - E_{x^2-y^2} = \Delta E_{xz,yx}$) are used to calculate the covalent bonding parameters α^2, β_1^2, and β^2 and the Fermi contact hyperfine interaction "constant" K (or κ). α^2 measures the covalency of the $d_{x^2-y^2}$–σ bonds, β_1^2 of the d_{xy}–π bonds and β^2 of the $d_{xz,yz}$–π bonds. These parameters are one for ionic bonds and are 0.5 for pure covalent bonds. One should refer to the original papers[8,9] for a more detailed discussion of the theory and parameters used therein.

There seems to be one fairly consistent trend resulting from the use of these theories, *i.e.*, a decrease in the value of $g_{||}$ implies an increase in the degree of covalent bonding. This behavior is predicted by the formalism[8,9] used to evaluate the covalent bonding parameters from the epr spectra. Also the experimentally measured values of $g_{||}$ for copper(II)–ligand complexes are reduced as the bonding becomes stronger. For example, $g_{||}$ is about 2.3–2.4 for copper–oxygen bonds, 2.2–2.3 for copper–nitrogen bonds, and 2.1–2.2 for copper–sulfur bonds. Table II gives the epr parameters for $Cu(en)_2(H_2O)_2^{2+}$, $Cu(3,2,3\text{-tet})(H_2O)_2^{2+}$, and $Cu(2,3,2\text{-tet})(H_2O)_2^{2+}$. The epr spectra imply that the covalent bonding is nearly the same in all three complexes but is slightly stronger in the 2,3,2-tet case. This is consistent with the visible spectral results.

The general theory[8,9] used to determine the covalent bonding parameters from the epr and visible absorption spectra does not, however, work well for these complexes. The problem encountered here is a common one, *i.e.*, the amount of π bonding predicted by the theory is greater than expected (see *e.g.*, ref 9–12). Reasonable results can usually be obtained if one assigns the band energies ΔE_{xy} and $\Delta E_{xz,yz}$ "correctly." For example, $\Delta E_{xz,yz}$ is often assigned an energy of about 25,000 cm^{-1} such that the out-of-plane π bonding is negligible ($\beta^2 = 1$). Usually this band cannot be confirmed because of a very intense charge-transfer band at an energy around 25,000 cm^{-1}.

Our experimentally measured and computer-analyzed g values and hyperfine constants for the copper complexes given in Table II. These results agree quite well with those of Alei, Lewis, Denison, and Morgan,[10,13] who have also measured the epr spectra of $Cu(en)_2(H_2O)_2^{2+}$. The epr data for the $Cu(en)_2$ complex have been analyzed using the theory of Kivelson and Neiman[9] and the results are reported in Table III. The epr data were treated in two ways: (1) (line a of Table III) values of α^2, β_1^2, and β^2 were calculated using the d–d band resolution of Procter, *et al.*,[5] with the ordering of energies of the states being $^2E_g > {}^2B_{2g} > {}^2A_{2g}$; and (2) (line b of Table III) we have assumed no in plane π bonding (*i.e.*, $\beta_1^2 = 1$) and have used the data to calculate α^2 and ΔE_{xy}.

Table III: Covalent Bonding Parameters for $Cu(en)_2(H_2O)_2^{2+}$

	α^2	β_1^2	β^2	$K = \alpha^2 P\kappa_0$, cm^{-1}	ΔE_{xy}, cm^{-1}	ΔE_{xz}, cm^{-1}
(a)	0.80	0.76	0.73	0.01258	17600	19400
(b)	0.79	1			24500 (409 nm)	

[a] The data from Table II have been used along with the following values for other parameters: $S = 0.093$, $T = 0.333$, $\lambda = -828$ cm^{-1}, and $P = 0.0360$ cm^{-1}.

The first treatment gives the covalent bonding parameter $\beta_1^2 = 0.76$ which, according to the theory, should indicate appreciable d_{xy}–π bonding. However, there are no orbitals available on the amine donors for such bonding, and thus β_1^2 should be one. The other π-bonding parameter, β_2^2, is calculated to be 0.73 thus indicating significant d_{xz}, d_{yz}–π bonding. This would have to involve the water molecule coordinating along the z axis perpendicular to the coordination plane of the amines. Bonding along this axis is usually considered to be weak, however; and furthermore, water is a poor π-bonding ligand. There is one other point in considering this treatment of the data. The σ-bonding parameter α^2 is 0.80 which would indicate more in and out-of-plane π bonding than in-plane σ–bonding which seems unusual.

In the other treatment we have assumed $\beta_1^2 = 1.0$ and have used eq 5d and e from Kivelson and Neiman[9] (KN) to determine α^2 (these are the equations for the hyperfine constants A and B). Using this value of α^2, then the KN equation (5b) (the equation for $g_{||}$) was used to find a consistent value for the d–d transition corresponding to ΔE_{xy} (24.500 cm^{-1}). As can be seen in Figure 2, there is no band at 24,500 cm^{-1} (24.5 kK). Using larger ΔE_{xy} results in $\beta^2 > 1$, a physically unrealistic value. Thus both treatments indicate that for the complex considered here the theory certainly does not work well. Attempts to use the theory

(7) A. S. Brill and G. F. Bryce, *J. Chem. Phys.*, **48**, 4398 (1968).
(8) A. H. Maki and B. R. McGarvey, *ibid.*, **29**, 31 (1958).
(9) D. Kivelson and R. Neiman, *ibid.*, **35**, 149 (1961).
(10) W. B. Lewis, M. Alei, Jr., and L. O. Morgan, *ibid.*, **45**, 4003 (1966).
(11) W. Schneider and A. V. Zelewsky, *Helv. Chim. Acta*, **48**, 1529 (1965); A. Van Heuvelen and L. Goldstein, *J. Phys. Chem.*, **72**, 481 (1968).
(12) S. Antosik, N. M. D. Brown, A. A. McConnell, and A. L. Porte, *J. Chem. Soc. A*, 545 (1969); H. R. Gersmann and J. D. Swalen, *J. Chem. Phys.*, **36**, 3221 (1962); E. M. Roberts and W. S. Koski, *J. Amer. Chem. Soc.*, **82**, 3006 (1960).
(13) M. Alei, Jr., W. B. Lewis, A. S. Denison, and L. O. Morgan, *J. Chem. Phys.*, **47**, 1062 (1967).

by juggling the values of λ (the spin-orbit coupling constant) and P, both of which have an $\langle r^{-3} \rangle$ dependence, have also failed.

Acknowledgment. We are indebted to the National Science Foundation and the Public Health Service for their support of this research.

Growth Patterns of Reaction Intermediates Produced by Self-Radiolysis of Tritiated Ethyl Iodide at 77°K[1a]

by Paul J. Ogren[1b] and John E. Willard*

Department of Chemistry, University of Wisconsin, Madison, Wisconsin 53706 *(Received April 8, 1971)*

Publication costs assisted by the U. S. Atomic Energy Commission

The trapped intermediates produced by the self-radiolysis of tritiated glassy and polycrystalline ethyl iodide at 77°K have been investigated with the aid of their esr and optical spectra. The initial growth rates are proportional to the specific activity but decrease with time at rates which are different for the different species. In glassy ethyl iodide, ethyl radicals grow to plateau concentrations which are proportional to less than the first power of the specific activity, the kinetics indicating that the radicals are removed by a process stimulated by the radiation, or that competing processes interfere with their production as the concentration of reaction intermediates increases. The average radical lifetime in the steady state at 101°K, the highest temperature at which radicals could be observed in competition with thermal decay, is *ca.* 15 sec. Between 77 and 95°K the radical decay rates increase with an Arrhenius factor of 2.5 kcal mol^{-1}, but increase much more rapidly above 95°K. Illumination of γ-irradiated samples in the 400–500-nm range removes trapped C_2H_5 radicals. Tritiated glassy samples emit a steady-state luminescence with an intensity approximately proportional to the specific activity. The synthesis of C_2H_4TI from T_2, C_2H_4, and I_2 is described.

Introduction

γ Irradiation of glassy or polycrystalline ethyl iodide at 77°K produces a number of trapped reaction intermediates observable by their visible-uv[2] or esr spectra.[3] Ethyl radicals have been clearly identified. Other tentative assignments include ions and charge transfer complexes. The stabilities of the species differ, and there is evidence that some are precursors of others. The present paper reports more extensive investigations of their growth and decay including evidence on photobleaching, temperature effects, and recombination luminescence. β Rays from tritium, present as C_2H_4TI, rather than γ rays, have been used for irradiation. This method of irradiation allows convenient continuous observation at a variety of dose rates and temperatures, avoids the interfering spectra which γ rays induce in the walls of the sample container, allows an evaluation of LET effects by comparison with γ-irradiation studies, and allows easy calculation of varied dose rates from a knowledge of the tritium concentration.

Tritium has previously been employed as a source of radiation in solid state radiolyses by Spinks and coworkers using HTO dissolved in H_2O, D_2O, and organic materials such as C_2H_5OH at 77°K and by Damerau and coworkers, who examined the decomposition products of tritiated tryptophane and dimethyldiethyltin at low temperatures.[4]

Experimental Section[5]

Synthesis of C_2H_4TI. C_2H_4TI was synthesized from T_2 (half-life 12 years, maximum β energy 18.6 keV) using the apparatus of Figure 1. The reaction sequence was $T_2 + I_2 \rightarrow 2TI$, activated by a hot wire, followed

(1) (a) This work has been supported in part by the U. S. Atomic Energy Commission under Contract AT(11-1)-1715, by the W. F. Vilas Trust of the University of Wisconsin, and by NSF and Danforth Foundation fellowships held by P. J. Ogren; (b) present address: Department of Chemistry, Maryville College, Maryville, Tenn. 37801.

(2) R. F. C. Claridge and J. E. Willard, *J. Amer. Chem. Soc.*, **88**, 2404 (1966).

(3) (a) H. Fenrick, S. V. Filseth, A. L. Hanson, and J. E. Willard, *ibid.*, **85**, 3731 (1963); (b) H. Fenrick and J. E. Willard, *ibid.*, **88**, 412 (1966); (c) G. L. Hermann and L. A. Harrah, Technical Report AFML-TR-65-333 (1966); (d) R. J. Egland and J. E. Willard, *J. Phys. Chem.*, **71**, 4159 (1967).

(4) (a) J. Kroh and J. W. T. Spinks, *J. Chem. Phys.*, **34**, 1853 (1961); (b) J. Kroh, B. C. Green, and J. W. T. Spinks, *Can. J. Chem.*, **40**, 413 (1962); (c) W. Damerau, G. Lassman, and H. G. Thom, *Z. Phys. Chem. (Leipzig)*, **223**, 99 (1963).

(5) Further details are available in the Ph.D. Thesis of Paul J. Ogren, University of Wisconsin, 1968.

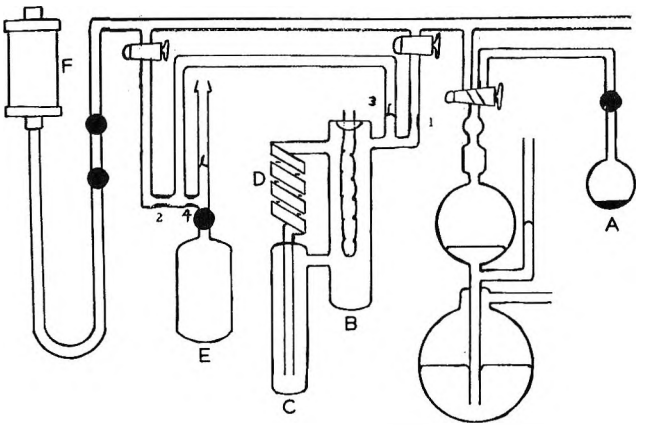

Figure 1. Vacuum manifold for synthesis of tritiated ethyl iodide. All connecting tubing was of 2 mm i.d. capillary. Solid circles indicate greaseless stopcocks.

by $TI + C_2H_4 \rightarrow C_2H_4TI$, catalyzed by AlI_3. Tritium stored as UT_3 on the uranium bed[6] (A) was released by heating and transferred by the Toepler pump to reactor (B). The reactor contained several grams of carefully dried I_2 in the bottom. In a typical synthesis, 1.5 Ci (2.6×10^{-5} mol) of T_2 was mixed with 7×10^{-4} mol of H_2 giving a total pressure of 30 Torr in the reactor, which was then sealed at 1. Reaction proceeded for an hour with the platinum wire electrically heated to a red-yellow glow. HI present in the $H_2 + I_2 \leftrightarrows 2HI$ equilibrium mixture was continuously removed by the 77°K trap (C), using convective circulation induced by warming coil (D). Fresh I_2 from the warmed solid in B mixed with the returning H_2, T_2 stream. After completion of the synthesis, point 2 was sealed, the break-seal (3) was opened, and the mixture of HI and TI was condensed into reactor (E) which contained *ca.* 1 g of AlI_3 and 2.3×10^{-3} mol of C_2H_4 (*ca.* 420 Torr at 25°). The AlI_3 was prepared by heating an excess of Al with thoroughly dried I_2. After addition of the TI to E and sealing at point 4, reaction was allowed to proceed for 90 min at 40–45°. The C_2H_5I–C_2H_4TI mixture was then purified by distilling from −250°K to 77°K to remove I_2, pumping at −78° for 6 hr to remove HI and low-boiling hydrocarbons, and passing through silver powder to remove residual I_2. The product was water white. Yields of *ca.* 70% of the H_2 used and 75% of the theoretical specific activity were commonly obtained. These samples of *ca.* 100 μl were of a convenient size for optical and esr measurements. Specific activity measurements on gaseous aliquots (3.83 ml at 40 Torr) in the ionization chamber (F) containing 30–40 cm of Ar[7] were reproducible to ±3% and agreed within 10% on an absolute scale with liquid scintillation counter measurements.[8]

In this paper specific activities are given in units of Ci ml^{-1} of C_2H_5I at 25°. For 1 Ci ml^{-1} the dose rate is 6.6×10^{15} eV g^{-1} min^{-1}. Samples of 5–10 Ci ml^{-1} were usually synthesized. To obtain lower specific activities they were diluted with inactive C_2H_5I. At 10 Ci ml^{-1} a sample contains *ca.* one T atom per 40 C_2H_5I molecules. Samples which had undergone significant decomposition on storage were repurified before use.

Safety Precautions with Tritiated Samples. External exposure to tritium β radiation is not hazardous, but the radiation may be a hazard if tritiated compounds are inhaled or ingested. All syntheses and spectrophotometric examinations of tritiated samples were carried out in an independently vented fume hood. Samples for esr measurements were prepared in 3 mm o.d., 2 mm i.d. Suprasil tubes which could be inserted into a Kel-F protective sheath (4 mm o.d., 3.4 mm i.d.) that would fit into the Varian liquid nitrogen dewar used in the esr cavity. The sheath, fabricated from a Kel-F rod, encased both the Suprasil sample tube and its quartz-to-Pyrex seal-off tube and was closed with a threaded aluminum cap and O-ring. Alternatively, protective sheaths can be fabricated by machining and heat sealing 0.25 in. o.d. Kel-F tubing.[9] Kel-F was found to be much less brittle at 77°K than Teflon, nylon, or polyethylene.

Esr Measurements. A Varian V-4500 X-band spectrometer operating with 100-kHz modulation and a microwave power of *ca.* 15 mW was used for esr measurements. Absolute concentrations of unpaired spins were determined by electronic integration[5] and comparison with DPPH and galvinoxyl standards. A few measurements were made at 4°K in an esr cavity designed for this purpose.[10]

Spectrophotometric Measurements. Spectrophotometric measurements on the 0.1-ml samples of tritiated ethyl iodide glass were made with a Cary 14 spectrophotometer using optical cells of 0.25–1-mm path length which could be reproducibly positioned in the light path while held under liquid nitrogen in a dewar with flat windows. Thin cells were used because of the limited sample volumes available, the high optical densities to be measured, and the necessity for minimizing the cracking which occurs when thicker samples of ethyl iodide glass are cooled to 77°K. The cell bodies were made by drawing down hot quartz tubing over stainless steel forms (*e.g.*, 0.5 mm × 1 cm × 4 cm).[11]

Luminescence Measurements. The steady-state luminescence resulting from self-radiolysis of tritiated ethyl iodide glasses was measured by an IP21 photomultiplier

(6) (a) J. J. Katz and E. Rabinowitch, "The Chemistry of Uranium," 1st ed, McGraw-Hill, New York, N. Y., 1952, pp 183–213; (b) R. W. Ahrens, Ph.D. Thesis, University of Wisconsin, 1959.

(7) K. E. Wilzbach, A. R. Van Dyken, and L. Kaplan, Argonne National Laboratory Report ANL-5143 (1953).

(8) We are indebted to Professor C. Heidelberger for the use of his facilities for these counts.

(9) M. A. Long and J. E. Willard, *J. Phys. Chem.*, **74**, 1207 (1970).

(10) H. W. Fenrick, Ph.D. Thesis, University of Wisconsin, 1966.

(11) Using techniques devised by W. J. Wheeler of the University of Wisconsin Department of Chemistry Glass Shop.

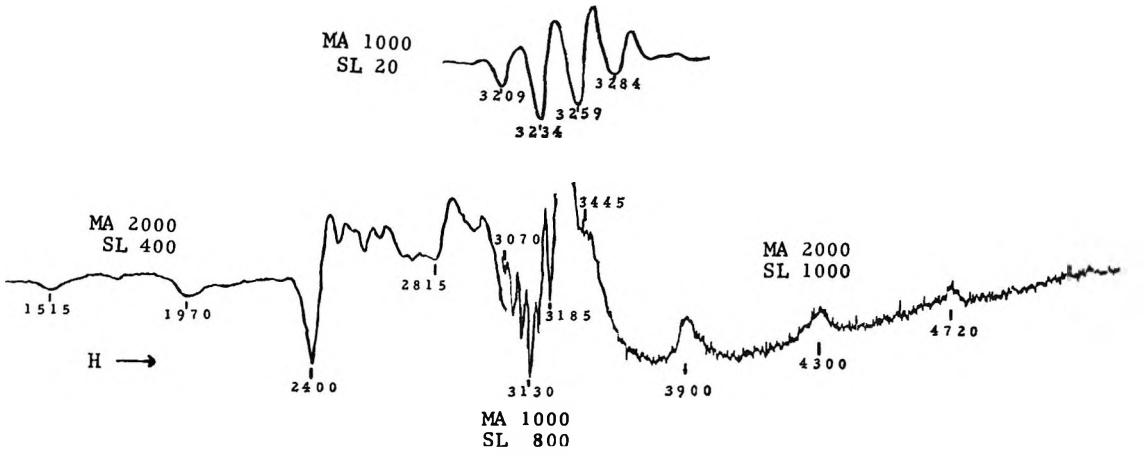

Figure 2. Esr spectrum of tritiated ethyl iodide glass (3.3 Ci ml^{-1}) after 600 hr at 77°K. The six-line C_2H_5 spectrum is shown above, and three sections of the low- and high-field spectrum, measured at different sensitivities are below. The absolute values of the fields indicated on the lower spectra are subject to an uncertainty of ±30 G. The microwave power was 15 mW in each case. MA = modulation amplitude; SL = signal level.

tube positioned *ca.* 2 cm from a sample held under liquid nitrogen in a dewar with a flat unsilvered window. The phototube has a maximum response at 400 nm with half maxima at 320 and 550 nm. Its signal-to-noise ratio is 1:1 or greater when exposed to 3×10^6 photons sec^{-1} at 400 nm and operated at 500 V. The dark currents of *ca.* 10^{-4} μA and photocurrents of *ca.* 10^{-3} μA through a 48K resistor were measured with a microvoltmeter.

Results

Esr and Optical Spectra of Glassy Samples. Radiolysis of ethyl iodide glass at 77°K by the β rays of tritium produces species which give esr spectra (Figure 2) and visible spectra (Figure 3) identical with those from γ irradiation of C_2H_5I glass.[2,3]

The six-line spectrum of the uper portion of Figure 2 is attributable to C_2H_5 radicals. It grows linearly in a freshly frozen sample at a rate proportional to the specific activity of the sample (Figures 4 and 5), but with decreasing rate at longer times, until a steady-state concentration is reached (Figure 6). Figures 7 and 8 show growth curves for all of the spectral features.

Glassy tritiated ethyl iodide gave the same six-line ethyl radical esr spectrum at 4°K as at 77°K, with no evidence of the doublet to be expected if trapped H atoms were present. Ethyl iodide glass γ-irradiated in a Cryotip unit[12] at 20°K in an optical cell with 0.40-mm path length gave the same 405- and 520-nm lines produced at 77°K (the dose was too low to produce observable absorption at 750 nm at either temperature).

Temperature Effects. The highest temperature at which ethyl radicals could be detected in the steady-state measurements on a 10 Ci ml^{-1} glass sample was 101 ± 1°K. The steady-state concentration was *ca.* 1×10^{-5} mol %, indicating an average radical lifetime of about 15 sec if $G(C_2H_5) = 2$[13] and first-order decay

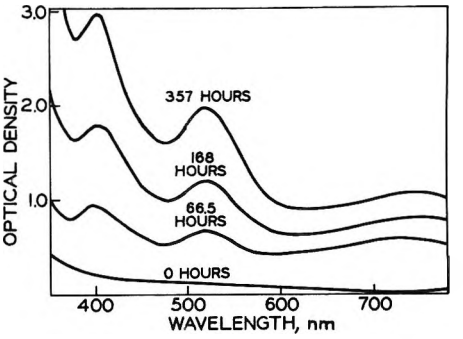

Figure 3. Optical spectrum of tritiated ethyl iodide glass (2.4 Ci ml^{-1}) as a function of time at 77°K. Cell thickness 0.40 mm.

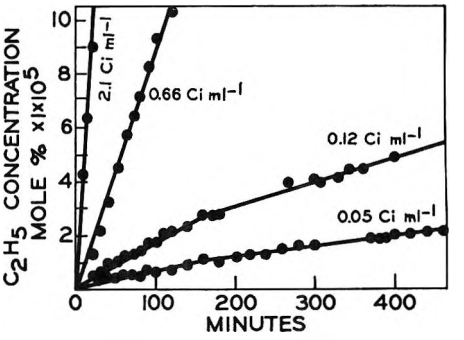

Figure 4. Growth of C_2H_5 concentration in tritiated ethyl iodide glasses of different specific activity, as a function of time at 77°K.

is assumed. The shape of the radical spectrum was the same at 101°K as at 77°K.

Ethyl radicals produced in C_2H_5I glass at 77°K by γ irradiation disappear within less than 5 min at 102 ±

(12) R. F. C. Claridge, R. M. Iyer, and J. E. Willard, *J. Phys. Chem.*, 71, 3527 (1967).

(13) P. B. Ayscough and C. Thompson, *Trans. Faraday Soc.*, 58, 1477 (1962).

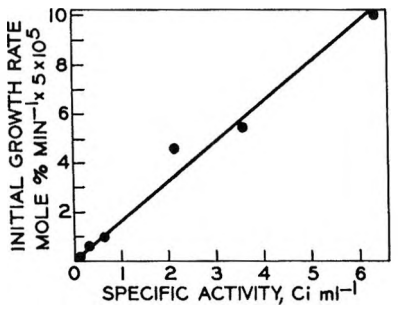

Figure 5. Initial growth rates of C_2H_5 radicals in tritiated ethyl iodide glass at 77°K as a function of specific activity.

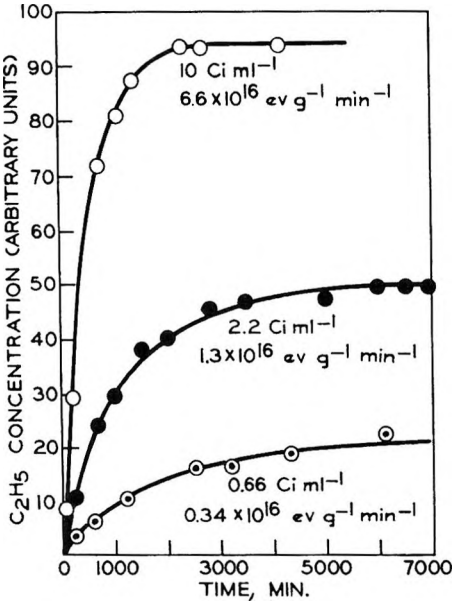

Figure 6. Concentration of C_2H_5 in tritiated ethyl iodide glasses of different specific activity as a function of long times of standing at 77°K; 100 units on the ordinate $= 1.4 \times 10^{-2}$ mol %.

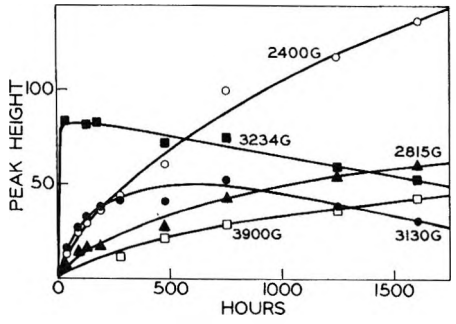

Figure 7. Change in concentration of paramagnetic species in tritiated ethyl iodide glass (3.3 Ci ml^{-1}) at 77°K as a function of time. See Figure 2 for spectral features at the indicated magnetic fields and for modulation amplitudes and signal levels used.

1°K. The esr spectrum near 3100 G is somewhat more stable, but is removed by 10 min of annealing at the same temperature. The peak at 2400 G decreases by less than 30% in 10 min at 102°K. The optical absorption peaks at 520 and 405 nm can be observed for several minutes at 99°K, while the 750-nm peak decays somewhat more rapidly.

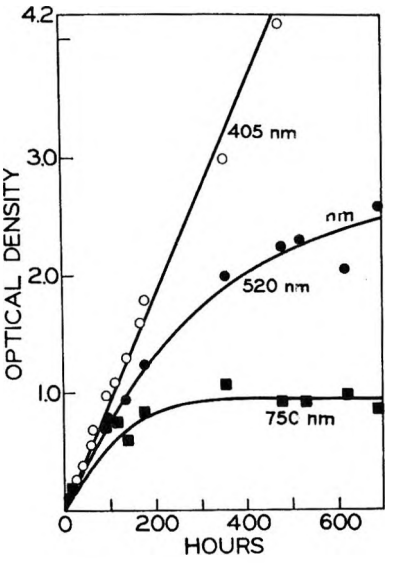

Figure 8. Growth in absorption maxima of visible spectrum (Figure 3) of tritiated ethyl iodide glass (1.4 Ci ml^{-1}) at 77°K as a function of time. Uncorrected for overlap of peaks; cell thickness = 0.40 mm.

Decay rates of radicals in tritiated samples at several temperatures were compared by observing their steady-state concentrations and assuming $R = kN$, where R = the rate of C_2H_5 production (assumed to be independent of temperature) and N is the concentration. This method of evaluating the data is, of course, somewhat arbitrary because of the complexity of the radical decay kinetics in these systems.[5] The steady-state plateaus were achieved both by warming samples from 77°K, with accompanying decay of the radical concentration to its new plateau and by cooling from the liquid with accompanying growth to the plateau. Between 77 and 95°K the decay rate increases by a factor of about 25, and over the next 5° by an additional factor of 50 (Figure 9). The slope of the curve of Figure 9 from 77 to 95°K yields an "E_A" value of 2.5 kcal mol^{-1}.

Luminescence and Optical Bleaching. When measured with the photomultiplier tube, samples of 10 and 1.4 Ci ml^{-1} gave ratios of luminescence current to dark current of 10:1 and 1:1, respectively, with a dark current of 10^{-4} μA. After corrections for self-absorption and solid angle, it is estimated that photon emission in the 320–550-nm range (pm bandwidth) is less than 2×10^{12} sec^{-1} and that G(photons) is not more than 0.2.

To test whether such luminescence could be responsible for the faster decay of radicals during irradiation than in its absence (see Discussion), we have monitored the radical concentration during illumination of a γ-irradiated sample of glassy C_2H_5I in the esr cavity (Figure 10) using several wavelength regions. The illumination intensity was 10^{16} photons sec^{-1} or more in

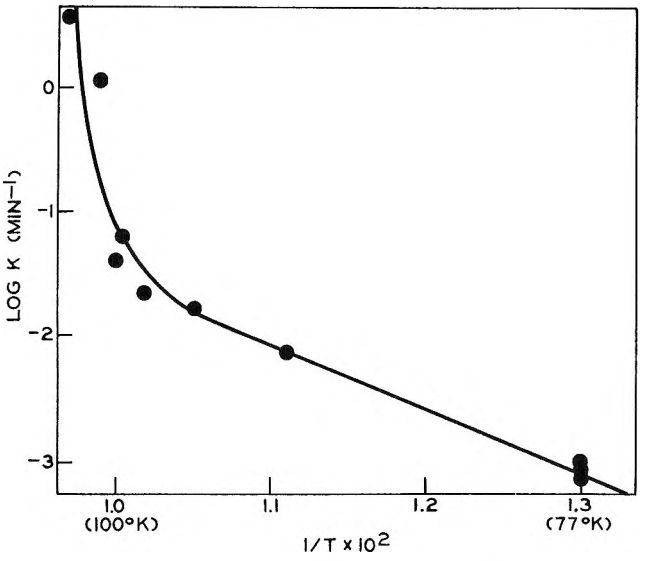

Figure 9. Arrhenius plot for C_2H_5 decay in tritiated ethyl iodide glass.

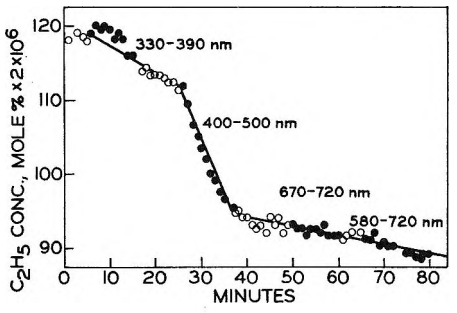

Figure 10. Effect of illumination at different wavelengths on C_2H_5 concentration in γ-irradiated ethyl iodide glass at 77°K. Open circles are for times when the light source was off and closed circles for times when it was on. The wavelength ranges indicated were filtered from the output of an AH4 lamp using Corning filters 7-51, 4-72, 2-64, and 3-66, in each case coupled with a 1-69 filter, for the 330–390, 400–500, 670–720, and 580–720-nm bands, respectively. Prior to the illuminations, the sample was stored 70 hr following a 1-min, 2×10^{18} eV g^{-1} γ dose.

all cases. At the start of illumination the radical concentration was *ca.* 6×10^{-5} mol % and the o.d. of the sample was *ca.* 0.5 at 520 nm. Radicals were removed with an estimated quantum efficiency of *ca.* 0.002 by light of 400–500 nm.

Effects of Additives. Iodine present at 0.3 mol % during γ irradiation of C_2H_5I glass reduced both the growth rate and plateau concentration of C_2H_5 radicals by 20%. Impurities produced by a 3-hr γ irradiation of C_2H_5I glass at a dose rate of 2×10^{18} eV g^{-1} min^{-1} followed by melting and refreezing lowered the growth rate and plateau by 10%. The irradiation and melting adds about 0.1 mol % each of C_2H_4, C_2H_5, I_2, and HI to the system.[3c] No effect on subsequent ethyl radical formation was observed for 1.2×10^{20} eV g^{-1} irradiations followed by 2 min at 99°K, which removed most

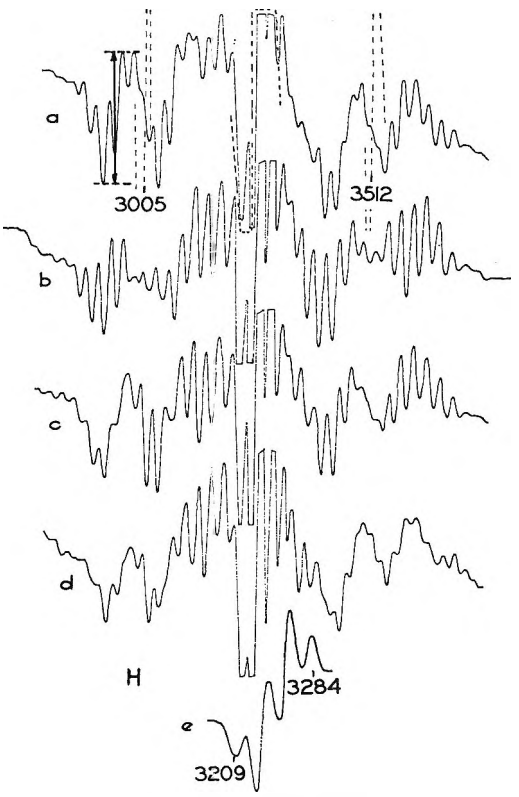

Figure 11. Esr spectra of tritiated polycrystalline ethyl iodide (10 Ci ml^{-1}) 50 hr after freezing. All spectra are from same sample. Spectra b, c, and d taken after rotating the sample around a vertical axis by 45 90, and 135° relative to a. Spectrum e shows central portion of signal at signal level 50 compared to 400 used for a, b, c, d. All modulation amplitudes 1250. Dotted lines on spectrum a show portion of spectrum which is obscured by container signal when activation is by γ irradiation.

of the ethyl radicals, or 30-min illumination at 660–900 nm, which removes the 750-nm peak.

G Values. *G* values reported for the production of C_2H_5 radicals by the γ radiolysis of C_2H_5I glass are 2.0 ± 0.4,[13] 2.2 ± 0.4,[14] and 1.5.[3c] The present work gave 2.2 ± 0.5. The radical concentrations shown in the figures of this paper have been calculated assuming $G = 2.0$.

Esr Spectra of Polycrystalline Samples. Figure 11 shows esr spectra generated in tritiated polycrystalline ethyl iodide by self-irradiation. The portions of the spectrum which are obscured by signals from the sample tube when γ irradiation is used[15] (dotted lines of Figure 11a) can be examined without interference. The bottom spectrum taken at eightfold lower sensitivity than the upper spectra suggests that the ethyl radical is responsible for the large central signal. The width of the individual lines of the central signal is greater than the width of the ethyl radical lines in ethyl

(14) R. J. Egland, Ph.D. Thesis, University of Wisconsin, 1968.

(15) R. J. Egland, P. J. Ogren, and J. E. Willard, *J. Phys. Chem.*, **75**, 467 (1971).

iodide glass or γ-irradiated polycrystalline ethyl iodide. The growths of both the C_2H_5 signal and the wide signal are shown in Figure 12 for each of two specific activities. Uncertainties in reproducibly positioning the samples in the cavity relative to rotation around the vertical axis lead to some of the scatter observed.

Discussion

Absence of LET Effects. In ethyl iodide glass the average energy (5.6 keV) tritium β particles[16] have a track length of about 3000 Å with spurs every 75 Å on the average, while the average (500 keV) Compton electrons produced by ^{60}Co rays have 1-mm tracks with average spur separations of 2000 Å.[17] The agreement of the $G(C_2H_5)$ values for the irradiation of C_2H_5I glass with tritium β's and with ^{60}Co γ's, and the similarity of the esr and optical spectra indicate that the greater proximity of spurs in the tritium case does not significantly alter the nature or concentration of the trapped reaction intermediates.

Species Responsible for Esr and Optical Spectra. Differences in the rates of growth (Figure 7) of different parts of the esr spectrum (Figure 2) of tritiated ethyl iodide glass at 77°K indicate the presence of at least three trapped paramagnetic radiolysis products, including ethyl radicals (six-line pattern in the upper portion of Figure 2); the species which gives the broad low- and high-field pattern with which the lines at 2400, 2815, and 3900 G are associated (tentatively identified as I_2^- [3d,14]); and the species responsible for the group of lines around 3130 G. The three optical absorption peaks of Figure 3 for which the growth curves are plotted in Figure 8 appear to correspond to three species. In addition, the visible tail of a further species absorbing in the uv region appears to grow. The 405-nm peak and the lines of the very broad esr spectrum both show continuing growth at 77°K during the periods observed, but the 405-nm absorption grows on warming in the range up to 102°K,[2] whereas the broad esr spectrum decays at 80°K,[14] indicating that they are due to different species. The growth curves of Figure 7 have not been followed for sufficiently long times or with sufficient accuracy to rule out the possibility that the 520- or 750-nm peak may result from the same species that is responsible for the very broad esr absorption or for the 3130-G pattern. The temperatures of onset of rapid decay (*i.e.*, disappearance in 5 min) differ for the three species observed by esr spectroscopy.

Of the four or more species responsible for the esr and optical spectra of glassy ethyl iodide, only the ethyl radical is identified with certainty. The 750-nm peak has been assigned[18] to a positive species $[(C_2H_5I)_n^+$ or $C_2H_5IC_2H_5^+]$, and later investigators have considered this plausible.[3] I_2^-, formed by $I + I^-$, has been suggested[3] as the species responsible for the 405-nm peak, while evidence on the effects of scavengers on the similar 395-nm peak in solutions of alkyl iodides in hydrocarbons suggests that it is due to a neutral species, and $C_2H_5I \cdot I$ has been proposed.[19] The evidence[3d,14] that I^{2-} is responsible for the broad esr spectrum argues against its being the species responsible for the 405-nm peak. The species responsible for the 520-nm peak is not known; $C_2H_5I \cdot I^-$ has been suggested as a possibility.[2]

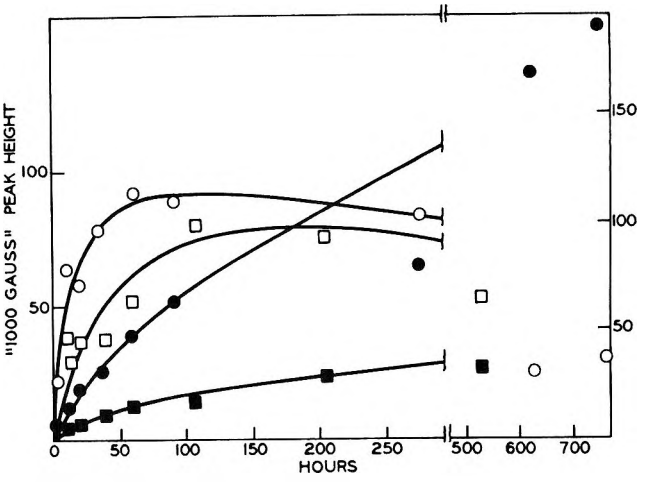

Figure 12. Change in concentrations of central signal attributed to C_2H_5 and the "1000-G species" in tritiated polycrystalline ethyl iodide as a function of time at 77°K. Circular points, 11 Ci ml^{-1}; square points, 3.3 Ci ml^{-1}. Solid points, C_2H_5 signal; open points "1000-G signal" measured by line X of Figure 11a. The height indicated by the arrow in Figure 11a was used to monitor the "1000-G species."

The predominant spectrum produced by γ-irradiated polycrystalline samples of C_2H_5I (Figure 11) is not observed in glassy samples. There is evidence which suggests that it may be due to electrons trapped in the polycrystalline matrix in such a way as to be coupled with both iodine atoms and methyl group protons.[15]

Growth Kinetics of Ethyl Radicals; Radiation Catalysis. Assuming that the rate of production of radicals (R) is constant for a given dose rate, the plateaus of Figure 6 indicate that some process (or processes) which remove radicals increases in rate with radical concentration until the rate equals R, *i.e.*, $dN/dt = R - kf(N_\infty) = 0$. If the removal process is first order, then N_∞, the radical concentration at the plateau, must be directly proportional to R (*i.e.*, $R = k(N_\infty)$. If the process is second order, N_∞ must be proportional to the square root of the specific activity ($R = k(N_\infty)^2$). For radical removal wholly by a first-order process stimulated by the continuing radiation ("radiation-catalyzed decay"), N_∞

(16) E. A. Evans, "Tritium and its Compounds," Van Nostrand, Princeton, N. J., 1966.

(17) (a) C. M. Lederer, J. M. Hollander, and L. Perlman, "Table of Isotopes," Wiley, New York, N. Y., 1968; (b) D. E. Lea, "Actions of Radiations on Living Cells," Cambridge University Press, New York, N. Y., 1955, p 24.

(18) E. P. Bertin and W. H. Hamill, *J. Amer. Chem. Soc.*, **86**, 1301 (1964).

(19) J. P. Mittal and W. H. Hamill, *ibid.*, **89**, 5749 (1967).

would be independent of the specific activity ($dN/dt = 0 = R - kRN_\infty$; $N_\infty = k^{-1}$).

The ratio of the plateau concentrations of Figure 6 is 1:2.5:4.7. If the concentrations were proportional to the first power of the specific activity, the ratio would be 1:3.4:15.2, and if to the square root, it would be 1:1.84:3.9. These data eliminate the possibility that radical removal at the plateau is solely by either first- or second-order thermal decay or by radiation-catalyzed decay. In γ-irradiated ethyl iodide glass at 77°K, the fraction of the radicals which decays per unit time at any given time after irradiation is independent of the initial concentration (*i.e.*, of the dose).[20] This "composite first-order"[21] decay indicates that each radical is removed by a process independent of the presence of other radicals and eliminates the possibility that a process proportional to $(N_\infty)^2$ contributes to the steady state of Figure 6. Therefore, radical removal at the steady state must occur by a combination of composite first-order decay and radiation-catalyzed decay. This is confirmed by the observation that the rate of decay of radicals in a γ-irradiated sample immediately after cessation of irradiation at doses in the plateau region is slower than the rate of radical production determined from the initial slope of the growth curve. For a sample irradiated to a dose of 3×10^{20} eV g^{-1} at a dose rate of 2×10^{18} eV g^{-1} min^{-1}, this decay rate was 30–50% slower than the growth rate.[18]

Quantitative evaluation of the dependence of plateau concentration on specific activity is not feasible, with the information available, because of the complexity of the interrelationships of the composite first-order decay and the radiation-catalyzed decay. Immediately after γ irradiation of a glassy ethyl iodide sample at 77°K the fractional decay rate is 1.3×10^{-2} min^{-1}, after 25% decay it is 3.4×10^{-3} min^{-1} and after 50% decay 1.0×10^{-3} min^{-1}. Thus the initial radical population contains a continuum of subpopulations which have different first-order decay rates. During prolonged irradiation, radiation-catalyzed removal of the slower decaying radicals occurs preferentially relative to removal of the more rapidly decaying radicals because of the difference in residence times in the matrix. This effect is illustrated by the fact that radical decay curves for ethyl iodide glass samples which have received a 1-min γ dose and a 60-min γ dose are superimposable after normalization for the 40-fold higher initial radical concentration in the latter.[18] This could not be the case unless the more thermally stable radicals were preferentially removed by radiation-catalyzed processes during the 60-min irradiation.

Mechanism of Thermal Decay. Ethyl iodide dissolved in liquid or solid hydrocarbons acts as an electron scavenger, undergoing dissociative electron capture ($C_2H_5I + e^- \rightarrow C_2H_5 + I^-$). The evidence indicates that in solid hydrocarbons the fragments remain in the parent cage and undergo geminate recombination at a measurable rate, with composite first-order kinetics.[21] Since the G value for ethyl radical production in pure ethyl iodide glass (*ca.* 2) is of the same order as in 1 mol % solutions in solid hydrocarbons (1.1), it is reasonable to assume that the same processes of formation and decay predominate, although additional processes may occur.

Decay of the free radicals by intraspur diffusion rather than geminate recombination would give composite first-order kinetics, for a portion of the decay, but is inconsistent with the experimental observations that (1) over 98%, and perhaps all, of the radicals decay by a process which is independent of the concentration of other radicals in the system;[20] (2) ethyl iodide glass at 77°K is stable for 2 years or more with respect to conversion into the thermodynamically more stable crystalline form, indicating that diffusion must be extremely slow.

Mechanism of Radiation Catalysis. For the experiment in which the rate of radical decay from the plateau following γ irradiation at 2×10^{18} eV g^{-1} min^{-1} was found to be about 50% of the rate of radical production,[20] G(radiation-catalyzed radical removal) = *ca.* 1. The concentration of radicals at the plateau was 5.2×10^{-4} mole fraction. If the radicals were equally spaced throughout the matrix, the average separation would be *ca.* 13 molecular diameters, and the average distance between the site of a new energy deposition event and that of a previously trapped radical would be *ca.* four molecular diameters (*ca.* 20 Å). This is an order-of-magnitude estimate of the distance over which the radiation catalysis effect is felt. Possible origins of the effect include (1) heating of the matrix by the radiation; (2) photobleaching by the luminescence emitted during irradiation; (3) reaction of H atoms, electrons, positive holes, or other radiolytic products with the growing concentration of radicals; (4) activation of recombination of geminate pairs, or of other combination processes, by energy transferred through the matrix; (5) scavenging of electrons by trapped positive holes as the concentration of these builds up, in competition with prodution of radicals by dissociative electron capture. Of these the first three appear unlikely for reasons noted below. The fourth cannot be ruled out; there is evidence that thermal decay of ethyl radicals in glassy ethyl iodide at 77°K occurs as the results of vibrations or rotations of matrix molecule groups necessary for geminate recombination, but very little is known about energy transfer through glassy matrices. The fifth is plausible and similar to the mechanism believed to be responsible for the plateau and subsequent decline in trapped electron concentration with increas-

(20) H. Fenrick, N. B. Nazhat, P. J. Ogren, and J. E. Willard, *J. Phys. Chem.*, **75**, 472 (1971).

(21) For other examples of this type of decay see: (a) W. G. French and J. E. Willard, *ibid.*, **72**, 4604 (1968); (b) R. F. C. Claridge and E. Willard, *J. Amer. Chem. Soc.*, **87**, 4992 (1965).

ing dose in γ-irradiated hydrocarbon[22a] and alcohol glasses.[22b] With increasing dose there is increasing probability of newly formed electrons encountering a trapped positive charge and becoming neutralized, in competition with dissociative capture. If this does not produce new radicals, it will decrease the level of the plateau of radical concentration.

Energy of 100 eV deposited in the matrix and converted into heat would raise the temperature of a sphere of 35 Å radius by 10°K assuming a heat capacity of 1 cal g^{-1} and no heat loss from the region. Since much of the energy is used for ionization and bond breaking and since such a temperature rise, if it occurred, could persist for only a fraction of a second, it appears improbable that thermal effects are responsible for the radiation-catalyzed radical removal (although a large uncertainty rests in the assumption as to the volume heated). According to the data of Figure 9, a 10°K rise in temperature from 77°K would increase the recombination rate by about sixfold.

The low quantum yield ($\leqq 0.002$) for removal of radicals by illumination in the 330–720-nm range (Figure 10) and the low G value for photon production by radiation-induced luminescence in the sample ($\leqq 0.2$) preclude the possibility that such luminescence contributes significantly to the radical removal responsible for the steady state.

Reaction of H atoms, electrons, or positive holes with free radicals might remove the radicals at a rate proportional to the radical concentration. The absence of a trapped H-atom esr signal in ethyl iodide glass undergoing self-radiolysis at 4°K and evidence against H-atom production in the radiolysis of hydrocarbon glasses argue against the H-atom reaction.[23] If electrons react with radicals ($R\cdot + e^- \rightarrow R{:}^-$), each such event removes a radical and prevents production of a new radical by dissociative capture. For this effect to be significant would require the cross section for e^- capture by radicals to be high relative to that for capture by C_2H_5I. The contribution of positive hole migrations to radical removal would require a charge mobility which seems improbable.

The experiments with added I_2, and with C_2H_5I exposed to prior irradiation and melting or annealing to generate stable products, indicate that such products of irradiation cannot account for much of the radiation catalysis, although they may be responsible for the slow decrease in ethyl radical concentrations at very long times (Figure 7).

Radical Growth in Polycrystalline Ethyl Iodide. Both the "1000-G" esr signal and the central signal attributed to ethyl radicals grow in tritiated polycrystalline ethyl iodide as rates which decrease with time. The broad spectra reach pleateaus (Figure 12) which are not greatly different in intensity for 3.3 and an 11 Ci ml^{-1} samples, consistent with predominant removal of the species by radiation catalysis. The maximum concentration of the 1000-G species produced by γ irradiation at a dose rate of 2×10^{18} eV g^{-1} ml^{-1}, which is 30 times that in the 11 Ci ml^{-1} tritiated sample, is not more than twice as high as in the 11 Ci ml^{-1} sample. The decrease in the 1000-G species at times greater than about 100 hr observed in this work and earlier[3c] suggests the increasing competition for the species or its precursor by another radiation product which is growing in concentration with time of irradiation. Evidence as to the identity of the species responsible for the broad spectrum has been discussed.[15] It may be physically trapped electrons coupled with both iodine atoms and CH_3 protons. Momentary warming of such samples to 147°K decreases the intensity of the broad signal while increasing the ethyl radical signal, as might occur if dissociative capture can compete for electrons with neutralization and retrapping processes. The continued increase in ethyl radical concentration with increasing dose, while the broad spectrum decays (Figure 12), is consistent with this model, although by no means proving it.

In addition to the differences in the nature and kinetics of trapped intermediates produced in polycrystalline ethyl iodide as compared to glassy ethyl iodide, discussed here, major differences in product yield obtained on melting have been reported.[24]

Related Investigations. Experimental investigations of limiting concentrations of free radicals in trapping matrices have indicated concentrations of N atoms in N_2 at 4°K of *ca.* 0.1%,[25] of 0.5% in polar aromatic compounds, and of 5% in nonpolar aromatic compounds.[26] If it is assumed that radicals are stably trapped unless they have a radical as a nearest neighbor, the maximum possible concentration may be estimated to be several per cent.[27] In the work of the present paper the maximum concentrations achieved were less than 0.1%. The relatively low limiting concentration may result from the production of each C_2H_5 radical in the same solvent cage with an I^- geminate partner[18,19] with which it is predestined to combine.

Previous examples of radiation catalysis include observations on a variety of biologically related organic solids,[27] on glassy and polycrystalline ethylene glycol,[28]

(22) (a) A. Ekstrom, R. Suenram, and J. E. Willard, *J. Phys. Chem.*, **74**, 1888 (1970); (b) S. Fujii and J. E. Willard, *ibid.*, **74**, 4313 (1970).

(23) D. Timm and J. E. Willard, *ibid.*, **73**, 2403 (1969).

(24) (a) E. O. Hornig and J. E. Willard, *J. Amer. Chem. Soc.*, **79**, 2429 (1957); (b) T. O. Jones, R. H. Luebbe, Jr., J. R. Wilson, and J. E. Willard, *J. Phys. Chem.*, **62**, 9 (1958); (c) H. J. Arnikar and J. E. Willard, *Radiat. Res.*, **30**, 204 (1967).

(25) (a) D. W. Brown, R. E. Florin, and L. A. Wall, *J. Chem. Phys.*, **66**, 2602 (1962); (b) B. J. Fontana, *ibid.*, **31**, 148 (1959).

(26) V. I. Trofimov, I. I. Chkheidze, and N. Ya. Buben, *Russ. J. Phys. Chem.*, **39**, 881 (1965).

(27) For examples and further references, see W. Snipes and P. K. Horan, *Radiat. Res.*, **30**, 307 (1967).

(28) V. K. Ermolaev and V. V. Voevodsky, "Effect of the Phase State on the Radiolysis of Organic Solids," in Proceedings of the Second Tihany Symposium for Radiation Chemistry, Akademiai Kiado, Budapest, 1967.

and on polycrystalline C_2Br_6.[29] By selective deuteration of radicals it has been shown that in γ-irradiated L-alanine crystals the radical plateaus are due to radical removal by radiation rather than to the onset of processes which compete with radical production.[27] Voevodsky and Ermolaev found that the initial growth of radicals in γ-irradiated solid ethylene glycol appears to consist of two linear portions,[28] suggesting two types of sites one of which is removed by effects of continuing radiation more readily than the other. The breaks occurred at doses of *ca.* 10^{20} eV g^{-1} and radical concentrations of *ca.* 0.1 mol %. The ratio of slopes of the two regions was independent of dose rate, and the breaks occurred at the same dose in different experiments. In the present work the initial growth of radicals often appeared to consist of two different linear portions at low dose rates and low ethyl radical concentrations (Figure 4) but the ratio of the slopes, and the dose at which the breaks occurred, changed with increasing dose rate. It is probable that in the ethyl iodide system the apparent breaks result simply from the early saturation of the population of ethyl radicals[20] which undergoes relatively rapid thermal decay.

γ Irradiation of polycrystalline C_2Br_6 produces Br_2 with differential G values which change from 4 at doses less than 2×10^{18} eV g^{-1} to 0.2 at 10^{20} eV g^{-1}. Additional data suggest that the $G(Br_2)$ values fall because two radiation-catalyzed processes ($C_2Br_5 + Br_2 \rightarrow C_2Br_6 + Br$, and $C_2Br_4 + Br_2 \rightarrow C_2Br_6$) remove Br_2.[29]

(29) R. M. Iyer and J. E. Willard, *J. Chem. Phys.*, **46**, 3501 (1967)

Ultrasonic Absorption as a Probe for the Study of Site Binding of Counterions in Polyelectrolyte Solutions

by C. Tondre and R. Zana*

C.N.R.S.-C.R.M., Strasbourg, France *(Received March 5, 1971)*

Publication costs borne completely by The Journal of Physical Chemistry

It is shown that ultrasonic absorption is selectively sensitive to site bound counterions and should therefore permit the study of this type of binding. Experimental results are reported showing an increase of the ultrasonic absorption of solutions of tetramethylammonium polyphosphate (PP), poly(ethylene sulfonate) (PES), poly(styrene sulfonate) (PSS), and carboxymethylcellulose (CMC) upon addition of alkali chlorides. These increases are interpreted in terms of site binding processes involving the alkali ions. For a given counterion site binding effects are found to increase when the minimum distance d between two charged sites is decreased. For PP, PES, and CMC the ionic sequences obtained in this work are quite similar to those obtained by others, using "static" methods. To explain these results it is assumed that the binding of a counterion involves two charged sites when d is small (chelation), and only one charged site when d is large (ion pairing).

I. Introduction

Ultrasonic absorption techniques have proved to be a useful tool for the study of aqueous solutions of simple electrolytes.[1] However, in the field of polyelectrolytes their use has been limited to studies of conformal transitions and H bonding in solutions of electrically charged polypeptides[2] and of polycarboxylic acids.[3,4] Recently we have shown[5] that ultrasonic absorption measurements may also provide informations on the nature and kinetics of counterion binding by polyions. The reasoning following was employed. In aqueous polyelectrolyte solutions there exist various chemical equilibria which involve counterions and charged sites on polyions. When sound waves are propagated through such solutions these equilibria are perturbed by the pressure changes due to the waves. This interaction gives rise to a relaxational ultrasonic absorption

(1) J. Stuehr and E. Yeager, "Physical Acoustics," Vol. IIA, W. P. Mason, Ed., Academic Press, New York, N. Y., 1965, p 351.

(2) G. Schwarz, *J. Mol. Biol.*, 11, 64 (1965); T. Saksena, B. Michels, and R. Zana, *J. Chim. Phys. Physicochim. Biol.*, 65, 597 (1968).

(3) B. Michels and R. Zana, Proceedings of the 7th International Congress on Acoustics, Akademiai Kiado, Vol. 2, paper 20M6, p 41, Budapest, 1971.

(4) B. Michels and R. Zana, *Kolloid Z.*, 234, 1008 (1969).

(5) C. Tondre and R. Zana, IUPAC Symposium, Book of Abstract Vol. I, paper IIa9, p 387, Leiden, 1970.

provided that a volume change ΔV_0 is associated with the perturbed equilibria.[1] When only one equilibrium is involved the excess absorption is given by[1]

$$\delta\alpha/N^2 = A/(1 + \omega^2\tau^2) = A/(1 + N^2/N_R^2) \quad (1)$$

where $\delta\alpha = \alpha - \alpha_0$ is the difference between the absorption coefficients for the polyelectrolyte solution and for the solvent, *i.e.*, water ; $\omega = 2\pi N$ is the angular frequency of the ultrasonic wave; $\tau = (2\pi N_R)^{-1}$ is the relaxation time associated with the equilibrium under study; N and N_R are the ultrasonic frequency and the relaxation frequency, respectively; and A, is a quantity independent of N. It has been shown that both A and τ are function of the two rate constants k_1 and k_{-1} characterizing the equilibrium and of the concentrations, c_i, of the species involved in the equilibrium. A can be written in the form[1]

$$A = \Delta V_0^2 \tau f(k_1, k_{-1}, c_i) \quad (2)$$

Equations 1 and 2 indicate that $\delta\alpha/N^2 = 0$ if $\Delta V_0 = 0$. For counterion binding reactions ΔV_0 is essentially due to the release by the counterion and the charged sites of the polyion of part of their hydration water. This release occurs only if counterions come close enough to polyion charged sites in order to bring about a strong decrease of the electrostatic field in the space surrounding ions and charged sites and containing the electrostricted water molecules (*i.e.*, the "A" region in the Frank and Wen's model[6]). Clearly, such counterions are those usually referred to as "site bound" or "specifically bound" counterions. In the following, site bound counterions are those whose hydration shells overlap those of charged sites. On the other hand, it can be safely assumed that counterions which constitute the ionic atmosphere of a polyion ("ionic atmosphere binding") retain practically all of their hydration water. Thus no volume change should be associated with this type of binding.

As was shown in an earlier paper,[5] the study of $\delta\alpha/N^2$ as a function of frequency and concentration may give the detailed mechanism of site binding and permit the determination of the rate constants. The purpose of this paper is to present additional results which substantiate those already reported[5] on polyethylenesulfonic acid (H-PES) and which show the effect of various parameters on site binding as detected through absorption measurements. These new results have been obtained mostly with solutions of polystyrenesulfonic acid (H-PSS), polyphosphate (PP), and alternating copolymer of maleic acid and methyl vinyl ether (Gantrez). A brief account of results concerning carboxymethylcellulose (CMC) is also given; a more thorough study on this polyelectrolyte will be published later.[7]

II. Experimental Section

Samples of Na-PES, Na-PSS, and Na-CMC were gifts from Hercules Powder Co., Dow Chemical Co., and Dr. M. Rinaudo (Grenoble, France). Solutions of these polyelectrolytes were purified and obtained in the acid form by passing them through columns of anion and cation-exchange resins. The acid content of the resulting solutions was determined by potentiometric titration. Tetramethylammonium (TMA) hydroxide was then added to obtain a neutralization degree of 0.95. Finally the TMA-polyelectrolyte solutions were diluted to the desired concentration. The polymerization degrees (*PD*) of CMC and PSS samples were unknown; that of PES was about 800.

Gantrez was purchased from Borden Chemical Co. in the form of an alternating copolymer of maleic anhydride and methyl vinyl ether. This copolymer was washed with ether, dissolved in acetone, reprecipitated in ether, and dried under vacuum. It was then dissolved in water and quantitatively hydrolyzed by heating at 60° for a few hours. The resulting solution was then purified and titrated as above. The *PD* of this copolymer was unknown.

A sample of K-PP ($PD > 1000$) was donated by Dr. U. P. Strauss. It was dissolved and transformed in TMA-PP by stirring with a TMA-neutralized cation-exchange resin (TMA-resin) and by passing the resulting solution through a column of TMA-resin. The concentration of this TMA-PP solution was determined by potentiometric titration of the hydrolyzed H-PP solution obtained by passing quantitatively a given volume of the TMA-PP solution through a cation-exchange resin and heating at 80–90° for 15 min to ensure a sufficient hydrolysis.

All stock solutions of TMA-polyelectrolytes were stored at 5°. The salts used in this work were of reagent grade purity and used without further purification. Throughout this paper concentrations are expressed in equiv/l.

The ultrasonic absorption coefficients were measured at 25° and 2.82 and/or 5.04 MHz using a two-crystal interferometer which has been described elsewhere.[8]

III. Results and Discussion

1. Existence of an Excess Absorption Due to Site Binding of Counterions. Figures 1 and 2 show the variation of $\delta\alpha/N^2$ *vs.* θ' = added salt concentration c_{XCl}/TMA-polyelectrolyte concentration c_p, for solutions of TMA-PP and TMA-PSS. These results are quite similar to those obtained for the effect of added alkali chlorides on the absorption of TMA-PES[5] and TMA-CMC[7] solutions.

These increases of $\delta\alpha/N^2$ with θ' may be interpreted: when alkali ions are introduced into TMA-polyelec-

(6) H. Frank and W. Wen, *Discuss. Faraday Soc.*, **24**, 133 (1957).

(7) R. Zana, C. Tondre, M. Rinaudo, and M. Milas, *J. Chim. Phys. Physicochem. Biol.*, in press.

(8) R. Cerf, *Acustica*, **13**, 417 (1963); S. Candau, *Ann. Phys. (Paris)*, **9**, 271 (1964).

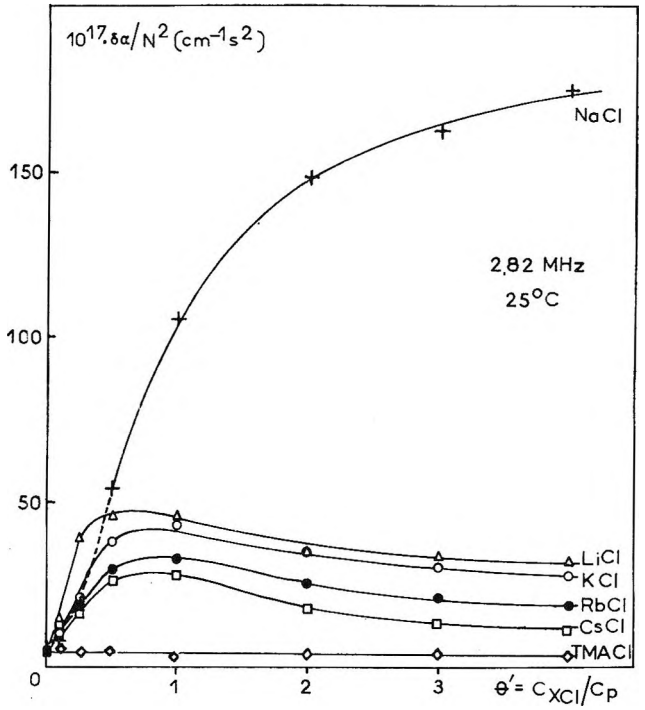

Figure 1. Tetramethylammonium polyphosphate: variation of $\delta\alpha/N^2$ with θ' upon addition of alkali chlorides and TMACl, $c_p = 0.035$ N.

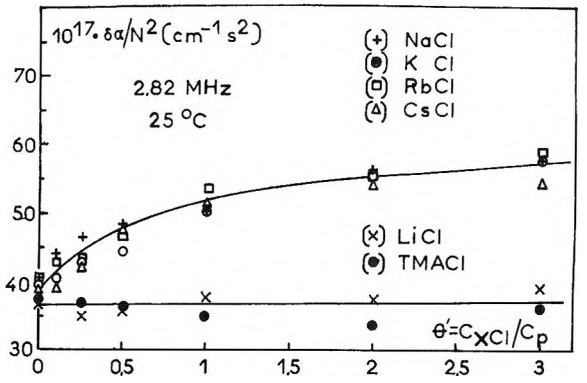

Figure 2. Tetramethylammonium polystyrenesulfonate: variation of $\delta\alpha/N^2$ with θ' upon addition of alkali chlorides and TMACl, $c_p = 0.1$ N.

trolyte solutions they may become site bound, in contrast with TMA ions which are not site bound because of their large radius.[5,9] This gives rise to a new absorption process and results in an increase of $\delta\alpha/N^2$ with θ'. However, before going any further one must consider the possible contributions of the three following processes to the increase of $\delta\alpha/N^2$.

(a) Relaxation processes involving the ionic atmosphere of the polyion[1] include electrostatic binding of the counterion as well as the relative movement of a polyion and its ionic atmosphere in the velocity field due to the sound wave. Such processes can be readily dismissed since in the Debye–Hückel approximation (which can be used for the moderately concentrated solutions used in this work: c_p ranging from 0.035 to 0.1 N) their contribution should not depend on the nature of the counterion, while our results show a strong dependence on this parameter[5,7] (Figures 1 and 2).

(b) Viscoelastic relaxations[10] which are related to the viscosity of the solution are known to be significant at frequencies well below 1 MHz,[11] *i.e.*, outside the frequency range investigated in this work. Moreover, their contribution should increase with the solution viscosity[10] while Figures 1 and 2 show that addition of salts which bring about a decrease of viscosity[12–14] result in an increase of $\delta\alpha/N^2$.

(c) Relaxation associated with conformational modifications of polyions occuring upon salt addition[12–14] may result in absorption changes in the megahertz range.[2,3] However, for polyphosphates no volume changes were observed upon addition of TMA-Cl to TMA-PP and of LiCl to Li-PP[9] although such additions bring about changes of conformation.[12] Volume change measurements have not yet been performed on the other polyelectrolytes studied in this work, but changes of conformation are known to occur for PES[13] and CMC[14] upon additions of salts. On the basis of Strauss, *et al.*,[9] results one should not expect any volume change and therefore, according to eq 1 and 2, any increase of absorption associated with conformal changes. Our results confirm this prediction since we found that for all TMA-polyelectrolytes studied so far[5,7] (Figures 1 and 2) $\delta\alpha/N^2$ is not modified upon TMACl additions up to $\theta' = 3$ and that additions of LiCl to Li-Gantrez and of NaCl to Na-CMC's[7] bring about only small changes of $\delta\alpha/N^2$.

Moreover, the striking behavior of NaCl on Figure 1 might be taken as an indirect evidence that the increase of $\delta\alpha/N^2$ is not due to conformal changes since the work of Strauss, *et al.*,[12] did not reveal any Na-specific conformal change of polyphosphate.

From the above discussion we conclude that the increase of $\delta\alpha/N^2$ with θ' is due to site binding processes.

2. Influence of the Nature of the Polyion. For a given added salt, our results[5,7] (Figures 1 and 2) show that the increase of $\delta\alpha/N^2$ with θ' depends strongly on the polyion. The effect of NaCl on $\delta\alpha/N^2$ for TMA-PP, PES, and PSS solutions has been represented in Figure 3 where $(\Delta\alpha/N^2)_{\theta'} = (\delta\alpha/N^2)_{NaCl,\theta'} - (\delta\alpha/N^2)_{TMACl,\theta'}$. CMC was not included as for this polyelectrolyte the effects depend very much on the substitution degree.[7] Whatever the added salt, $\Delta\alpha/N^2$ has been found to increase in the order PSS < PES < PP. This sequence

(9) U. P. Strauss and Y. Po Leung, *J. Amer. Chem. Soc.*, **87**, 1476 (1965).

(10) T. Litovitz and C. Davis, "Physical Acoustics," Vol. IIA, W. P. Mason, Ed., Academic Press, New York, N. Y., 1965, p 282.

(11) B. H. Zimm, *J. Chem. Phys.*, **24**, 269 (1956); P. Rouse, *ibid.*, **21**, 1272 (1953).

(12) U. P. Strauss, *et al.*, *J. Phys. Chem.*, **61**, 1353 (1957); *J. Amer. Chem. Soc.*, **82**, 1311 (1960).

(13) H. Eisenberg and G. Mohan, *J. Phys. Chem.*, **63**, 671 (1959).

(14) C. Pierre, M.A. Thesis, University of Grenoble, October 1969.

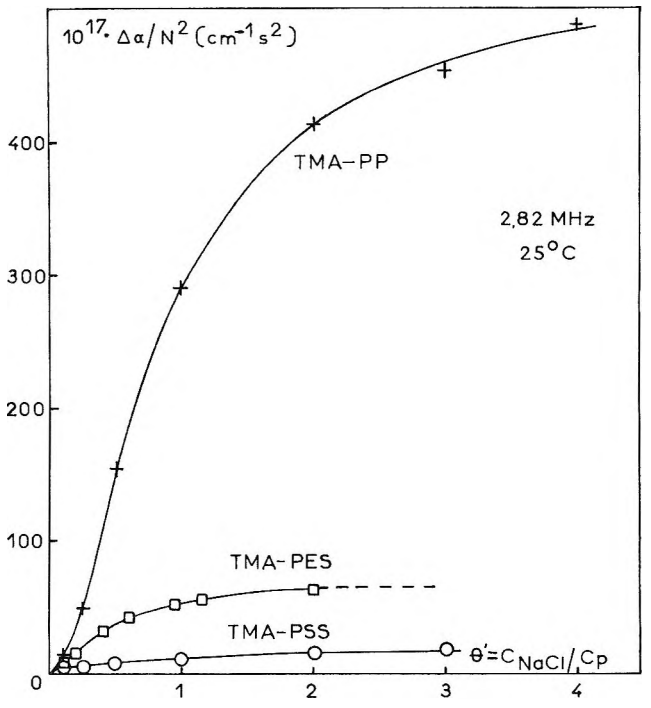

Figure 3. Effect of NaCl additions on $\Delta\alpha/N^2$ for TMA-PP, TMA-PES, and TMA-PSS, $c_p = 0.1$ N.

of polyions is the same as the one found by volume change measurements[9,15,16] and reflects the influence on $\Delta\alpha/N^2$ of the electrostriction of the polyion on the surrounding water molecules. This electrostriction depends on the intrinsic electrostriction of the charged site and on the minimum distance d between charged sites when one adopts the rod-like model[17] for polyions. The distance d which represents the actual distance between two charges on the cylinder equivalent to the polyion is different from the charge distance b which appears in the expression of the charge parameter λ, characteristic of the rod-like model[17] (b is related to the projection of d on the axis of the rod or cylinder). d depends on the polyion local conformation and on the distance between the charged group on the side chain and the polymer chain. Therefore, the differences in $\Delta\alpha/N^2$ for the three polyions cannot be explained in terms of λ since it has about the same value for PP, PES, and PSS. The average surface charge density cannot be used either because site binding is a local process in which the discrete nature of the charged sites must be considered. The results in Figure 3 indicate that the excess ultrasonic absorption due to site binding increases when d decreases since $d_{PP} < d_{PES} < d_{PSS}$.[18]

3. Counterion Sequences. The following sequences of counterions with respect to the resulting increase of $\delta\alpha/N^2$ have been obtained for $\theta' > 1$: TMA-PES,[5] H $\sim$ TMA $<$ Li $<$ Cs $<$ Rb $<$ Na $<$ K; TMA-PP, TMA $<$ Cs $<$ Rb $<$ K $<$ Li $\ll$ Na; TMA-PSS, H $\sim$ TMA $\sim$ Li $<$ Cs $\sim$ Rb $\sim$ K $\sim$ Na; TMA-CMC,[7] H $\sim$ TMA $<$ Cs $<$ Rb $<$ K $<$ Na $<$ Li.

It is striking that these ionic sequences are very similar to those obtained for PP,[12] PES,[13] and CMC[19] by other methods which may be referred to as "static" methods in contrast with ultrasonic absorption which is a "dynamic" method. The ionic sequence for PSS has not been reported yet. For TMA-PP an inversion similar to the one which can be seen in Figure 1 for the effects of Li^+ and Na^+ has also been found through intrinsic viscosity measurements.[12] These findings suggest that the ionic sequences obtained in this work may not be too modified when the ultrasonic frequency N is decreased although eq 1 and 2 predict a dependence of $\delta\alpha/N^2$ on the nature of the counterion through ΔV_0, k_1, k_{-1}, and the concentration of site-bound counterions. Our results may be taken as indicating that the relaxation frequencies, N_D, associated with the dehydration of counterions and polyions are of the order or larger than the narrow frequency range studied in this work (2.8–5.0 MHz), as was found for Na-PES.[5] On this basis, changes in the above ionic sequences must be expected at higher frequencies, when $N_D < N$, as the ratio N^2/N_D^2 (see eq 1) becomes significant and as the values of N_D are likely to depend on the nature of the counterion. At this point it must be remembered that in their ultrasonic absorption studies of alkali metal salts of small chelating agents, Eigen, *et al.*,[20] found ionic sequences which were shown to depend on frequency. This variation was attributed to differences in the binding of the various alkali ions by the chelating anions. It was also reported[20] that the relaxation frequencies were independent of concentration, varied very little with ionic strength, and increased only by a factor $\sim$5 in going from Li^+ to Cs^+. These results are quite similar to those reported in this paper and in others.[5,7,15]

The ionic sequences found in this work may now be explained if one assumes that site bound alkali ions are either fixed on one charged site (ion-pairing) or adopt an equilibrium position between two charged sites[9] separated by the distance d (see part III 2), depending on the respective values of the counterion radius and of d. The latter type of binding which is analogous to chelation would occur only when d is small enough. It may then be postulated that for a given polyion exists a counterion X whose radius is such that the binding of X results in a maximum neutralization of the elec-

(15) C. Tondre and R. Zana, unpublished results.

(16) M. Rinaudo and C. Pierre, *C. R. Acad. Sci., Ser. C*, 269, 1280 (1969).

(17) T. Alfrey, *et al.*, *J. Polym. Sci.*, 7, 543 (1951); G. Manning, *J. Chem. Phys.*, 51, 924 (1969).

(18) It is difficult to evaluate d without a model for the polymer chain. However the sequence $d_{PP} < d_{PES} < d_{PSS}$ is readily obtained when one adopts a planar zig-zag model for the polymer chain and sets the charge at the center of mass of the oxygen atoms.

(19) M. Rinaudo and M. Milas, *J. Chim. Phys. Physicochem. Biol.*, 66, 1489 (1969).

(20) M. Eigen, *Pure Appl. Chem.*, 6, 97 (1963); see also ref 1, p 450.

trostatic field in the counterion and charged site "A-regions"[6] and in turn, in a maximum release of electrostricted water molecules. Thus, the site binding of X should yield the largest volume change and the largest increase of $\delta\alpha/N^2$ at frequencies $N < N_{D,X}$ as indicated by eq 1. On the contrary, when d is large ion pairs would be formed and result in smaller increases of $\delta\alpha/N^2$. Polarization effects, invoked by others[21] to explain ionic sequences, may then be of importance.

The following facts are thought to give support to the above model. (a) Volume change measurements[9] have shown that, as expected the maximum volume change is obtained for a counterion which differs with the polyion under study.

(b) Our model predicts that the smaller d, the smaller the radius of the counterion for which the maximum increase of $\delta\alpha/N^2$ is observed, in agreement with our results on PP (Figure 1) and PES[5] for which $d_{PP} < d_{PHS}$: the maximum effects are observed, respectively, with Na^+ and K^+.

(c) For PSS, since d is large (>6 Å) the electrostriction is probably rather small and should therefore result in smaller $\delta\alpha/N^2$ increases than for other polyions. Moreover in this case only ion pairs may be formed with small ions while chelation may occur with large counterions. In the former case very small or no effects should be observed. Our results in Figure 2 seem to confirm these predictions since no effect is observed with Li^+ and H^+ while rather small effects can be seen for Na^+, K^+, Rb^+, and Cs^+.

(d) Results relative to Gantrez give evidence of the two types of site binding postulated in this work. It must be first remembered that Gantrez is a polydicarboxylic acid characterized by two well-separated pK_a's.[22] Therefore, at neutralization degree $\theta < 0.5$ at the most one CO_2H per monomer unit is ionized, and the distance d between charged sites is large (>5 Å at $\theta = 0.5$). At $\theta > 0.5$ the number of fully ionized monomer units increases linearly with θ. On these units d is small and chelation may occur. Figure 4 shows the variation of $\Delta\alpha/N^2$ with θ for the neutralization of Gantrez with NaOH and LiOH. $\Delta\alpha/N^2$ is defined as the difference between the values of $\delta\alpha/N^2$ at a given θ when the neutralization is conducted with XOH and TMAOH. Therefore, $\Delta\alpha/N^2$ may be assumed to represent the absorption term due to the binding of X. It can be seen that with both NaOH and LiOH, $\Delta\alpha/N^2$ remains quite small up to $\theta = 0.5$ and then increases rapidly and almost linearly with θ. The same ionic sequence was obtained with Gantrez and CMC.[7]

4. Case of H^+. H^+ has been dissociated from the other monovalent counterions because of its particular behavior.

In this work for PP and PSS and in ref 5 for PES it has been found that equimolecular solutions of H-polyelectrolyte and TMA-polyelectrolyte have the same value of $\delta\alpha/N^2$. Thus, in solutions of strong polyelectrolyte H^+ behaves as if it were not bound. Indeed, other techniques[23] have shown that there is no site binding of H^+ by PSS but preliminary volume change measurements seem to indicate that H^+ is somewhat site bound by PES.[15] On the basis of this last result one would have expected an absorption to be associated with the binding of H^+ by PES. Because of its extremely small size however H^+ may be expected to give rise only to ion pairs. That no absorption could be detected may indicate that the fraction of bound H^+ is too small to give rise to a measurable absorption.

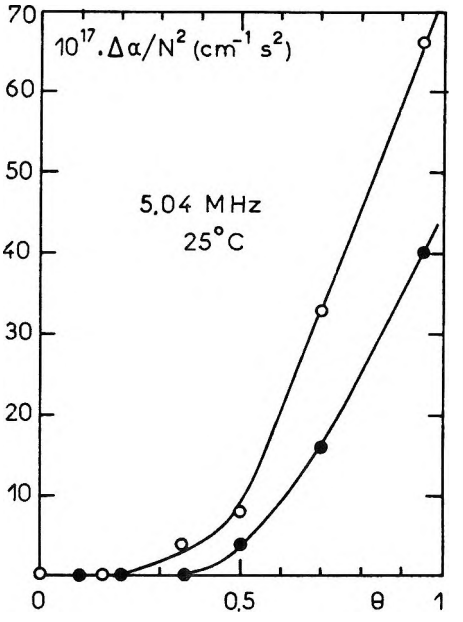

Figure 4. Gantrez: variation of $\Delta\alpha/N^2$ with the neutralization degree θ for the neutralization with NaOH (●) and LiOH (○), $c_p = 0.1$ N.

In a solution of weak polyelectrolytes, essentially polycarboxylic acids, we have shown[4,7] that a small although measurable absorption is associated with the binding of H^+ by $-CO_2^-$. This binding, however, results in the formation of a covalent bond and in a quite large ΔV_0 (up to 20 cm³/mol for polyacrylic acid[15]), and is probably different from the binding in solutions of strong polyelectrolytes.

In conclusion, it may be said that all the results given in this paper show that the observed increases of $\delta\alpha/N^2$ upon additions of alkali chlorides to solutions of TMA-polyelectrolytes are due to site binding processes involving the alkali ions. It is hoped that the results of volume change and ultrasonic absorption measurements

(21) H. Bungenberg de Jong, "Colloid Science," Vol. II, H. Kruyt, Ed., Elsevier, New York, N. Y., 1949, p 259.

(22) P. Dubin and U. P. Strauss, *J. Phys. Chem.*, **74**, 2842 (1970).

(23) S. Lapanje and R. Rice, *J. Amer. Chem. Soc.*, **83**, 496 (1961); L. Kotin and M. Nagasawa, *ibid.*, **83**, 1026 (1961).

now in progress in our laboratory will provide us with the detailed mechanism of site binding and with the values of the rate constants and of the fraction of site bound counterions.

NOTES

Determination of the Hindered Rotation Barrier in *Unsym*-Dimethylselenourea and Comparison with Similar Compounds

by L. W. Reeves,* R. C. Shaddick, and K. N. Shaw

The Chemistry Department, University of Waterloo, Waterloo, Ontario, Canada *(Received March 10, 1971)*

Publication costs assisted by the National Research Council of Canada

A recent review article by Kessler[1] collects the information regarding studies of the restricted rotation about C–N bonds in amido-type structures. It is evident that many of these data are reliable only as far as values of $\Delta G^{\ddagger}$, the free energies of activation, are concerned.[2,3] In amides and thioamides the order of these energies for hindered internal rotation about the C–N bond is now fairly well accepted. Consistency tests on the many studies can be made by plotting $\Delta S^{\ddagger}$ *vs.* $\Delta H^{\ddagger}$ and extrapolating the data for a given compound to $\Delta S^{\ddagger} = 0$. This gives the $\Delta G^{\ddagger}$ obtained from coalescence temperatures to a very good degree of precision and merely reflects the systematic errors in $\Delta H^{\ddagger}$ and $\Delta S^{\ddagger}$, which arise from the nmr experiment.[1,2,4]

Considering the general structure

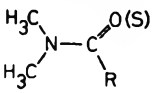

the following series of decreasing free energy of activation (in kcal mol^{-1} at 298°K) for amides with varying R has been measured

CN (21.4)	F (18.2)	CH_3(17.4)	Cl (16.8)
phenyl (14.8)	OCH_3 (15.2)		SCH_3 (11.4)

The corresponding series for the thioamides is

CN (23.4)	CH_3 (20.2)	Cl (19.1)
phenyl (18.4)	OCH_3 (17.8)	SCH_3 (15.7)

The data above have been assembled from ref 1–8 and some has come from our own unpublished studies.

With few exceptions, in the above series the barrier in the thioamides is about 2 kcal mol^{-1} higher than in amides for a given substituent. This can be attributed to the increased C–N π bond character expected for the thioamides in the ground state.[8] The phenyl group may differ because of the steric complications of the larger group. We shall be presenting these comparisons in more detail in a separate paper. Barriers in the corresponding urea compounds are not so well studied[4,6]

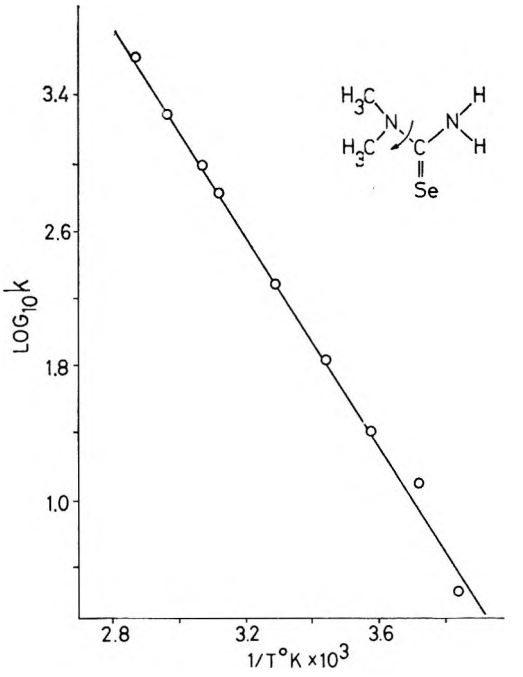

Figure 1. Arrhenius plot for the hindered internal rotation rates of *unsym*-*N*,*N*-dimethylselenourea.

(1) H. Kessler, *Angew. Chem. Int. Ed. Engl.*, 9, 219 (1970).

(2) A. Allerhand, H. S. Gutowsky, J. Jonas, and R. A. Meinzer, *J. Amer. Chem. Soc.*, 88, 3185 (1966).

(3) P. T. Inglefield, E. Krakower, L. W. Reeves, and R. Stewart, *Mol. Phys.*, 15, 65 (1968).

(4) J. Sandstrom, *J. Phys. Chem.*, 71, 2318 (1967).

(5) A. Lowenstein, A. Melera, P. Rigney, and W. Walter, *ibid.*, 68, 1597 (1967).

(6) A. S. Tompa, R. D. Barefoot, and E. Price, *ibid.*, 73, 435 (1969).

(7) R. C. Neuman and L. B. Young, *ibid.*, 69, 2570 (1965); R. C. Neuman, D. N. Roark and V. Jonas, *J. Amer. Chem. Soc.*, 89, 3412 (1967).

(8) L. W. Reeves and K. N. Shaw, *Can. J. Chem.*, in press, and unpublished work.

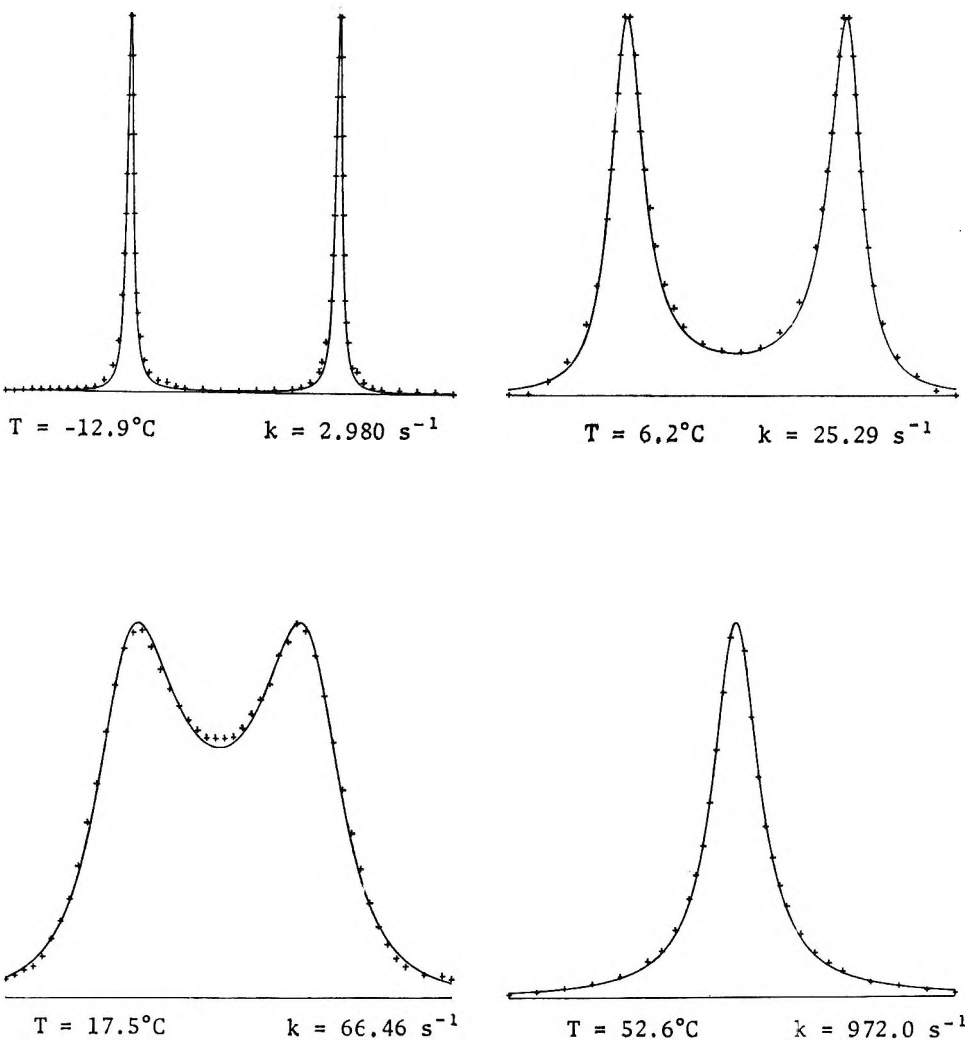

Figure 2. Selected line shape fit data for the nmr spectra of *unsym-N,N*-dimethylselenourea. The continuous line represents the computed line shape and the experimental data points are superimposed.

but it appears that *N*-methyl urea derivatives have extremely low barriers, such that spectral resolution by the nmr technique is not possible even at the lowest available sample temperatures ($\sim -160°$). The thioureas have a higher barrier to internal C–N rotation and estimates of $\Delta G^{\ddagger}$ for a series of methylthiourea solutions range from 13.2 to 14.4 kcal mol^{-1}.[6] The purpose of this present note is to report a study of *N,N*-dimethylselenourea (unsymmetrical) by a total line shape fit of the spectra of solutions 0.94 mol % in $CDCl_3$ at a series of temperatures between -12.9 and 74.7°. The compound was obtained from K and K Laboratories and recrystallized from chloroform before use. The residual $CHCl_3$ in the $CDCl_3$ was used as a line shape standard and 1% TMS was added as a lock signal. A Varian HA 100 with the standard variable temperature accessory was used for the study. Temperatures were defined by use of methanol and ethylene glycol samples,[9] in appropriate temperature regions. The spectra were especially simple to analyze, since no long-range coupling is observed and a trivial two site rate matrix suffices for the analysis.[8,10] The chemical shift difference between the equally populated methyl sites,

Table I: Kinetic Data for DMSeU (0.94 Mol % in $CDCl_3$)

Temp, °C	k, sec^{-1}
74.7	4360.0
63.9	1946.0
52.6	972.0
47.3	657.0
30.2	194.6
17.5	66.46
6.2	25.29
−4.4	12.47
−12.9	2.980

E_a = 14.31 ± 0.33 kcal mol^{-1}
$\Delta S^{\ddagger}$ = −2.88 ± 1.10 cal deg^{-1} mol^{-1} (298.2°K)
$\Delta H^{\ddagger}$ = 13.72 kcal mol^{-1} (298.2°K)
$\Delta G^{\ddagger}$ = 14.58 kcal mol^{-1} (298.2°K).

(9) A. L. Van Geet, *Anal. Chem.*, **40**, 2227 (1968).
(10) L. W. Reeves and K. N. Shaw, *Can. J. Chem.*, **48**, 3641 (1970).

2Ω,[10] was measured as 46.6 Hz and was conveniently independent of temperature.

The rate constants for internal rotation are set out in Table I which also lists the kinetic parameters extracted from the Arrhenius plot (Figure 1) in the usual manner.[2,3] Selected line shape fits are presented in Figure 2, where the continuous lines are computed line shapes and the data points from normalized experimental spectra are superimposed. The average spectral intensity deviation in all the line shape fits was less than 1.8%. In the table the value of $\Delta S^{\pm}$ is satisfactorily close to zero.

The contribution in simple amides of structure Ib which represents the π character of the C–N bond in the ground state is larger for thioamides than for amides because of the less efficient overlap of S 3p and C 2p orbitals.

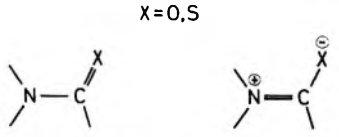

Ia Ib

The expected trend in urea compounds is analogous, but here the overall barrier is further lowered because of the sharing of π character between two C–N bonds, as shown by structures IIb and c.

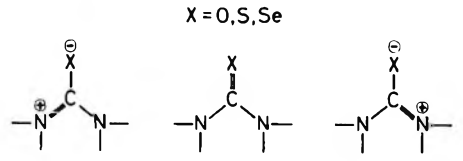

IIa IIb IIc

The previous study of thioureas was performed using coalescence temperatures in unsymmetrical ureas[6] and possibly on reexamination some downward adjustment of $\Delta G^{\pm} = 14$ kcal mol^{-1} would be expected.

Hologram Interferometry for Isothermal Diffusion Measurements

by Julius G. Becsey,* Nathaniel R. Jackson, and James A. Bierlein

Aerospace Research Laboratories, Wright-Patterson Air Force Base, Ohio 45433 *(Received March 18, 1971)*

Publication costs assisted by the Aerospace Research Laboratories

In this paper we report the use of hologram interferometry[1] for the study of isothermal diffusion from a boundary. The principal advantage of the method, aside from the simplicity of the optics, is that there is no need for optical-quality windows in the diffusion cell. Since the base hologram can be taken with the cell filled with a homogeneous solution, the real-time interferogram is formed between the reconstructed homogeneous cell image and the cell image with the diffusion in progress. Thus, all contributions due to optical retardation in the test zone are nulled out except those produced by the diffusion process. Traditional interferometric techniques such as Rayleigh,[2-4] Mach-Zehnder,[5] and wave-front shearing[6-11] do not possess this valuable characteristic.

Our finite fringe hologram interferometer is essentially the same as described before[12,13] with the exception of the laser (in this work we used a 15-mW CW He/Ne laser), collimator lenses (f.l. = 36 cm), recording camera (35-mm model, f.l. = 135 mm), and base hologram plate holder. To eliminate inevitable shrinkage due to atmospheric humidity changes, a wet-gate plate holder was used (Jodon Engineering Associates) which affords excellent fringe stability over long periods. The base holograms were recorded on Agfa Scientia 8E75 and 10E75 plates (about $^1/_{10}$ to $^1/_{50}$-sec exposures). The real-time interferograms were recorded on Kodak Pan-X film (about $^1/_{500}$-sec exposures). To minimize the skewness of the interferograms due to higher order aberrations in the cell, the recording camera was focused at a plane located within the cell at one-third of the cell length measured from the exit window.[14] The magnification of the recording camera was also determined at this plane. The measurements were taken in a flowing-junction cell[5] about 8 cm high, length 7.95 cm, width 0.8 cm. The beam deflector was adjusted so that five finite fringes appeared in the image of the cell.

To interpret the finite fringe interferograms, we need to know the optical path P in a free-diffusion cell at any distance x measured upward from the initial boundary (eq 1).

(1) L. O. Heflinger, R. F. Wuerker, and R. E. Brooks, *J. Appl. Phys.*, **37**, 642 (1966).

(2) J. StL. Philpot and G. H. Cook, *Research (London)*, **1**, 234 (1948).

(3) L. G. Longsworth, *J. Amer. Chem. Soc.*, **74**, 4155 (1952).

(4) H. Svensson, *Acta Chem. Scand.*, **4**, 399, 1329 (1950); **5**, 72, 1301 (1951).

(5) C. S. Caldwell, J. R. Hall, and A. L. Babb, *Rev. Sci. Instrum.*, **28**, 816 (1957).

(6) E. J. Ingelstam, *J. Opt. Soc. Amer.*, **47**, 536 (1957).

(7) O. Bryngdahl, *Acta Chem. Scand.*, **11**, 1017 (1957).

(8) O. Bryngdahl and S. J. Ljunggren, *J. Phys. Chem.*, **64**, 1264 (1962).

(9) O. Bryngdahl, *J. Opt. Soc. Amer.*, **53**, 571 (1963).

(10) W. J. Thomas and McK. Nicholl, *Appl. Opt.*, **4**, 823 (1965).

(11) C. N. Pepela, B. J. Steel, and P. J. Dunlop, *J. Amer. Chem. Soc.*, **92**, 6743 (1970).

(12) G. E. Maddux and J. G. Becsey, *Rev. Sci. Instrum.*, **41**, 880 (1970).

(13) J. G. Becsey, G. E. Maddux, N. R. Jackson, and J. A. Bierlein, *J. Phys. Chem.*, **74**, 1401 (1970).

(14) H. Svensson, *Opt. Acta*, **1**, 25 (1954).

$$P(t,x) \equiv L\mu(t,x) = L\bar{\mu} + (L\Delta\mu/2)\,\mathrm{erf}(x/2\sqrt{Dt}) \quad (1)$$

Here t is the time since the start of the experiment, L is the geometric length of the cell, μ is the instantaneous refractive index at any vertical distance x, $\bar{\mu}$ is the mean of the initial refractive indices of the diffusing solutions, $\Delta\mu$ is their difference, and D is the isothermal diffusivity. A fringe number j can be assigned to a selected fringe if one counts (in the direction of decreasing x) the number of the fringes intercepting the continuation of the vertical and straight portion of any fringe until the selected fringe is reached. Since the distance between the adjacent fringes corresponds to a path difference of one wavelength, the fringe number j can be expressed as a function t and x

$$j(t,x) \equiv P(t,x \longrightarrow \infty)/\lambda - P(t,x)/\lambda = (L\Delta\mu/2\lambda)[1 - \mathrm{erf}(x/2\sqrt{Dt})] = (L\Delta\mu/2\lambda)\,\mathrm{cerf}(x/2\sqrt{Dt}) \quad (2)$$

We index each interferogram serially in time by the subscript $m = 1, 2$, etc., and each fringe number on the interferogram by $n = 1, 2$, etc. In practice it is necessary to introduce a zero-time correction t_0 (applicable to all t_m) and a base-line correction B_m (peculiar to each interferogram) to account for error in locating the straight portion of the fringes. Hence eq 2 becomes

$$j(t_m,x_{m,n}) = j_{m,n} = (L\Delta\mu/2\lambda)\,\mathrm{cerf}[x_{m,n}/2\sqrt{D(t_m + t_0)}] + B_m \quad (3)$$

For each interferogram taken at time t_m the value of $x_{m,n}$ was measured for each $j_{m,n}$; the parameters D, t_0, $L\Delta\mu/2\lambda$, and a set of B_m were calculated by the minimization of the function

$$\sum_{\mathrm{ALL}\,m} \sum_{\mathrm{ALL}\,n} [(j_{\mathrm{calcd}})_{m,n} - (j_{\mathrm{obsd}})_{m,n}]^2 \quad (4)$$

where $(j_{\mathrm{calcd}})_{m,n}$ is given by eq 3. A grid-search type nonlinear least-squares method was applied in the data reduction process.[15]

The interferograms obtained during the interdiffusion of water and 0.03 M aqueous KCl solution are shown in Figure 1. Table I summarizes our results for several different systems. $\bar{M}$ is the mean of the initial molal concentrations and ΔM is the initial concentration difference between the interdiffusing solutions. The errors given are the standard errors of the mean obtained from independent measurements. The zero-time corrections ranged between 0 and 90 sec; the values of B_m were of the same magnitude as the average fringe number errors (about 0.08). All measurements were made at 25.0°. The experimental values are in reasonable agreement with other determinations.[16-18]

It is also possible to record the entire refractive field in the free-diffusion cell by taking holograms during the diffusion process. If these holograms are reconstructed by a collimated laser beam (incident from the same angle as the original reference beam), the real object beam can be studied by different optical methods. Figure 2 shows an interferogram obtained from a hologram (0.005 M aqueous KCl/water at 25.0°, t = 10.3 min) with a wave-front shearing interferometer.[7,8] Thus, the actual refractive

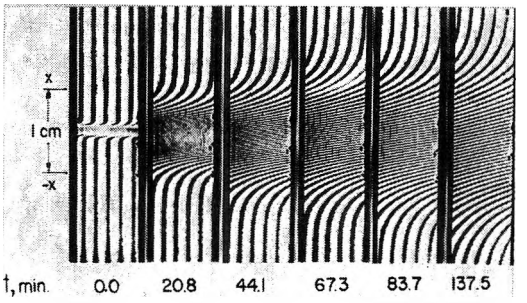

Figure 1. Finite fringe real-time hologram interferograms. Aqueous KCl (0.03 M) diffusing into pure water at 25.0°.

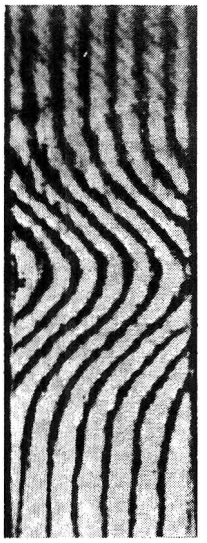

Figure 2. Wave-front reconstruction by holograms and analysis with wave-front shearing interferometer.

Table I: Isothermal Diffusivities of Various Aqueous Solutions at 25.0° Measured by Hologram Inferferometry

Aqueous solution	$\bar{M}$	ΔM	$D \times 10^5$, cm²/sec: This work	$D \times 10^5$, cm²/sec: Literature
KCl	0.0150	0.0300	1.872 ± 0.012	1.876[a]
D_2O	0.9973	1.9946	2.242 ± 0.014	2.264[b]
D_2O	0.4923	0.9845	2.284 ± 0.014	2.268[b]
CdI_2	0.4674	0.0287	0.808 ± 0.006	...

[a] References 16 and 17. [b] Reference 18.

(15) J. G. Becsey, L. Berke, and J. R. Callan, *J. Chem. Educ.*, **45**, 728 (1968).

(16) H. S. Harned and L. R. Nuttall, *J. Amer. Chem. Soc.*, **71**, 1460 (1949).

(17) H. S. Harned and L. R. Nuttall, *ibid.*, **69**, 736 (1947).

(18) L. G. Longsworth, *J. Phys. Chem.*, **54**, 1914 (1960).

index field can be recorded and reconstructed at any time for evaluation by various optical methods chosen at convenience.

Vibrational Deexcitation of Highly Excited Polyatomic Molecules. The Amount of Energy Transferred per Collision[1a]

by B. S. Rabinovitch,*[1b] H. F. Carroll,[1c] J. D. Rynbrandt, J. H. Georgakakos,

Department of Chemistry, University of Washington, Seattle, Washington 98105

B. A. Thrush, and R. Atkinson

Department of Physical Chemistry, University of Cambridge, Cambridge, CB2 1EP, United Kingdom *(Received June 1, 1971)*

Publication costs assisted by the Air Force Office of Scientific Research

The purpose of this note is to clarify the conclusions from some recent studies of collisional energy transfer involving highly vibrationally excited polyatomic molecules.

A study of the collisional quenching of vibrationally excited, ground electronic state cycloheptatriene (CHT), and of its deuterated analog CHT-d_8, has been reported by Atkinson and Thrush[2] (AT). From their treatment of the data, AT concluded that the average amount of energy removed from CHT per collision ($\langle\Delta E\rangle$) by various bath gases is (kJ mol^{-1}): CHT, 17.5; toluene, 11.5; SF_6, 5.9; CO_2, 3.8; He, 0.6. These magnitudes agree with earlier estimates based on fluorescence quenching experiments with β-naphthylamine.[3] However, they are much smaller than the *down-jump* steps reported at room temperature by Kohlmaier and Rabinovitch[4] (KR) from chemical activation studies of vibrationally excited *sec*-butyl radicals (kJ mol^{-1}): SF_6, ≥ 37; C_4H_8, ≥ 37; CO_2, 16.7; He, ≥ 3.3. The values of AT are smaller yet than those deduced for vibrationally excited cyclopropanes[5] chemically activated by methylene radical reaction.

Atkinson and Thrush suggested that their results would be better reconciled with those of KR if the latter's values had been incorrectly deduced: they proposed that an error by KR of a factor of 2 in the calculated magnitudes of the decomposition rate constants, k_E, could have led to an error of more than a factor of 2 in the deduced $\langle\Delta E\rangle$ quantities. In addition, they proposed that while k_E values were known accurately in the cyclopropane work, an incorrect value of $\Delta H_f°(CH_2)$ had caused an error in the assumed energy and treatment of cyclopropane; with use of the original data, but with a current value of $\Delta H_f°(CH_2)$, AT presented drastically revised $\langle\Delta E\rangle$ quantities for the cyclopropane system (kJ mol^{-1}): He, 0.6; Ar, 1.6; N_2, 1.9; C_2H_4, 2.5. The value so obtained for He is in striking agreement with the like quantity for CHT.

It is evident that some disagreements in interpretations and conclusions exist between the data treatment and results of the Washington and Cambridge groups. Setser, *et al.*,[6] have called attention recently to a difference in interpretation between their recent results on halogenated ethanes and that of AT. We wish here to examine these matters in some depth, albeit with brevity.

The data of AT were analyzed by them in terms of Stern–Volmer plots with multistep quenching, and with the assumption that a constant amount of energy was removed from CHT on each collision. We first wish to demonstrate that the discrepancy between the work of the Washington and Cambridge groups is not as large as was originally stated—especially for less efficient bath gases. We have applied the stochastic method of data treatment[4,7,8] to the He–CHT data. Theoretical values of k_E were similar to those used previously.[2] Two sets of weak collider calculations were made—one for a stepladder, and the other for an exponential distribution of down-transition probabilities. On the basis of a stepladder model, which was employed by AT, the average energy amount transferred per *down-step* from CHT is 1.9 kJ mol^{-1}. This quantity is three times larger than the original value of AT. The increase is due mainly to the fact that AT (as well as the earlier workers with β-naphthylamine[3]) neglected up-transitions; these have a probability relative to down-transitions which is governed by detailed balance. The correction is smaller for more efficient gases; thus, the original value of 3.8 kJ for CO_2 is raised to 5.0 kJ, while the values for toluene and CHT are essentially unchanged. Nonetheless, the values of $\langle\Delta E\rangle$ found for down-steps for He and CO_2 from the CHT work are now only two to three times smaller than those of KR, and any discrepancy is substantially reduced. Some discrepancy still remains and depends, in part, on the relative magnitudes of the collision cross sections used by

(1) (a) This work was supported by the Air Force Office of Scientific Research, Directorate of Chemical Sciences, under Contract No. F 44620-70-C-0012; (b) on leave, 1971; (c) on leave from Kingsborough Community College, The City University of New York, City University Research Fellow.

(2) R. Atkinson and B. A. Thrush, *Proc. Roy. Soc., Ser. A*, **316**, 131 (1970).

(3) M. Boudart and J. T. Dubois, *J. Chem. Phys.*, **23**, 223 (1955).

(4) G. Kohlmaier and B. S. Rabinovitch, *ibid.*, **38**, 1692, 1709 (1963).

(5) J. W. Simons, B. S. Rabinovitch, and D. W. Setser, *ibid.*, **41**, 800 (1964); D. W. Setser, B. S. Rabinovitch, and J. W. Simons, *ibid.*, **40**, 1751 (1964).

(6) W. G. Clark, D. W. Setser, and E. E. Siefert, *J. Phys. Chem.*, **74**, 1670 (1970).

(7) J. H. Georgakakos, B. S. Rabinovitch, and E. J. McAlduff, *J. Chem. Phys.*, **52**, 2143 (1970); J. D. Rynbrandt and B. S. Rabinovitch, *J. Phys. Chem.*, **74**, 1679 (1970).

(8) Y. N. Lin and B. S. Rabinovitch, *ibid.*, **72**, 1726 (1968).

AT.[9] Of course, there is no reason why $\langle \Delta E \rangle$ values should be identical for different substrates and systems.[2]

What meaning is to be attached to $\langle \Delta E \rangle$ quantities? Atkinson and Thrush suggested in their concluding remarks, as a preferred interpretation of the data obtained by them, that most collisions with inefficient bath gases are elastic and that a large amount of energy, perhaps an average vibrational quantum of ~16 kJ mol^{-1}, is removed on infrequent collisions, *e.g.*, 1 in 28 for He, say, rather than a much smaller amount on virtually each collision. On this basis, however, the remaining disagreement between the two groups becomes the question, how important is elastic collision? Is the elastic collision probability, p_{ii}, close to unity for He, for example, as suggested by AT?[10]

The Cambridge data offer no information on this matter since theirs is a "high pressure" study.[4,7] The work of the Washington group cited,[4,5] and later studies,[6,7] were made at both "high" and "low" pressures and do provide such information, as do thermal dilution studies.[8] We may recall (see ref 4 and 7) that the "high pressure" single-channel kinetics method for studying energy transfer gives values of $\langle \Delta E \rangle$ which depend, as required input, upon the magnitude of the inelastic collision cross section; by contrast, the "low pressure" method yields values of $\langle \Delta E \rangle$ which refer only to inelastic collisions and which require no knowledge of the inelastic collision cross section. The measurements to date which are diagnostic for this matter supply a consistent answer: "low pressure" single-channel reaction systems, of the kind considered above, and later work with multiple channel reaction systems[7,11] give concordant values for the behavior of a given inefficient bath gas in similar systems; these values of $\langle \Delta E \rangle$ when applied to the "high pressure" single-channel data show that p_{ii} has no special weight. In short, the relative magnitudes of inelastic collision cross sections for all gases appear to be closely similar to those of conventional[9] total kinetic collision cross section and, in the case of helium, say, is certainly not as low as $^1/_{28}$ of such magnitude. This conclusion is further supported by the consistency of relative effective cross sections found from energy transfer cross sections with those deduced from transport properties.[9,12] Thus, for helium, smaller amounts of energy are transferred on virtually every collision, rather than very large amounts at infrequent collisions.

Finally, it was suggested by AT that the calculated values of $\langle \Delta E \rangle$ in (1) the *sec*-butyl radical system and in (2) the cyclopropane system depend strongly on the magnitudes of the theoretical k_E used in the data interpretation in the first case[4] and on an error in the value of $\Delta H_f^\circ(CH_2)$ used[5] in the second case. We have reinvestigated this matter by detailed *ad hoc* stochastic calculations. The suggestion of AT proves to be greatly overdrawn. In the first case, the experimental magnitudes of KR depend principally on "low pressure" data, and the proposed error in k_E changes the deduced magnitude of $\langle \Delta E \rangle$ by only 10%. The error in $\Delta H_f^\circ(CH_2)$ in the second case[5] is actually irrelevant since the thermochemistry was specified in empirical manner as based on reasonably well known (within a factor of 2, say) values for k_E in the cyclopropane system. Moreover, the original $\langle \Delta E \rangle$ values for cyclopropanes[5] have recently been reconfirmed by a reinvestigation of the dimethylcyclopropane system,[8] while the *sec*-butyl data agree with a large number of recent investigations of other similar radical systems.[7]

There is no doubt that experimental error may affect some or all of the data under consideration. For instance, there is an inconsistency between the data reported by AT for CHT and CHT-d_8.[13] Some values for CHT-d_8 at lower energies are inaccurate but can be corrected.

Acknowledgment. One of us (B. S. R.) is grateful for the hospitality of Trinity College (Oxon) during his tenure there as a Visiting Fellow, and for that of the Department of Physical Chemistry, Oxford University.

(9) L. D. Spicer and B. S. Rabinovitch, *J. Phys. Chem.*, **74**, 2445 (1970).

(10) If this suggestion is correct, however, there should then not be nearly as much curvature in the calculated Stern–Volmer plots presented by AT for He, CO_2, and SF_6 (Figures 5 and 6 of ref 2), since the curvature depends on the magnitude of the average energy amount transferred per *inelastic* collision and not on the magnitude of the average amount per total number of collisions; elastic collisions do not affect the shape of the Stern–Volmer curve.

(11) D. C. Tardy, C. W. Larson, and B. S. Rabinovitch, *Can. J. Chem.*, **46**, 341 (1968); C. W. Larson and B. S. Rabinovitch, *J. Chem. Phys.*, **51**, 2293 (1969).

(12) Y. N. Lin, S. C. Chan, and B. S. Rabinovitch, *J. Phys. Chem.*, **72**, 1932 (1968); S. C. Chan, J. T. Bryant, L. Spicer, and B. S. Rabinovitch, *ibid.*, **74**, 2058 (1970).

(13) The experimental magnitudes of k_E for the two compounds diverge with increase of E in a manner contrary to the theoretical predictions for normal isotope effects in externally activated systems; see B. S. Rabinovitch and J. H. Current, *Can. J. Chem.*, **40**, 557 (1962).

The Reaction of Acetaldehyde and *tert*-Butyl Hydroperoxide[1]

by M. C. V. Sauer and John O. Edwards*

Department of Chemistry, Brown University, Providence, Rhode Island 02912 *(Received May 7, 1971)*

Publication costs assisted by U. S. Air Force Office of Scientific Research

The stoichiometry and thermodynamics of the addition reaction (eq 1) of acetaldehyde and *tert*-butyl hydroperoxide have been studied by proton magnetic resonance spectroscopy.

(1) Abstracted from a portion of the Ph.D. thesis of Maria C. V. Sauer at Brown University, 1970.

$$CH_3C(=O)H + HOOC(CH_3)_3 \rightleftharpoons CH_3C(OH)HOOC(CH_3)_3 \quad (1)$$

Nmr Spectra. The nmr spectrum of pure acetaldehyde consists of a quadruplet at δ 9.68 and a doublet at δ 2.15 (Figure 1). The quadruplet was assigned to the aldehydic proton and the doublet to the methyl group.

The nmr spectrum of *tert*-butyl hydroperoxide consists of a singlet at δ 1.25 assigned to protons of the *tert*-butyl group and a quite broad resonance at δ 7.97 assigned to the proton of the hydroperoxide group.[2]

The nmr spectra of mixtures of acetaldehyde and *tert*-butyl hydroperoxide show (in addition to the resonances of pure acetaldehyde and *tert*-butyl hydroperoxide) a quadruplet centered at δ 5.35 and a doublet centered at δ 1.24. The broad peak assigned to the hydroxy and hydroperoxy groups was shifted in this spectrum to about δ 5.

The assignments of the doublet and the quadruplet of the addition product were checked by measuring the coupling constants; it was found that $J_{\text{doublet}} = J_{\text{quadruplet}} = 5.50$ cps. Similarly, for acetaldehyde, the assignments were confirmed by the coupling constants: $J_{\text{doublet}} = J_{\text{quadruplet}} = 2.84$ cps.

The δ 1.25 resonance due to the *tert*-butyl group in *tert*-butyl hydroperoxide appears in the mixtures spectra as a slightly broad peak and apparently overlaps with the resonance due to the *tert*-butyl group in the addition product. By varying the total concentration of *tert*-butyl hydroperoxide it was found that under the experimental conditions the resonance was saturated. The saturation was noticed because with increasing concentrations of *tert*-butyl hydroperoxide the intensity of the peak remained unchanged and by decreasing the radiofrequency of the oscillator the intensity of the peak in a particular sample increased.[3]

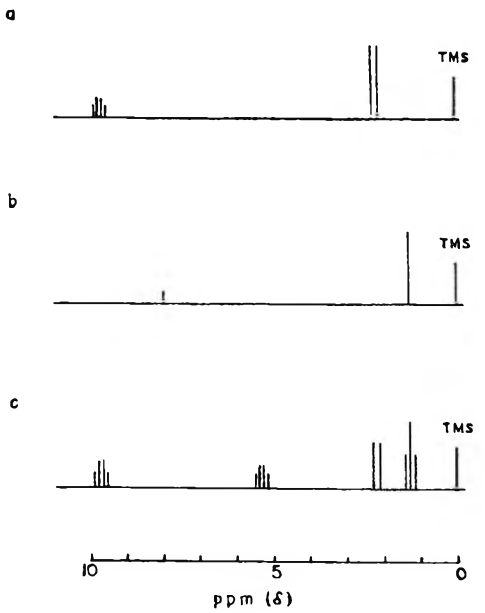

Figure 1. The nmr spectra of acetaldehyde (a), *tert*-butyl hydroperoxide (b), and a mixture of acetaldehyde and hydroperoxide (c) relative to tetramethylsilane; assignments are given in text.

To avoid the saturation problem, solvent benzene was added to the system and, when working at low temperatures, small concentrations of *tert*-butyl hydroperoxide were used. Under these conditions, the δ 1.25 resonance became narrower and it was possible then to distinguish the chemical shifts of the *tert*-butyl group in the free *tert*-butyl hydroperoxide and in the addition product; these shifts are less than 2 cps apart.

The product nature and stoichiometry of the reaction were checked in every spectrum by measuring the relation in intensities between the *tert*-butyl resonance, the methyl doublet, and the proton quadruplet of the addition product.

$$\frac{I_{tert\text{-butyl}}}{I_{\text{methyl}}} = \frac{3}{1} \qquad \frac{I_{tert\text{-butyl}}}{I_{\text{proton}}} = \frac{9}{1}$$

Results. The equilibrium constants K were calculated according to the equations

$$K = \frac{[\text{addition product}]_e}{[CH_3CHO]_e[tert\text{-BuOOH}]_e}$$

and

$$[CH_3CHO]_e = \left(\frac{I_{CH_3CHO}}{I_{CH_3CHO} + I_{\text{addition product}}}\right)[CH_3CHO]_0$$

wherein I refers to the intensity of the nmr signal for the respective quadruplets. Similarly, from conservation of mass, we have

$$[\text{addition product}]_e = [CH_3CHO]_0 - [CH_3CHO]_e$$

and

$$[tert\text{-BuOOH}]_e = [tert\text{-BuOOH}]_0 - [\text{addition product}]_e$$

The subscripts zero and e refer to initial and equilibrium states, respectively. The reaction was studied in the concentration range for acetaldehyde from 2.6 to 6.2 M, for *tert*-BuOOH from 1.7 to 2.5 M, and benzene concentration from 3.7 to 7.4 M.

At least four experiments at different concentrations were performed at each temperature. The equilibrium constants obtained, along with standard deviations, are presented in Table I. The corresponding Van't Hoff plot showed some scatter but no deviation from linearity. The derived thermodynamic parameters for finite concentrations are as follows: $\Delta H = -8.60$

(2) D. Swern, A. H. Clements, and T. M. Lwong, *Anal. Chem.*, 41, 412 (1969).

(3) J. A. Pople, W. G. Schneider, and J. H. Bernstein, "High-Resolution Nuclear Magnetic Resonance," McGraw-Hill, New York, N. Y., 1959.

kcal mol^{-1}, $\Delta G = -0.66$ kcal mol^{-1}, $\Delta S = -26.6$ cal mol^{-1} deg^{-1}, and $T\Delta S = -7.94$ kcal mol^{-1}.

Table I: Equilibrium Constants at Different Temperatures for the Reaction of Acetaldehyde with *tert*-Butyl Hydroperoxide (Eq 1)

Temp, °C	K, M^{-1}
−1.0	12.2 ± 0.8
5.5	9.3 ± 0.5
10.0	6.7 ± 0.5
12.0	5.6 ± 0.5
17.5	4.8 ± 0.4
25.5	3.1 ± 0.4

The value of K for the reaction of *tert*-BuOOH with acetaldehyde is slightly less (a factor of 4 at 0°; a factor of 2 after statistical correction) than for hydrogen peroxide and acetaldehyde. Since conditions could not be made identical, the difference is only an estimate; nevertheless, it is clearly small. Also there are small differences in the values of ΔH and ΔS (more negative for H_2O_2 addition). It seems clear that the addition process is essentially the same for H_2O_2 and *tert*-BuOOH; the replacement of H by a *tert*-butyl group has little significance on the reaction.

Acknowledgments. We are grateful to the U. S. Air Force Office of Scientific Research (Grant No. 70-1839) for continued support.

COMMUNICATIONS TO THE EDITOR

Dependence of the Glass Transition Temperature on Heating Rate and Thermal History

Publication costs assisted by Catholic University of America

Sir: In a recent paper Rasmussen and MacKenzie[1] have reported glass transition temperatures, T_g, measured by differential thermal analysis (dta) as a function of heating rate for water–alcohol solutions. Using a treatment proposed by McMillan,[2] they calculated activation entropies and enthalpies for the glass transition relaxation from their data. We wish to report here some preliminary results of an analysis of heat capacity measurements in the glass transformation region which indicate that no fundamental significance can be attached to the kinetic parameters derived by the method of the above authors.[1,2]

McMillan's treatment[2] is in error in that he considers the heat capacity, C, rather than the enthalpy, H, to be the relaxing quantity in the glass transition region. (McMillan's treatment cannot account, for instance, for the maxima commonly observed[3] in heat capacity–temperature plots near T_g.) The correct approach is to consider the total enthalpy of a glass-forming liquid to be the sum of a nonrelaxing part, H_0, and a relaxing part, H_r

$$H(T,t) = H_0(T) + H_r(T,t)$$

The heat capacity changes and the breaks in the dta curves observed near T_g are then associated with the time–temperature dependence of the relaxing part of the enthalpy, for which a corresponding relaxational heat capacity may be written

$$C_r(T,t) = \partial H_r(T,t)/\partial T$$

The simplest assumption for the time dependence of the relaxational enthalpy is the first-order kinetic expression

$$\frac{\partial[H_r(T,t) - H_r^\infty(T(t))]}{\partial t} = -\frac{[H_r(T,t) - H_r^\infty(T(t))]}{\tau(T(t))} \quad (1)$$

τ is the relaxation time and H_r^∞ is the equilibrium relaxational enthalpy, such that at constant temperature

$$H_{r,T}^\infty = \lim_{t\to\infty} H_{r,T}$$

In eq 1 it is presumed that the temperature–time schedule of the system is known, so that H_r^∞ depends ultimately only on T. This, along with the assumption of linearity, also makes τ a function only of T. Previous relaxation experiments have shown that eq 1 is generally inadequate both in that more than one time constant τ is needed to account for the observed data and in that first-order kinetic expressions fail at fairly

(1) D. H. Rasmussen and A. P. MacKenzie, *J. Phys. Chem.*, **75**, 967 (1971).

(2) J. A. McMillan, *J. Chem. Phys.*, **42**, 3497 (1965).

(3) U. E. Schnaus, C. T. Moynihan, R. W. Gammon, and P. B. Macedo, *Phys. Chem. Glasses*, **11**, 213 (1970).

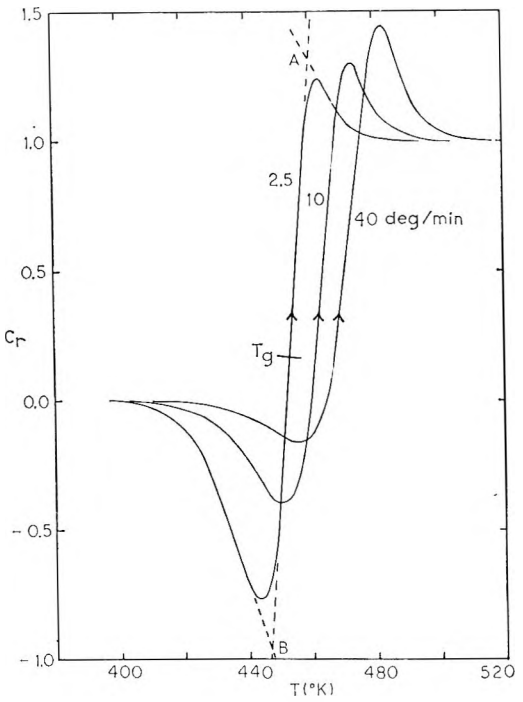

Figure 1. Calculated heat capacity curves for various heating rates of glasses quenched at a rate of −40 deg/min.

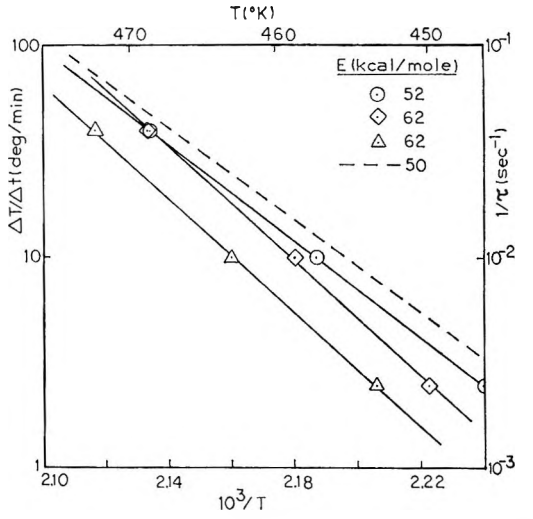

Figure 2. Arrhenius plots and activation energies for heating or cooling rate *vs.* T_g and relaxation time *vs.* temperature: ⊙, T_g measured for a cooling schedule starting above the glass transition region; ◇, T_g measured for a heating schedule of glasses quenched at −2.5 deg/min; △, T_g measured for a heating schedule of glasses quenched at −40 deg/min; – – –, Arrhenius plot for $1/\tau$.

small departures from equilibrium.[4-6] Since the calculations to be described here are intended only to be illustrative of the effect of thermal history and heating or cooling rate on T_g, however, it is sufficient for our present purposes to assume the simple relaxation kinetics given in eq 1.

Integration of eq 1, followed by differentiation with respect to T, allows calculation of C_r as a function of temperature. The value of H_r at the initial time and temperature is a required boundary condition for the integration and is determined by the previous thermal history of the system. In Figure 1 we show some C_r *vs.* temperature curves calculated in this fashion. (Details of the calculation will be presented in a future publication.) These are sample calculations using a value of

$$\tau = A \exp(E/RT)$$

with $A = 1 \times 10^{-22}$ sec and $E = 50{,}000$ cal/mol, which gives a glass transition around 200°. The C_r values are normalized to zero and unity at the respective low- and high-temperature limits.

The C_r curves shown in Figure 1 were calculated for various heating rates of glasses which were first quenched at a rate of −40 deg/min from a temperature well above the glass transition region to a temperature well below it. T_g has been taken as the midpoint of the line AB, to correspond with the T_g definition of Rasmussen and MacKenzie.[1] In Figure 2 Arrhenius plots of heating rate *vs.* T_g are shown for the curves of Figure 1, along with similar plots for glasses of other thermal histories and for the relaxation time τ. The activation energies, E, for the various plots are given in the figure.

Two important points may be gleaned from Figure 2. The first is that the T_g values measured for a given rate of change of temperature with respect to time depend both on the thermal history of the glass and on the direction of temperature change (heating or cooling). Hence it is not a fruitful exercise to concern oneself overly with the assessment of an exact and "correct" T_g value at a given heating rate for a given substance, as Rasmussen and MacKenzie[1] have attempted to do for the case of water. That is, T_g values at 5 deg/min outside their limits of −137 ± 1° can be obtained for water samples subjected to different thermal histories, as is suggested by the scatter in their Figure 7.[1] (We do not mean here to denigrate the value of T_g *vs.* composition studies for glasses of identical thermal history, as conducted by Rasmussen and MacKenzie[1] and numerous others.)

Second and more important, the activation energies (and other kinetic parameters) assessed from the dependence of T_g on heating rate also depend on thermal history and type of heating or cooling schedule and do not necessarily correspond to the activation energy for the relaxation time controlling the glass transformation phenomena. For the sample calculations summarized in Figure 2, the apparent activation energy for T_g was

(4) M. Goldstein and M. Nakonecznyj, *Phys. Chem. Glasses*, **6**, 126 (1965).

(5) P. B. Macedo and A. Napolitano, *J. Res. Nat. Bur. Stand.*, **71A**, 131 (1967).

(6) L. Boesch, A. Napolitano, and P. B. Macedo, *J. Amer. Ceram. Soc.*, **53**, 148 (1970).

found to deviate by as much as 25% from the relaxation time activation energy.

It should be evident from the foregoing that the extraction of fundamental kinetic parameters for the glass transition from the temperature dependence of the heat capacity will require analysis of the entire C *vs.* T curves in the transition region, taking into account the thermal history of the glass. Such an analysis will also require the use of kinetic expressions more realistic than eq 1. We are currently at work on this problem and hope to be able to report its solution in a future publication.[7]

Acknowledgment. This research was supported by a grant from the Air Force Office of Scientific Research.

(7) EDITOR'S NOTE. Drs. D. H. Rasmussen and A. P. MacKenzie (Cryobiology Institute, RFD 5, Box 137, Madison, Wis.), the authors of ref 1, comment as follows. We are very pleased to learn of the work of Moynihan and Macedo. Lest we appear from their paper to have endorsed a particular theory of the nature of glass relaxation phenomena, we wish to take this opportunity to say we believe we made ourselves clear concerning our reservations regarding McMillan's treatment. In the absence of a treatment founded upon more generally accepted concepts of the glassy state, we restricted ourselves to the derivation of empirically useful information.

CHEMICAL ENGINEERING AND MATERIALS SCIENCE DEPARTMENT AND VITREOUS STATE LABORATORY
CATHOLIC UNIVERSITY OF AMERICA
WASHINGTON, D. C. 20017

CORNELIUS T. MOYNIHAN
PEDRO B. MACEDO

RECEIVED JUNE 14, 1971

Electron Transfer Reactions of Ferrocenes[1]

Publication costs assisted by the Ames Laboratory of the U. S. Atomic Energy Commission

Sir: The rate of electron exchange between ferrocene and ferricenium ions, as in reaction 1, has been of long-

$$Fe(C_5H_5)_2 + {}^*Fe(C_5H_5)_2^+ = Fe(C_5H_5)_2^+ + {}^*Fe(C_5H_5)_2 \quad (1)$$

standing interest. Successful kinetic studies using radiotracer methods have been limited to low temperatures (−70°) in methanol;[2,3] even there the rate is so high as to be barely measurable. The use of nmr line broadening has likewise been frustrated owing to the high transverse relaxation time of ferricenium ion.[4]

Our approach to this problem has been to evaluate the rates of *net* electron transfer reactions between substituted derivatives, rather than the exchange process itself. These data may then permit, under certain theoretical models, the calculation of a value for the exchange rate constants.

For example, one reaction studied is reaction 2.

$$Fe(C_5H_5)(C_5H_4\text{-}n\text{-}Bu)^+ + Fe(C_5H_4CH_3)_2 = Fe(C_5H_5)(C_5H_4\text{-}n\text{-}Bu) + Fe(C_5H_4CH_3)_2^+ \quad (2)$$

Although also quite rapid, these cross reactions give rise to net observable chemical change, making them more amenable to study. In the present studies, the rate constants were evaluated, typically within a standard deviation of 5–10%, using the stopped-flow method with very low reactant concentrations, (1–10) × 10^{-6} M, under reversible second-order conditions.[5,6]

In all, ferrocene and seven of its substituted derivatives of the type $Fe(C_5H_5)(C_5H_4X)$ and $Fe(C_5H_4X)_2$ were studied. The formal electrode potential for each compound was determined in the same medium by potentiometric titration. These values, summarized in Table I, permit the calculation of the equilibrium constant for each of the cross reactions as in eq 2.[7] Rate measurements were made on 22 reactions. Figure 1 depicts the results of these determinations in the form of a plot of log k_{ij} *vs.* log K_{ij} (where i and j refer to the numbers 1–8 assigned the ferrocenes in Table I). The data appear to be reasonably linear, and the slope of the line shown is 0.55.

This graphical treatment is suggested by the Marcus relation[8] for adiabatic, outer-sphere electron transfer

Table I: Electrode Potentials and Calculated Electron Exchange Rate Constants for Ferrocene and Substituted Ferrocenes, $Fe(C_5H_4X)(C_5H_4Y)$[a]

	X, Y	$E°'$, V *vs.* sce	10^{-6} k_{ii},[b] M^{-1} sec^{-1}
1	CH_3, CH_3	+0.1899 ± 0.0005	6.6
2	n-C_4H_9, n-C_4H_9	+0.2353 ± 0.0004	6.7
3	H, n-C_4H_9	+0.2556 ± 0.0005	6.5
4	H, H	+0.2719 ± 0.0005	5.7
5	H, HgCl	+0.2797 ± 0.0004	5.3
6	H, CH_2OH	+0.2806 ± 0.0005	4.2
7	H, C_6H_5	+0.3267 ± 0.0010	18
8	H, I	∼+0.427	14

[a] $E°'$ and k refer to 25.0°, in 1:1 v/v n-PrOH/H_2O with μ = 0.050 M, $Ba(ClO_4)_2$ electrolyte. [b] Electron exchange rate constant, as in reaction 1, computed fitting experimental k_{ij} values to eq 3.

(1) Work performed in the Ames Laboratory of the U. S. Atomic Energy Commission. Contribution No. 3044.

(2) D. R. Stranks, *Discussions Faraday Soc.*, **29**, 73 (1960).

(3) G. Lang, M.S. Thesis, Washington University, St. Louis, Mo., 1956.

(4) M. Dietrich, Ph.D. Thesis, Washington University, St. Louis, Mo., 1962.

(5) A Durrum stopped-flow spectrophotometer having a Kel-F mixing chamber with a 2-cm optical path was used for these determinations. The reactions were followed at wavelengths in the region 230–270 nm where the difference in molar absorptivity between the two ferrocenes was the greatest. The data were fit to the kinetic equation for reaction 2 using standard relations.

(6) A. A. Frost and R. G. Pearson, "Kinetics and Mechanism," 2nd ed, Wiley, New York, N. Y., 1961, pp 187, 188.

(7) As a matter of convention the cross reactions in eq 2 are all written such that $K > 1$. The rate constants referred to are those for the reactions proceeding in the forward direction, although in many cases kinetic determinations were carried out from both sides.

(8) (a) R. A. Marcus, *J. Phys. Chem.*, **67**, 853 (1963); (b) W. L. Reynolds and R. W. Lumry, "Mechanisms of Electron Transfer," Ronald Press, New York, N. Y., 1966, Chapter 6.

$$k_{ij} = (k_{ii}k_{jj}K_{ij}f_{ij})^{1/2} \quad (3)$$

where k_{ii} and k_{jj} are the electron exchange rate constants between the respective ferrocene and its oxidized form, k_{ij} the (experimental) rate of net electron transfer as in eq 2, K_{ij} is the equilibrium constant, and f_{ij} is the quantity defined by $\log f_{ij} = (\log K_{ij})^2/4 \log (k_{ii}\, k_{jj}/Z^2)$, Z being the collision frequency of neutral molecules, $10^{11}\ M^{-1}\ \text{sec}^{-1}$. The success of eq 3 in correlating other outer-sphere electron transfer processes has been noted by Sutin and wcoorkers.[9-12]

In this case, the validity of the treatment of the data implied by Figure 1 depends upon the eight electron exchange rate constants (k_{ii}, k_{jj}) being the same and f_{ij} remaining close to unity. The data are not in bad agreement with this model. More quantitatively, however, the 22 values of k_{ij} can be used according to eq 3 to derive "best" values for the exchange rate constants, assuming that the form of the Marcus relation

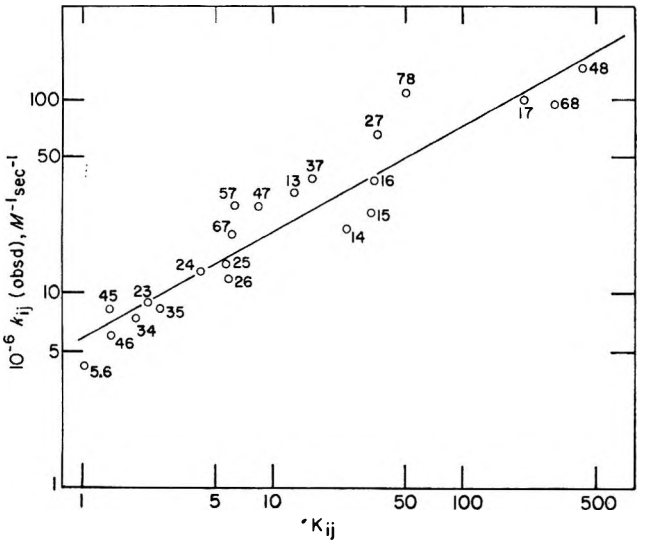

Figure 1. A plot of the log of the experimental rate constants k_{ij} *vs.* log K_{ij} for the net electron transfer reaction as in eq 2. The compounds are identified by the numbers in Table I, with the convention as stated.[7]

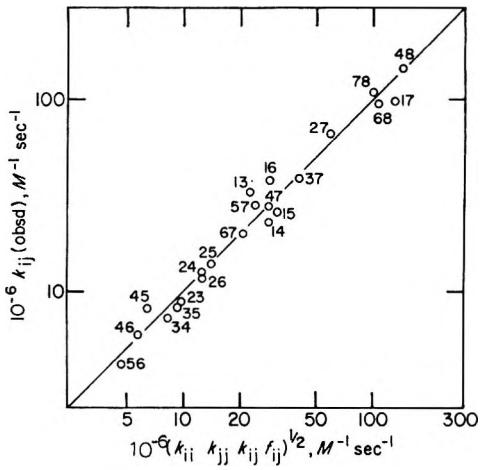

Figure 2. A plot of the log of the experimental rate constants k_{ij} *vs.* log $(k_{ii}\ k_{jj}\ k_{ij}\ f_{ij})^{1/2}$, the latter calculated from the parameters given in Table I. Same legend as in Figure 1.

is correct. These calculated rate parameters are also listed in Table I and are seen to cover but a factor of 4 in magnitude. Using these eight parameters and the electrode potentials, the 22 cross-reaction rate constants are recalculated to within an average deviation of 13%. The agreement of theory and experiment are shown in Figure 2, where the experimental values of log k_{ij} are plotted against the log of the right-hand side of eq 3 using the parameters given in Table I.

(9) M. H. Ford-Smith and N. Sutin, *J. Amer. Chem. Soc.*, **83**, 1830 (1961).

(10) G. Dulz and N. Sutin, *Inorg. Chem.*, **2**, 917 (1963).

(11) H. Diebler and N. Sutin, *J. Phys. Chem.*, **68**, 174 (1964).

(12) R. J. Campion, N. Purdie, and N. Sutin, *Inorg. Chem.*, **3**, 1091 (1964).

(13) Fellow of the Alfred P. Sloan Foundation, 1968–1970.

INSTITUTE FOR ATOMIC RESEARCH AND DEPARTMENT OF CHEMISTRY
IOWA STATE UNIVERSITY
AMES, IOWA 50010

JOHN R. PLADZIEWICZ
JAMES H. ESPENSON*[13]

RECEIVED JUNE 28, 1971

Molecular Sieve Zeolites

ADVANCES IN CHEMISTRY SERIES No. 101 and 102

Seventy-seven papers from a symposium co-sponsored by the Divisions of Colloid and Surface Chemistry, Petroleum Chemistry, and Physical Chemistry of the American Chemical Society and Worcester Polytechnic Institute, Edith M. Flanigen and Leonard B. Sand, co-chairmen.

Do you need a group of substances that can remove radioactive isotopes from nuclear wastes, remove ammonia from secondary sewage effluents, remove sulfur dioxide from waste gases, foster formation of actinides, or disrupt bacterial cells? These and many other possibilities are available through research on molecular sieve zeolites. For example, they are used for

- separating hydrogen isotopes
- solubilizing enzymes
- carrying active catalysts in curing of plastics
- transporting soil nutrients in fertilizers
- filtering tars from cigarette smoke

"Molecular Sieve Zeolites" reports recent advances in this rapidly developing field. Volume I offers 41 papers devoted to the synthesis, structure, mineralogy, and modification of sieve zeolites. These are followed in Volume II by 36 papers discussing sorption and catalysts.

Volume I: 526 pages with index. Cloth bound (1971) $16.00
Volume II: 459 pages with index. Cloth bound (1971) $16.00
No. 101 and 102 ordered together $30.00
Postpaid in U.S. and Canada; plus 35 cents elsewhere.
Set of L.C. cards with library orders upon request.

Other books in the ADVANCES IN CHEMISTRY SERIES of interest to colloid and surface, petroleum, and physical chemists include:

No. 97 Refining Petroleum for Chemicals
293 pages Cloth bound (1970) $11.50

No. 89 Isotope Effects in Chemical Processes
278 pages Cloth bound (1969) $13.00

No. 87 Interaction of Liquids at Solid Substrates
212 pages Cloth bound (1968) $9.50

Order from:

Special Issues Sales
American Chemical Society
1155 16th St., N.W.
Washington, D.C. 20036

HARPER & ROW

1817

JUST PUBLISHED

Procedures in Nucleic Acid Research Volume II

Edited by GIULIO L. CANTONI and DAVID R. DAVIES
National Institutes of Health

Sixty articles describe methodologies in nucleic acid research. Encompassing the latest advances in the field, this volume stresses methods of general applicability. Focus is on physical, physiochemical, and chemical techniques used to analyze and characterize nucleic acids—spectroscopic and hydrodynamic methods, centrifugation techniques (including a specialized technique for measuring the length of lambda DNA), and physiochemical techniques ranging from temperature-jump methods for the chemical modification of nucleic acids and for the study of nucleic acid-protein interactions. Special section on the preparation and purification of nucleic acids. October, 1971. Tentative: 900 pp.; $35.00.

Modern Theory of Polymer Solutions

HIROMI YAMAKAWA, Kyoto University

Systematically describes the theoretical advances of the last 20 years in the study of the equilibrium and nonequilibrium properties of dilute polymer solutions. Emphasis throughout is on physical pictures and theoretical methods, which are carefully developed and explained. June, 1971. 619 pp.; $19.95.

RECENTLY PUBLISHED

Introductory Quantum Chemistry

S. R. LA PAGLIA, Georgetown University

This modern text emphasizes observables and real chemical systems. Recent contributions of computer calculations are introduced to increase understanding. Covered in depth: the chemical bond, development of the wave theory of matter, principles of quantum mechanics, atoms and the periodic system, the diatomic molecule, molecular spectra and molecular structure, polyatomic molecules, PI electron theory, Ligand field theory. Prerequisite: One year of college calculus. Other necessary mathematics incorporated in opening chapters. 1971. 416 pp.; $13.95.

For more information on these and our other texts write Dept. 275C, Harper & Row, 49 East 33rd St., N.Y. 10016

Get your 8¢ worth.

Here is our ESR and our Laser Raman Spectrophotometer. Low cost, expandable, and worth knowing more about. A note and an 8¢ stamp will bring complete information from JEOL, 235 Birchwood Ave., Cranford, N. J. 07016

ESR

Console – Solid state modular design.
Magnet – 6″, 9″, and 12″-wide gap.
Frequency – X, K and Q band available.
Standard Cavity – X band cylindrical type, UV irradiation port, g-value marker.
Recorder – XYT type synchronous display with oscilloscope.
Accessories – Rapid field scan, variable temperature, plus 26 more.

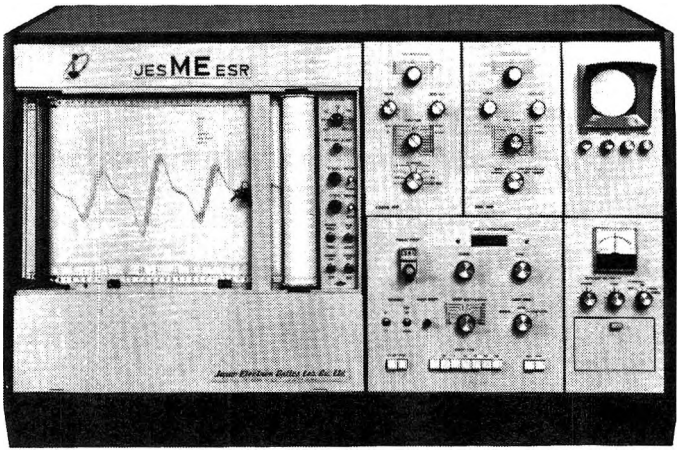

Laser Raman

Console – Push button solid state design.
Optics – Ghost-free monochrometer.
Laser Source – All commercial models available.
Sample Chamber – Oversized area for sample versatility.
Detection System – Wide Photon-counting range.
Recorder – Dual pen, providing simultaneous Raman spectrum and depolarization ratio measurement.
Resolution – 1cm^{-1} guaranteed.

NMR Spectrometers/Mass Spectrometers/ESR Spectrometers/Laser Raman Spectrophotometers/Laboratory Computers/Scanning Electron Microscopes
Electron Microscopes/X-ray Diffractometers/Amino Acid Analyzers.